Development of a Machine-Tooling-Process Integrated Approach for Abrasive Flow Machining (AFM) of Difficult-to-Machine Materials with Application to Oil and Gas Exploration Components

A thesis submitted in partial fulfilment for the degree of Doctor of Engineering

by

Mitchell James Howard

School of Engineering and Design, Brunel University

June 2014

Abstract

Abrasive flow machining (AFM) is a non-traditional manufacturing technology used to expose a substrate to pressurised multiphase slurry, comprised of superabrasive grit suspended in a viscous, typically polymeric carrier. Extended exposure to the slurry causes material removal, where the quantity of removal is subject to complex interactions within over 40 variables. Flow is contained within boundary walls, complex in form, causing physical phenomena to alter the behaviour of the media. In setting factors and levels prior to this research, engineers had two options; embark upon a wasteful, inefficient and poor-capability trial and error process or they could attempt to relate the findings they achieve in simple geometry to complex geometry through a series of transformations, providing information that could be applied over and over.

By condensing process variables into appropriate study groups, it becomes possible to quantify output while manipulating only a handful of variables. Those that remain un-manipulated are integral to the factors identified. Through factorial and response surface methodology experiment designs, data is obtained and interrogated, before feeding into a simulated replica of a simple system. Correlation with physical phenomena is sought, to identify flow conditions that drive material removal location and magnitude. This correlation is then applied to complex geometry with relative success. It is found that prediction of viscosity through computational fluid dynamics can be used to estimate as much as 94% of the edge-rounding effect on final complex geometry. Surface finish prediction is lower (~75%), but provides significant relationship to warrant further investigation.

Original contributions made in this doctoral thesis include; 1) A method of utilising computational fluid dynamics (CFD) to derive a suitable process model for the productive and reproducible control of the AFM process, including identification of core physical phenomena responsible for driving erosion, 2) Comprehensive understanding of effects of B_4C-loaded polydimethylsiloxane variants used to process Ti6Al4V in the AFM process, including prediction equations containing numerically-verified second order interactions (factors for grit size, grain fraction and modifier concentration), 3) Equivalent understanding of machine factors providing energy input, studying velocity, temperature and quantity. Verified predictions are made from data collected in Ti6Al4V substrate material using response surface methodology, 4) Holistic method to translating process data in control-geometry to an arbitrary geometry for industrial gain, extending to a framework for collecting new data and integrating into current knowledge, and 5) Application of methodology using research-derived CFD, applied to complex geometry proven by measured process output.

As a result of this project, four publications have been made to-date – two peer-reviewed journal papers and two peer-reviewed international conference papers. Further publications will be made from June 2014 onwards.

Executive Summary

Industrially-supported academic research is critical to enhancing the precision engineering capability of UK manufacturers. This summary is intentionally written in business-level technical language, from the perspective of the sponsor organisation.

The abrasive flow machining (AFM) process is a niche precision engineering part finishing technique. It, therefore, satisfies Mollart Engineering's strategic view of business development as a specialist service. There is not a great deal of competition for AFM processes in the precision engineering marketplace in which Mollart Engineering operates. The AFM process was brought to Mollart by buying a machine from Micro Technica in Germany to develop a process to eliminate burrs in Mollart's oil and gas work. The AFM process is ideally suited for the media to act on sharp corners and profiles of machined features in the complex titanium deep-hole-drilled parts for which the company is well known. The effect of the AFM media smoothing and eliminating burrs in specific locations was identified as a process that could be developed further.

Unfortunately, the lack of experience, part complexity and unusual media fluid behaviour conspire to make the process difficult to understand and control. This provided the business case for Mollart to apply for EPSRC and TSB support in order to understand the process better by conducting a formal research and development programme. The AFM process has been developed in a scientific manner, and stands to highlight Mollart's technical ability to take a promising manufacturing process which has earned itself 'black-art' status and remove the mystery surrounding its effects, for Mollart's own business development.

Mollart's current two major oil and gas partners, Schlumberger and Weatherford, where currently approximately £1.5M of business per annum is obtained, have both shown an interest in the process that would result in Mollart winning more business. This is provided the current product quality is improved by the AFM process against competitors. These two customers have direct revenue benefits to Mollart's existing business. The key question now remains as to how far an AFM business can be developed beyond Mollart's traditional core competency of deep hole drilling.

There is a more general market for better quality deburred components than presently being offered by two competitors Extrude Hone in Milton Keynes, and Deburring Services in Cheltenham, England. Beyond this, there are international export sales potential for AFM. It is also possible that Mollart could extend its current machine tool business by buying Micro Technica in Germany or becoming an agent for an AFM machine manufacturer. Mollart is already a global machine tool business with a network of agents available to help develop AFM machine sales. Media sales as a consumable product are also a viable avenue of exploitation.

There are also some industry specific businesses that Mollart have identified as being of possible interest. Medical industry bone ball joints are a good example of just one medical part that demands good surface finish that AFM offers. Smith & Nephew and Johnson & Johnson are already customers of Mollart deep hole drilling machines. The plastic mould industry and the optics industry also have componentry that demand high surface finishes that could be offered by Mollart as either a subcontract or a machine sale business. To develop a market in these highly specialised industries would necessitate Mollart working with a partner. Mollart could develop a consultancy service for AFM processes in specialised industries.

The AFM process is synergistic with the rapidly growing market of 3D printing technologies, which is an additive machining process. Metal layer forming by laser technology are becoming acceptable competitors to traditional subtractive machining methods. Build times are reduced, particularly on prototype work, and the benefits of the 3D process will increasingly be seen by a number of manufacturing companies. This could be developed to the point where traditional manufacturers may have to readjust their manufacturing process focus. To take advantage of this advancement in technology, a partnership with a 3D machine manufacturer could be established where they produce the net shape and Mollart would complete the product to a closer tolerance and finer surface finish. Currently, the surface finish generated by the 3D process is very poor. The nature of 3D printing means geometries can be produced that would not be possible with current machine shop technologies, which in turn means that traditional final-machining or finishing operations will not always be suitable. In conclusion, as a ‘liquid sandpaper’ tool, AFM is the perfect partner-technology to ensure surface finish is of an engineering standard for components used in many industries from oil and gas, medical, aerospace, plastics, optics, semiconductors, 3D printing and automotive industries.

Attempts by Mollart to win market share in complex part manufacturing is the key to their future, and is a reliable source of future revenues and profit that this project can help develop. The mechanical nature of the process ensures a repeatable result, which is a critical advantage over traditional manual work. It is also evident that in a situation where the process is optimised and working with good repeatability, Mollart can be certain that the operation cycle time and output will be consistent when using AFM. As the service operator, Mollart could form a series of new relationships required to support, develop and sell the service. Suppliers have been defined throughout the project. In a commercial implementation, work has already been attracted away from Kennametal Extrudehone upon demonstration of improved technical understanding. Target markets for Mollart’s aforementioned subcontract service exist initially in-house, with the process set to be applied initially to complex high value oil and gas parts. Target markets are still under research and will be driven largely by opportunity.

Acknowledgements

I would like to express my gratitude to the staff of Mollart Engineering, in particular Mr Guy Mollart and Mr Mike Pragnell, for supporting the Engineering Doctorate programme and providing their guidance, support and insight throughout the project. Without their support this research would not have been possible.

For their supervision and assistance in navigating academic challenges and academic-industrial relationships, I would like to thank Professor Kai Cheng and Professor Luiz Wrobel. I would also like to thank Mrs Janet Wheeler for her administrative support.

Playing a key role in the funding of the research, I would like to thank the Engineering and Physical Sciences Research Council (EPSRC) and the Technology Strategy Board (TSB).

Without the encouragement and patience instilled in me by my parents James and Shelley Howard, I would not have reached this point – I once read that being ‘smart’ does not earn one a doctorate, but perseverance, tenacity and cogency do – I know I can attribute that to my parents.

Valuable assistance from subcontractors is recognised in the form of training by Dr Mike Slack (Ansys Fluent) and in rheological characterisation by the staff of Escubed Ltd.

Author's Declaration

I declare that this thesis is my own unaided work. It is being submitted for the degree of Doctor of Engineering (EngD) at Brunel University, Uxbridge, Middlesex, UK. It has not been previously submitted for any other degree or examination in any other university.

Mitchell James Howard

Snarestone, June 2014

Contents

Reader's Guide

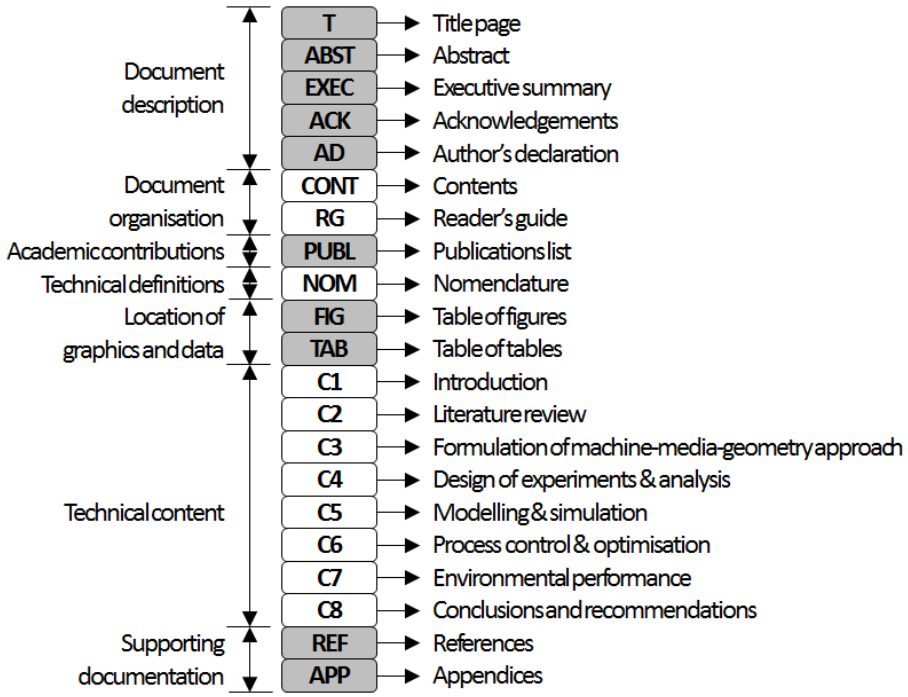

The figure above is designed to help guide the reader through the structure of the document in a single page, starting with the document description – title page, abstract, acknowledgements and the author's declaration preface the document contents. Document organisation is presented in a traditional contents page, followed by this page. The academic contributions made during the project are highlighted on the next side, followed by technical definitions should the reader be unfamiliar with some of the terminology used throughout the document. A separate reference is made to the location of figures and tables.

The document body is laid out in a logical, flowing manner; the introduction provides background to the process, its reason for existence and how the project came into being. Literature is then analysed to describe the state-of-art and make a case for the approach to the project – the highly-integrated system is described in chapter three. Initial technical works and empirical data collection are described in chapter four, while chapter five begins to produce an in-silico copy of physical systems. Chapter six defines the method for controlling the physical-virtual relationship and chapter seven discusses the approach and implementation perspectives when working with practical setups. Chapter eight discusses the environmental aspects of the process, considering the tools and processes it aims to replace, while chapter nine draws conclusions and looks at opportunities for further research and commercial implementation strategies. References and appendices are also provided.

Publications list

During the period of registration on the Engineering Doctorate programme, the author has produced several pieces of peer-reviewed work;

- Abrasive flow machining: R&D strategy and challenges in industrial applications.
  Published in Advances in Manufacturing Technology XXVI Volume 1 (Tenth International Conference on Manufacturing Research), published 11/SEP/2012.

- An industrially-feasible approach to process optimisation of abrasive flow machining and its implementation perspectives.
  Published in Proceedings of the Institution of Mechanical Engineers, Part B: Journal of Engineering Manufacture, volume 227, issue 11, November 2013, pp. 1744-1748.

- An integrated systematic investigation of the process variables on surface generation in abrasive flow machining (AFM) of Titanium alloy 6Al4V.
  Published in Proceedings of the Institution of Mechanical Engineers, Part B: Journal of Engineering Manufacture (2014) 0954405414522210.

- Energy and resource efficiency in the abrasive flow machining process: an assessment of environmental and economic viability within a UK precision machining SME.
  Accepted 22nd March 2014, due to be published in Proceedings of the ASME 2014 International Design Engineering Technical Conferences & Computer and Information in Engineering Conference, IDETC/CIE 2014, Aug 17-20, Buffalo, New York, USA. Paper number DETC2014-34110.

- Mollart Engineering; Abrasive flow machining of complex geometry. Technology Strategy Board (TSB), 'Smart' Award, Proof of Concept (PoC) category.
  Application submitted directly to TSB, successfully awarded on 25/JUN/2012. Blind peer-review was carried out by five anonymous reviewers, followed by an internal panel of eight appropriate industrial technologists. Application was one of ~60 successful from ~800 applicants.

Nomenclature

i. Abbreviations

AFF	Abrasive Flow Finishing
AFM	Abrasive Flow Machining
AJM	Abrasive Jet Machining
AJP	Abrasive Jet Polishing
AMEE	Advanced Manufacturing and Enterprise Engineering
AMMG	Abrasive Micromachining and Microgrinding
ASTM	American Society for Testing and Materials
AWM	Abrasive Water Jet Machining
B_4C	Boron Carbide
BB	Box Behnken
BCC	Body-Centred Cubic
BP	Back Propagation
CAE	Computer-Aided Engineering
CCD	Central Composite Design
CFD	Computational Fluid Dynamics
CIP	Carbonyl Iron Particles
(C)NC	(Computer) Numerical Control
CSA	Cross Section Area
CSD	Cross Section Diameter
CTE	Coefficient of Thermal Expansion
DBGAFM	Drill-Bit Guided Abrasive Flow Machining
DPM	Double Planetary Mixer
DPM	Discrete Phase Model
EAFM	Extrusion Abrasive Flow Machining
EBM	Environmentally Benign Manufacturing
ECM	Electro-Chemical Machining
EDM	Electron-Discharge Machining
EH	Extrude/Extrusion Honing
EPDM	Ethylene Propylene Diene Monomer
EPSRC	Engineering and Physical Sciences Research Council
FCC	Face-Centred Cubic
FEPA	Federation of European Producers of Abrasives
FF	Full Factorial
FTIR	Fourier Transform Infrared Spectroscopy
GA	Genetic Algorithm
GCMS	Gas Chromatography Mass Spectrometry
GF	Grain Fraction
GS	Grit Size
GUI	Graphical User Interface
HAV	High Added Value
HAZ	Heat Affected Zone
HCP	Hexagonal Close Packed
HV	High Viscosity
IA	Included Angle
ID	Inner Diameter

IIR	Isobutylene Isoprene Rubber
LCA	Life Cycle Analysis
LV	Low Viscosity
MMC	Metal Matrix Composite
MMG	Machine-Media-Geometry
MMI	Man Machine Interface
MP	Modifier Percentage
MR	Material Removal
MR	Magneto-Rheological
MRAFF	Magneto-Rheological Abrasive Flow Finishing
MRP	Magneto-Rheological Polishing
MRPF	Magneto-Rheological Polishing Fluid
MRR	Material Removal Rate
MSDS	Material Safety Data Sheet
MTS	Modified Tabu Search
MTT	Micro Technica Technologies GmbH
MV	Medium Viscosity
NC	Numerical Control
NN	Neural Network
NR	Natural Rubber
OA	Orthogonal Array
OD	Outer Diameter
OEM	Original Equipment Manufacturer
OPEC	Oil Producing and Exporting Countries
PBSO	Polyborosiloxane
PDMS	Polydimethylsiloxane
PHR	Peak Height Reduction
POI	Point of Interest
PV	Peak-to-Valley
PVA	Polyvinyl Acrylate
RBFN	Radial Basis Function Network
RE	Research Engineer
RGA	Real-coded Genetic Algorithm
RMS	Root Mean Square
SA	Simulated Annealing
SAFM	Softness Abrasive Flow Machining
SBR	Styrene Butadiene Rubber
SEM	Scanning Electron Microscopy
SI	Systéme International
SG	Spheroidal Graphite
SOD	Stand Off Distance
SPE	Solid Particle Erosion
TEM	Thermal Energy Method
TEM	Transmission Electron Microscopy
TIG	Tungsten Inert Gas
TGA	Thermogravimetric Analysis
TSB	Technology Strategy Board
UDF	User Defined Function
WEDM	Wire Electron-Discharge Machining
WLI	White Light Interferometry

WM	Washington Mills
WP	Work Package
XRD	X-Ray Diffraction

ii. Symbols

α	Alpha, commonly refers to an angle or CTE value.
~	Approximately.
˚c	Degrees Celsius.
ΔRa	Difference in average roughness (pre- to post-process).
ΔH	Change in enthalpy.
Ø	Diameter.
η	Eta, symbol for dynamic viscosity.
#	Used in place of the word ‘number’.
<	Less than.
>	More than.
µm	Micrometres, 1_{x10}^{-6}m.
%wt	Percentage by weight.
±	Indicates a tolerance value balanced about a nominal value.
ρ	Density, SI unit.
σ	Sigma, symbol for stress.
A	Area.
A	Amperes, unit of electrical current.
Bar	Industrially accepted metric for pressure.
CO_2E	Carbon Dioxide equivalent.
C_p	Specific heat.
cSt	Centistokes, 1_{x10}^{-2}St.
CrMo	Chromium Molybdenum.
dt	Difference in temperature.
D_H	Hydraulic diameter.
E	Energy symbol.
F	Force, SI unit.
g	Grams, 1_{x10}^{-3}kg.
g/cm^3	Grams per cubic centimetre, unit of density.
g/ml	Grams per millilitre, a unit of concentration.
g/s	Grams per second, a unit of mass flow.
GJ	Gigajoules, 1_{x10}^{9}J.
h	Hours.
i.e.	Latin, “id est”; “that is”.
J	Joules, unit of energy.
J/t	Joules per tonne. Energy expended per unit weight of produce.
K	Kelvin, SI unit of temperature.
kg	Kilograms, SI unit for mass.
kg/m^3	SI unit of density.
kg/cm^2	Unit pressure, not SI.
$kJ/kg^{-1}/K^{-1}$	Unit of specific heat, kilojoules per kilogram per Kelvin.
$kJ/kg^{-1}/c^{-1}$	Unit of specific heat, kilojoules per kilogram per Celsius.
kW	Kilowatts, 1_{x10}^{3}W.
kWh	Kilowatt-hours, 1_{x10}^{3}Wh.
L	Litres, industrially used unit of volume.

m	Metres, SI unit for length.
m	Mass, in kg.
m^2	Square meters, unit of area.
m^3	Cubic meters, unit of volume.
mm	Millimetres, $1_{x10}{}^{-3}$m.
m/min	Meters per minute.
mm/min	Millimetres per minute.
m/s	Metres per second.
mm/s	Millimetres per second.
MPa	Megapascals, $1_{x10}{}^{6}$Pa.
MJ	Megajoules, $1_{x10}{}^{6}$J.
MJ/L	Megajoules per litre; energy consumed per unit volume produce.
n	Number.
nm	Nanometres, $1_{x10}{}^{-9}$m.
N/mm^2	Newtons per millimetre.
P	Wetted perimeter.
Pa	Pascals, SI unit for pressure.
Pa.s	Pascal Seconds, SI unit for dynamic viscosity.
Q	Quantity of energy.
R^2	R-squared value denotes goodness-of-fit.
Ra	Average roughness (arithmetic mean of total sample length).
Re	Reynolds number.
Rz	Average roughness (mean of 5 deepest troughs, 5 tallest peaks).
s	Seconds, SI unit of time.
s^{-1}	Reciprocal seconds, unit of shear rate.
St	Stokes, unit of kinematic viscosity. Not SI.
t	Time, quantity.
T	Tesla, unit of magnetic field strength.
U	Heat transfer coefficient.
V	Volts, potential difference.
v	Volume in m^3.
v	Mean velocity in m/s.
Ɵ	Theta, commonly refers to an angle.
$W/m^{-1}/K^{-1}$	Unit of thermal conductivity / heat transfer.
W	Watts, unit of electrical power.
Wh	Watt-hour, unit of total power consumed.
$\bar{x}$	Bar-x, arithmetic mean.

List of Figures

List of Tables

Chapter 1 – Introduction

This research concerns the identification and solution development for a highly integrated machine-tooling-process approach for application in high value manufacturing. Mollart's (sponsor organisation) business holds multiple opportunities for R&D, and this research is focused in their subcontract division. As a producer of high value machined metal components for the oil and gas, telecommunications, nuclear, aerospace and general engineering industries, Mollart's subcontract division are under ever-increasing pressure from competitors to improve lead times and product quality, and to cope with increasing administrative requirement and reduction of cost by customers. Their strategic decision-making, both at board-level and senior management level is always aimed at reduction of these impacts; reduction can involve, i.e. updating of business management software to ease administration tasks, increase employment to introduce new skills/capacity or purchase of new/updated machinery to better cope with manufacturing challenges.

The oil and gas components produced in Mollart's subcontract business are typically used in the exploration activities of companies like BP, Chevron and Shell, while the tools are hired out by Mollart's customers (the tool OEMs), such as Weatherford, Baker-Hughes and Schlumberger. Oil exploration is a lucrative business; the planet's energy needs are increasing in unison with the spread of technology, population growth and expansion of the middle classes. The perceived 'peak oil' phenomena has driven up prices due to declining extraction rates, regional security concerns and a future where energy resources are controlled by a limited number of oil producing and exporting countries (OPEC). These factors are a contributor to the high value of nearly all elements of the crude oil exploration and refining process. The performance (reliability, accuracy, durability) of these tools is of paramount importance to the OEM.

In this research project, Mollart's need is derived from the functional requirements of oil and gas industry components; as a turnkey manufacturer, Mollart are responsible for managing the application of numerous manufacturing technologies – some old, some new, some in-house, some subcontracted. The value of the parts increases as production progresses – the initial cost of the raw material is just the baseline, with further operations adding to the workpiece value. The manufacturing environment in the subcontract division is highly modernised – almost 100% of production machinery contains some form of numerical control (NC), inspection facilities are temperature controlled, extensive use of software for 3D visualisation is made and lean strategies for error-avoidance are incorporated into the day-to-day running of all divisions. However, Mollart is not a fully-automated mass-producer working in high-volume, low-value parts and still must manage the risk of human error which can occur at *any* manufacturing stage. In terms of risk, the higher the value of the part and the greater the number of labour hours invested in it, the greater the impact when a mistake is made.

Upon receipt of finished parts from Mollart, the OEM installs hydraulic fluids, wiring, solenoids, pistons, seals, motors and more – the preparation of these sub-assemblies accrues cost to the OEM in materials and labour. Where the features merge, several phenomena negative to part performance are noted;

- Sharp edges; where sharp edges are created, the installation of wire-looms and piston seals can be difficult – these materials are polymeric (or polymer-insulated) and soft, leading to damage when caught on sharp edges. In deep-hole drilling activities, it is often necessary to drill a through-hole from both ends, thereby halving the positional error where the holes meet. This practice always leaves a minor tolerable mismatch, but must be rounded to prevent damage to wire insulation.
- Varied surface finish; the application of different manufacturing processes leaves a variety of different surface finishes which may require a secondary manufacturing process to correct – welding and electro-discharge machining (EDM) are such examples. There is also a less important issue with finish aesthetics – while a given surface finish may be technically acceptable, a bright, clean scratch-free one sends a positive signal to a customer.
- Varied surface texture; occasionally a surface is prescribed a direction of finish orientation or a pattern conducive to a functional requirement – efficiency of piston bores and channels for oil or air flow can be improved if the surface texture is controlled. Mating surfaces are usually improved if a cross-hatched texture is applied.
- Burrs; remaining material bent or hanging into one feature from another. Similar to sharp edges, but larger and varied in size – a sharp edge is sharp in a predictable location, whereas a burr is a manufacturing flaw that if missed, can cause damage to wiring, seals and pumps during installation or operation.
- Localised surface stresses; subtractive manufacturing processes release stress as material is removed. This is most frequently exhibited by long cylindrical parts or thin-wall circular features distorting when made from large solid billets. Surface stresses can lead to reduced fatigue life, binding of installed components and reduced ductility.

Measurement and inspection operations frequently identify manufacturing errors – this saves the financial and administrative burden associated with return-shipping, re-working and re-shipping. The complexity of workpieces is such that hundreds of features are under inspection and not all components require 100% checks. A separate issue is that of inspection methods and tools – small or complex internal features rarely lend themselves to easy insertion of tools and gauges and as such are not capable of proper assessment. When machined features are found to be out-of-tolerance (or machining is deemed an inappropriate means of geometry creation) the manual ‘by-hand’ processes are used, which introduce the potential for further human error (distinguished from human error when operating machinery).

1.1 Application of the abrasive flow machining (AFM) process.

In 2008, Mollart began investigating means of edge-rounding a number of features in complex geometries. Their options were narrowed to ECM (electro-chemical machining) and AFM, the former falling by the wayside after a difficult phase working with a subcontractor. The complexity of tooling and high power requirements were a concern. The AFM process was developed through trials with a German machine tool manufacturer – Micro Technica Technologies (MTT) GmbH, whose specialist experience, geographical location and willingness to carry out development work made them a more attractive proposition than their competitor, Kennametal Extrudehone.

The AFM process is a mechanical one, used to deliver an abrasive grit to a workpiece surface, or more accurately, to a point of interest (POI). It is consisted of two vertically-opposed cylinders, where the base of each is connected to a hydraulic ram, capable of delivering 46bar pressure over the piston cross-section area (CSA). Within the lower cylinder, approximately 20L in capacity, an abrasive media fills the volume – this media is comprised of a liquid phase (known as carrier) and a dispersed solid phase (grit). The upper cylinder is controlled in a single axis, where it can be brought closer to the lower cylinder or pushed further away. The purpose of this motion is to allow a workpiece to be clamped between the two open cylinder-ends which are capped off with adapter tooling to allow the introduction of abrasive media into the job.

In all implementations of the AFM process, there are three fundamental elements necessary to put a system together – machine, media and tooling; process setup is largely driven by the geometry the user is attempting to process – the POI must be exposed to media flow, which is achieved by a tooling setup. In complex geometry, there can be numerous plugs, sheaths and caps used to control the direction of flow, but to-date there are no reliable and transferable methods of controlling the effects on the job. By establishing tooling, the restrictions to flow are defined – the machine and media work in unison to deliver a velocity, quantity and level of indentation to the POI. The variables in the entire system number approximately 40, the majority of which are numerical (as opposed to categorical) which increases the system complexity.

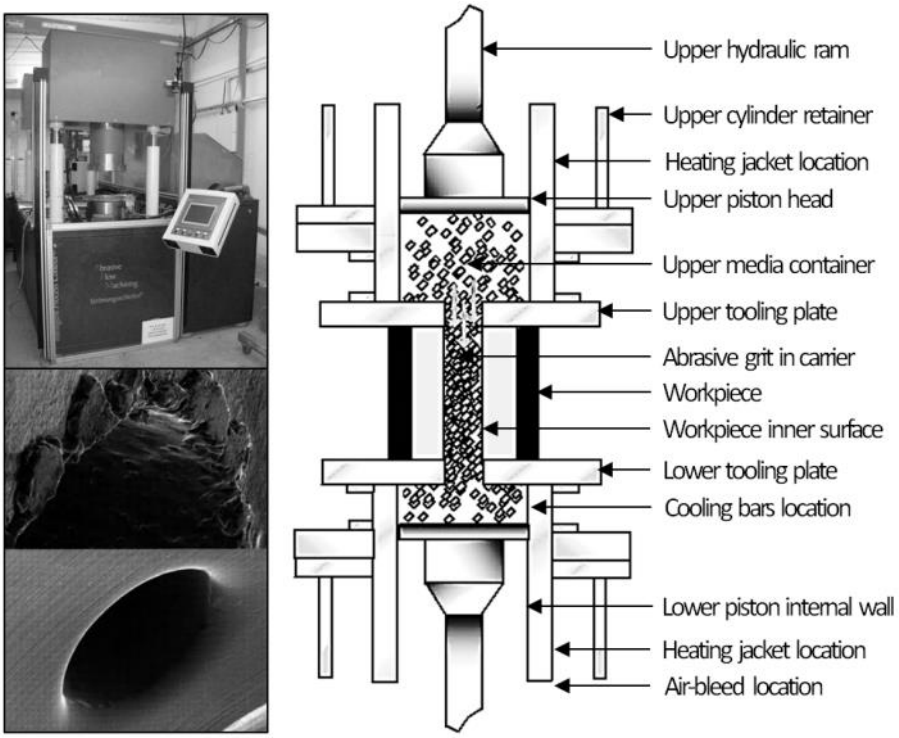

Figure 1.1 – Schematic of machine structure and critical components.

AFM's popularity is firmly based within manufacturers that have seen the flexibility offered by the process – it is capable of honing, edge-rounding, surface finishing and removal of recast layer. Its strength however, is in the processing of POIs where traditional tools cannot reach, and where complex forms mean human labour would result in poor repeatability.

1.1.1 Mechanical design.

The machine structure is as shown in figure 1. The maximum velocity at the machine piston face is 0.005m/s, the maximum pressure 46bar and maximum stroke 0.3m. The velocity of the upstroke can be set independently to the velocity of the downstroke for the purposes of preventing erosion in one direction by reducing velocity on a return stroke. The temperature can be controlled within a range between 0-50˚c for the purposes of altering the behaviour of the media, where the carrier viscosity will increase in lower temperature and reduce in higher temperature. The clamping pressure is approximately 200bar, set by the manufacturer using their '1:4' rule for operating:clamping pressure ratio. As a system whose primary purpose is to migrate 20L of abrasive slurry around metallic containers, the prospect of wear on critical parts is great – the piston head is constructed of a metallic ring with a proprietary moulded polymeric seal around the edge. This is designed to prevent leakage between cylinder wall and piston head; when grit particles force past, a channel is opened which allows further (and more) particles to squeeze past, causing eventual seal failure. The

temperature is applied by means of two inductive heating mats, wrapped around each cylinder – the cooling is applied by sealed bars running the top of the lower cylinder containing refrigerant gas. A temperature probe signals to the controller when the refrigerant should be sent through the tubes, but the heating mats are permanently switched on.

1.1.2 Media configuration options.

Media is the consumable product in the system – comprised of a carrier and grit, the MTT product is wholly proprietary and kept private. The carrier is the liquid phase, pumped by the machine, which in turn provides momentum to the grit. Carrier exhibits both shear thinning (pseudoplastic) and shear thickening (dilatant) properties, dependent upon shear condition, although the grit content also plays a role. Grain fraction is a media variable, as are grit size and grit material. Typically Boron Carbide is used to process exotic metals, whereas Silicon Carbide and Aluminium Oxide are used in softer substrates. Grit remains dispersed, even when the media is under no-load.

1.1.3 Tooling design and related issues.

Tooling is specific to the job – if the features to process are internal, there must be a sealed internal passage with inlet(s) and outlet(s). This passage is known as the flowpath. The geometry of the tooling affects the angle of attack and magnitude of pressure loss; tooling design for AFM can only be as flexible as the geometry allows, so in cases where POI processing requires additional work relative to other surfaces, an experienced designer will already have an idea of how the media flows. Tooling is not only used to direct media; it can be used to protect surfaces, to change the nature of the media's work or to prevent clogging or 'flow dead-spots'. Design of tooling is pure estimation – the media and machine settings can normally accommodate for tooling deficiencies, but all three elements must work together. Considerations when designing include understanding machine pressure capacity and the pressure drop through a designed cavity, whether cavities are in serial or parallel, whether the desired grit size will flow without clogging, whether the chemistry of the carrier will allow sufficient velocity and whether a set of features are balanced in exposure to flow (as opposed to one processed more, usually as a result of differing reduction ratios).

1.1.4 Problems with current process approach.

When all machine, media and geometry (MMG) decisions have been made, it is said that a 'process model' exists – these three elements are depicted in figure 1.2 below. As a manufacturing process, the number of variables makes it difficult to understand and control. Continuing with trial and error model development helps neither industrial

practitioners nor academics. Knowledge about the effects of a single variable cannot be gained without changing levels of others, preventing isolation of effects.

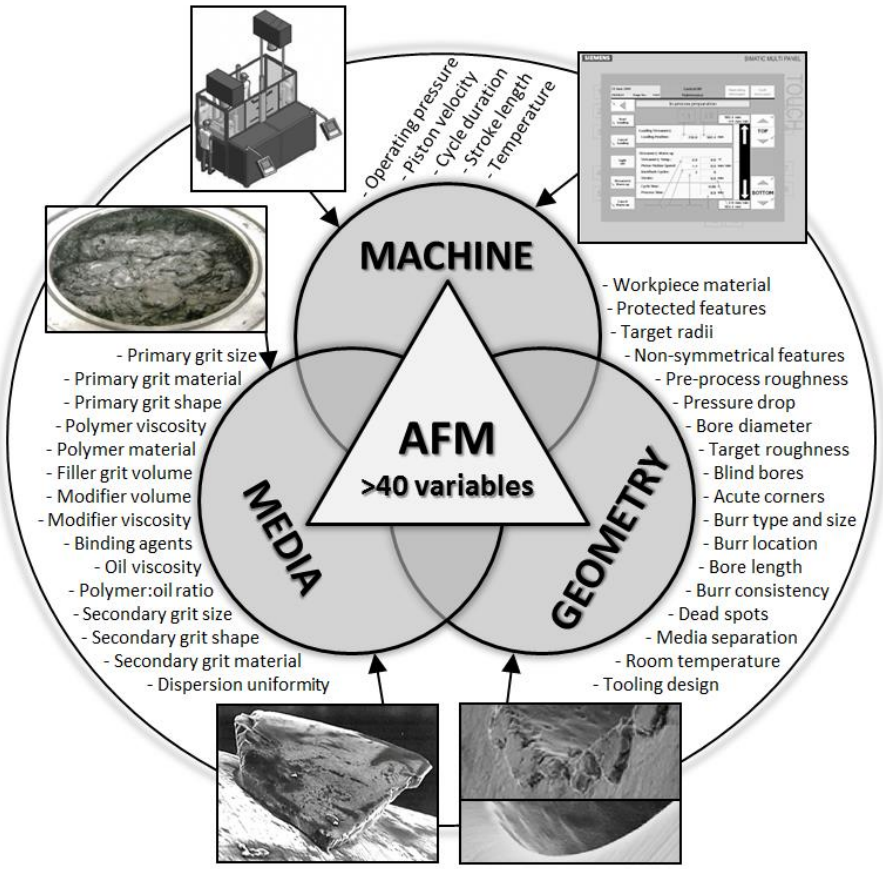

Figure 1.2 – Process variables within the abrasive flow machining ‘triangle’.

It helps to view AFM as a simple hydraulic circuit; except the material and pipe sizes are highly unconventional. Prior to this project, Mollart had no significant experience in the process and were reliant upon the machine supplier to provide machine parameters, media configurations and tooling design. These services incur cost; internal design engineers developed fixtures; while some worked, several concepts were misunderstood – chief amongst these is the MMI (man machine interface) relating only to the machine cylinders. The velocity, pressure and quantity of processing, while successful in one part, would yield different results in another. The principle of pressure drop, whereby long or narrow cavities coupled with high viscosity fluid means the machine cannot attain levels set on the MMI. The process is one of many considered a ‘black art’ by industrialists, often providing inconsistent results or unconventional behaviour.

1.2 Aims and objectives of the research.

There are four core technical aims in the project, but the overarching goal is to produce a capable and practical AFM process, suitable for a precision manufacturing environment. It is of great value to remove any element of trial and error from the process setup phase, to have confidence in the MMG configuration and to provide a proven method capable of reapplication to further arbitrary geometries.

1.2.1 Critically assess the effects of machine parameters.

As the multi-variate nature of the process prevents the design of a high-factor high-level experiment (due to an uneconomical number of trials) an experiment to describe the effects of the machine is produced to ensure the corner of the triangle is independently understood. Objectives are;

- To use a designed experiment to develop and test a model for the prediction of surface roughness, material removal and peak height reduction, to explain the effects of velocity, temperature and quantity.
- To design a standard testpiece and testpiece environment to allow collection of results in geometry that will be reapplied elsewhere, for maintaining transferability of results.
- To control the surface finish and degree of edge-rounding in testpieces, gaining understanding of expected error and method for balancing the parameters to control response magnitude.

1.2.2 Critically assess the effects of media parameters.

Control of the media is core to controlling the entire process – the proprietary nature of the media sold by MTT limits process understanding by preventing the attribution of responses to a particular factor within the media. Media behaviour is developed and assessed for this reason. Objectives are;

- To work with a third party to characterise and manufacture an abrasive media for the purpose of fulfilling production requirements and to complete the analysis exercise.
- To use a designed experiment to develop and test a model for the prediction of surface roughness, material removal and peak height reduction, to explain the effects of modifier percentage, grain fraction and grit size.
- To understand and improve the media’s performance and provide options for extreme surface finishing and extreme edge-rounding, to extend process capability beyond that of competitors.
- To recognise which factors drive testpiece form-change, whether all factors are significant and whether media formulation should be job-specific.

1.2.3 Correlate results from physical testpiece with virtual environment.

Ability to simulate a production process is a valuable and viable tool if real data is applied. To redefine the method of parameter selection away from trial and error and into a predictable, producible and productive alternative, results from a controlled system must be transferred and realised in an arbitrary system. Objectives are;

- To configure a computational fluid dynamics (CFD) system whereby media flow in the testpiece environment can be inspected and analysed and flow patterns can be compared to physical samples.
- To correlate the output from simulation with physical data collection as a means of determining which physical phenomena are responsible for formation of a surface.
- To model and evaluate the accuracy of the simulated system, each for those independent machine-simulations and for media-simulations. Correlation must be analysed to prove its existence using goodness-of-fit metrics.
- To devise a method of integrating the output from aims 1.2.1 and 1.2.2, in order to create a 'meta-simulation' where proven correlated machine simulations are joined with proven correlated media simulations.

1.2.4 Apply technique to production components.

Simulation of the testpiece environment prepares the data and models for reapplication to an arbitrary geometry such as a production component. The method works on the basis that generic phenomena such as temperature, velocity or strain rate can be present in any geometry, any fluids and any machine; if conditions that achieved a response in part 'A' are replicated in part 'B', then the same result is expected. Objectives are;

- To simulate a production component using a previously verified virtual media and machine, but changing the geometry to that of the new component. The hypothesis states that manipulation of virtual machine and media properties to achieve desired flow conditions will result in the physical geometry change as shown in aim 1.2.3.
- To develop a system termed 'abrasive potential index (API)', which acts as a descriptor for the grit size and grain fraction in an abrasive media. These factors cannot be simulated; therefore their effects must be tied to a flow condition and their abrasive potential considered as variable based on flow condition. The API is also limited to the geometry in which it is tested.
- To ensure research carried out is transferred to the shopfloor with machinery operators in-mind, and difference in process-understanding acknowledged. Develop quick reference tools to make appropriate simulation-based decisions for media and machine configurations.

1.3 Scope of research.

Defined in two stages, the scope of the research is considered as the activities required, performed and expanded-upon in order to achieve the project aims and objectives – the *project* scope considers only the elements necessary to define tools and techniques and the *product* scope considers the elements necessary to limit the final output.

1.3.1 Project scope.

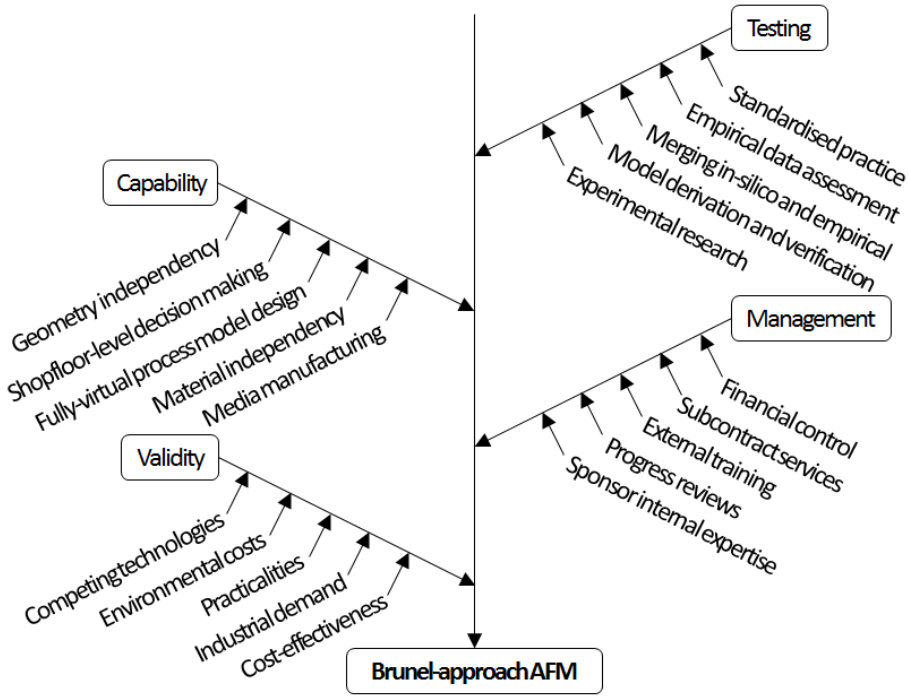

Figure 1.3 – Ishikawa diagram representing project scope.

Throughout the course of the project, decisions are made based on whether they, 1) directly or indirectly ease the experimental testing of concepts and processes, 2) increase the capability of final project output, 3) make best use of internal or external support or available budget, and 4) allow the process to tackle more practical concerns of validity, i.e. cost-effectiveness. The project aims to collect empirical data through physical testing exercises – experiments are designed specifically for this purpose – they do not aim to provide immediate solutions for complex geometries, instead collecting data to be reapplied in further in-silico study, *then* applied to complex parts. As the project aims to provide a service to Mollart's subcontract division, capability is core to project output in the HAV environment – in-scope is geometry independency for applying empirical data across a broad range of parts, media manufacturing for complete process control and the conversion of complex process concepts into shop-floor level tools to improve knowledge-transfer. Managerially, the scope includes financial control to maintain budgets and project progression, use of external services for metrology and exploitation of industrial contacts to reduce decision making risks.

While the AFM process is undoubtedly well-rooted, how *valid* the process is moving-forward as a manufacturing tool is called into question by current capability – scope of the project includes assessment of costs, competing technologies, but more importantly cost-effectiveness, practicality and demand. 'Green-credentials' of the process are considered in-line with EngD requirements, review the impact caused by moving from manual 'by-hand' processes to automated 'AFM-type' processes.

1.3.2 Product scope.

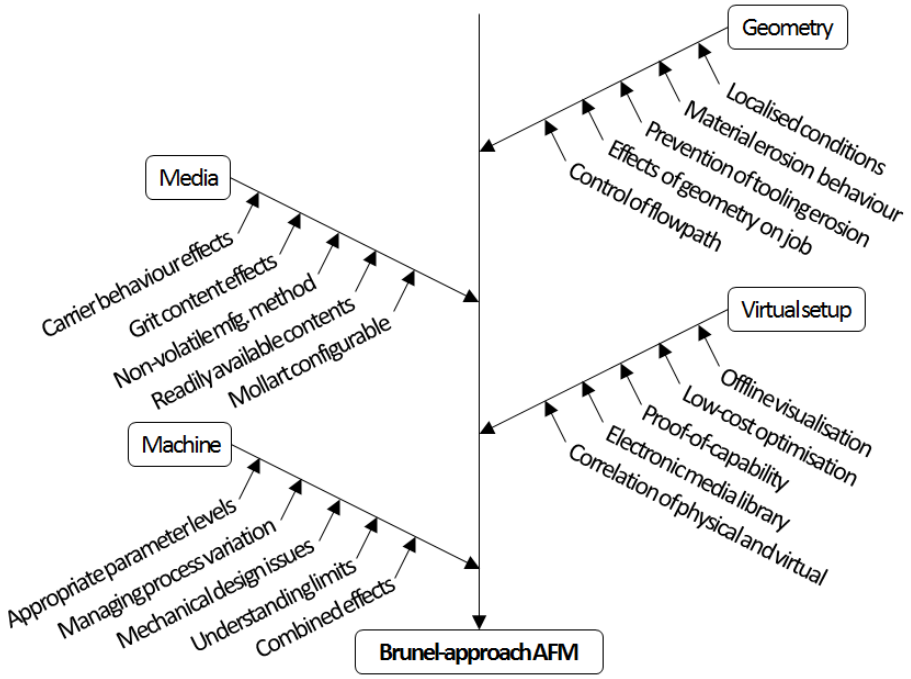

Figure 1.4 – Ishikawa diagram representing product scope.

Product scope differs from *project* scope by defining the constraints for the final product, i.e. the output to be applied in the commercial environment. These are grouped similarly to project scope – output is considered in categories of machine, media, geometry and the main area of originality, virtual setup. Core to project success is the control of the three corners of the AFM triangle – starting with media, the flexible tool must be characterised, designed, analysed and data generated to allow the reapplication of the substance. Geometry is key to process understanding and future profitability – materials in contact with the abrasive flow are used for different purposes – some provide mechanical support, some control the direction of flow and some prevent damage to workpiece surfaces. As the machinery is simple, but of importance to repeatable delivery of the media to the geometry, variation about delivery, the machinery limits and interaction between parameters at varying levels is considered – product scope limits research activities to those conducive to understanding these phenomena. The novel element in this project is the integration of CFD simulation by identification of parameters which bear strong scalar correlation between those

measured results and virtual outputs. The strengths of developing a system whereby simulation can provide a process model are numerous; 1) offline visualisation is a by-product of the simulation environment and has great potential in fault-finding and marketing efforts, 2) optimisation is possible by geometry manipulation and re-simulating, 3) customer confidence can be built by demonstrating previous successes and simulation of their component is useful for gaining prospective work, 4) media configurations behave differently – with basic rheological testing, an electronic form of the media can be stored and applied at will in simulation, and 5) correlation of physical and virtual results leads to the ability to develop a connection between media, material and simulation results, thus providing a back-calculation method of media specification.

1.3.3 Out of scope.

For both project and product, out of scope items are those which are neither technically rewarding nor financially viable nor practically achievable. Research is based on delivering a highly increased capability, process knowledge and offline setup procedure so that technical ability is not made broadly available. Out of scope items include;

- Changing the machine hardware to control the results; the AFM process must be developed in its normal state, with no modifications to the machine or process.
- Multiphase modelling in software simulations; while readily useful for liquids and gases, the same systems are not useful for particulate matter with unique mechanical properties, size distributions and dispersion phenomena.
- Control of production inconsistencies that cause AFM to be useful in the first instance; while AFM's presence is a 'sticking plaster' for machining issues, the project is not concerned with removal of these occurrences and aims to develop AFM to overcome them more effectively.

1.3.4 Technology readiness level.

Research presented in this thesis considers the drawbacks of the AFM process and aims to derive new solutions starting with understanding basic technological concepts. This equates to NASA's (National Aeronautics and Space Administration) technology readiness level (TRL) scale at level one. Progression to designed experiments in order to prove existing research and ensure process validity in materials and machinery used at Mollart Engineering is considered at level two and three. Application of data in a technology development phase is considered TRL three to five; in real terms, the novelty of the project is derived at this stage by working to combine physical data collected empirically with field variables obtained from simulation – the analysis, interpretation and subsequent integration with computer models are developed here. Verifications to prove the work from TRL3 and TRL4 is shown in the form of case studies on arbitrary geometries and through arbitrary level processing during the course

of experimental work – this is considered TRL5, while more detailed simulations of complex production parts are considered TRL6. The development of accompanying tools and charts for shopfloor usage, structures for application of the technique and refinement of processes in considered TRL7 and TRL8.

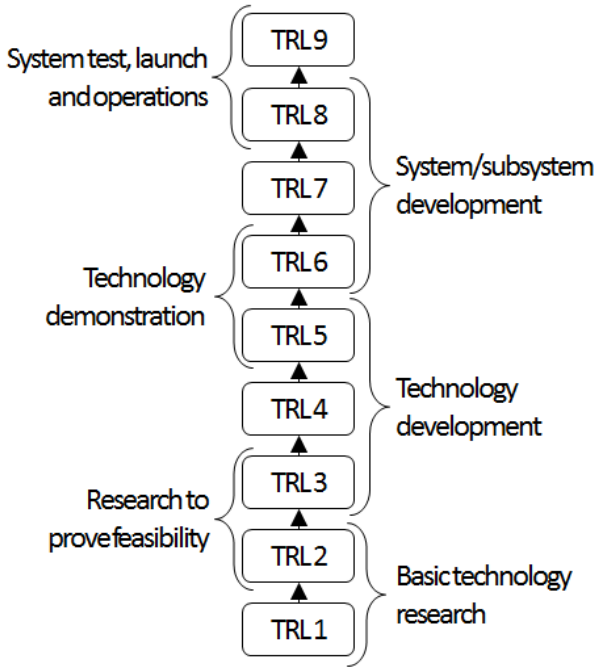

Figure 1.5 – Technology readiness level (TRL) scale. *Adapted from NASA standard.*

1.4 Thesis structure

This document is prepared in line with the guidelines as provided by British Standard BS 4821:1990. Withdrawn in 1998, this document is still recommended for use by Brunel University amongst other institutions. This thesis is presented in nine individual chapters as illustrated in the table below.

Table 1.1 – Overview of thesis structure.

Chapter	*Title*	*Content*
1	Introduction.	Considers the background of the research, sponsor information, brief process description, process problems, aims and objectives, scope, document structure and management aspects.
2	Literature review.	Identifies the main themes of current and past research, including the state-of-art, historical perspectives, current process modelling methods, hardware development and simulation efforts.
3	Formulation of machine-media-geometry approach.	Presents the logic-driven and systematic approach for collecting empirical data. The structure for application, transferability and development behind the method are discussed.
4	Design of experiments and analysis.	Data collection is comprised of exercises designed to understand fundamental process principles. Experiment design, metrology systems, variance and prediction models are presented.
5	Modelling and simulation.	Converting physical results into virtual results requires a bridging solution in the form of software. The package, its setup and integration methodology is presented, while the findings are discussed in terms of system optimisation.
6	Process control and optimisation.	Combining the simulations of machine and media behaviour, a framework for generating a specific surface finish and edge-geometry is provided. Limits and practicalities are discussed.
7	Environmental performance.	A comparison of competing technologies is made, while the environmental costs of Mollart's current activities are assessed against the costs of AFM – its sustainability, life cycle impact and future design for environment is considered.
8	Conclusions and recommendations.	Further applications, exploitable outputs, contributions to knowledge and recommendations are made in this final chapter.

1.5 Pre-project development

Before the EngD project began, Mollart's engineers had been working with German machine tool manufacturer, 'Micro Technica Technologies GmbH' (MTT). A specialist manufacturer of AFM machinery, their strengths are in experience-based process development, special-purpose machinery design and in media manufacturing. Prior to machine purchase in 2008, MTT carried out developmental work for Mollart on a specific component.

1.5.1 Machine structure and relationship with supplier.

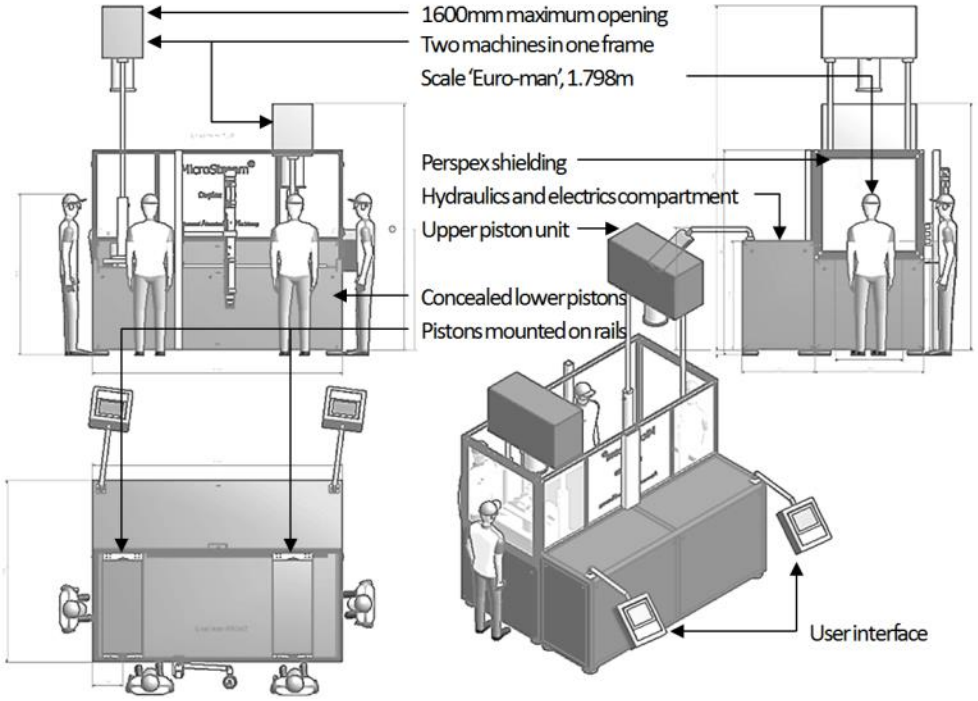

Figure 1.6 – Micro Technica Technologies Duplex 250. *Adapted from MTT Manual.*

Mollart's experience with MTT leading up-to and following delivery is of critical importance to several areas of project focus – the potted history begins in late 2007 when following a tradeshow, Mollart foresaw an opportunity to automate their deburring processes with an MTT electro-chemical machining (ECM) process. After several visits to MTT, by March 2008 Mollart had discounted the ECM process after learning of high power requirements and inflexible tooling options. AFM had been proposed and Mollart shipped a test component with deburring requirements for MTT development. Mollart defined several key features within the part that would require processing and by July 2008, had split the processing into four stages. A contract was raised and by December 2008, the design of two machines in one frame was complete and all component orders placed – testing was carried out at MTT in late December

2008. Mollart provided a component in January 2009 for final acceptance of the machine and finalised the floorplan and power requirements by March 2009. The machine was delivered and positioned by Mollart, but not commissioned nor training provided until June 2009 – following this, Mollart made efforts to understand the process, develop more tooling and run the setups as formulated with MTT.

Shortly after the commissioning, errors began to appear. In June 2009, a temperature sensor error meant the refrigerant-based cooling system was running permanently due to an excessively high reported temperature. Noise levels and high temperatures from the hydraulic power pack (also in June 2009) meant the entire pack was replaced due to underspecified pumps and radiators leading to overheating. The first refrigerant leak occurred in July 2009, followed by excessive force on O-rings causing media to leak in September 2009.

By November 2009, the process wasn't performing as expected and Mollart had been unsuccessful in manipulating the results on complex jobs. MTT claimed insufficient media aggression was the cause and proposed to increase flow speed by softening the media. Modification of tooling to change flow direction would also increase aggression, but would increase pressure drop; the capacity of the machine to run at a given velocity is controlled by the pressure it can deliver – the component in question was already consuming 40bar of a maximum 45bar. The chemistry of Mollart's current media would not allow further softening, so MTT developed a new type. Still in November 2009, the new media gave the component a reflective surface after having been pre-process shot blasted to remove larger burrs. This was not a surface finish or edge-rounding result, but a surface texture change, ultimately superficial for the requirements of the workpiece. Further testing with the same media in January 2010 was less successful and as a result, the failures led to a missed opportunity for the first subcontract work in March 2010. In July 2010, MTT sent a new British applications engineer to see fixtures and setups. While generally okay, several elements could be improved to reduce pressure drop and encourage the correct angle of impact – despite the recommendations, Mollart had little luck with the changes made and eventually the process was removed from several route cards, meaning components were no longer being scheduled for AFM. Nine months later in April 2011, the EngD candidate started work on the process.

The process had become stagnant at Mollart – when the EngD candidate began research, it became clear that the process required more than simple trial and error to make it commercially useful, and current efforts had been centred about best-guesses and manufacturer suggestions. Contemporaneous 'testing' was of an industrial nature, i.e. of no proven experimental design and certainly could not be considered to be controlled or reasonably measured. Following a brief analysis of the process carried out through literature searches and discussions with staff involved, an approach was formulated to try to understand and control the process variables.

Chapter 2 - Literature Review

Previous research in the area of abrasive flow machining is analysed and cross referenced to identify the approaches taken by other researchers, to 1) critique the existing analytical methodologies, 2) understand the greater application and purpose of their work, 3) generate novel and useful ideas to solve the AFM process shortfalls, 4) isolate important papers, from authors whose work appears to be industrially applicable or strong industrial-consideration made, and 5) to ensure sufficient replication is achievable if similar experimentation must be carried out in the course of this project.

Over 168 sources are used in this review; the vast majority (75%) are recent sources from 2000 or later (figure 2a). Primary sources (peer-reviewed journals, peer-reviewed conference proceedings, reports, theses and patents) are preferred, accounting for 160 sources, while secondary sources (textbooks and periodicals) account for the remainder (see figure 2b). The authorship is global, although there can be considered to be hotbeds of development in the USA initially, followed by India since 1990 and in Europe and China since 2000.

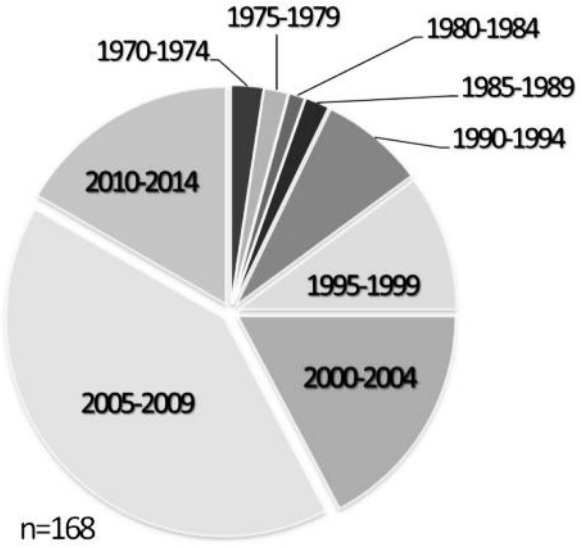

Figure 2.1 – Research intensity, 1970-present (quantity of publications made).

Papers are found using the databases within the subscriptions of Brunel University, where searches are performed using the Google Scholar search engine, Arxiv pre-print server and Brunel University's Library Databases to identify suitable article hosting sites such as ScienceDirect (Elsevier). Where papers are found to be inaccessible, they are ordered from the British Library using Brunel University's access service. The review is broken into nine sections where the literature is summarised before being compared to both equivalent and interrelated papers – the sections are based on the main research themes as described in the introduction; while many works cover one or more

themes, structure is defined in the review by ‘binning’ papers according to section themes through their titles, abstracts and conclusions.

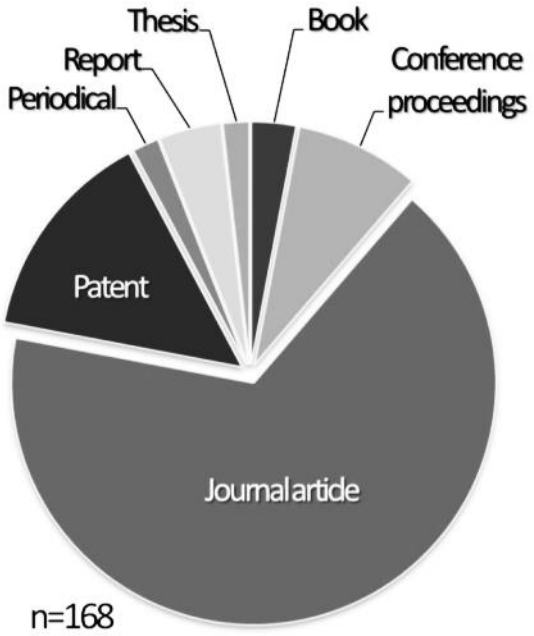

Figure 2.2 – Publication type, 1970-present (literature as used in this review).

The majority of papers are based on the technical behaviour of the AFM process rather than distantly-related concepts – concepts such as ‘design of experiments’ specifically-related to AFM process application are given greater consideration than concepts such as ‘lean manufacturing in SMEs’ or ‘non-Newtonian fluid flow simulation’. Where these concepts *are* discussed, is in direct relation to one of the important section themes.

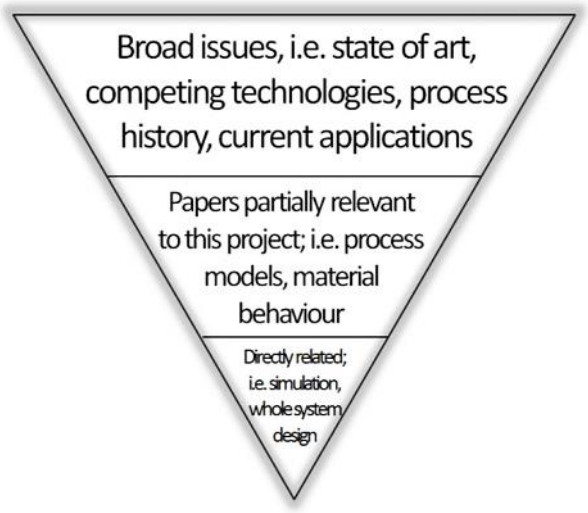

Figure 2.3 – Literature review paper relevance visualisation.

2.1 Introduction

The themes covered in this review are based on thorough searches of academic and high-quality sources of information and knowledge – the review is structured with the following headings;

- Abrasive flow machining; the state of art
  Eight dedicated review papers, written between 2001 and 2012 are available for initial source material, each focusing on the state of art. Additionally, topics include nano-scale abrasive finishing processes, polishing advanced materials, industrial challenges in grinding and general state of art of AFM papers.
- History of industrial and academic development
  Patents are used to describe the early contributors to the process, while the historical interaction between AFM suppliers is described through a combination of internal Mollart knowledge and conversations with MTT. Focus is also placed on the nature of patented works, and the transition between mainly industrial research into academic research.
- Current areas of active research
  Recent papers (2010-) show a variety of research activity, ranging from trials with non-standard machinery and media through to simulation and effects of standard AFM parameters.
- Applications and process capability
  Papers containing significant justifications for application of the AFM process are reviewed first in this section – secondly, a section referring to specific areas of academic interest is provided, including; application to rapid prototyped parts, ceramics processing, micro-hole processing and complex surfaces.
- Process models
  The greatest volume of current research is within process model development. The section covers the approaches taken by authors to generate data and model it, including in-process monitoring and offline non-computerised simulation. Empirical studies are analysed, while alternative abrasive machining processes are compared in terms of capability and optimisation methods.
- Fluid dynamics
  Research related to the effects of abrasive:surface interaction as a result of rheological properties is discussed in this section. Work is distinguished as either studying the effects of ‘concentrated suspension’ or attempted manipulation of the environment to study the effect of geometry change. The section also covers studies of micro-grits, carriers and media as a whole.
- Hardware development
  Significant efforts have been made to increase AFM process efficiency between 2000 and 2010 – this section covers alternative hardware, analysis and optimisation of that hardware, novel machine control and some conceptual adaptations of AFM.

Objectives in the ‘machine parameter study’ (1.2.1) include utilising designed experiments to model the prediction of response variables, design a standard testing environment and to control the error and response magnitude. Numerous works deal with experimental approaches – the most prolific area of study in AFM is the attempted process modelling of all fundamental variables, those thought to affect the process significantly. These papers also describe their test environments, although the comparability of hardware and the value of material selection is highly questionable. It is hoped that the standard testpiece is not simply a means-to-an-end for this research project, but something that can be further applied by the sponsor and future academic works. Error in process setup is tackled indirectly by works involved in physical testing.

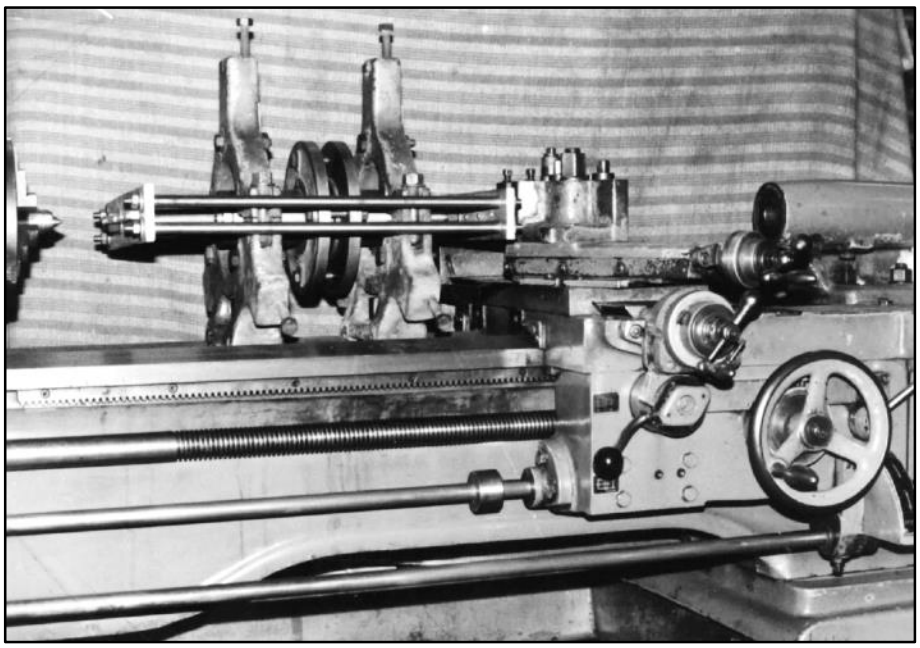

Figure 2.4 – Modified lathe bed used by Jain & Adsul (2000). Materials used are soft metals, aluminium and brass – uncommon in HAV manufacturing; the testpiece is a simple 12x6x2.5mm plate.

Objectives in the ‘media parameter study’ (1.2.2) include a subcontracted activity to have a supplier develop an abrasive media, to use designed experiments to gain knowledge of independent variables within that media, to determine the configurations of that media allowing extreme but controlled responses and to recognise the factors that drive testpiece form-change. Most papers dealing with process model development use surface finish as their output, although the difference between whether researchers use percentage change or outright finish values muddies the water. Certain pre-process finishes and textures define the improvement-value, and this contrasts with those studies using the ‘final value difference’ approach. There is a significant amount of literature available for the control of surface condition by fluid flow alone and equally a volume of research on new and capable media carriers. Ultimately, Mollart will not be able to

synthesise these products on the shopfloor – the products must be cold mixed at room temperature.

Objectives in the ‘physical to virtual correlation’ (1.2.3) section include the configuration of a CFD environment to represent the physical testpiece environment, to determine which simulated phenomena correlate with measured results, to evaluate the simulation accuracy and to devise a technique for integrating the data from both machine and media parameter studies. Elements of this approach have been performed in simple geometry previously, but to-date no solutions have been shown. There are limited and incomplete studies looking at the effects of tooling in simple geometries, including a simulation, but using no repeatable definitions for machine, media behaviour or practical verification of results. There is no inference that an erosion location and quantity model could be developed; the research papers collected focus largely on the effects of various flow phenomena on the erosion rates, but are missing elements that require a greater overarching study to ensure completeness.

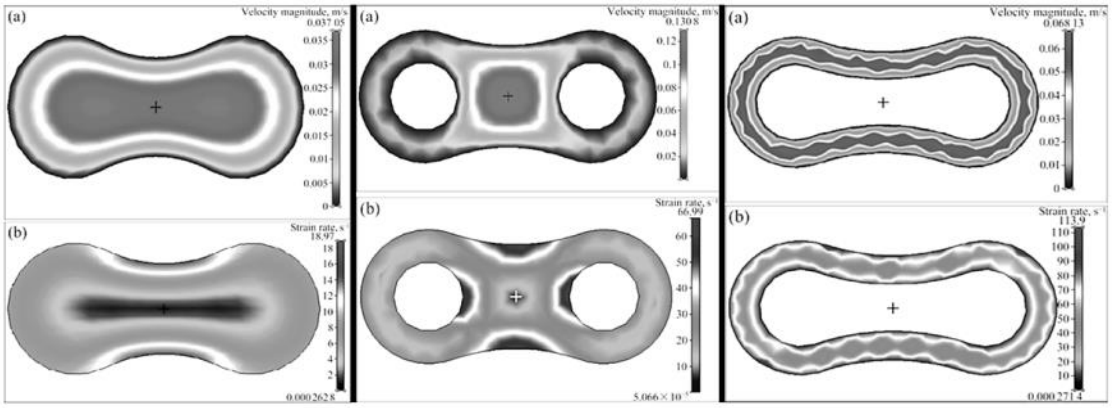

Figure 2.5 – Simple geometry simulation, showing effect of plugging geometry difference on velocity and strain rate responses. System is not practically verified. *Adapted from Wang et al., 2009*.

Objectives in the ‘application to production parts’ (1.2.4) section include the transition of the method to complex geometry using simulation, to develop a method of characterising the abrasive potential of the media and to ensure the results are useful and appropriate for application on the shopfloor. Obtaining literature in this section is difficult – complex geometry is vacant from academic research, primarily due to the inability to gain quantitative and logical findings when so many unknown effects are present in the system. This project develops the CFD-integrated methodology, and applies it to components which are important to the sponsor’s production activities and also to those applications found in secondary literature sources (textbooks and periodicals).

2.2 Abrasive flow machining; the state of art

State of art studies are used to highlight the current progress in a field of research. Three papers have been produced directly assessing the state of art in AFM.

2.2.1 Dedicated literature review papers

The first (Mali & Manna, 2009) reviews the contributions of authors in terms of process variable identification; number of cycles, extrusion pressure, media flow volume, media flowrate, media viscosity, abrasive particle size and concentration, media rheology and initial surface condition. Comparatively, the second state of art review (Brar, et al., 2010) does not directly identify the process variables, instead referring to fixture effects, temperature dependence, mechanism of MR, rheological properties, substrate material, cutting forces and active grain density. The third paper (Cheema, et al., 2012) focuses on the principle machine configurations of traditional AFM, i.e. one-way (pumping media through the part and out the other side, not to be returned), two-way (reciprocating the media load) and orbital (fixture allows the workpiece to move in circular eccentric motion, approx. 5mm). Cheema et al. extend their review to the area of HMPs (Hybrid Machining Processes), identifying eight unique AFM HMPs. These are covered in more detail in section 2.8;

- MAAFM – Magnetically-Assisted AFM
- MRAFM – Magneto-Rheological AFM
- ECAFM – Electro-Chemical AFM
- CFAAFM – Centrifugal-Force Assisted AFM
- DBGAFM – Drillbit-Guided AFM
- RAFF – Rotational Abrasive Flow Finishing
- SFAAFM – Spiral Flow Assisted AFM
- UAAFM – Ultrasonic Assisted AFM

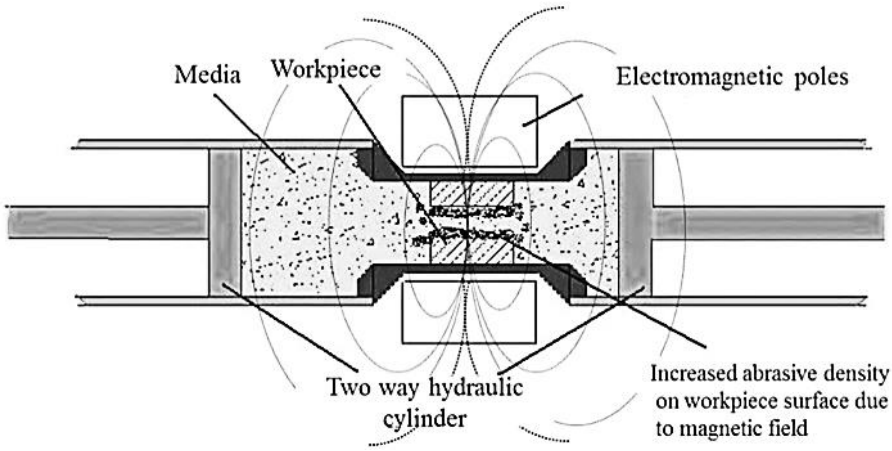

Figure 2.6 – Schematic of MAAFM (Magnetically-Assisted AFM) (Singh, et al., 2002)

Mali and Manna's (Mali & Manna, 2009) efforts are then focused on collating the 'special techniques' used to study the AFM process. This is the first review-type evidence of how fragmented and incomplete the existing work is – from 11 methodological approaches, the authors can only find one paper (from 1992) that describes their findings in a measureable quantity conducive to further application in a practical environment. Their review then identifies four of the eight HMPs as listed by Cheema et al. (2012).

Table 2.1 – Collated findings for controlling magnitude of significant responses

Author(s)	Material removal rate (MRR)	Material removal (MR)	Final surface finish (Ra)	Surface finish improvement (ΔRa)
Mali and Manna, 2009	Increases with extrusion pressure and percentage concentration of abrasives.	Increases indefinitely relative to number of cycles.	Control of abrasive mesh size, abrasive concentration, cycles and pressure.	Pre-process finish can be improved by 60-70% with only one cycle.
Brar et al., 2010	Improved significantly by the magnetically-assisted method.	Can be improved by centrifugal force, through a rotating rod.	Values of <0.01µm are possible with orbital motions.	Orbital workpiece motions improve finish by 20-30 times.
Cheema et al., 2012	CFAAFM improves angle of attack, improves with increasing speed.	SFAAFM increases grit travel, improving per-cycle work.	Improved by ultrasonic vibrations perpendicular to flowpath.	Improved by tooling and higher initial surface roughness.

Mali and Manna (Mali & Manna, 2009) propose that the process can be made more efficient by the application of the HMPs, although they state that the only reason is due to greater control of the abrasive media. Brar et al. (Brar, et al., 2010) suggest that future directions for the process should be toward simulation of the systems to increase automation and to optimise the process responses. Cheema et al. (Cheema, et al., 2012) recognise the research avenues of finishing external surfaces and control of complex

tooling, but they also recognise that current work will only be picked up by industry when complexity and performance are suitable for industrial implementation – however, their criteria for industrial suitability are somewhat skewed, as they write, "the prime requirements for industry are high precision products with a fine surface finish at relatively lesser processing costs". In Mollart's case (likely not representative of *all* industrial uses of AFM), high precision is not required, nor is fine surface finish, nor are rock-bottom costs. In edge-rounding requirements, the target values are within a large 1-1.5mm range, while surface finishing is 90% a 'no-more-than' target. The work is almost exclusively high value, meaning processing time and cost are of lesser importance than job quality. While the generalised findings of current literature (as surmised by these papers) is technically useful, the research target is not so well-focused – there remains, unrecognised as a general direction, the solution to guaranteed process capability from a dead start in complex geometry (where dead start implies the engineer has nothing but customer geometry). It is therefore logical to suggest that any method by which an engineer can gain greater control of the system, primarily through media as suggested by Mali and Manna (2009), is of practical usefulness.

2.2.2 Abrasive-based advanced finishing techniques

Jain (VK) is a surname that is frequently seen in AFM-based literature – his (and his co-authors) efforts have significantly advanced the field of micro-scale advanced finishing processes, usually in the modelling field. This section of the review covers four papers, published between 2001 and 2008, each discussing recent advances in the field of surface finishing with abrasives, focusing on the output of the authors relative to AFM.

The first paper (Jain & Jain, 2001) identifies four groups of finishing processes, mechanical, chemical, electrochemical and thermal, to which AFM belongs to mechanical (see figure 2.7). Their tone attempts to draw relevance to industrial challenges, and they consider the key driver in achieving economic and efficient process performance (in all HAV finishing operations) to be the optimal setting of process parameters. They state, "[the AFM process] cannot repair surface defects and taper problems because it removes the material uniformly", a statement later repeated (Jha & Jain, 2006). This phenomena is not recognised in Mollart's current AFM process experience – the opposite is true; potential reasons for this disagreement include the design of Jain's testpieces – commonly, testpieces in empirical studies are tubular and sometimes thin metallic plates are used, which provide only 2D data. Jain & Jain also note the importance of pre-process surface roughness, "the amount of stock removed from milled surfaces and surfaces produced using wire electro-discharge machining (WEDM), is statistically different from that of turned and ground surfaces". Concurrent with numerous applications-based studies, the WEDM process is a violent cutting process which leaves a heat affected zone (HAZ) known as white layer. This rough finish (~2µm) has been shown to be conducive to a greater percentage improvement in finish compared to more widespread primary forming processes such as turning and

milling (Tzeng, et al., 2007). They also make the inherently practical observation of, "higher workpiece hardness gives relatively higher MRR and better surface finish". The authors quote, "increase in abrasive concentration increases MRR and decreases surface roughness because more abrasive grains come into contact with the workpiece surface causing more abrasion". This statement is in logical agreement with conventional wisdom of grinding. Closing statements approach the more industrially-useful, "in the absence of analytical models, optimum selection of process parameters requires extensive experimentation, which is time and money consuming" – as recognised by Mollart in order to begin this research project. It can be taken that in 2001, there was little drive toward an all-encompassing model, with key authors choosing to study elements rather than drive toward a complete system, although then, as today, multi-variable regression analysis is the preferred modelling technique for the AFM process when attempting to gain empirical data.

Existing classification of advanced machining processes

Type of energy	Main process	Energy source	Tool	Transfer media	Mechanism of material removal
Mechanical	USM	Ultrasonic vibration	Sonotrode	Abrasive slurry	Erosion or Abrasion
	AJM	Pneumatic pressure	Abrasive jet	Air	
	WJM	Hydraulic pressure	Water jet	Air	
	AWJM	Hydraulic pressure	Abrasive-water jet	Air	
	IJM	Hydraulic pressure	Ice jet	Air	
	AFM	Hydraulic pressure	Abrasives	Putty	
	MAF	Magnetic field	Magnetic abrasives	Air	
Chemical	CHM	Corrosive agent	Mask	Etchant or reactive environment	Chemical dissolution or ablative relation
Electrochemical	ECM	High current	Electrode	Electrolyte	Anode dissolution through ion displacement
Thermal	EDM	High voltage	Electrode	Dielectric	Melting and vaporization
	EBM	Ionized material	Electron beam	Vacuum	
	IBM	Ionized material	Ion beam	Atmosphere	
	LBM	Amplified light	Laser beam	Air	
	PAM	Ionized material	Plasma jet	Plasma	

Figure 2.7 – Classification of advanced machining processes. (Jain & Jain, 2001)

Jha & Jain's 2006 review entitled 'nano-finishing techniques' (Jha & Jain, 2006), introduces the principle of nano-technology in the context of how far the manufacturing industry can take manufacturing processes – i.e. down to atomic, or nano-scale. Manufacturing tolerances are becoming tighter and tolerances of 1µm, while not widespread are certainly more prevalent than in previous years. It is recognised that advances made since the 1960s have been driven by industry's own internal ability within standard design practice, making novel mechanical improvements – with the transition to the knowledge economy, those machinery and process developers must turn to more advanced process development methods in order to ensure their processes are competitive.

The authors (Jha & Jain, 2006) highlight current mechanised applications of abrasives, defining grinding, lapping and honing as the three core defined technologies. Grinding can be split into stock removal grinding (SRG) and fine finishing grinding (FFG) – grinding is capability-wise weaker than AFM – it can only be applied to simple continuous surfaces. Its major variables of abrasive size, abrasive material, abrasive support matrix (bond) wheel speed and feedrate are highly comparable to AFM.

S. No.	Finishing process	Workpiece	Ra value (nm)
1.	Grinding	–	25–6250
2.	Honing	–	25–1500
3.	Lapping	–	13–750
4.	Abrasive Flow Machining (AFM) with SiC abrasives	Hardened steel	50
5.	Magnetic Abrasive Finishing (MAF)	Stainless steel	≈8.0
6.	Magnetic Float Polishing (MFP) with CeO_2	Si_3N_4	4.0
7.	Magnetorheological Finishing (MRF) with CeO_2	Flat BK7 Glass	0.8*
8.	Elastic Emission Machining (EEM) with ZrO_2	Silicon	<0.5
9.	Ion Beam Machining (IBM)	Cemented carbide	0.1

*RMS.

Figure 2.8 – Comparison of surface finish obtainable by different finishing processes. (Jha & Jain, 2006)

The second technology of lapping consists of loose abrasive used to fine finish a surface – the ‘lap’ is a flexible but thick pad used to retain the slurry and create three body abrasion. It can be applied to flat or slightly concave or convex surfaces. The final group as distinguished by Jha & Jain (2006) is honing – used primarily for sizing and surface finishing in internal bores, pressure is applied to a mandrel and grinding stones are rotated against the surface creating a cross-hatched finish. These techniques are limited to between 0.013-0.025µm Ra minimum surface roughness. AFM is said to reach 0.05µm according to the authors, with the added ability of travelling into workpieces where gas, liquid or other slurries can travel. The authors note the AFM of mould and die industry parts, whereby the inlet flow behaviour and conformance to features is similar to the non-Newtonian behaviour of many polymeric materials formed in moulds, aiding the flow and fatigue life of the parts. Unattended operation is also possible, which is particularly useful in high volume automated production, especially in the automotive environment – recent successful applications include AFM systems for ‘flow tuning’ i.e. surface finishing for precise airflow behaviour.

The third paper (Zhong, 2008), takes a deeper look at the tools used by researchers when dealing with polishing processes – while the paper provides numerous examples of electrochemical, this review is more concerned with mechanical achievements; Mollart have never been in the surface finishing business, but the abilities of the AFM process present a strong case for approaching this subsection of the UK precision manufacturing sector. Zhong (2008) notes that parameter determination in process setup

is often a trial and error task – AFM is not the only loose abrasive process limited by this fundamental restriction – it is seen in nearly all the AFM HMPs and in those chemically- and thermally-driven processes also. Complex geometry is increasingly being processed by industrialists using liquid-suspended abrasives. As a further illustration of the knowledge economy, Zhong (2008) describes developers of these new technologies as belonging to a new group of academic-engineers whose abilities in mathematical modelling and simulation techniques are providing answers to the complex multivariate interactions in polishing processes.

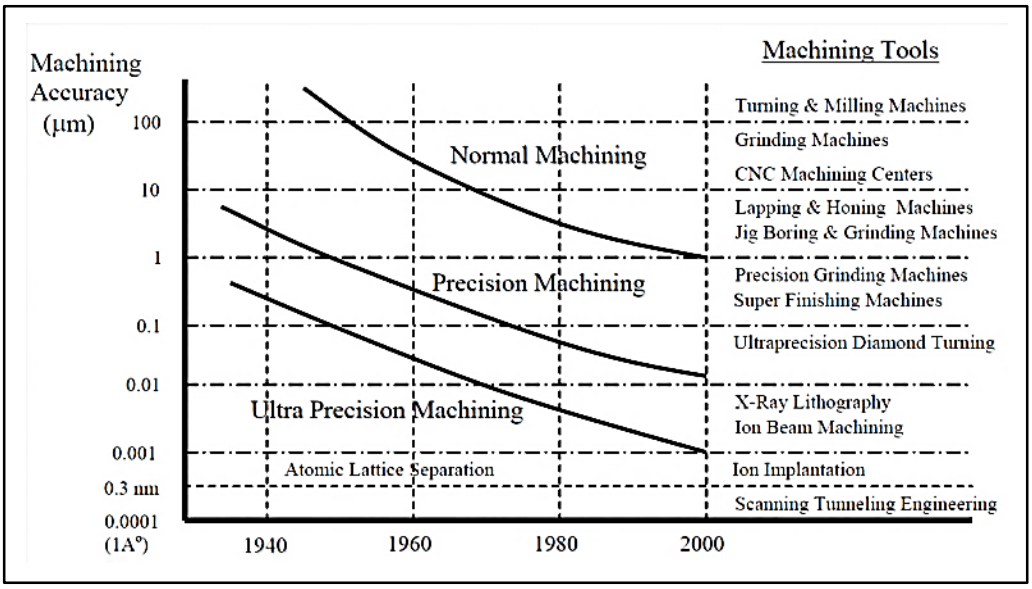

Figure 2.9 – Achievable machining accuracy. (Jha & Jain, 2006).

The fourth paper (Jain, 2008) echoes the previous three papers – figure 2.9 shows how the decades since 1930 have moved the boundaries of what is considered precision machining. Jain (2008) states that the initial use for AFM was in the deburring and surface finishing of aerospace hydraulic and fuel system parts, which is where Extrudehone's modern day expertise in Aluminium may stem from. Common to the other papers, this review gives little more than "active grain density has been found to influence finishing rate and depends on the machining parameters such as abrasive concentration, extrusion pressure, abrasive mesh size and medium viscosity". While not in the paper explicitly, it would also be true to say that a wide variety of other parameters also affect surface finish; authors Gorana et al. (2004) modify AFM using a centrifugal force system to increase active grain density (fig. 2.10) – as will be described in the process model section, the common feature is that no authors make an attempt to understand further geometry changes, preferring to work with tubes and small flat samples. Interestingly, a paper (Jain, et al., 2001) self-referenced within this review paper considers effects of parameters on the viscosity of the medium – abrasive concentration, media temperature and mesh size have a significant effect on the

rheological behaviour of the media as a whole – this has significance to further work. Jain recognises that the model weaknesses are based on the 2D nature of the stochastic models in existence – they only account for theoretical interactions in the XZ or YZ planes, whereas a more complex, likely software based solution would be needed in order to describe 3D 'XYZ' interactions.

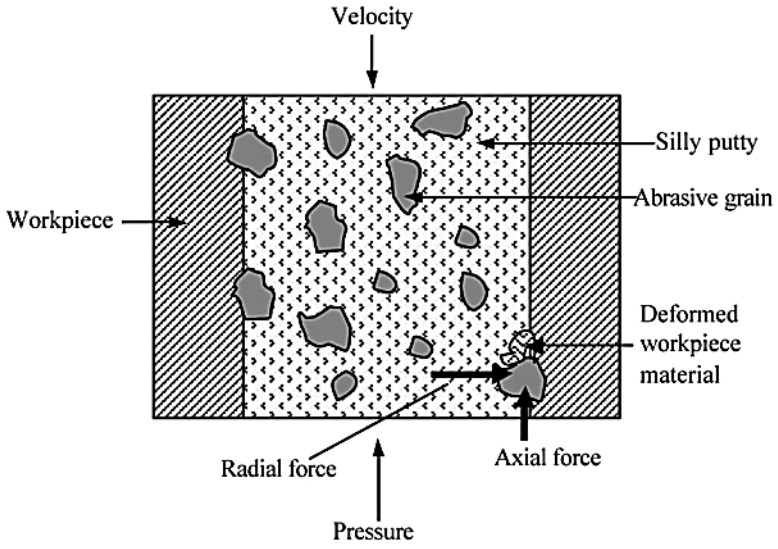

Figure 2.10 – Types of forces acting on a grain. (Gorana, et al., 2004)

2.2.3 Higher-level considerations

Industrial demand should be the driver for all engineering research, and the many parallels between traditional grinding and non-traditional loose-abrasive processes such as AFM are illustrated in the 2009 paper by Oliveira et al. (Oliveira, et al., 2009). The authors question whether grinding research matches the industrial demand for the research output, a question that can also be asked of AFM research – while Oliveira et al. (2009) draw the conclusion that traditional grinding certainly is ahead of demand, the practical implementation of AFM-based research is not, suffering mainly from incomplete and difficult-to-replicate work with connotations for industrial feasibility.

In Oliveira et al.'s research, they define process improvement requirements for grinding end-users – these include material removal and roughness measurement, in-process gauging and better predictability; as seen in AFM, these opportunities have not been solved due to complexity. As modern HAV manufacturing is highly discipline-specific, commonly manufacturers prefer to purchase turnkey solutions, where the term turnkey means 'ready-for-use' or 'a complete package'; skills remain within the turnkey provider and the customer gains the capability as supplied – traditional grinding and AFM are comparable in this sense.

All abrasive systems are used to generate a specific surface – recent developments in traditional grinding have been focused on production of surface textures as-well-as surface finishes – explosive growth in this area is primarily a result of research into extending service life of components by producing textures that cooperate with part function. The authors identify three natural segments for abrasive finishing processes, which can also be applied to AFM;

- Rough-finishing – strives to achieve high productivity.
- Ultra-precision – strives to achieve highest level of functionality.
- Precision – struggles for trade-off between functionality and productivity.

As pictured in figure 2.9, while technology progresses and overcomes the challenges of today for the application of tomorrow, the emergence of new materials and operating environments can also push the curves back, leaving the three segments in a static position over the years, giving the impression of no-progress. Currently, the challenges facing grinding and AFM equally are metal matrix composites (MMCs) and laminate-type composites, both covered later in this review.

AFM and traditional grinding differ in the technological approach taken by researchers – grinding research appears to be implemented into practice not by redesigning the machinery and methods of tool application (as with AFM recent developments, see 2.2.1), but by upgrading the control systems, monitoring the process and understanding parameters in new applications – the relevance of AFM to industrialist could be increased in this approach was taken. Oliveira et al. (2009) identify opportunities for industrially-relevant research in grinding;

- Critical tolerances – robust monitoring and control.
- Machine developments – stiffness, control and readjustment of worn tools, in-situ metrology, acoustic emissions, key technology for processing large parts.
- Information and database systems – integrated process analysis and knowledge management systems.
- Educational concepts – human resources and training material.
- Cost analyses – energy efficiency, cost-benefit compared to other technology.
- Surface integrity – prediction ability, achievement of microstructure, metallurgical properties.

Many of these are viable approaches for AFM research, perhaps none more so than information and database systems and surface integrity – combined, these challenges in grinding technology. Process reliability and capability (required by industry) can be vastly improved by generating structured ways to control and monitor machining operations.

2.3 Areas of active research

Historically, the human race has used abrasives to form materials up until the development of iron – the earliest stone forming tools were used to rub a slightly softer workpiece material. The civilisation of ancient Greece is known (Scott, et al., 1991) to have impregnated bronze with carborundum grit to produce makeshift files. These artefacts have survived the test of time due to the hardiness of the stone, far in excess of modern historic treasures.

2.3.1 Historical beginnings of the AFM process

AFM begins with the patenting of the process by Ralph William McCarty of the Extrude Hone Corporation, based on an application (McCarty, 1970) started in 1965 but abandoned in favour of a more developed solution. Commonly, the invention is attributed to Lawrence James Rhoades, the founder of Extrude Hone, entrepreneur, inventor and mechanical engineer. Following the receipt of the first patent, the company gained a competitor in the shape of 'Dynetics' – their 1977 patent (Perry, 1977) (filed in 1975) for a new method of applying the abrasive media, potentially in two formulations, while also describing a new method of forming the polymeric carrier from precursors.

Extrude Hone gained other patents throughout the 1970s for machinery and media, but the next significant patent comes in 1987 (Rhoades, et al., 1987) concerning the development of a system for achieving a specific resistance to flow, as gas and liquid management components benefit from accurate size and finish. Their first European competitor in the machine tool arena forms in 1992 in Germany; Micro Technica Technologies was formed from several ex-employees of Dynetics that disagreed with elements of the mechanical design at Dynetics.

In 1994, the Extrude Hone Corporation patented a process for 'unidirectional AFM', comprised of a hopper and plunger arrangement for cyclical processing of components which suited only a single flow direction, i.e. return of the media would produce unwanted erosion effects. Rhoades and Extrude Hone then began an interest in the 3D printing processes being developed at MIT in 1996 – taking a particular interest in metal printing, the technology was licensed to Extrude Hone and development began. To maintain growth, the business also made its own acquisitions – they invested in alternative finishing technologies such as thermal energy method (TEM) and electro-chemical machining (ECM) but also sought to develop the AFM side of the business – in 2001, they acquired Dynetics.

Subsequently in 2002, Extrude Hone developed a system (Walch, et al., 2002) comprised of hardware allowing the separate storage and application of two media formulations in a hybridisation of theirs and Dynetics' systems. By this point (2005), Extrude Hone had become a USD80m turnover business – their surface finishing expertise was noticed by Kennametal and bought for USD137m. Rhoades declined to

stay on at the business, turning to the directorship of the now ~10 years matured 'ExOne' additive layer manufacturing (ALM) business. Under Kennametal, Extrude Hone were awarded a world patent (Lunn, et al., 2006) in 2006 for a new type of thermoplastic carrier with increased resistance to compression and a faster relaxation time, but no patents appear to have been released since. Figure 2.11 presents the path of Extrude Hone formation to present day.

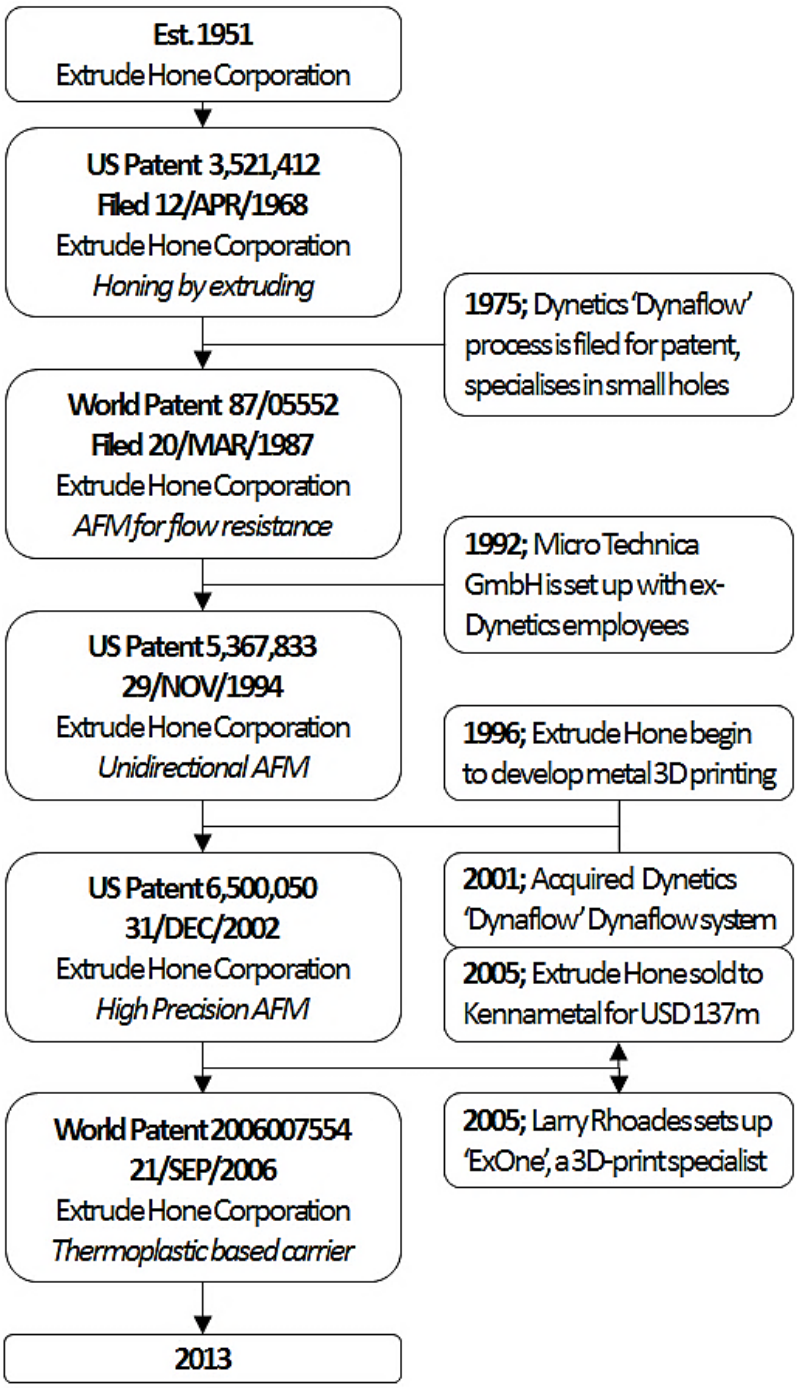

Figure 2.11 – Extrude Hone Corporation's main stages of development.

2.3.2 Applications and process capability

AFM was developed to serve the same purpose it still serves today – to reach and process features that no other process can reach with a gentle mechanical action, while competing processes require chemical processing (precluding certain metals and potentially inducing corrosion), violent processing (thermal energy method charges a component with gas and ignites it, which has the potential to damage thin wall sections) or unreliable processing (such as vibratory finishing, which struggles to reach tight areas, and cannot guarantee abrasive action in complex geometry).

Historically, the earliest applications-based paper is a 1994 example by Lawrence Rhoades himself, detailing the applications encountered by Extrude Hone. Thereafter, the majority of work is easily divided into categories of, 1) complex metallic geometry, 2) additive layer manufactured parts, 3) micro-holes, 4) ceramics, and 5) composites. Within each category, there is a spread of papers without any form of publication date trend, ranging between 2000 and 2012. The content of each, irrespective of category is heavily industrially-driven. Research appears to be driven by a sponsor in almost every case, with the exception of the micro-hole work. Reasons for this are explained in part by three periodicals referenced in this section – AFM is viable industrial technology, for pre-existing industrial problems; the periodicals refer to the difficulty in surface finishing and achieving efficient and economic deburring.

2.3.3 Process models

Fundamental approaches to solving machining problems are the natural way to attempt to solve challenges – the process model section is intended to separate those authors producing the low-level numerical models which utilise known-scientific effects of abrasion, from those authors carrying out empirical data collection studies. There are unfortunately several similarities between the two approaches – they both suffer from traditional economic costs associated with experimental complexity, both are limited to generating data in a single geometry and both produce end results that are qualitative in nature, not quantitative.

Neural network approaches appear to be the first attempts at process modelling with the first examples appearing in the late 1990s – the research continues into 2010, alongside classical abrasion theory application, radial basis methods and desirability functions. The in-process measurement heading in this section discusses papers which attempt to study energy and temperature as factors conducive to work-done. By far the largest body of work is in the production of empirical studies; these works are formulated with a great degree of similarity – an introduction (usually referencing a previous study using different parameters), an equipment description, an experimental design, a data collection step and an analytical argument preceding conclusions – these studies provide useful data to correlate against one’s own studies or against other works. However, development of a comprehensive AFM process model means that these works are not

useful enough to be considered as ready-made sources of data. The vast majority are published between post-2000, with the exception of neural networks.

2.3.4 Fluid dynamics

A third method of studying the AFM process, one which makes comparative sense in the study of complex parts, is through the use of established principles of fluid flow and erosion. A body of research is available that studies the effects of abrasive flow on substrate materials, but not specifically referring to the AFM process; studies include those assessing impingement angles of abrasive media (i.e. the effect of media direction onto a surface) and those assessing fixturing modifications (i.e. the effect of geometry on media flow). Importantly, the previous works involving computational fluid dynamics (CFD) are explored, produced between 2009 and 2013, the works remain in an early, non-industrialised and incomplete condition, but show promise in developing a 'green-button' process. Significantly, the volume of research into media component design and media configuration is well-represented – different streams of research are put-forward between 1995 and 2010 (with the exception of an Extrude Hone document from 1975) including study of;

- Media properties as an aggregate product
- Carrier properties as an aggregate of modifier and base product
- Modifier properties as synthesised from precursors
- Commonplace and alternative polymeric carriers
- Media modified for use in HMPs, i.e. iron-shot-loaded (magnetorheological use)

2.3.5 Hardware development

Characterised by two vertically-opposed cylinders pumping media into the part through a fixture, the 'standard AFM' process is the most developed, most industrially-accepted, most-studied and most-practically viable. However, some authors have noted new ways of increasing its efficiency and starting in 2002 with magnetic field assisted AFM, researchers based in India sparked a total of eight hybrid AFM systems. None have come to commercial fruition, (it can be speculated) due to the additional layer of media management complexity on top of a complex fixturing arrangement. These technologies are not a core element of this review, but their success and failings can be noted for future use. Literature shows several key phases for each – publications outline the technology proposed, then ~2 years after, an effects analysis is carried out and thirdly, an optimisation stage occurs. Two further subsections covering novel control solutions and conceptual solutions are presented, containing research by authors between 1989 and 2012 – investigations are niche in nature and largely conference-paper sourced.

2.4 Applications and process capability

Often, the academic study of a manufacturing technology can be misaligned with the requirements of industry – this section of the review is focused on extracting the valid industrially-useful findings.

2.4.1 Basis for application of AFM

Stemming from industrial demand for better internal finishes, the AFM process finds its most successful application in the polishing of relatively small and difficult to reach features, usually internal and used as flow passages in function. Kao and Shih (2007) present a study looking at how AFM effects the roundness of micro-holes when used as a post-process (or secondary) technique. After forming the holes with an EDM machine and carefully studying the variation with a gauge R&R study, they use an Extrude Hone machine running with 0.015mm silicon carbide (SiC) abrasive, running at 276bar. They witness three effects as shown in figure 2.12, despite running at the same parameters – this points to stochastic phenomenon within the work.

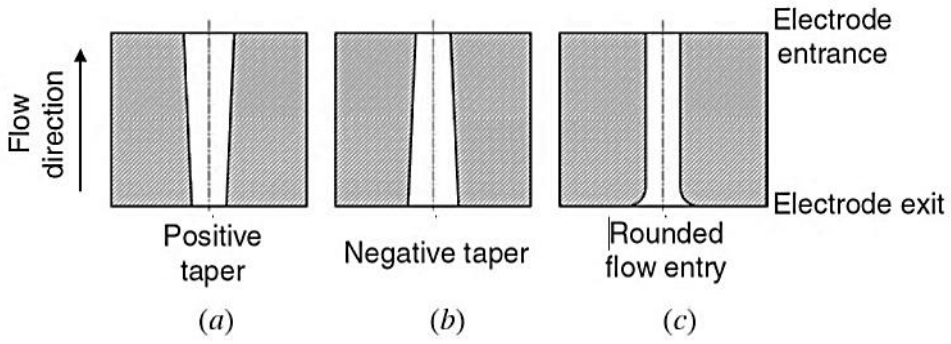

Figure 2.12 – Classification of the shape of a micro-hole for the fuel injector: (a) positive taper, (b) negative taper and (c) rounded flow entry. (Kao & Shih, 2007)

Heisel and Schaal (2008) (Heisel & Schaal, 2008) identify the circumstances of initial burr creation and recognise the need for a technology such as AFM, "due to the difficult accessibility, the deburring of drill hole edges is problematic here and requires a lot of time as well as money". AFM is capable of only low levels of MR – burr minimisation is a useful precaution to take to ensure the uniformity and success of the process. The authors describe their findings – increased drill feedrate increases burr size, burr formation increases with reducing exit surface angle and cutting speed of the drill does not affect burr generation.

Lawrence Rhoades produces a general case study paper in 1991, outlining process elements, process suitability and process structure – the work is well illustrated providing insight into the application as seen by its designer. Rhoades (Rhoades, 1991),

describes the method by which machine parameters can affect the media which in-turn effects a change within the media-geometry interaction. See figures 2.13, 2.14 and 2.15.

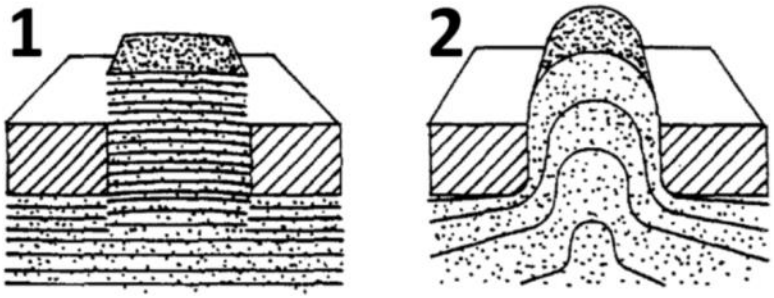

Figure 2.13 - The media flow pattern can be varied to achieve different results (*adapted from Rhoades, 1991*)

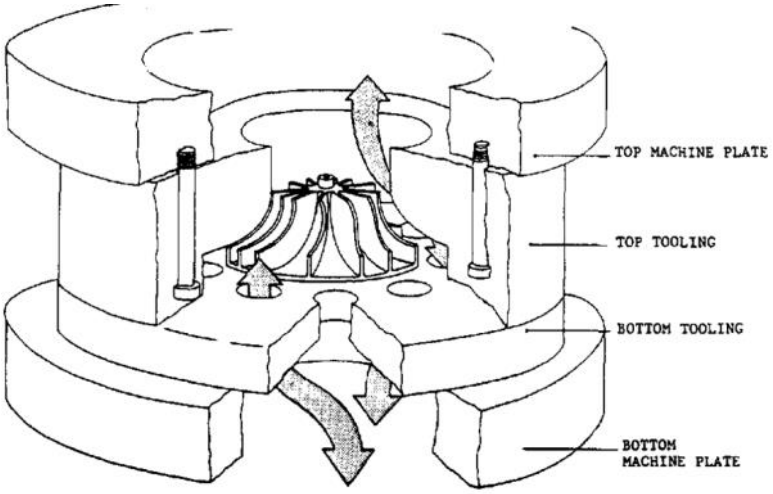

Figure 2.14 - For processing external edges, the part is contained within a fixture to form a flow restriction between the outside of the part and the inside of the fixture. (Rhoades, 1991)

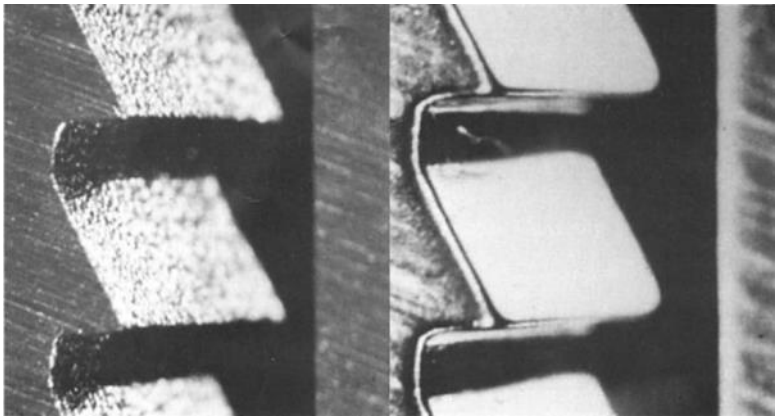

Figure 2.15 - Close-up of the teeth on an extrusion die shown before (L) and after (R) processing. (Rhoades, 1991)

Summarising the author's main points about the process strengths, many conjectural ideas are witnessed, borne mainly from the entrepreneurial nature of the process development at this stage. Rhoades writes;

- Process is abrasive only where the flow is restricted.
- Materials from soft aluminium to nickel alloys.
- For processing walls normal to the flow direction, media should maintain a uniform flow rate. For edge-rounding, less viscous media that increases in velocity once with the feature.
- Flow condition is driven by machinery, media, workpiece and tooling.
- When forced into a restrictive passage, the viscosity of the media temporarily rises, holding the abrasive grains rigidly in place.
- Low velocity is better for uniform removal, high rates produce larger radii.
- Depth of cut depends on media viscosity and extrusion pressure.
- Approximately 90% improvement in surface finishes with tolerances of 10% of material removed.

A group of authors (Aurich, et al., 2009) between three institutions produce a comprehensive review entitled, 'burrs – analysis, control and removal'. They help to make the case for AFM by describing it thusly, "holes with diameters less than 2mm is possible by using … abrasive flow machining (AFM)". Burr complexity influences the technology used to remove it – burr location, length of edges to deburr, number of edges and burr size are significant factors determining complexity. They recognise that manufacturing costs are increased in industries where burr removal and cleaning are paramount, but also recommend that burr control is better than burr avoidance because it aids the application of an automated finishing technology, such as AFM.

Authors Yang and Zhao (2010) (Yang & Zhao, 2010) provide another detailed overview of the AFM process, processing their own design of nozzle with a 0.3mm aperture. Their system provides 70bar to the diameter and using their own media and machine design, they provide an analysis of the surface roughness results, but without any apparent structure – the structure of the test table implies a three-level two-factor fractional factorial design (9 trials), whereby the experimental goal is to increase flow rate in the nozzle, but the increase in flow rate scales with the processing time, which is known to scale proportionally with material removal.

Describing the methods of material removal in aluminium and brass, the authors Yadav, Singh and Singh (2011) (Yadav, et al., 2011) identify shearing, ploughing and rubbing as MR modes, whereby shearing is the traditional process as seen in turning and milling (producing chips), ploughing is a material displacement technique and rubbing is a surface modification process. While aluminium is used widely in the aerospace industry, neither it nor brass are particularly common engineering materials – certainly not for mechanical strength or resistance to corrosion. Following a short study of process behaviour in these soft metals, the authors present their assessment of process

capability – low finishing rate is widely accepted, but their statement, "incapability to correct the form geometry" is misleading – if tooling and flowpath are controlled, processing time is the only limitation.

Figure 2.16 – 500x micrograph showing complete removal of EDM recast layer (1) surface before AFM, (2) surface after AFM (*adapted from Yadav et al., 2011)*

Applications are presented by the authors in a range of industry sectors – they are;

- Aerospace
    - Adjusting flow resistance of blades, vanes, combustion liners, nozzles and diffusers.
    - Improving airfoil surface conditions on compressors, turbine sections, spray nozzles, fuel control bodies and bearing components.
    - Edge finishing of holes, attachments to improve mechanical fatigue strength of blades, disks, hubs and shafts.
    - Removal of milling marks and improvement of finish on complex profiles of impellers and blades.
- Automotive
    - Polishing of bores in engine blocks for improved performance
    - Polishing of intake ports and exhaust manifolds to improve airflow, increases power and efficiency.
    - Finishing of fuel spray orifices, injector nozzles.
    - Removal of stress risers, cracks, rounding of sharp edges to enhance component life.
- Die and Mould
    - Polishing machined dies to remove machining marks, in direction of material flow. This produces a better quality and longer lasting mould.
    - Complete removal of EDM recast layer (see figure 2.16).
    - Processing of multiple passages simultaneously.

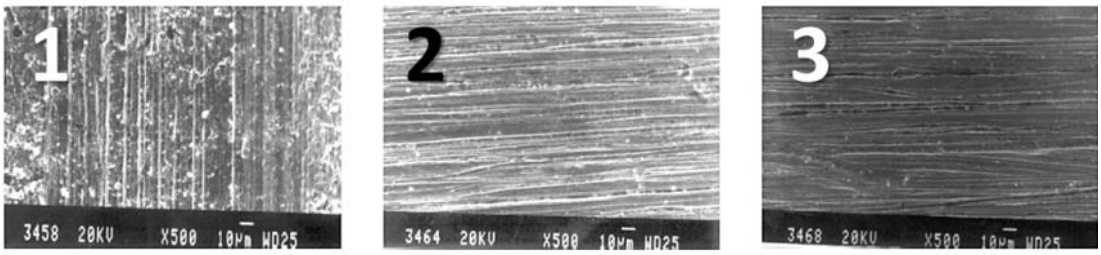

Figure 2.17 – Scanning electron micrographs of surface at different stages of AFM (1) before AFM, (2) after 5 cycles, (3) after 10 cycles. (*adapted from Narayanasamy et al., 2004*)

The use of AFM is largely driven by those users working in a 'precision' environment (trade-off between functionality and productivity) and as such the authors Narayanasamy et al. (2004) have identified behaviour within AFM whereby diminishing returns are seen in terms of surface finish past the first few cycles. Practically useful, the conclusions suggest there is a stage whereby roughness improves, stabilises and then becomes worse – this can only be taken as accurate for the circumstance within which the authors tested – the known-to-be-high number of variables in AFM prevent this scenario from ever truly leaving the laboratory.

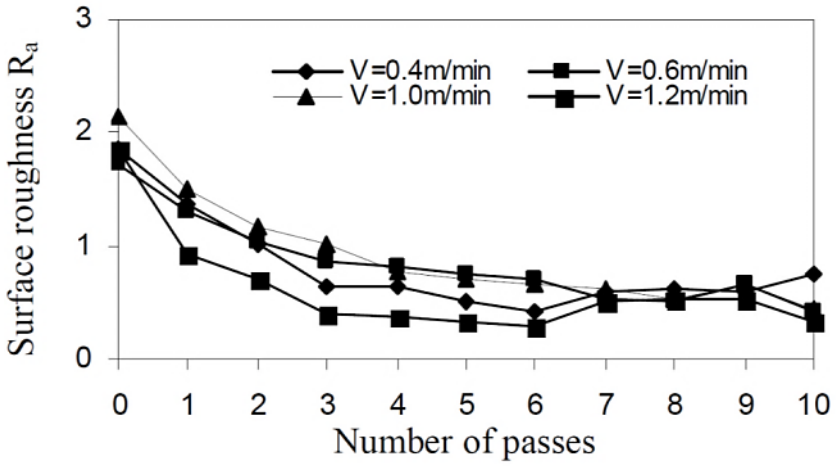

Figure 2.18 – Parametrical influence on surface roughness characteristics of AISI 4419 steel. (Narayanasamy, et al., 2004)

2.4.2 Applications and capability

In contrast to 2.4.1, this section presents numerous dedicated studies of the AFM process in specific applications rather than discussing the need and existing applications.

2.4.2.1 Applied to complex metallic parts

Academic research papers have been produced on the topic of complex part finishing with AFM – in 2007, Wilk and Tota (Wilk & Tota, 2007) produce a paper focused on turbine blade machining. They identify AFM as an unconventional technology suitable for the secondary processing of turbine blades and blisk finishing. Comparable technologies are expected to meet a processing time of five minutes. Cooling holes on the blade surfaces are approximately 0.5mm. It is noted that abrasive machining processes are the only way to achieve the narrow tolerances of surface roughness.

In the die and mould sector, there are several uses for the equipment – some may be used in polymeric injection moulding, some in metal injection moulding (MIM) (increasingly popular following development of metal matrix composites (MMCs)) amongst other processes designed to form metals, ceramics, polymers, natural fibres and laminate-type composites. Even low-volume production with these components is highly stressful and damaging to the mould surfaces – Brinksmeier et al. (2004) (Brinksmeier, et al., 2004) discuss the requirements for high tolerance work such as structured optical elements, machined initially by diamond or precision grinding tools – they investigate the ability of AFM to finish the mould; they state the material removal rate is in direct proportion to the media velocity. Running the process for 15min at 15bar delivered values of 0.06µm Ra in a 150˚ V-groove. AFM is identified as a technology suitable for the production of structured surfaces.

Two authors work with AFM as a potential process in gear cutter (hob) manufacture – one author (Rech, 2006) identifies the influence of hob cutting edge form and influence on wear resistance and the second (Claudin & Rech, 2009) assess numerous processes and their performance. Gear cutters are different to traditional mills, drills and turning tools – these tools work by producing continuous chips, with a steady load on the cutting point. Gear cutters interact with the billet through intermittent cutting – they still aim to shear the workpiece in order to produce chips, but there is no continuous contact – these tools are subject to higher impact load, all located on the tool tip. If sharp edges were to be used, the tool tips would brittle fracture from the body of the hob and the tool would be useless. Instead, before coating, the finish-machined hobs have a small radius (5-30µm) applied to the cutting tip to spread the load – Rech (2006) shows that using AFM to produce the radius as opposed to ‘micro-sandblasting’ produces a better homogeneity of finish, a surface texture conducive to improving the actual surface area in contact with the substrate and as a consequence, improved coating adhesion and increased resistance to fatigue cracks. The later paper (Claudin & Rech, 2009)

strengthens the argument for AFM of gear hobs; the size of the radius is better achieved with the abrasive process. It is verified as more wear resistant when using 9.83L of media compared to 19.66L – this means AFM should be calibrated to deliver the correct amount of media to ensure 10µm cutting edge radius.

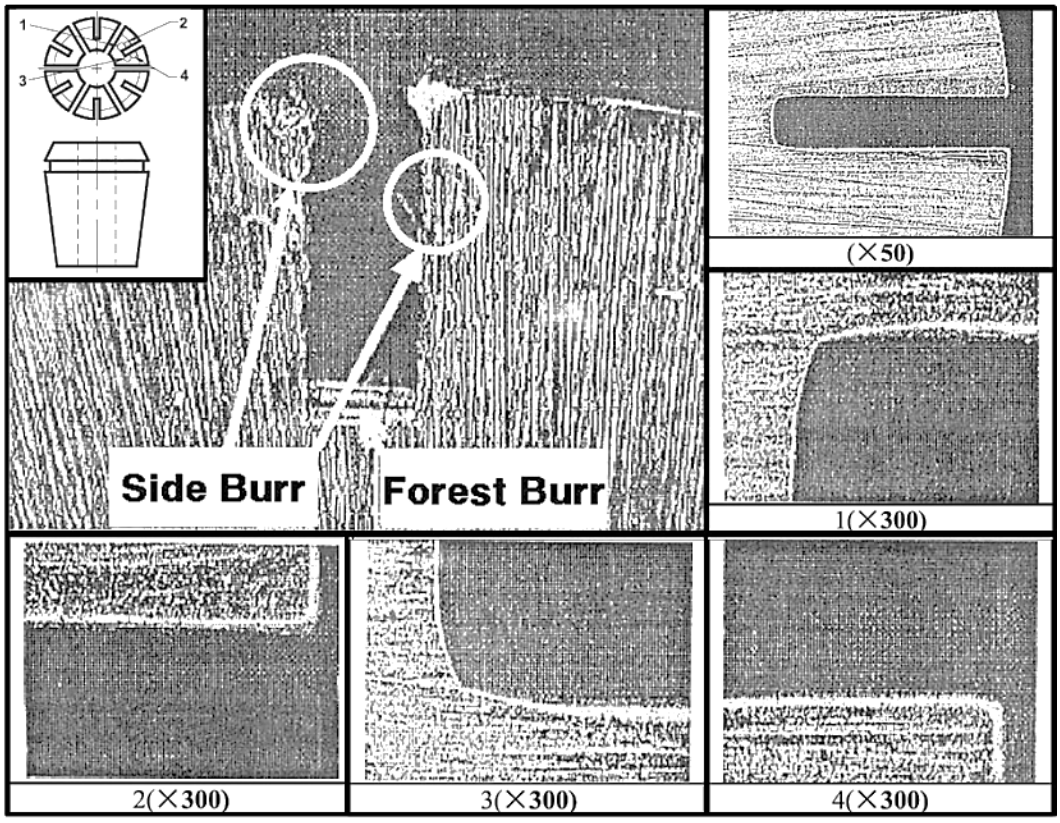

Figure 2.19 – Result of deburring spring collets (top left – before AFM, right and bottom edge, after AFM). (*adapted from Kim & Kim, 2004*)

As previously shown, burrs are a significant problem, potentially causing up to 15% additional costs within a manufactured part. Kim and Kim (2004) (Kim & Kim, 2004) investigate the burr generation and burr removal process using AFM in spring collets – these tools are used to hold cylindrical shank tools on-centre in a rotating spindle to better than 5µm concentricity – burrs can prevent the insertion of round bar and/or lead to concentricity errors, as their presence offsets the round bar, allowing it to rotate in an eccentric path. The authors find that AFM is effective at finish machining, that SiC is more effective than aluminium oxide (Al_2O_3) in high hardness chrome-molybdenum (CrMo) alloy, concentricity is not affected by AFM pressure, high viscosity media is more effective at deburring (in direct contradiction to Rhoades, 1991) and surface roughness is improved despite the target being material removal.

2.4.2.2 Applied to additive layer manufactured (ALM) parts.

The extents of process uptake in ALM manufactured components is accelerating – the technology has the potential to wipe out a number of more traditional machining operations, save for three core issues that remain today, even after approximately 20 years of development; 1) surface finishes are still incredibly poor - 8µm Ra is not uncommon, and the best that can be achieved is ~2µm Ra. Engineering finishes should be at a maximum of 1µm Ra, 2) mechanical properties are still not equal with cast or wrought product of the same constitution – this forces ALM manufacturers to work with the constraint that their components need a further heat treatment process following manufacture, and 3) geometrical accuracy is not engineering-acceptable – while the metal process is the most well-controlled, typically building in 40µm layers, the powder sintering process does not isolate the part cross section from the surrounding loose powder well-enough to prevent additional power adhering to the side of the profile. There are four major ALM processes;

- FDM (Fused Deposition Modelling) – solid ABS material is deposited through a nozzle – accuracies of ±0.25mm.
- SLA (Selective Laser Ablation) – solidifies photosensitive liquid polymer in a drum – accuracies of ±0.125mm.
- SLS (Selective Laser Sintering) – solidifies layers of dry powder, typically a grade of polyamide (Nylon) – accuracies of ±0.1mm.
- DMLS (Direct Metal Laser Sintering) – solidifies layers of dry metallic powder, typically nickel-, titanium- or iron-alloy – accuracies of ±0.05mm.

Stereolithography (SL) is synonymous with ALM – the parts are ‘built’ (bottom-up/additive) as opposed to cast and machined (top-down, subtractive). This means their properties are not isotropic, and the degree of anisotropy is varied dependent on the strength of bonds in the direction of build. AFM study of these materials requires an appreciation of the usage scenario of ALM-built parts in order to understand and mitigate the effects of build orientation on erosion rates.

Williams and Melton (1998) (Williams & Melton, 1998) use a proprietary early grade photopolymer resin, in a cuboid form and design a two-level full factorial experiment to study effect of grit size, pressure, build style and surface orientation. The authors acknowledge the stair-stepping effects of the build method, and that AFM can remove the effects within one or two cycles dependent upon setup. Inspection using an SEM (scanning electron microscope) showed the researchers that no flowlines were present on the surface of the substrate, suggesting the material was being removed by brittle fracture. They also note evidence of tearing and debris between the layers when magnified by 80x – for functional components, this makes AFM difficult to clean from plastic ALM parts with porosity shown to be present to a depth.

PEL (profiled edge laminae) are used for large soft metal forming (such as aluminium aerospace panels) and for thermoplastic softening (for plastic enclosure forming). They

incorporate heating and cooling channels – a manufacturing challenge exists where the laminae forms require finishing on the 'conformal' channels. Figure 2.20 references the structure of these devices. The authors Williams et al. (2007) (Williams, et al., 2007) design a full factorial experiment to study two factors at two levels; pressure (69bar and 90bar) and material (aluminium and steel).

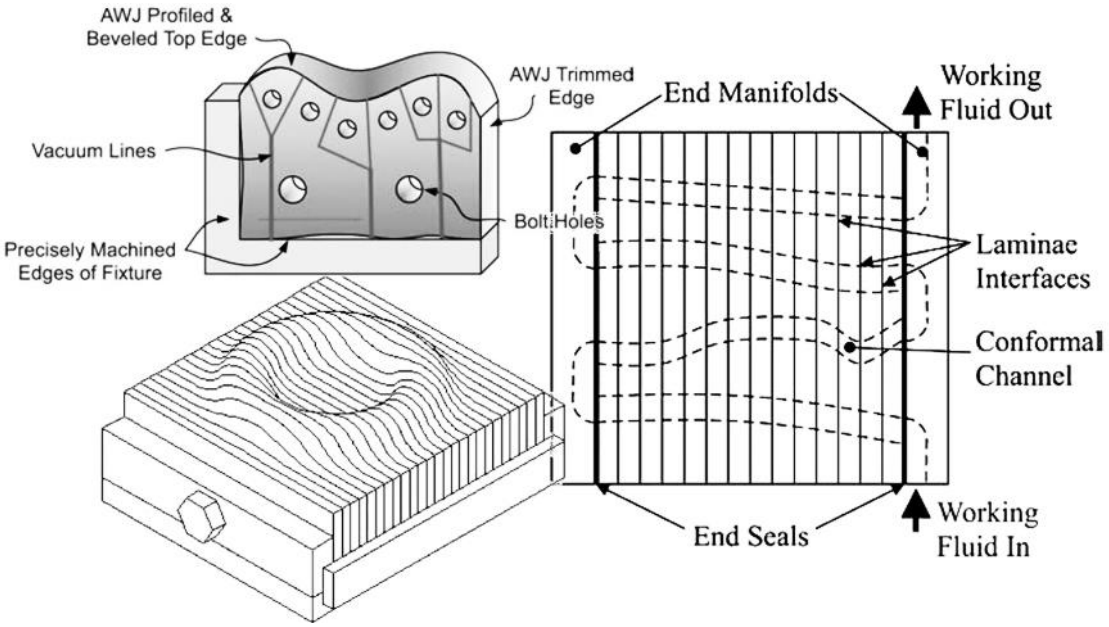

Figure 2.20 – Schematic of profiled edge laminae (PEL) tooling, fixturing method and conformal channel location. (*adapted from Williams et al., 2007*)

The tooling itself forms the flow cavity for the AFM process which removes much of the fixturing design from control – 'sealing' refers to the effect achieved by the MR mechanism of AFM – ploughing and rubbing mode means the joins between laminae are blended internally, effectively smearing material between laminae. The degree of sealing achieved by smearing was sufficient to maintain pressurisation for 15mins, and proves the concept that AFM can be used as an alternative to glues, seals and metal joining techniques such as brazing.

Fused deposition modelling (FDM) is arguably the most economically affordable ALM process – both the machinery and consumables are now well within reach, with consumer-level FDM machinery available from high street electronics stores. The coarse tolerances of the process mean that surface finish is somewhat undesirable, at 15-20µm Ra (Galantucci, et al., 2009). The authors attempt to manipulate the roughness through build strategy and a chemical post-processing stage, which proves successful – but they are alone in their remarks concerning uniformity, "AFM has been experimented with also for the manufacture of holes or small complex shaped surfaces, but this is limited by poor precision of the viscous agent pressure distribution, that can lead to non-homogenous material removal from the workpiece".

A report by Slovakian authors Duleba and Sikora (2011) (Duleba, et al., 2011) illustrates the relative strength of the direct metal laser sintering process (DMLS) – materials available (and therefore should be considered targets for AFM researchers) are aluminium AlSi10Mg, cobalt-chrome CCMP1, Inconel 718, maraging steel 1.2709MS1, stainless steel 15-5PHSSPH1, stainless steel 316L and titanium 64. These materials are all used in powder form, and therefore are pre-alloyed. The authors note the standard finish of the DMLS process as 8.75µm, and amongst others consider AFM to be a viable finishing process, "this is an inexpensive option for DMLS projects that are not tolerance dependent, and a more uniform surface roughness. The extent to which AFM is successful depends upon the degree of preparation of the treated surfaces". Unfortunately, the authors describe neither why they deem AFM to only be suitable for loose tolerance work nor their ideas of an AFM 'preparation' step.

2.4.2.3 Applied to 'micro-hole' electro-discharge machined (EDM) parts.

Commonly, the AFM process is considered an effective process in cleaning the surface of substrates treated with electro-discharge machining (EDM). The hardened residual layer is typically rougher than surrounding finishes, making it susceptible to the flow of concentrated abrasives of AFM. A key application for the EDM process is in the subtractive manufacture of micro-features in difficult to machine materials – the process is an electro-chemical means of MR and thus produces little stress during operation. The electrode (EDM tool) is typically copper or graphite, and is produced as a form to be sunk (hence the differentiation between sink- and wire-EDM) into the workpiece. Holes or forms can be produced as small as the electrode can be manufactured. Four papers are identified which approach the subject of AFM of micro-bores and AFM of micro-bores produced by EDM.

In a biomedical-justified application, the authors Tzeng et al. (2007) (Tzeng, et al., 2007) analyse the AFM of micro-'slits' produced by EDM by inspecting the quality of edge-rounding and the shape-precision. Employing a four-factor experiment, studying the abrasive particle size, abrasive concentration, extrusion pressure and machining time, the authors opt for a cylindrical billet with a repeated 'S' form micro slit with 0.23mm gap and manufactured from stainless steel. They find the optimum combination to remove recast layer is 150µm grit size, 50% concentration, 67bar and 30mins processing time – however, their experimental output is limited by the structure of the experimental design and results are not predictable beyond the experimental process space. The parameters chosen above are full factorial 'maximise response' choices. A higher concentration of abrasives is found to increase performance due to increased media viscosity, and the increased number of grains also results in an improved surface roughness. The authors find that a higher extrusion pressure is also liable to reduce precision.

Authors Lin et al. (2007) study a stainless steel substrate with an EDM-drilled 0.3mm hole. The EDM process produces debris which causes secondary discharges and pitting on the surface as illustrated in figure 2.21. With an L18 Taguchi-based experiment (fractional factorial), they identify six process variables; motion mode, extrusion pressure, extruding period, abrasive concentration, abrasive grain size and machining time. Machining time is shown to affect MRR with greatest significance, optimum grain size to finish titanium 6Al4V is 20µm and a stainless steel substrate is found to be more improved when processed for 40mins as opposed to Ti6Al4V. Unfortunately there are many simple criticisms that can be levelled at the output – chief among these is transferability – in order for the study to apply to other applications, the same media, geometry and workpiece materials would need to be applied. The extents of dissimilarity prevent the work from being recognised as anything more than proof of concept or as a starting point for another researcher.

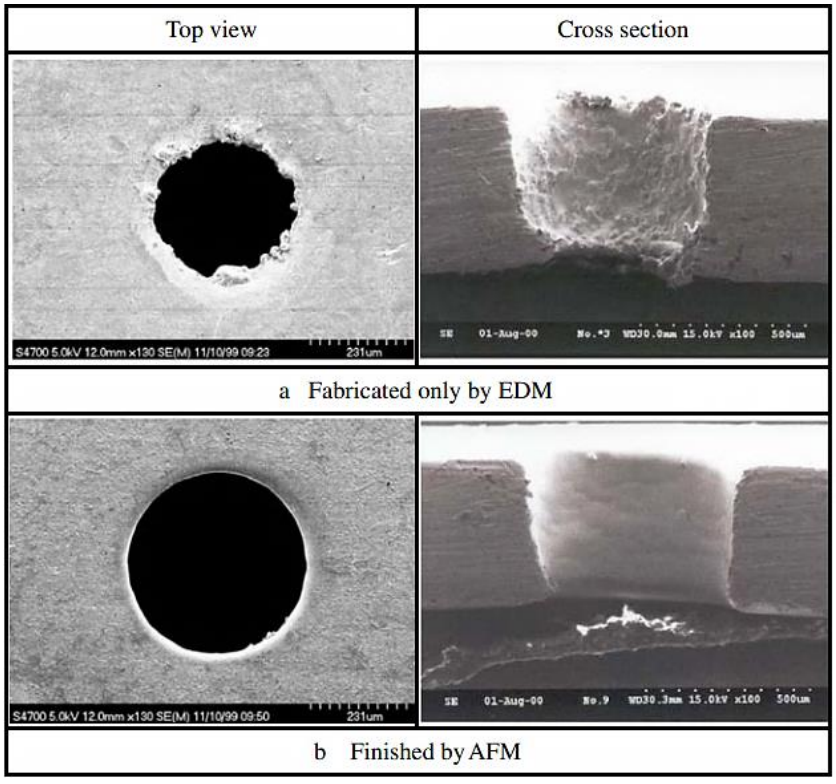

Figure 2.21 – Scanning electron microscopy (SEM) micrographs of the microholes (conditions: rotational motions, 5bar extruding pressure, 0.25s extruding period, 1g/ml abrasive concentration, 3µm abrasive grain size, 60min machining time. (Lin, et al., 2007)

Yin et al. (2004) (Yin, et al., 2004) present more applications in their paper focused on the AFM of micro bores in stainless steel and zirconia substrates with less than 1:25 aspect ratios. Stainless bores are 500µm in size while zirconia are 260µm – applications for these parts include fluidic filters, grids, biomedical filters, inkjet nozzles, optical ferrules, high-pressure orifices, standard defects for testing materials, micro-pipettes,

pneumatic sensors and manipulators, guides for wire bonders, spinning nozzles and fuel injectors. Critically, the authors recognise that inspection of these bores is as important as their machining and gather their results using both stylus interferometry and white light interferometry in multiple planes. The findings show that over both substrates, a 60% improvement was seen – interestingly, their setup contains a 100bar operating pressure, 17.5µm grit at 3.44% of media volume; the carrier fluid is water. Their results are certainly MMG-specific but the fact they successfully operated a carrier with Newtonian rheology is useful for operating the AFM process at the high-pressure/small-feature end of the spectrum. Surface finishes for these parts, irrespective of material or diameter-influenced-velocity reached 0.6µm Ra, which is comparably short of the 0.05µm suggested as the process best-effort by many authors.

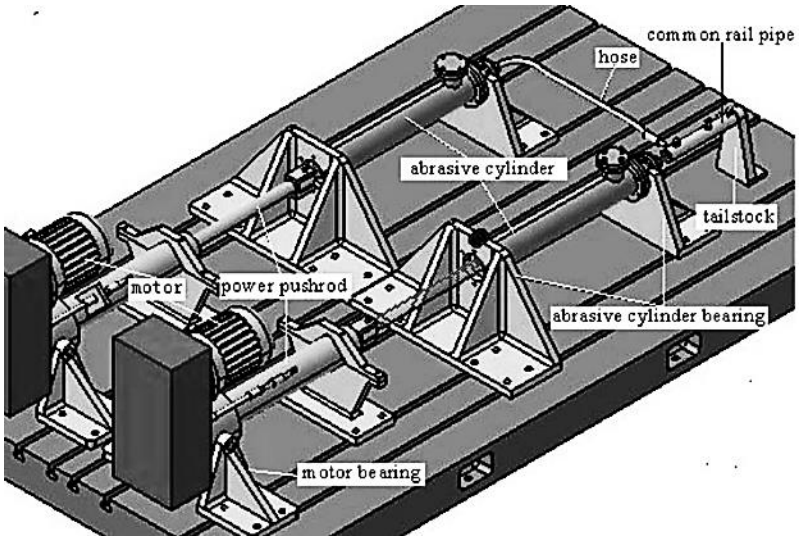

Figure 2.22 – Overall structure and design of abrasive flow polishing equipment. (Li, et al., 2009)

Diesel component machining is a popular application of the AFM process. The performance improvements sought by manufacturers of ICEs (internal combustion engines) are now in the order of <5%, meaning small changes such as surface finishes and gas/fluid flow optimisation is a viable target for automotive sector research. The authors Li et al. (2009) (Li, et al., 2009) develop a basic machine design for 1-off processing of a common rail diesel pipe – see figure 2.22. The authors identify the need for identical finishing on four small inlets feeding into a central bore running perpendicular to the inlets; in order to achieve uniform roughness and edge-rounding, the authors recognise the requirement to control the pressure and velocity distribution. The key finding in an applications and capability context are that component fatigue life would be vastly improved, although it should be noted that the authors appear to have only carried out a simulation of the work, and no practical verification or figures are provided.

2.4.2.4 Applied to ceramic materials

Technical ceramics have been in use for several decades – primarily in physics research, automotive, oil and gas and medical industries, their hardness, resistance to wear and high temperature stability make them a workable alternative to harder metals. Processing these materials is made more difficult by the resistance to erosion exhibited, but given the correct combination of parameters, the authors Uhlmann et al. (2009a and 2009b) present the options for users working with commercial ceramics such as ZTA ceramic, comprised of aluminium oxide with <30% titanium carbide by volume. They utilise a diamond-laden ($\bar{x}$=44.5µm) abrasive, of the same polymeric carrier as commercial AFM operators. They study the effects of temperature, pressure and processing time.

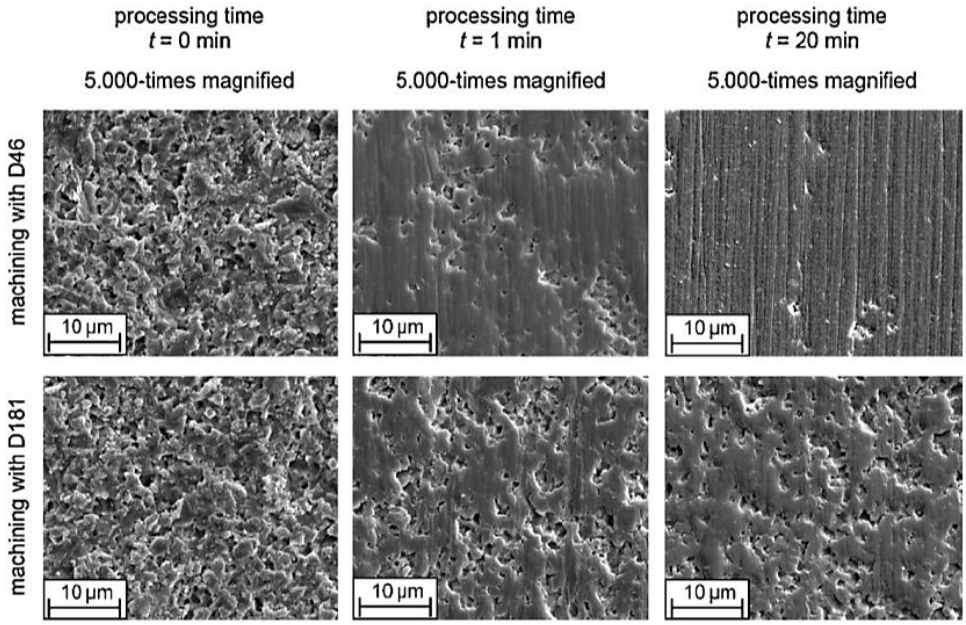

Figure 2.23 – Surface formation on aluminium oxide ZTA ceramic. (Uhlmann et al., 2009a)

The machining process is found to produce "washed-out" surface finishes, which may be interpreted as 'non-reflective', a result of scattered finish orientation. The authors (Uhlmann et al., 2009a) find the MR mode to be 'ductile', implying a primary ploughing deformation action followed by ductile fracture. Material defects are smoothed on the surface, but when erosion removes the outer layer, sub-surface defects are exposed. Brittle MR mode can be achieved with diamond abrasive above 185µm.

In the second paper, Uhlmann et al. (2009b) work in the area of substrate pre-treatment prior to coating – similar to the methods applied in the hob (gear-hobbing) pre-treatments, the authors are applying AFM and thermal laser ablation to cemented carbide, typically used as substrate for high quality drills and mills. It is suggested that controlled edge-rounding prior to coating improves the tool life. Their findings indicate AFM provides a better surface quality, removing peaks, reducing peak spacing and

removal of cobalt binder. While surface quality is lesser with thermal laser ablation, the coating fails in adhesion with AFM, whereas laser ablation increases strength between substrate and results in a cohesive failure mode through tensile cracks.

2.4.2.5 Applied to composites

Research is published on two forms of composite materials – fibre-reinforced and particulate-reinforced. The authors Ravikumar et al. (2012) (Ravikumar, et al., 2012) focus on carbon-carbon (C/C) composites, i.e. carbon fibre reinforcement in a carbon matrix, while the authors Mali and Manna (2010) (Mali & Manna, 2010) focus on silicon carbide particulate reinforced aluminium. Process variables in the C/C material study are grit size, extrusion pressure, process oil (viscosity modifier), abrasive concentration and number of cycles. Like so many experimental investigations, the MMG combination is unique and difficult to replicate elsewhere. The substrate is pre-treated, ground in this instance – grit size of mesh 220 achieves a 30-35% improvement in finish, 60bar achieves a 30% improvement in finish, 12% by weight oil content achieves a 30% improvement in finish, 70% by weight abrasive content achieves a 30% finish improvement and 150 cycles achieves a 45% improvement in finish. In criticism of this work, the effects of processing time could be to blame for the lack of finish achieved with smaller grit mesh size, and from an industrial perspective, the only reason for pre-processing with grinding would be to achieve a given form, i.e. to remove any undulations that AFM may exaggerate.

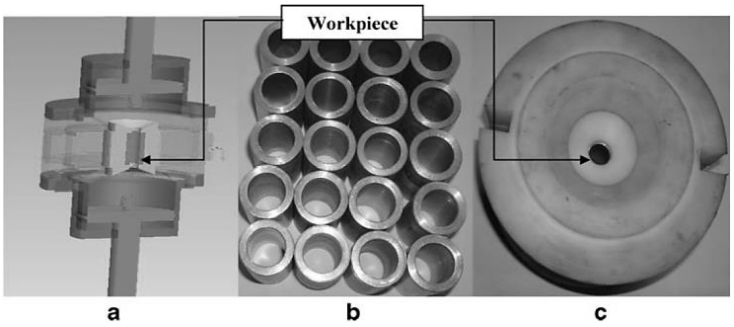

Figure 2.24 – Detailed mechanics of AFM, workpiece and tooling, where (a) CAD model shows the mechanism of AFM, (b) Al/15 wt% SiC-MMC workpieces and (c) AFM tooling with workpiece. (Mali & Manna, 2010)

Authors Mali and Manna (2010) opt for a mixed-level factorial design – grit size is studied with five levels, while cycles, pressure, grain fraction and viscosity are set at three levels each. Their findings are industrially useful – in this material, ploughing and rubbing may be observed leading to a degradation of surface quality. While their optimal parametric combination is expressed much like in a ‘Seito-method’ experiment (i.e. maximise response instead of a mathematical model), they are able to identify significant parameters; grit size is most significant to processing this type of material,

for both surface finishing and edge-rounding. Grain fraction (% of abrasives) is most significant to average roughness. Their final concluding comment is somewhat inaccurate, "mathematical models … are successfully proposed for proper selection of AFM parameters during finishing of [MMC] workpiece".

2.4.3 Recognised competing processes

Table 2.2 – Competing technologies.

Process	Strengths relative to AFM	Weaknesses relative to AFM
Centrifugal Vibratory Finishing	• Clean and dry process • Inexpensive, easy to change media • Zero setup requirements	• External surfaces only • Ineffective in large components • Ineffective edge rounding
Electro-chemical Machining	• No mechanical load • Higher productivity; <20s for a roughing and finishing cycle combined • Consistency in overcoming random burr formations	• High power requirements • Limited by accessibility of tool • Cannot process non-conductive materials, i.e. polymer composite and some ceramics
Thermal Energy Method	• Instant random burr removal • Chamber filled with gas and action performed equally over entire job • No scratching nearby features	• Unsuitable for thin walls • Increased burr size demands more aggressive explosion • No finishing or rounding ability
Abrasive Water Jet Machining	• Minimal post-process cleaning • High stock removal • Reduced processing time	• Geometrically inaccurate • Cannot travel around corners and maintain cutting ability • Poor surface roughness, not designed for the task
Sand Blasting	• Good levels of material removal, suitable for paint and other thick coatings • Low-cost replaceable media in form of iron shot	• Inaccurate, typically applied by hand, holding part by hand • Only removes material in line of sight of gun • Surface roughness or edge rounding is not repeatable
Wet Finishing	• Wide area of application • Can process very thin walls • Secondary processing is achievable by replacing water for a chemical agent	• Cannot be carried out on internal surfaces of a complex part • Abrasive collects in cracks, ledges and pockets
Manual Finishing	• Zero setup time or cost • Tooling is cheap • Unknowns, i.e. large burrs or swarf may be discovered by eye, or even machining error	• Expensive • Non-automated, human-error • Requires only a slip and a job can be scrapped, after all machining hours have gone in

2.5 Process models

Modelling in engineering can take many forms – numerical, uncertainty, in-silico, conceptual and statistical to name but a few. Their purpose is to take thoughts/ideas and formalise them into a structure to communicate concepts/findings to stakeholders. The models presented in this section are mainly numerical models (those attempting to define the underlying behaviour of the AFM process) and empirical models (those presenting specific findings derived from experimental investigation).

2.5.1 Numerical methods

Authors studying the AFM process have long sought a mathematical representation of the process behaviour and its interaction with a workpiece surface – this subsection presents works relevant to the AFM process and makes comparison to real-time captured process data.

2.5.1.1 Neural network methods (expert systems).

Strongly related to computer science, the neural network is an alternative to rule-based programming, and imitates basic animal brain functions using 'nodes', interconnected and sharing information about the condition of the system by different metrics. They are popularly used in machine learning applications.

Lam and Smith (1997) (Lam & Smith, 1997) produced a conference paper detailing the approach to using a neural network for prediction of surface condition. The literature review suggests the authors feel that previous work has not encompassed enough AFM process variables in order to fully understand the process, and those previous authors did instead opt to study a subset which restricted model accuracy. Interestingly, they make no mention of substrate material, nor attempt to understand that operating pressure is not uniform through the part; therefore maximum operating pressure is not defined by the target feature size. The model is not applied to other geometry, and achieves only a 65% explanation of outgoing average air (the response variable).

Authors Petri et al. (1998) (Petri, et al., 1998) develop two neural network approaches for surface finishing and for edge-rounding. They are utilising some basic data collected by Extrude Hone's subcontract department and attempting to develop a predictive model where geometry and material are combined to model the process. The authors have not collected the data themselves, and for the range of variables covered, it is proportionally very small and contains no repetitions. This may be the reason for the lack of R-squared value for the predictive model – this reinforced by their closing 'further work' statement, "application of statistical approaches to analyse correlations among input variables with the intention of reducing unnecessary inputs".

Jain et al. (1999) (Jain, et al., 1999) discuss the element of ‘system training’ using response variables to allow the system to recognise the factor settings which lead to a given response. The term ‘high dimensional space’ is important, sometime also referred to as ‘multi-variate’. Neural networks do not require any assumed structure of model form – they are based on error correction ‘back propagation’ learning rules, fed with real data running with given input parameters, combined with a cross-reference step in a ‘hidden layer’ and utilising real output data to verify against experimental input conditions. The systems are normally software-based, and error corrections are referred to as iterations as is common in modern ‘iterative’-type calculation software – the authors run ~4000 corrections. The authors (Jain, et al., 1999) combine the neural network (NN) with multivariable regression analysis (MVRA) and compare NN, empirical and MVRA obtained results. Error in prediction by NN was 0.25-8.95% but in favour of NNs, the MVRA results were 0.09% to 25%.

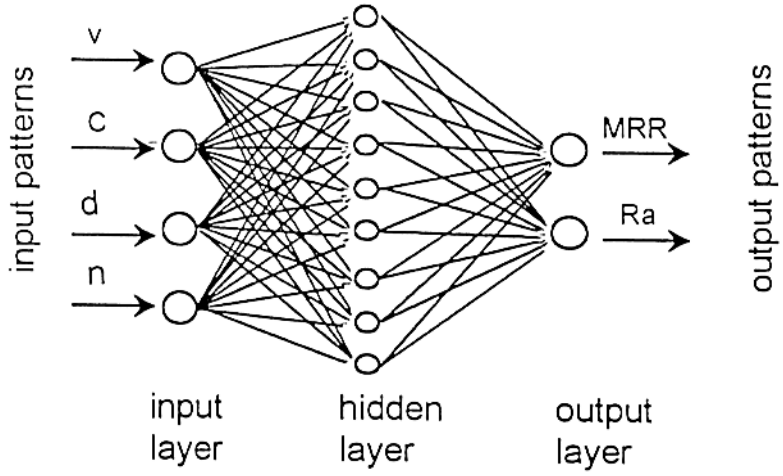

Figure 2.25 – Structure of three layered neural network. (Jain, et al., 1999)

One year later, Jain and Jain (2000) (Jain & Jain, 2000) apply a genetic algorithm (GA) technique and compare to NN and empirical data once more – an optimised NN achieves 6.44% surface finish error and 6.23% MRR error. Authors Ali-Tavoli et al. (2006) (Ali-Tavoli, et al., 2006) have two datasets they use for testing their NN and GA tools – a training set and a testing set. Factors are number of cycles and concentration of abrasives, with responses of surface finish and material removal. They have identically processed sets for aluminium and brass substrate materials, showing the flexibility of input data where cycles is recorded at five levels and concentration is recorded at four, while material type is at two. The authors frequently refer to ‘multiobjective optimisation’, whereby an end user may require two or more outputs to be maximised or minimised, while the condition of other factors may be restrictive. The ‘Pareto’ method of optimisation eliminates the requirement to perform iterations as certain parameters are labelled as non-dominant where conflicting outputs may favour extreme settings.

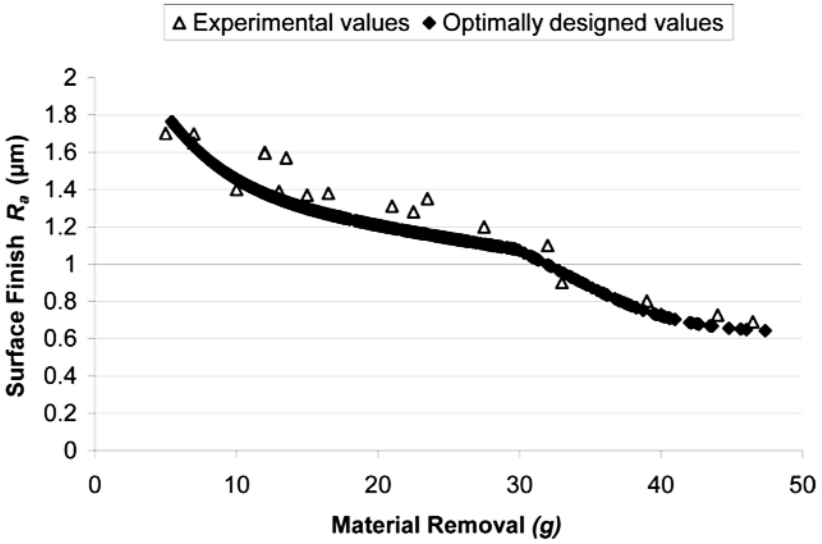

Figure 2.26 – Overlay graph of the obtained optimal Pareto front with the experimental data of aluminium AFM process. (Ali-Tavoli, et al., 2006)

Reviewing the status of NN usage for modelling of surface roughness, Pontes et al. (2010) (Pontes, et al., 2010) find many inconsistencies and gaps in the body of research which prevent the thorough and logical comparison of NNs as a tool. They identify the strengths of NNs as, 1) universal function approximation, 2) resistance to noisy or missing data, 3) accommodation of multiple non-linear variables with unknown interactions, and 4) mapping complex relationships whose representation in analytical terms would be difficult. As the authors only reference two papers relating to AFM NNs, the discussion is based on numerous other machining technologies, and discussed in general terms – approaches are transferable, i.e. between data collection, definition, fitting and validation.

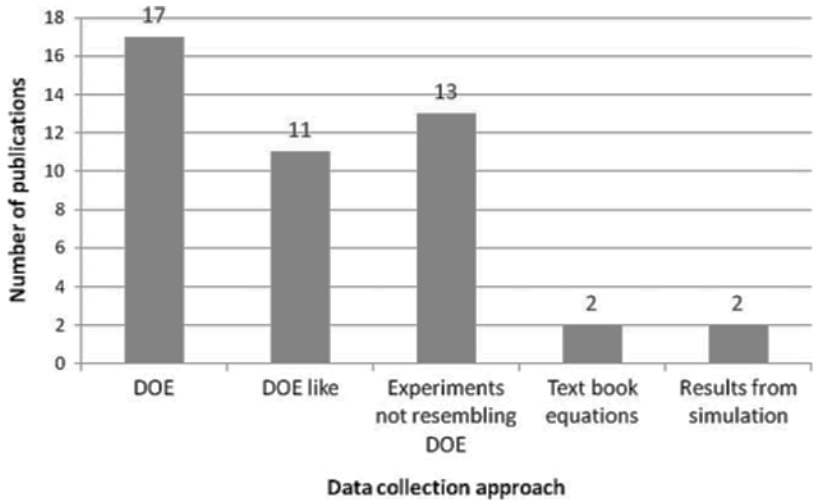

Figure 2.27 – Approaches adopted to build neural network training datasets. (Pontes, et al., 2010)

Figure 2.27 illustrates how critical DOE knowledge is to extending an experimental exercise into a modelling one. The inputs into the DOE and consequent collected data are directly transferred into the two NN datasets – however, in the light of AFM's MMG system, it becomes apparent that NNs cannot identify shape beyond simple representations, any complexity/arbitrariness is difficult/impossible to represent numerically. The authors note that basic information required to replicate the studies are missing – this is further verified by the papers referenced in this review, containing poor numerically quantified figures, i.e. conclusions without reference to process capability and for goodness of fit values between models and empirical data.

2.5.1.2 Finite element / classic abrasion theory methods.

The authors Jain, Jain and Dixit (Jain, et al., 1999) apply standard fluid dynamics equations in the development of a finite element model. Assumptions made tally with work presented further in this document whereby media is isotropic and homogenous, although media flow may not always be steady, nor are media properties independent of temperature and time as suggested by the authors. Mechanisms of material removal are not widely agreed upon at this stage (1999), but summarily the authors describe two modes – plastically impressed grooves, not involving material removal (MR) and that shape of particles determines whether chip cutting and rubbing occur. Spherical particles are shown to aid transition from rubbing to partial chip formation, adopting the terms 'microploughing' and 'microcutting'. MR occurs not by a single ploughing particle, but by multiple particles tracing over ridges formed from prior particles tracks – the peaks are effectively a series of microfatigue inducing actions. The authors note, "microploughing and microcutting are the dominant processes on ductile material while microcutting becomes important on brittle materials".

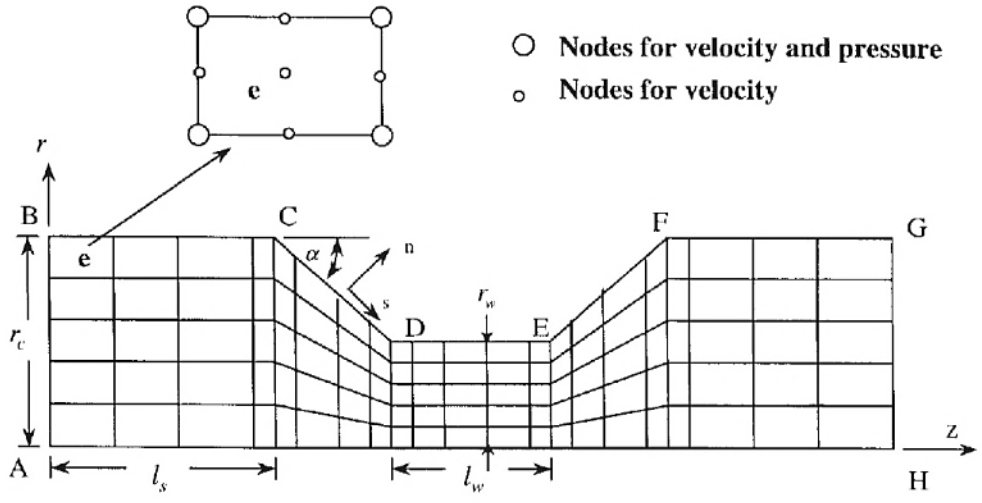

Figure 2.28 – Finite element mesh produced by (Jain & Jain, 2003).

Numerical simulation with a comparable model is presented by the authors Jain and Jain (Jain & Jain, 2003). They find that average piston velocity of between 0.2mm/s and 0.8mm/s is linear to extrusion pressure, whereby their FEM model agrees to over 90%; they also find that (as shown in figure 2.28) that increasing the angle (i.e. pumping toward a flat face perpendicular to flow incurs the greatest extrusion pressure necessary to overcome the feature. This defines an additional complexity in the process where features are responsible for incurring pressure drop, not only the wall friction and media internal friction. With a silicon carbide abrasive the process also shows velocity to be linear to stress, reduction ratio to be non-linear to extrusion pressure and hardness of workpiece material to be non-linear to depth of indentation.

In a further 2004 paper, Jain and Jain (Jain & Jain, 2004) work with a square box section for testpiece geometry, attempting to establish the effect of continuous scratching in a stochastic simulation. The principle of establishing how many grains are actively involved with contact at the surface is useful to determine potential abrasive action. The author's results show that, for a particular grain fraction, reducing grit size increases active particles, although a conflict in results suggests that once grit is broken down through continued use, active grain density takes a downturn.

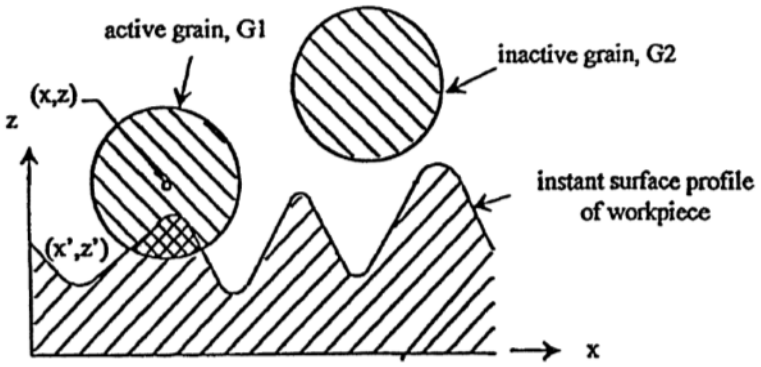

Figure 2.29 – Interaction of presumed spherical abrasive grains with surface. (Jain & Jain, 2004)

For the first time in 2009, the authors Jain et al (Jain, et al., 2009) attempt to provide a model for processing of complex workpieces with AFM. Each stroke is considered to remove the same amount of material, all grains are the same size, force on the grain is normal to the surface and equal, grains are uniformly dispersed and temperature is assumed to be constant. The analysis uses RSM to predict the responses, but seemingly infers that unless force is known/calculated at a given POI in a job, grain action cannot be translated into a MR value. The plots of theoretical MR against experimental do not characterise the behaviour adequately, in some cases showing the model of parameter 'no. of cycles' to deliver only 33% of actual experimental MR. The same is true of pressure plots. The deviation may have been caused by, "fixture design alteration", and, "simplified assumptions in models".

An apt description of the classic abrasion theory is Levko's 2009 (Levko, 2009) paper considering AFM's effect on surface roughness on the basis of a 'contact-interaction' model. Adopting a similar 'force-based' interpretation as in figure 2.29, the 'micro-asperities' are noted and spherical shape is not assumed. Contour area, pressure, material hardness and elasticity are considered as factors, whereby an assumption is made that a single grain's resultant effect can be multiplied by the volume of grain in a body of media – recognised as 'mass-contact'. The author is aware that grains may come into contact with the surface between "500-12,000" times, although the models appear to make no concession for the ploughing mode of MR where multiple grains cut through the heightened fatigue stress peaks of previously ploughed grooves.

2.5.1.3 In-process measurement.

While pre-process and post-process actions are simplest to enforce, they are rarely economical – a continuous inspection method, checking for part condition by electronic means without measuring the feature itself is seen as a reasonable approach by authors. Authors Jain and Jain (Jain & Jain, 2001), adopt the test geometry as pictured in figure 2.28, while mentioning a fourth mode of MR in addition to a 1999 paper by the same authors – 'microcracking' occurs mainly in brittle material where high concentrations of grit incur greater levels of MR leading to larger debris detaching from the surface. The authors' inspection method is based on principles of heat and energy transfer; energy transfer uses the force model as applied by the authors previously and the heat transfer model applies to a one-dimensional scenario where heating the workpiece allows the transfer of heat into the media – the conclusion states, "the model is capable to predict the change in workpiece temperature", considered useful as the temperature of media alters with viscosity and further, affects grit support ability, although the authors do not state whether the effect is due to chemical makeup or as a result of viscosity itself.

In 2009, authors Fang et al (2009) attempt to determine a link between machining efficiency and temperature of media. The work is based on a test system which does not allow temperature control, and thus is of questionable potential for replication in industry-based work. However, their conclusion notes that increased cycles are responsible for increasing media temperature as a result of friction between shear planes. Efficiency is considered to be reduction of rolling particles; increase in rolling particles occurs in parallel with greater velocity and pressure – sliding is the opposite.

Practical application of AFM is given by Baehre et al's 2012 paper (Baehre, et al., 2012) attempting to use in-process measurement of axial forces – the process is justified for use on marine propellers, to reduce effects of cavitation; the same reasons apply to fuel injection systems, hydraulic actuators and stress-sensitive intersections. The authors apply axial force sensors to a traditional AFM setup for the purpose of accumulating data correlating force with response variables. Findings include force increasing linearly with passage length and applied pressure, negating any useful output for complex

geometry – in addition the length of the passage was shown to be the leading influence, not geometry. A friction factor is hand-calculated and axial force is shown to correlate the most, while higher piston pressure is shown to generate a finish faster – although results are affected by geometrical bellmouthing at the entrance to the bore.

2.5.1.4 Radial basis / network methods.

Mollah and Pratiha ((Mollah & Pratihar, 2008) attempt to model TIG (tungsten inert gas) welding and AFM using 'radial basis function networks' (RBFNs) using back propagation (BP) and genetic algorithm (GA) as methods of training a so called 'soft computing' approach, utilising fuzzy logic. Their input data is not specified, but the GA-trained RBFN performed slightly better than the BP-trained, although error in input data was cited as a limiting factor. Plots show an increase in deviation from the model's predicted value line as response magnitude increases, for both MRR and Ra.

2.5.1.5 Desirability function and metaheuristic technique.

Mukherjee and Ray (2008) identify multiple-objective response problems relevant to CNC honing – mode of MR is comparable to AFM, as it is a grinding process. The authors note the variety of responses attributed to grinding processes almost always contain different units. Three response optimisation techniques are used – RGA (Real-coded Genetic Algorithm), SA (Simulated Annealing) and MTS (Modified Tabu Search); MTS is considered to be best at providing accurate results to solve single-stage grinding problems. It is unclear how the results from the system input are altered when the model (figure 2.30) is applied to an arbitrary geometry; it appears to present good agreement between model predicted values and actual values, with model failure at the extremities of the prediction space. The results are spread throughout a high roughness value range, questioning the usefulness of the model.

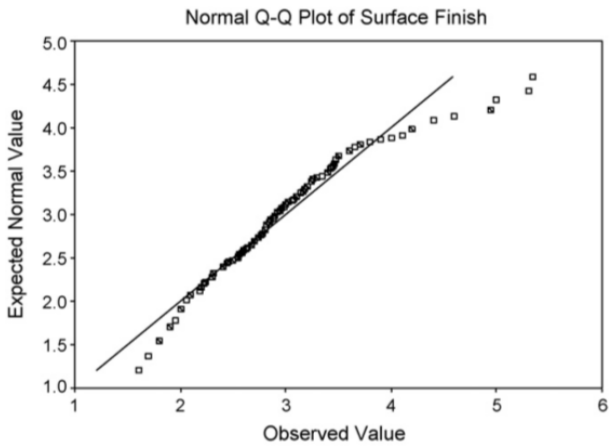

Figure 2.30 – Q-Q plot of surface finish variable. (Mukherjee & Ray, 2008)

2.5.2 Approaches to modelling used in unrelated processes.

Two groups of authors present techniques used to model a process similar to that of AFM – Momber et al. (Momber, et al., 1999) use acoustic emission as an online 'real-time' method of in-process measurement in 'hydro abrasive erosion' (HAE) and Patel et al. (Patel, et al., 2009) use a 'trust region' method to optimise an RSM designed empirical study of surface roughness drivers in ceramic composite machined by EDM.

The HAE operation is similar to abrasive water jet machining (AWJM) whereby a high velocity (>100m/s) stream of deionised water is fed toward a component – the stream contains abrasive of given mechanical properties, size, shape and volume where variables affect MRR and surface finish. The authors (Momber, et al., 1999) identify that temperatures are localised at the point of erosion after testing with a garnet abrasive in five different types of concrete. Acoustic emission (AE) results are collected and plotted for several variables – in figure 2.31, the AE response is plotted against abrasive flow in g/s. Plot 'a' to 'c' represents mechanical properties increasing in terms of compressive strength, Young's modulus and fracture energy. The results are inconclusive – either there is no linearity (plot b) or no gradient (plot a, c).

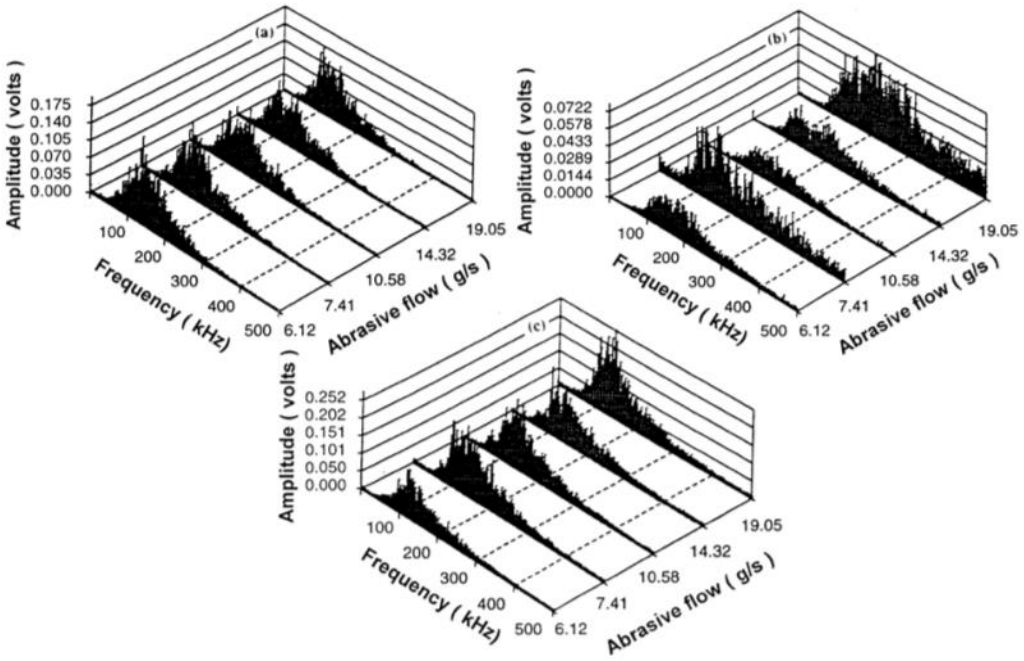

Figure 2.31 – Frequency domain AE-signals with change in abrasive mass flow rate. (*adapted from Momber et al. 1999*)

Authors Patel et al. (Patel, et al., 2009) consider EDM for surface finishing of electroconductive ceramics as a solution to machining problems with conventional approaches. Process parameters are selected as part of an RSM design formed using 'design expert' software to perform regression analysis and ANOVA tasks – the model is considered useful by the authors who find the dominant parameters, significant

interactions, anomalous behaviour and develop a prediction model for results within 95% confidence interval. Cost reduction is cited as the most useful application of the research, for those involved in EDM of ceramics. Unfortunately, the vast majority of the results plots show a response of between 0.8µm and 3µm Ra – these finishes are extremely poor, and it should be noted that anything above 0.8µm would be polished by hand in a precision machining environment.

2.5.3 Empirical studies.

A majority of AFM-related papers consider the effects of the surface in a specific material or subset, and the process parameters that users attempt to control. Across the board, widespread recognition of the number of variables and interactions is noted.

2.5.3.1 AFM in metals.

Authors Jain and Adsul (Jain & Adsul, 2000) identify parameters; 1) cycles, 2) concentration of abrasive, 3) mesh size and 4) media flow speed. Through their experiments, they find their system has little effect on MR as they are using a low-pressure one. They find increased cycles to improve Ra value, although the percentage increase reduces with increasing cycles. This is due to the availability of peaks in the early case. Higher abrasive concentration increases rate of improvement in Ra, likely due to greater volume of abrasive edges. All findings are true for both aluminium and brass workpiece materials.

In a 2005 paper, Raju et al. (Raju, et al., 2005) focus on AFM of SG (spheroidal graphite) iron primitives, a type of iron used for strength and ductility. In a one-way bench system, the authors fix pressure, velocity, grain fraction, temperature and stroke length – their process variable is number of passes. They find that the material suits a lower pressure (10bar), until their seventh pass, where the surface starts to deteriorate. They note that a rough surface may be subject to clogging (valley filling up). They also state, contrary to conventional wisdom that out-of-roundness form is improved and that their system has produced a varied finish at different points of the bore.

Zhang et al. (Zhang, et al., 2009) operate a self-built one-way machine whereby a testpiece is designed with three 0.15mm holes drilled into the end face. Under a pressure of ~980bar, grit of F1200 (~8µm) at a concentration of 45-50% in a mineral oil carrier is fed through the system and out through the part as pictured in figure 2.32. After sacrificing the testpiece, a drilled finish is said to be improved from 2.5µm Ra to 0.2µm. The authors agree with the assessment of Raju et al. (Raju, et al., 2005) that beyond a certain time period, the results are poorer. Greater machining efficiency is seen from using larger particles; however accuracy of form is reduced and it is recommended that abrasives should be selected based on desired finish.

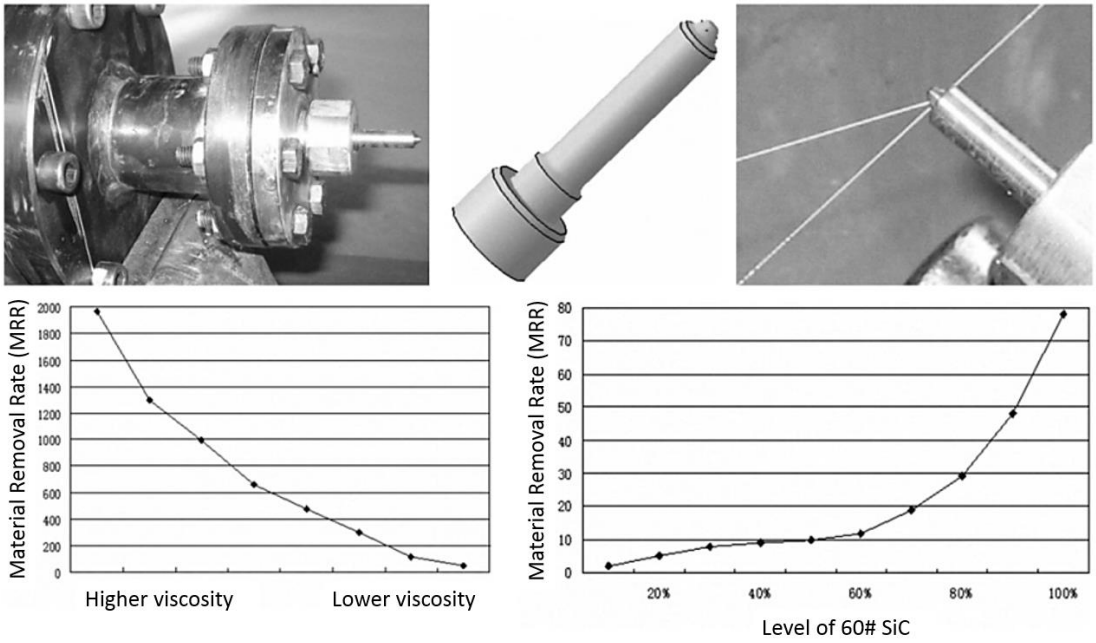

Figure 2.32 – Effects of viscosity and grain fraction in micro-AFM. (*adapted from Zhang et al. 2009)*

A small study was performed by Kumar and Manna in 2010 ((Kumar & Manna, 2010) where the authors utilise a screw-driven AFM (extrusion AFM, EAFM) system similar to that used in injection moulding. A die is affixed to the exit of the screw where a 15mm bore allows the exit of the slug. Pre-process roughness is found to be in the range of 2.1µm to 2.8µm Ra; under 45bar pressure, pumping through a cylindrical 40mm long bore, the finish is shown to be best at the largest grit size in the test and 20 cycles – due to the unconventional nature of the pumping apparatus, what constitutes a cycle is unclear. Surface finish also shows an almost linear improvement with increased pressure.

Kenda et al. (Kenda, et al., 2011) study the process in D2 tool steel, pre-machined with an EDM process – they attempt to show that EDM surface damage can be cleared and induction of compressive residual stress is possible. With a two-way AFM machine, they process samples at 35bar and 60bar. Using a media with F80 (165µm) grit, the pre-process EDM finish of 1.68µm is reduced to between 0.23µm and 0.94µm following AFM. Residual tensile stress (undesirable) is applied by the EDM process to approximately 550MPa – AFM removes this and creates a 10µm layer of 200-350MPa compressive stress (desirable) – this is proportional to operating pressure, although layer thickness is constant. X-ray diffraction (XRD) is used to measure residual stress.

2.5.3.2 AFM in ceramics.

Three authors present empirical studies based on ceramics processing; Sankar et al. (2009) discuss the processing of MMCs, or metal matrix composites (see figure 2.33) – an evolution of polymeric homogenous composites. In this instance, the testpieces – an

aluminium alloy loaded with 10%wt and 15%wt silicon carbide particles, are ground to a predefined starting roughness to prevent any influence on percentage improvement figures. However, this leaves the issue of surface texture, finish orientation and dislodged/torn particulate reinforcement unanswered. The authors determine an optimum finishing pressure of 60bar, where a new styrene butadiene rubber (SBR) carrier is used to transfer momentum of F220 (65µm) grit.

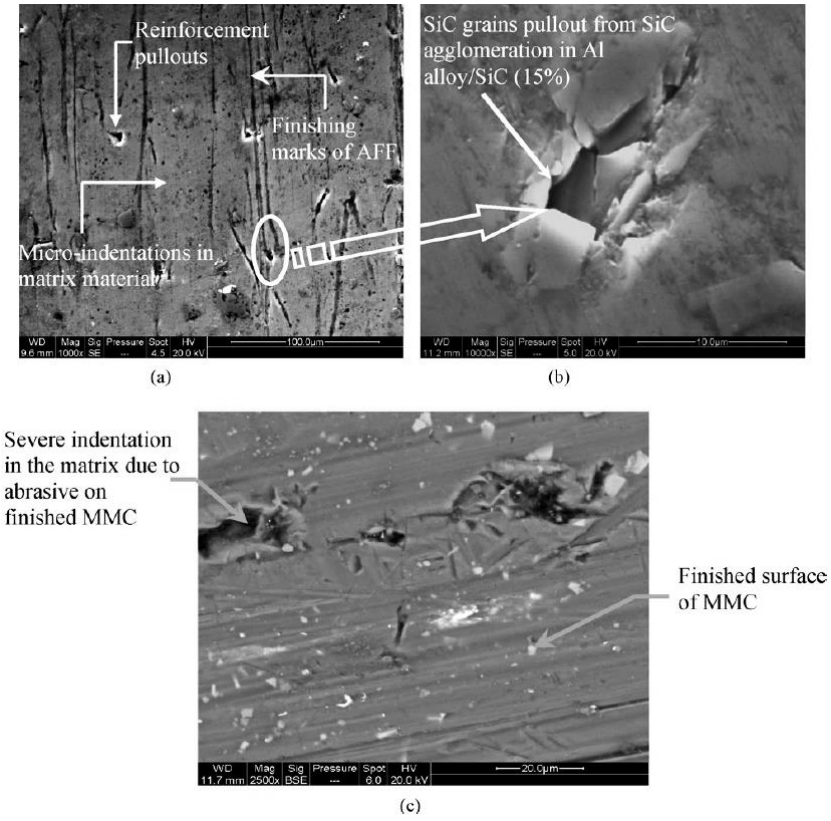

Figure 2.33 – Micro indentations in matrix material. (Sankar, et al., 2009)

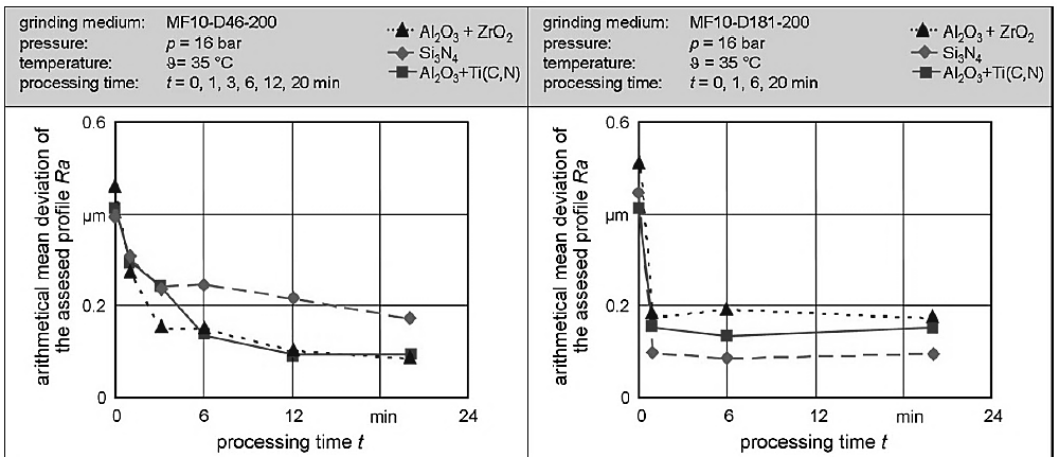

Figure 2.34 – Average roughness response for grit size against time. (Uhlmann et al., 2009a)

Authors Uhlmann et al. (Uhlmann et al., 2009a) apply diamond-loaded media to three grades of ceramic – an aluminium + zirconium grade, a silicon grade and an aluminium + titanium grade. Figure 2.34 shows the effects of processing with two grit sizes – the right hand plot uses smaller size diamond particles, which explains the better overall finish, but not the reasons for reaching that finish sooner than the larger D181 particles.

Mali and Manna (Mali & Manna, 2010) use the same material as Uhlmann et al (Uhlmann et al., 2009a), while recognising the same effect as Raju et al. (Raju, et al., 2005) whereby a limit is met and the surface becomes rougher. The authors present an optimal parameter combination, although the results are only valid for the MMG combination presented in the paper. Abrasive mesh size is considered to be the driver for MR and reduction in PV (peak to valley) height, while grain fraction is considered most important for surface finishing. Media viscosity drives workpiece form, although the authors make no mention of model validity following a change in geometry.

2.5.3.3 AFM mechanisms of MR, forces and process variables.

Loveless et al. (Loveless, et al., 1994) study the effects of AFM upon different surfaces; different microstructures and different machining methods are shown to deliver markedly different effects. Their key findings are; 1) initial surface condition affects MR, 2) WEDM is particularly well suited to post-processing with AFM, 3) uniformity is subjectively improved, 4) roughness profiles are improved – the authors do not recognise that AFM can roughen a surface given an acceptable pre-process roughness.

In a 2002 conference paper, Szulczynski and Uhlmann (Szulczynski & Uhlmann, 2002) identify the MR modes present in AFM – MR modes are critical to ensuring that process behaviour is able to be optimised and that grit is placed into the correct regime to ensure MR (or regime conducive to surface finishing). High viscosity is recognised to facilitate "extremely high MR", while the media (apparently supplied by Micro Technica Technologies) contains their standard 'filler' grit whereby a stronger MR response is seen as a result of greater normal force.

Authors Gorana et al. (Gorana, et al., 2004) employ a two-component axial dynamometer to measure forces when varying pressure, grain fraction and grit size. Axial force is increased by greater pressure, while reduced by grain fraction and grit size – it explains over 85% of total variability in the dataset. Radial force is increased by pressure and grain fraction, but reduced by grit size – the two positive effects contribute over 73% of total radial force responsibility. The ratio between two forces measured has a linear relationship with surface roughness, although values are of little further use.

Volume of *active* grit in a media configuration is studied by Gorana et al. (Gorana, et al., 2006a) in a bid to predict surface roughness. Extrusion pressure is shown to correlate linearly with average number of active grains up to 70bar, "beyond which it starts declining". Theoretically, the authors suggest that the two metrics are directly

proportional and *should* scale – the authors acknowledge the difference between their theoretical and experimental models are high. Correlating with other authors (Gorana, et al., 2006b) (Jain & Jain, 2004) percentage reduction of Ra is achieved by increased grain fraction and that rubbing and ploughing are mechanisms of MR. Figure 2.35 shows the disagreement.

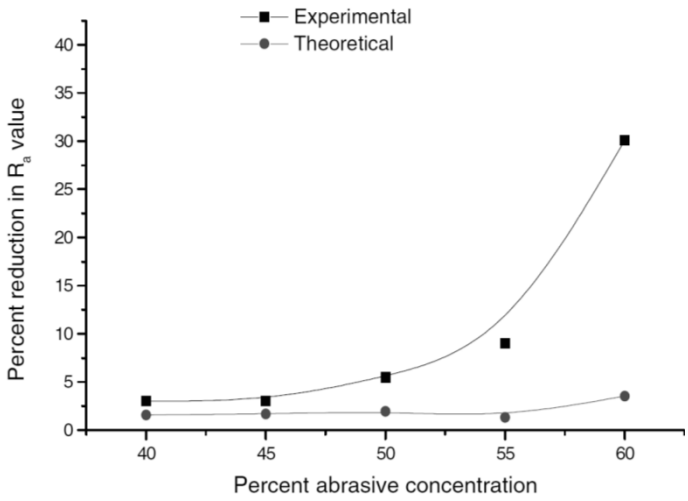

Figure 2.35 – Variation between theoretical model and experimental data. (Gorana, et al., 2006a)

In what appears to be an extension of their paper published in the same year, the authors (Gorana, et al., 2006b) add scratching experiments to establish mode of MR. Figure 2.36 presents two materials under the same conditions; "considerable care should be taken when evaluating and interpreting the force on a single grain" – the authors note a minimum load for chip formation correlates well with experimental MR. They find that rubbing dominates, but ploughing exists – at this stage, it seems prudent to suggest that Gorana et al. (2006b) are simply using operating conditions that are not conducive to alternate modes of MR.

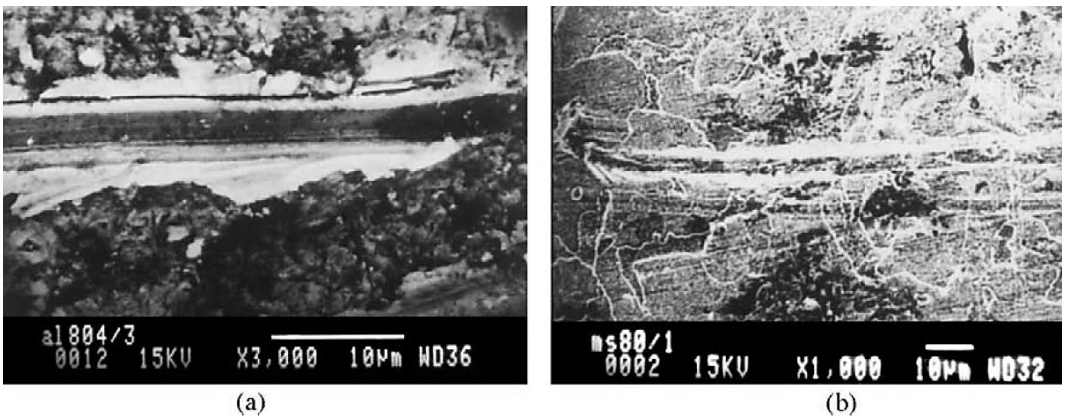

Figure 2.36 – SEM image of scratching experiment. (a) aluminium, (b) mild steel. (Gorana, et al., 2006b)

Cherian and Isaac (Cherian & Issac, 2013) study the effect of process variables of hardness, grit size, grit hardness, extrusion pressure and carrier properties. They find that roughness can be improved by keeping the extrusion pressure high, grit size low and grain fraction high. The authors also find that when force ratio between axial and radial is at a maximum, the percentage reduction in roughness is at a maximum – one can only assume that acceptable roughness is still driven by grit size, as placing greater force behind larger grit has the potential indent to a greater extent.

2.5.4 Comparison to alternative abrasive machining processes.

The textbook 'micromachining of engineering materials' contains a chapter entitled 'abrasive micromachining and microgrinding' (AMMG) (Cheng, 2001) – this serves as a good overview of abrasive technologies mode of surface-interaction in modern industrial abrasives use. Three modes of MR are noted; brittle, ductile and smeared;

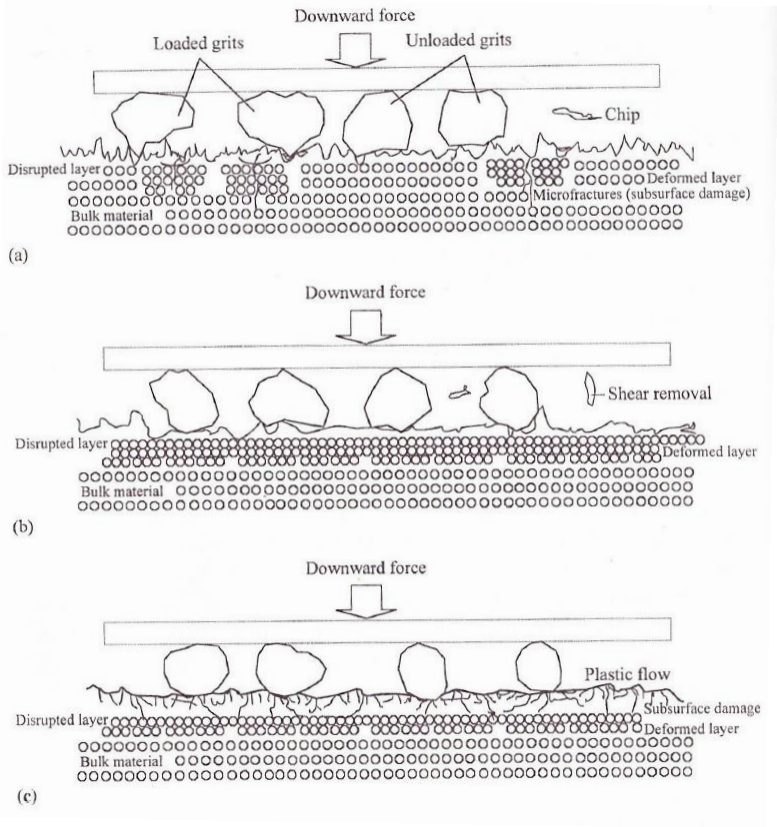

Figure 2.37 – Three types of micromachining modes in abrasive micromachining. (Cheng, 2001)

Brittle mode (figure 2.36, (a)) generally occurs in abrasive machining processes where grit is fired, either in a stream of gas or liquid over a surface and impacts over the same spot, causing cracks. Shot blasting and AWJM are examples of such mode. Ductile mode (figure 2.36, (b)) occurs when abrasives shear off workpiece material, preventing subsurface damage and physically removing material as opposed to smearing. Depth of

cut and use of lubrication are key factors in determining efficiency. Creep-feed grinding is an example of such mode. Smeared mode (figure 2.36, (c)) (commonly called ploughing) occurs when a surface is plastically deformed and peaks are pushed into troughs. Low levels of MR are achieved, but damage from previous processes can be repaired. The mode occurs when the machining process is inhibited by bonding – in the case of AFM (an example of this mode) the polymeric carrier inhibits.

Authors Gessenharter et al (Gessenharter, et al., 2003) compare 'chemo-mechanical' polishing with AFM and laser polishing for preparation of surfaces used to injection mould optical elements. While the comparisons are not abrasive processes, the authors state that laser polishing achieved between 0.3-0.45µm Ra, while AFM achieved 0.1µm Ra. The closing statement argues that AFM rounding cannot be avoided and may be inappropriate in certain applications – the chemo-mechanical technique achieved 0.0072µm Ra, although the PV (peak-to-valley) value is missing from the paper for the other technologies, but rests at 0.47µm for this technique. The authors make no consideration for optical surfaces inaccessible by traditional means.

Arief and Cheng (Arief & Chen, 2010) provide an overview of loose-abrasive machining processes – common inputs are identified as kinematics, abrasives, slurry composition, coolant, machine and workpiece properties. Common outputs include forces, temperatures, vibrations, vibrations, surface properties and size errors. Polishing using abrasive processes is described, "the main purpose of polishing is to modify the surface texture, rather than the shape".

Deburring is known to be a difficult, yet achievable task for AFM – authors Balasubramaniam et al (Balasubramaniam, et al., 1998) study the abrasive jet machining (AJM) process, which benefits from higher velocity particles and open access to workpiece features to deliver improved deburring performance. Burr root thickness is considered a key parameter, and following a Taguchi experimental design, the authors present a linear correlation between jet SOD (stand-off distance) and radius generated. SOD may be equated to pressure-drop in AFM, whereby energy exerted on abrasives is reduced or increased depending on controlled restrictions in the system.

Insightfully, the author (Mazurkiewicz, 2000) sees abrasive machining processes requiring, "dedicated software systems [to] obtain information from data banks about materials to be cut", and consequent machining parameters. With specific reference to AWJM, he notes reliability must be driven by improvements in pumping equipment, something seen frequently in AFM – steady flow rate and minimised pulsation lead to increased tool and machine life.

The author (Szabo, 2001) recognises the recent trend of polygonal bores in engineering tooling and fixtures – Sandvik Coromant's 'Capto' modular tooling system is a prominent example, utilising a rounded triangle to provide orientation to parts. To provide a tight fit to avoid coolant leakage, the surface finish and size are important – manual finishing is possible with grinding and abrasive belts, although in serial, one

after the other. Finishing the surface and rounding the edges to improve function are performed internally by Szabo's patented flexible honing system, although limited to 0.2mm total material removal allowance.

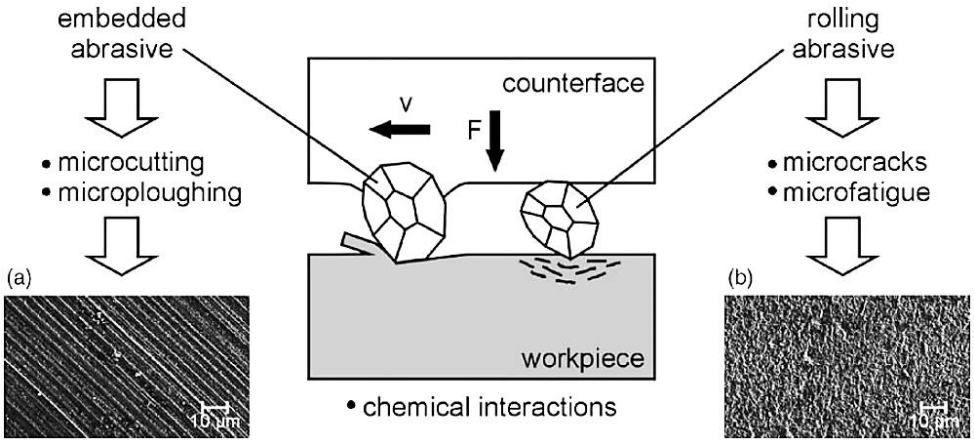

Figure 2.38 – MR mechanisms in machining with loose abrasives. (Brinksmeier, et al., 2006)

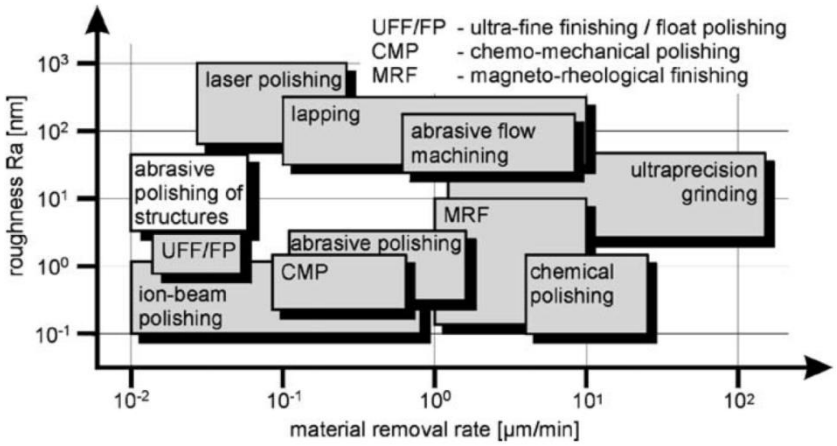

Figure 2.39 – Classification of MRR for new abrasive polishing processes. (Brinksmeier, et al., 2006)

Brinksmeier et al (Brinksmeier, et al., 2006) discuss multiple abrasive polishing techniques and highlight in figure 2.38 that abrasives share common modes of application. Figure 2.39 identifies finishing techniques and their relative position in terms of MRR (µm/min) and final roughness (Ra, nm). Only chemical polishing and ultra-precision grinding can best the AFM process in terms of MRR while final roughness is not competitive (in this operation).

Surface generation is shown to be proportional to grit mesh size by Barletta et al (Barletta, et al., 2007) in the process 'fluidised bed abrasive jet machining (FB-AJM)', where a tubular workpiece has its ends sealed, creating an inlet and outlet, forming a system comparable to AFM, except horizontally. The phases of the media are air, fluid and grit, combined by introducing a flow of air between 5m/s and 50m/s. Fluid is also

introduced, providing additional motive force to the grit, introduced in a tertiary stage. Like AFM, the process is reversible, and material is reclaimed. Key parameters include the shape of the jet and abrasive feed rate, easily compared to shape of flow field and grain fraction in AFM. The transitory nature of the very low viscosity carrier raises the question of finish uniformity, and whether particle velocity is constant along the bore length.

Chastagner and Shih (Chastagner & Shih, 2007) describe AJM in such a way that it becomes apparent it is a refined, miniaturised and localised version of shot blasting. They experiment with inconel 718 (nickel-alloy) square edges, and produce 0.14mm radii – in contrast to AFM, extension of processing time does not create ever larger radii, but surface damage *does* occur. The authors note a circular arc does not fit the resultant post-process form (non-tangential results), while the angle of impingement is seen to affect MRR; for brittle materials, a jet of abrasive perpendicular to the surface increases MRR, while in their inconel samples (more ductile) a shallower angle increases MRR.

2.5.4.1 Optimisation methods of alternative abrasive machining processes.

Author Stephen Malkin (Malkin, 1981) discusses the objectives in cylindrical grinding operations; to satisfy geometric, metallurgical and surface quality requirements. He considers two strategies – a conventional cycle, whereby cycle time reduction is king and a second where a fixed spark-out time is observed. He finds that off-line optimisation is sensitive to abrasive edge condition and that, after evaluating a number of industrial grinding methods, that the typical efficiency of non-optimised setups is less than 50%. His system comprises a transducer used to optimise the in-feed parameters of the wheel and a micro-processor (of undescribed nature) to control feed rate – his offline method is a numerically derived balance between wheel RPM and wheel force.

Gopal and Rao (Gopal & Rao, 2003) consider the factors at play in efficient grinding of SiC ceramic material and the issues associated with excessive force causing cracking. They develop a genetic algorithm to maximise material removal with the following findings; SiC is primarily influenced by feed rate, depth of cut and grit size – the percentage area of surface damage decreases with an increase in feed rate and is unaffected by grit concentration.

Using the wet abrasive jet polishing (AJP) system, the authors Mao et al (Mao, et al., 2010) identify three geometries – a linear microgroove (starting at 0.24μm Ra), a linear microchannel (starting at 0.36μm Ra) and a curved microchannel (starting at 0.36μm Ra). While the surfaces are essentially freeform and contained, the work focuses on investigating technique performance – experiments are performed using ANSI mesh size abrasives - #3000, #2000 and #1000 is used on all three geometries. The microgroove is improved down to 0.06μm Ra, while the linear microchannel is improved down to 0.08μm Ra. However, the overriding finding is that each of the sizes

require over 1h to reach comparable levels of roughness as seen in AFM (~0.1μm Ra), but there is inconsistency with other abrasive processes – the larger grit offers the better ultimate finish, a trend which passes through the two smaller sizes in the work.

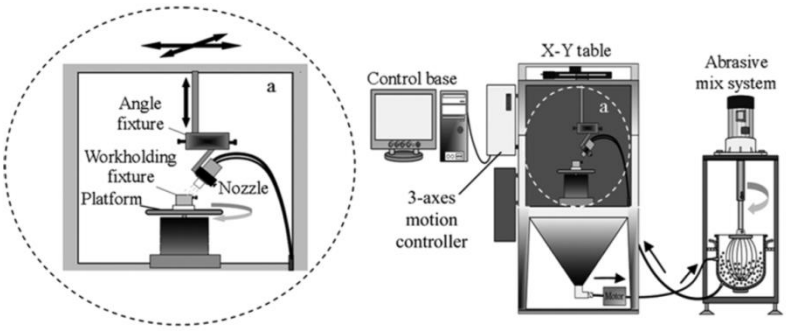

Figure 2.40 – Schematic illustration of basic experimental AJP system. (Mao, et al., 2010)

Deepak (Deepak, 2012) offers a review of optimisation methods for metal cutting operations – the methods covered are described previously in this chapter, however figure 2.41 surmises the basis for all optimisation techniques quite succinctly. Their closing statement re-states how different optimisation methods should be selected based on inherent potential in the application under study.

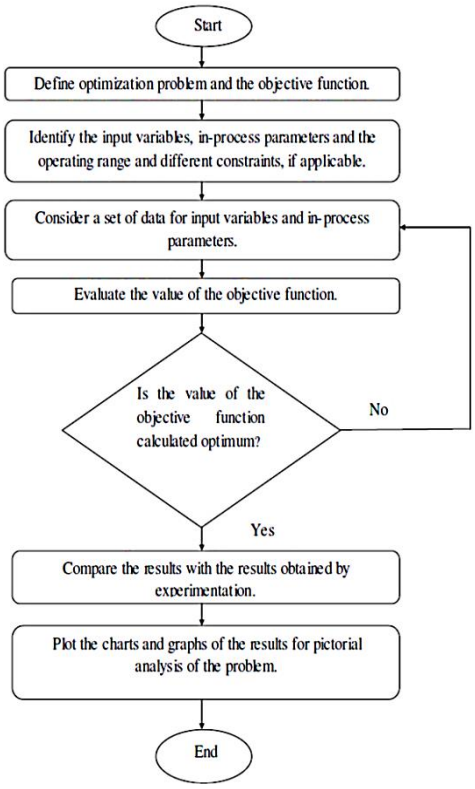

Figure 2.41 – Optimisation algorithm. (Deepak, 2012)

2.6 Fluid dynamics.

Motion study of liquid and gas is dealt with in the discipline of fluid dynamics. In this research, the interest in fluid dynamics is largely due to the transport mechanism employed by the abrasive particle used to generate abrasion in workpieces. Within this subsection, papers are summarised to identify those principles useful to the project goals – the sections are split into; surface condition change as a result of fluid flow, computational fluid dynamics, chemical descriptions and analysis of micro-grits, and, chemical descriptions and analysis of carriers (grit transportation fluid).

2.6.1 Surface condition change as a result of fluid flow.

Fluid flow is largely recognised to be controlled by surrounding geometry, however, when fluid flow also means the delivery of abrasive particles, many authors have attempted to understand the relationship of fluid flow and erosion of (typically) metals. Authors Finnie, Stevick and Ridgely (Finnie, et al., 1992) study the effects of angle of impingement – figure 2.42 presents the actual and predicted relationship between a particle of 120 mesh size SiC being fired at aluminium 1100 (a ductile metal) at 158m/s through air. The graph presents the relationship of erosion at angles between 0˚ and 90˚, where the solid line and long dashed lines are probability density functions, the short-dashed line is a prediction for a single particle on a smooth surface and dotted line shows the experiment values.

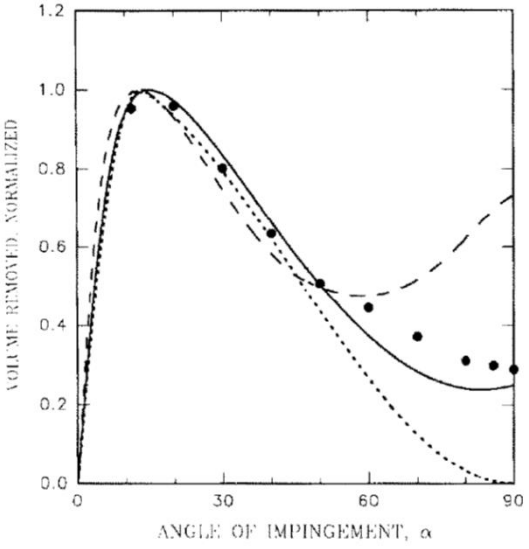

Figure 2.42 – Erosion predictions for a single particle striking a smooth surface. (Finnie, et al., 1992)

Importantly, the authors find that angle of attack is a significant factor in erosion magnitude – while results will alter if materials and transport methods are changed, the concept that erosion values can be predicted based on angle of attack has been proven.

Finnie (Finnie, 1995) provides an insightful history of erosion research, and while highly specific and perhaps not helpful for understanding the quantitative effects of erosion studies, issues of importance are raised, such as particle velocity change as a result of diameter, material microstructure particle size, particle shape and hardness.

Polishing compound containing Polyborosiloxane (PBSO) mixed with abrasives is considered by authors Fioravanti and Fletcher (Fioravanti & Fletcher, 1996) to polish mould surfaces, with special interest in temperature distribution. They acknowledge that silicone polymer viscosity alters with temperature flux and in turn increases flowrate. Their system is pressure driven and thus believe there is a link between pressure and viscosity. They also note that viscous heating is a dominant passive variable over the heating provided by the sonotrode used to vibrate the media – 28% of the resultant energy gained by the PBSO could be attributed to the application of ultrasonic waves, while the remainder is friction from viscous heating. Using ultrasonics is shown to be inappropriate to heat the material.

Specific to AFM, authors Haan and Steif (Haan & Steif, 1998) consider the literal ‘slow flow of concentrated suspension’ in action in AFM and its significant differences to that of transport of particles by air. They find particle force per unit area to be related to stress in the suspension, and critically, that particle-wall forces (those interactions between particle and surface of workpiece) are not related to the pressure used to drive the suspension at the entrance to a cavity.

2.6.1.1 Erosion behaviour in alternative abrasive wear processes.

Campos-Amezcua et al (2007) study undesirable erosion – solid particle erosion (SPE) as occurs in the operation of steam turbines for power generation. Efficiency losses are the result in a commercial application, but in this field, several cross-over issues exist – 1) engineers wish to view the flow and measure behaviour, but cannot as the flow is interrupted or instruments damaged, 2) fluid-solid interaction is difficult to model, and 3) the numerous factors at play when considering modelling limits. As with other work (Finnie, et al., 1992) angle of impingement is a recognised cause of SPE, and modelled as such, shown in figure 2.43.

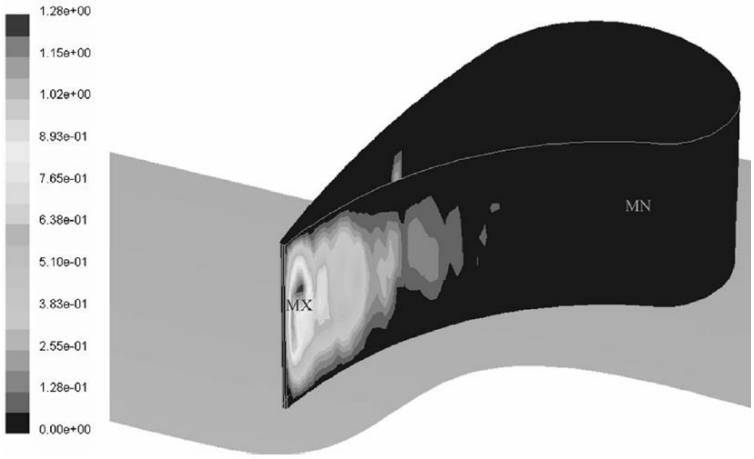

Figure 2.43 – 3D erosion rate contours on the nozzle (kg/m^{2}s). (Campos-Amezcua, et al., 2007)

2.6.2 Computational fluid dynamics (CFD).

Complex features as an area of AFM research is very limited – this sub-section more than others describes the four papers that attempt to come close to a viable and industrially-applicable model.

Wang et al (Wang, et al., 2009) consider the known issues surrounding modelling of abrasion and also recognise the futility of attempting to model particle-surface interaction in AFM, as the delivery method contains such great variation in force, angle and velocity. Their method assumes the power law relationship of an arbitrary 'bouncing putty', filled with 50% SiC grit – they aim to use CFD to create a uniform surface finish in a hole chain (should not really be considered as a complex form), and the power law behaviour is not replicated elsewhere – this may be a genuine characteristic of the media, but not one described by others. Figure 2.5 shows the simulation of the fluid with various combinations of tooling – ensuring uniform strain rate was their target, but no practical verification is performed. If it was, then the results would not be valid – their model contains no lead-in, i.e. the force starting from the media chamber itself is not present, meaning any non-uniformity in the flow profile leading up to the part is not accounted for.

In a similar exercise, authors Li et al (2009) view distribution of pressure and velocity to attempt equal processing on a common rail diesel part (see figure 2.44). Using Ansys Fluent, they model a 2D section of the rail, assuming an equal feed into each rail – there are several problems with this approach that are not tackled in the conclusions. The processing of a 'T' junction requires equal flow from around the entrance of the stalk to the 'T', while their model shows only flow coming from the stalk of the T.

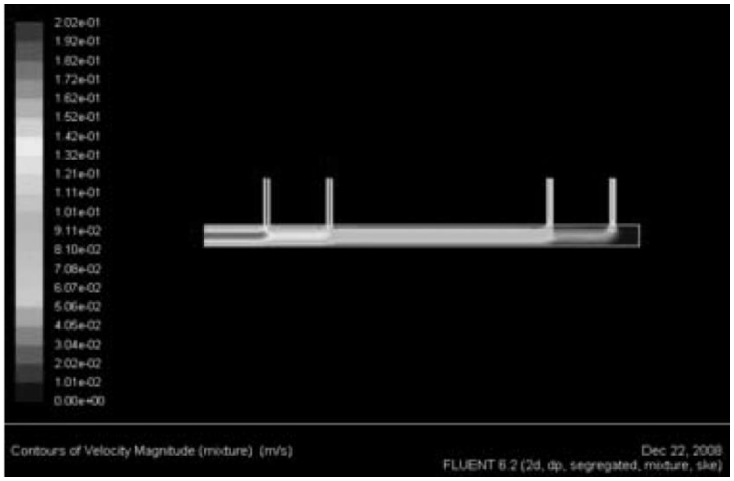

Figure 2.44 – Velocity distribution in common rail diesel component. (Li, et al., 2009)

They make no adjustment for velocity at each inlet. Flow behaviour as a result of having one outlet means mass flow rate increases toward the outlet, almost certainly resulting in different rounding results for each 'T' in the profile. Their media programming consists of simply defining a Newtonian (known to be invalid) fluid of high viscosity. The final finding of machining only one branch at a time is derived from another simulation, pumping in the wrong direction, with no physical verification.

Using COMSOL®, authors Schmitt and Diebels (Schmitt & Diebels, 2013) attempt a bona fide simulation of AFM. Significantly it is known that in the year 2013, this work is the peak of capability in simulating AFM. The authors acknowledge there is no validated model to control AFM and that the proprietary nature of the media prevents them from understanding behaviour in its entirety. As with Wang et al (Wang, et al., 2009), they use a power law model to model media. Considering the implementation of CFD, they find wall slip realism (tribological relationship between particle and surface) to be a problem, as simulation systems normally consider the wall to be of zero velocity. In conclusion, they note the lack of study into media behaviour, but appear to have a viable virtual method in COMSOL's Arbitrary Lagrangian-Eulerian (ALE) model, which, while not explicitly clear, appears to move the mesh based on exposure to a field variable, but can result in unrealistic and strong distortions. It should be noted that the work does not appear to be practically verified.

As a by-product of developing a process model for AFM of ceramic bushes, authors Uhlmann et al (Uhlmann, et al., 2009) state they use simulation (CFD specifically), but upon closer inspection, the text reads, "Finally it is possible to determine local velocities through a CFD-simulation within a **single application system**. A work result can therefore be anticipated through the **analysis of the technological data**. The functional capability of the **process model has still to be proved** through a selection of complex-shaped workpieces". At the time of writing, this work appears to have reached a dead stop – 2009 is the last mention of having developed a system to predict complex workpieces, but the sum total of the described method is presented in figure 2.45,

which, it can be seen, is little more than a conceptual diagram, that requires additional work to establish a model for every new geometry, hasn't been proven in practice and claims unknown 'technological data' as being used to define output. The work also assumes that velocity is the driver for erosion.

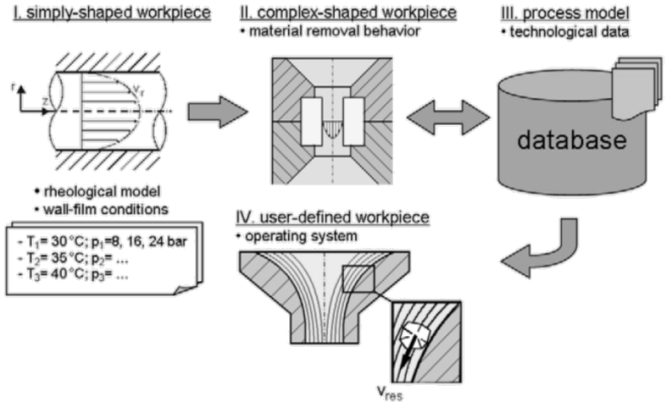

Figure 2.45 – Flow chart showing development of process model. (Uhlmann, et al., 2009)

2.6.3 Chemical descriptions and analysis of micro-grits.

Abrasive slurries are comprised of carrier fluids and abrasive grains, each catering to transport and erosion respectively. While this area of study is highly specific and largely chemistry-based, there are two interesting papers produced that offer some insight into material choice effects on the metallic substrate under test.

Samsonov and Gaevskaya (Samsonov & Gaevskaya, 1975) work with a lapping machine to provide a repeatable system, whereby ingots of niobium and vanadium were re-melted and ground to a class 8 surface finish. Under a pressure of 0.82kg/cm^2 for 5min, the metals were lapped by TiC, ZrC, HfC, VC, NbC, TaC and WC. Findings conclude that with increases in plasticity of the carbide grit, material removal falls and surface finish improves – the opposite is also true; with reducing plasticity, material removal is less effective, material removal increases while surface roughness increases.

Specific to AFM, the authors Mitchell and Laufer (Mitchell & Laufer, 1980), tackle abrasive wear of the ExtrudeHone process, in titanium alloy Ti6Al4V – a popular material at Mollart Engineering. This work (in the opinion of the author) contains the greatest technical depth of any subsequent workpiece-grit interaction study. The findings are summarised as follows;

- High compressive stress left on surfaces of ~420±45MPa, in all directions parallel and perpendicular to abrasive flow direction.
- Using TEM microscopy, a subsurface layer of 10μm is known to be deformation free.
- Thin sub-grains are generated in the size range of tens of nanometres.
- Surface condition indicates high plastic flow has occurred in the surface layer.

2.6.4 Chemical descriptions and analysis of carriers.

Several groups of authors discuss methods of manufacturing media and the properties synonymous with particularly suitable media for AFM applications. The first of which is Kuo (Kuo, 1999), writing in the polymer data handbook, the predominant material in silly putty is polydimethylsiloxane (PDMS). He describes the characteristic of the fluid form as liquid at low molecular weight and solid gum at higher weight. Mechanical and thermal properties are also provided, and may be considered useful ersatz values in lieu of data from silly putty manufacturer, Dow Corning. See table 2.3 for properties.

Numerous polymers are employed in the production of carrier materials – authors Kulikov and Hornung (Kulikov & Hornung, 2005) present their work aiming to create a 'more manufacturable' version of silly putty by using linear low density polyethylene (LLDPE). While this work does not refer to the AFM process, it does reference the characteristic of silly putty, a known component in early AFM media, and certainly a viable route for those wishing to manufacture their own media.

Table 2.3 – Important properties of PDMS polymer.

Property	Unit	Condition	Value
Density (ρ)	g/cm^3	PDMS (1,000-12,500cSt)	0.970
CTE (α)	(K^{-1})	PDMS ($M=1.5_{x10}^{-4}$) at 30˚c	9_{x10}^{-4}
Specific heat (C_p)	$kJ/kg^{-1}/K^{-1}$	PDMS (M=400,000)	1.552
Thermal conductivity	$(W/m^{-1}/K^{-1})$	PDMS (1,000-60,000cSt) at 50˚c	0.1591

Kulikov and Hornung note the material's behaviour, "if rolled into a ball and dropped, the material bounces like rubber", "the material sags under its own weight and flows…but not indefinitely". Silly putty is more technically known as Dow Corning 3179 compound.

While Kulikov and Hornung's statement of apparent material stiffness suggests there is more than one value for viscosity of the material, Davies and Fletcher (Davies & Fletcher, 1995) describe the viscosity of three modified variants of an unknown PBSO polymer at 222Pa.s (LV), 1869Pa.s (MV) and 6659Pa.s (HV), suggesting a useful region of viscosity for practical application, as the work is performed in conjunction with ExtrudeHone UK. The authors calculate the viscosities by rearranging the Hagen-Poiseuille equation, as they have a known hydraulic diameter, bore length and velocity.

In addition to Fletcher and Fioravanti's (Fioravanti & Fletcher, 1996) previous comments concerning working temperature and effect on viscosity, the author's also note that the abrasive concentration affects specific heat – this raises the point that polymer properties are not the sole driver of viscosity or material rheological response – inter-particle contact is also said to be ineffectual when attempting to model heat input.

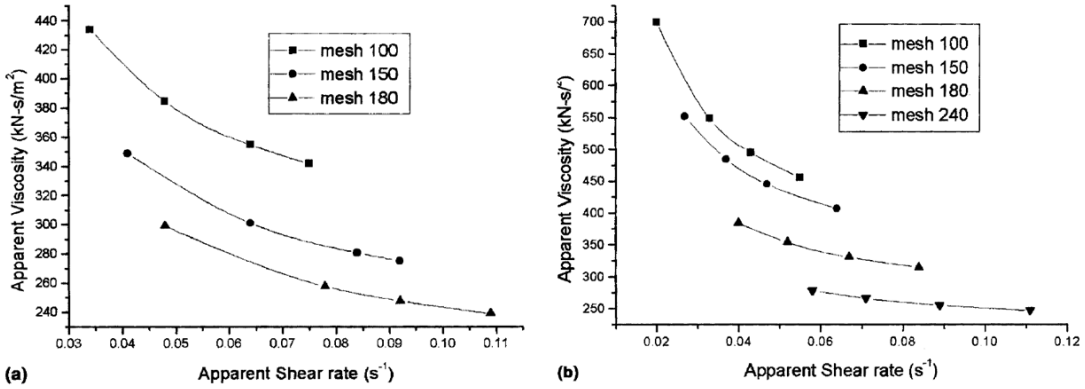

Figure 2.46 – Effect of apparent shear rate on apparent viscosity. (Jain, et al., 2001)

Presented in figure 2.46 (Jain, et al., 2001) is the effect of abrasive concentration on apparent shear rate, whereby (a) is 33% abrasive concentration and (b) is 45% concentration. The difference in viscosity between the two is evidence of abrasive concentration and abrasive size affecting the media behaviour – it can be stated as fact that viscosity is seen to reduce with reducing particle size and rate of change of viscosity is greater at higher grain fraction. The plots also show increasing shear rate to indiscriminately reduce viscosity, suggesting that shear-thinning behaviour is prevalent; this conflicts with information from commercial suppliers and conventional wisdom.

Author's Tzeng et al (Tzeng, et al., 2007) describe a media formed of undisclosed polymer, wax, silicone oil and SiC abrasive. Their term, 'self-modulating', appears arbitrary and is likely used to describe the viscosity change seen under different working conditions. The authors are essentially testing the response of their media against metrics such as abrasive concentration and extrusion pressure as many before have done, except there are two significant inconsistencies – 1) "as AFM processing abrasive particle size becomes coarse, the machined surface becomes better", and 2) "burrs are visible and AFM can remove these to produce a recast layer".

Without describing their polymeric carrier and modifying agent, authors Wang and Weng (Wang & Weng, 2007) offer a study where two polymers are filled with 50% abrasive grit. Figure 2.47 presents the behaviour as studied in a 'rheological apparatus'. It should be noted the higher viscosity product also offers greater elongation properties. Shear thinning is also demonstrated in this plot, for both media.

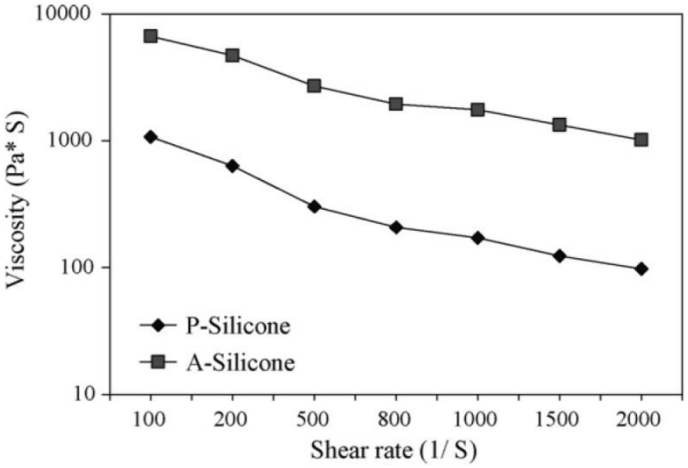

Figure 2.47 – The effects of shear rates on the viscosity. (Wang & Weng, 2007)

Power law is used by Wang et al (Wang, et al., 2007) to describe the media behaviour to simulate in finite volume CFD-ACE^{+} software. They find that there is an arbitrary link between increased polishing ability when a high strain rate is achieved, but no quantification of erosion, temperature, error, verification or hysteresis effects. Their power law model may or may not reflect the media in-use, but it is known through conventional wisdom that AFM media thickens upon greater load, in contrast this work.

Kar et al (Kar, et al., 2009a) utilise alternative carrier materials in the form of a natural rubber (RMA-4) and a butyl rubber (IIR) as a means of deviation from the expensive silicone-based polymers used in most media. A two-roll mill is used to mix additives into a media compound, whereafter process variables are studied, followed by characterisation, specific to their developed product. 9-12% oil loading is considered appropriate for the rheology of the product, while loading with abrasives to ~47% increases complex viscosity behaviour. Butyl rubber and naphthenic oil are considered to have been successful in material removal trials.

In later work, Kar et al (Kar, et al., 2009b) state that there are three requirements when developing one's own media – 1) attempting to match properties of commercial products for functional purposes, 2) chemical compatibility of ingredients with each other and with substrate material, and 3) economical cost. Authors adopt base polymers; 1) natural rubber (NR), 2) ethylene propylene diene monomer (EPDM), 3) butyl rubber (IIR), 4) silicone rubber (Si), and 5) styrene butadiene rubber (SBR). Serving as a lubricant and viscosity modifier, naphthenic oil is compatible and used to modify the rubbers. Concluding, the authors find the rubbers more mechanically stable, and that SBR is the most viable of the group – interestingly, the authors find an ExtrudeHone Corporation commercial product to degrade only at 390˚c, whereas SBR degrades at 475˚c. Mollart's existing advice recommends no higher than 50˚c – perhaps the authors are accounting for full degradation and not rheological property change over time/use.

In extension of Kar et al (2009a, 2009b) work concerning polymers modified with naphthenic oil, Rajesha et al (Rajesha, et al., 2010) study the composition of the media

in order to characterise it – they find it to be comprised mainly of esters, alkanes and alkenes (therefore an ester group polymer), that its viscosity is sufficiently low to be used as a carrier in AFM and that 640Pa.s offers a threshold where material removal rates used to improve surface finish peaks; it can be considered a material removal operation thereafter (i.e. stock removal, honing, recast layer removal).

Sankar et al. (Sankar, et al., 2010) develop a styrene polymer-based carrier using a hydrocarbon oil as a plasticiser – their work varies the quantity of plasticiser between 2.5% to 17.5% as a process variable. Using a steady-state flow approach to rheological testing, the authors test for viscosity against shear rate amongst other comparisons.

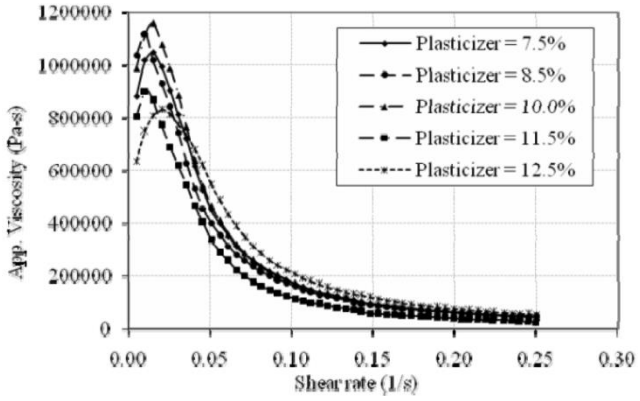

Figure 2.48 – Variation of apparent viscosity of AFF medium with shear rate. (Sankar, et al., 2010)

Testing over a *very* short shear rate range, they note a significant reduction in viscosity, although this appears to settle at the same value for all levels of plasticiser content, and only shows a shear-thinning response. A better resolution over a larger range may reveal much more of interest.

A report paper produced by Wan et al (Wan, et al., 2010) of the Singapore Institute of Manufacturing Technology presents a local subcontractor-driven media development programme for cost reduction purposes. The authors use an additive 'Hydrocut' in an aqueous solution, capable of suspending F200 sized particles. The additive is commonly used to improve the coherence of AWJM streams. Using a 2-6bar air-driven system, the authors use a full factorial (2^4) DoE to study capability in an EDM-cut aluminium bore. Predictably, they find viscosity (and shear stress, in-turn) to vary with Hydrocut percentage; they also find abrasive action to correlate with normal shear stress coefficient.

2.6.4.1 Media for non-standard AFM process.

Over the course of the last 10 years, authors have attempted to improve the efficiency and control over the standard AFM process – one of the most significant and potent

developments is the use of magnetism to influence carrier behaviour, the carrier containing a magnetically-sensitive element (typically iron-shot) and an electromagnet positioning to invoke field lines through the part where increased erosion is desired.

Jha and Jain (Jha & Jain, 2009) describe an MR (magnetorheological) fluid as that of a Bingham plastic, i.e. shear thinning, but requiring a 'kick' to begin flowing, but continues-on to correct the assumption based on the variation in process shear rate being partially responsible for breaking the chain of carbonyl iron particles (CIP) used to control local viscosity. The authors obtain experimental data and find that three models fit; Bingham plastic, Herschel-Bulkley and Casson fluid – the latter two however provide better R^2 values.

Seok et al (Seok, et al., 2009) demonstrate that a CIPs form a columnar structure and that a linear relationship exists between 'ratio of particle velocity to imposed pressure' and 'effective friction coefficient' ranging between 0.2 to 0.9. They establish that the dominant wear mechanism is abrasion.

Finally, the authors Sidpara et al (Sidpara, et al., 2009) find a strong goodness-of-fit with the Herschel-Bulkley model. Performing an ANOVA activity, they find magnetic field to have the highest contribution on the yield stress (93%) and viscosity (50%). Their work is performed using a water carrier, loaded with CIP and an abrasive, but it is not clear whether the authors attribute CIP mechanical properties to the erosion effect, or whether the force exerted on abrasive are assumed. A magnetic field of 0.6T is applied as the upper end of the experimental range – this increases viscosity, but can be metered by controlling abrasive concentration (increase reduces viscosity).

2.7 Hardware development.

Multiple incarnations of the standard vertically-opposed piston design are developed in the literature – while some degree of increased capability is globally achieved, increased tooling/machinery complexity and geometry constraints limit the potential technical and commercial implementation of the work. This section briefly discusses the alternatives, their developmental stage and relative success.

2.7.1 Magneto-Rheological Abrasive Flow Finishing (MRAFF).

Early work into the process by authors Jha and Jain (2004) are descriptive and helpful – figure 2.49 illustrates the simple adjustment to the setup, although it becomes instantly clear that coil position and thus, field orientation are only finitely adjustable and perhaps beyond acceptable economic costs when considering complex geometry.

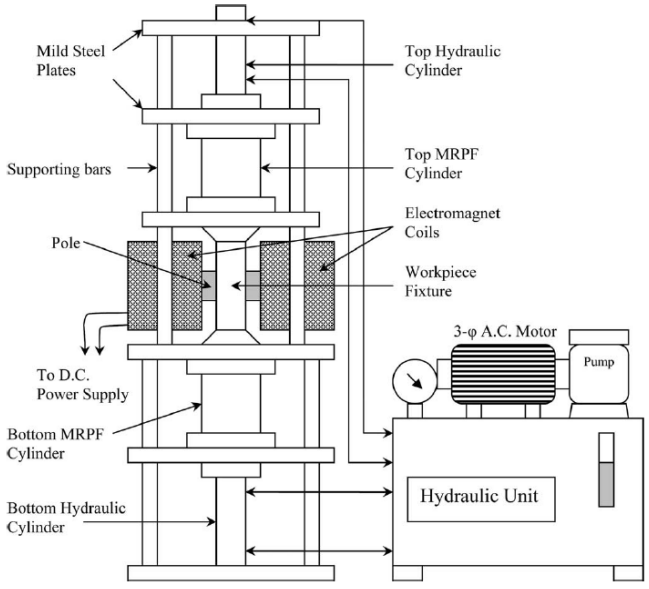

Figure 2.49 – Schematic of MRAFF experimental setup. (Jha & Jain, 2004)

Singh et al (Singh, et al., 2004) prepare a study to identify the key process parameters. Based on the process schematic above (Jha & Jain, 2004) Singh et al find voltage to be the most significant parameter, followed by working gap. Other parameters such as grit mesh size are not significant, suggesting the range of control afforded by the 'MR' equipment of the MRAFF process is greater than without.

In terms of process maximums, authors Singh and Walia (Singh & Walia, 2012) determine that material removal increases with field strength and that 0.4T can be considered a threshold, with marginal improvement up to 0.6T. These statements are only valid for the machine, media and geometry conditions under study.

In an extension of much standard-AFM work, authors Singh et al (Singh, et al., 2002) find that field strength has a strong interaction with number of cycles – somewhat predictably-so, as logically an improvement in material removal will occur every stroke of the piston, cumulating into a final, higher MR value. They do however note a scatter in roughness values, which they acknowledge is not the case in standard-AFM.

S.No.	Process Parameter	Range	Unit
1	Magnetic Flux	0.2-0.7	Tesla
2	Extrusion Pressure	5	N/mm^2
3	Number of cycles	4	No.
4	Abrasive particle size	60-65	Micron
5	Media Flow Volume	290	cm^3
6	Abrasive to media concentration	1:1	% by weight
7	Polymer-to-Gel Ratio	1:1	% by weight
8	Aluminium Oxide -to- Iron Powder	3:2	% by weight
9	Temperature of media	32 ± 2	°C
10	Reduction Ratio	0.90	---
11	Initial Surface Roughness	0.6-1.1	µm

Figure 2.50 – Process parameter of MRAFF. (Singh & Walia, 2012)

The principle of abrasive action in MRAFF is described by Das et al (Das, et al., 2008) as CIP wrapping around the abrasive particle to provide a local support, controlled by the operator. The authors note a significant improvement in surface roughness under increased magnetic field strength.

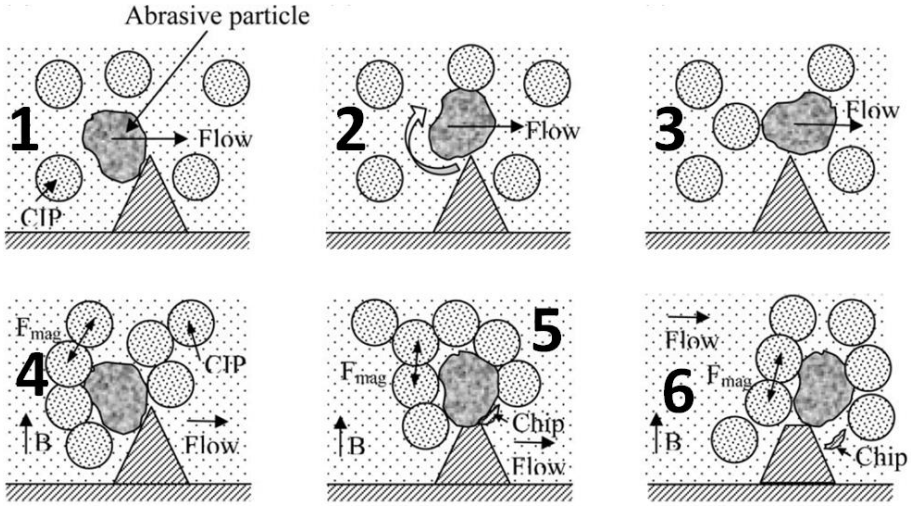

Figure 2.51 – Finishing in absence of mag. field (1-3) & presence (4-6). (*adapted from Jha & Jain, 2004*)

Application of the MRAFF process allows authors (Das, et al., 2010) to finish internal bores of stainless steel to 16nm while authors (Sadiq & Shunmugam, 2009) reach 80nm in the same material. Parametrically, the contribution of variables in MRAFF do not appear to reflect the same percentages as found in standard-AFM (Singh, et al., 2002) –

second order interactions such as abrasive grit size and grain fraction are not as effective as magnetic field and workpiece material. In 2005, authors Jayswal et al (Jayswal, et al., 2005) develop a numerical simulation model – the conclusion suggests that the results compare favourably well with experimental values, but at four discrete points, (0-4 mins) their surface roughness values are calculated at; 1.5µm (start value), 1min=0.9µm (actual=0.55µm), 2min=0.65µm (actual=0.35µm), 3min=0.45µm (actual=0.3µm) and 4min are identical, but given the trend, it is likely to continue negatively, suggesting this work is not accounting for some significant process variables.

2.7.2 Electro-Chemical Abrasive Flow Machining (ECAFM).

Authors Dabrowski et al produce two papers in 2006. The first (Dabrowski, et al., 2006a) considers the use of electrically-conductive media as a means of performing a process similar to ECM but with AFM hardware. Such issues arise as breakdown of carrier and pastes adhering to the workpiece, which does not occur in standard-AFM. Feasibility of this system is somewhat limited by material of workpiece and geometric limits of electrode position. The second paper (Dabrowski, et al., 2006b) concludes that while electrochemical influence is ambiguous, there is a notable improvement in finish, although type of abrasive media is a process driver.

2.7.3 Centrifugal-Force Assisted Abrasive Flow Machining (CFA-AFM).

Shear rate has been shown to be a driver for increased erosion by several authors – Walia et al produce three papers discussing the CFA-AFM process, using a tool to invoke a higher shear rate at local point of interest. The first paper (Walia, et al., 2006) details a finite element model and experimental results to prove out the process – they achieve reasonable agreement between a numerical simulation of a rotating rod, a model of forces between rod, media and part, but only in a two-dimensional example.

The second (Walia, et al., 2008a) aims to prove that increasing the number of dynamically-active particles is possible through the CFA system – they conclude that their low-viscosity trial improves active particles by 62%, but as viscosity increases, there is negligible return. As in standard-AFM, Walia et al (Walia, et al., 2008b) show that surface condition is not damaged by the use of a centrifugal rod, and reflects an improved micro-hardness and compressive stress proven by XRD analysis. It should be noted that this phenomena also occurs with standard-AFM technology, without additional tooling and constraints as required with CFA technology.

2.7.4 Drill Bit-Guided Abrasive Flow Finishing (DBG-AFF).

In a comparable development to CFA-AFM, authors Sankar et al (Sankar, et al., 2009a) essentially add geometry to the centrifugal rod and name it 'Drill Bit Guided', as the geometry resembles that of a helical drill flute. Experientially, this technique appears to be aimed at creating a flow field shape that is conducive to greater erosion.

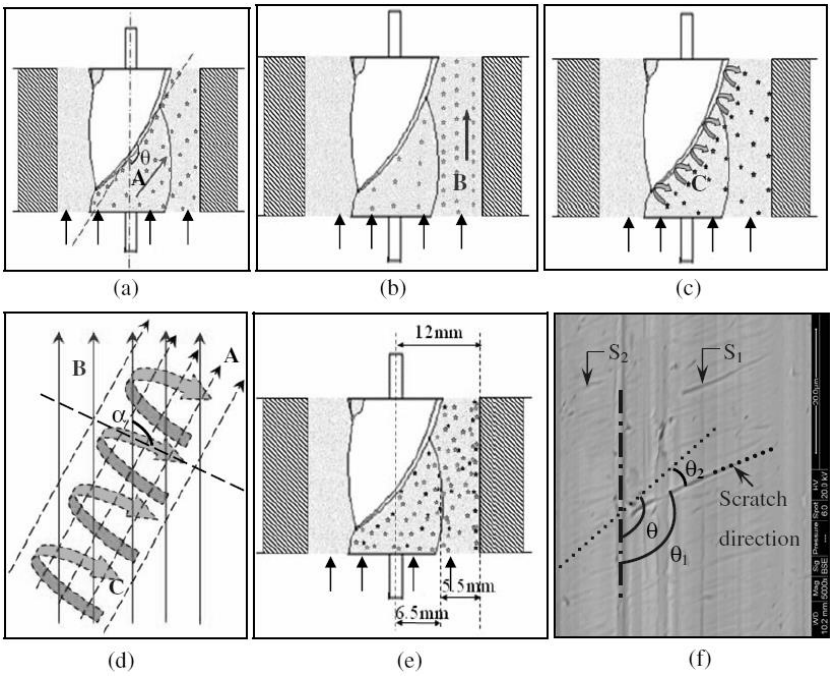

Figure 2.52 – Possible flows of the media in the finishing zone. (Sankar, et al., 2009a)

Similarities in results are found with CFA and standard-AFM – logical extensions are agreed in Sankar et al's conclusions; the helical path increases cycle-on-cycle work (increasing efficiency), while increasing media oil content reduces improvement in average roughness. Decrease in drill bit diameter causes a decrease in MR – it could be reasoned that a lower viscosity exists and thus less support for abrasive.

2.7.5 Rotational Abrasive Flow Finishing (R-AFF).

R-AFF considers the application of fixturing to invoke a rotary motion on the outside of a component. Per cycle, the rotary motion allows abrasives a longer flow path, one where the tangential force is higher, thus permitting greater indentation and lateral force against surface peaks. The process is trialled in three materials, but the authors (Sankar, et al., 2009b) find most success with an MMC – Al alloy / SiC(10%).

A follow-up paper produced in 2010 (Sankar, et al., 2010) aims to determine optimum process parameters, including finding the optimum rotation speed to produce desirable topology in the form of unidirectional 'micro-scratches'. As their machinery is

comprised of reciprocating media cylinders, a cross-hatching effect is seen, with angles formed as a result of rotational speed and media velocity, agreeing by up to 82.5%. They claim 44% improvement in roughness and 80% improved in MR values; greater resistance to penetration (fewer voids) translates into higher hardness readings – the opposite is an issue when abrasives tear out MMC reinforcement creating voids.

2.7.6 Novel machine control solutions.

In two conference papers, authors Li et al (Li, et al., 2009) discuss a motion control system development for maintaining a constant pressure through an orifice, and Bin et al (Bin, et al., 2012) discuss the issues surrounding in-process monitoring and control. It appears that the authors both use Delphi diesel injection nozzles and one-way AFM machinery, with Bin et al (2012) developing a prototype machine that monitors output flow rate as a process variable, using it as one of a number of variables to maintain a repeatable (±1%) output. Li et al's (2009) contribution is somewhat ambiguous – their concluding statements are generic requirements and applications of AFM; as a conference paper, this work appears to have developed a viable AFM control system, supposedly at low cost, but already in existence.

2.8 Summary

The literature is wide-ranging, and describes numerous established techniques, adaptation of existing techniques and niche techniques, relying on material removal by loose or rigidly-bonded abrasive particles – the following points aim to clarify the way in which this research project should move forward.

- Contradiction exists in whether AFM uniformly finishes surfaces in all applications; (Galantucci, et al., 2009) against (Jain & Jain, 2000) (Jain & Adsul, 2000) (Gorana, et al., 2006b).
- Contradiction exists between authors the link between viscosity and deburring effect; (Kim & Kim, 2004) (Rhoades, 1991).
- Design of Experiments (DoE) knowledge is critical for surface roughness modelling (Pontes, et al., 2010).
- 'Offline' setup failure is common (Momber, et al., 1999) and it could be postulated that iterative breaking-down and inspecting 'after-the-event' is the cause. If post-process checking and in-process measurement are likely to fail, the only logical approach is to get the process right before running.
- Conventional wisdom suggests that loose abrasives will vector equal and opposite to input kinetic energy. Some authors (Raju, et al., 2005) appear to claim contrarily that irrespective of geometry/defective-features (out-of-roundness) that AFM unifies finish/features, which would require a uniform vector and force upon each surface (highly unlikely).
- Response values, however collected, sourced or interpreted (empirically or mathematically), are never useful apart from in the reapplication to the arbitrary geometry in which they were gathered (Howard, et al., 2012).
- Initial surface condition is given as a major factor by many authors (Loveless, et al., 1994) and while percentage improvement can be garnered from this, it is also logical to note that roughness may increase as a result of process variable selection. The work already performed only considers small areas – roughness will vary throughout the part based on MMG condition at the POI.
- Authors (Gorana, et al., 2006b) show nearly all their experimental parameters have significant effects. If this is the case, and they have only recognised a subset of available variables to minimise their experimental cost, it is highly likely they have excluded contributory factors, or perhaps even more significant factors. Ultimately, a lack of awareness/potential control results.
- Loose abrasives used in the AJM process as demonstrated by (Barletta, et al., 2007) (Chastagner & Shih, 2007) (Balasubramaniam, et al., 1998) occupy the other end of the scale to traditional bonded grinding wheels – the middle ground of 'semi-bound' (i.e. AFM) is well-researched, but relatively inconclusive. It is not possible to conclude from the literature which factors (combinations of abrasive and workpiece material) define wear.

- Does ductility (as opposed to brittleness, resistance to tensile load) define wear? Impingement angle of 90° is perpendicular – continuous impact-strikes chip away at a brittle material, but ductile material requires a shallower angle for effective MR.
- Solving major erosion problems in the past has been down to characterising the particle trajectories as a result of understanding the fluid carrier mechanisms (Finnie, 1995).
- Plasticity of abrasive material is a key driver of surface finish in lapping operations (Samsonov & Gaevskaya, 1975) – this goes some way to confirming the experiential preference of MTT to use AlO_2, then SiC, then B_4C, then as a last resort, diamond, to effect a trade-off between MR and Ra.
- Tzeng et al. (2007), claim that AFM can remove tool marks and burrs, "to produce a recast layer" – this is factually incorrect.
- Some work (Schmitt & Diebels, 2013) considers extrusion pressure to be the key determining factor in erosion, and location of pressure determines local erosion by extension. A key oversight would seem to be that pressure does not equate to viscosity, and thus cannot be considered a metric of abrasive grit support.
- No authors class the process as capable of peening, although many describe the creation of a layer of compressive residual stress. This could be considering peening, although peening (dependent upon method) creates layers between 200-700µm thick, whereas AFM is ~10µm thick.

Environmentally, AFM is not discussed in the literature in a context sufficient to define environmental credentials – this is a notable knowledge gap, alongside the ambiguous and incomplete technical capability knowledge gaps. AFM has the potential to make high-volume processing of deburring operations more efficient, less costly and quicker. It could also be considered as a means of preventing the manufacture of arguably less flexible machinery, reducing overall machine tool manufacturing requirement.

Perhaps most critical of all points overlooked in the literature is that of fluid flow condition being the driver behind abrasive delivery to the workpiece surface. Without this knowledge (i.e. impingement angle, local velocities) and without the ability to determine the amount of support provided by the matrix, existing work does not allow application to complex geometry, nor does it allow the reapplication of existing data.

Overall, literature agrees largely upon the following points;

- Erosion ***magnitude*** highly linked to particle force on surface.
- Erosion ***location*** linked to fluid flow and resultant condition at a POI.
- Erosion ***uniformity*** should be described by uniformity of field variables.
- Erosion ***potential*** is limited by viscosity-temperature relationship.
- Erosion ***repeatability*** is controlled by machine, media and hysteresis effects.
- Erosion ***accuracy*** is not currently predictable within disclosed works.

Chapter 3 - Formulation of the Machine-Tooling-Process Integrated Approach

3.1 Overview

This chapter presents the route taken to build a methodology that allows the researcher to integrate empirically-collected, inferred, correlated and numerically-derived data into a grand framework which removes the majority of investigative work from subsequent production tasks. It also attempts to describe the divide between three elements of project output; 1) the bulk of doctoral exploratory and analytical work, 2) the subsequent research requirement in some process setups, and 3) the recurring 'new part' model development steps.

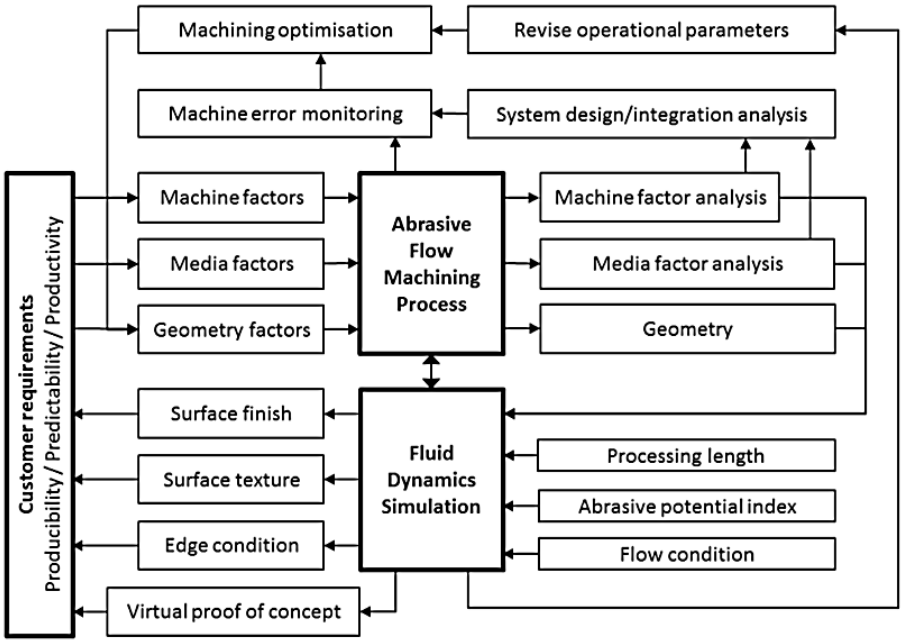

Figure 3.1 – CFD-integrated AFM process map.

Manufacturing standards require technologies to be robust and repeatable, in order for them to be considered useful. In this section, research interests are identified – those key research questions which allow formulation of an approach. The machine structure and the pre-existing constraints of the project are also considered - the concept of transferability is important – without defining the changes in momentum and processing quantity when pumping media between machine and part, a researcher may fail to appreciate the change in behaviour when setting machine levels on a console and the subsequent real conditions in the part.

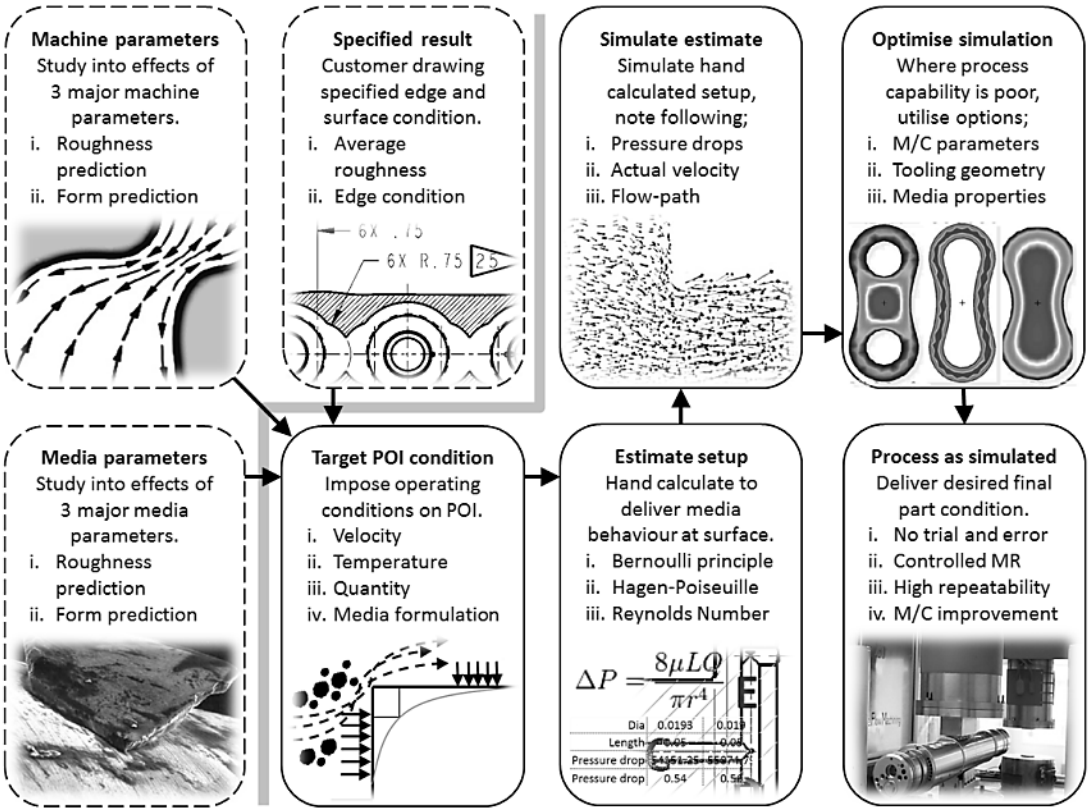

Figure 3.2 – Early scheme of data collection framework.

A framework is designed whereby these items are studied and understood, in terms of the effects of machine and media configuration on a testpiece in a controlled environment – the framework is designed to build knowledge of process effects and aid the transition into a virtual system that allows infinite geometrical testing. Some elements of the framework are less integrated – these augmented items are critical to developing the production tools necessary to commercialise the technique. Also discussed in this chapter are the scientific concepts and how they are applied in a physical and software environment to provide true engineering confidence.

3.2 Research interests

By working in association with Mollart, the content of this thesis is based on the application of AFM in components manufactured over the last three years. Although the application is mainly to oil and gas exploration tool bodies, techniques are easily transferred to aerospace, medical, defence and automotive applications. In operation, the (frequently) cylindrical components (measuring up to Ø0.2x1.6m) contain hydraulic fluid, electrical cabling, solenoids and crude oil housed within an array of over 100 ports, through-holes, blind-holes and cross-holes. Critically, it is very difficult to obtain consistent finish across all features and intersections; remaining sharp edges encourage wire insulation to be stripped, loose flashings of workpiece material can break loose (damaging pumps and hosing), and samples of oil or gas can become contaminated. Human labour is a very inconsistent method of finishing such a complex part and errors are frequently made, resulting in increased transportation and re-work costs.

3.2.1 Challenging production part examples

Technical challenges that require a research approach are seen in a multitude of parts;

1) Features may not always be symmetrical – invariably, media is fed toward the component from a cylindrical container and through a symmetric adapter ring. After the media has entered, invariably the flow-path (the sealed cavity through which media flows) is asymmetric – therefore, if the intention is to ensure a uniform flow field approaching the feature to be processed, flow-path modification through tooling insertion is the only option. The flow-field (velocity, temperature, viscosity) profile of the cross section approaching the feature) is also capable of manipulation and affects the rate and location of erosion. Figure 3.3 is an example of features that carry wires with soft insulation – the inlets are asymmetric to the features.

2) Features may not be sympathetic to erosion by abrasive flow. Features with shallow angles and features behind an acute angle are likely subject to low surface strain rates, pockets of low pressure and heated lower-viscosity material flow. The flow-field may not be conducive to the feature (or POI, point of interest) as illustrated below in circle 2 of figure 3.3. Through research, the project aims to visualise the passage of media through the component and determine the post-process effect. The same technique would be useful for checking new tooling designs and allows a fully-virtual process setup.

3) Features may be out of position by up to 5mm – the variance within the metal-cutting process, particularly on long components and deep holes, means the joins between features may not be to nominal drawing dimensions and therefore not to where the AFM tooling was designed to aid the flow. Research interests include studying the effects of flow surrounding the POIs and the subsequent effect of tooling and geometry combinations.

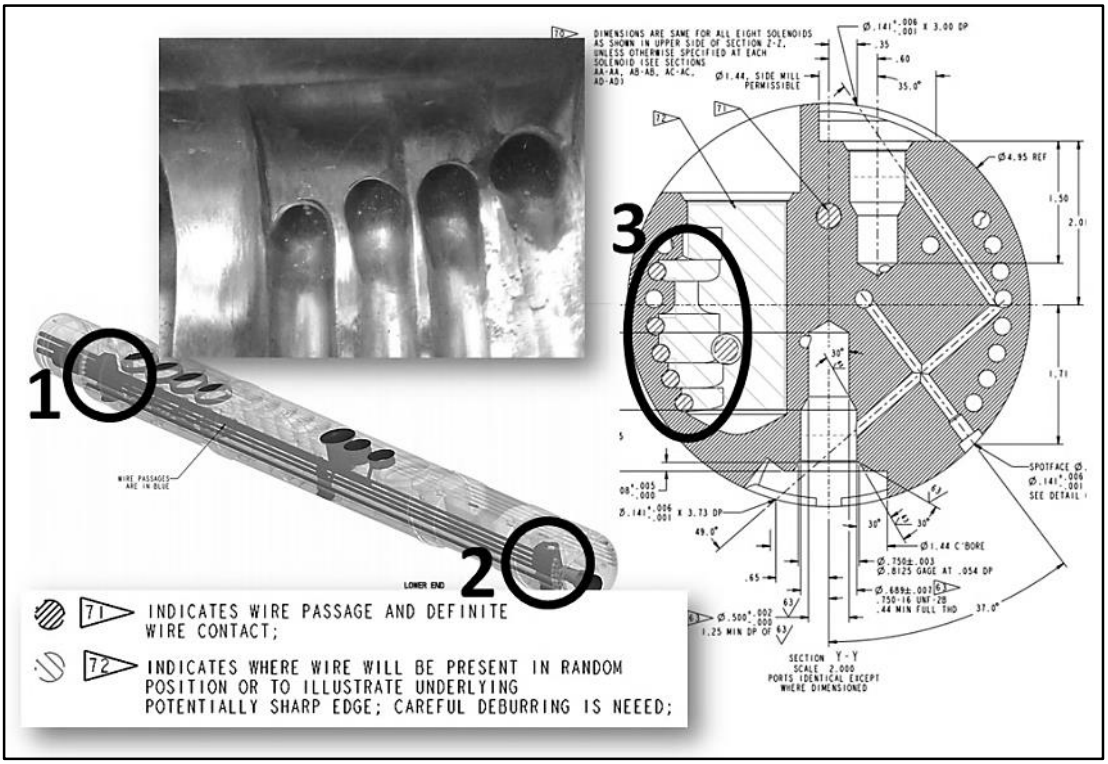

Figure 3.3 – Example of AFM-viable end-ports from oil and gas exploration tool.

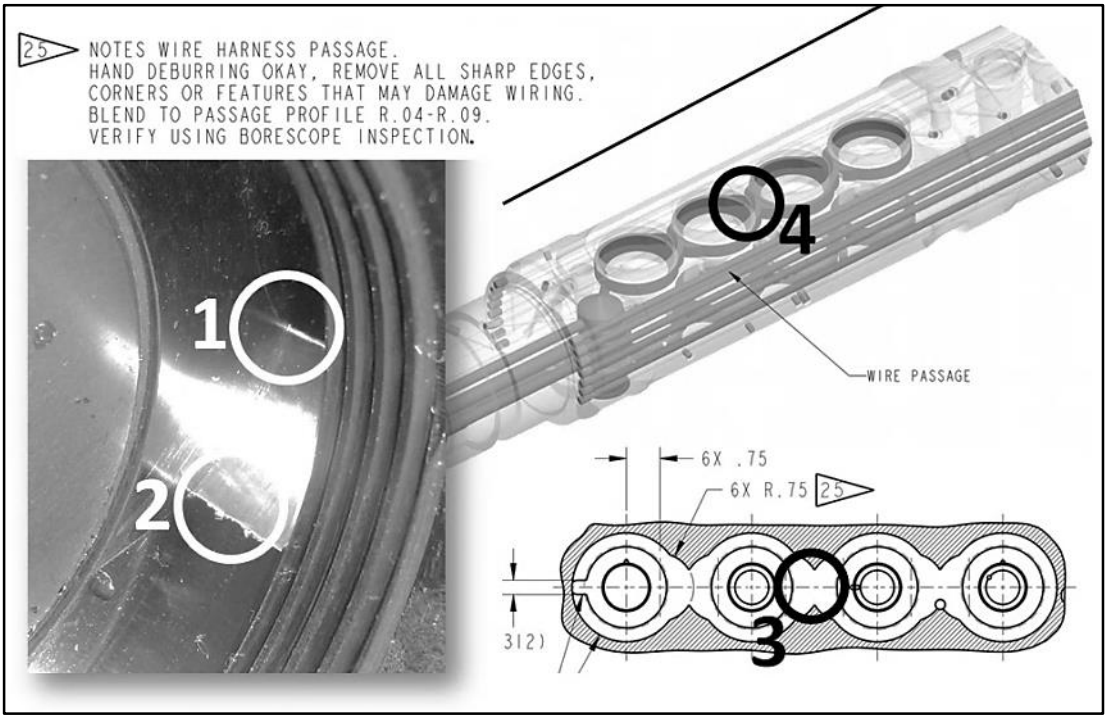

Figure 3.4 – Example of AFM-viable internal wire passage from oil and gas exploration tool.

4) It is not uncommon to find holes which are deep, but ‘blind’ (finished to a drilled depth, not drilled through) – the AFM tooling designer may be required to formulate a method of tooling a feature at the end of the bore, perhaps entering from a cross-hole as

shown in circle 1 of figure 3.3. These features are both difficult to measure and difficult to produce by hand – to improve AFM process capability, this project must provide the business with a viable means (through research) of determining processing parameters to provide the desired result, one which requires no measurement due to process confidence.

5) Pre-existing machined surfaces may not permit further material removal (MR) – just as edge-rounding and surface finishing are key variables to control at the POI, those same responses are important at areas where erosion is to be avoided – AFM is typically carried out in the latter stages of part production – surfaces may already be finished to specification and at risk of surface damage caused by media flow, post-AFM cleaning or where media may leak between tooling and surface (where close contact is required). This is exemplified by the tooling shown in figure 3.5 in a fracking tool – using a solid model cut-through section, the numbers 1-4 are additions to customer geometry used to control direction of media passage.

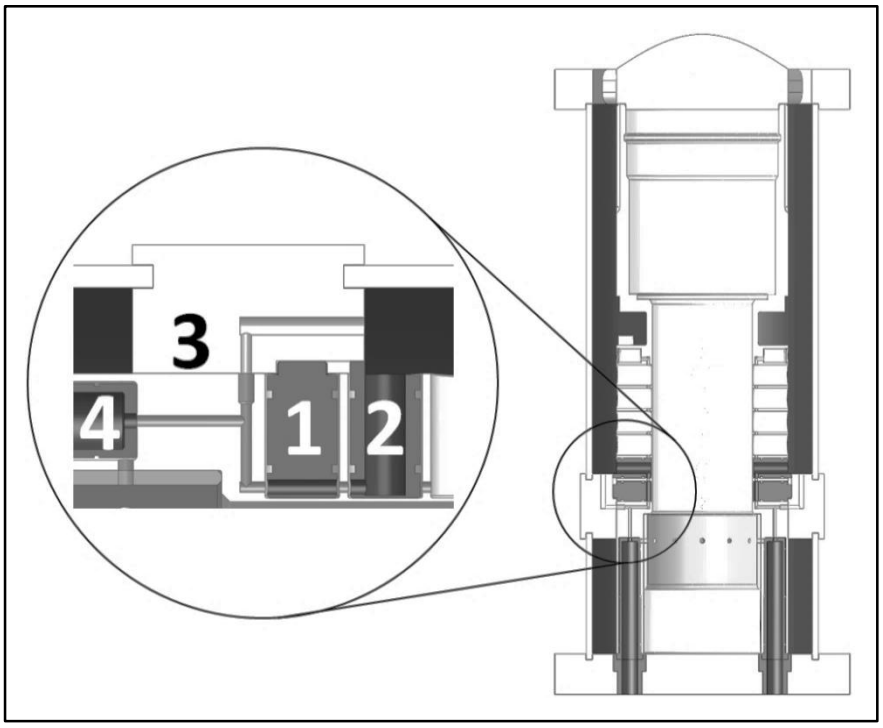

Figure 3.5 – Section view through hydraulic fracturing tool.

6) Tooling access is frequently an issue in components where small bores and inaccessible features are found – this is typically AFM's strongest application, as humans also struggle to reach these areas, but it should be noted that as shown in figure 3.6, the difference between 'media access' and 'tooling access' are constraints in their own rights. In this scenario, the research interest is in understanding the minimum requirement for tooling and whether internal near-feature tooling is required, or whether the flow can simply be regulated to provide the right conditions.

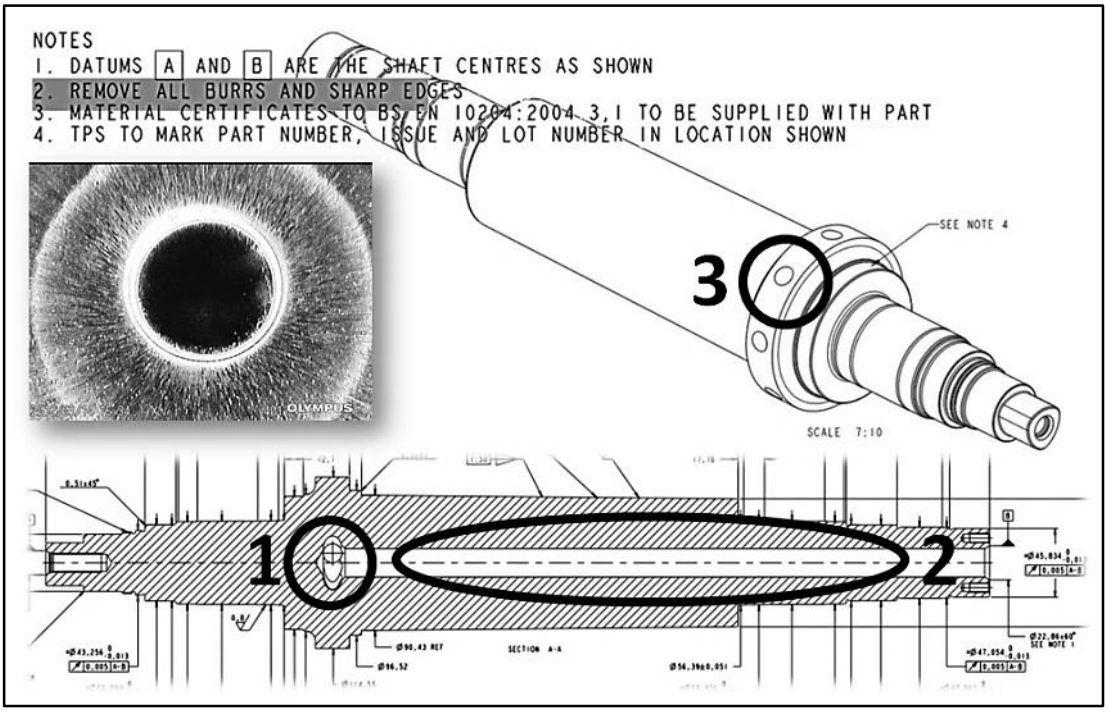

Figure 3.6 – Example of AFM-viable features from turbomachinery component.

7) Alongside completed surface finishes, figure 3.7 has sharp edges to protect that are customer stipulated – workpiece physical size and strength should be considered in tooling as the clamping force of the machine holds the potential to distort geometry, especially when the sharp features (circle 3, 4) are on a suitable clamping surface.

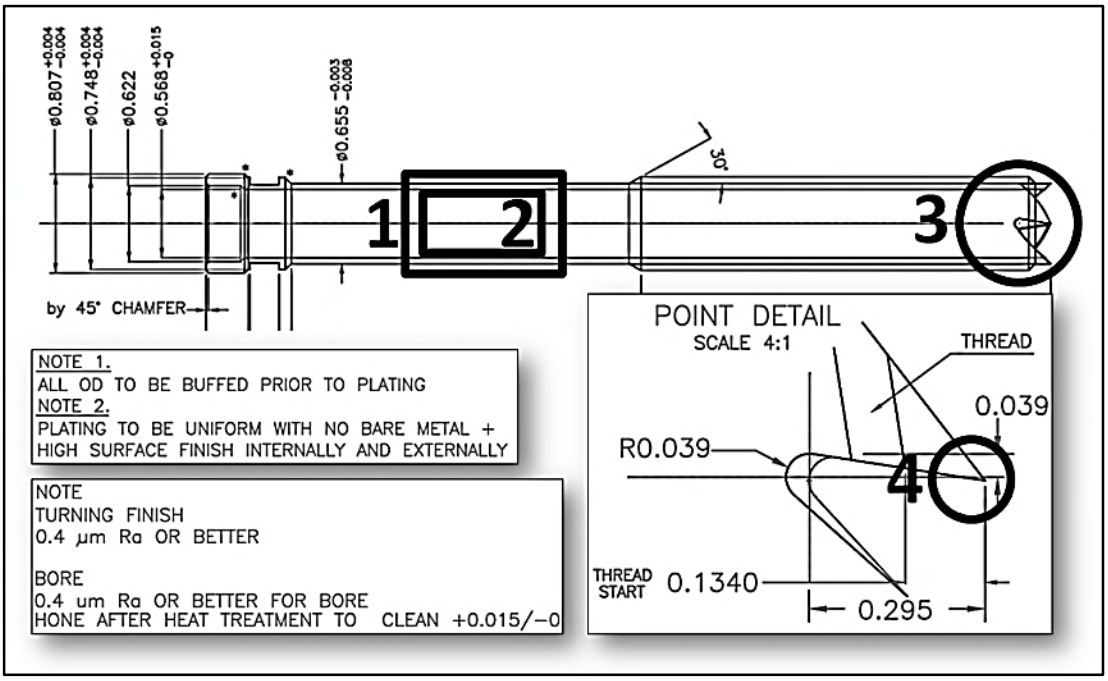

Figure 3.7 – Example of AFM-viable features from consumer product.

3.2.2 Non-production related research interests.

While the commercial viability of the process is of paramount importance to Mollart, the potential for novel research is high – the intention to gain control over the process with new geometry, before the start button is pushed drives the non-production related research interests. Five are noted below;

1) Can simulation output be correlated with physical measured results, to an extent that erosion can be irrefutably tied to a field variable value in a testpiece and then replicated in a complex part? There must be a method developed to control the process before components are put-up on the machine – anything else is continuing with trial and error.

2) Can those predictions be effectively proven in testpiece geometry, trialled in a complex geometry, implemented in a manufacturing environment, complete with machine error and unforeseen circumstances? Robustness of output ensures process uptake and is a measure of project viability and success.

3) Can process variables be grouped and studied in such a way that makes practical and economic experimentation possible, but also that variables in existing literature are considered, quantified, studied and critiqued? Existing work does not include 'enough' variables, but nor does it study the 'right' variables.

4) While effects on the roughness and edge condition are varied and a result of a number of interacting factors (primarily the carrier-grit-flowpath-surface interaction), it is thought that velocity and extrusion pressure offer the greatest control. However, the route to achieving a given media surface speed is controlled by many factors, starting with the ability of the machine to deliver sufficient pressure to overcome viscosity of media and part through-hole diameters.

5) It has been determined that Mollart's most difficult to process part with a 5.6mm diameter bore and with ~60,000cSt viscosity media, requires a pressure of nearly 170bar for the machine to reach maximum piston speed. How can the developmental work in this project assist with overcoming the fundamental limits of existing machinery?

3.3 The importance of transferability

Given a particular set of machine or media parameters, it is currently difficult/impossible to predict a tangential radius, or provide *any* estimate of material removal quantity or from which location. To progress, this incurs trial and error work for a production component which remains part, media and tool specific, and may only be transferrable to other components by experience. In practical terms, the current state of the technology prevents the user from carrying out a single operation with certainty of outcome which, in turn, prevents an economic and efficient means of delivering a customer's desired finished part condition.

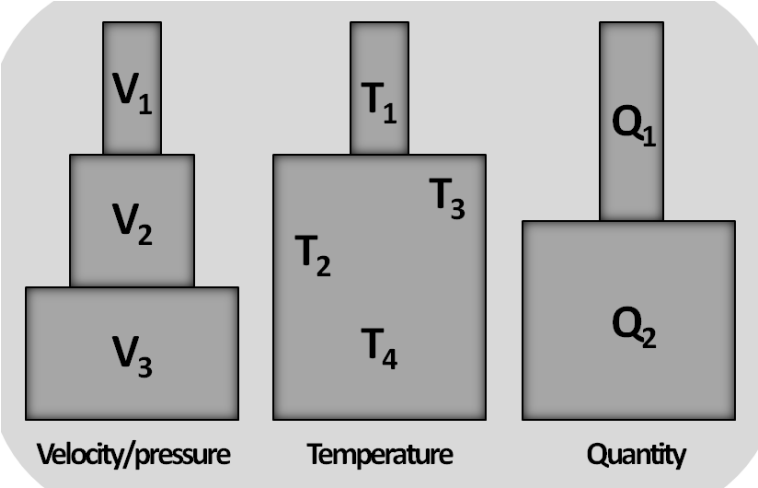

Figure 3.8 – Simplified schematic of key quantity variation throughout machine.

As economic reasons prevent the use of complex parts in study activities, research can only move forward by defining a new data collection environment, formed of a standardised testpiece and fixturing – in this system, the machine and media are pre-existing, and come with their own inherent factors and levels which must be taken into account when presenting results obtained using the system. Figure 3.8 depicts the simplest level of machine parameters, velocity, temperature and quantity (V, T and Q) where the leftmost image describes the principle of cross sectional area (CSA) influencing velocity as CSA reduces. This is relatively easy to calculate in tubular sections or sections made of simple shapes, however when the approach is applied to geometry such as that depicted through figures 3.3 to 3.7, it becomes markedly more difficult and that variation across the CSA profile is also difficult to predict. The example of temperature is equally perplexing, as in AFM, sources of heat can be active or passive and often undergo machine-initiated correction cycles using active sources. Temperatures T_1 to T_4 depict temperature influence by temperature of workpiece (T_1), influence by active cooling apparatus (T_2), influence by correction attempts (T_3) and through dissipation (T_4). Knowledge of local temperature is exceedingly difficult to see in a sealed and dynamic system such as that of AFM. Lastly, the same can be said of

quantity – that in a container of ~20L, the machine user panel will define a stroke of 300mm, equating to 20L; the question must be asked – how much media rests inside the part as a dead zone (AFM fills a component and empties the lower reservoir before pumping media back), making the 300mm/20L figure highly variable when considering part volume. If a component of internal volume 20L were processed alongside one of 1L, the degree of processing would be significantly different. Complex geometry can be time-consuming and likely uneconomical to calculate volumes – it is simpler when using modern CAD systems, however the change in local volumes in the workpiece affect other process variables such as viscosity.

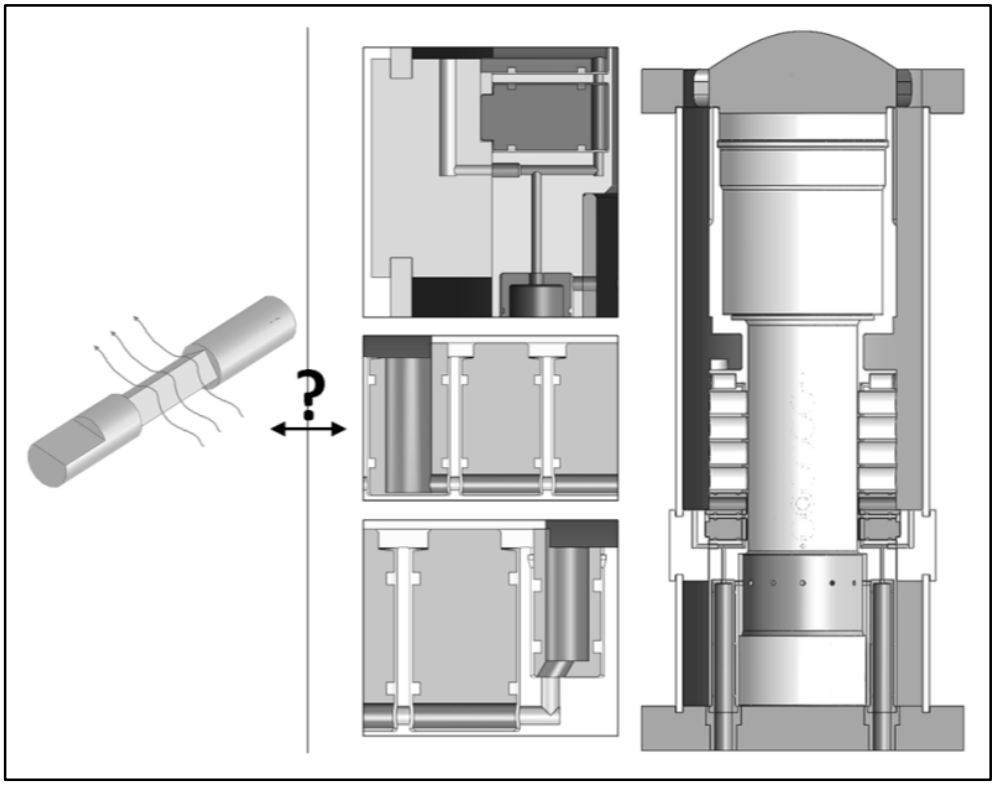

Figure 3.9 – How can the results from a testpiece be employed in a complex component?

An overarching question that this research attempts to answer (as previous literature has not done-so), is whether a system can be formulated that allows the prediction of post-process geometry without performing trial and error work. A critical system requirement is that of ensuring testpiece environment data is applicable to real, customer geometry and that findings 1) do not remain in the academic domain, 2) are production-viable, and 3) are fully transferable to infinite geometrical possibilities.

3.4 Approach framework.

Figure 3.10 presents a structured approach to obtain the necessary data. Boxes 1-5 obtain machine knowledge and boxes 6-10 obtain the same but for media knowledge.

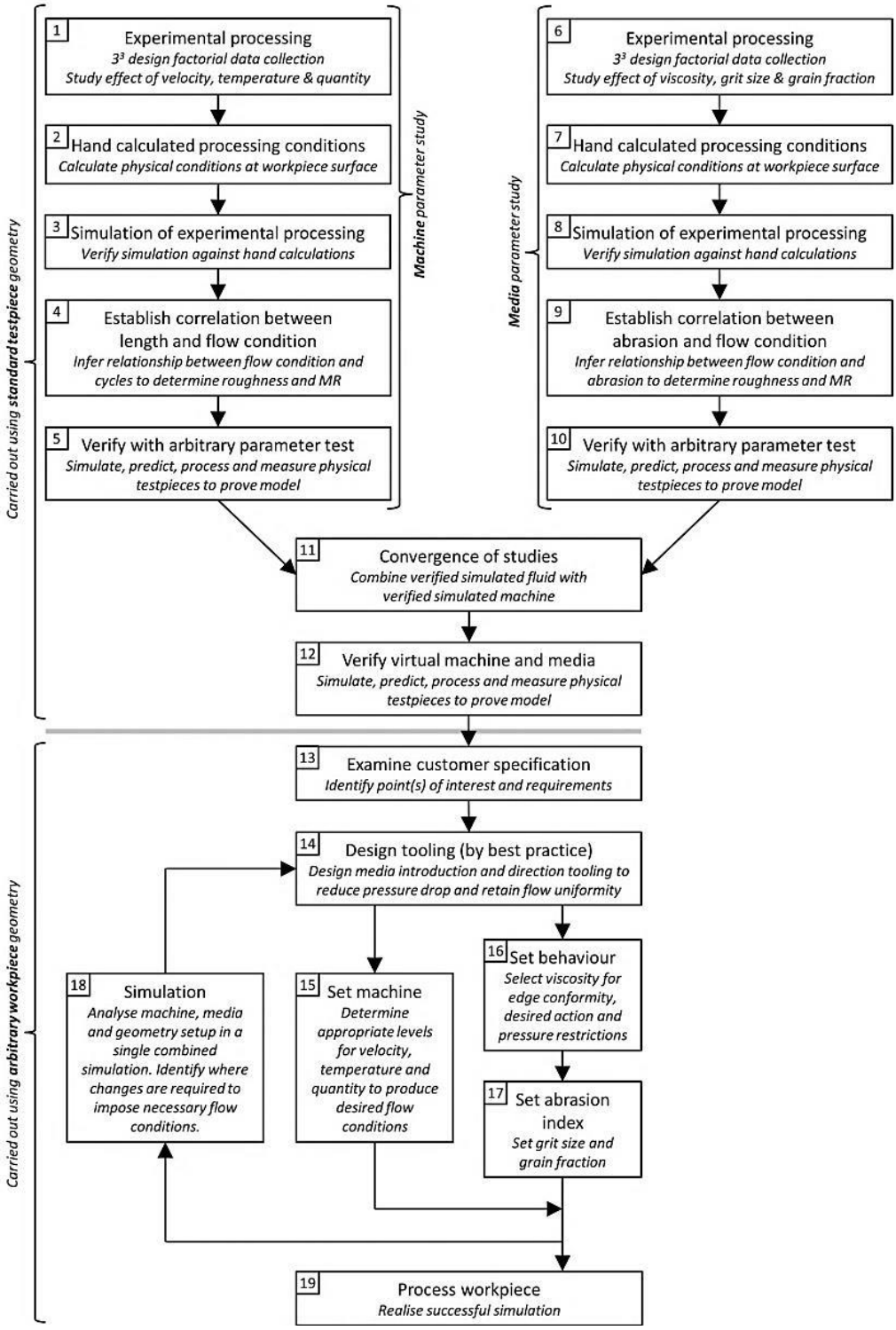

Figure 3.10 – Transfer of experimental results to arbitrary geometry through CFD simulation.

3.5 Scientific concepts.

Abrasive flow machining can be likened to a self-contained hydraulic circuit, comprised of two reservoirs with built-in pumps, transferring fluid through a complex-shape restriction. Additional complexity is provided by sources of heat input and extraction, viscous heating, frictional effects, ambient temperatures, variation in material specific heat and mechanical properties of the flow's bounding walls. This subsection aims to apply scientific principles to the process so it may be described at a fundamental level. Principles are applied numerically throughout chapters four and five, but their suitability to the AFM process is debated in this chapter.

3.5.1 Fluid dynamics.

Defined as the study of fluid behaviour in motion, fluid dynamics is core to process output – the energy absorbed and transferred to abrasive particles, the vector of travel and velocity, pressure, etc. differential throughout the part is exceedingly difficult to calculate and frequently in modern computer-aided engineering (CAE) the answer is to use software to simulate a fluid flow. In AFM, the following equations are appropriate for partial description of flow phenomena;

- Reynolds (Re) number; the ratio of inertial forces to viscous forces, i.e. resistance applied by the material being pumped in counter-effect to the momentum carried from a source of kinetic energy. Three regimes are accepted; laminar, transition and turbulent. Turbulent defines an unstable flow where rapid change between velocity and pressure occur in close vicinity. Technically, the cause is a lack of supporting kinetic energy. Before turbulent flow can become laminar (assuming additional momentum is applied) a 'transition' regime is observed, between Re=4000 and Re=2300. Laminar flow occurs when momentum overcomes internal forces. Media flow in AFM is laminar, with further work suggesting a value of Re=0.003, due to high viscosity of media.
- Eddy currents; as flow passes by an obstruction, whether flow is turbulent or laminar, the momentum prevents the material from conforming to the geometry on the trailing edge of the obstruction. This leads to the formation of an area of low pressure, sometimes extending to vacuum levels, but the end-effect is that an area of surface fails to be processed, or is processed with different flow conditions. Vortices share similar dynamics, although more commonly a component of turbulent flow, therefore not as applicable to AFM as the formation of eddies. Flow instabilities (turbulence) cause the output of the AFM process to be unpredictable as the streamlines are chaotic.
- Preston's equation; stipulates that rate of material removal in grinding operations is proportional to velocity multiplied by pressure. This, while not an absolute rule and derived from empirical study, gives some accepted meaning to the significance of extrusion pressure seen in the literature. In AFM, the context

is similar to grinding in that the rate of exposure to abrasive (velocity) and driving force behind it (pressure) delivers the same effect – dwell time in grinding is synonymous with processing quantity in AFM – while the equation calculates material removal rate, total MR can be easily estimated. The equation is written as ‘r = k P v’, where k is a coefficient determined by type matrix, abrasive grit and workpiece material.

- Hagen-Poiseuille equation; can be used as a generalised model for calculating pressure-drop in long, full-bore pipe flow. Terms include length of pipe, dynamic viscosity, volumetric flow rate (or velocity) and radius – AFM benefits from this equation in a number of ways; estimation of pressure drop to determine machine capacity for a component, calculation of maximum viscosity media suitable and estimation of velocity achievable. As a generalised model, the Hagen-Poiseuille is not intended for use with non-Newtonian substances, however it holds very well – it can be derived from the Navier-Stokes equations, themselves derived by adding viscous stress and pressure terms to Newton’s own laws of motion.
- Bernoulli’s principle; defines the change in fluid pressure and velocity in a streamline and describes the principle in AFM that kinetic and potential energy varies throughout the workpiece based on flow conditions. Velocity increases where pressure decreases, although AFM may operate with a continuously adjusting source of mechanical energy – however, the principle that where input mechanical energy is continuous and unadjusted, the pressure in a constriction is reduced as Bernoulli’s principle states that fluid flowing through a wide pipe and entering a narrower pipe will increase in speed and reduce in pressure – the effect appears counter-intuitive as it could be conceived that pressure would increase to force the fluid through, but in terms of energy density, the kinetic energy of the narrower pipe is higher and in line with the conservation of energy principles from Bernoulli’s principle can be derived, the corresponding potential (pressure) energy must reduce.

3.5.2 Rheology.

In traditional grinding technology, the wear properties of the bond may be studied for degradation rate to control rate of new grain exposure and thus surface finish. Likewise in loose abrasive AWJM, the coherence of the fluid stream contributes to final geometry quality; in AFM, the complexity of abrasive delivery is focused on the polymeric carrier – chemistry indiscriminate, the behaviour of these fluids is largely thought to determine the final geometry. Factors of the carrier behaviour are discussed in the area of ‘rheology’ – the study of fluid motion, distinct from the term ‘fluid dynamics’ as it applies more readily to the study of ‘sludge’, ‘mud’, ‘slurry’ and other multi-phase materials, but primarily those in a ‘soft-solid’ state as opposed to fully liquid.

Two major groups of liquid behaviour exist – Newtonian and non-Newtonian. A Newtonian behaviour describes the tendency of a fluid under-load to exhibit the same strain rate as the input stress, resulting in deformation at the same rate as displacement. The non-Newtonian will exhibit a variable rate of strain when input stress is equal, changing shape at a rate slower that the displacement occurs. Often, a non-Newtonian fluid can be generalised into either shear-thickening (where viscosity increases under shear force) or shear-thinning (where viscosity reduces). These materials may thicken and thin at different shear rates, but complexity in description is unavoidable – the following definitions are noted for integrity;

- Dilatant; the umbrella term for a shear thickening material, the action of thickening is seen mainly is particle-suspended materials, where it is thought that the colloids (those particles in suspension) are responsible for increased interaction and reduce the motion potential of the liquid/semi-solid supporting matrix/carrier. The term dilatant does not define the material's viscosity at a given shear rate, the rate of change of viscosity or any viscosity-limit effect. The effect described by dilatancy is that only of viscosity connected to shear rate.
- Thixotropy; comparable to dilatancy and often confused, thixotropy describes the same effect as dilatancy except shear rate is not the driver for viscosity change; shear rate *over time* is, however. For example, if a thixotropic material underwent a change in shear condition, but remained at a very low shear, i.e. a shaking action, extended exposure to the low shear would result in higher viscosity. The same action with a dilatant would result in a far less significant increase in viscosity in the same time-period.

The opposite of these material behaviours is their 'thinning' equivalents; when referencing the terms 'pseudoplastic' (the direct opposite to a dilatant, sometimes described as power law-governed) and rheopecty (the direct opposite to thixotropy). Additional complexity in describing non-Newtonian fluids arises when considering some of the other branches of the previously described four terms;

- Bingham plastic; starting at high viscosity and reducing under shear force, it could be considered a pseudoplastic or potentially a rheopectic, but Bingham plastics define a sub-group of shear-thinning materials that require a kick to begin flowing.

Viscosity is thought to be caused by one chemical and one mechanical phenomena; inter-molecular relationships between shear-planes within the material and between suspended colloid-interaction in the material.

3.5.3 Tribology and mechanical properties.

Scientific principles of interacting surfaces in relative motion are studied under the banner of tribology. Encompassing satellite disciplines such as scientific application of

principles of lubrication, wear and friction are included. AFM has historically (see literature review) been considered a technology that warrants the study of substrate-abrasive relationship, however this project aims to develop the flow-substrate relationship knowledge that has been postulated may lead to better process control.

Mechanical properties of substrate materials are a viable avenue of research where individual characteristics of both abrasive and substrate interact to deliver a specific rate of MR. Of particular scientific interest is the clarification of whether AFM is more suited to processing of harder materials through being predispositioned to flow conditions that encourage the brittle fracture of the surface, or whether softer materials are more easily processed due to AFM's delivery of abrasive being prone to cause plastic flow (ploughing). Cutting efficiency is not a core driver for the work. The truth may be that different materials are likely to interact with different abrasives to varying extents, and thus provide no clear picture of which mechanism AFM uses to perform MR. In any event, the area of contact mechanics, indentation hardness and crystal structures are valid explanatory tools and terminology sets for describing project output.

3.5.4 Thermodynamics.

Application of the laws of thermodynamics to AFM is multi-faceted, with multiple sources of energy input and output – it is helpful to consider the hardware and phenomena that the researcher has the ability to monitor/control;

- Zeroth law, heat capacity; while the media in the lower cylinder, workpiece and upper cylinder is a single physical volume, thermal and kinetic energy are applied only at certain points. The lower piston has an additional source of heating and cooling in the form of bars running through the cylinder. During the process, the time and quantity of media in any one location can have varying kinetic and thermal energy input - while the kinetic energy input is equal from either cylinder, the distribution of heating elements provides more energy from the lower end of the system, but also greater regulation. During processing, the requirement for physical motion prevents any of T_1, T_2 and T_3 (figure 3.8) from reaching a state of equilibrium, despite being part of a closed three-part system.
- First law, enthalpy; process energy consumed is equal to the input energy (thermal and kinetic) less the work done by the system. In the AFM process, input energy can be calculated through the combined temperature and kinetic energy applied, although the variations in temperature are the cause of difficulty in hand calculations - the solution may be to model the system as it heats using a simulation package. The kinetic energy input is significantly simpler, as it relies only on the force required to accelerate the media mass. In practice, the energy applied can be lost through convection through friction forces on the container walls and by passing the media through restrictive passages. The ΔH (change in

enthalpy) value can be considered a key performance indicator for the processes' environmental performance.

- Second law, entropy; describes the tendency for a system to homogenise the energy within its boundaries – i.e. high energy areas will transfer to areas of lower energy. This principle is present in a number of solar-thermal systems whereby the density of a heated fluid is reduced, causing a reservoir of cooler fluid (mounted at a higher point) to displace the volume of heated fluid. In the AFM process, the purpose of the warm up cycles (run before processing a part) is to homogenise the media, both in terms of uniformity of particle distribution and in terms of temperature distribution. Energy in the system is constantly drained by the convection of heat from the external walls of the cylinder - in order to conserve more energy, insulation of these surfaces would be prudent, although the temperature of the media will affect its viscosity and reduce its ability to do work.
- Third law, entropy approaching absolute zero; while the process is unlikely to ever be used at less than 0c, the third law considers the effects on a thermodynamic system of the removal of thermal energy. Since the AFM process utilises a viscoelastic fluid, the reduction in temperature (reduction in thermal energy input) requires an equal energy input from the kinetic energy delivering piston to overcome the system entropy heading towards zero.

3.5.5 Kinematics and impingement angles.

Literature has shown that the angle of impingement (vector) and motive force (velocity/pressure magnitude) can combine to explain depth and nature of indentation of abrasives – the scientific issue in AFM is that of the supporting matrix and its condition at the time of impact. The principles involved in describing vectors of flow include complex flow theories that are typically described by CFD software. Discussed in the literature review, the theories behind angle of attack and erosion rate is a common connection made by those studying solid particle erosion in gas streams containing particulate matter. Authors have previously found that some materials with relative ductility are more prone to MR when processed with shallow impingement angles, as their structure is more prone to plastic deformation, whereas relatively hard materials are more effectively processed using angles approaching 90°.

Technical principles to consider in this area are the shape of abrasive, the angles that may be seen on said abrasive, traditional principles of cutting mechanics in the shearing modes (seen in milling and turning), brittle fracture (grinding for polishing) and in burnishing (material displacement, no removal). Mixed mode effects, i.e. rolling and skidding, may also affect surface texture and in the largely chaotic AFM abrasive delivery process, may be caused by combinatorial effects which can be analysed using surface micrographs and careful experiment design.

3.6 Summary.

Development of a feasible process begins with understanding the factors affecting the final results – some can be determined by reason and logic, others by experimentation; ultimately, a numerical value must be placed on the surface finish and edge-rounding results driven by customer requirements, and an overriding academic influence in order to ensure validity, a systematic approach and a comprehensive output.

Philosophically, the system discussed in this chapter should be considered a precursor to a fully-software controlled machine; the vision is that a conceptual proof is required in this research, which leads onto a grander implementation of a proven methodology. At some point in the future, an AFM machine exists where collected data from testpiece geometry may be analysed by on-board metrology, having been processed overnight by an automatic testpiece loader. Such data would be fed straight into an integrated database whereby material erosion data would be reapplied and simulation data collated and cross-referenced. For new media types, unmanned rheometry would characterise new compounds and automatically simulate the behaviour to extend the abrasive potential knowledge of the media. To further the vision, it is conceived that solid model geometry be marked up by a human to highlight features to process, fed into a software package and optimised tooling be the output. This work attempts to establish the feasibility of using a CFD-driven process-prediction methodology and applies it stepwise to complex geometry found in Mollart Engineering Ltd's own subcontract division – the work is highly industrially-relevant, and it is known that the wider engineering market will benefit from the technology.

This research differentiates itself from previous and current commercial/academic attempts at controlling the AFM process by occupying a space where industrial viability is king, closely followed by academic scrutiny, and (perhaps importantly) that those without the background to perform this work are aware of the processes and can obtain further information using this document as a guide. Much is known of the AFM process through academic study, but like so many processes that remain unseen in action by the naked eye, the development of tacit knowledge by a lay-person or machine operator is constrained to experience, therein involving the costly and time-consuming trial and error approach. Generation of new process knowledge is the ultimate goal.

The author intends to have this work viewed as a framework where the reader should attempt to understand the connections between work elements by understanding the inputs and outputs, i.e. the variables controlled, the parameters collected in metrology exercises, the values obtained in simulation. Armed with this understanding, the author feels that, after discussing the methodology with colleagues, that a reader will more readily comprehend the aims, objectives, project output and understand how further work with different machinery, materials, geometry can easily be performed.

Chapter 4 - Design of Experiments (DoE) and Analysis

4.1 Introduction

This chapter's goal is to understand the effects of machine and media variables on the surface of the workpiece in preparation for simulation tasks – there are three key response variables in each of machine and media studies; using a developed standard testpiece design, over 130 parts are processed in two phases – firstly, with machine parameters acting on the testpiece where the media and naturally the geometry are fixed, and secondly, where machine is fixed and media is varied - the same testpiece design is used. These are measured using two systems; roughness as a metric is simple to devise a comparative measurement system, i.e. measure samples at the same point with the same technology. Secondly, considering material removal, quantification of radius size and accuracy is required. Working with two experimentally-derived datasets, analysis activities aim to uncover the driving forces behind the resultant surfaces, and identify data to be taken forward to chapter 5, modelling and simulation.

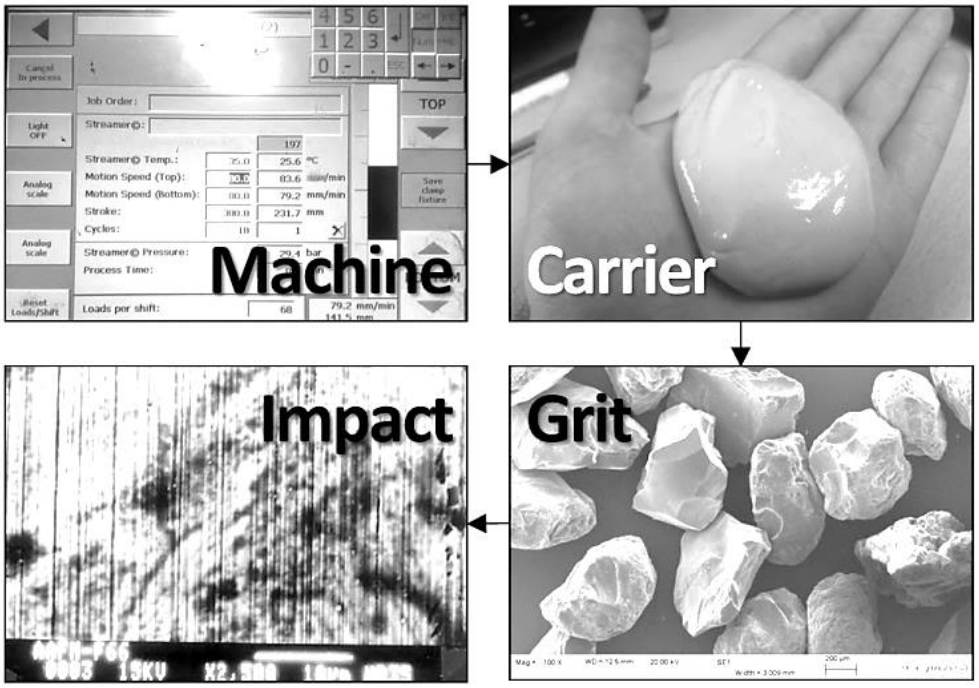

Figure 4.1 - Transfer of momentum between system elements.

At the lowest and simplest level, an end user can only dictate the conditions at a point of interest (POI) by means of core user-controlled inputs; velocity of media, quantity of processing and angle of attack. It is important to distinguish between use of the term '*POI environment'* and '*process variables*'; a POI environment refers to the conditions present at the surface an engineer is attempting to process – these will likely be far

removed from the conditions present at the machine, i.e. the process variables as user set. As summarised from the literature, there is no truly transferable way of determining process effects in a simple geometry, then successfully realising the same results (with the same inputs) in a complex geometry. POI environment change is the cause, as influenced by changes in velocity, quantity and angle of attack (process variables) caused by the part geometry.

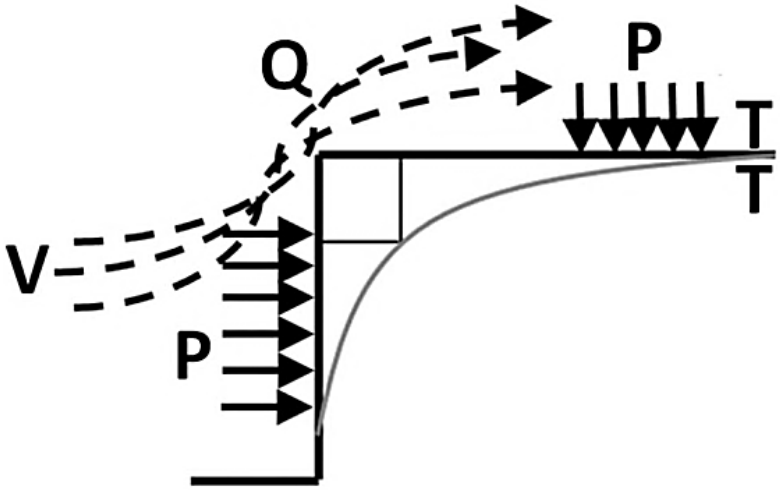

Figure 4.2 - Schematic of low-level principles on substrate surface. Where V is velocity, Q is quantity, P is pressure and T is temperature.

When approaching the setup of a new component, engineers have two options – 1) they can embark upon a wasteful, inefficient and poor-capability trial and error system, hoping for the best in a complex and highly-varied process, or 2) they can attempt to relate the findings they achieve in simple geometry to complex geometry through a series of transformations. This project takes the second option. Given a particular set of machine and media parameters, it is currently difficult/impossible to;

- Achieve tangential radii or uniform surface finishes
- Provide estimates of material removal or radius size
- Estimate the material removal location

Trial and error is incurred when a production component (part, media and tool specific) may only be transferrable to other components by experience. In practical terms, the current state of the technology prevents the user from carrying out a single operation with certainty of outcome which, in turn, prevents an economic and efficient means of delivering a customer's desired finished part condition. Controlling the outcome by means of hand-calculations is feasible in simple components, and estimates can be made in slightly more complex geometry, but as soon as varied diameters, varied shape, boundary forms, flow field non-uniformity (at inlet and outlet), changes of direction and stacked features are present over long lengths, realistic and repeatable predictions as to

where AFM process erosion will take place become difficult/impossible to state. Figure 4.3 shows traditional fluid dynamics flow boundaries, where non-erosive, Newtonian, 'Reynolds-laminar', 'Reynolds-transition' and full-bore flows can be reliably calculated for volume, pressure and velocity.

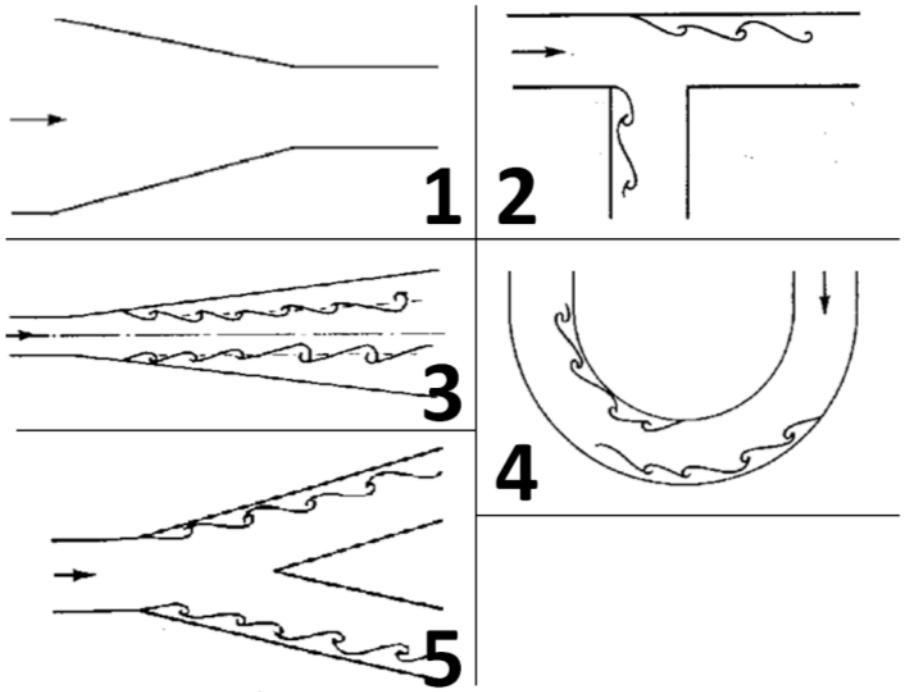

Figure 4.3 – Common flow boundaries. (1) Convergent flow, (2) T-junction, (3) Divergent flow, (4) Bend, and (5) Y-junction. (*adapted from Sleigh & Noakes, 2009*)

As per chapter 3 methodology, in order to migrate findings from simple geometry in a controlled POI environment, data must be collected within the 'process space' of machine settings and from media configuration options. A process space is a three-dimensional concept, consisting of a cube (or cuboid) with three axes labelled as three variables to be studied (Euclidean). Within the process space, the extents are finite – for a given combination of XYZ, an experiment may be carried out to determine its result as compared to another XYZ point. When performed comprehensively over a multitude of statistically positioned XYZ points, the process behaviour and interactions can be explained and effects of each axis can be described, even when three factor interactions are in-effect. DoE is used to describe experimental test conditions and analysis options – the strength of DoE is its logical and systematic approach, incorporating error assessment to understand effects precision. While these types of studies have been previously carried out, there are several highly important (and novel) differences that warrant re-testing to characterise effects for controlled re-application in chapter 5;

- Data from the literature comes from unknown machinery, with unknown natural parametric inaccuracy – error replication difficult without excessive effort.

Trials also carried out in a mixture of horizontal and vertically-oriented structures, sometimes mounted on lathes or self-supporting.

- Difficult to replicate, either partially or fully – access to material specifications, machined surface textures and finishes and media composition unavailable. The number of process variables each with unknown out-of-specification quantity makes the task nearly impossible to adopt current work.
- Cannot perform rheological tests on, nor replicate, media manufactured by authors 5-20 years ago – media is also inaccessible, or guaranteed to be deteriorated. Uncertainty surrounding configuration.
- Form and function of existing author's testpieces not useful for re-application in simulation or to describe edge-rounding, considering the requirement in Mollart's complex part – literature parts adopt flat surfaces and inner walls of tubes, with measurement points as defined by the authors.
- Previous work has not isolated variables according to respective MMG groups – machine and media are isolated from geometry to allow appropriate reapplication in chapter 5.

While it is recognised that output from studying the machine and media variables will only be applicable to the testpiece and test material, data and analysis will provide useful assessments of error, repeatability and causal relationships useful for production 'firefighting' tools. Analysis aims to deliver;

- Response distributions, standard errors, interaction between first order terms;
- Main effects (ANOVA);
- A verified predictive model;
- Contour plots for rule-of-thumb tools;
- Verification of acceptable levels of deviation from prediction and why;
- A visualisation of how achievable high-magnitude responses are;
- The behaviour of responses subject to changes in two others;
- Discussion of phenomenological effects and likely reasons for the behaviour;
- Three numerical responses values for all trials, critical to simulation;
- General observed effects and methods for improving media parameter study technically and economically;
- Production-valuable 'firefighting' tools.

4.2 Early investigations into machine-based variables.

Arriving at the final methodology to collect data from the process was achieved through an iterative and time-consuming chain of events. There are four distinct stages between starting and successfully designing and testing the final testpiece geometry and experimental methodologies. Initially in July 2011, a study was carried out using an optimisation-driven experimental design. Thereafter, the same geometry and a more appropriate two-level four-factor design was designed and tested. The effects in the geometry were extreme and difficult to measure with repeatability – those results that *were* collected, presented poor geometrical form and high variation amongst repetitions. Thirdly, the geometrical influence and machine limitations were understood and a new testpiece was designed. While showing minor signs of experimental usefulness, the feature within the part was not exposed to the flow in a method that would create measureable features, nor was the geometry conducive to reducing experimental error from unmonitored variables. The fourth attempt is the final and most successful design, used in the designed experiments and simulation environments over the next pages.

4.2.1 Final iteration of early investigations.

Following two preliminary designs and three experimental attempts, the testpiece is machined from a single 116mm length of Ø16mm round bar in the material under study; the research carried out in this document uses titanium 6Al4V grade 5, a prevalent choice in medical and oil and gas industries, and one known to be susceptible to AFM in the correct conditions, and media using boron carbide (B_4C) abrasive grit.

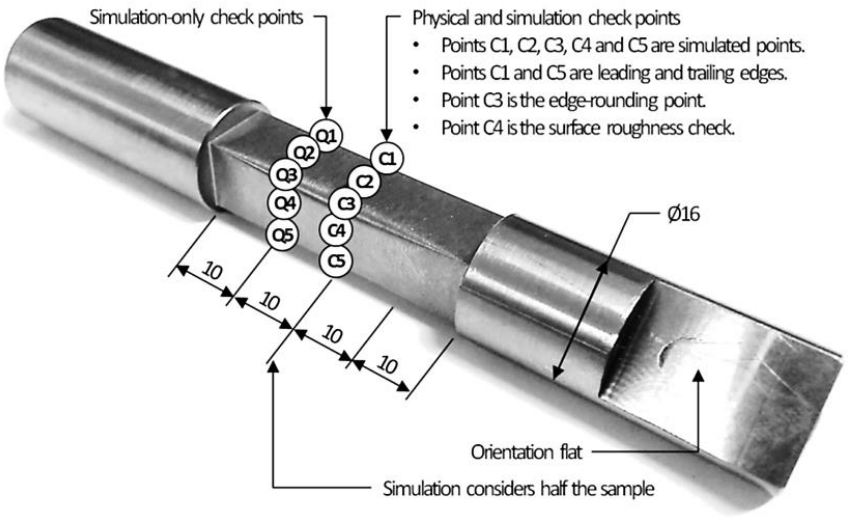

Figure 4.4 – Final testpiece design. Ø16mm x 116mm long, manufactured from the material under study.

Compared to previous geometries, this one is easily manufactured, requiring only a quick outer diameter ‘clean-up’ operation and a two-step milling operation whereby the

orientation flat and 10mm^2 centre section is machined. The testpieces are light, easily handled and stored, but perhaps most importantly easily removed and exchanged within retention fixtures without damage. The AFM machine also requires no unclamping to swap samples, in the instance a repetition should be performed immediately following another. With reference to figure 4.4, the most obvious difference is the form - previous forms have clearly represented the bores and steps within production parts, but only to a very limited extent (a counterbore). As per the framework described in chapter three, and in more detail in chapter five, the role of the testpiece geometry is not to replicate production part features – it is to provide an environment where process data is easily collected with repeatability, so that simulation data may be correlated to validate an electronic version of the testpiece environment so that extension of the findings is possible by application to more complex geometry. The sample is inserted into the side of a fixture block which holds the sample on centreline, secured in angular position by a flat bottom grub screw. This system aids inspection requirement - previously, a contact-based probe was used with poor reproducibility (re-position and re-measure), but this testpiece is capable of being measured without requirement for post-AFM machining, particularly suited to non-contact optical inspection techniques. Due to the inaccessibility of the point of interest in the previous work, the roughness was given a higher importance in the analysis. The edge form results are the descriptor of material removal (and thus capability of machine, media and geometry to produce a desired result). As roughness improvement has been shown to be linked to pre-process roughness (a characteristic controlled by initial manufacturing method (i.e. drilling)), and very difficult to achieve consistently, the importance of roughness results should be considered as secondary to material removal results.

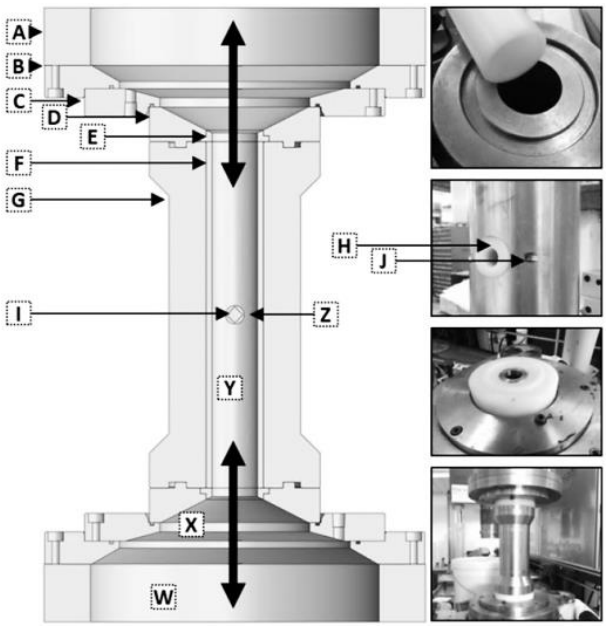

Figure 4.5 – Final design experimental setup in section view.

Re-using attempt three's support tooling (with modified main body, (figure 4.5, G)), the model and photographs in figure 4.5 conclude the revised setup. The lettered components are; A – machine cylinder body, B – EN24T steel adapter ring (250mm>260mm), C – EN24T steel adapter ring (260mm>150mm), D – nylon location adapter ring (150mm>40mm), E – nylon sacrificial ring, F – nylon liner tube, G – EN1A steel main body, H – nylon testpiece support, I – titanium testpiece, J – testpiece orientation and retaining grub screw. Also marked are; W – area of constant velocity, X – region of acceleration into workpiece, Y – constant velocity increased by a ratio of cross section area at W and cross section area at Y, Z – testpiece region, reduced area increases velocity and pressure about the edge by a function of cross sectional area at Y and minimum cross sectional area about Z. These parts are now used in section 4.3 and 4.4 for the main body of data collection activity.

4.3 Experimental setup for machine parameter study.

The experimental design detailed in this section firstly considers the error-inducing elements observed throughout previous attempts. These sources of error are listed, together with mitigation methods under section 4.3.1.

Typically, factorial designs are set at two levels for each factor, whereby minimum and maximum levels are determined by the factor's limits. Factors operating within a finite capacity (velocity and temperature) are normally set by finding the maximum and minimum levels possible - at this stage, previous experience has shown that machine levels are not comparable to levels within the part and in some instances, the viscosity of media and bore size of the geometry prevented the machine from delivering an upper level for velocity, which had the effect of running the upper and lower level for velocity at the same value – this is overcome by calculating the projected velocity beforehand by estimating media viscosity as in 4.3.3. Factors and levels are derived based on the expectation of non-linear response – three levels are derived by what can be achieved in the part and codified into a 3^3 design.

The test order is randomised and repeated three times under 27 different combinations of factors and levels. This totals 81 runs, and must be carried out in the order listed. Measurement consists of two metrics; 1) quantifying the final roughness (as pre-process roughness is irrelevant), and 2) material removal achieved at a given location, not for the purpose of defining the radius generated, but to profile the material removal over a given length for application in simulation. As the design is fully-crossed (full factorial), it is possible to analyse each factor individually (main effects) or each interaction, whether second or third order. Samples processed in this section are measured with processes described at 4.5 and analysed with processes described at 4.6. Data is collected for the purpose of;

- Comparing, 1) hand-calculated pressure and velocity, and 2) observed pressure and velocity, to the simulated equivalent.
- Combining total processing length with the field variable as determined in the simulation, so a relationship between simulation and measured values can be formed.
- Identifying process phenomena, generating rules-of-thumb and carrying out statistical analysis.

4.3.1 Identifying and designing out main sources of error.

Mollart's AFM machine is a production machine and was built with a production mentality – cost reduction was most important and built to the customer's specification limit to fulfil the application. During the time period leading up to the start of this project, sources of process variation were recorded – natural process variation is generally caused by modern manufacturing's limited ability to deal *economically* with variation such as ambient temperature or necessity of engineering tolerances – i.e. it is typically assumed that without difficulty, a hole can be drilled to a nominal diameter ±0.2mm. Reducing natural variation in order to ensure an improvement on ±0.2mm could be achieved by ensuring material quality is consistent or that tools are centred sufficiently before running.

4.3.1.1 Experiment variables.

Figures 4.23 and 4.24 illustrate the experimental setup; the design of the surrounding fixtures is intended to allow introduction of media into the testpiece at a constant rate, constant direction and create a constant surface condition. Achieving good data for further application in simulation and comparison to hand calculations is reliant on a process that repeats output within a repeatable margin of error.

Table 4.1 – Identified variables.

Category	Machine variables	
Independent variables	Piston speed, mm/min (Velocity, m/s)	
	Temperature, ˚c (Temperature, ˚c)	
	Cycles, n	(Quantity, m)
	Stroke, mm	
Dependent variables	Average roughness (Ra, μm)	
	Edge-rounding (n/a)	Material removal (MR, mm^2)
		Peak height reduction (PHR, mm)
Control group	Tooling, supporting the testpiece	
	Testpiece geometry	
	Testpiece material	
	Media configuration	
	Measurement method	

To aid the building of numerical models, precision can be increased if sources of passive change in the system are identified and isolated – controlling them requires uneconomical adjustments to machine hardware, whereas isolation is a design process that allows the variables to remain, but in a very non-influential way. Experimentally, machine performance is assessed using repetitions, over every cell (unique combination of factors and levels).

4.3.1.2 Difficult to control variables.

Those variables identified to be difficult to control or uneconomical to constrain are listed below;

- Passive temperature increase.
  Friction, load and machine temperature control are free to affect media temperature. Factor and level selection prevent rapid increase in heat through friction and combined with testpiece bore size, the effect of work increasing temperature is reduced. Once media is homogenised, the machine is able to maintain equilibrium.
- Pre-process edge condition out of square.
  Poor tool condition or poor alignment when carrying out milling operation during testpiece manufacture can lead to a failure to produce a 90˚ edge. Square edges can be inspected on samples without damaging surface integrity. To ensure general machining accuracy, flats are machined in a single operation with automatically indexed workpiece.
- Pre-process roughness.
  Generated by a multitude of manufacturing processes, roughness is very difficult to control – it is a function of tool condition, machine vibration, machine setup and workpiece properties - representative samples can be taken every n-off manufactured, but roughness improvement is a very impractical unit to work with when considering results.
- Geometric consistency of media inlet and outlet tooling.
  Wear on media introductory tooling through erosion may affect media speed and pressure upon entry or exit. Tooling designed for testpiece processing includes a sacrificial bush to ensure replication of entry diameter into testpiece. If this is not done, the centre pipe may begin to widen, altering the media flow field.
- Machine pressure delivery.
  Rises when increased velocity is set, temperature is reduced or viscosity is increased. A common misconception is that pressure delivered is only a function of the velocity set on the machine. Pressure as a parameter is not set on the machine, and despite the reported value from the transducer frequently changing (through changing head weight and viscoelastic behaviour change), once in a stable condition, i.e. the media in a constant shear condition, the back pressure remains constant.
- Material hardness variation between samples.
  Homogeneity of testpiece caused by manufacturing process - materials are produced in a given size through extrusion or casting processes; all bars were ordered at the same point in time and belong to the same batch, representing the same properties. Materials used in 4.3 and 4.4 are from the same batch.

- Machine stroke.
  Quantity of media in the cylinder may vary, causing unpredictable stroke length. Media quantity passing through the part is controlled by the stroke length of the machine – the stroke length is controlled by a machine-based sensor which starts recording length when the pressure rises after air is bled from the system. Since the stroke length record is fixture-independent, once the machine completes a cycle (two strokes) (i.e. with a warm-up fixture), it reports a stroke length that a user can set to be the maximum, ensuring a repeatable processing length.
- Active temperature change.
  The machine possesses two large 400V heating mats and a refrigerant delivery system which chills rectangular bars over which media passes. The machine's media temperature control system is actively managed through use of sensors, and while the user sets a temperature, the working conditions determine the variance about the set nominal. Given appropriate testpiece sizing and continuous operation with the warm-up fixture to the point where the desired running temperature has been reached – the machine should run stably.
- Wear on abrasive grit.
  Operation of machine incurs workpiece-grit interaction. Initial shape of abrasive grit is controlled by the grit manufacturing process, but after mixing with carrier and applied in the AFM process, the grains become rounded and less aggressive. To mitigate, samples of grit will be taken from used media, new media, and fresh new grit from a supplier for comparison.

4.3.2 Objectives and techniques.

Previous experience in the three attempts in section 4.2 has led to clear experimental design requirements, mostly an evolution of the previous attempts.

4.3.2.1 Objectives.

The experiment must show the effects of the machine parameters on the surface of the workpiece – the critical output of this experiment is to provide empirical data that can be applied in statistical analysis and simulation software. Objectives are as follows;

- Provide method of generating predictable surface finish and radius within testpiece by varying machine parameters.
- Rank the ability of parameters to improve surface finish and radius; describe the limits of each.
- Show consideration of variables throughout system and mitigate/remove where possible.
- Generate dataset whereby every combination of parameter is assessed for radius and roughness results for application in simulation.

4.3.2.2 Techniques.

The purpose of this experiment is to provide response variable output values that can be correlated with simulated field variables, except there is a key technical block; simulation cannot accommodate the reciprocating nature of the pistons, and therefore is only a snapshot of piston motion, in one direction, at one moment in time. In order to correlate findings with simulation when processing with a given velocity and temperature, experimentation must be performed with all combinations of factor and level, realising a total of 27 unique cells, in order to identify the effect of quantity, and integrate it outside a simulation environment. Samples for all datapoints are required. For this reason, fractional factorial is neither economical nor technically feasible, but it can be acknowledged that as a tool to show estimates of main cause and effect it is very useful as shown in earlier attempts. It does not allow the construction of a reliable model, and when entering into three level designs, the response surface methodology (RSM) provides a better tool.

A three-level design is proposed to model possible curvature in the response function and to handle the case of nominal factors at 3 levels. This test order was generated by a statistical software package. It comprises a three-factor, three-level (3^3) general full factorial design with three repetitions for each run. The run order is randomised to minimise systematic error. The data collected allows formulation of a Box-Behnken (RSM) design, providing a basic predictive model, discussed in 4.6.

4.3.3 Calculation of experimental levels.

The aim in deriving factors and levels is to ensure two things; a) processing parameters are capable of being delivered by the machine, and b) the values used transfer to any other part without further significant transformation. Following principles of transferability set out in chapter 3, the values in table 4.2 are found through the calculation activities performed from 4.3.3.1 to 4.3.3.4.

Table 4.2 – Factor coding for machine parameter study.

Factors	Levels	Derived	Machine value
Velocity (V)	+1	0.325m/s	280mm/min
	0	0.230m/s	195mm/min
	-1	0.100m/s	85mm/min
Temperature (T)	+1	45°c	45°c
	0	35°c	35°c
	-1	25°c	25°c
Quantity (Q)	+1	250m	Stroke; 150mm, Cycles; 42
	0	145m	Stroke; 146mm, Cycles; 25
	-1	40m	Stroke; 144mm, Cycles; 7

4.3.3.1 Capability to deliver velocity levels.

Levels for velocity are controlled by two very limiting factors; media viscosity and testpiece internal diameter. Testpieces will need to be manufactured, and thus represent a significant material and labour cost – the media configuration is also fixed, and without significant cost, cannot be replaced for another variant. These both affect the processing parameters that the machine can deliver, most notably the piston speed (velocity). In order to ensure that the viscosity (fixed) and hydraulic diameter (value to set) imposed do not prevent the successful completion of all trials, levels are estimated as per the following calculations. Hydraulic diameter is useful for likening flow in non-circular tubes to that of circular tubes where $D_H = D$. Two semicircles are the fluid flow cross section and hydraulic diameter is calculated in equations 4.1 to 4.6.

$$A = 0.001257 – (0.014 \times 0.04) \quad (4.1)$$

$$A = 0.000697 \quad (4.2)$$

$$D_H = 4A / P \quad (4.3)$$

$$D_H = 4\ (0.000697) / (0.177664) \quad (4.4)$$

$$D_H = 0.002788 / 0.177664 \quad (4.5)$$

$$D_H = 0.015693m,\ 15.7mm \quad (4.6)$$

Where D_H is hydraulic diameter (m), A is cross section area (m^2) and P is wetted perimeter (m).

The term D_H is employed in the Hagen-Poiseuille equation for estimating the pressure drop in a long cylindrical pipe. As the entire pipe length in the experimental system has a larger D_H compared to the short length around the testpiece, the restriction is only in effect over a maximum of 14mm. The Hagen-Poiseuille equation is experimentally derived, and should only be used as a generalisation of a non-Newtonian fluid. It also assumes a constant velocity and that the flow is laminar. Density is a required term, and is estimated by weighing a known volume of media from the supplier MTT.

$$p = m / v \quad (4.7)$$

$$p = m / (\pi\ 0.142)\ x\ 0.26 \quad (4.8)$$

$$p = m / (0.06157\ x\ 0.26) \quad (4.9)$$

$$p = 25.86 / 0.016 \quad (4.10)$$

$$p = 1616.25 kg/m^3 \quad (4.11)$$

Where p is density (kg/m^3), m is mass (kg) and v is volume (m^3).

Dynamic viscosity is required by Hagen-Poiseuille to incorporate the fluid's internal resistance to flow, which is of great importance to this work – as a non-Newtonian fluid, the viscosity will change with shear condition; for this experiment, the media is placed in nine separate shear conditions as stipulated by the testpiece geometry and combinations of velocity and temperature (quantity has no effect on shear condition). Kinematic viscosity is known to be approximately 1,200,000cSt, although this changes dependent on shear condition.

$$v = \mu / p \quad (4.12)$$

$$\mu = vp \quad (4.13)$$

$$\mu = 1.2\ x\ 1616.25 \quad (4.14)$$

$$\mu = 1939.5 Pa.s \quad (4.15)$$

Where μ is dynamic viscosity (Pa.s), v is kinematic viscosity (m^2/s) and p is density (kg/m^3).

As the Hagen-Poiseuille applies only in a laminar regime, the Reynolds number must be found to determine its suitability; laminar is Re=<2000 or turbulent is Re=>3000. Reynolds number is found using Reynolds formula $Re=pVD_H/\mu$;

$$Re = pvD_H / \mu \quad (4.16)$$

$$Re = (1616.25\ x\ 0.3\ x\ 0.015693) / 1939.5 \quad (4.17)$$

$$Re = 7.609 / 1939.5 \quad (4.18)$$

$$Re = 0.003923\ (laminar) \quad (4.19)$$

Where p is density (kg/m^3), v is mean velocity (m/s), D_H is hydraulic diameter and μ is dynamic viscosity (Pa.s).

Reynolds number through the Ø0.04m tube approaching the testpiece is calculated as follows;

$$Re = pvD_H / \mu \quad (4.20)$$

$$Re = (1616.25 \times 0.3 \times 0.04) / 1939.5 \quad (4.21)$$

$$Re = 19.395 / 1939.5 \quad (4.22)$$

$$Re = 0.01 \text{ (laminar)} \quad (4.23)$$

Where p is density (kg/m^3), v is mean velocity (m/s), D_H is hydraulic diameter and μ is dynamic viscosity (Pa.s).

To determine the pressure drop incurred in the system with geometry as pictured in 4.24, the Hagen-Poiseuille is used to estimate the required pressure at machine's maximum velocity. Viscosity is generalised to 1950Pa.s and the exercise is performed twice to cater for ΔP around the testpiece (4.25 to 4.27) and ΔP through the remainder of the pipe (4.28 To 4.30). For this exercise, d=D_H.

$$\Delta P = 32\mu Lu / d^2 \quad (4.24)$$

$$\Delta P_{testpiece} = (32 \times 1950 \times 0.014 \times 0.3) / 0.015693^2 \quad (4.25)$$

$$\Delta P_{testpiece} = 262.08 / 0.000246 \quad (4.26)$$

$$\Delta P_{testpiece} = 1{,}065{,}366Pa,\ 10.65bar \quad (4.27)$$

$$\Delta P_{tube} = (32 \times 1950 \times 0.286 \times 0.3) / 0.04^2 \quad (4.28)$$

$$\Delta P_{tube} = 5353.92 / 0.0016 \quad (4.29)$$

$$\Delta P_{tube} = 3{,}346{,}200Pa,\ 33.46bar \quad (4.30)$$

Where ΔP is difference in pressure (Pa), μ is dynamic viscosity (Pa.s), L is the length of the pipe (m), u is mean velocity (m/s) and d is the pipe diameter (m).

While it may seem coincidental that the combined loss through tube and testpiece total the effective maximum capacity of the machine of 45bar (33.46+10.65), the viscosity of media was back calculated using the geometry and velocity. The media was set to 25˚c and velocity in the part estimated to be at ~0.3m/s through a transformation described in 4.3.3.2. These conditions placed the maximum stress on the hydraulic system and provided the experiment with top levels through which lower and median levels could be selected.

4.3.3.2 Transfer of velocity levels.

The machine's graphical user interface (GUI) requires piston speed input in mm/min, relative to the machine piston head. Where part geometry and media viscosity permit the machine to deliver the requested piston speed (velocity), and is not throttled by lack of machine pumping capacity (potential for this ruled out through velocity level

selection in 4.3.3.1), the velocity in simple geometry (such as a tube) can be calculated using cross sectional area (CSA). Below are set m/s levels for the piston speed factor. In order to effect a set velocity in the part in mm/min, the following approach is used;

Table 4.3 – Piston to testpiece velocity transfer.

	-1	**0**	**+1**
Desired part velocity (m/s)	**0.100**	**0.230**	**0.325**
Part internal diameter (m)	0.04	0.04	0.04
D40 CSA (m^2)	0.001257	0.001257	0.001257
Part obstruction area (0.014x0.040) (m^2)	0.00056	0.00056	0.00056
Part final CSA (m^2)	0.0006963	0.0006963	0.0006963
Machine piston diameter (m)	0.25	0.25	0.25
M/C CSA (m^2)	0.049	0.049	0.049
Ratio between part and m/c	70:1	70:1	70:1
Piston speed velocity (m/s)	0.001417	0.00325	0.004667
Conversion m/min (x60) (m/min)	0.085	0.195	0.280
Conversion mm/min (x1000) (mm/min)	**85**	**195**	**280**

Assuming the velocity at the tip of the testpiece (point C3, figure 4.4) is the desired area where geometry should be controlled, table 4.3 is organised into three groups of rows – as cross section area (CSA) is the driver for velocity change, the top group determines the area of the cross section about point C3. The second group establishes the equivalent figure for the machine CSA, while the third calculates the ratio; 70:1 means that velocity about point C3 is 70 times greater than at the piston face.

4.3.3.3 Capability of quantity levels.

Quantity of processing allows the effects of temperature, velocity and media configuration to manifest themselves on the surface of the workpiece – without prior knowledge, it is difficult to estimate how much processing is required, but experimentally, it must be ensured that sufficient metres are applied to allow the process to take effect to a suitable extent. Using experiment tooling and sacrificial testpieces, levels are set based on best practice for the harshest material removal conditions – high velocity (280mm/min) and low temperature (25˚c).

Delivery of a particular quantity of media over a set duration has little physical requirement of the machine; the only minor consideration is the build-up of hydraulic oil temperature after a period of sustained load. The effects of this raise the overall temperature of the piston motion system and place greater demand on the machine's cooling system; although this is detached from affecting the media temperature, the machine has a hydraulic oil temperature sensor that can automatically shut down the machine in the event of excessive load. Risk of excessive load has been all but eliminated following the calculations in 4.3.3.1. Table 4.4 shows the iterative process

used to reach an appropriate set of quantity levels – the ‘cum.’ Column lists the total metres and number of cycles used to reach the level of edge-rounding desired by the researcher and Mollart. The process is concluded once 250m is reached and a 1.5mm radius is estimated by a sight-based radius gauge.

Table 4.4 – Iterative processing to determine quantity levels.

Run	m/c V	T	Q	Str.	Cyc.	Cum.	Comments
n	mm/min	˚c	m	m	n	Q/Cyc.	
1	85	35	5	0.15	1	5/1	Removed sharp edge from milling operation. No rounding.
2	280	35	35	0.15	6	40/7	Minor rad evident, <0.5mm, machining marks gone.
3	280	35	35	0.15	6	75/13	Increased rad, ~0.5mm.
4	280	35	35	0.15	6	110/19	Further increased, <0.75mm.
5	280	35	35	0.15	6	145/25	Approx. 1-1.25mm.
6	280	35	35	0.15	6	180/31	Roughly 0.25mm improvement.
7	280	35	70	0.15	12	250/43	Minor improvement over last run.

4.3.3.4 Transferability of quantity levels.

In the production environment, media quantity available for a job may vary and part volume will vary; in order to ensure any single point within any arbitrary geometry is worked with the same quantity (not at the same speed) of abrasive grit, the approach below must be used to determine a new metric; ‘metres of media’. This is not to be confused with velocity effects – within any part, the media can travel at a variety of different velocities, although the distance travelled is an entirely separate metric.

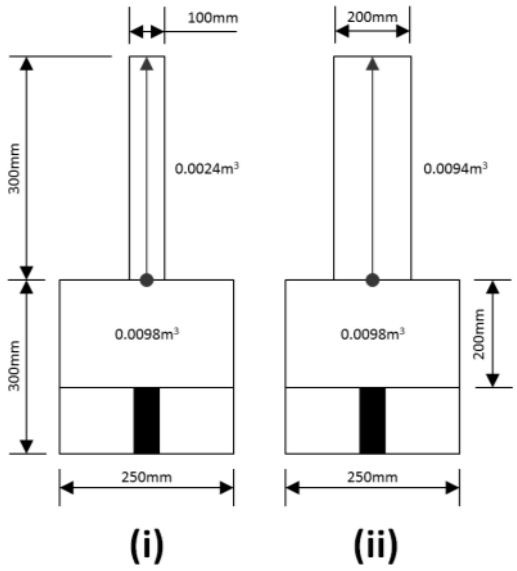

Figure 4.6 – Example media volume against part volume. Demonstrates quantity of surface processed.

Referring to figure 4.6, system ‘i’ on the left takes a part of volume 0.0024m^3, while system ‘ii’ on the right assumes a part volume of 0.0094m^3. Media volume for both systems is 0.0098m^3. In order to ensure cycles and stroke are set to deliver a number of ‘metres of media’ over any single point of interest, it is assumed that grit is uniformly dispersed. It is necessary for the operator to determine the machine’s stroke using the GUI and to determine the part internal volume, by way of a solid modelling program, or by hand where complexity allows. Table 4.5 offers an example of the difference that part volume makes to the quantity of processing on a surface.

Table 4.5 – Example quantity conversion.

	System (i)	System (ii)	Comments
Media volume / part volume	0.0098 / 0.0024	0.0098 / 0.0094	
1 stroke (exchange) equal to	4.08333	1.043	exchanges of media in part
1 stroke	200mm	200mm	
1 cycle	2 strokes	2 strokes	
1 cycle	400mm	400mm	
Total stroke x exchanges	400 x 4.08333	400 x 1.043	
Processed length	1633mm	417mm	after one cycle

Therefore, a method is required to set the stroke and cycles for equal processing where two points of interest (POI) in parts of differing volume are presented. Table 4.6 assumes a desired processing length of 5m.

Table 4.6 – Processing quantity

	System (i)	System (ii)	Comments
Desired processing length	5000mm	5000mm	At POI
Max available stroke	200mm	200mm	
Media volume / part volume	0.0098 / 0.0024	0.0098 / 0.0094	
1 stroke (exchange) equal to	4.08333	1.043	exchanges of media in part
Length / exchanges	1225		(A)
(A) / (max avail. stroke x 2)	1225 / (200 x 2)	4794 / (200 x 2)	
Number of cycles	3	12	to do equal POI processing

In this experiment, the geometry will always remain the same – however, the media volume may change, depending on losses when reclaiming media. The method proposed allows the user to maintain the consistency of the ‘metres of media’ unit irrespective of available media volume. Current media levels allow the experiment to guarantee that 150mm can be delivered per stroke (artificially capped to ensure media delivery is consistent) - this corresponds to total processing as in table 4.7.

Table 4.7 – Total quantity conversion.			
	-1 system	0 system	+1 system
Desired part processed length	40m	145m	250m
Media volume / part volume	$0.0074m^3$ / $0.000373m^3$	$0.0074m^3$ / $0.000373m^3$	$0.0074m^3$ / $0.000373m^3$
Ratio of media:part volume	19.84	19.84	19.84
Total m/c travel required	2.016m	7.308m	12.6m
Stroke available on machine	0.15m	0.15m	0.15m
Total stroke per cycle (x2)	0.3m	0.3m	0.3m
Exact no. cycles required	6.72 (7)	24.36 (25)	42. 00 (42)
Total m/c req. / rounded cyc.	2.016m / 7 = 0.288m	7.308 / 25 = 0.292m	12.6 / 42 = 0.3m
Divided by 2 for stroke	0.144m	0.146m	0.15m
Final settings	Stroke 144mm, Cycles 7	Stroke 146mm, Cycles 25	Stroke 150mm, Cycles 42

4.3.4 Key issues.

This experiment plan is the fourth evolution of previous geometrically and physically incapable designs. Every experimental design is a compromise, whether that be in the number of factors studied, the limits of a potentially infinite process space or the accuracy of the levels delivered. Most of these concerns are addressed, as is the future application of the data, with particular effort placed in ensuring transferability.

Table 4.8 – Processing time estimate.					
Run	Order	Velocity	Quantity	Minutes	Hours
#	*#*	*m/min (m/c)*	*m (m/c)*	*#*	*#*
1	29	0.085	7.3	85	1.4
2	70	0.195	2	10.3	0.2
…	…	…	…	…	…
81	37	0.195	2	10.3	0.2
			Total	4038min	67h 20m

To calculate processing time, an excel spreadsheet was assembled to estimate the entire run-time. Working on 8/hrs day, 40hrs/week and 175hrs/month, the total run time is 67.3hrs – this excludes the significant time saving made by running the longer duration trials overnight, overtime and Saturday hours. Processing should be completed within 7-10days.

4.4 Experimental setup for media parameter study.

Limited understanding is held over the effects of abrasive media/slurry on the surface of the workpiece – the media is comprised of two phases; the first is a highly viscous liquid (semi-solid carrier/putty/polymer), which is known to exhibit non-Newtonian rheological properties, and a second solid phase of abrasive grit in various sizes. The problem is multi-faceted, requiring rheological characterisation of the current product, an economical manufacturing method for a new product, sourcing of suppliers and mixing equipment and a similar factor and level decision-making process to that of section 4.3.

4.4.1 Overview.

Media availability is only through one source - commercially, Mollart are restricted to purchasing media from a Germany-based supplier at a cost of approximately ~£4300/25kg. The supplier is 'Micro Technica Technologies GmBH' (MTT) (also the machine manufacturer) and it is in their interests to keep their media manufacturing method out of the public domain; as such, Mollart have little more than codified product numbers and material safety data sheets to provide information on how the media is produced.

As the only company that Mollart is aware of producing the substance on a commercial basis, Mollart are beholden upon MTT for trialling different configurations, which is a real limitation in developing and understanding the process. To date, Mollart have only seen fit to purchase ~8 containers, one configuration was purchased with (relative) high viscosity and large grit - purportedly ideal for material removal and edge rounding (media used in 4.3 experiment). A second configuration was also purchased, of lower viscosity and smaller grit, although still for the same purpose, but in smaller diameter bores. Media reverse engineering is necessary due for two reasons - for subcontract purposes when the project is over and for ensuring that a number of configurations are tested to provide data for reapplication.

Academic literature has been collected on the topic of media manufacture as presented in chapter two. While several principles can be derived through cross-referencing articles, there are two major problems with the literature; 1) the entire machine configuration is not explicitly disclosed so the reader is left without the ability to repeat the work based on replication of the machine-media-geometry triangle, and 2) pre-process condition of researcher's workpieces are not fully characterised - it is common to use 'wire electro discharge machining' (WEDM) to machine samples, which produces a rough surface (conducive to AFM producing a large improvement), but also a hardened, brittle surface (occurring through heat affected zone (HAZ), also known as re-cast layer or white layer), which increases AFM process capability more so. While data can be gleamed from these setups to formulate generic statements about process behaviour when changing a single parameter, unfortunately they do not provide

information which can be applied in an industrial scenario. Several elements of the test systems are not applicable to industrial challenges, such as developing parts of process models without due regard to material selection, description of impingement angles, exact media formulation or the most critical element - total processing and velocity at the point of interest (POI) which varies for every machine and testpiece setup.

Within the media, variables are as numerous as in the other two corners of the AFM triangle, but aside from the incomplete and unrepeatable academic literature, several key principles may still be drawn, such as increased grain fraction will increase bulk viscosity and in turn, will increase material removal rate (MRR). It is also known that larger grit sizes will deliver an ultimately poorer finish than smaller grits, while achieving greater MRR. Carrier viscosity has a relationship with MRR by providing additional support to the grit. The overarching problem is with the lack of information on relationships between media variables, and how they can be quantified to aid prediction models. The research question that must be posed is, "if all else is equal, and <insert media variable here> is increased/decreased, what will the surface finish and edge geometry results be?".

4.4.2 Research interests.

This element of the project is important for determining the effects of the media parameters - without it, future work assumes Mollart (or its customers) have only a single configuration of media, which may be ideal for processing a specific part and achieving a particular finished condition, but will also severely restrict the flexibility of the machine, system and process. The ability to predict the final surface condition with a given machine and geometry environment is critical to making the process industrially viable. Several schools of thought exist about media behaviour and its interaction with the surface - these are developed by general assumptions of fluid behaviour and (more useful) existing knowledge of the traditional grinding process which utilise grit of similar size in a more rigid matrix. The experiment, once complete, must provide a broad range of 'rule-of-thumb' knowledge, charting of two-factor interactions, contour plots and response surface plots. A predictive equation must also be developed, although the usefulness is limited due to relevance only to fixed machine and geometry levels.

Traditionally, the mesh size of the abrasive is steadily reduced to achieve a better finish, however, AFM's semisolid grit delivery system is unlike other abrasive machining processes – this section must gain data to establish the relationship between grit size and surface condition. The size of the cutting edge in the media is inexorably linked to three explanatory variables – academic literature has shown less MR can be expected with smaller mesh size grits and vice versa. These statements are generally considered true in any grinding discipline – this work is interested in quantifying their effects - it is not enough to simply say, "increase grit size for greater edge-rounding" - it is critical to

develop the relationship between machine parameters and media parameters using simulation, hand-calculated conditions and simpler erosion metrics.

A theory exists that a less viscous carrier is more inclined to conform to complex geometry than a more viscous carrier. While the experimental setup occludes finish uniformity data, the establishment of machine parameter effects (as presented in section 4.6) has determined the effects of velocity, temperature and quantity on surface finish. With this in mind, one could state for certain that surface finish is controlled by machine-based forces (velocity, strain, pressure, etc) (also quantified), and combined with simulated confirmation of viscosity behaviour, results of simulated flowpath and actual roughness can be compared to a number of other POIs in simulated geometry. While precise surface finish over complex geometry is less important in Mollart's main business, there is demand for it within mould & die, medical and aerospace industries. Where this does help Mollart (and is sector indiscriminate) is in the prevention of material removal across points/surfaces in a part where that feature should be left unprocessed.

Relationships between grain fraction, material removal and viscosity hold the potential to control finish uniformity and conformity, particularly in small holes. When discussing viscosity, four metrics are used to describe the factor; 1) base polymer viscosity, 2) modifier percentage, 3) carrier viscosity, and 4) bulk viscosity. Media is comprised of grit and polymeric carrier - the carrier is formed of a base polymer which is mixed with a modifier to set desirable properties. Carrier is mixed with grit to form the media to be used in the machine - the carrier:grit ratio is referred to as the grain fraction, and provides a bulk viscosity, which differs in viscosity to the carrier alone due to the increased proportion of solid phase material. In use, the geometry of the workpiece will affect local stresses within the media which, as a non-Newtonian fluid, will effect a local change of viscosity - this is exacerbated by repeated working of the media (as AFM is a cyclical process) which generates thermal energy through viscous heating. While the factors affecting viscosity appear complex, complete control over viscosity is held by the operator by configuring media as appropriate. Potential to gain greater control exists through selection of high specific heat carrier constituents, requiring more energy to heat the carrier, resulting in more stable chemical behaviour. In terms of research interests, the grain fraction factor will allow this experiment to analyse and quantify the effect of increased volume of grit, whilst viscosities will be known for each of variant of media by the modifier percentage and its different stages of assembly.

For the three factors under scrutiny (percentage modifier, grit size and grain fraction), performance will be gauged against surface average roughness (Ra), material removal (MR) and peak height reduction (PHR). Performance for the range of levels tested (three levels) will vary - an absolute limit may exist, or returns may diminish. In any case, the limits of the factor coupled with their associated finishing and material removal abilities will prove useful in Mollart's subcontract plans. The choice of

experimental design and knowledge of the process determines the confidence that the researcher has in extrapolation of results – where this experimental design differs from that of section 4.3 is in the nature of the parameters – in this design, factors have hard limits which remain intact, irrespective of geometry and machine parameters. The grit sizes are limited in terms of commercial availability and the grain fraction and modifier percentage are limited in terms of media stability and desirable behaviour – this was not the case previously, where parameters such as velocity and quantity could be extended or reduced ad-infinitum by altering test geometry.

4.4.3 Media manufacture.

This section contains input from a subcontractor, but it should be stressed that their work is necessary on a skills, cost, timeframe and access-to-equipment basis (in disciplines abstract to the author of this thesis), rather than knowledge-generation. At all stages, they were guided, critiqued, questioned and pushed by the author of this thesis, frequently extending to visitation, performing research related to their goals, completing their work and altering/approving their methodologies. To summarise, their contribution/input (to which no claim is made by the author of this thesis) is the selection of a base polymer and identification of a modifying agent. The subcontractor is referenced where appropriate.

A third-party subcontractor specialising in chemical analysis techniques have been instructed to work in collaboration with Mollart and the TSB funding, by participating in two phases of work; the first phase describes the viscosity of the media under different strain rates and temperatures. It also looks at the constituent parts of the product and analyses the grit size numerically and the grit shape by-eye. The second phase was to create a viable production-ready method of manufacturing the media for the purposes of analysis through experimentation and for the planned production service. They produced two small 120mL containers of polymer alone and grit suspended in polymer. Their reports are available in the appendices, although the major points concerning production are discussed below.

4.4.3.1 Abrasive grit – materials, volume and size.

Variables within the grit include its size, the material, the fraction of secondary grits, their size, distribution of sizes within the total grain fraction and the shape. Several principles of the grit choice have been carried from the experience-derived levels in MTT products – for example, all MTT media issued to Mollart for work in Titanium, Inconel and Stainless Steels is comprised of Boron Nitride material – amongst the materials MTT offer, Boron Nitride is the hardest grit available bar diamond, and logic dictates that softer material will reduce effective material removal, one of the

experimental response variables. Therefore, grit material is fixed to boron carbide for the entirety of the media parameter study, as it was in the machine parameter study.

To ensure grit shape and size distribution are common between manufacturers, and thus, cater for eventualities such as supplier business failure, disputes or natural disaster, Mollart obtained grit from one unknown source and two known sources – some F80 (see appendix for reference sizes) left behind by MTT after a service visit, several sizes from Washington Mills (USA) and several from ABSCO (China). Escubed carried out some SEM work on the samples using a Malvern Mastersizer 2000 for the size distribution and a Zeiss Evo MA15 scanning electron microscope for visual shape comparison and further shape and size assessment (found in Escubed reports in appendices). One interesting finding was that both manufacturers were oversize on the FEPA specifications, although by a similar amount for each grade. Their shapes are virtually identical, signalling a similar manufacturing process in use (see figure 4.7).

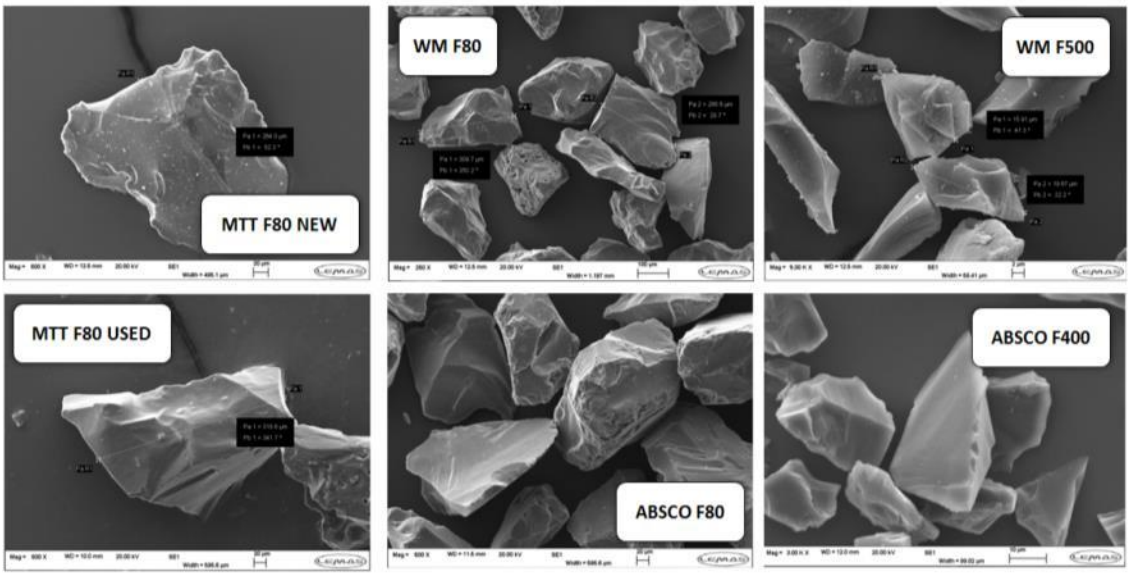

Figure 4.7 – Supplier comparison of B_4C microgrits.

4.4.3.2 Polymer – rheology, availability, modifiability.

Polymer and modifier combinations are numerous, and literature (inclusive of patents) has shown multiple successful compounds – the concern in this project is to gain a product of similar behaviour to the MTT product, but without carrying out chemical reactions in its manufacture due to the undesirable health and safety consequences of working with volatile materials. Modification with a secondary chemical was known to be possible following a service visit by MTT where they added an unknown gel to soften the media – gels are discussed in the literature. Challenges in development of the product are 1) the sourcing of a non-Newtonian silicone polymer that lends itself to modification, 2) ability to support a solid grit phase, uniformly dispersed, 3) ensuring ability to work at high temperature (<70˚c) without producing dangerous gases, 4) using

a cold-working manufacturing process, negating the need to operate ovens, work with chemical precursors and synthesis techniques. The final polymer selected was supplied to Escubed by Mollart prior to Escubed commencing work, following research resulting from this project – the Dow Corning 3179 dilatant compound rests at a total viscosity of 11,400Pa.s, an exceptionally high starting viscosity. This value means that mixing with a modifying agent may be awkward – a high-viscosity mixer is required. Figure 4.8 illustrates the position of the base polymer in the system.

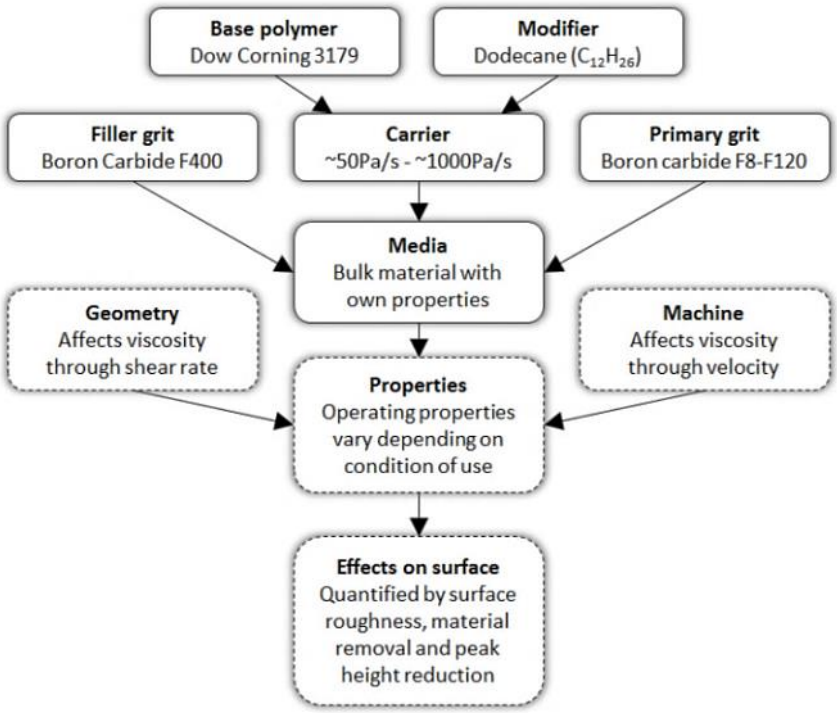

Figure 4.8 – Media construction and factors affecting static and dynamic properties.

DOW CORNING(R) 3179 DILATANT COMPOUND

9. PHYSICAL AND CHEMICAL PROPERTIES

SAFETY DATA SHEET
According to article 31 and Annex II of the EU REACH Regulation

Version: 1.4
Revision Date: 13.04.2012
Superseded date: 30.01.2008

DOW CORNING

Form	:	Viscous Liquid
Colour	:	Pink
Odour	:	None
Boiling point/range	:	> 100 °C
Flash point	:	> 93.8 °C (Closed Cup)
Explosive properties	:	No Vapours may form explosive mixtures with air.
Specific Gravity	:	1.14
Viscosity	:	10000000 cSt at 25°C.
Oxidizing properties	:	No

Figure 4.9 – Data from Dow Corning 3179 dilatant compound MSDS.

4.4.3.3 Modifier – identification, miscibility.

Initial hopes for controlling viscosity rested with the purchase of off-the-shelf silicone polymers of varying viscosities – however, following research into potential suppliers and products, it was found that none were of the consistency of putty and none were non-Newtonian in behaviour. This led to the assumption that the oil samples collected from the top of the MTT product were playing a part in the final behaviour of the product, and that a base polymer with desired behaviour would need to be modified from a greater to lesser viscosity. Escubed identified through a fourth-party GCMS (gas-chromatography mass spectrometry) subcontractor that mixed hydrocarbons were in the oil, however the dominant one was 'dodecane' ($C_{12}H_{26}$). After hand mixing trials, small samples (200mL) were shown to be stable, rheologically very similar and after a period of relaxation it was found that the properties were retained. By hand, the samples were mixed with 3179 compound and the oil used as a diluent. The identification of dodecane is shown in Escubed's stage one report, in the appendix.

Figure 4.10 – Samples of media (L) and carrier (R) provided by Escubed.

4.4.3.4 Lab-scale mixing results.

Test samples have been made by hand, and their rheological behaviour analysed in terms of viscosity against strain rate – this data is required in order to begin profiling an electronic version of the media – only rheological behaviour is necessary as the study aims to divorce the carrier from the grit content. These small scale examples provide the first evidence that using Dow Corning 3179 modified with dodecane can provide rheological properties similar to that of MTT's product. The samples show terminal viscosities – between 30% and 40% concentration of modifier, each additional 5% reduces the polymer by 500Pa.s, except this does not extend to the increased oil content of 47.5%. It has been previously discussed between Mollart and MTT that small

samples are not always representative of a larger body of media – the increase in viscosity without addition of grit strengthens this viewpoint. The figures below show the viscosity reduction with increased modifier percentage – starting with figure 4.11 at 4000Pa.s, the viscosity reaches 1500Pa.s and stabilises. The stress curve allows the operator to gauge where the fluid may start to flow under its own weight.

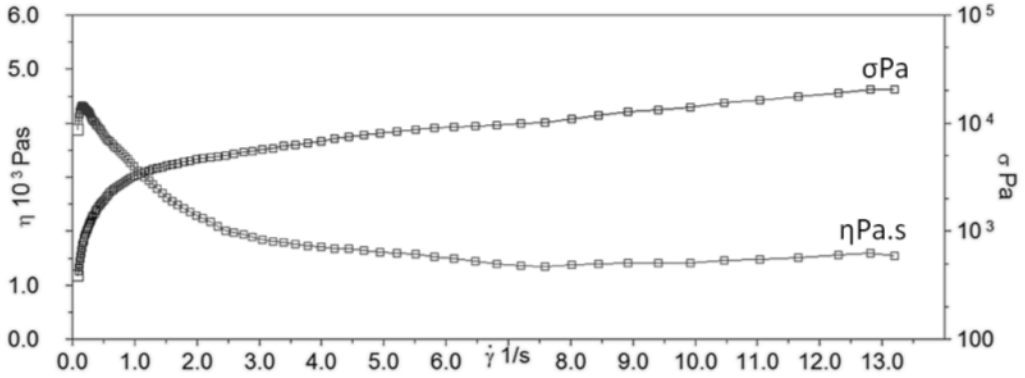

Figure 4.11 – Flow curve of 3179 modified 30% by weight at 25˚c.

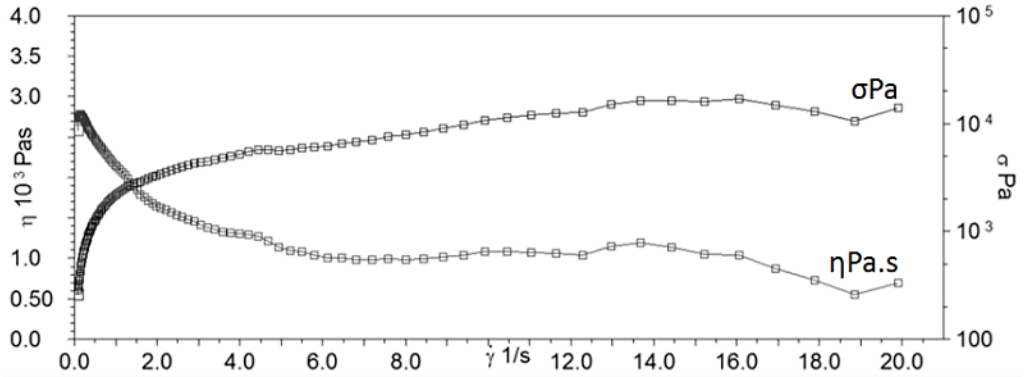

Figure 4.12 – Flow curve of 3179 modified 35% by weight at 25˚c.

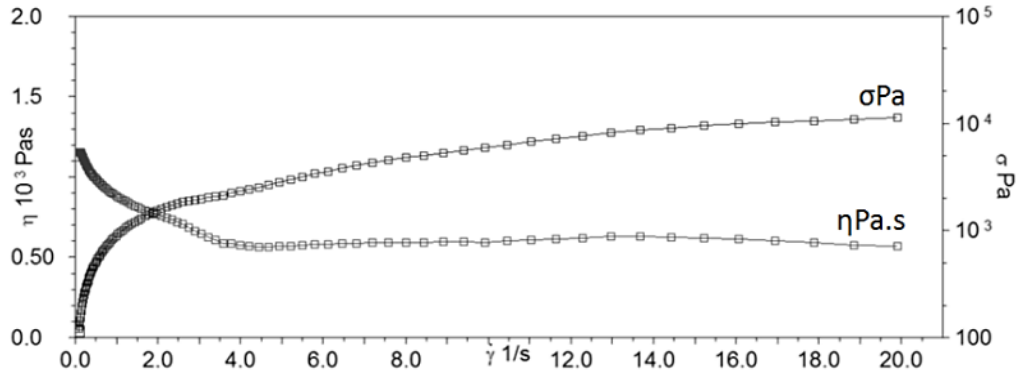

Figure 4.13 – Flow curve of 3179 modified 39% by weight at 25˚c.

Looking at the viscosity (dynamic, η) curve of figure 4.12, a starting viscosity of 2750Pa.s is recorded, tapering down to 1000Pa.s. This places a theoretical Mollart 'M35' carrier squarely within the behaviour of MTT's MF20 media. So far, there is no dilatant (shear thickening) response. Referring to figure 4.13, starting viscosity of 1200Pa.s is recorded, tapering down to 500Pa.s. This places a Mollart 'M39' carrier squarely within behaviour of MTT's MF10 media, which is unexpected given the more viscous to-the-touch feel of the product. There is a slow dilatant response from $4s^{-1}$.

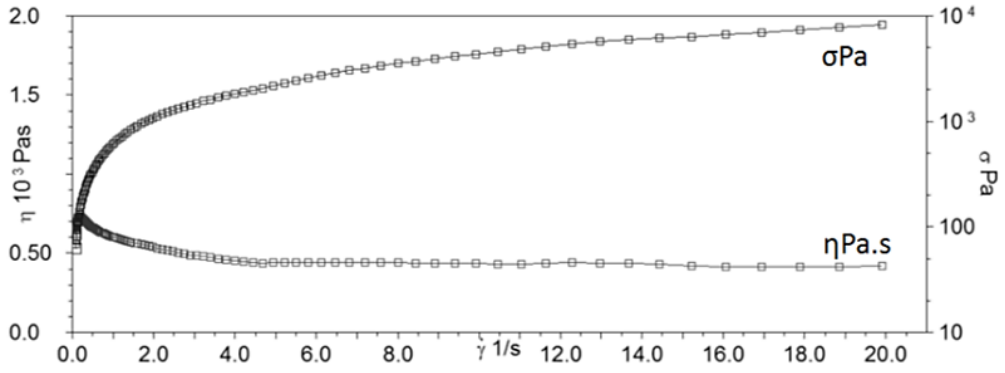

Figure 4.14 – Flow curve of 3179 modified 47.5% by weight at 25˚c.

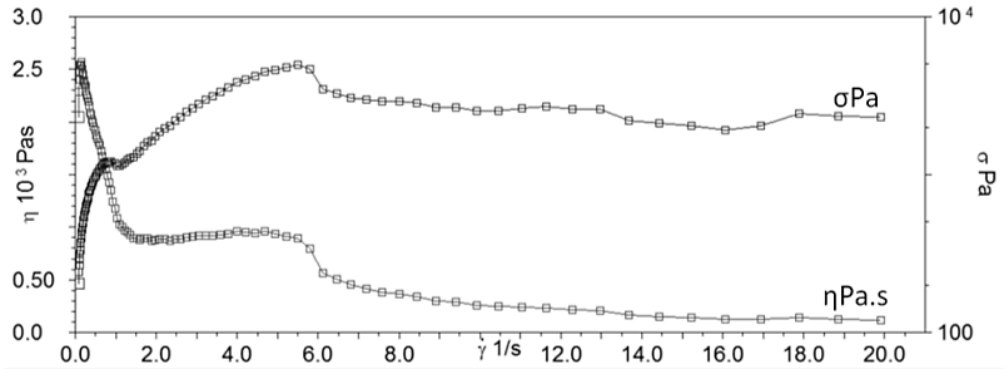

Figure 4.15 – Flow curve of 3179 modified 47.5% by weight at 25˚c, including 50% by weight of grit.

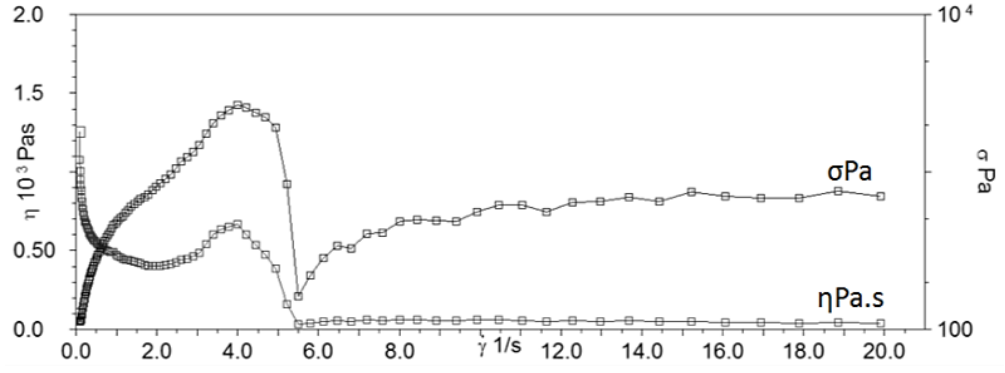

Figure 4.16 – Flow curve of MTT MF10-based media, at 25˚c.

Figure 4.14 starts at 700Pa.s and tapers down to 400Pa.s. There is a slow dilatant response from $4s^{-1}$, whereas the change with figure 4.15 is significant, and can be attributed to the addition of grit - a starting viscosity of 2500Pa.s is recorded, tapering down to 900Pa.s. This example shows a response more typical of the MTT 'with grit' samples. Grit content appears to strengthen the shear thickening response, and the measurement is lost at $6s^{-1}$, as is the case with other 'with grit' samples. For comparison, figures 4.35, 4.36 and 4.37 characterise the behaviour of MTT's MF10 sample, at three different temperatures – the temperatures used in the machine parameter study. The shape is comparable, and ultimately, the Mollart-manufactured media offers greater flexibility than MTT's product through academic study.

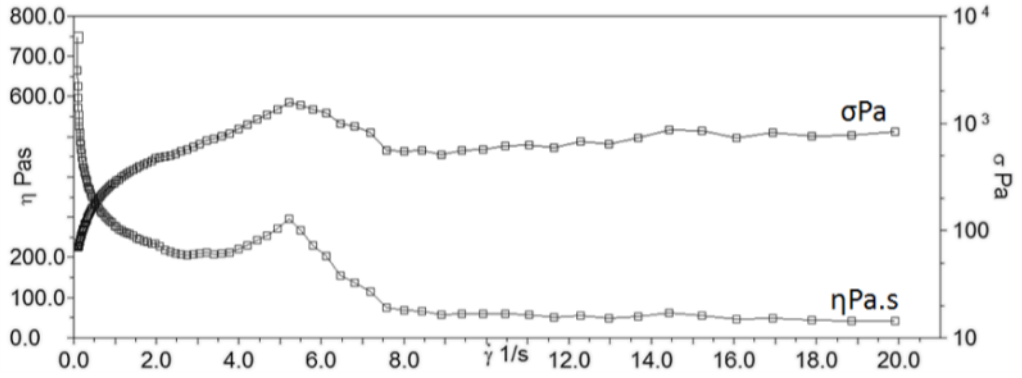

Figure 4.17 – Flow curve of MTT MF10-based media, at 35˚c.

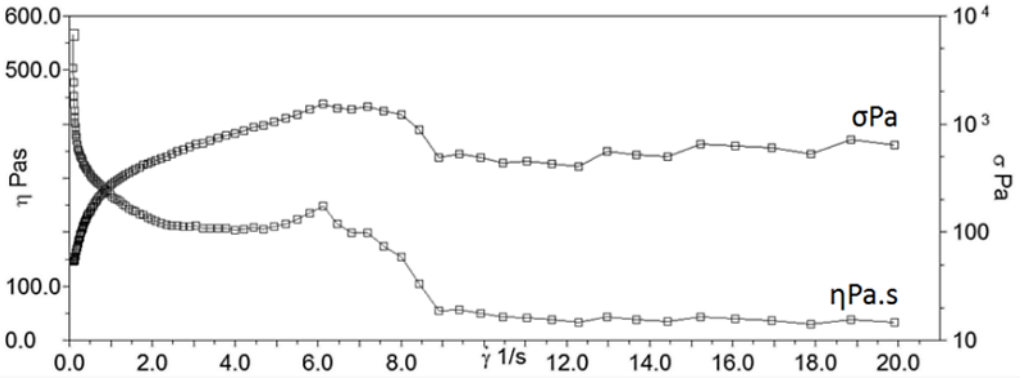

Figure 4.18 – Flow curve of MTT MF10-based media, at 45˚c.

4.4.3.5 Production-scale mixing results.

A day was spent at Winkworth Machinery in Reading, Berkshire. The company manufactures the 'Z-blade' mixer and offers a hire service required to remain within the TSB's project budget. Several key tasks were proposed for the day to ensure that the mixer was an appropriate tool and that experimental levels were appropriate. Aims of the visit were to 1) determine capability of the mixer to mix HV silicone polymer, 2)

check that Escubed's lab samples were scalable and 3) to check the stability limit of dodecane addition.

There are two options to aid the mixing process with this type of machine. The first is to fill the drum with ingredients, covering the blades and starting the mixer; the second option is to drip feed the ingredients and build up the volume slowly. The researcher started with the latter option and found the polymer and oil to mould themselves to the cavity on each blade – this was directly due to a lack of material in the drum. After adding a greater volume of polymer, the mixture began to homogenise and work itself through the two blades consistently. The mixer is therefore suitable to mix the highly-viscous base polymer with zero modifier percentage and achieves homogeneity within approximately 8 minutes of addition of modifier.

Figure 4.19 – Mixing activity illustration.

Fortunately, the viscosity of 3179 will reduce with temperature, and 10% of dodecane reduces viscosity to a more manageable level. The Z-blade has an optional heating jacket to reduce the 3179's viscosity to a level where it mixes easier with the rheologically distinct dodecane. While the behaviour of Escubed's hand-kneaded samples certainly appears to be comparable to the touch and the rheology almost identical in behaviour, there was doubt over whether a 120mL sample could be manufactured in a production-useful quantity. The drum in the research machine at Winkworth is 11L in capacity – through oil addition, a batch of 7.5L was made whereby the grit was added to the mixer after polymer had reached the desired condition. The resultant mixture (see figure 4.19) was extremely similar to MTT's product, in the shear thickening aspect (brittle fracture), colour, consistency and ability to peel away from a surface with no residue or material left behind. Escubed's method is certainly scalable.

The modifying agent dodecane is used to reduce the resting viscosity of the 3179 compound. The samples provided by Escubed without grit contain 50%wt of dodecane, and it was considered to be relatively soft. The sample including grit was noticeably more viscous. To ensure the viscosity limit was not a 'hard-limit' and that the dodecane

could saturate in the 3179 at a higher percentage, a simple strategy was employed during the trial. Throughout the mixing process, the intention was to add ingredients to achieve a 70% MP. This was achieved until 60% was reached where the media was increasingly soft, softer than the MF20 product of MTT's. The decision was taken to add grit to the 60% MP, knowing that additional oil content could be added in case of a severe thickening effect. There was no severe thickening, and a 50% GF (grain fraction) was put together, which remained on the softer side of the MF20 product. The MP level of 70% is now known to be excessive and MP levels will be revised to 60%, 50% and 40%.

Figure 4.20 – Biro pen reflected in blade of mixer following mixing process.

4.4.3.6 Naming convention and handling.

Using the media as designed above for experimentation requires naming schemes, costing, manufacturing requirements and quantities. Main considerations at this point are to ensure that enough of the product is produced in each batch. The machine contains a Ø250mm cylinder at 300mm long, including the extended length around the heating and cooling fixture. Without the heating and cooling fixture, cylinder volume is $0.01473m^3$ (14.73L), and including the fixture, a capacity of $0.01964m^3$ (19.64L). Average density of the product is ~$1700kg/m^3$, varying dependent on the grain fraction and modifier percentage, translating to approximately 19L/25kg. Manufacturing quantities will need to allow the machine stroke length ability of >200mm for comparable results with the machine parameter study, translating to a batch size of 19.5L each.

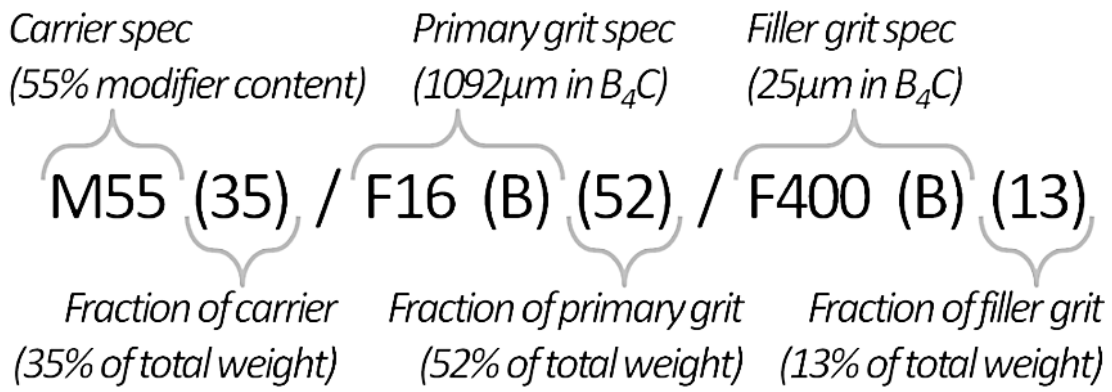

Figure 4.21 – Media naming convention.

A media naming convention has been devised to describe each batch, following a similar style to MTT's, although with some simplification. Figure 4.21 displays the method. There are 3 individual components split by forward slashes. The first is the carrier specification (M55 is 55% modifier percentage), the second is the primary grit (F16(B) is FEPA standard F16 grit in boron carbide material) and third is the filler grit (F400(B) is FEPA standard F400 grit in boron carbide material). The numbers in brackets denote the percentage by weight of each element within the batch, i.e. for the example in figure 4.21, a 10kg batch would contain 3.5kg carrier (35%), 5.2kg primary grit and 1.3kg filler grit. This system allows the calculation of grain fraction (add the grit elements together) (65%) and the 80/20 split between primary (100/65*52=80%) and filler (100/65*13=20%).

4.4.4 Objectives and techniques.

Instead of developing a mammoth 3^{40} full factorial experiment, careful planning and pre-testing has brought the variable count down to three within this sub-experiment, justification for which is provided later. In the machine parameter study, the levels selection was driven by the requirement to operate the machine within the machine's pressure limit, thereby ensuring that each level was attainable in the test system. In the media parameter study, the factors are not affected by in-process control, meaning their levels are set before the experiment begins and remain as such throughout. Factors and levels are derived based on the expectation of non-linear response – three levels are derived by the MTT media benchmark (using it as a guide), as opposed to simple selection of physical media component limits. A key factor in this experiment that was of no concern previously is the number of experiments. Assuming the three levels of each media factor as a bare minimum for experimental design selection, we must give consideration to the number of factors and the relationship between number of runs and resultant requirement for 25kg media batches.

4.4.4.1 Objectives for media parameter study.

Output from this experiment is designed to be used for providing a method of generating repeatable and predictable surface finish and edge-rounding within the same design of titanium 6Al4V testpiece by varying media parameters. A ranked list of parameters' ability to improve surface finish and edge-rounding is also required, describing the limits for each. Given the errors noted in the last experiment, the media parameter study should show consideration of variables throughout the system and mitigate/remove where possible. For the purposes of simulation, the samples used in the experiment must cover full factorial data points, but in consideration of economic constraints, the experiment must use repetition to ensure good model accuracy, so that untested remaining full factorial data points can be predicted.

4.4.4.2 Experimental design-type critique.

In order to describe the impact of each media factor on the surface of the testpiece, a methodology that addresses the factors across the entire process space must be considered, but one that does not incur an uneconomical number of runs. The design must also provide the required rule of thumb data, consider its own internal error, provide a robust predictive model and ideally offer a route for extension of the study.

Table 4.9 – Experimental design types.

Type	Subgroup	Use	Positive	Negative	Rank
Factorial design	2-level factorial	Estimating main effects and interactions	Economical	Insufficient levels	5
Factorial design	Taguchi OA	As a 'fraction' of a full factorial design	Estimation of main effects	No interactions or effects magnitude	4
Factorial design	General factorial	All possible combinations of factors	Fully crossed	Number of runs	3
Response surface	Central Composite	Good description of edge of process space, less efficient than BB for 2-way interactions	Better (although linear) estimates outside process space	Inefficient vs. Box-Behnken <4 factors	2
Response surface	Box-Behnken	Estimation of quadratic effects, where 2-way interactions are needed	Fewer runs than 3k full factorial, rotatable	Requires multiple centre points for improved accuracy	1

The Box Behnken design is most appropriate, however in standard form, only contains a single point at the edges. It is prudent to add additional edge- and centre-points into the design, which should provide a greater degree of accuracy with a minimised number of

runs. In the standard form, only the centroid provides the error estimation – by averaging repetitions at the edge-points increases experimental cost, but also increases validity. In comparison to the machine parameter study, the Box-Behnken design was completed as an adjunct to the full factorial experiment – something that was chosen to ensure all process points were covered and measured values had been collected so that correlation to simulations could be established. In this study, attempts to minimise the number of media batches have led to an experiment design that does not cover all possible combinations – this means that certain combinations will be missing when attempting to correlate response values with simulated-equivalent values. The technique will now require the prediction of the missing points using the response surface model, and a brief verification activity will follow to prove the accuracy. The final result will be a complete 3^3 structure full factorial table which would normally have required 27 media configurations, instead of the 13 in the Box-Behnken design.

Whereas the machine parameter study looked at the machine actions and how it affected the surface, thus requiring conversions from machine inputs to effects at the testpiece surface, a simpler, different approach can be taken. Issues of transferability are not dominant - the experiment must ensure data collected is capable of transferal to another AFM system. To do this, it must be considered how the experiment factors can be defined to allow universal application. Media properties aren't as problematic as machine properties – firstly, they remain as set, irrespective of external conditions (in a static environment) and have no requirement for conversion from a derived unit. The levels remain set for each configuration, as machine volume, part volume, part cross-section area and machine cross-section area don't play a role in the POI conditions.

4.4.5 Experimental design.

Previously, Mollart's Duplex machine offered many thousands of combinations of the machine piston motion actions such as velocity, stroke length, cycles and temperature – the previous goal was to study their effects – the system made changing experimental levels simple as it was a case of altering values through the GUI. Now, this luxury is not available – changing experimental levels is now a case of emptying the machine of a batch of media, cleaning and filling with another. Added to the load-homogenise-unload cycles, the economic cost of working with the previous experiment structure is considered unsuitable – the three level, three factor full factorial design requires a minimum of 27 unique runs to arrive at a complete dataset. To reduce the media configurations necessary to populate the required datapoints, a method of reducing unique configurations is required – not necessarily the number of runs, but certainly to reduce the cost and manufacturing lead time for the consumable product under investigation. The Box-Behnken design is capable of fitting a second order quadratic model.

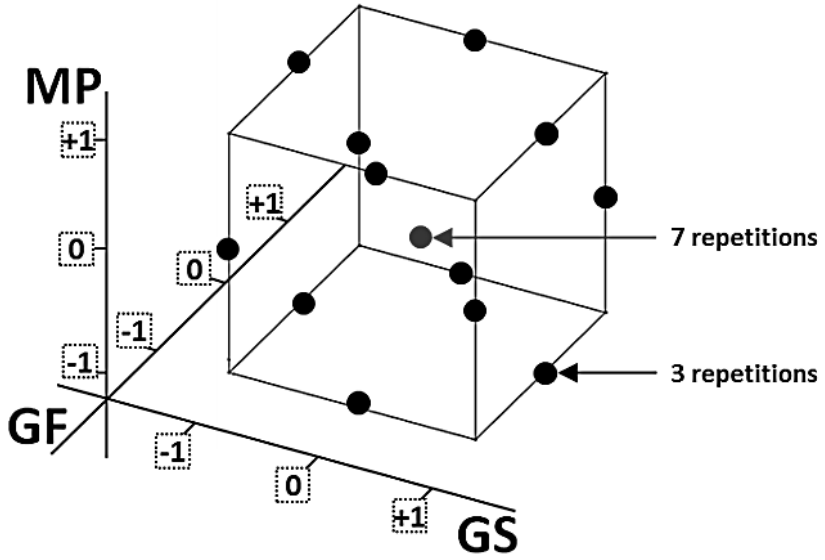

Figure 4.22 – Experimental design structure.

This design is far more efficient than the CCD (central composite design) response surface alternative as only three factors at three levels are studied - where four or more are concerned, the CCD is more appropriate. In contrast, the previous design would have required the manufacture of 27 different batches of media. In this design, unique combinations of factors and levels exist on each edge of the cube, plus one in the centre (see figure 4.22). This totals 12 edge-points and one centroid. The centre point in this exercise requires seven repetitions (seven total runs) for predictive model accuracy, three repetitions at the edges, totalling 13 media batches and 43 separate runs. The CCD design also captures a better model at the extremities of the process space, however, the Box Behnken is more representative of the space under investigation, as the factors – modifier percentage (MP), grain fraction (GF) and grit size (GS) – two from three are categorical factors and cannot be scaled indefinitely (MP and GF). In this vein, grit size (GS) can also be thought of as limited – experience suggests that grit sizes above and below certain thresholds are impractical, particularly if MTT's 5/diameter rule-of-thumb for maximum grit size (to avoid clogging) is adhered to. Further comments on media levels are made in the next section.

In the media corner of the AFM triangle, variables number 11. In the process of reducing potential experiment length, the quantity has been reduced to three that remain adjustable on the shop floor and consolidate two or more variables into a single factor which will be referred to as a consolidated variable. The following are considered to be root variables - those variables which cannot be considered in a more fundamental way; 1) base viscosity, 2) volume of primary grit, 3) volume of secondary grit, 4) volume of filler, 5) grit material, 6) primary grit size, 7) secondary grit size, 8) filler grit size, 9) volume of modifier, 10) volume of polymer, and 11) volume of carrier. Figure 4.23 shows three rows where 'true variables' are listed on the top row. Variables which are deemed to be incapable of influencing the process in a significant manner, but still must

be set are fed into the ‘fixed’ box, and final test variables are retained in the bottom row. In order to deliver suitable levels for the experiment and maintain the transferability concept important to ensuring wider industrial application, the consolidated variables are scalable and universal.

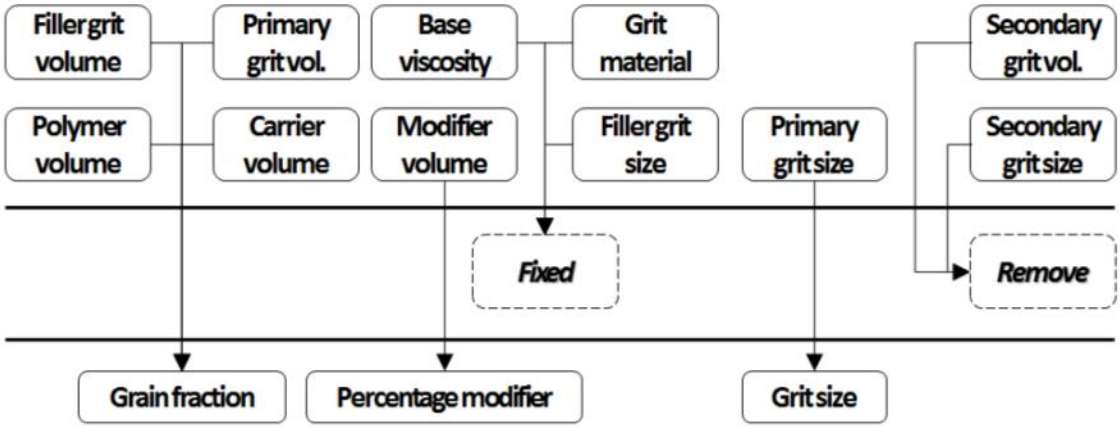

Figure 4.23 – Route to final variables.

One of the key elements of the media’s behaviour in an industrial scenario is its viscosity - the property which determines its resistance to flow. Due to the complex behaviour of the base polymer, it is impossible to place a single value on the media’s viscosity - only a rheogram can be used to show its true behaviour. A logical approach is to take ‘percentage modifier’ as the first factor in the experimental design. This provides a single percentage value of modifying agent as a rheological property manipulation method, irrespective of weight or volume.

The second factor is the percentage of grit to carrier, or grain fraction. Industrially, the quantity of grit versus quantity of carrier is significant due to the volume of potential cutting edges - pumping a workpiece full of carrier without grit will not remove material. As grain is added and uniform dispersion is assumed, grit to grit interaction is increased. The alternative to ‘grain fraction’ as a factor is to state a weight of grit or a weight of polymer, but these are counter-intuitive – they do not scale unless knowledge of the original media volume is available.

Grit size is the third factor – this selection can be convoluted with filler grits, secondary grits and reduced volume of grit due to an increase in particle size and weight. Filler grit is retained as a fixed variable - given that all MTT configurations contain a ~20% (of total grain fraction) fraction of F400 filler grit, the configurations will all continue to retain the same percentage by weight (only in grit). The secondary grit is excluded as an unnecessary variable, deemed to only have an effect comparable to the primary grit. Mass in kilograms is used as the measured quantity.

4.4.6 Calculation of experimental levels.

43 runs are required – in table 4.10, a number of issues are presented, concerning the balancing of the three major variables in the media. A benefit of working with the Box-Behnken experimental design is that factor and level combinations are typically only 'slightly-less-than-extreme' relative to final product levels within the process space. Because of this, confidence is held that values obtained in the Box-Behnken will outweigh statistical error induced by working with atypical levels.

Table 4.10 – Presumed effect of factors.

Factor	Level	Machine	Media	Geometry
Modifier percentage (MP)	High	Lower pressure requirement	Stability reduced	Reduced MR
			Reduced viscosity	More edge conformity
	Low	Higher pressure requirement	Increased grit support	Greater MR
			Increased viscosity	Less edge conformity
Grain fraction (GF)	High	Higher pressure req.	Higher viscosity	Greater MR
		Shorter cylinder life	More clogging	Poorer finish
	Low	Lower pressure req.	Lower viscosity	Reduced MR
		Longer cylinder life	Less dilatant effect	Less homogenous
Grit size (GS)	High	No effect	Larger particles	Greater MR
				Poorer finish
	Low		Smaller particles	Poorer MR
				Better finish

Experimental levels should consider the stability of the product as a whole to ensure that individual factors do not become overly influential in the process model. Looking at the first variable, 'modifier percentage (MP)', the middle level is representative of Escubed's relatively soft 50% (wt) carrier – the middle level in this case should be representative of current media behaviour, so as experimental levels observe the effects of reducing and increasing the volume of modifier. Levels must be set to maintain a stable product – as the values must be equally spaced, the base level must suit the machine's ability to pump, as reducing modifier content will increase viscosity. Judging by the graphs in 4.4.3.4, an appropriate -1 level is 40%, especially considering that addition of grit content leads to increased viscosity. The upper level is set by stability of the media – the mixing trial showed 50% modifier when mixed with 50% grit displayed comparable properties to MTT's MF10 products – this mixture is in the stiff region of MTT bases, but varying grain fraction and grit size have the potential to reduce, as well as increase the viscosity, leading the researcher to set 50% for the 0 value. The response in the rheograms of 4.4.3.4 when adding just 5% modifier leads to a significant reduction. The upper level is shown to be stable at 60%, yet very soft – the addition of grit makes the softer carrier easier to handle and more viscous.

Previously it has been thought that rheological testing of the carrier after modification was necessary to ensure consistency in carrier behaviour. Not only is this option costly, both financially and time-wise, it is counter-intuitive. The variable under study is the

percentage modifier, not viscosity. Viscosity cannot be described with a single value, but given the consistent benchmarked properties of the media's component parts, the measuring, mixing and temperature conditions should be maintained as consistently as possible.

Table 4.11 – Methods for MTT grain fraction naming.

		kg	Grit:carrier ratio	(Pri+Sec.):Fill
A	MF20-80B(125)-400B(25)	10	Grit 150 : carrier 100	P 125 : F 25
			15:10 , 1.5:1, 60/40	12.5:2.5, 5:1, 83/17
	MF7.5-30S(100)-36S(100)-400B(40)	10	Grit 240 : carrier 100	P 100 : S 100 : F 40
			24:10, 2.4:1, 71/29	200:40, 5:1, 83/17
	MF10-24B(60)-40B(60)-400B(40)	10	Grit 160 : carrier 100	P 60 : S 60 : F 40
			16:10, 1.6:1, 62/38	120:40, 3:1, 75/25
B	MF20-80B(125)-400B(25)	20	Grit 150 : carrier 200	As Above
			15:20, 1:1.33, 43/57	
	MF7.5-30S(100)-36S(100)-400B(40)	30	Grit 240 : carrier 300	
			24:30, 0.8:1, 44/55	
	MF10-24B(60)-40B(60)-400B(40)	30	Grit 160 : carrier 300	
			16:30, 0.53:1, 35/65	

When considering 'grain fraction (GF)', academic literature and MTT's previous configurations lead to viable suggestions – previously, MTT's naming structure added to confusion over the content of their products, but as shown in table 4.11, there are two interpretations of the MTT product code system, not clarified by their manual. In the examples under method A, the grit fraction is assumed to be referenced to 100 total parts of base, except it could be the case that they are all referenced to 100 parts, i.e. three bracketed fractions relate to 300 parts of base. If this were the case, the percentage would be calculated as per method B. The calculations do not allow clarification through common sense – the percentages are too close to determine which is correct by simply handling and observing the media, and there is no way of separating the two parts (reliably). Despite difficulties in obtaining information that explains whether method A or B is correct, ultimately the grain fraction levels can vary between 35% and 65% in the experiment, thereby covering all bases. To reinforce method B, a trend in academic literature leans toward higher carrier fraction, as shown in table 4.12.

Table 4.12 – Academic literature grain fraction trend.

Fraction	Author(s)
35%	Fang et al, 2009
40-60%	Gorana, Jain and Lal, 2006
40, 55, 60%	Gorana et al, 2006
56-78%	Jain and Jain, 1999
66%	Loveless et al, 1994

Levels are selected based on three main arguments, 1) that sufficient material removal occurs to provide testpiece geometry useful for data collection, 2) that levels are achievable in terms of media stability, and 3) they bear resemblance to levels used by MTT and those in academic literature. Grain fraction is set to 35%, 50% and 65%.

As per the previous two factors, 'grit size (GS)' does not change when swapping machine or part - it is fixed upon assembly. Grit size is thought to be the determining factor in material removal (MR) and ultimate surface roughness. Grit size selection within this experiment is important to ensuring that a range of material removal and surface roughness improvements are achieved on the testpieces, to begin to determine the GS:surface-condition relationship. As the filler grit is set at a constant 20% of all grain fractions, the -1 level for grit size must rest somewhere above that size (F400/25µm). The +1 level should ideally rest somewhere above the primary grit in the machine parameter study to prove an extension to grit size theories obtained from that dataset. The 0 value is equally spaced between these, and given that grit size in micrometres is the true scalable quantity (not the FEPA mesh size), it must be ensured that the median between +1 and -1 levels rests within 0-30µm of another mean FEPA standard size distribution. This limits the options somewhat - the most suitable distributions are in table 4.13. The preferred distribution is F16, then F14, then F20. Within those groups, the best have the smallest delta, although all are tolerable. Since standard mesh sizes grow exponentially, the 1346µm grit is deemed too large and the 940µm too close to the machine parameter study's material.

Table 4.13 – Grit size distribution and median value.

#	FEPA		Actual		Median	Level	Δ
	+1	-1	+1	-1	µm	0	µm
	F-grade		µm				
1	F16	F240	1092	50	571	F30 (559)	12
2	F16	F220	1092	63	578	F30 (559)	19
3	F16	F280	1092	42	567	F30 (559)	8
4	F20	F240	940	50	495	F36 (495)	0
5	F20	F80	940	165	553	F30 (559)	6
6	F14	F240	1346	50	698	F24 (686)	12
7	F14	F280	1346	42	694	F24 (686)	8

The machine and geometry are the fixed corners of the AFM triangle in this experiment – machine levels for the experiment need to be determined such that sufficient material removal is achieved for a significant measureable response to be provided, and that a range of surface roughness and edge-rounding values are recorded. To test these conditions, the configurations in table 4.14 will be used first.

Error between runs seen from parameters in machine parameter study should be minimised (see section 4.6) – target machine values for this study should present

minimal deviation, however selection of those levels should not predispose the media configurations to a specific type of surface. For example, increased velocity universally increases roughness and increased temperature universally reduces roughness. Since the media viscosity and ease-of-pumping is unknown, the velocity will be set to the maximum achievable when running with batch nine (see table 4.14). Considering temperature, its effect is universal and requires no conversion from machine to part, leading us to set a mid-range 35˚c.

Table 4.14 – Batches of media to manufacture first for pumping and abrasion level checks.

Run	MP	GF	GS	Comment
12	+1	-1	0	Easiest to pump, checks MP upper and GF lower levels.
	60%	35%	F30	
9	-1	+1	0	Most difficult to pump, checks MP lower and GF upper levels.
	40%	65	F30	
13	+1	0	-1	Least abrasive, checks for high degree of surface finishing.
	60%	50%	F240	
15	-1	0	+1	Most abrasive, checks for sufficient degree of sample edge rounding.
	40%	50%	F16	

Sufficient processing time must elapse to allow the media to enact its abrasive potential. This is controlled by the machine value of ‘quantity’; too short and the media will not have long enough to affect the surface condition, too long and the process can become too expensive in terms of time. It is important to retain a similar level to the machine parameter study for the purpose of direct comparison of media effects, and also that a mid-range value is used, so as not to bias the likely trade-off between MP and GF & GS. Factor coding for the media parameter study is given in table 4.15.

Table 4.15 – Factor coding for media parameter study.

Factor	Level	Derived	Actual
Modifier percentage (MP)	+1	60%	60%
	0	50%	50%
	-1	40%	40%
Grain fraction (GF)	+1	65%	65%
	0	50%	50%
	-1	35%	35%
Grit size (GS)	+1	F16	1092µm
	0	F30	571µm
	-1	F240	50µm

4.4.7 Extension of Box-Behnken to full factorial

Previously, simulation input includes machine conditions as variables – everything apart from processed length is able to be simulated. This means that temperature and velocity are the experimental levels which vary the simulation output – effectively leaving a human stage thereafter to determine the relationship between simulation results, response variable and processing length. This is made possible by having real physical results describing every interaction between velocity, temperature and quantity – where the experimental cost is acceptable, this is a viable method. However, fundamental constraints in the experiment design lead to the requirement to predict certain values for simulation using a mathematical model. The prediction model is a source of potential error in itself, but nonetheless, the blanks must be filled in. Examples of missing datapoints are given in figure 4.24, marked '!'.

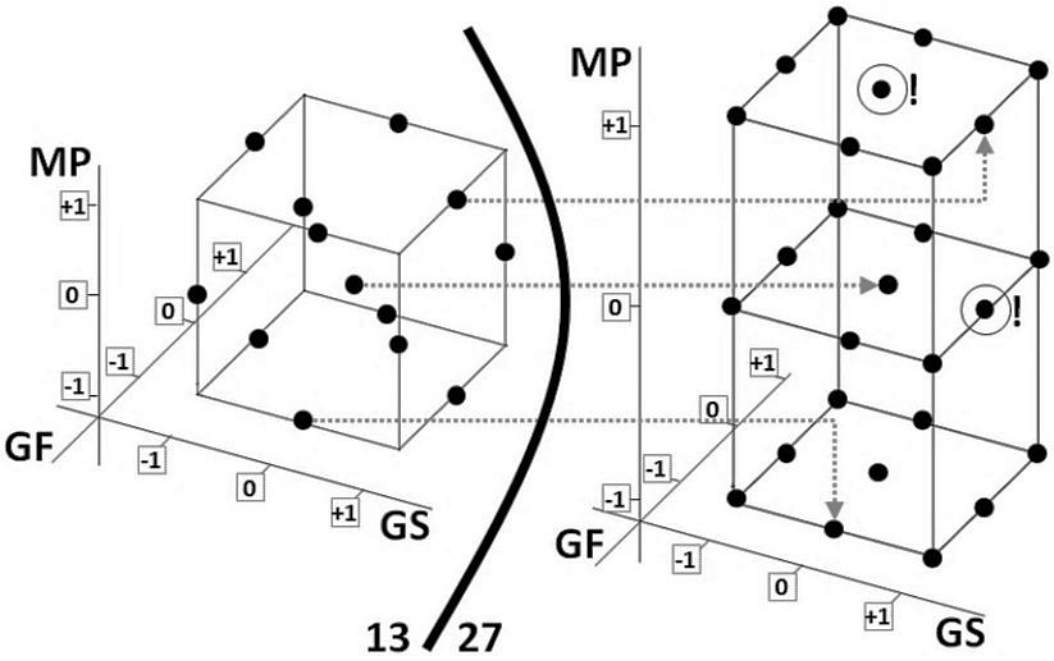

Figure 4.24 – Box-Behnken (L) design transferred to full factorial (R).

Fluent (simulation software) typically requires the same input data as selected for experimental levels in the physical world – three concerns are held about the re-application of experimental data in the simulation activity;

- Cost of experimental materials and media assembly.
  If mistakes are made in the specification of media and these products are found to not provide a spread of data, then polymers cannot be separated from modifiers or grits and media/time is wasted. To reduce risk, levels can be based on previously seen setups for factors such as grain fraction and grit size and polymer behaviour comparisons can be made by hand and rheogram. As per table 4.14, certain batches may be manufactured and tested first. The cost of a

unique combination of three variables is just over £1000. Using 13 unique combinations instead of 27 has economic benefits, but does not cover the process space in the same way as in the machine parameter study. This design is more suitable as the extremities of the process space are not included in experimental levels, and the researcher has chosen to replicate several points to ensure accuracy. Once analysed, the experimental design will provide a predictive model with an estimate of error – this will allow the researcher to predict the values up to the total 3^3 (27) quantity, and allow human integration of media parameter simulation results, response variables and processing length.

- Prediction reliability.
  As with all numerical models, there is an element of error and data out can only be as good as data in. The standard Box Behnken design requires only 12 edge points and 1 centre point, but between 5 and 7 centre points are recommended for better resolution. The design offers no facility for edge point replication, so the researcher has opted to carry this out separately to the Box Behnken requirements. Three replicates from edge points will be used to calculate averages, standard deviation, spread of data and repeatability.
- Rheology information from 14 batches (13 experimental, 1 verification).
  Simulation requires a table of strain rate against viscosity for the purposes of completing a lookup table in order to simulate the fluid behaviour. Data collection must be performed in the same way as Escubed in section 4.4.3.4.

4.4.8 Key issues

To minimise risk of poor data, the following process, environmental and phenomenological issues are identified.

Table 4.16 – Identified variables.

Category	Media variables	
Independent variables	Modifier percentage, %	
	Grain fraction, %	
	Grit size	
Dependent variables	Average roughness (Ra, μm)	
	Edge-rounding (n/a)	Material removal (MR, mm^2)
		Peak height reduction (PHR, mm)
Control group	Tooling, supporting the testpiece	
	Testpiece geometry	
	Testpiece material	
	20% F400 filler grit	
	Boron carbide (B_4C) grit material	
	Machine parameters (V, T, Q)	
	Pre- and post-process measurement methods	

Control group variables are similar to the machine parameter study – the tooling remains in order to direct media over the testpiece at constant rate, constant direction and constant surface condition. The testpiece design remains, for the purpose of achieving good data for further application in simulation and comparison to hand calculated pressures and velocities. Workpiece material is retained, for results comparison – titanium provides a suitable level of erosion in the test environment, which is of interest given that all batches contain boron carbide. Media contains the same percentage and size of filler grit - all of MTT's media that Mollart have purchased in the past have contained almost exactly 20% of total grit weight in a smaller size – always F400 (25µm). All MTT media purchased by Mollart in the past has contained exclusively boron carbide grit material, as MTT's advice is to use the harder material in Mollart's mainly titanium, stainless steel and nickel-alloy workpiece materials. Contrary to the machine study, the effects of media variables are studied in this section, with further application of results in a simulation environment – the machine corner of the triangle must remain fixed in order to isolate the effects of the media variables.

4.4.8.1 Difficult to control variables

- Temperature dependant viscosity.
  Chemical behaviour of Dow Corning 3179 base polymer drives the media's viscosity change as a result of heat – different batches contain grit and modifier volumes that displace 3179 volume, reducing the predictability of specific heat. To mitigate, the media is pre-heated, and from preliminary trials, appears to heat slower and retain temperature better than MTT's product.
- Load-unload contamination.
  Swapping batches leaves traces of previous media – media will be exchanged 19 times in total, potentially damaging media rheology – mitigation is by employing a standard cleaning practice of using IBS200 to remove waste and panel-wipe to remove residual IBS200, as it evaporates.
- Warm-up cycle shear history variance.
  Difference in warm-up duration and periods of media relaxation may cause behavioural change. Media manufacture will consist of a mixing activity and unloading into storage buckets. Upon starting the experiment, media will be loaded straight from the bucket and homogenised at the machine's full stroke length for 15 cycles. Escubed's work found that MTT media will stabilise after 4-5 cycles. It is recommended to use experimental parameters for the warm-up (35˚c and velocity to reach 35bar working pressure).
- Ambient temperature.
  During the warm-up cycle the machine will be set to the experiment temperature – if processed long enough (15 cycles should suffice) the media will reach the machine temperature. When working within machine pressure limits, the cooling system is effective at maintaining the user-specified temperature.

4.5 Data collection and metrology solutions

Following sample processing, their surface- and edge-conditions are crucial to understanding the effects of the AFM process. As all sample geometry, material and application is the same, the same measurement and inspection steps are used for samples processed as part of sections 4.3 and 4.4. This section discusses the required data, the method of obtaining it and instrumentation used.

4.5.1 Measurement system requirements

Surfaces of the testpiece are treated by the AFM process according to the orientation in the fixture (orientation flat facing 9 o'clock), whereby the flow in one direction is split into two by the V-form straddling the centre Ø40mm bore. The media is under less pressure when it passes over the V than when it reaches the area of smallest cross section – this causes a differential in work at the two areas. The orientation of the sample and 2D faces exposed to media are symmetrical in all four quadrants of the pipe.

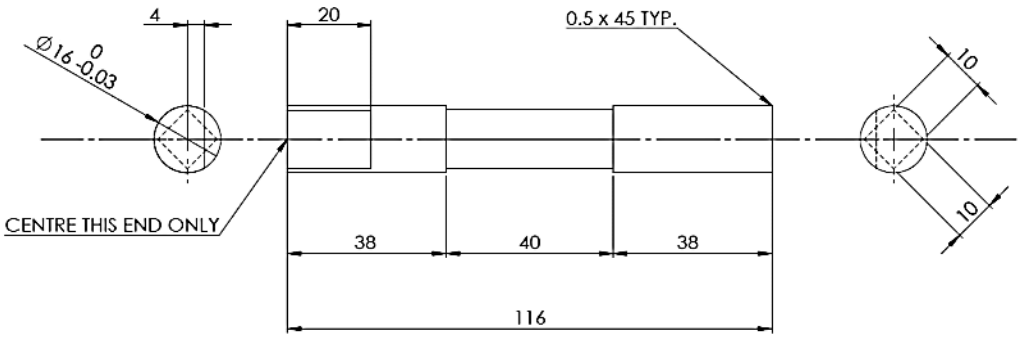

Figure 4.25 – Testpiece manufacturing drawing.

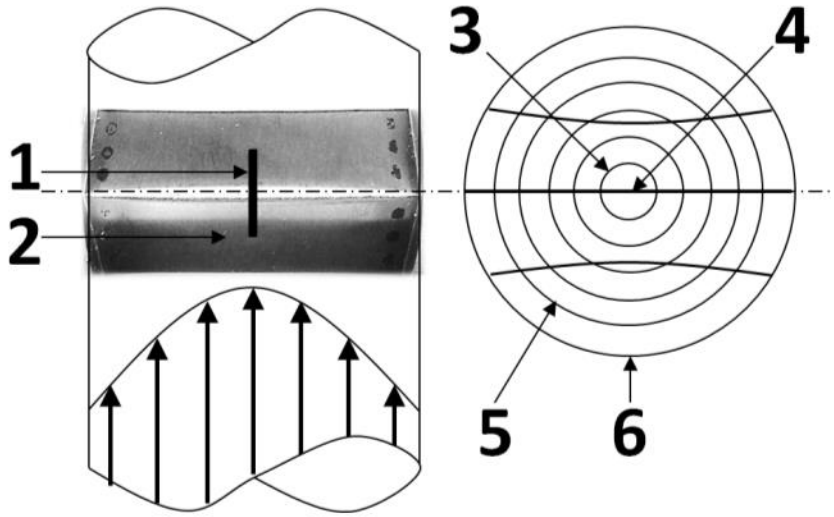

Figure 4.26 – Test assembly side view (L) and top view (R).

Present in all processed testpieces is the effect of velocity profile as shown in figure 4.26. Point three shows the centre of the profile in the full-bore flow – this is where the media flows fastest, or alternatively where the media flows at the velocity as set on the machine. Point four depicts the top V of the testpiece where the media approaches first – very little work is done here, nor is it expected to. Point five highlights the outer zone where the velocity (and pressure) is reduced – the side view shows the effect differential between media approaching at 0˚ and approaching at 45˚. Point six is the boundary wall, where, over time, the testpiece form encourages greater erosion on the support body about the testpiece location as pictured in figure 4.27.

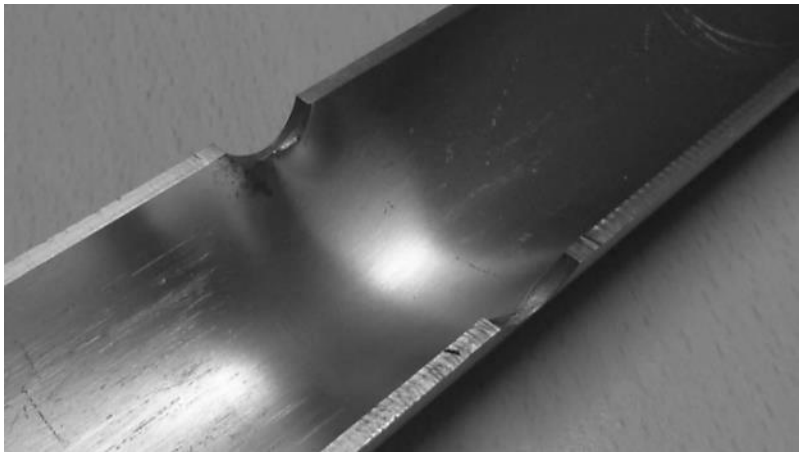

Figure 4.27 – Sectioned steel testpiece body liner

To encourage a meaningful degree of edge-rounding in an easily-simulated geometry, the features inspected in this research is the edge exposed to flow (figure 4.26, point one) and a surface exposed to flow (figure 4.26, point two). While a difference between measured roughness results over the surface of the sample is evident, and the degree of edge-rounding is different along the length of the edge, the results are 1) being collected at the point where the machine is doing most work (i.e. the centreline), and more importantly, 2) the field variables (physical conditions of the fluid) are easily visualised in simulation, wherever the datapoint may be.

4.5.2 Conversion into numerical values.

In order to characterise and analyse the two features, metrics must be chosen to provide a single numerical value that describes the edge. Here, the transition from data to information to knowledge is described, in terms of physical steps carried out. While the instruments collect data, readings are contextualised (converting data to information) by describing a location and quantity, while knowledge is generated in the analysis (sections 4.6 and 4.7).

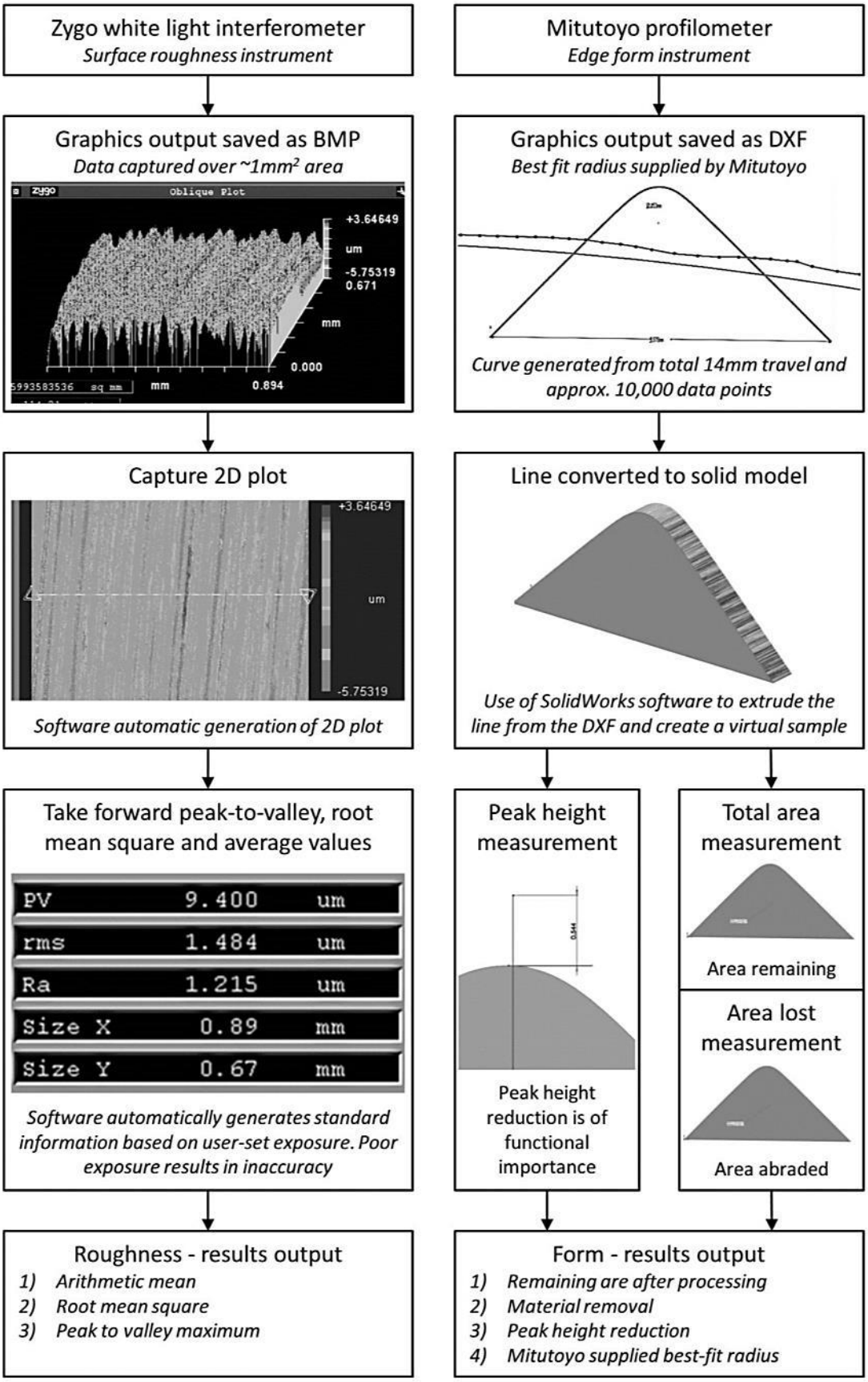

Figure 4.28 – Transformation of results into numerical response variables.

Surface roughness and edge form are collected through a physical interaction, both providing an electronic file as output. While surface roughness is displayed instantly, edge form requires some translation into useable values. Seven outputs are available, although not all are critical – the three main responses to be applied in the analysis are arithmetic mean surface roughness (Ra, μm), total material removal (MR, mm^2) and peak height reduction (PHR, mm).

Average roughness is common, however the implementations of material removal values are not; initially, a radius value was intended, but as experience with the process increased, the realisation that truly tangential radii were uncommon began to materialise. Radius (r, mm) is frequently found on manufacturing drawings to denote a specific degree of edge-rounding, whether to allow for a mating feature, edge-clearance or as a deburring avoidance method. Tooling, media and process parameters are controlled to allow the flow to create a (near) tangential radius, however this may be throttled by geometry and pre-existing features. In the absence of a widely recognised unit, two are presented (see figure 4.29) and used in the analysis activities. The first is material removal (MR) usually measured in grams, but in this instance, the concern is only for the material removal about the point of interest in a 2D plane which provides a mm^2 value. This unit is useful for characterising the overall extent of MR, but could be misleading in cases where the angle is shallow between edge '1-2' and the radius is effectively small – inferring that a high MR value does not always mean a suitable degree of deburring.

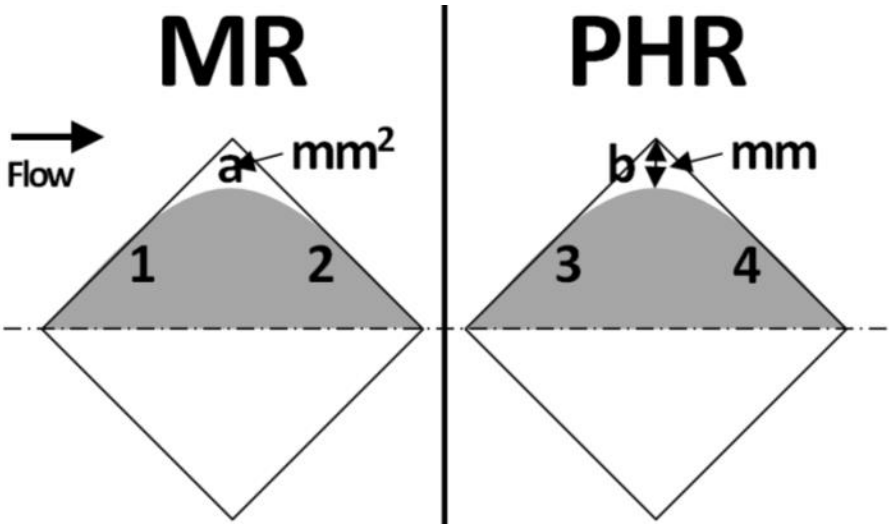

Figure 4.29 – Difference between MR and PHR edge-rounding.

The counterpart unit, peak height reduction (PHR), offers a solution – irrespective of total MR, the PHR unit defines the extent of removal from the theoretical pre-process edge, in a straight line down to the post-process tangent (the shortest possible line). This

unit guarantees what MR does not; that material has been removed from the point of a non-tangentially rounded feature.

In surface roughness collection, the sample is measured at point E (as depicted in figure 4.30) which is the centre of the face as exposed to the media – gravity effects have been ruled out in previous work, so a measurement taken from any of the four faces should yield a virtually identical result. This was determined to be accurate after checking one of the samples in detail by measuring the nine positions on each of the four faces. The points at 'E' measured 1.260µm, 1.236µm, 1.269µm and 1.254µm, with a mean of 1.254µm and standard deviation of 0.014µm – a deviation so small that it has no functional significance if, for example, the testpiece was a customer component requiring an equal finish on all four sides, then an increase in deviation of 100% would still not affect quality (by shopfloor manufacturing standards).

Looking at corner quality in the fast regions (eight points), those points at A, C, G and I measured a mean of 0.620µm with a standard deviation of 0.047µm, approximately 3.5 times greater than the centre points – for the slow regions, a mean of 0.511µm and standard deviation of 0.069µm, a marginal increase in error compared to media travelling at higher velocity. It is therefore reassuring that centreline data is of greater accuracy considering its importance as the area at which the machine has imposed the true operating conditions.

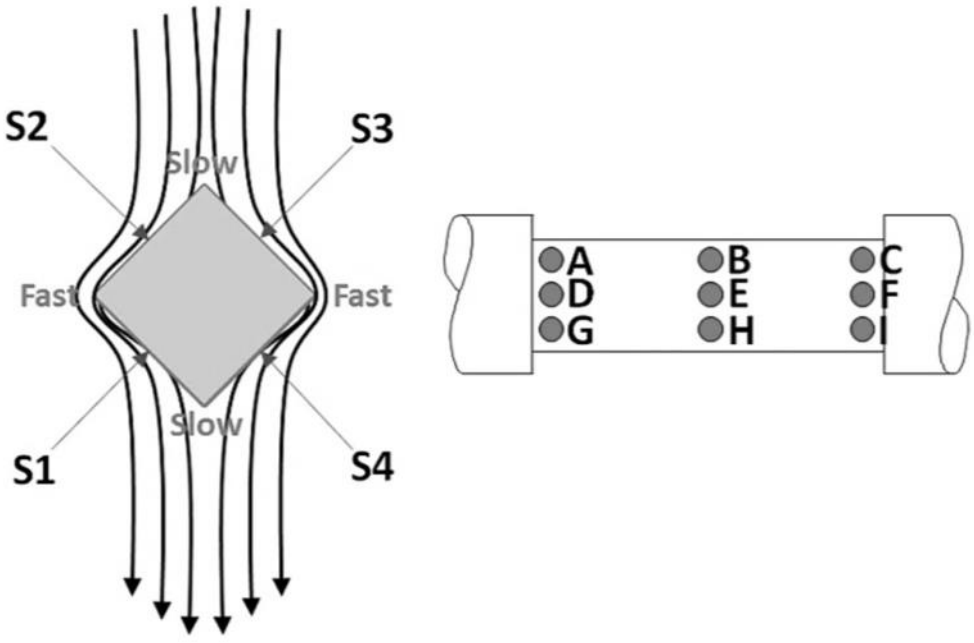

Figure 4.30 – Whole-face roughness assessment.

In the edge form data collection exercise, the samples are measured by a trained user of profilometer machines and worked with Mollart to determine the most suitable method of data collection. The samples are mounted at 45˚ to their position as processed so that

the peak of the edge is the highest point measured. The operator sets the carbide tip of the stylus to the top of the sample in the Z axis, finding the highest point at an almost arbitrary position across the length of the peak. The operator then finds the lowest point along the peak using the Y axis hand wheel to move the sample under the stylus (moved in direction of sample centreline) – this positions the stylus at the point of the flow field which was at maximum velocity as set on the machine, and directly at the edge of the sample.

The stylus is then sent to +5mm from the peak, leaving it resting somewhere about point 'E'. The stylus is then dragged (very minor surface force, approximately 3 grams, no impact on geometry) a total length of 10mm, through point 'B', over the peak and back down to -5mm. Total length travelled is approximately 14mm over the surface, and the machine registers its position every ~1.4µm, providing a curve with approximately 10,000 nodes. The operator then applies a re-orientation correction by drawing lines of best-fit along the two flat faces, ensuring the sample is orientated perfectly.

As an addition, a best-fit radius is supplied in the DXF file as a default output from the software. This best fit appears to be inconsistent on several samples, periodically appearing as a far smaller radius with a very poorly fitted curve. For this reason, best-fit radii are not included in the analysis stages, but it should also be remembered that tangential radii are uncommon as radii form is subject to flow condition which may not always be conducive to tangential radii.

The secondary operations are carried out by a solid model as produced from the DXF curve – this allows SolidWorks 2012 to report the surface area, which the researcher can then lay the original form over using the centre of the base of the triangle as a reference point (because gravity effects are not present, and part geometry is mirrored perpendicular to the faces (within described error)).

Upon completed processing, samples were cleaned in a 'panel wipe' degreasing solution (naptha and n-hexane based clear fluid) commonly used on Mollart's customer components, then re-marked with the same number marked during processing. Samples are wiped with a non-abrasive cotton cloth, and samples with significant amounts of contamination are dipped and shaken in panel wipe before wiping. Samples are neither re-useable nor re-manufacturable. After processing, they are only useful for three things; further measurements in different locations, re-measurements and storage for future erosion knowledgebase plans.

4.5.3 Measurement instrumentation.

Two technologies are used in the sample measurement process – profilometry and interferometry. The equipment in figure 4.31 is used, the white light interferometer (WLI) to the left is owned and operated by Brunel University and the profilometer to the right is used under hire agreement with Mitutoyo UK initially, and following

availability issues, with Salcey Precision Engineering. Both instruments are used in a calibrated state and use fixtures to repeat the position of the samples.

The WLI is a ‘Zygo’ instrument, capable of measuring to accuracies of 0.001µm (1nm) – reference figure 4.31, magnification is set to 20x throughout the process (A), the testpiece is positioned with the flat facing 1.30, positioned according to a recess on the side of a steel block (B). The testpiece is positioned on the block laterally using the edge of the 16mm diameter where it meets the square section (C) – sample movement is then achieved by traversing the table forward and back with a dial (D), and sideways (E). The granite worktop is automatically levelled by air cushions at each of the four corners (F), and tilted if required by the dial (G). A calibration sample is always on-hand at (H).

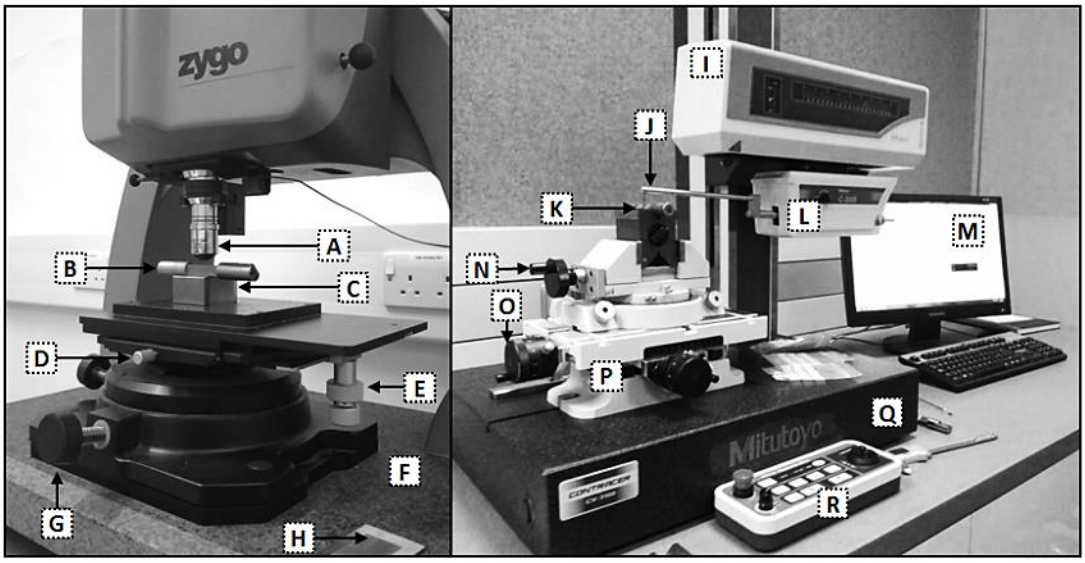

Figure 4.31 – Zygo WLI (L) and Mitutoyo CV3100 formtracer (L).

The profilometer is a Mitutoyo CV3100-series ‘formtracer’. It uses a stylus, dragged in a 2D plane over a surface to provide an electronic version of the form in a ‘line’ drawing, which allows the fitment of various standard shapes, and/or measurement of these shapes. In contrast with radius gauges or best-fit microscope software, the profilometer collects thousands more (one every 1.4µm) datapoints and insensitive to standard forms, i.e. it does not expect to see a straight line or a tangential radius – it collects and represents the trace of the probe using the software ‘Formtracepack 5.303’. As pictured in figure 4.31, the main beam (I) is visible behind the stylus motion assembly (L) – it is rooted to a granite table (Q). This provides Z height control, critical to allowing various sized workpieces on the table. It remains stationary during operation. The stylus motion assembly allows ±25mm travel, limiting the maximum peak to valley value to 25mm. The motion assembly drags a stylus (J) with a tungsten carbide tip of <12µm diameter. A V-block with clamp for the testpiece’s orientation flat is used to constrain and repeat the orientated position of the sample (K), while the

traversing wheel at (N) moves the upper stage and the wheel at (O) moves the lower stage, both in a sideways motion. The traversing wheel at (P) moves the lower stage forward and back in order to find the lowest point on the peak. Control-wise, a conventional PC (M) is used to output data in DXF format for further application and the stylus is positioned using the pendant-type control (R) to allow the operator to watch the machine while they make adjustments.

Measured outputs for each sample include; 1) average roughness (µm), 2) root mean square roughness (µm), 3) peak to valley maximum roughness (µm), 4) area remaining (mm^2), 5) area removed (mm^2), 6) peak height reduction (mm); 7) software-derived best-fit radius (mm).

4.6 Analysis of machine parameter study data

Analysis is first achieved by determining the error through mean and standard deviation of the measured values. Secondly, a predictive model, analysis of variance (ANOVA), main effects plots and interactions plots are required – this is achieved by the population of results generated by the full factorial design into a response surface method, namely the Box-Behnken experimental design. This technique delivers a predictive model using ANOVA to determine significant model terms, a numerical constant and a weighting for each factor.

Several verification experiments are carried out using the model as a prediction device, utilising the remaining runs of the full factorial design as markers for values the RSM-derived model should be predicting. Results are compared between iterations of the model, the exclusion of terms with high noise factors and higher order interactions. It is not possible to create a prediction model with the factorial design, but its 'fully-crossed' structure is critical to obtaining a comprehensive dataset for application in figure 3.10, box 4 (establish relationship between length and flow condition).

It is important to note that the ability of the model to predict the outcome of a response variable is not a critical element of the project, rather an exercise in developing a greater understanding of the process by how it affects the functional features of a workpiece. At this stage, all work is tied to the testpiece geometry and material, which is not representative of a complex geometry (nor is it supposed to be) – its ultimate purpose is a means by which a given flow condition can be used to infer a generated surface condition (through any of Ra, MR or PHR responses).

Aims for the analysis include (but are not limited to); 1) the description of interactions between parameters, 2) to predict the surface finish and edge form, 3) to determine the model accuracy through physical verification, 4) verify results against existing experience and literature, 5) to compare the prediction against physical results using the process window concept, 6) to aid the selection of media parameters through reduction of process error, and 7) provide data vetted for unexpected error before inferring relationship between CFD-derived flow conditions, actual conditions and measured responses.

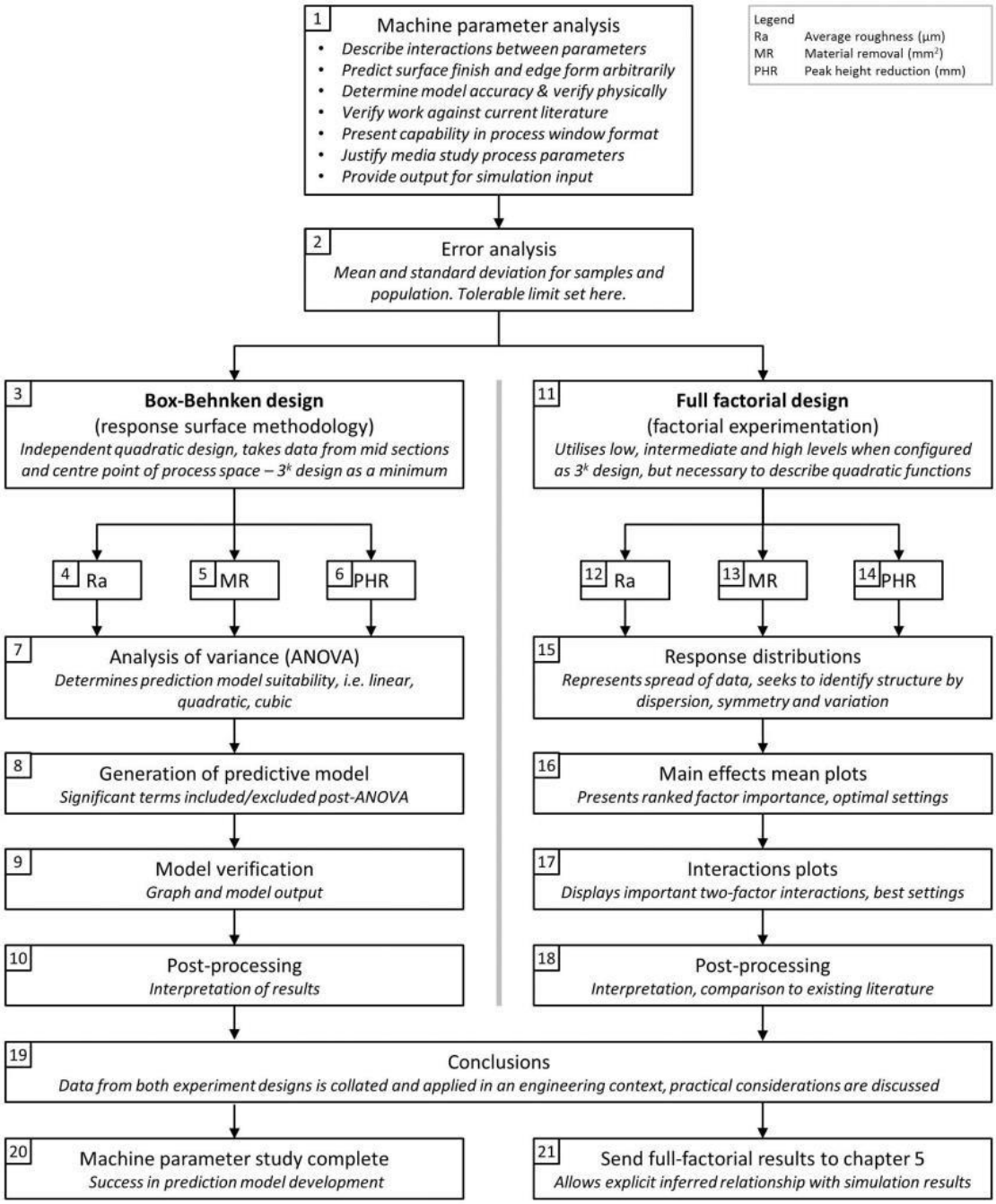

Figure 4.32 – Overview of machine parameter analysis activity.

4.6.1 Error and acceptability.

Experimental data often contains error, whether system-induced or user-induced. It is important to carry out an analysis of error before undertaking further in-depth analysis before errors are brought forward and model inaccuracy results. Section 4.6.1.1 discusses and presents an initial look at the data, the full error assessment and what the results mean for subsequent modelling activities – in practical terms, the dataset error should be a fraction of the error acceptable in model and subsequent verification checks.

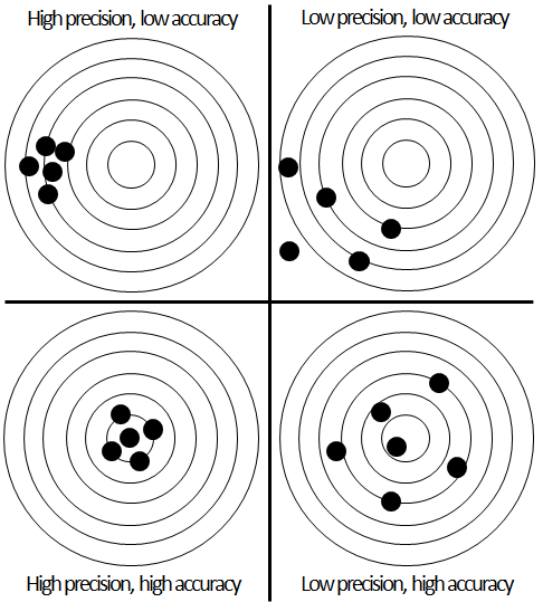

Figure 4.33 – Definition of accuracy and precision.

Figure 4.33 illustrates typical error types in four sketches– the experimental data collected in section 4.3 should fall into 'low precision, low accuracy' as it is desirable to have the values cover the process space under study. Resultant models developed through this section will be attempting to derive predictions in the 'high precision, high accuracy' range.

4.6.1.1 Initial look, histograms of responses.

The initial look at the data is used to screen out any major flaws in the experiment or data collection exercise by checking for expected datapoint distribution and whether the results conform to expectations when studied in simple pairs. Histograms, run plots and contour plots are used to determine whether responses are clustered, to view spread of results and to view general two factor effects. It is desirable to see a spread of values – if results are clustered at one end of the scale, or clustered in several locations, then the setting of the factors and levels are unbalanced and influencing process outcome.

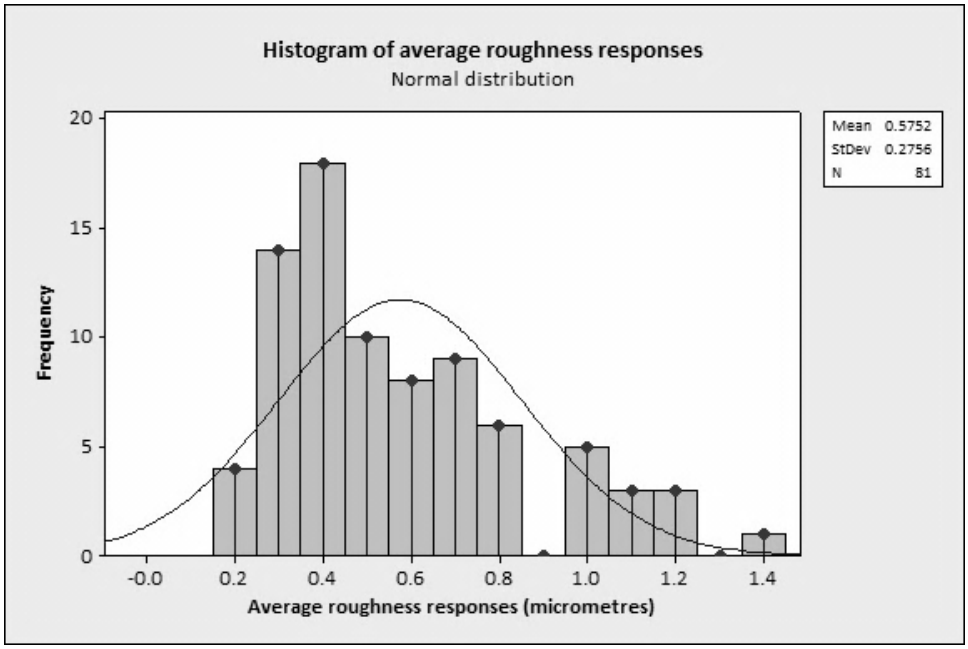

Figure 4.34 – Histogram of average roughness responses.

Showing a normal distribution, the data in figure 4.34 is skewed to the right, which means there is no 'typical value' as would be expected for an experiment which operated over the entire process space. The most prolific return for average surface roughness is the 0.35-0.45µm bin, but is certainly not at the centre – there appear to be no significant outliers, although there are no responses for 0.85-0.95µm, which may be unusual if the trend was any more evident.

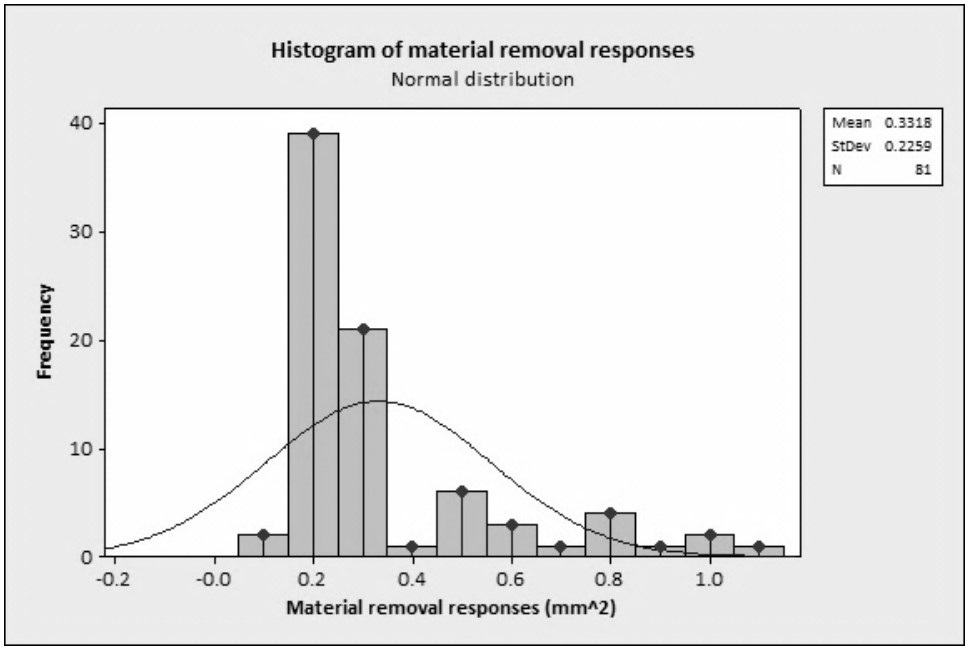

Figure 4.35 – Histogram of material removal responses.

Showing a normal distribution, the data in figure 4.35 is more heavily skewed to the right, indicating that material removal is difficult to achieve once a specific quantity is removed. Naturally, this is only applicable to the geometry, media and material used in the test environment. The highest frequency bin is 0.15-0.25mm^2, consisting of half the results, followed by another 20 results in the 0.25-0.35mm^2 bin. There are no significant outliers or gaps in the data.

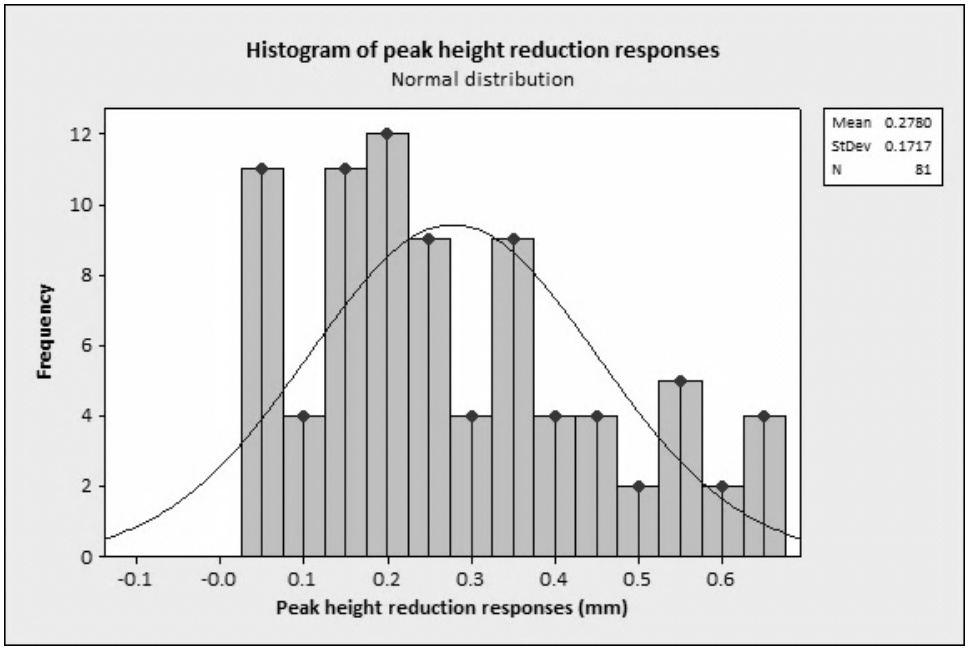

Figure 4.36 – Histogram of peak height reduction responses.

Showing another normal distribution, albeit skewed to the right again, figure 4.36 shows an interesting difference between the PHR and MR behaviour – while the overall MR falls off sharply, the PHR tapers to a lesser extent. Not only does this justify using the unconventional PHR unit as planned, it illustrates the action of the abrasive wear as being focused on the tip of a geometry. PHR appears to be disconnected from the MR relationship. The bulk of the results remain in the area of lesser effect, at around 0-0.35mm, whereas a quarter (21) of the results fit into the >0.4mm range.

4.6.1.2 Initial look, run sequence plots.

Charting average roughness of each sample against its run order should present a spread of points across the process space. There should be no relationship between sample run order and resultant roughness measurement. Plot figure 4.37 presents a greater density of points beneath 0.8µm, with no relationship between X and Y. There is no linear relationship, nor any non-linear relationship. The highest datapoint appears to be an outlier, as there should be two other points in horizontal alignment. This value has since

been re-measured and found to be dissimilar to the other two points with the same processing condition, whereby those points are comparable.

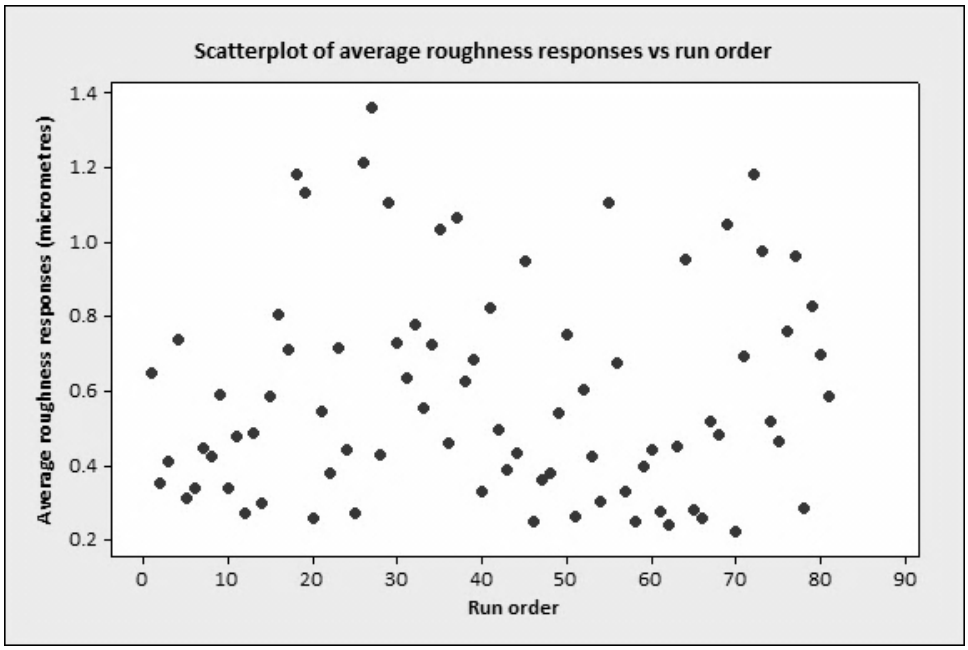

Figure 4.37 – Run sequence plot of average roughness responses.

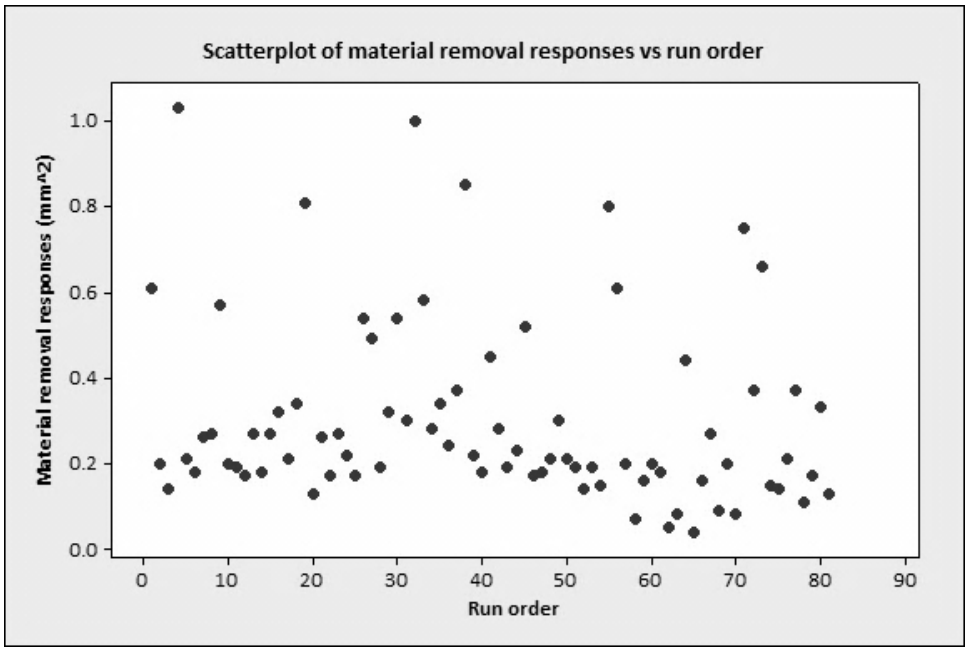

Figure 4.38 – Run sequence plot of material removal responses.

Evidence of machine-based influences would be highlighted by clustered points. In figure 4.38, points are spread throughout the lower end with greater density beneath 0.4mm^2. This points to a systemic limit of media when combined with titanium material

in this geometry – it can be deduced that material removal is not best achieved by varying machine parameters, as there is a cap imposed by geometry and material.

Figure 4.39 – Run sequence plot of peak height reduction responses.

The greater vertical spread depicted in figure 4.39 indicates that peak height reduction can be effectively manipulated within the testpiece setup. X and Y are unrelated, both linearly and non-linearly. There are no apparent outliers, and points appear to be evidently horizontally arranged in 3s, 6s or 9s. The lack of structure is the ideal outcome in this scenario.

4.6.1.3 Initial look, contour plots for average roughness.

Contour plots analyse the effects on Z (average roughness) as a function of X and Y (independent variables). A clear demonstration of the relationship between velocity and temperature is provided in figure 4.40; increasing temperature results in a lower average roughness while increasing velocity results in a rougher surface. What remains unclear is how well these graphs will scale – the definition between the lines and consistency of direction is helpful, but as long as the machine operates within its physical limits, these interactions will be valid. A misconception with these plots is the idea that surface finish may be predicted as a result of reading off and applying two values from the X and Y axes for a desired value of Z. The approach should be to use the graphs as a rule of thumb, as the interaction will change based on the value of the third (unnamed) factor (set to average in all figures). Figure 4.41 demonstrates an increased velocity once more increasing roughness, while increased quantity of processing on a surface is linked quite

clearly to an increase in roughness. Contour plots are obtained through Minitab software and significance is limited to two factor interactions.

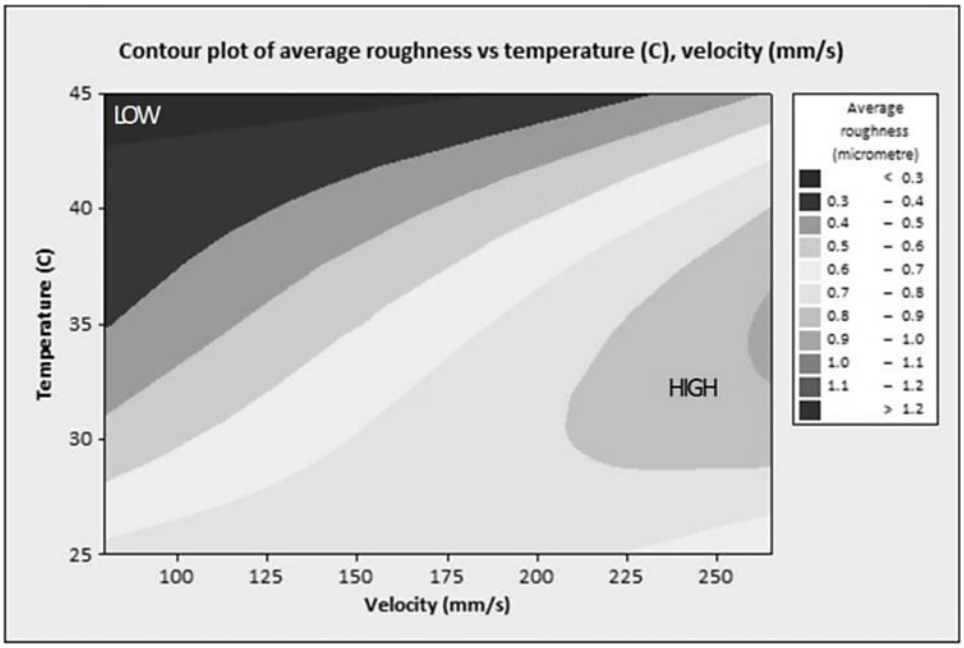

Figure 4.40 – Contour plot of velocity vs. temperature for average roughness responses.

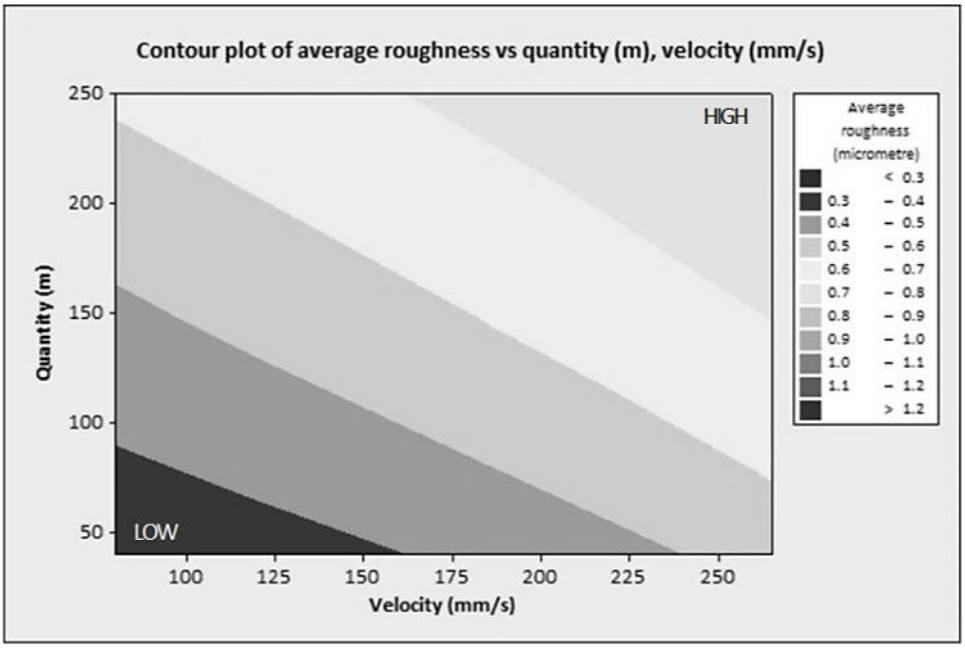

Figure 4.41 – Contour plot of velocity vs. quantity for average roughness responses.

Figure 4.42 is particularly useful for describing the case whereby low quantity provides a better finish, but only to a point where an increase in temperature is required to improve the surface further. All surface finish plots suggest that ‘no-processing’ would

be the solution for best surface finish, but it must be remembered that these results are with a set grit size and grit material, and thus deal only with the potential of one media configuration to erode. Should an end-user require a finish better than the milled pre-process of ~0.35Ra, the grit size used in this experiment would be the wrong choice. Conventional wisdom would suggest smaller and softer grit, but results from section 4.7 confirm this. This plot confirms that increasing temperature improves surface finishing ability, while reducing processing quantity also improves finish.

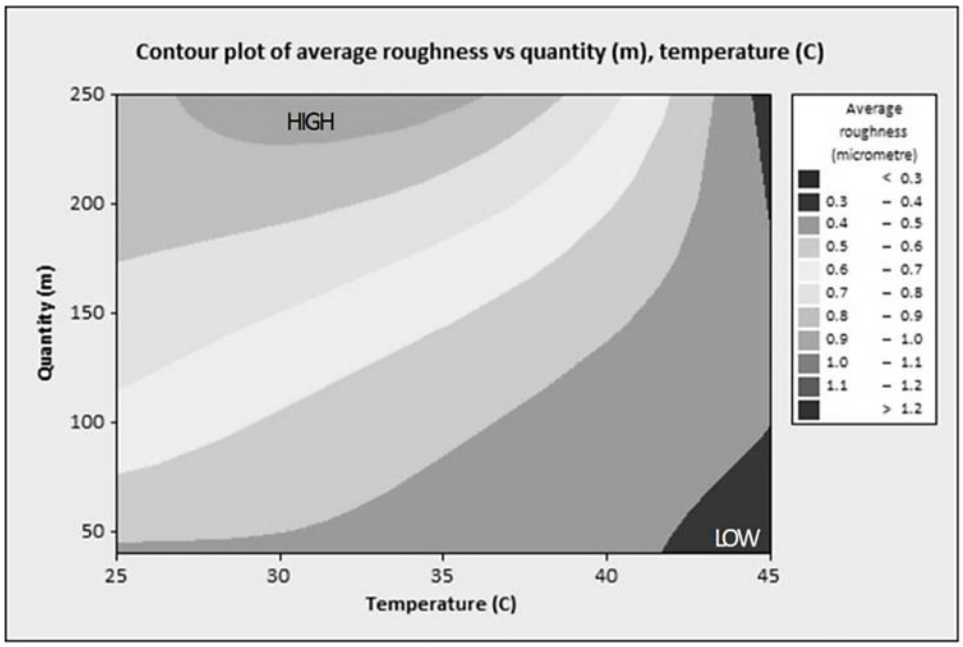

Figure 4.42 – Contour plot of temperature vs. quantity for average roughness responses.

4.6.1.4 Initial look, contour plots for material removal.

Figure 4.43 displays the increased material removal ability of a lower temperature. The temperature appears to dominate in this two factor relationship whereby the degree of material removal is observed to be less manageable after velocity reaches 175-200mm/s. This finding resonates with academic work and conversations with MTT where an optimum operating pressure exists to maximise material removal. The general rule-of-thumb relationship shows a clear tendency for softer less-viscous media to be unsuitable for stock material removal which may be an issue in honing and edge-rounding applications. Showing quantity to be dominant with respect to velocity, figure 4.44 makes a strong argument for the manipulation of media properties (not machine parameters) to achieve a given level of MR in time-critical applications. The relationship is not entirely as expected, with increases in velocity failing to provide a meaningful change in material removal. An extended version of this figure may be useful, but considering the machine levels used in this experiment, the maximum allowable working pressure had already been reached. In practical terms, the

relationship suggests that a velocity is best set to create a flow field suited to the desired final geometry, whereas quantity is the factor that allows the process to reach that geometry.

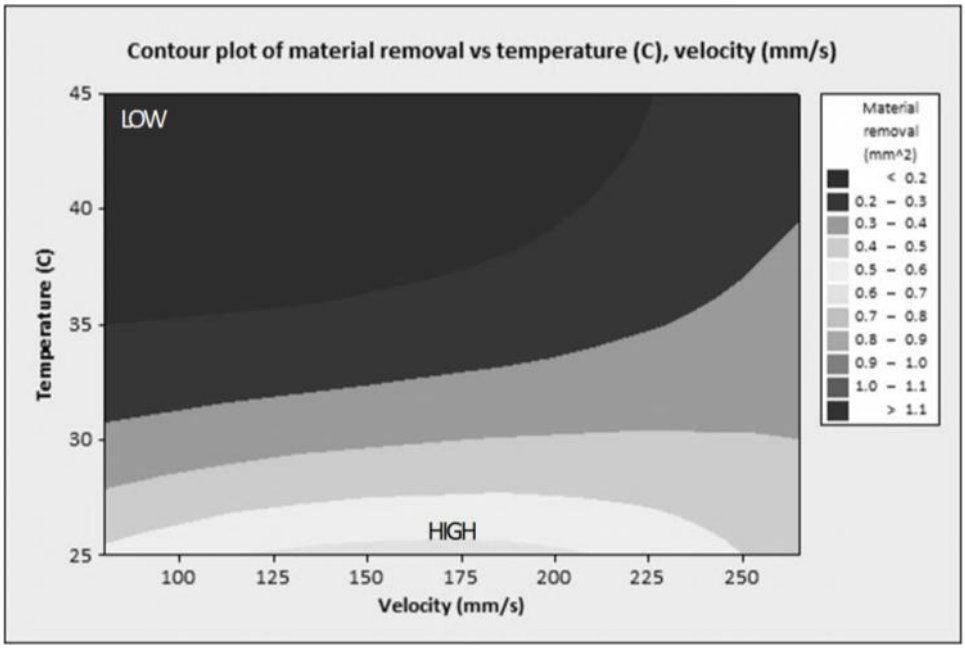

Figure 4.43 – Contour plot of velocity vs. temperature for material removal responses.

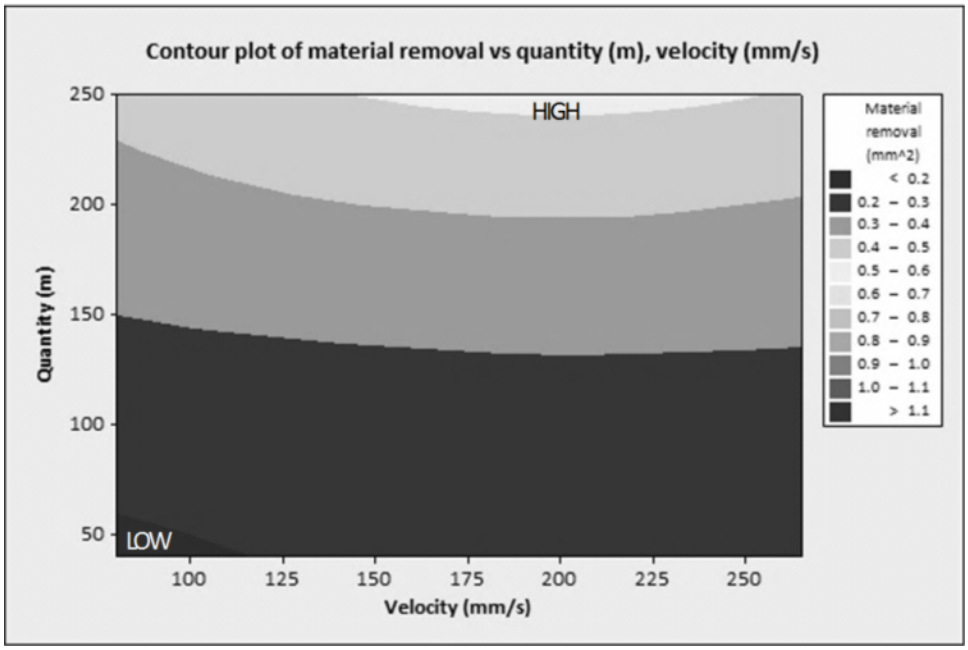

Figure 4.44 – Contour plot of velocity vs. quantity for material removal responses.

Figure 4.45 shows material removal is limited by low-viscosity media and limited processing quantity, in complete agreement with figure 4.44. The material removal

effect is significantly amplified by reducing temperature; in practical terms, the only two factors of significant influence are quantity and temperature, whereas figure 4.44 shows that ~200mm/s should be a target surface speed in titanium. Figure 4.45 shows with increased quantity, exponentially greater levels of MR can be achieved, but increasing temperature limits the rate of change. This is likely due to a throttling effect over the testpiece POI whereby quantity reduces efficiency on a per-cycle basis.

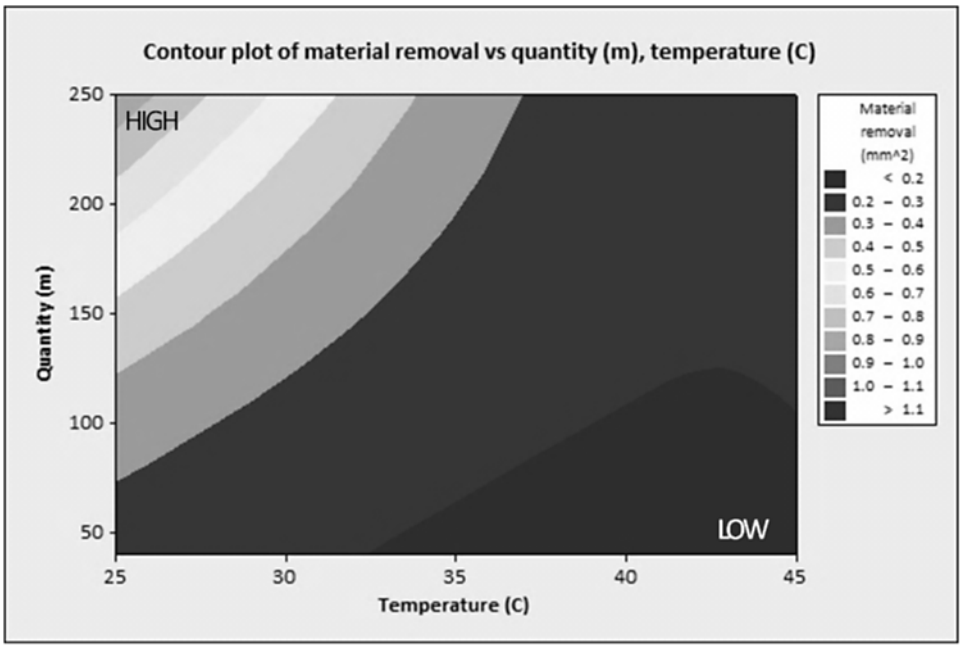

Figure 4.45 – Contour plot of temperature vs. quantity for material removal responses.

4.6.1.5 Initial look, contour plots for peak height reduction.

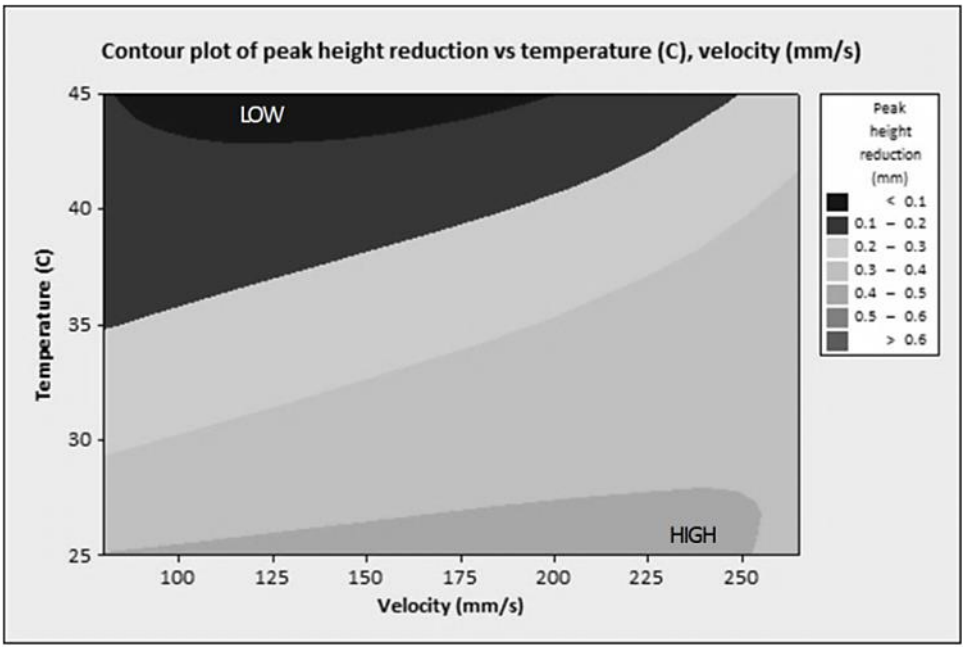

Figure 4.46 – Contour plot of velocity vs. temperature for peak height reduction responses.

Focusing on the LHE of figure 4.46, diminishing returns are seen by increasing processing quantity; however, if velocity is increased, those returns are amplified when moving to the RHE. When proposing rule-of-thumb changes to a process model, the effects of changes on other features should be considered – an increase at one POI may push another feature out of tolerance – this is especially true with regards to quantity – the flow condition is manifested for longer with increased quantity.

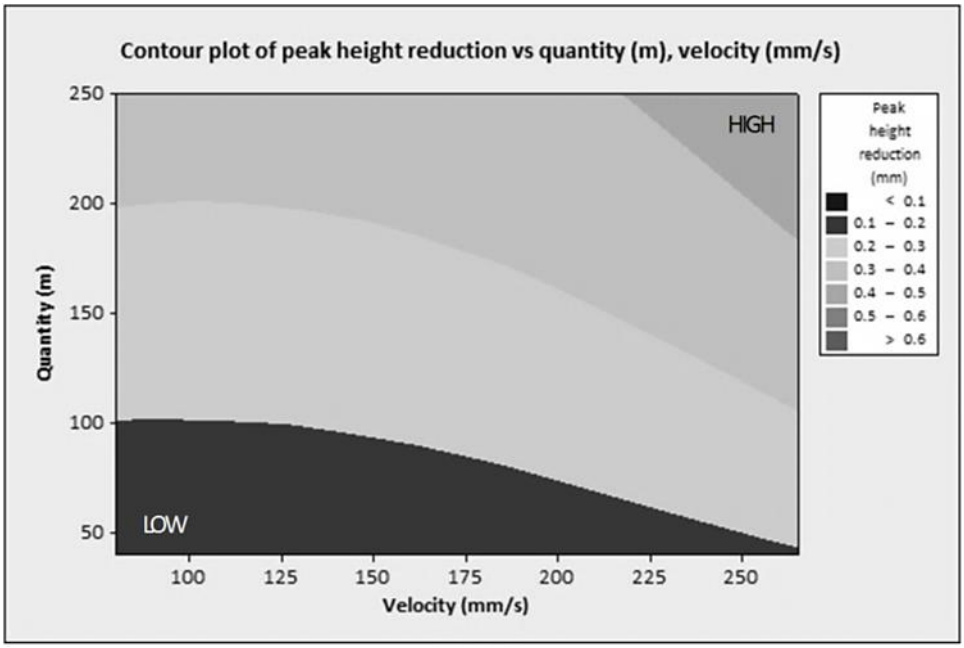

Figure 4.47 – Contour plot of velocity vs. quantity for peak height reduction responses.

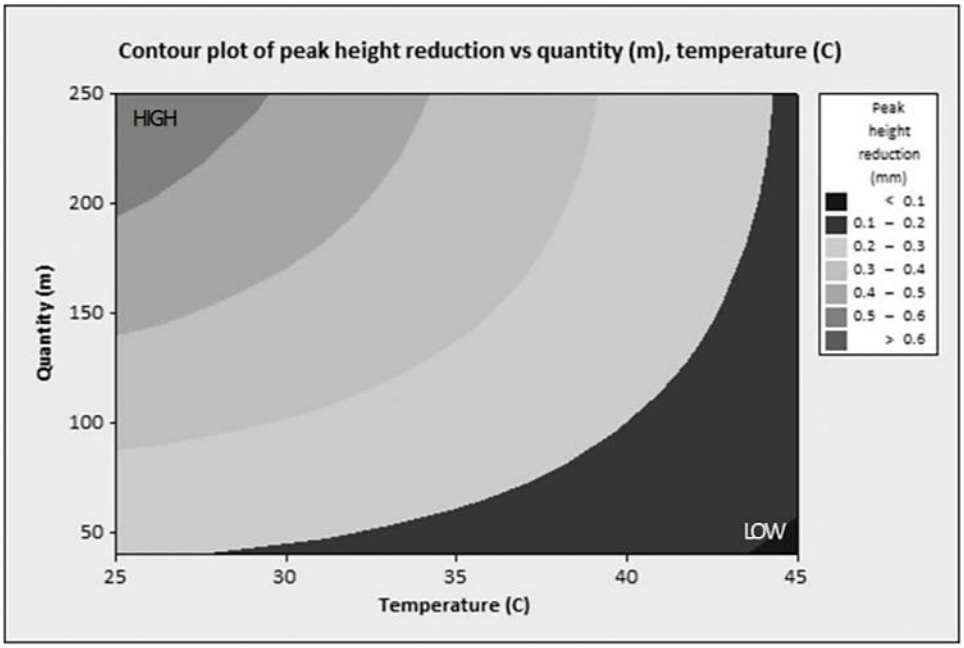

Figure 4.48 – Contour plot of temperature vs. quantity for peak height reduction responses.

A relationship between higher velocity and lower temperature appears to be conducive to reduction of peak height on a sample edge as illustrated by figure 4.47. Peak height is different to material removal, as the AFM process is a ‘constant-contact’ manufacturing method whereby an edge is exposed to a flow condition which, in a majority of cases, will not naturally produce a tangential radius. Peak height is useful to determine the actual location between a pre-process POI on an edge and processed POI on an edge. This plot shows agreement with the previous material removal plots, although the

widths and continuity of the contours are not so well defined. Similar to the quantity vs. temperature MR plot (figure 4.45), a quadratic relationship is seen between the two factors in figure 4.48, but the underlying finding is the requirement for a more viscous media to be worked over a longer duration to achieve the greatest PHR. As temperature is increased, the matrix softens and reduces the grit support, but perhaps most interesting is the difference between this and the material removal equivalent – as quantity increases, MR slows but doesn't stop – as far as this plot shows, PHR stops altogether, meaning that MR will continue to increase, but PHR does not.

4.6.1.6 Average roughness error assessment.

Average roughness mean responses vary between 0.242µm and 1.252µm, while standard deviation varies between 0.006µm and 0.08µm. As a percentage of the mean, deviation of individual runs vary between 0.66% and 9.61%. Population mean shows an average roughness response of 0.569µm, average deviation for the whole dataset at 0.031µm and average percentage deviation of 5.79%. Boxplot Y axis values are noted in three values; velocity, temperature and quantity, comma separated and in that order.

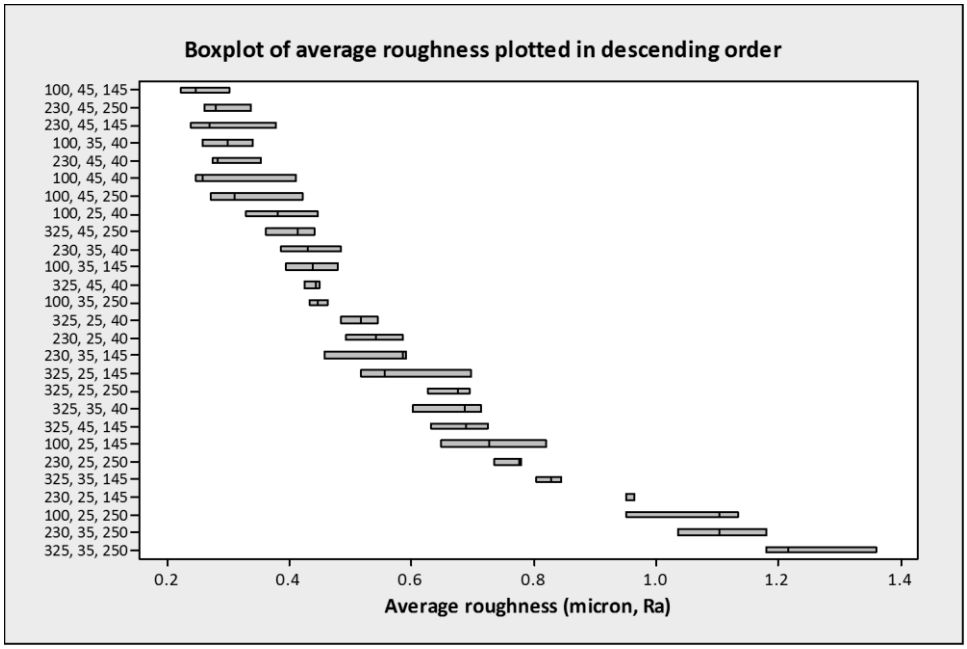

Figure 4.49 – Boxplot of average roughness plotted in descending order.

The data is represented graphically below in figure 4.49 which shows that the error is not linked to processing parameters that resulted in a higher average roughness, nor to any specific level of velocity, temperature or quantity, as all 27 combinations are randomly spread throughout the Y axis, ordered by average roughness response.

4.6.1.7 Material removal error assessment.

Material removal mean responses vary between 0.15mm^2 and 1.05mm^2 while standard deviation varies between 0.004mm^2 and 0.059mm^2. Standard deviation as a percentage of the mean varies between 0.51% and 8.36%. Average MR response is 0.330mm^2, average deviation for the whole dataset at 0.016mm^2 and average percentage deviation of 4.89%. The data is represented graphically in the boxplot (figure 4.50) which shows that the error is linked to processing parameters where temperature is lower and processing quantity is higher. It could also be taken that greater material removal results in greater error, which is something to consider when planning to 'hit a target' in production planning. MR does not appear to be exclusively linked to greater quantity however – the V100, T25, Q250 run, second from bottom shows a minimal deviation. There is empirical evidence here that potentially describes the machine's tendency to fail to process parts with repeatability when user-chosen operating parameters force the machine to work harder, for longer.

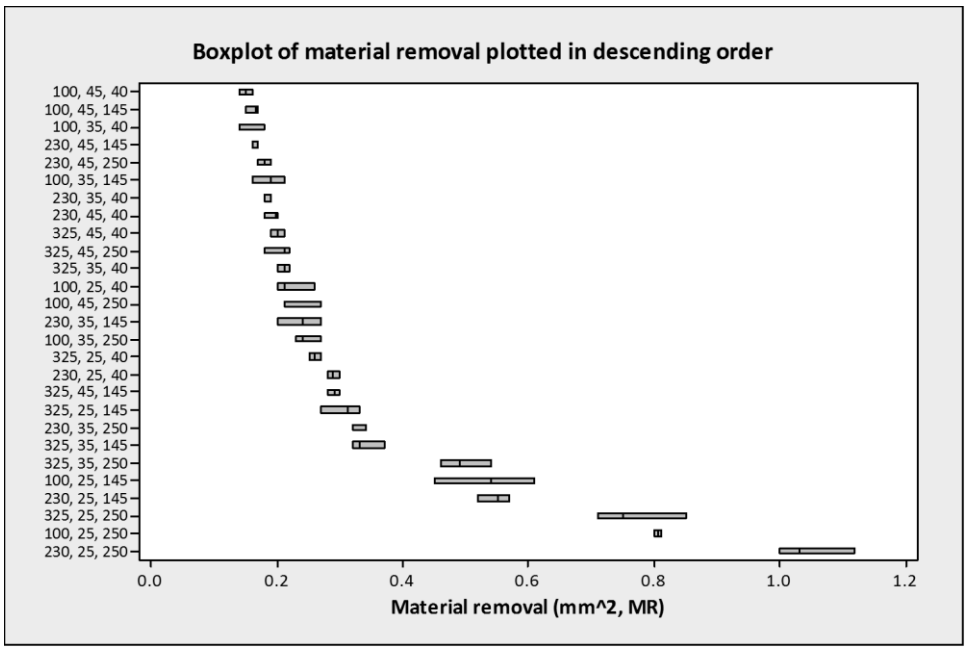

Figure 4.50 – Boxplot of material removal plotted in descending order.

4.6.1.8 Peak height reduction error assessment.

Peak height reduction mean responses vary between 0.039mm and 0.646mm while standard deviation varies between 0.002mm and 0.057mm. Standard deviation as a percentage of the mean rests between 0.89% and 9.78% for individual runs. Average peak height reduction response is 0.279mm, average deviation for the whole dataset is 0.016mm and average percentage deviation is 5.34%. The data is represented graphically below in figure 4.51 – it shows that the error increases in proportion with the magnitude of the response, a feature in common with figure 4.50. The same

argument can be made with the peak height reduction as with material removal – higher quantity appears conducive to greater error, which may be linked to mechanical load on the machine. Errors are relatively well distributed, but difference is greater and centre points more spread with increasing PHR. Practically speaking, the only way to improve upon these results is to adopt a more academic approach to the machine control – the boxplot suggests there is an error in processing quantity that is compounded as the workpiece is processed over a longer period.

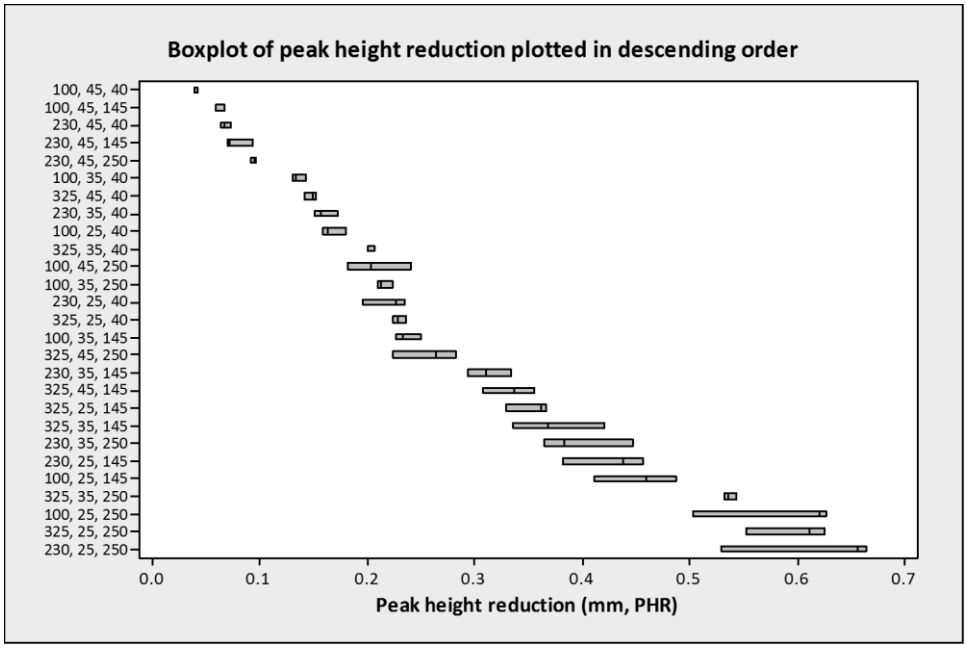

Figure 4.51 – Boxplot of peak height reduction plotted in descending order.

4.6.1.9 Acceptability.

The results collected from the samples have been assessed for error and while there are anomalies in certain places, the data is useful for taking forward into a more detailed analysis and for predictive model development. The initial look and error assessment activities have provided several items for discussion;

- Effects of data error on further work.
  Across all three response variables, there is an average population deviation of ~5%, and no more than ~10%. This error may be compounded in a model, but in the event of the model proving to be beyond usefulness, there should be consideration given to the true application of the data;
    - For surface finish work, Mollart are typically dealing with a ‘no more than’ type of tolerance limit – this means that a customer drawing will define an upper limit or a maximum roughness. To combat error in a roughness prediction model, one would simply select the parameters that

met the criteria of the lowest level with confidence. The deviation achieved above is an average of 0.031µm Ra.

- For edge-rounding and peak height reduction work, Mollart are dealing with a 'range' value, i.e. 1-2.5mm radii – this means the customer are looking for a value that rests between these two. The accuracy of the data is perfectly sufficient for this. The data shown above achieves standard deviation of 0.016mm^2 and 0.016mm for material removal and peak height reduction respectively.

- Application of data to further process models.
  This project deals with the application of AFM process parameters in order to hit a specific target value of a desired response variable. This type of process model is known as prediction, but the data may eventually be used in an optimisation model (one which aims to maximise or minimise a specific response) or in a calibration model (one which may be used to duplicate the behaviour and subsequent effects of a batch of media or a refurbished machine). Accuracies may change job to job, but assuming a worst case error of 10% on a prediction model output using the above data is reasonable.
- Pre-process roughness and surface roughness results.
  The majority of experimental combinations used in this experiment have been shown to generate a rougher surface than the pre-process machined roughness. As surface-finishing and edge-rounding ability appear to be at odds with one another, the lay-person may ask whether 'AFM' can polish titanium at all – this is a gross over-simplification – clear evidence has been shown that AFM is a technique which requires the engineer to make constant trade-offs between factors. Empirical evidence has been presented that a weaker media matrix (achieved through increased temperature) will provide a better finish – this minimises the depth of indentation as illustrated in white light interferometer results. The conventional wisdom, influenced by academic work and traditional grinding knowledge states that a small grit will indent even less, providing a better finish. Therefore, the conclusion can be reached that the experimental conditions shown here are only conducive to improving finish at the edge of the process space explored – section 4.7 will utilise smaller grit, which should yield a more impressive surface finish, but poorer material removal.
- Philosophy of machine parameter influence.
  The three variables controlled on the machine had been used prior to this work at Mollart as the only way of manipulating the process. The initial look has shown that VTQ are used to reach a given geometrical form – one that the media has the potential to reach, while providing a small level of flexibility in media behaviour manipulation.

4.6.2 Full factorial analysis.

Analysis is carried out as per the steps in figure 4.32. For each of the responses (Ra, MR, PHR), the contribution made by V, T and Q is studied.

4.6.2.1 Factor effects assessment for surface roughness.

The half normal plot in figure 4.52 is used as a graphical representation of the significance of model terms. In this example, the full factorial experiment presents 80 degrees of freedom, whereby two thirds are error terms. Terms of significance are found to the right hand side of the plot, and further up the Y axis. This plot shows factor B to be the most effective, followed by AB, C, etc. This data can be copied from the graph to produce a ranked effects list. AC is close to the guide line (leftmost line with triangular points) – it is considered insignificant. Analysis of variance is used to determine whether the model proposed is significant –table 4.17's F-value of 116.3 implies the model is significant – there is only a 0.01% chance this could occur due to noise. Values of Prob>F less than 0.05 indicate model terms A, B, C, AB, BC and ABC are significant. Values greater than 0.1 indicate a lack of significance, such as the interaction relationship of AC. In table 4.18, the strong significance of terms above, a deviation of 0.045µm (Ra) and excellent agreement between R-squared values, means the values collected in the experimental work are good to ascertain the main effects, residuals and interactions. Adequate precision should read at least 4; 38.743 is a very good signal to model the design space.

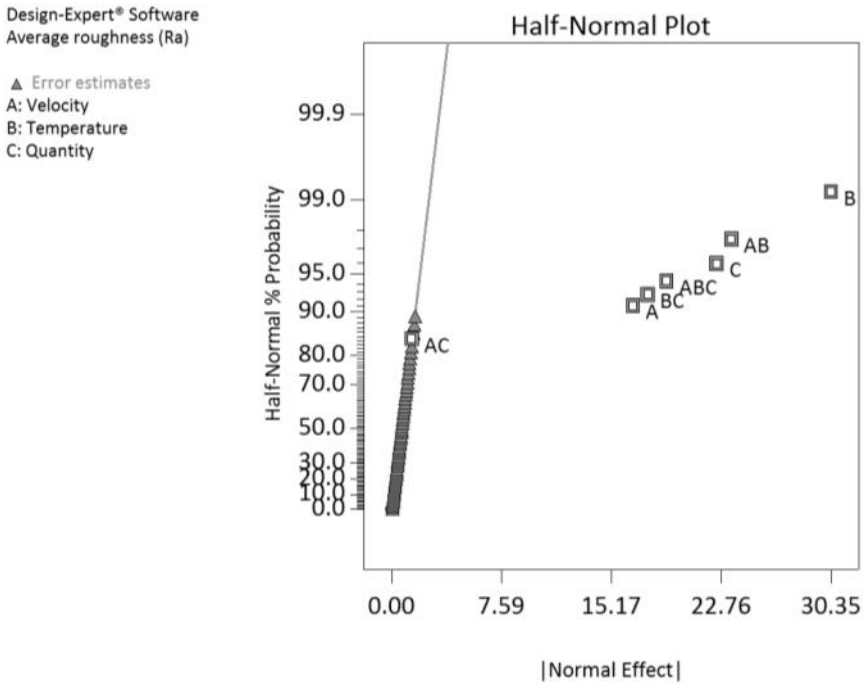

Figure 4.52 – Half normal plot for average surface roughness.

Table 4.17 – ANOVA classical sum of squares type II.					
Source	Sum of squares	Degrees of freedom	Mean square	F value	P value (prob>F)
Model	6.170	26	0.24	116.30	< 0.0001
A – Velocity	0.580	2	0.29	142.12	< 0.0001
B – Temperature	1.890	2	0.95	464.05	< 0.0001
C – Quantity	1.040	2	0.52	255.52	< 0.0001
AB	1.160	4	0.29	142.32	< 0.0001
AC	0.013	4	0.003307	1.62	0.1823
BC	0.670	4	0.17	82.35	< 0.0001
ABC	0.810	8	0.10	49.41	< 0.0001
Pure error	0.110	54	0.00204		
Corrected total	6.280	80			

Table 4.18 – Deviation and predictability figures.			
Standard deviation	0.045	R-Squared	0.9825
Mean	0.57	Adjusted R-squared	0.9740
Coefficient of variation (%)	7.94	Predicted R squared	0.9605
Predicted residual sum of squares	0.25	Adequate precision	38.743

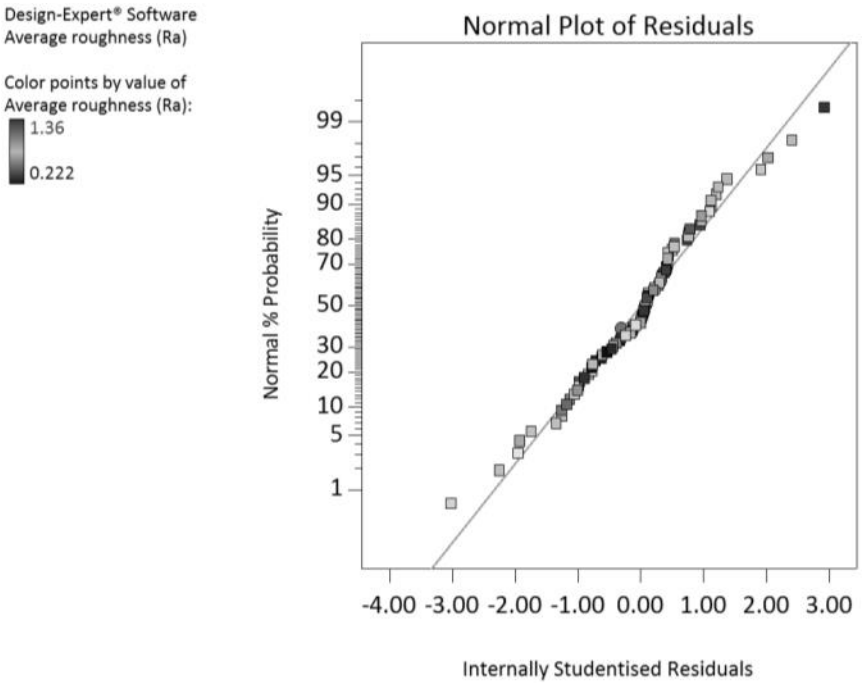

Figure 4.53 – Normal probability plot of residuals for surface roughness.

Residuals are errors in the fitted model that are not accounted for by significant factors and standard error combined. The normal plot in figure 4.53 shows whether error values follow a normal distribution, depicted by points marked on the line. This plot

demonstrates a good fit to the distribution, with some points breaking away at either end – if residuals are normal, model errors are considered predictable, which increases confidence in further analysis.

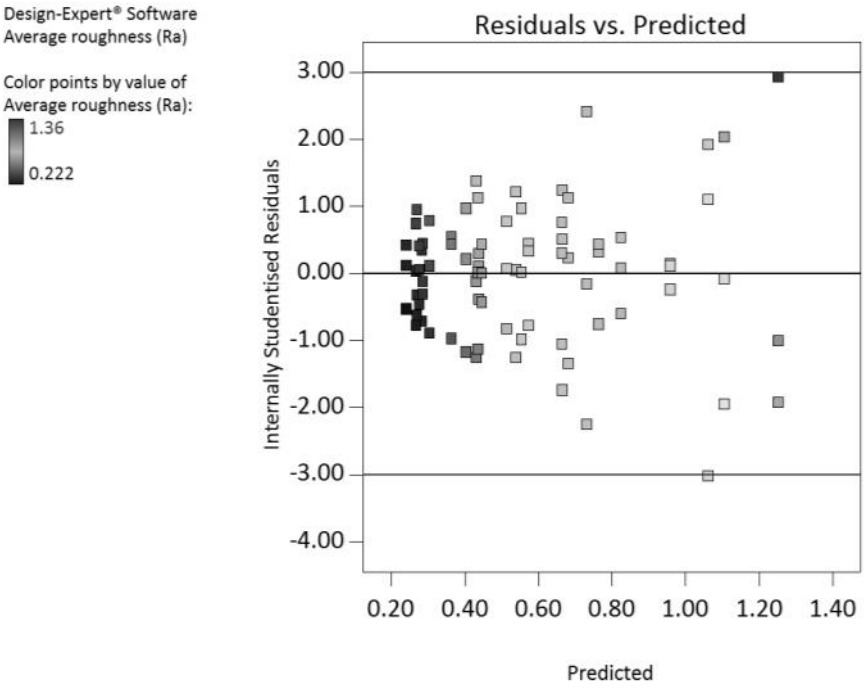

Figure 4.54 – Internally studentised residuals versus predicted values.

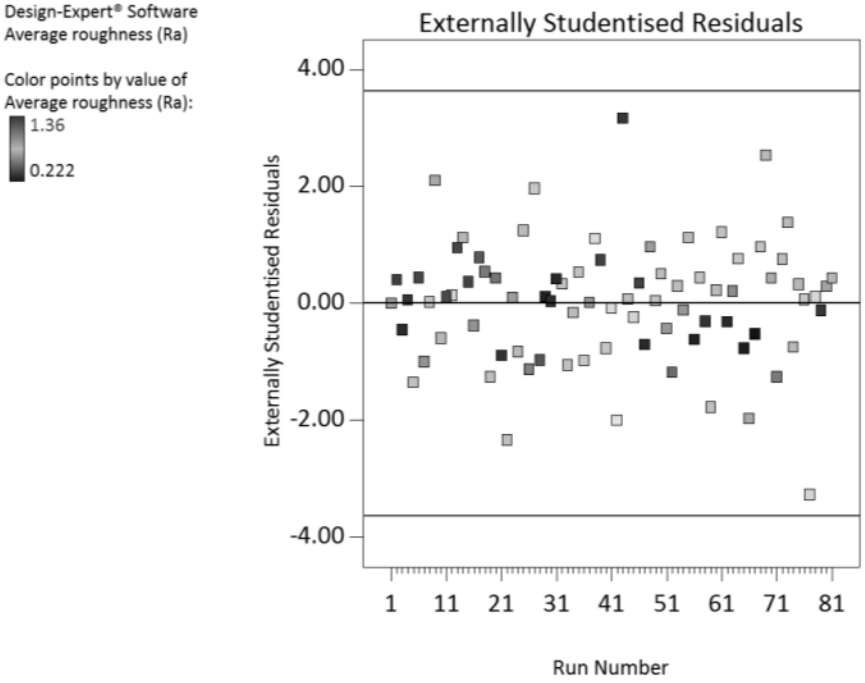

Figure 4.55 – Externally studentised residuals versus run order.

Presented in figure 4.54, the plot shows residuals against the predicted response using actual values from design input – in this case, the residuals are evenly scattered about the centre until 0.8Ra is reached on the X axis – this is representative of previous boxplots shown in the initial look phase, suggesting that error increases with increased response magnitude, something which requires increased machine capability to correct. Plot 4.74 presents the number of standard deviations that the actual value deviates from the predicted value after removing the point from calculations – this allows the identification of abnormal runs, of which there appear to be three in this example – the dark outlier is high roughness (bad) and the light outlier is low roughness (good).

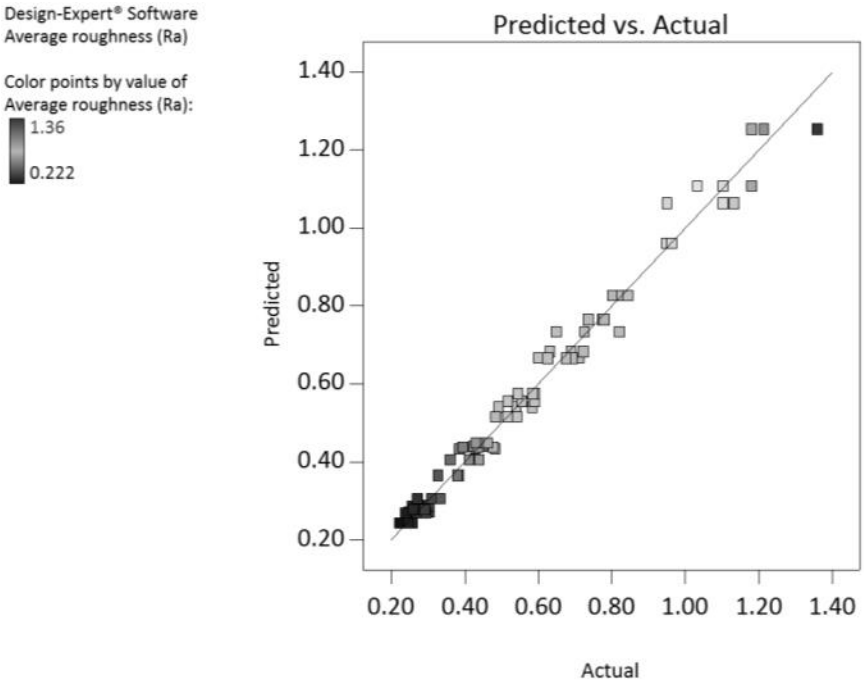

Figure 4.56 – Predicted versus actual average roughness response.

While the response surface design presents an input value independent system for response prediction, the full factorial also predicts values, but only with the provided repetitions and only for levels used in the experiment. Figure 4.56's purpose is to detect a value or group of values which are not well described by the model. Given the consistent spread about the line of best fit, it can be assumed that model terms shown in the ANOVA table are representative of effects seen on the samples and thus, interactions and main effects will be reliably produced, as will be accompanying error estimates. In the full factorial design, multiple interacting factors exist – single factor analysis in this case is not helpful as the resulting line plots are subject to vast change when manipulating levels of other values. For this reason, it is interesting to view VT (AB), VQ (AC) and TQ (BC) relationships within the average roughness dataset as presented in figure 4.57. This plot shows that (with average quantity) roughness will linearly increase with velocity when processed at 35˚c, but velocity has no effect until

230mm/s is reached when processed at 25˚c and 45˚c. Increasing velocity to 325mm/s at 25˚c will reduce roughness, while the opposite is true when running at 45˚c.

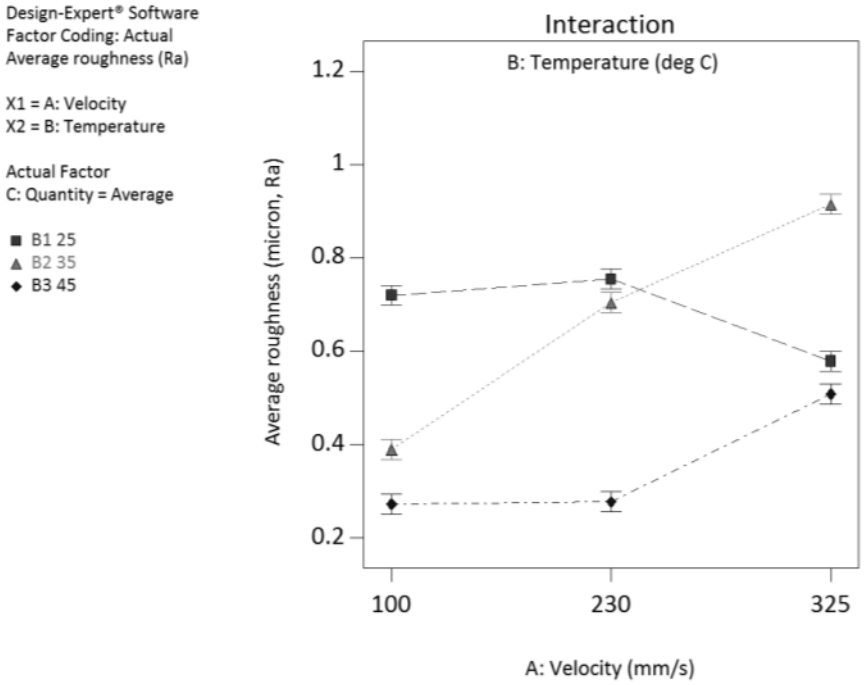

Figure 4.57 – Two-way interaction, effects of velocity and temperature on average surface roughness.

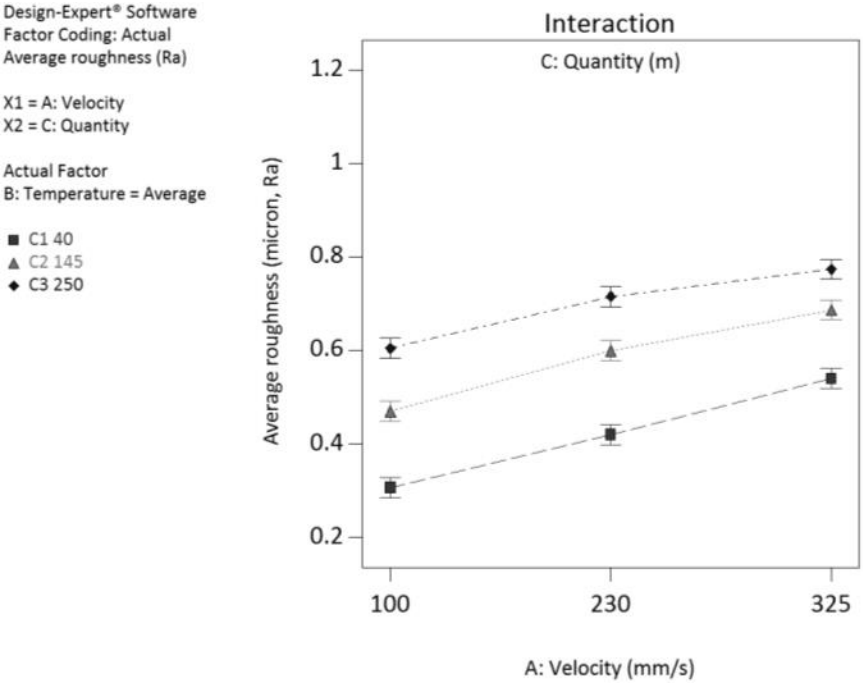

Figure 4.58 – Two-way interaction, effects of velocity and quantity on average surface roughness.

The VQ (AC) relationship shown in figure 4.58 is insignificant according to the ANOVA table – irrespective of levels, the VQ effect means roughness increases with

velocity, but all three levels for quantity have no effect on the finish. As there is no real change, this two factor interaction becomes a poor option when attempting to control finish in a production environment – it is limited in both magnitude of response and rate of change. Reasons for this may be grounded in the 'sandpaper theory' whereby the grit within the media is a predetermined size that isn't going to change during operation – continually using this grade of sandpaper (or media) will indent surface to same level every time until the surface indentations match the protruding length of sandpaper grit. This theory is reinforced by the slight declining trend in the triangular and diamond lines (145m and 250m) after the velocity passes 230mm/s, as the longer the surface is processed, the less change we are likely to see.

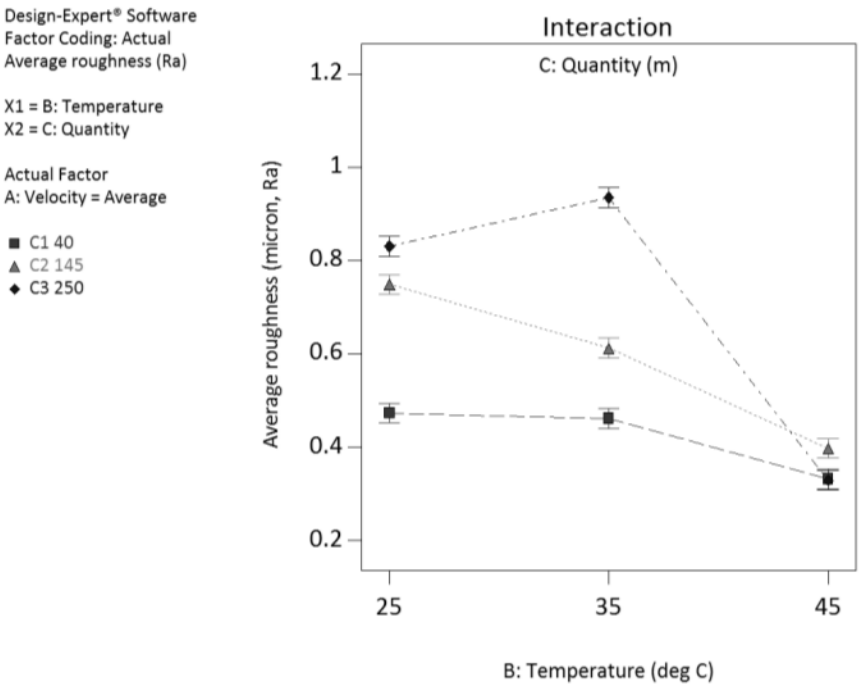

Figure 4.59 – Two-way interaction, effects of temperature and quantity on average surface roughness.

Figure 4.59 displays an interaction that is considered significant, and can be seen quite clearly to be temperature dominated – with a set average velocity, a low quantity of processing (40m) will show minimal change in surface roughness across the range of temperatures, although a slight improvement is clear. Increasing the processing quantity gives a rougher surface when starting the processing, but decreases linearly as temperature increases, providing a greater magnitude of change. The diamond line (longer processing, 250m) tells a different story – when processing a component for a longer duration, a lower temperature will still promote a rougher surface, but as temperature increases (supposedly weakening the grit support), the surface becomes rougher – the only explanation in this case, bearing in mind velocity is constant for the entire plot, is to suggest that the 35˚c temperature when processed over a longer duration is more aggressive, perhaps by way of rheology or some kind of hysteresis

effects. It is likely that the materials ability to store energy is improved at 35˚c, and the increased processing duration increases the number of total shear cycles the polymer is exposed to. This behaviour however does not translate directly to the two lesser quantities beneath. Irrespective of this behaviour, all quantities of processing are subject to the same effect at 45˚c. They plummet to the most effective surface finishing temperature – if the project/customer/user required a surface finish in their workpiece, a high temperature is almost certainly a prerequisite.

4.6.2.2 Factor effects assessment for material removal.

Figure 4.60 presents the significant factors for material removal as the two factor interaction of BC, temperature-quantity. By quite some margin, the AB (velocity-temperature) relationship trails, running at the head of the group leading to guide line. The error terms are neatly lined up and make a tiny fraction of the model's pure error. As with surface roughness, the velocity-quantity term is relatively insignificant, albeit less-so that in the average roughness dataset.

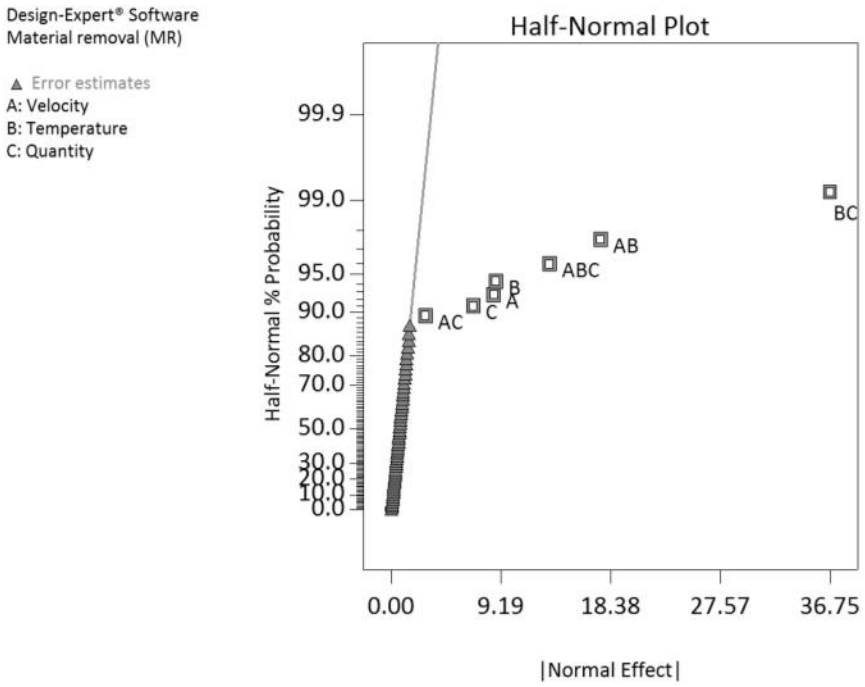

Figure 4.60 – Half normal probability plot for material removal.

The model F-value of 225.46 in table 4.19 implies the model is significant – there is only a 0.01% chance that the model has occurred due to noise. Where Prob>F values are less than 0.05, the model terms are significant, which in this case includes all terms, although the AC term stands apart in terms of probability.

Table 4.19 – ANOVA classical sum of squares type II.					
Source	Sum of squares	Degrees of freedom	Mean square	F value	P value (prob>F)
Model	4.01	26	0.15	225.46	<0.0001
A – Velocity	0.054	2	0.027	39.25	<0.0001
B – Temperature	1.64	2	0.82	1196.70	<0.0001
C – Quantity	1.01	2	0.5	736.43	<0.0001
AB	0.22	4	0.055	81.12	<0.0001
AC	0.010	4	0.002624	3.84	0.0082
BC	0.94	4	0.23	342.88	<0.0001
ABC	0.14	8	0.018	25.73	<0.0001
Pure error	0.037	54	0.000684		
Corrected total	4.05	80			

Table 4.20 – Deviation and predictability figures.			
Standard deviation	0.026	R-Squared	0.9909
Mean	0.33	Adjusted R-squared	0.9865
Coefficient of variation (%)	7.91	Predicted R squared	0.9795
Predicted residual sum of squares	0.083	Adequate precision	59.603

The predicted R-squared is in good agreement with the adjusted R-squared (shown in table 4.20) and adequate precision reads greater than 4, ensuring the model terms are suitable to describe the factor interactions.

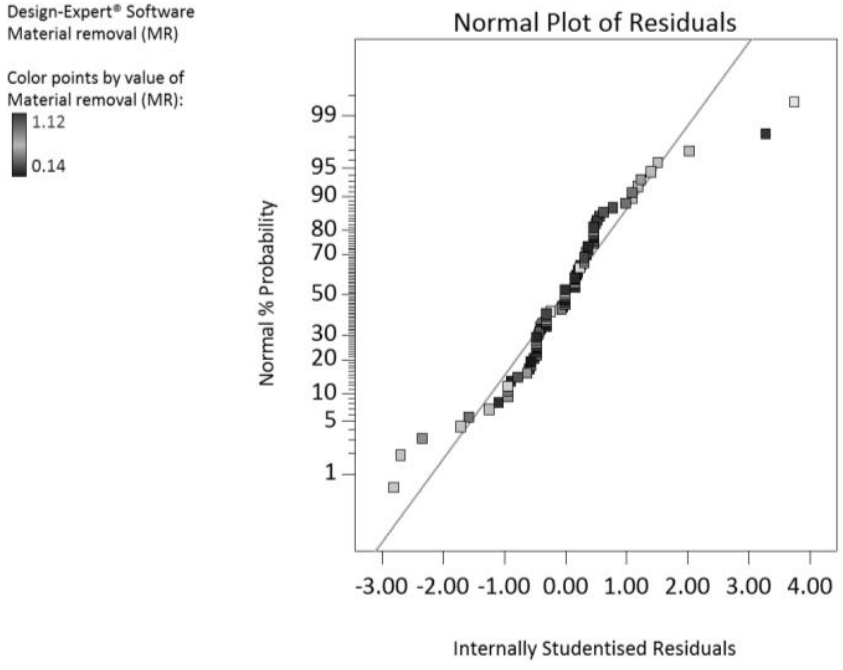

Figure 4.61 – Normal probability plot.

In figure 4.61, the points form a slight ‘S’ shape, but ultimately returns back to the line. The presence of outliers only truly exists at the top end, once more with the greater response magnitude, highlighting that surface roughness is not the only response variable to see this effect – further reinforcing the need for greater machine axis control.

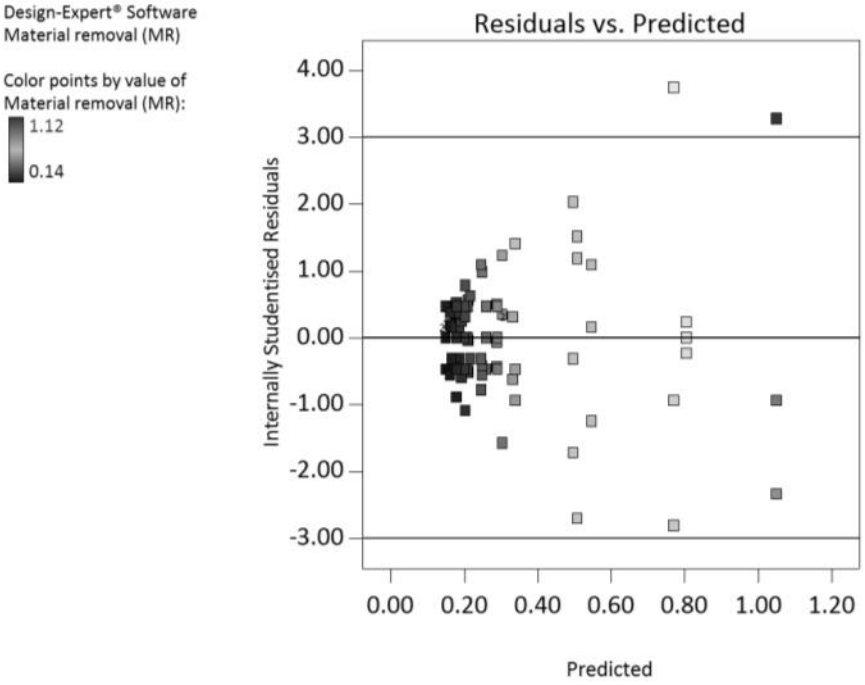

Figure 4.62 – Internally studentised residuals versus predicted values.

The homogeneity of the scatter shown in figure 4.62 begins to break up at 0.4mm^2 (predicted MR value), and comes back online to within 1σ at 0.8mm^2, but is far from regular, exceeding 3σ between 0.8mm^2 and 1.1mm^2. There is little that can be done with this at this stage, but may benefit from a different strategy of obtaining a greater spread of results – i.e. initial experiment planning may benefit from checking a spread of test samples to better fill the process space. Normally a transformation should be applied to the ‘megaphone’ pattern seen here to ensure assumptions of constant residual error do not affect the ANOVA results, however, using a base 10 log transformation, the data does not affect results. In addition, the error shown in figure 4.63 is well spread about the centre, with outliers as previously seen with other error visualisation tools. Material removal responses are clustered at the lower end of the response range, i.e. 0mm^2 to 1.2mm^2 as described by the legend – this doesn’t affect the ability to check interactions with the model, as a range of responses (acknowledged to be fewer) are generally seated well on centre.

Material removal values as collected rest in a lower range as illustrated by figure 4.64, suggesting experimental values should have been somewhat extended to increase the effect, however, there were two other responses to consider and there was little knowledge of the apparent diminishing returns present in this MR dataset. Ultimately,

there were some combinations of factors and levels which provided the mid- and upper-datapoints, and it is helpful to see they fit well on the same line as formed primarily by the lesser (higher quantity) responses.

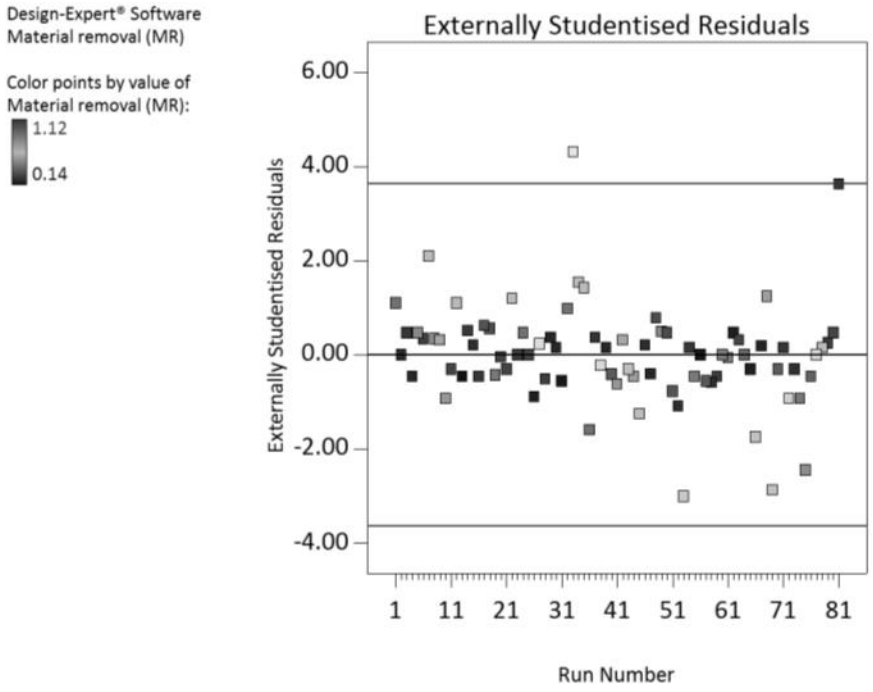

Figure 4.63 – Externally studentised residuals versus run order.

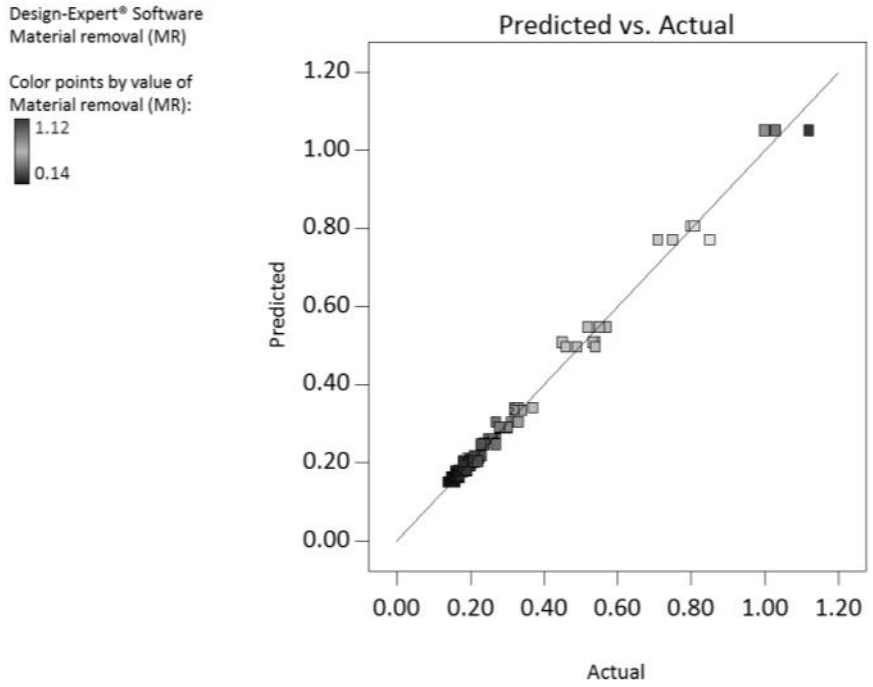

Figure 4.64 – Predicted versus actual response.

Figure 4.65 considers a constant quantity, and represents the three levels of temperature with square-, triangular- and diamond-marked lines. The X axis represents velocity in mm/s and the Y, material removal in mm^2. Focusing on the two upper temperature levels, increasing velocity exponentially increases material removal, however this does not translate when working with 25˚c. Starting at 100mm/s, material removal registers a $0.5mm^2$ response, and as expected, increasing the velocity to 230mm/s continues to increase the degree of material removal to the greatest level on the plot. However, the theory does not hold as the media reaches up to 325mm/s – MR drops by $0.15mm^2$ to $0.45mm^2$. This may be an example of the lack of edge conformity that occurs when the media is stiff and the velocity attempts to force it past a feature at speed. The unit of MR is an area based one which, given greater conformity, would see a greater surface area exposed to the flow. It is likely that the more viscous, cooler media travelling at 325mm/s is simply not making contact with the surface.

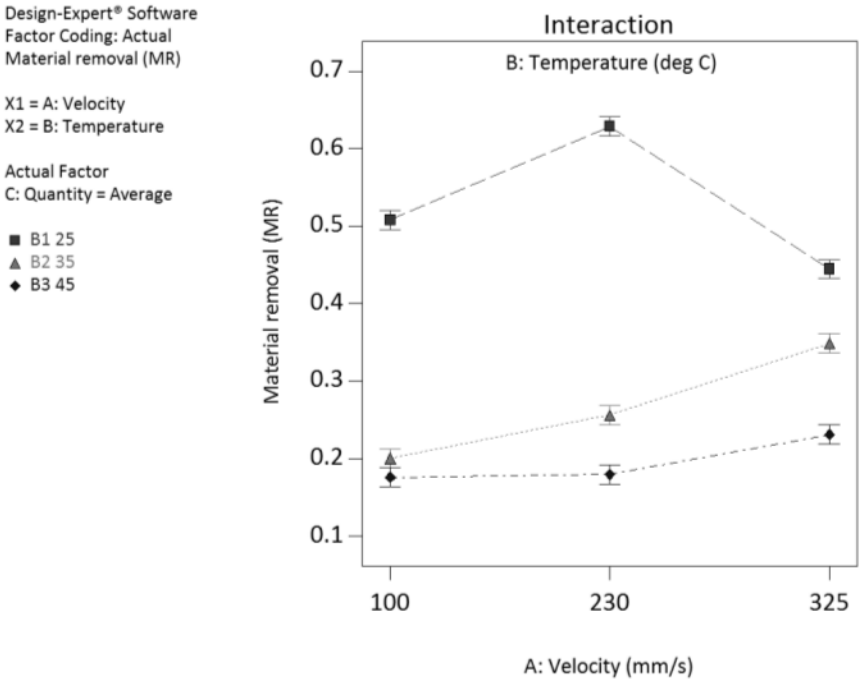

Figure 4.65 – Two way interaction, effects of velocity and temperature on material removal.

Temperature is the constant in figure 4.66 – three lines of varied processing quantity are plotted, and their effect on MR as velocity changes are assessed – the term AC (VQ) is far less significant than others and shares a similar form to the previous surface roughness AC plot. Material removal is driven initially by processing quantity, with only marginal improvements when velocity increases by another 130mm/s. Perhaps symptomatic of the previously derived relationship, none of the processing quantities increase MR further when paired with increased velocity – if the interface between part and media is separating, an area of extremely low velocity will be seen in the simulations of chapter 5.

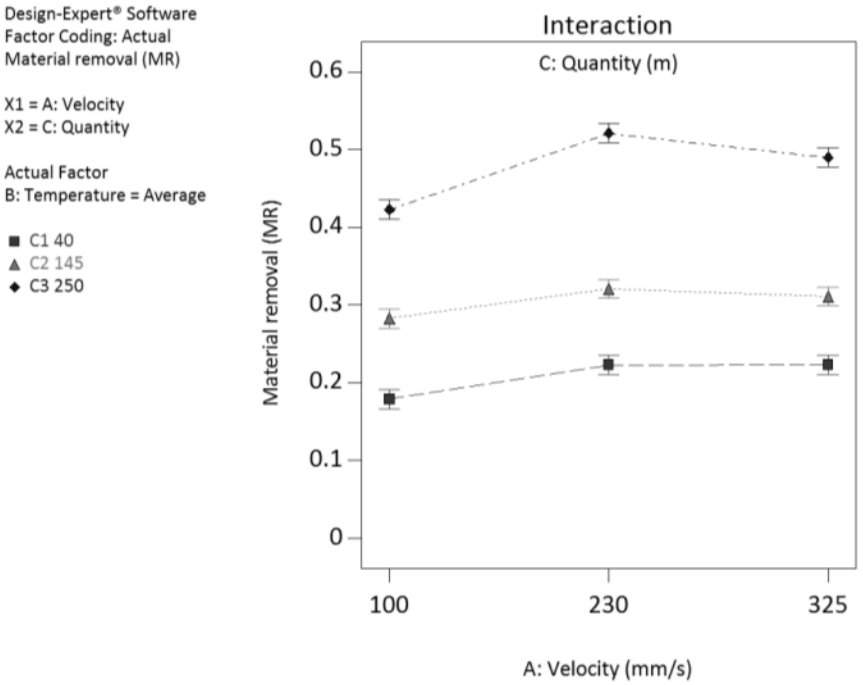

Figure 4.66 – Two way interaction, effects of velocity and quantity on material removal.

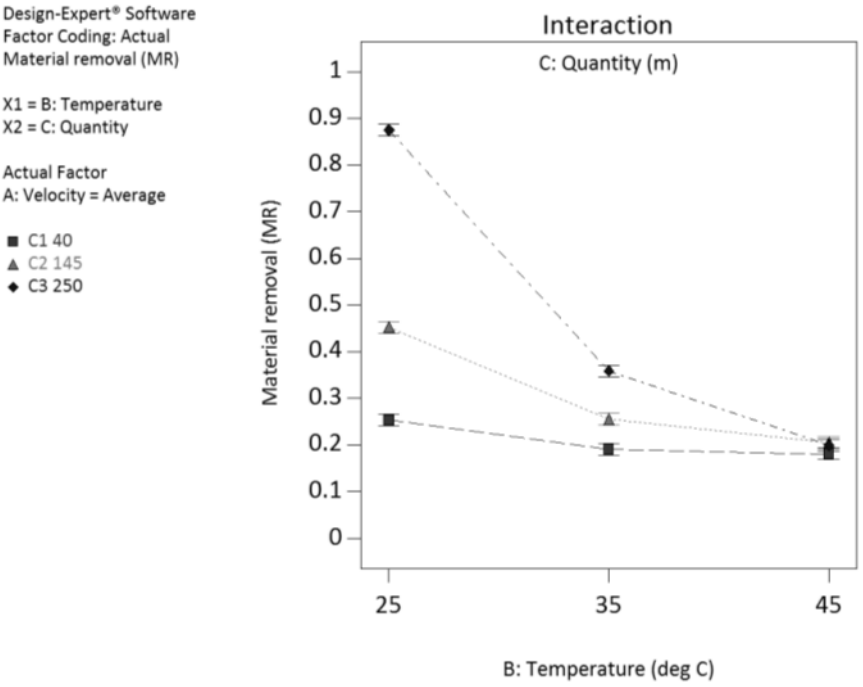

Figure 4.67 – Two way interaction, effects of temperature and quantity on material removal.

The most significant interaction in the material removal dataset is seen in figure 4.67. As velocity is held constant, the starting temperature shows the expected effect of low temperature and high quantity, generating a >0.85mm^2 MR response. Practically speaking, the relationship is important in applications where stock material removal is the target, whether that be bore honing or edge rounding. Upon a 10˚c increase to 35˚c,

the effect of processing quantity magnitude is reduced to within 0.2mm^2 of each other, which is reduced to functionally zero at 45˚c. The ability to chill the media is something present in the most basic of AFM machines; however the workpiece-induced pressure drop may cause problems when trying to pump the chilled highly-viscous product. While this plot displays a clear message that MR is best achieved by a high viscosity matrix, it is believed that a trade-off can be had between lower viscosity and larger grit – something that section 4.7 aims to prove. Mollart's production geometries contain flowpath features down to Ø3mm, which do not predispose themselves to low pressure pumping, so this figure may also make a case for the purchase of an uprated machine.

4.6.2.3 Factor effects assessment for peak height reduction.

In the PHR dataset, the plot shows media quantity (C) to be most conducive to achieving peak height reduction (mm) and as noted previously, the velocity-quantity relationship to be of comparative insignificance. Terms BC, A and AB should also prove to reveal process effects for helping to understand peak height reduction causes.

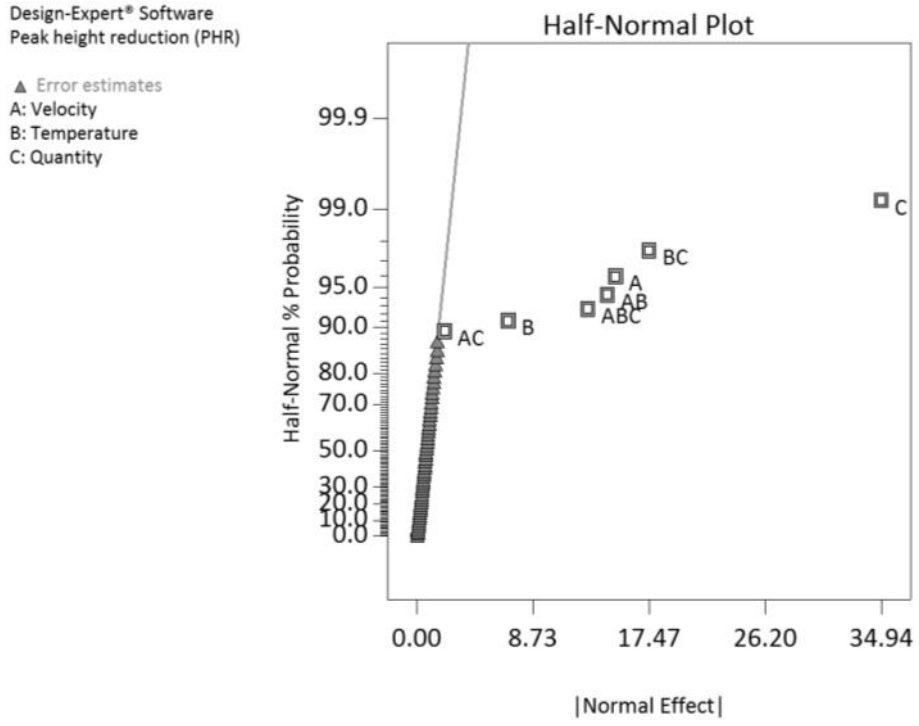

Figure 4.68 – Half normal probability plot for peak height reduction.

The model's F value of 140.98 in the ANOVA table 4.21 suggests excellent significance of the model – there is only a 0.01% chance that the model is formed by chance. All terms are significant, although AC is only 0.0008% from being insignificant, and will be treated as such.

Table 4.21 – ANOVA classical sum of squares type II.					
Source	Sum of squares	Degrees of freedom	Mean square	F value	P value (prob>F)
Model	2.38	26	0.091	140.98	<0.0001
A – Velocity	0.15	2	0.074	114.63	<0.0001
B – Temperature	0.95	2	0.47	730.66	<0.0001
C – Quantity	0.80	2	0.40	614.04	<0.0001
AB	0.14	4	0.036	55.15	<0.0001
AC	0.00663	4	0.00166	2.55	0.0492
BC	0.21	4	0.052	80.26	<0.0001
ABC	0.13	8	0.016	24.37	<0.0001
Pure error	0.035	54	0.000648		
Corrected total	2.41	80			

Table 4.22 – Deviation and predictability figures.			
Standard deviation	0.025	R-Squared	0.9855
Mean	0.28	Adjusted R-squared	0.9785
Coefficient of variation (%)	9.12	Predicted R squared	0.9673
Predicted residual sum of squares	0.079	Adequate precision	41.287

The predicted and adjusted R-squared values (table 4.22) are in good agreement with each other and the adequate precision ratio is 10 times greater than needed for confidence that signal is sufficient to continue working with this full factorial design model. Despite the slight S-curve, transformation provides no significant change to the ANOVA table or the following interaction plots. A range of PHR values are spread along and tightly conforming to the guide line in figure 4.69. There is one outlier, and as with previous response groups, it is of greater response value, but it is alone, and other values of a similar magnitude are fitted to the line well.

Taking a similar form to previous plots of this type, the residuals shown in figure 4.70 are virtually all within 3σ, although higher response magnitudes appear to be resting on the over-estimated side of the centre. In practical terms, these values are expected residuals of predicted values, so of little practical importance, but of interest in seeing where a bias in the data lies – as the graph is formed of predictions from actual values, the spread within 2σ and in the values up to ~0.6mm give confidence in the application of the terms used to construction interaction plots.

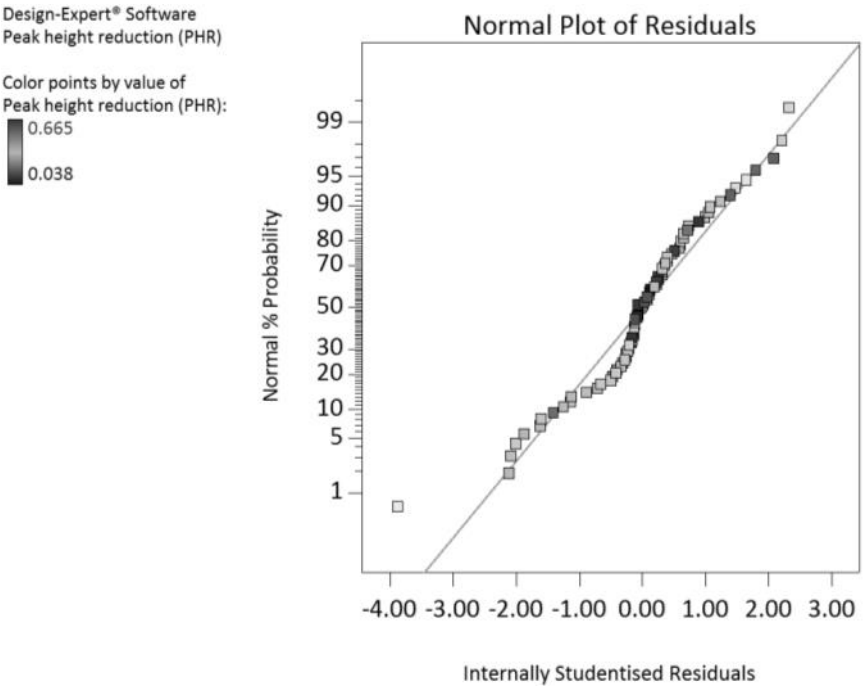

Figure 4.69 –Normal probability plot for peak height reduction.

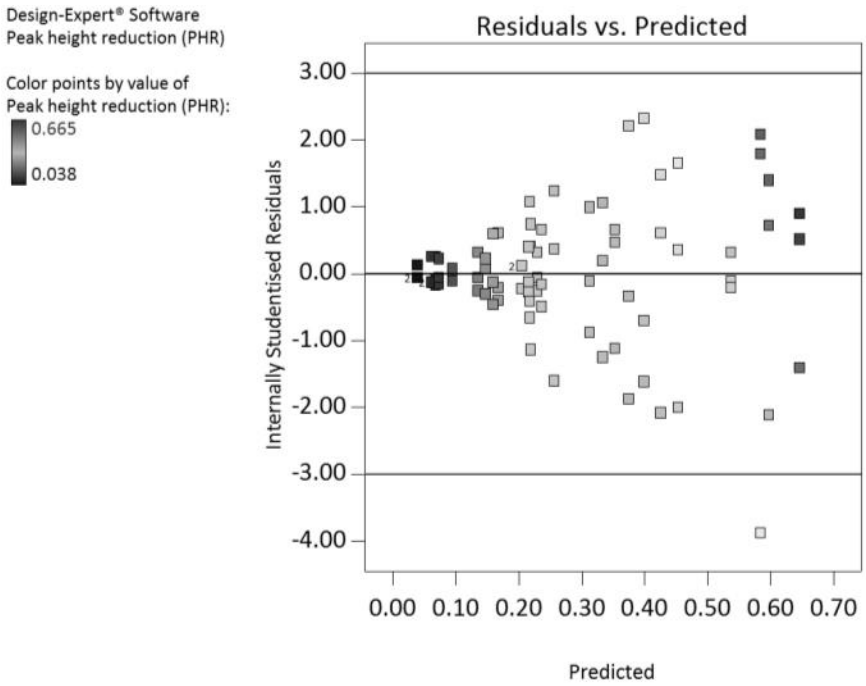

Figure 4.70 – Internally studentised residuals versus predicted values.

The purpose of figure 4.71 is to identify the number of standard deviations that the actual values deviate after removing the actual value and replacing it with a predicted one – the distribution appears relatively consistent about the centre with a good spread of points, both in location and magnitude. There is one outlier that may represent an abnormal run, but its influence is vastly reduced in its current position.

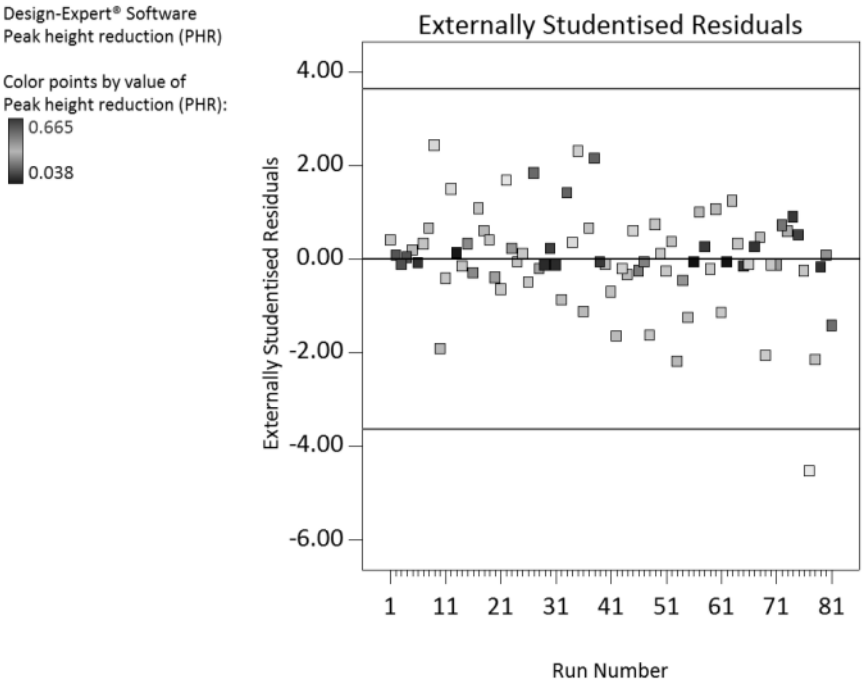

Figure 4.71 – Externally studentised residuals versus run order.

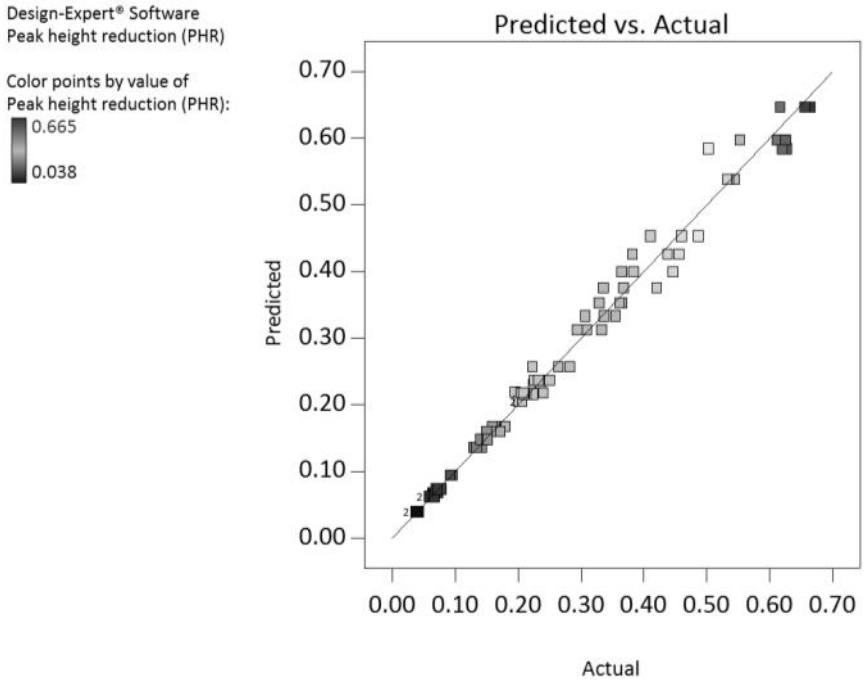

Figure 4.72 – Predicted values versus actual response for peak height reduction.

PHR presents the greatest spread of datapoints over the range of measurements, which should lead to a robust model. There are no clusters at the lower end of figure 4.72 and a good range distributed through the median response of ~0.35mm. A similar effect is seen in the greater response magnitudes as other figures (4.75, 4.83) pertaining to machine control accuracy, but not significantly deviated from the line of best fit.

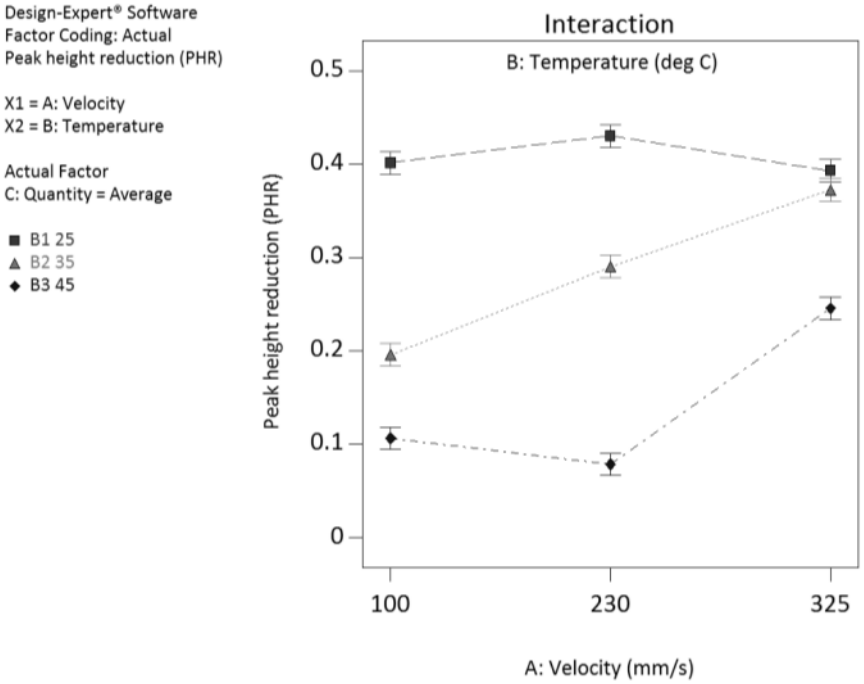

Figure 4.73 – Two way interaction, effects of velocity and temperature on peak height reduction.

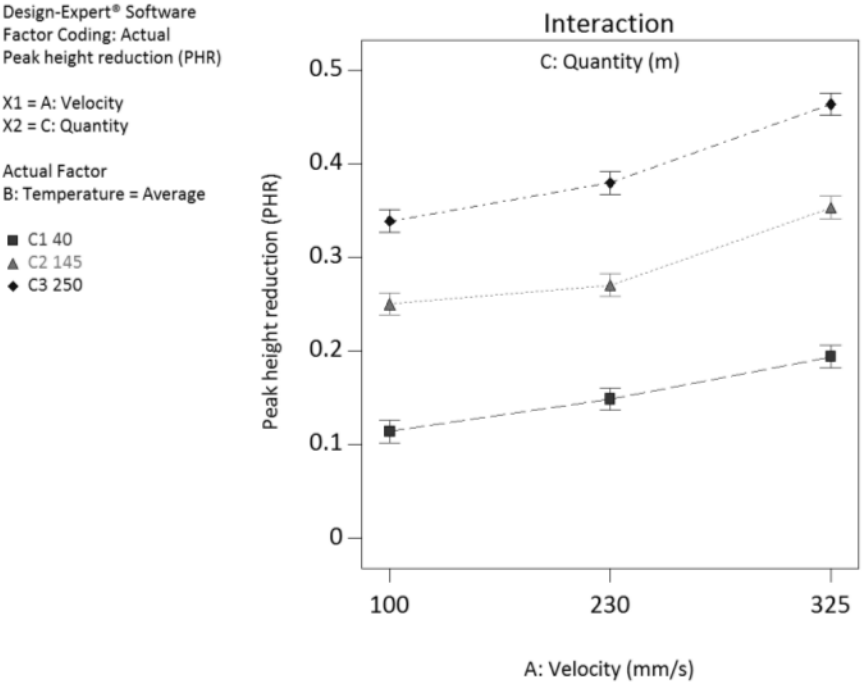

Figure 4.74 – Two way interaction, effects of velocity and quantity on peak height reduction.

In the interaction plot at figure 4.73, quantity is the constant and the response of PHR is driven by temperature and velocity – as expected, the lower the temperature, the higher the PHR, based on the well-established grit support theory. With an increase in velocity, PHR capability is further increased when working at 25˚c and 35˚c, but undergoes a reduction when moving faster in a 45˚c environment. This may be due to internal media

factors whereby 100mm/s at 45˚c allows transfer of momentum from matrix to grit, whereas moving faster at 230mm/s, the grit tumbles or moves around more within the polymer. By 325mm/s, the 45˚c trial shows a marked increase in PHR, suggesting a critical velocity is reached between the 0 and +1 levels where inertia is transferred once more and PHR can continue. A potentially similar effect as with MR is seen on the 25˚c line – as the media velocity increases to 325mm/s, the PHR ability is reduced. Viscosity effects and prevention of media-surface conformity may be to blame, but simulation of the more viscous lower temperature media will help identify the effects.

As the insignificant effect once more, the AC interaction displayed in figure 4.74 shows that for a constant temperature, the velocity has an almost universal effect on PHR – processing quantity only determines the start point, but the effects as velocity increases are no different to each other, only differentiated by the offset PHR levels as determined by the processing quantity. This VQ interaction in respect to PHR is only really useful if the user needs to ‘gear down’ and provide fine control where the user may need to achieve a specific target – other interaction plots present sharp changes, but in a radius generation application, it is useful to know that velocity provides a steady camber when temperature and quantity are fixed.

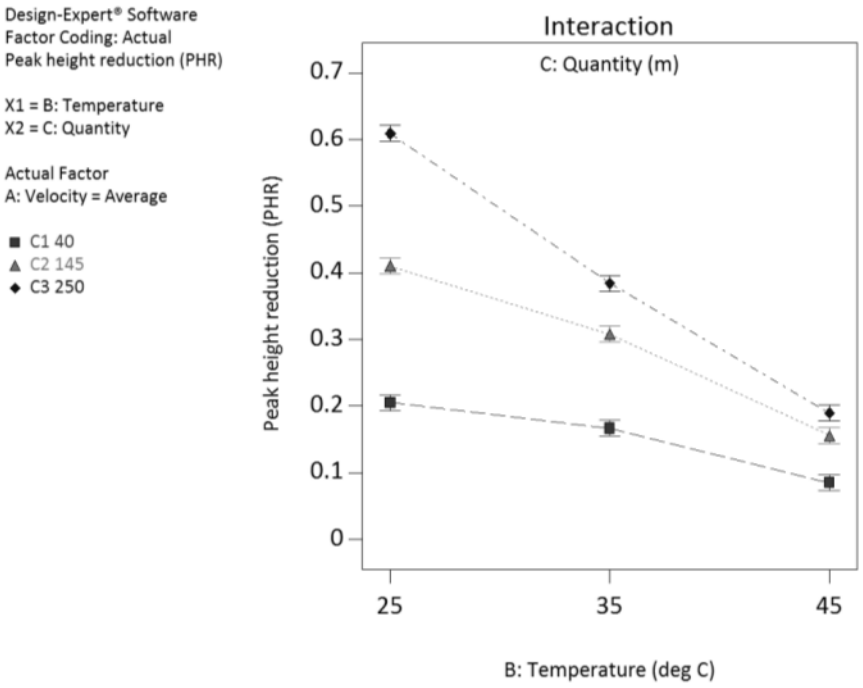

Figure 4.75 – Two way interaction, effects of temperature and quantity on peak height reduction.

When velocity is fixed, the most effective and predictable behaviour in PHR response is noted – in line with other work and prior interaction plots, behaviour shown in figure 4.75 illustrates why low temperature and high quantity are conducive to PHR. The rate of decrease is greater in the longest processing quantity, followed by the 145m and the 40m, showing the importance of temperature in the reduction of peak height – looking

at the start values, they are split by the same distance (0.2mm) as are the quantities – therefore it can be assumed that at 25˚c, PHR is reduced by 0.2mm in our test geometry for every 100m of processing. As seen previously, the increase in temperature gradually reduces the power of the media to grind away the peak of a feature. Of course, this plot is only valid for the material, media and geometry tested, placing critical importance on simulation for determining the actual flow condition and how it might affect the peak in an arbitrary geometry – we do now know that a 90˚ edge with a 45˚ flow prefers a more rigid media to increase PHR.

4.6.2.4 Full factorial generated data interpretation.

In figure 4.76, plots are shown at 25˚c, 35˚c and 45˚c. The most significant effect on surface roughness is temperature – increasing the temperature is thought to weaken the grit's supportive polymeric matrix – the evidence agrees with this as a systematic reduction of roughness is achieved by moving through the temperature range; however there are erroneous increases after moving from 25˚c to 35˚c – this may support the theory that in a given setup, the weakening of the polymer through heat may increase media-surface interaction. This theory is reinforced by the effect being strongest in high-velocity high-quantity environments. After 35˚c, the matrix loosens to the point that grit support is lost and depth of indentation is reduced.

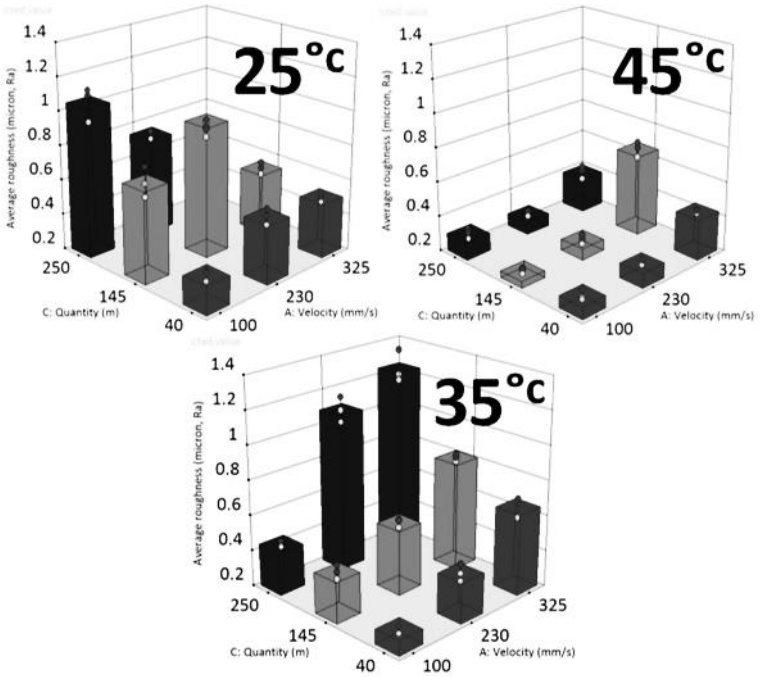

Figure 4.76 – Surface roughness plots. VQ interactions at three levels of temperature.

The second-most significant factor for material removal is not a single factor – it is the velocity-temperature interaction. It is possible to generate an MR response by

manipulating these two factors; this is inherently useful to know – in a production environment, there may not be scope to increase machine maximum pressure capacity, resulting in lower flow speeds – this can be counteracted by using a lower temperature or higher quantity as pictured in figure 4.77.

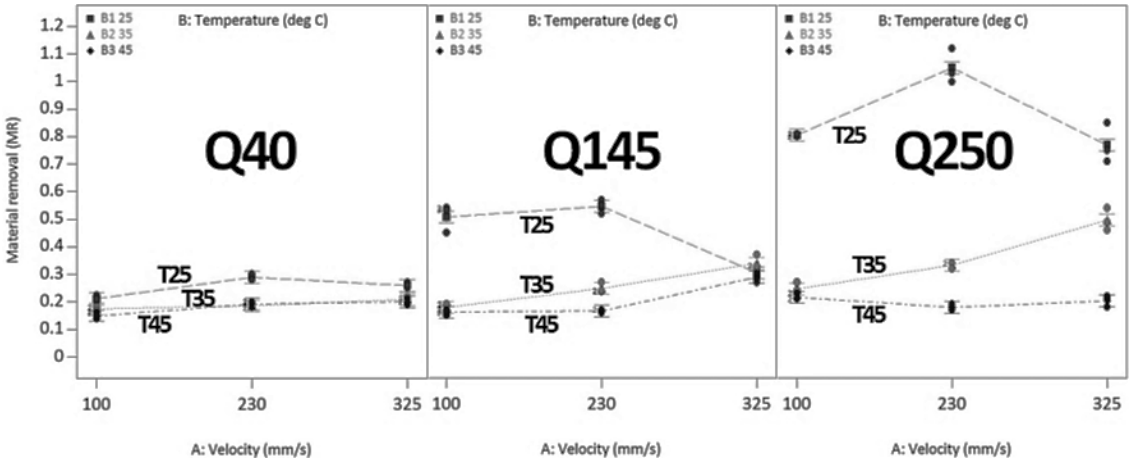

Figure 4.77 – Material removal plots, VT at 40m, 145m and 250m.

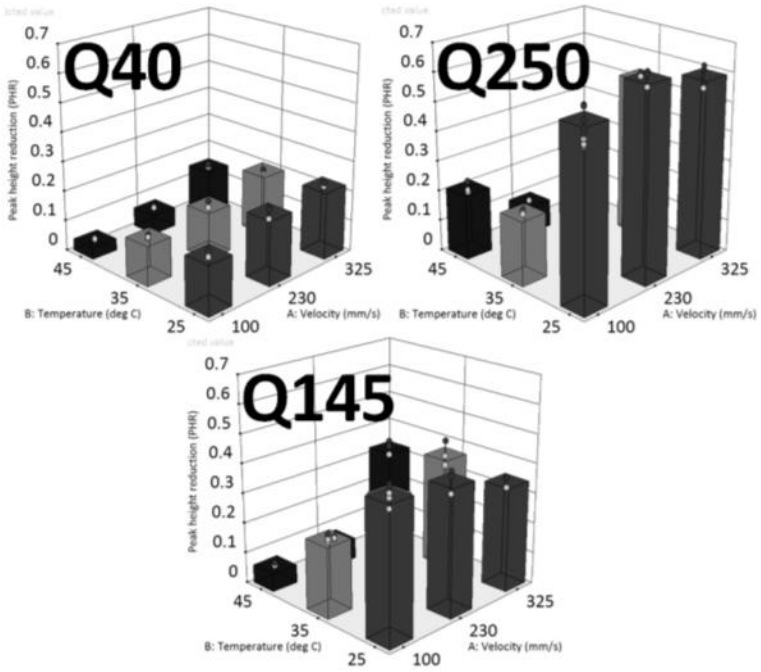

Figure 4.78 – Peak height reduction dataset showing surface plots for velocity-temperature interactions.

The most significant factor affecting peak height reduction is quantity, shown at 40m, 145m and 250m in figure 4.78. Practically, velocity can be set to a moderate value, whereafter temperature minimisation and quantity maximisation are proven to be most effective at PHR.

4.6.3 Response surface methodology (RSM) analysis.

Using the Box Behnken type RSM design through a software package, the prediction model is formulated by observing 13 runs (figure 4.24 (L)), which, in this case, are extracted from the full factorial experiment. The steps are to define the experiment structure, in this case opting for a response surface method design, followed by entering the process variables together with units, titles and levels. The software evaluates the standard error of the design and moves forward to identify model terms for checking in an analysis of variance (ANOVA) exercise (not presented). As a result of ANOVA, we are left with a table that presents the most suitable terms to fit the model. The software is able to present the model's influence on response variables by altering the values of velocity, temperature and quantity – multiple graphing options are provided, but most importantly, the point-prediction tool is used as is displayed throughout 4.6.3.

Table 4.23 – Runs extracted from full factorial design.

#	V	T	Q	$\bar{x}$Ra	$\bar{x}$MR	$\bar{x}$PHR
	mm/s	˚c	m	µm	mm^2	mm
1	230	25	250	0.764	1.050	0.646
2	100	35	40	0.284	0.176	0.135
3	230	35	145	0.574	0.249	0.312
4	325	25	145	0.554	0.304	0.352
5	325	35	250	1.252	0.497	0.537
6	230	45	250	0.277	0.180	0.094
7	230	45	40	0.287	0.193	0.068
8	100	25	145	0.732	0.508	0.453
9	325	45	145	0.682	0.290	0.333
10	100	45	145	0.242	0.162	0.062
11	100	35	250	0.447	0.247	0.216
12	230	25	40	0.539	0.289	0.219
13	325	35	40	0.667	0.210	0.205

Experimental runs extracted from full factorial results are used to form the response surface design input dataset. From 27 runs in the full factorial set, the Box-Behnken design requires 13 points as model input – these points are assembled from the full factorial experimental design – cells (unique combinations) required are listed in table 4.23 together with average Ra, MR and PHR responses.

4.6.3.1 Surface roughness prediction model.

In order to verify the model described below in equation 4.31, some verification experiments must be performed; however, the availability of an additional 14 experimental runs from the full factorial experiment (cells unused in the Box Behnken

assembly process) provides us with ready-made verification samples. Equation 4.31 presents a linear model derived from ANOVA table, type III, partial sum of squares, where Ra is average roughness in µm, V is velocity in mm/s, T is temperature in degrees Celsius and Q is quantity in metres.

$$Ra = 0.5409 + (0.0015 \bullet V) - (0.0138 \bullet T) + (0.0011 \bullet Q) \quad (4.31)$$

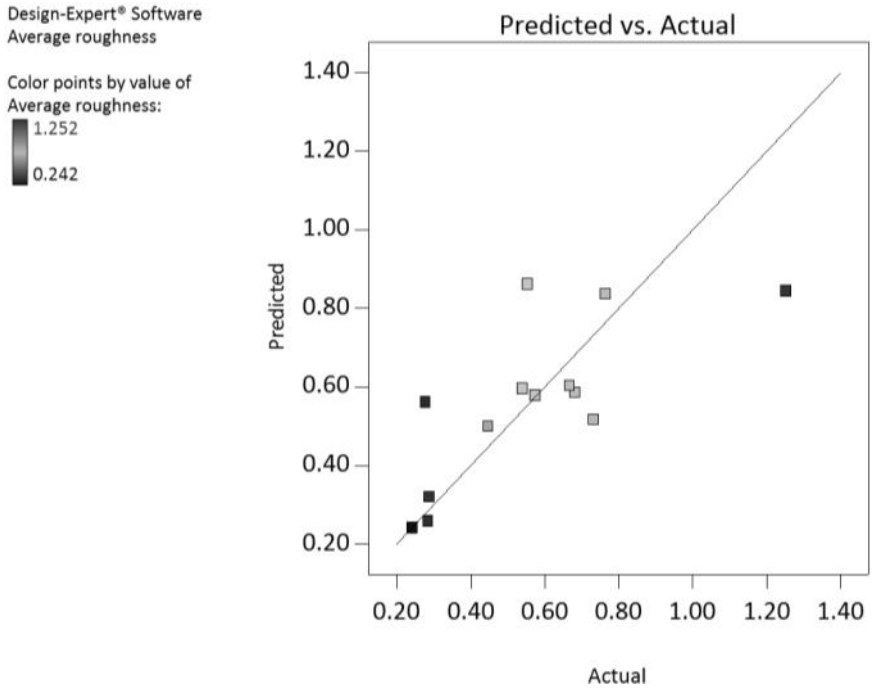

Figure 4.79 – Predicted values versus actual responses using model in eq. 4.31.

Figure 4.79 displays the best fit according to the predictive model (equation 4.31) generated by the ANOVA analysis, using significant terms – in this case V, T and Q are only-just significant (resting on p-value of 0.1) and offer a linear model. Predicted versus actual values are shown, but it is known from the scatterplots that data is clustered into the lower-mid end of the effects range and thus any model may find it difficult to describe the behaviour at the top of the response range. The number of points available in the full factorial experiment make this behaviour easier to diagnose. Data fitting in this exercise is not ideal – the R^2 value of 0.5508 suggests 55% of the effect is explained by the linear model. The design model is quadratic, and while a better fit is seen, the significance is reduced and confidence in predicted values is lower.

Table 4.24 shows 14 VTQ cells from the full factorial experiment that weren't used in the formation of the Box-Behnken design. Focusing solely on the ΔRa column in table 4.24 four values are marked in grey – the values between 0.3Ra and 0.42Ra prove where the model is weakest, reducing prediction accuracy. Common between the worst error is the extended processing duration – another run at 250m is provided, and

exhibits less error, however this is accompanied by low velocity and high temperature, reducing strain on machine. Several iterations of this model have been produced using 2 factor interaction terms, quadratic and cubic terms, although this linear version remains the most accurate. For the most part, the accuracy of ~0.2Ra is sufficient for any re-application of data, but this table reinforces the fact that a minor inaccuracy in either velocity or temperature can manifest itself and compound over a long processing duration. Ultimately, the knowledge of surface speed, temperature and processed length will still apply to the simulation work, albeit the findings from this subset of the data may require more modelling work to increase the accuracy in the testpiece environment, should it ever be needed. The full factorial analysis in section 4.6.2 is a clearer demonstration of data quality.

Table 4.24 – Point prediction using model eq. 4.31.

#	V	T	Q	Measured $\bar{x}$Ra	Predicted $\bar{x}$Ra	ΔRa	Comment
	mm/s	˚c	m	µm	µm	µm	
1	100	25	40	0.364	0.396	0.032	Good
2	100	25	250	1.062	0.638	-0.424	Bad
3	100	35	145	0.437	0.379	-0.058	Good
4	100	45	40	0.270	0.121	-0.149	Good
5	100	45	250	0.305	0.362	0.057	Good
6	230	25	145	0.959	0.714	-0.245	Poor
7	230	35	40	0.432	0.456	0.024	Good
8	230	35	250	1.106	0.696	-0.410	Bad
9	230	45	145	0.268	0.438	0.170	Good
10	325	25	40	0.515	0.743	0.228	Poor
11	325	25	250	0.665	0.984	0.319	Bad
12	325	35	145	0.825	0.726	-0.099	Good
13	325	45	40	0.438	0.464	0.026	Good
14	325	45	250	0.404	0.709	0.305	Bad

4.6.3.2 Material removal prediction model.

As above, a linear model derived from an ANOVA table (type III, partial sum of squares) is presented. MR is material removal in mm^2, V is velocity in mm/s, T is temperature in degrees Celsius and Q is quantity in metres. Only three terms are used in the model as reduction was required for statistical significance and sufficient signal to noise ratio.

$$MR = 0.6633 + (0.0003 \cdot V) - (0.0166 \cdot T) + (0.0013 \cdot Q) \quad (4.32)$$

Figure 4.80 displays predicted values versus actual response values based on the linear model shown in equation 4.32 and is of R^2 value 0.5416, indicating 54% of effects are explained by the model. As with the previous model, the ANOVA table p-value has determined a significant model is found with factors V, T and Q alone, and not with interactions. This is as reduced as the model can become – the outlier at '1.1 actual' represents the V230, T25, Q250 experimental combination – considering the boxplot for error presented earlier, this combination shows the greatest level of material removal, but also one of the greatest levels of error. Despite the error in the point position, a worst case prediction error of $0.2mm^2$ is shown in table 4.25.

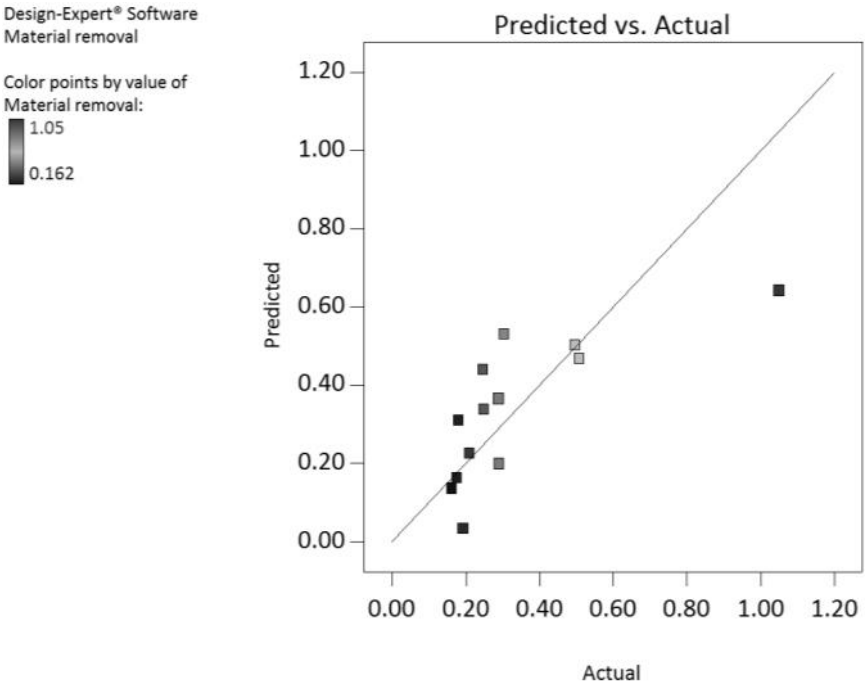

Figure 4.80 – Predicted values versus actual responses using model in eq. 4.32.

Table 4.25 displays a manageable range of error, well within shop floor levels for deburring and radii accuracy – especially considering the previous manual operations were carried out by hand with manual and power tools. The material removal data is a quantity which refers to an edge exposed to flow at 45˚ to the part face, which will produce a virtually tangential radius – the data collected in section 4.6.2 in the full factorial analysis is a pre-requisite for simulation work, where the flow field will allow the user to calculate the material removal without concern over asymmetrical geometry.

Table 4.25 – Point prediction using model eq. 4.32.							
#	V	T	Q	Measured $\bar{x}$MR	Predicted $\bar{x}$MR	ΔMR	Comment
	mm/s	˚c	m	mm^2	mm^2	mm^2	
1	100	25	40	0.211	0.330	0.119	Good
2	100	25	250	0.805	0.607	-0.198	Poor
3	100	35	145	0.179	0.303	0.124	Good
4	100	45	40	0.150	0.000	-0.150	Good
5	100	45	250	0.217	0.276	0.059	Good
6	230	25	145	0.547	0.503	-0.044	Good
7	230	35	40	0.187	0.337	0.150	Good
8	230	35	250	0.333	0.476	0.143	Good
9	230	45	145	0.167	0.171	0.004	Good
10	325	25	40	0.260	0.391	0.131	Good
11	325	25	250	0.770	0.668	-0.102	Good
12	325	35	145	0.340	0.364	0.024	Good
13	325	45	40	0.200	0.060	-0.140	Good
14	325	45	250	0.203	0.337	0.134	Good

VTQ values in table 4.25 are those from the full factorial experiment that weren't used in the formation of the Box-Behnken design. Note typical error of <0.12mm2 from a range of results up to 0.8mm^2 highlighted grey – model improvement would be possible with a greater number of points to integrate into the model. For the purposes of this task, the accuracy is perfectly sufficient.

4.6.3.4 Peak height reduction prediction model.

Peak height reduction is arguably the most helpful metric to re-apply to industrial components – the unit is directly comparable to any other 90˚ edge with flow hitting it at 45˚, and (in this geometry) describes the reduction in material at a tangent to the flow direction. This is useful for the removal of material from edges which may damage wire insulation, or contain large burrs.

$$PHR = 0.7633 - (0.0028 \bullet V) - (0.017 \bullet T) + (0.0032 \bullet Q) + (0.000077 \bullet V \bullet T) + (0.0000053 \bullet V \bullet Q) - (0.000095 \bullet T \bullet Q) \quad (4.33)$$

Equation 4.33 presents a two-factor interaction model derived from ANOVA table, type III, partial sum of squares. Terms of V, T, Q, VT, VQ and TQ are significant outputs from the ANOVA table. Where PHR is peak height reduction in mm, V is velocity in mm/s, T is temperature in degrees Celsius and Q is quantity in metres. Model reduction was not required with the peak height reduction data, retaining a better fitting and more complex model for the prediction equation.

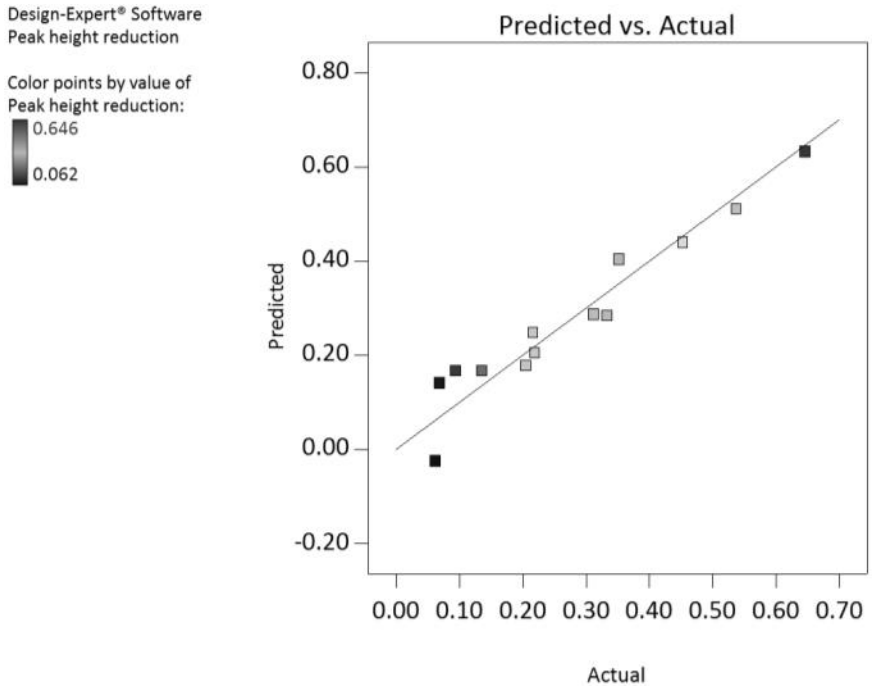

Figure 4.81 – Predicted values versus actual responses using model in eq. 4.33.

Predicted values versus actual response values based on two factor interaction function are fitted to the data in figure 4.81. The most accurate and significant of the three response variables, the PHR model contains significant terms V, T, Q, VT, VQ, QT. Error is well distributed about the line of best fit. Points are distributed along the length, not clustered. The worst case is found at the lower end of the line – this is represented by row 5 in table 4.26. Prediction error of 0.2mm is the worst point, where maximum reductions of 0.6mm were achieved, but this value is highly erroneous – typical prediction accuracy is <0.1mm, best case 0.004mm, which is 0.06% error. The three predicted versus actual plots have poorly fitting points at the extreme upper and extreme lower end of their best fit lines – this may point to machine repeatability problems in these areas – upon further inspection of the processing parameters that were used – it appears to be low velocity and high quantity that combine to cause the worst case error in all three response variables. It has been thought previously that machine piston travel is not collected as accurately as it could be, and velocity tracking techniques by the software are not capable enough – this work shows a relationship, but cannot determine causality – in any event, the modification of machine is out of scope and the work presented here is for the purposes of developing a simulation capability.

Table 4.26 – Point prediction using model eq. 4.33.

#	V	T	Q	Measured $\bar{x}$PHR	Predicted $\bar{x}$PHR	ΔPHR	Comment
	mm/s	˚c	m	mm	mm	mm	
1	100	25	40	0.167	0.298	0.131	Poor
2	100	25	250	0.584	0.580	-0.004	Good
3	100	35	145	0.236	0.207	-0.029	Good
4	100	45	40	0.039	0.034	-0.005	Good
5	100	45	250	0.218	0.000	-0.218	Bad
6	230	25	145	0.425	0.418	-0.007	Good
7	230	35	40	0.160	0.173	0.013	Good
8	230	35	250	0.399	0.398	-0.001	Good
9	230	45	145	0.073	0.152	0.079	Good
10	325	25	40	0.229	0.135	-0.094	Good
11	325	25	250	0.597	0.669	0.072	Good
12	325	35	145	0.375	0.344	-0.031	Good
13	325	45	40	0.147	0.220	0.073	Good
14	325	45	250	0.256	0.353	0.097	Good

4.6.3.4 Box Behnken generated data interpretation.

Figure 4.82 illustrates the effect of temperature on average roughness. The plane of prediction surface is manipulated by temperature, the source of main effect in surface roughness control; 25˚c on the left and 45˚c on the right. As previously suggested, the error bars are larger on the left side where the machine undoubtedly must work harder under the increased viscosity of the media at lower temperature – as a linear model was the best fit for the data, both surfaces are completely flat and contain no second order interactions – however, the general effects are accurate, both figures illustrating the increase in surface roughness with increased velocity and quantity, which reduction in both improves the finish – the limits of the effects are temperature driven, as the offset Z height of the 45˚c shows.

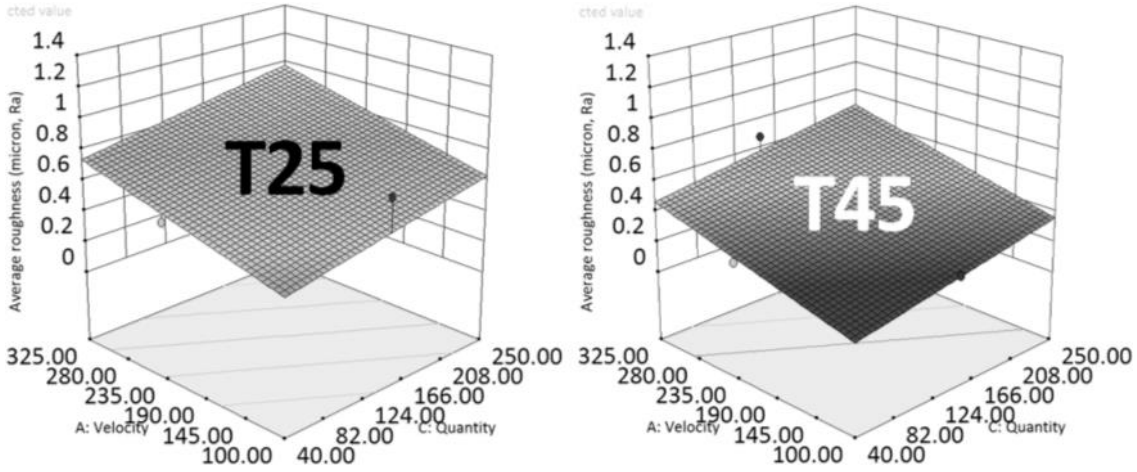

Figure 4.82 – Predictive model response surfaces sourced from average roughness dataset.

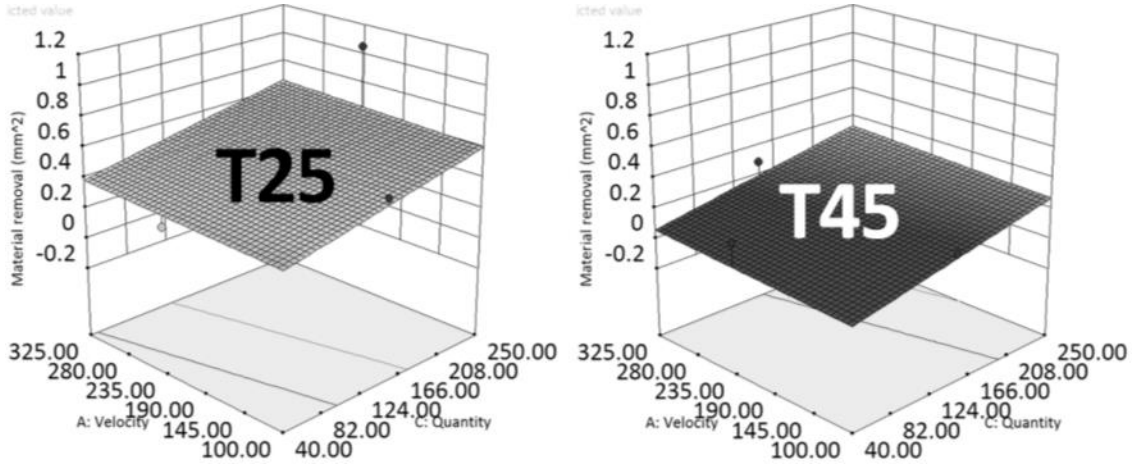

Figure 4.83 – Predictive model response surfaces sourced from material removal dataset.

The prediction plane of the surfaces in figure 4.83 depicts increased removal where quantity is increased, but velocity is shown to have minimal effect – the effect is driven by a temperature-quantity interaction whereby the figure to the right (45˚c) limits material removal, likely due to a less viscous media.

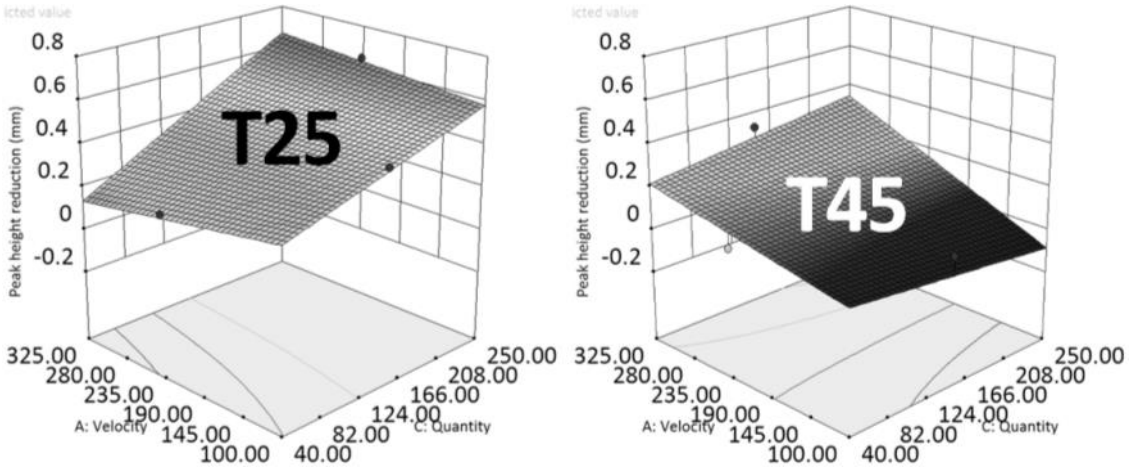

Figure 4.84 – Predictive model response surfaces sourced from peak height reduction dataset.

The surface in figure 4.84 is curved, formed of two factor interaction terms within the model. The left side at 25˚c shows increased velocity to reduce peak height at a more effective rate when coupled with greater quantity. When increasing the temperature, as much as 0.7mm of PHR can be lost when the entire right side of the surface reduces. A higher velocity can combat this loss, beneficial for processing of small bores when media viscosity must be reduced to reduce pressure drop in the system.

4.6.4 Conclusions.

Throughout the factorial and RSM analysis activities, several phenomena have been noticed. These incidences may be useful tricks for production, or simply methods of understanding the process better.

4.6.4.1 Phenomena.

Figure 4.85 presents means of three cell repetitions – plotted with respect to their individual run, i.e. each of the three responses are plotted vertically. It can be seen that while MR and PHR crossover in multiple locations, roughness is virtually always offset from the MR or PHR. It is interesting to note however that two runs appear to flout that trend – V230/T25/Q250 and V325/T25/Q250 – the two most difficult to pump combinations. In both cases, MR is higher, not PHR – reasons for the trend reversing in these two cases may be due to the suggested reduction in media-surface interaction that potentially results from high-speed high-viscosity flow.

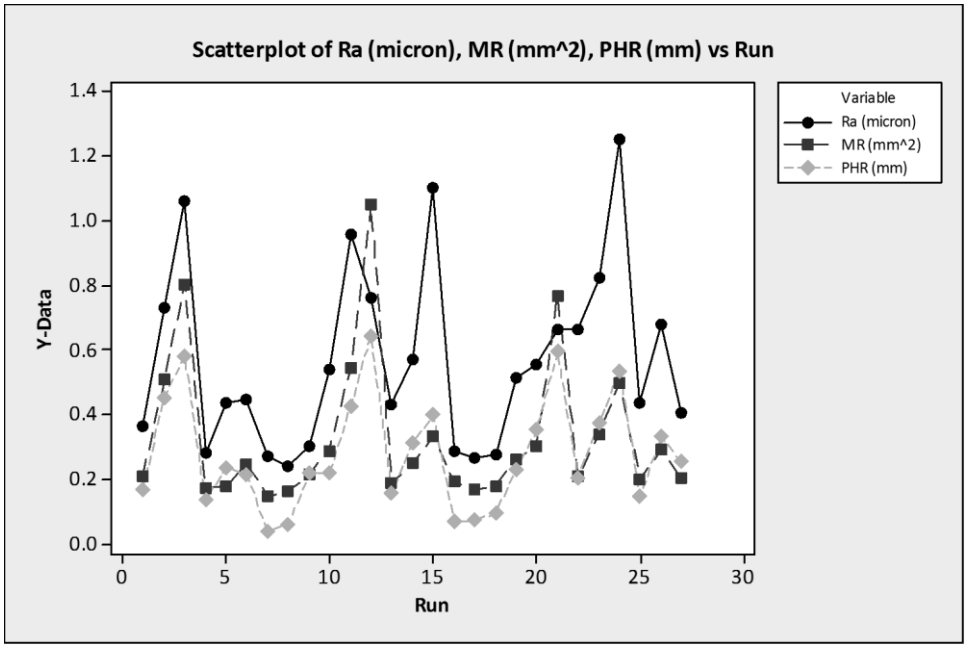

Figure 4.85 – Scatterplot of Ra, MR and PHR against run order.

As described in 4.6.3, Ra and MR linear models for RSM are not good – too few datapoints are likely the cause. This is proven by the same cells for PHR providing a naturally better fit for occupying a 2FI (two factor interaction) model and providing a R^2 93% accuracy.

AFM uses machine parameters to manipulate the ability of the media to indent on the workpiece surface. Media has a pre-determined range of 'effect-magnitude' capability, determined by rheological behaviour of carrier and grit size – in numerous trials, the phenomenon of increased quantity responsible for increased surface roughness is exhibited – often providing an argument for not using AFM at all to improve surface finish. Surface finish is a measurement used to describe the distance between peaks and troughs over a sample area or sample length depending on chosen instrument. In this experiment, media, geometry and material was fixed – testpieces were machined to ~0.35µm Ra (a good machined finish). It has been established that while machine levels can vary the response of surface roughness through velocity temperature and quantity, the vast majority of responses were seen to increase roughness. Pre-process roughness and texture orientation are arbitrary within production workpieces – it is controlled by the machining technology used and the sequence of operations – however, unless large gradients exist, it has been shown that AFM 'overwrites' the previous finish with its own. Pre-process roughness is caused by the milling operations used to create the 10mm square – with typical 0.35µm surface features, the AFM grit at ~700µm indents the titanium workpiece to a greater extent than 0.35µm over the range of experimental parameters.

4.6.4.2 Recognised mechanisms.

Of useful application in production components, the VT and TQ interactions in MR are useful for identifying cycle time reduction and levels trade-offs whereby compensations can be made to reduce energy usage or reduce media overheating. The experimental findings show quite clearly that temperature and quantity are primary drivers for feature alteration, and while it would be useful to place a numerical ratio on the effect these factors have on the response, the reality is that the ratio would change with virtually any change in another factor.

AFM's potential to 'overwrite' a pre-process roughness is often misrepresented as 'percentage improvement' in surface finish, particularly in research consisting of electro-discharge machining (EDM) where pre-process roughness is high. Equally, the opposite end of the spectrum is shows a different story – AFM upon a good finish has the potential to roughen it. There is an intrinsic limit for any media configuration – controlled by the type of polymer behaviour, grit size, material, concentration and potential to indent the workpiece – the media formulation in this experiment was not 'wrong'; it was simply the incorrect choice should surface finishing have been the desired outcome.

4.6.4.3 Limits.

Velocity has little effect on material removal in terms of response magnitude; however, velocity can define the shape of the flowfield, and thus media edge conformity. Temperature plays a significant role in the removal of material – too warm and grit is not supported, too cold and it will not conform to a feature's edge.

4.7 Analysis of media parameter study data.

Due to the expense of media and effort involved in loading, homogenising, processing and unloading 20L of material every run to a total of 43, the Box-Behnken model provides the economic reduction of experimental effort, whilst maintaining the required experimental resolution and desired numerical outputs. Several improvements in the modelling process are integrated over the analytical steps adopted in section 4.6, primarily to overcome the statistical influence of error increasing with response magnitude – ANOVA is usually valid only when certain assumptions are made about input data, the first being that error is considered to be constant throughout the range of responses.

While the previous full factorial design allowed the population of a Box-Behnken design (albeit at the most reduced number of runs possible), the activity in this section utilises the Box-Behnken model's own internal error estimations, coupled with the repetitions of the edge-points and centroid. Tolerable limits for error and acceptability are noted in section 4.7.1, while further error assessment is made toward the rear of 4.7 for the purpose of assessing the performance of the model.

Prior assessment of datasets used in 4.6 showed no appreciable difference in ANOVA results, prediction models or standard deviation when applying a power transform to the data. Three datasets in this activity do see an improvement, as illustrated in section 4.7.2. Distribution of error is discussed, while ANOVA results are presented to identify the significant factors in this experiment – this is followed up with interaction plots to determine the relationship between two factors for a single level of another, best fit analysis to determine outliers in the prediction model and whether a justification for retesting certain samples can be found and response surface plots to provide a graphically-helpful projection of interactions of three variables (two independent, one response).

Interpretation of results provides a discussion of the potential effects on the system and geometry in a production environment, and identifies key findings to act as firefighting tools or to provide greater flexibility when economic considerations must be made, resulting potentially in committing raw materials to a batch of media in a mixing process or to ensuring the properties and abrasive potential of a batch suit multiple defined purposes.

As a final step, the data is funnelled into the full factorial structure and populates the 14 missing runs from the Box Behnken using the predictive model. The resulting full factorial dataset is not analysed as any useful extrapolations have been made using Box Behnken analysis as making predictions from predictions is poor practice.

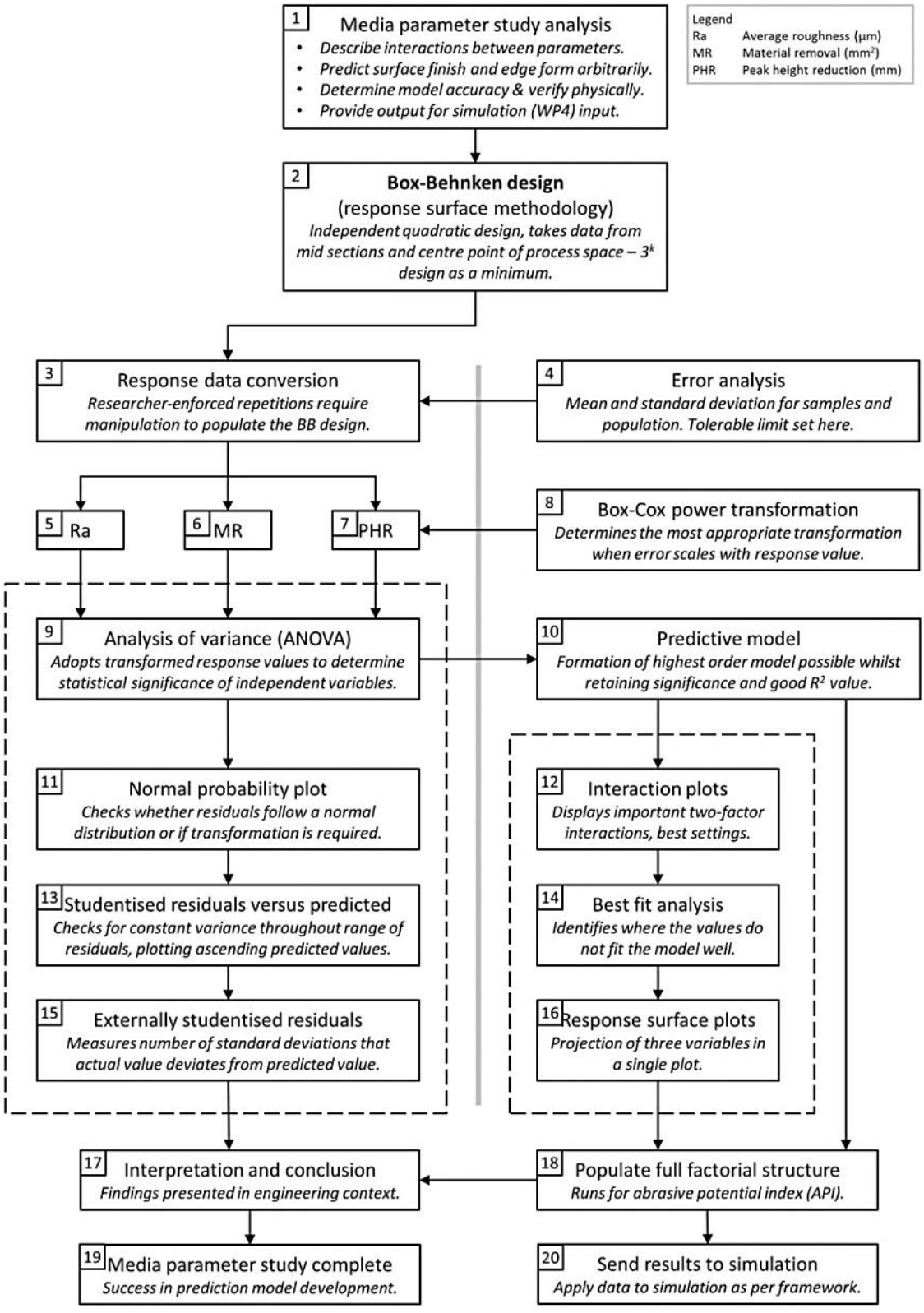

Figure 4.86 – Overview of media parameter analysis activity.

4.7.1 Error and acceptability

In contrast to the data obtained from the full factorial experiment, the data from the Box-Behnken experiment is not necessarily required to fill the process space, as the design does not test every possible configuration, but a subset thereof. Nonetheless, the error assessments are completed by simple means, standard deviations and statistical technique to understand variance.

4.7.1.1 Initial look at average roughness dataset.

Collating all 43 response values and plotting them in a histogram allows the visualisation of results 'spread'. The average response is 0.48µm Ra – approximately 0.2µm from the centroid datapoint, although there are no reasons to expect the average to rest on the centroid average. Figure 4.87 shows the values to conform to a normal distribution, as would be expected from a experimental design representing a spread of process levels.

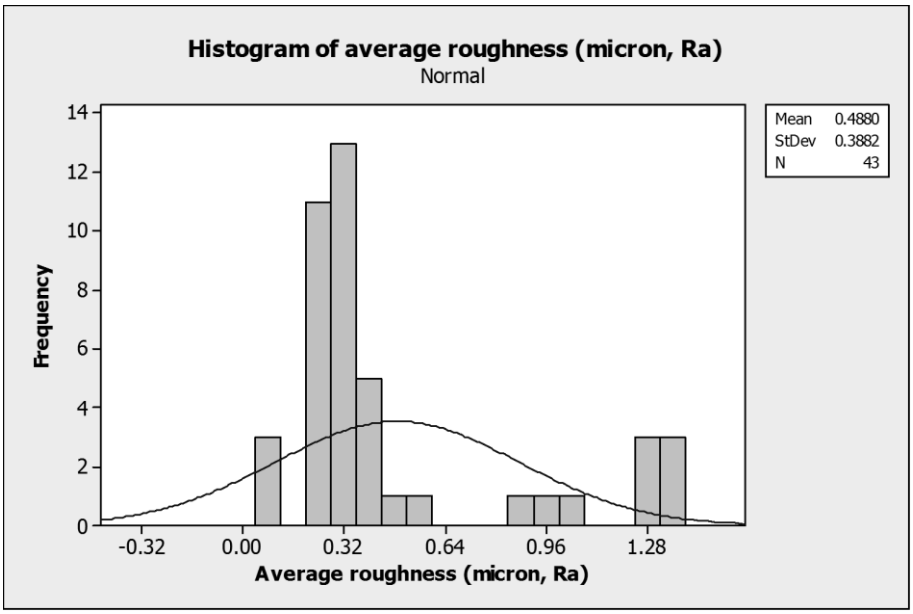

Figure 4.87 – Histogram of media study average roughness responses.

In the interest of analysing repeatability, the plot in figure 4.88 presents the measured roughness response against the experimental cell combination. Without reference to the actual levels, there are no significant outliers, with the groups of three remaining tightly bunched – except for the centroid repetitions, run independently throughout the experiment to ensure geometrical effects of worn tooling or worn media did not affect the processing capability of the machine. To understand general effects, figures 4.108, 4.109 and 4.110 are used to view the effect of each two factor interaction, with the third

variable set to maximise the response (maximise in this case means lowest Ra for surface roughness and highest mm^2 and mm values from MR and PHR).

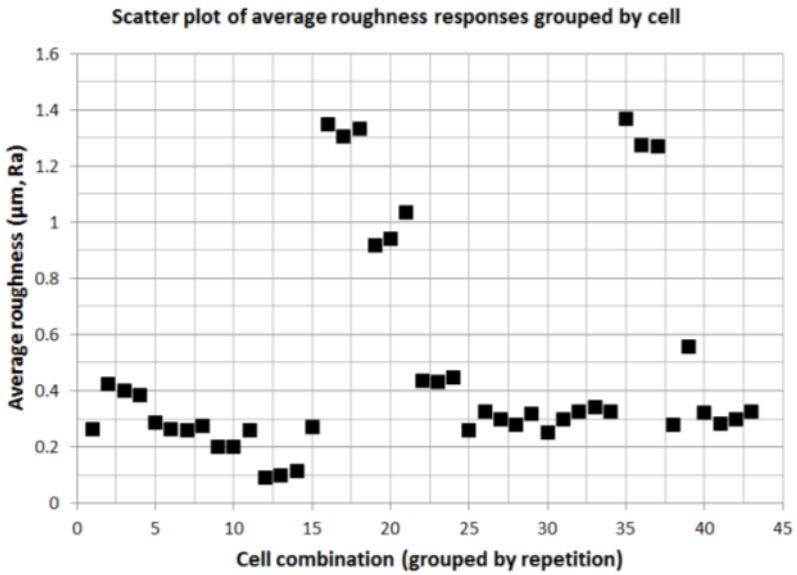

Figure 4.88 – Scatter plot of average roughness responses from media parameter study.

In figure 4.89, modifier percentage is plotted against grain fraction. Grit size is 51µm (F240) for the entire plot. Ra improves, but only as a simultaneous function of GF and MP increase; improvement only comes when the two factors are increased in unison.

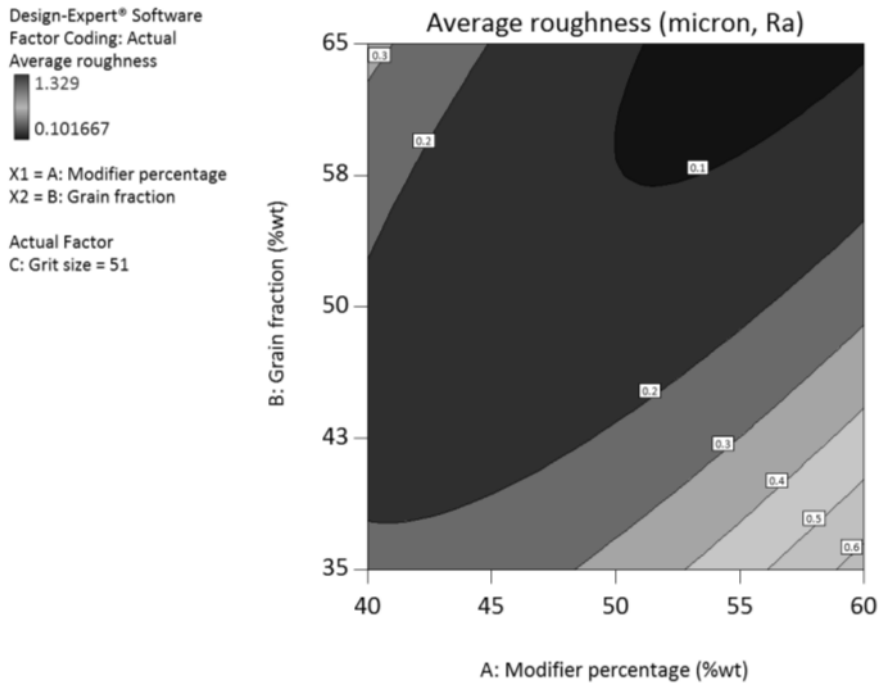

Figure 4.89 – Contour plot of modifier percentage against grain fraction.

Average roughness is shown to be reduced almost linearly by grit size in figure 4.90, with grain fraction set to 54%wt. As expected, the larger grit is more effective when the carrier is stiff (40%wt modified) but the benefits taper down when grit size reduces, hinting that the F240 product meets its limit to improve surface finish under these flow conditions.

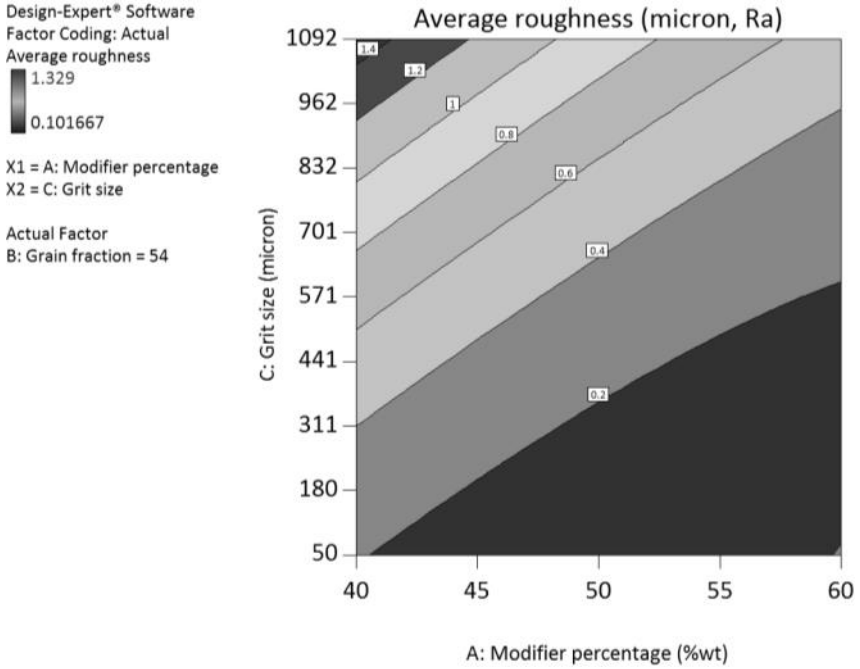

Figure 4.90 – Contour plot of modifier percentage against grit size.

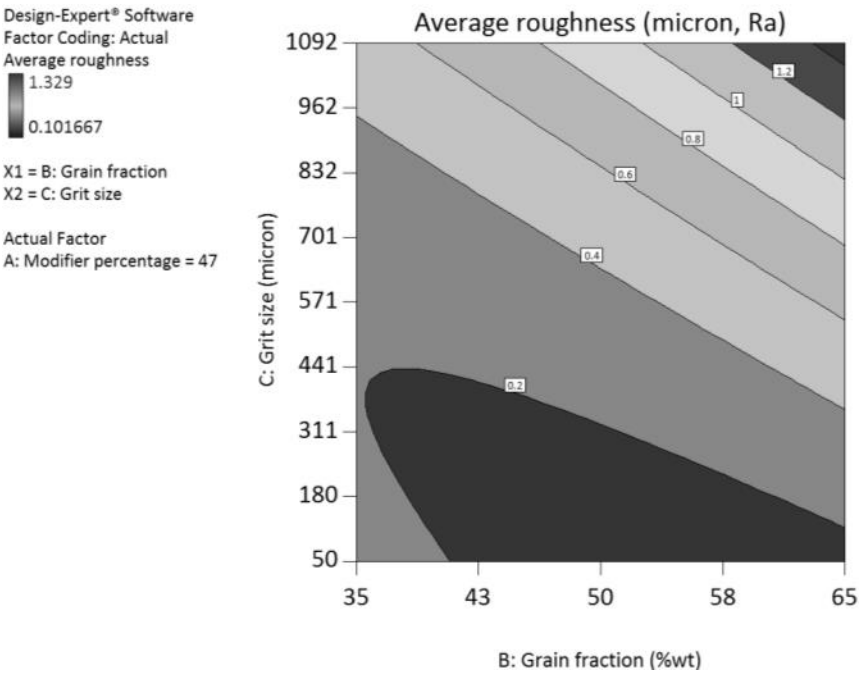

Figure 4.91 – Contour plot of grain fraction against grit size.

Figure 4.91 presents a constant modifier percentage of 47%wt, illustrating that too much grit appears to have the effect of roughening the surface – it could be suggested that increased grain fraction increases grit-grit interaction and tessellates grains, compounding with modifier percentage to increase viscosity and remove material. However, the lower left quadrant shows the beginnings of a reverse in the trend, highlighting that insufficient grit could allow loose grains to affect surface in isolation.

4.7.1.2 Initial look at material removal dataset.

Material removal is a 'optimise'-type target – whereas surface finish is a no-more-than value, material removal corresponds to a given edge condition following a machining process, albeit in the methods described in section 4.5. Figure 4.92 presents the responses in mm^2 showing an average value of $1.034mm^2$ over the 43 responses. Few values reach the top, suggesting experimental levels should be tweaked to increase edge-rounding if trials were to be re-run. The histogram is biased toward the centroid as seven values are collected for it; regardless, the plot shows the edges of the process space are captured by at least *some* runs with repeatability.

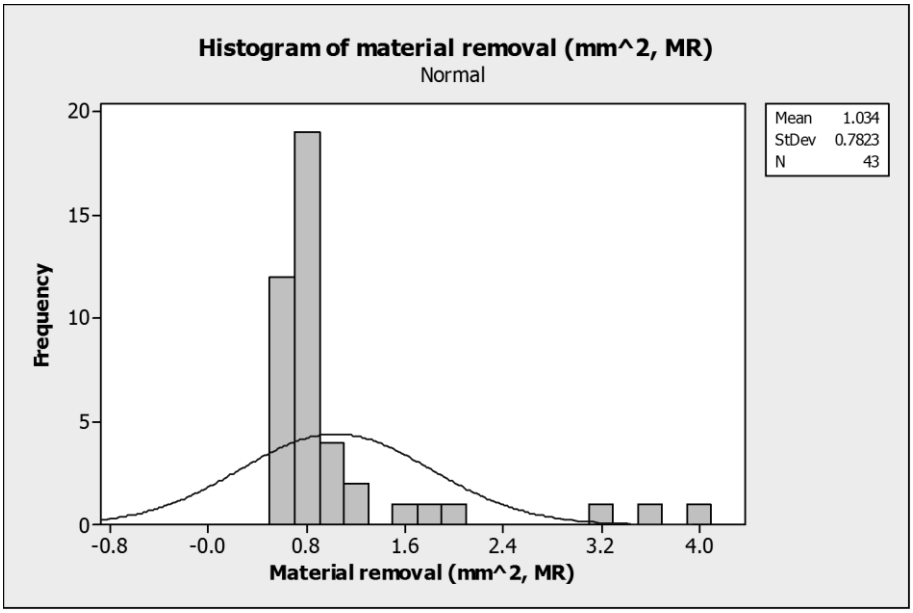

Figure 4.92 – Histogram of media study material removal responses.

Extreme responses are common to only one configuration of MP, GF, GS as pictured in figure 4.93; three more groups show a greater than average response while the remainder are relatively flat, which may be a function of the experimental levels chosen – the groups of three do however remain distinct and are suitably grouped to distinguish between erroneous non-repeatable values and reliable values for modelling.

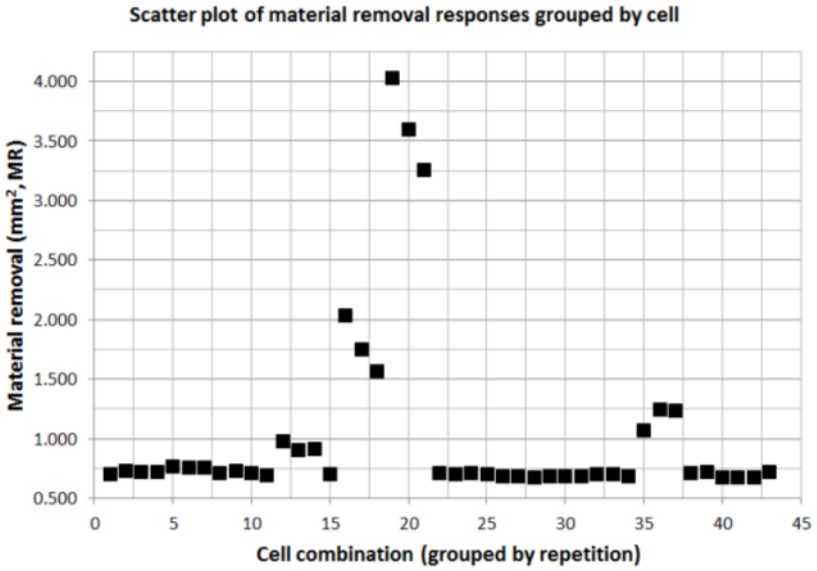

Figure 4.93 – Scatter plot of material removal responses from media parameter study.

Three contour plots are presented to show two factor interactions pertaining to material removal values – figure 4.94 shows that higher MR can be achieved by increasing grain fraction and reducing modifier percentage, in effect increasing viscosity. The constant in this plot is grit size at 416μm, closest to F40 mesh size. Grain fraction appears to require a threshold of above 50% to begin to make a change to total MR, but grit size provides a manipulator for this effect as shown in figure 4.96.

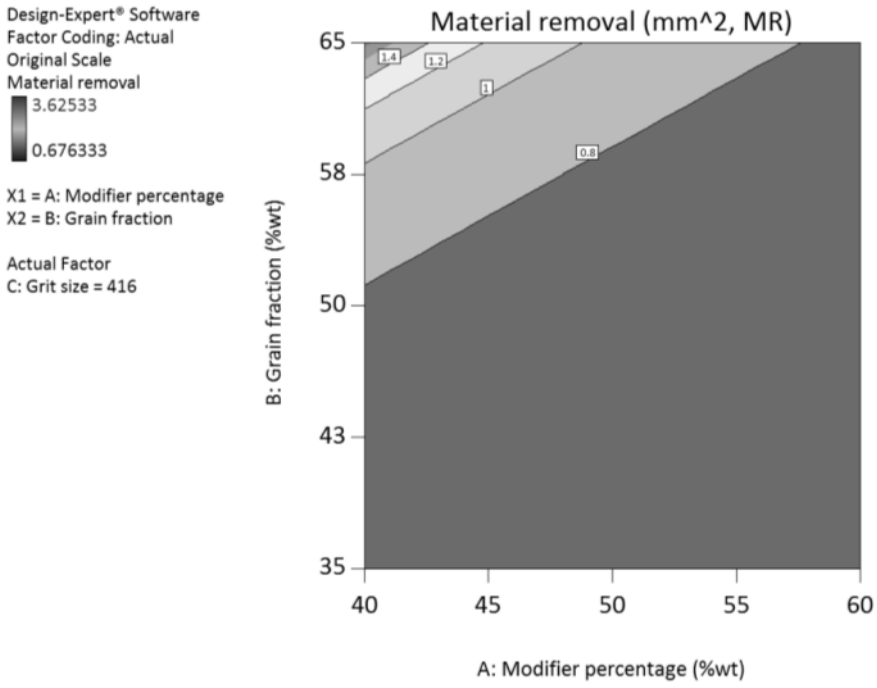

Figure 4.94 – Contour plot of modifier percentage against grain fraction.

Interaction between media viscosity and grit size is illustrated in figure 4.95 – grit size is only effective at MR where the media is stiff enough to retain grit orientation and prevent rolling. A higher percentage modifier (potentially for flow field control) can be counteracted to maintain MR by increasing grit size.

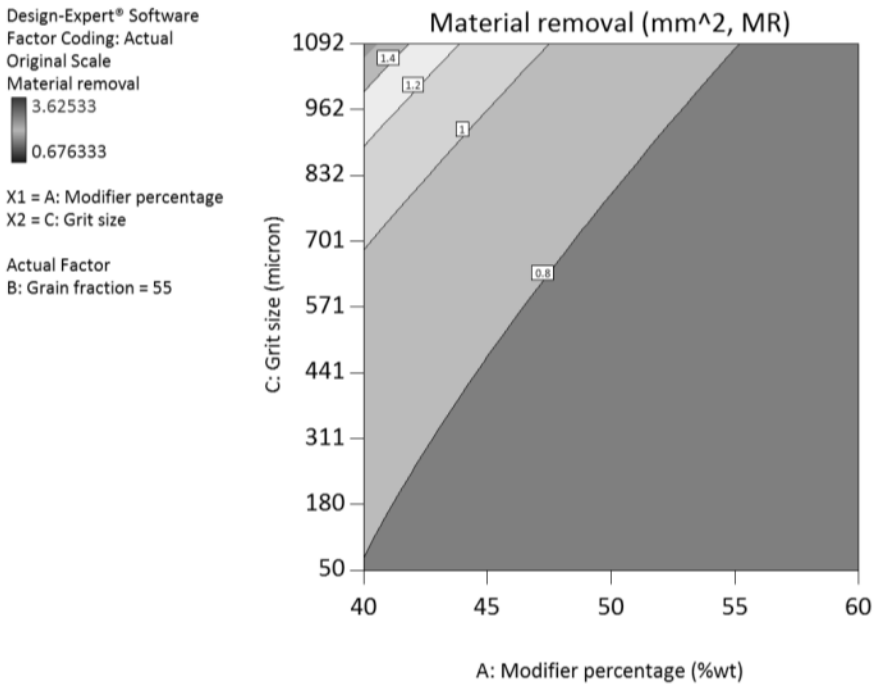

Figure 4.95 – Contour plot of modifier percentage against grit size.

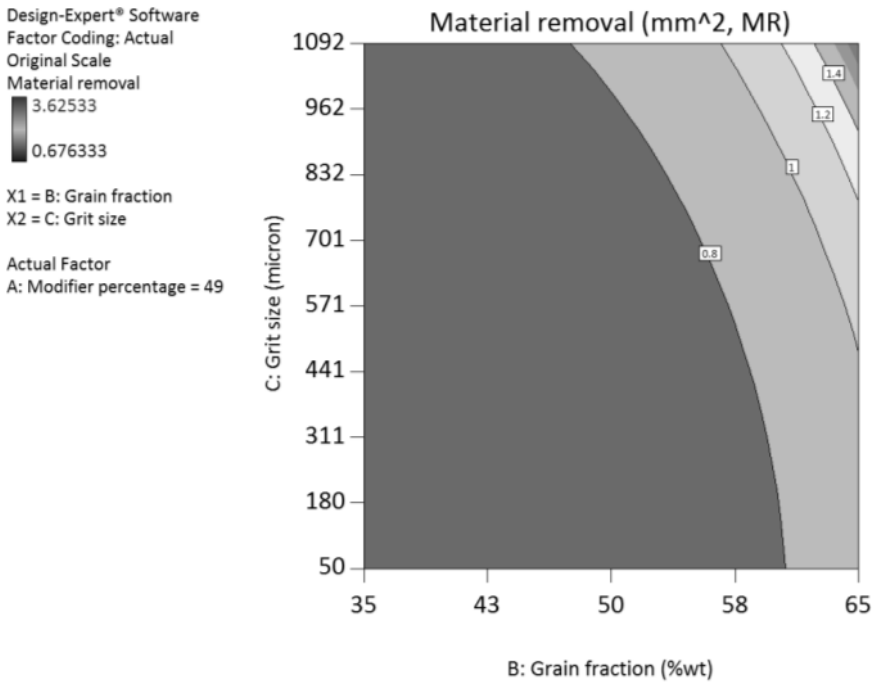

Figure 4.96 – Contour plot of grain fraction against grit size.

In situations where MR is insufficient, figure 4.96 shows a potential avenue to improving performance by addition of grit, without comprising grit size or type or needing to remove modifier, the additional of grit is shown to be effective at increasing MR. Despite this, the gradient in figure 4.96 suggest that addition of a second, larger grit would be a more efficient means of achieving the target.

4.7.1.3 Initial look at peak height reduction dataset.

As an alternative to MR to describe edge-rounding in a single value, PHR offers a more effective means of describing the '*functional*' rounding – i.e. that required to avoid damaging wires or disrupting fluid flow. The distribution of results is more helpful than Ra and MR, as a shorter distance between collected values is seen, providing the ability to strengthen the prediction models in the middle of the response range.

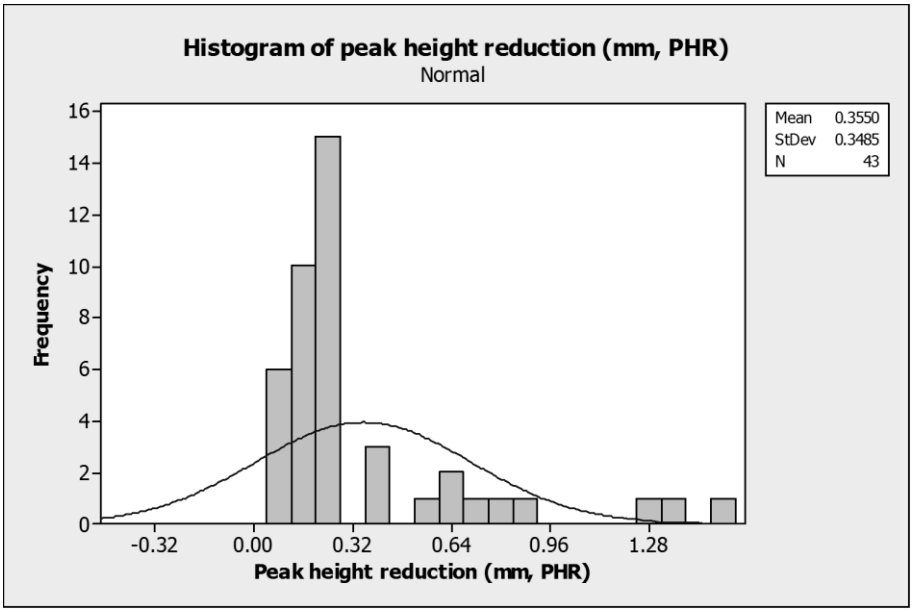

Figure 4.97 – Histogram of media study peak height reduction responses.

Figure 4.97 presents responses ranging between 0.09mm and 1.39mm – control of both ends of the spectrum is a useful capability to have to aid feature protection. Average response is 0.35mm, while naturally the pre-process PHR is 0, placing the average at approximately 25% of maximum response. Values follow a normal distribution, and contain the same bias toward the centre as the histograms before.

Compared to the MR dataset, the scatter plot in figure 4.98 presents a string of points with greater response magnitude and better separation from other runs, once more proving the worth of the PHR unit as defining a feature uncharacterised by the MR unit. Greater variance is visible at greater response magnitude, pointing to a similar effect as seen in the machine parameter study; more work causes greater variation.

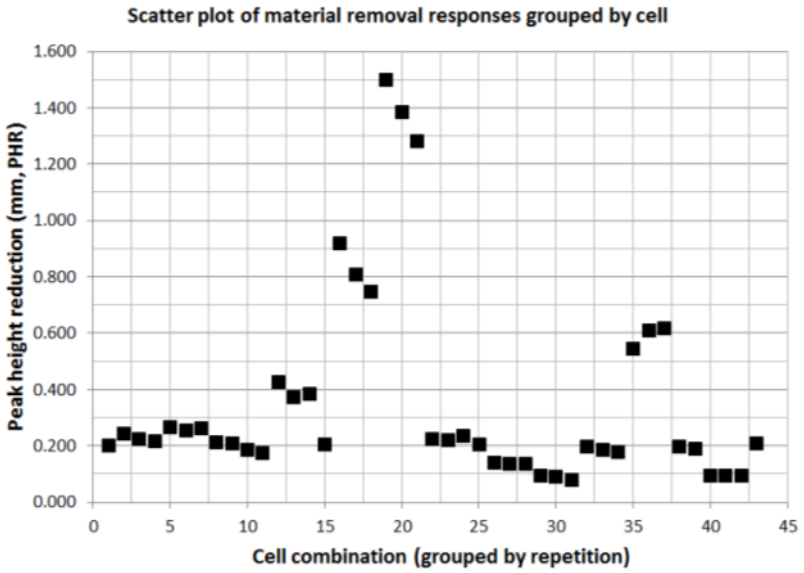

Figure 4.98 – Scatter plot of peak height reduction responses from media parameter study.

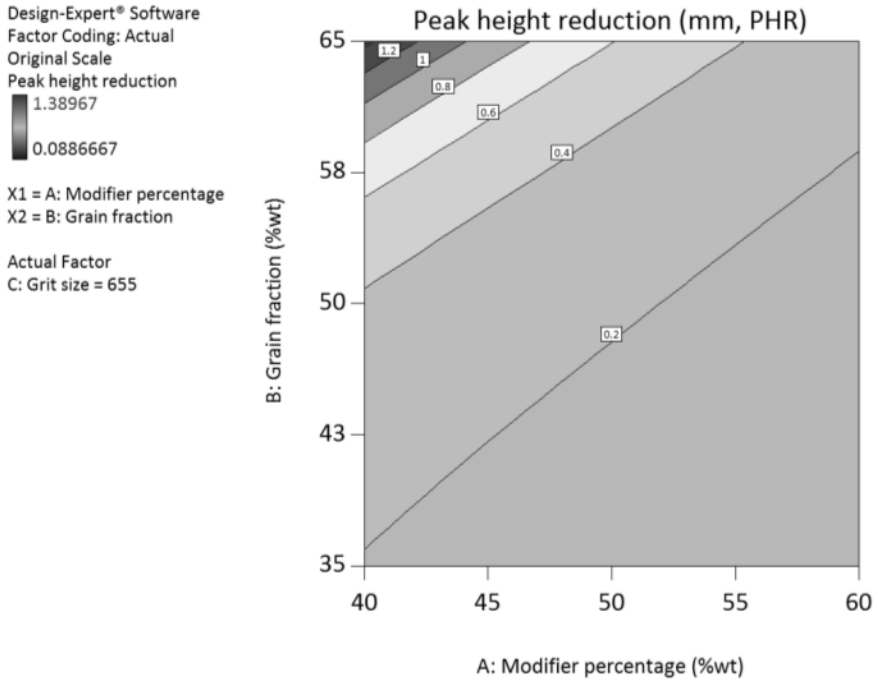

Figure 4.99 – Contour plot of modifier percentage against grain fraction.

Adopting a value of 655µm (F24), the response of PHR in figure 4.99 is seen to increase with additional grain fraction and reduce with additional modifier percentage. These findings are aligned with MR, whereby additional grit concentration increases the number of cutting edges and grit-grit interaction, while additional modifier reduces the ability of the carrier to support the abrasive grains, further suggesting the key physical driver for surface condition change is viscosity. Reducing grit size is seen to lessen the ability of media to remove material, although as figure 4.100 shows, modifier percentage can be more effective at controlling PHR. Grain fraction is constant at

61%wt in this example, but the trend would not be affected by this factor. Practically speaking, this plot shows the importance of ensuring a desirable flow field is simulated, as (dependent on grit size) the difference of 10%wt modifier percentage can affect the PHR by a factor of three.

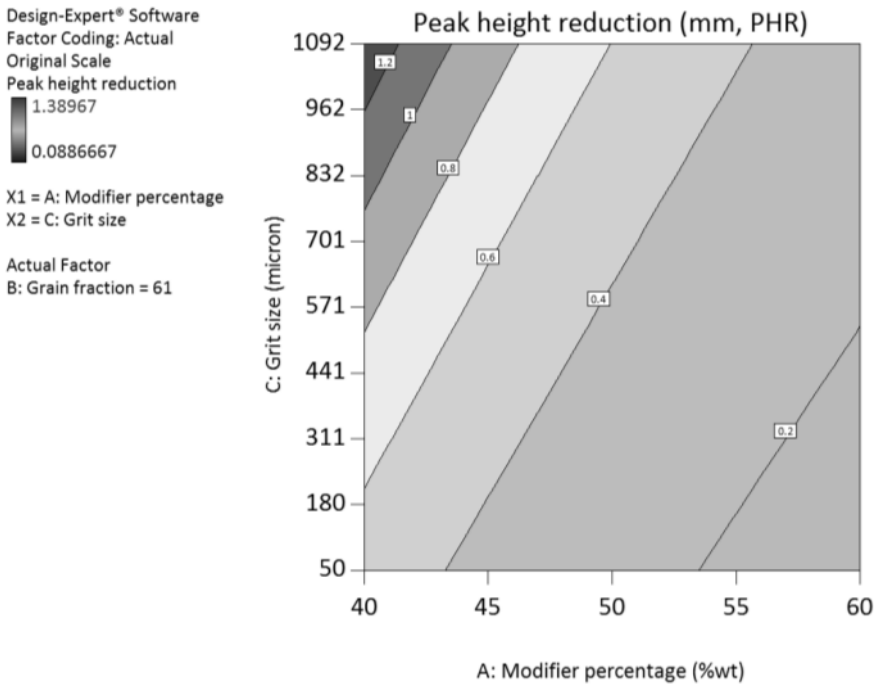

Figure 4.100 – Contour plot of modifier percentage against grit size.

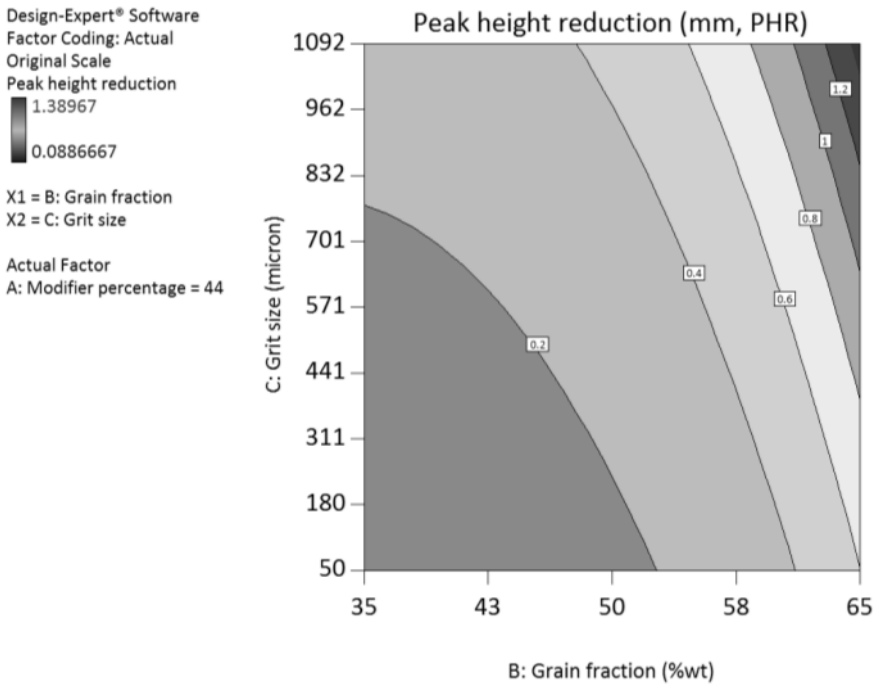

Figure 4.101 – Contour plot of grain fraction against grit size.

The relationship between grit size and grain fraction is important – with modifier percentage set at 44%wt, the effect of grain fraction increase is one of steady displacement of grit size's contribution to PHR. As in the other metrics, the rate at which MR or PHR are achieved is driven by combinatorial effects.

4.7.1.4 Boxplots from average roughness dataset.

With much in common with the boxplots in the machine parameter study, the effect of error increasing with increased response magnitude reoccurs here in figure 4.102. The worst case standard deviation is 0.05 on the MP40, GF65, GS571 run – while the error is perfectly acceptable, and is far above average levels of control in industrial surface finishing operations, the run is one of three significantly rougher surfaces, all presenting greater variation, apparently as a product of doing more work. This is a machine control issue, and while these results for surface finish are unlikely to be target values, the repeatability must be considered when the machine is working harder.

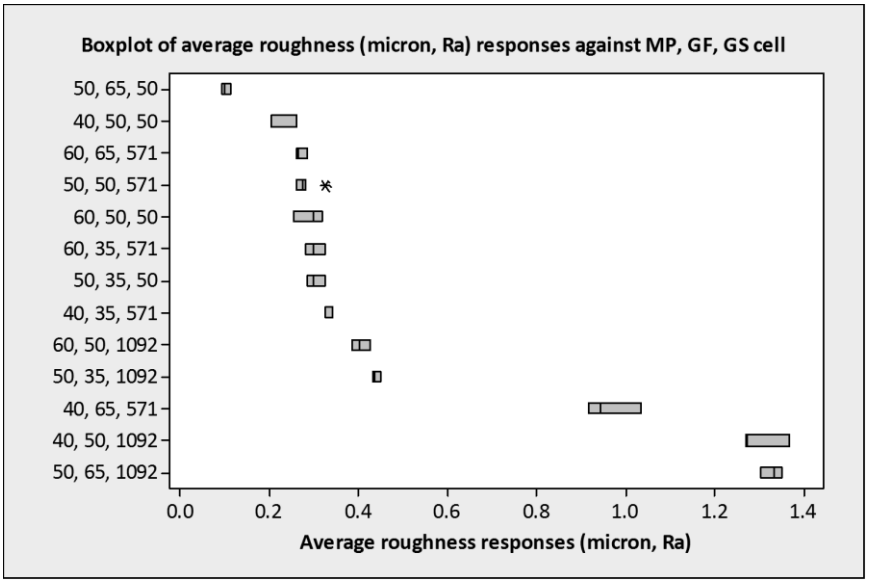

Figure 4.102 – Boxplot of average roughness responses against cell combinations.

The second most deviated is the run below – MP40, GF50, GS1092. The run contains the same carrier but less grit, although larger and required a comparable back pressure to the MP40, GF64, GS571 run to operate at the experimental levels for VTQ.

4.7.1.5 Boxplots from material removal dataset.

Significantly larger deviation is seen in the runs most stressful (for the machine hardware) for the MR dataset – the most demanding is MP40, GF65, GS571 with a standard deviation of 0.318mm^2. The run MP50, GF65, GS1092 sits at 0.196mm^2,

although it is possible to say the deviation is well spread about a centre point indicating random phenomena are unlikely to have caused it, further strengthened by the increasing error of the four greatest magnitude runs. It is also possible to speculate from figure 4.103 that viscosity is not only increased by reduced modifier percentage, but also by increased grain fraction, irrespective of grit size.

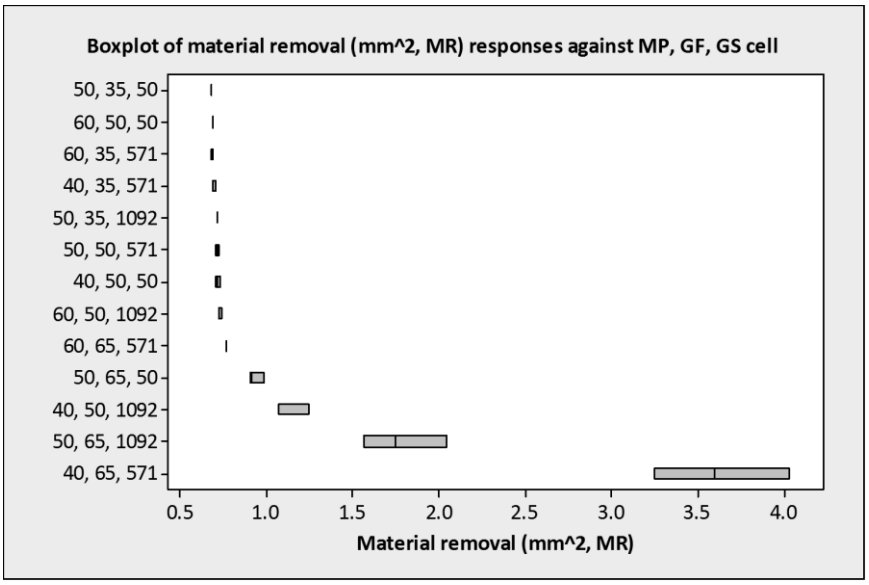

Figure 4.103 – Boxplot of material removal responses against cell combinations.

4.7.1.6 Boxplots from peak height reduction dataset.

Akin to previous boxplots, greatest error is 0.09mm, followed by 0.07mm and 0.03mm.

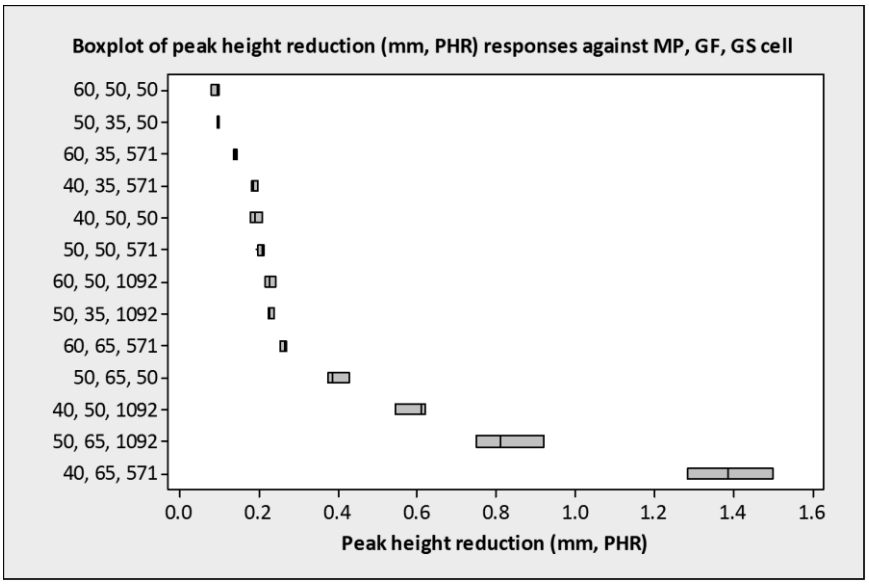

Figure 4.104 – Boxplot of material removal responses against cell combinations.

4.7.2 Significant factors and variance.

To establish the quality of the data and quadratic model derived from the experiment, plots of residuals against predicted values are used to identify distribution, residuals are plotted against predicted values to assure constant variance and normal distribution (assumptions made by ANOVA) and the externally studentised residuals plot identifies abnormal runs. In addition, the Box-Cox power transform plot is used to identify whether data should undergo a transformation, i.e. a value, be it a power or logarithm, applied to all values in the dataset to help it conform to the requirements of ANOVA.

4.7.2.1 Significance and variance in average roughness dataset.

Figure 4.105 shows none of the defined S-curve associated with a need for transformation – the points are clearly based on the guide line, within expected scatter.

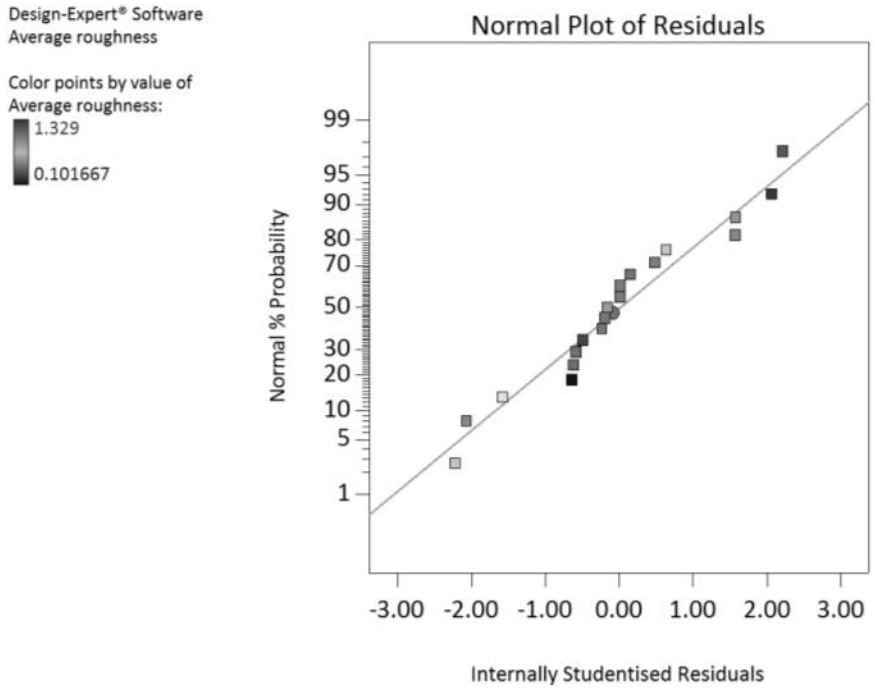

Figure 4.105 – Normal probability plot of average roughness datapoints.

When using a software-derived predictive model, the plot in figure 4.106 arranges the predicted responses in order of magnitude and tests for consistency of variance – it should be a random scatter pattern; megaphone patterns indicate a need for transformation. Values are accumulated in the 0.3µm area, although variance does not expand with increase in response magnitude. The plot at figure 4.107 presents values as deviations between actual and predicted when actual values are deleted from calculations – this is useful for identification of abnormal runs; in this example, no outliers are found and all 19 values are scattered randomly within the space.

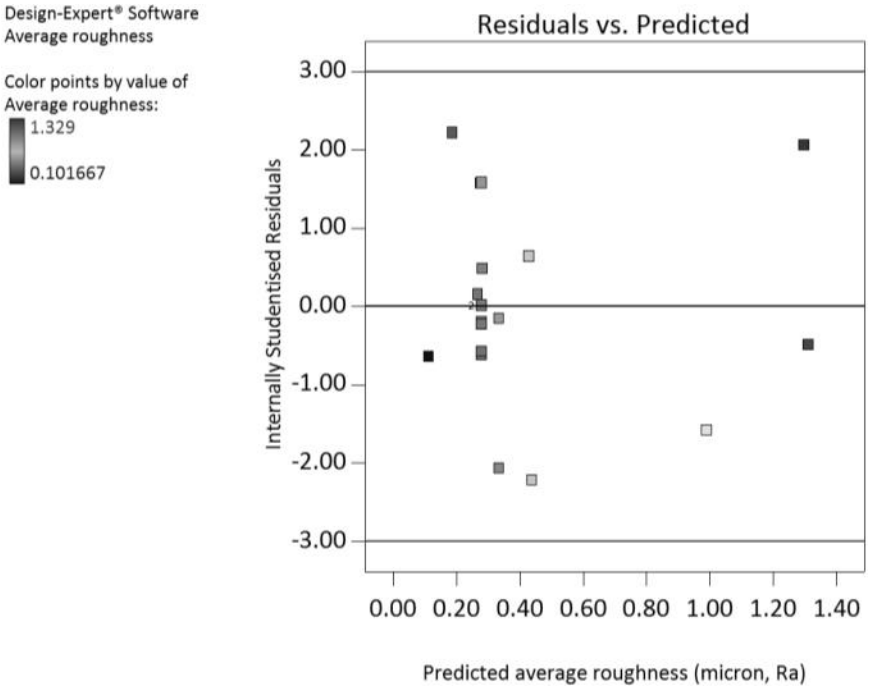

Figure 4.106 – Studentised residuals against predicted average roughness.

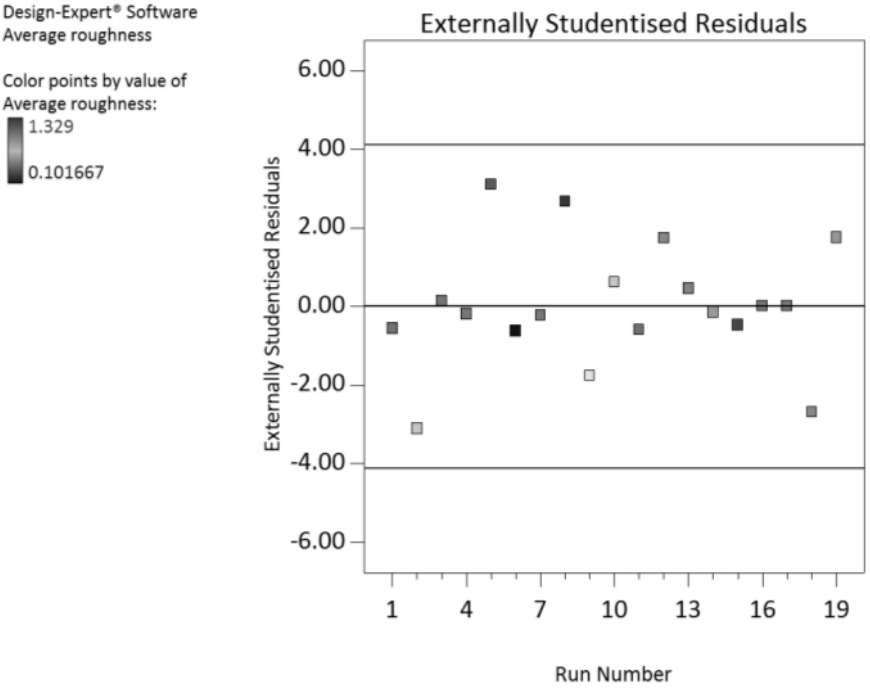

Figure 4.107 – Externally studentised residuals against run number.

The Box-Cox in figure 4.108 makes no recommendation for transformation – if the 95% CI (confidence interval) about the vertical line straddles the '1' value, then no recommendation is made. The lowest point of the curve is used to identify the value.

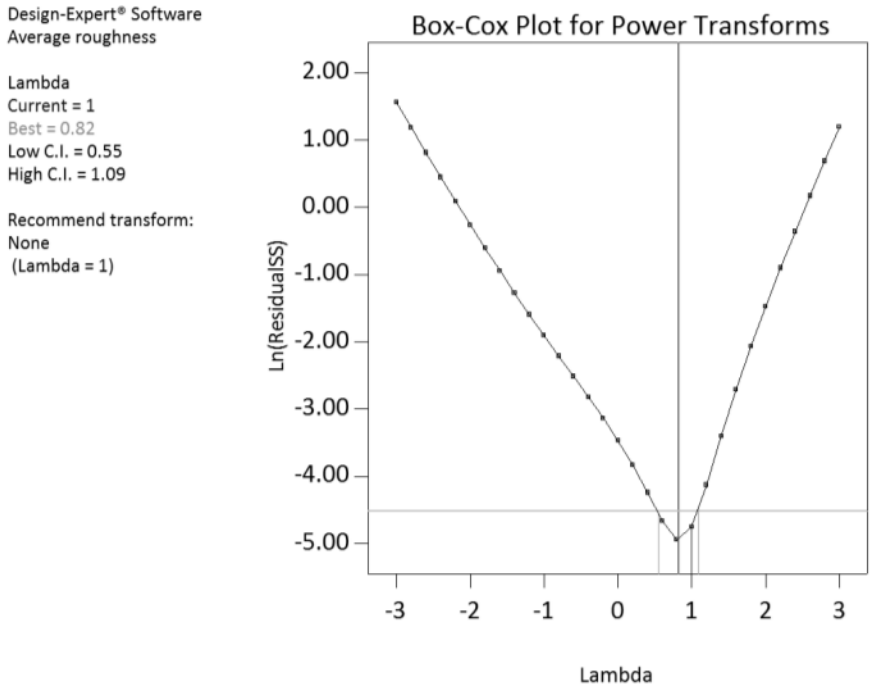

Figure 4.108 – Box-Cox power transform plot for average roughness dataset.

4.7.2.2 Significance and variance in material removal dataset.

Present in figure 4.109 is a slight S-curve that could be viewed as random scatter – the values at the extremities of the guideline do not conform to the shape. This plot shows data following a transformation applied as per the recommendation in figure 4.112.

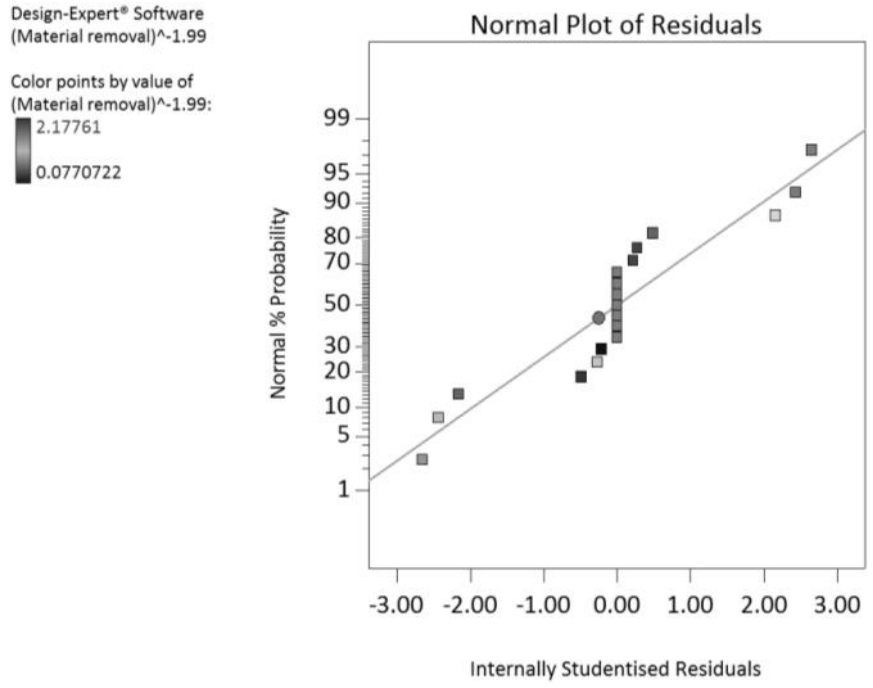

Figure 4.109 – Normal probability plot of material removal datapoints.

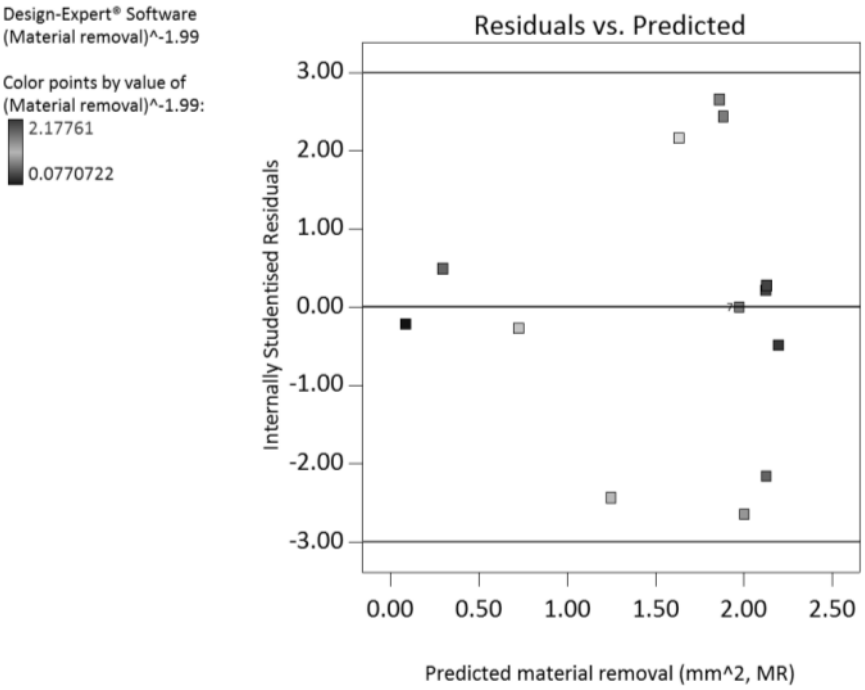

Figure 4.110 – Studentised residuals against predicted material removal.

Also with figure 4.112's recommended transformation, figure 4.110 shows a very slight megaphone pattern, although less so than pre-transformation and with greater scatter. The transform is applied to all data and analysis upon transformed values – actual values are not affected and further plots are representative of real-world MR values.

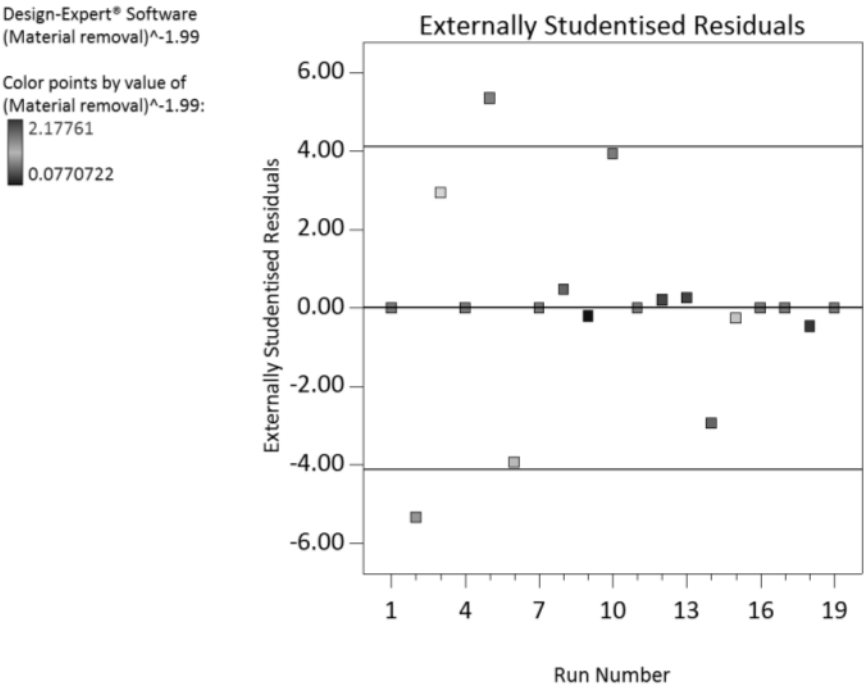

Figure 4.111 – Externally studentised residuals against run number.

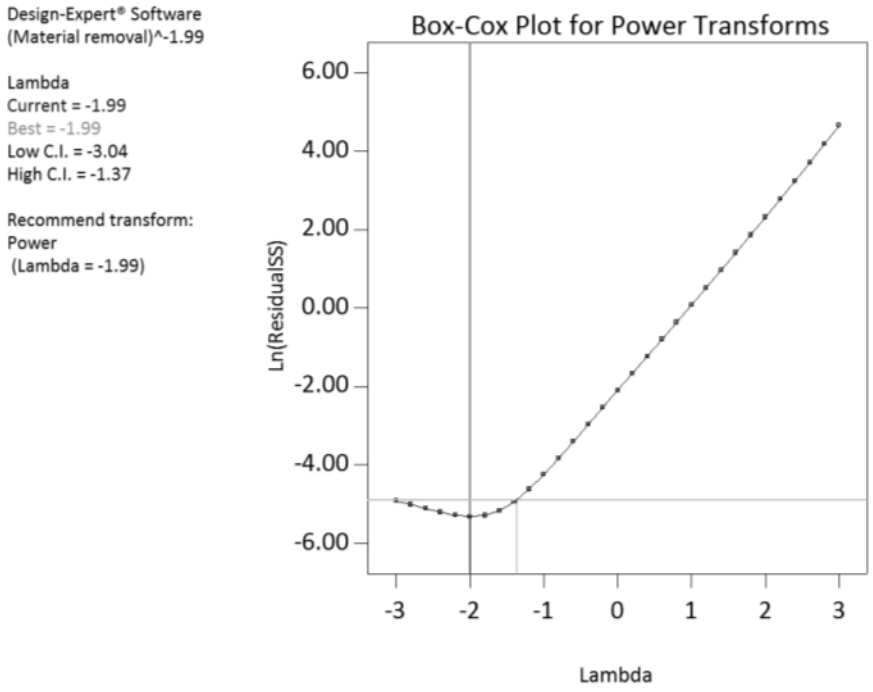

Figure 4.112 – Box-Cox power transform plot for material removal dataset.

4.7.2.3 Significance and variance in peak height reduction dataset.

The log10 transformation applied to this dataset (see figure 4.116) is the most effective and as found in the machine parameter study, the PHR dataset is once more the most statistically robust unit.

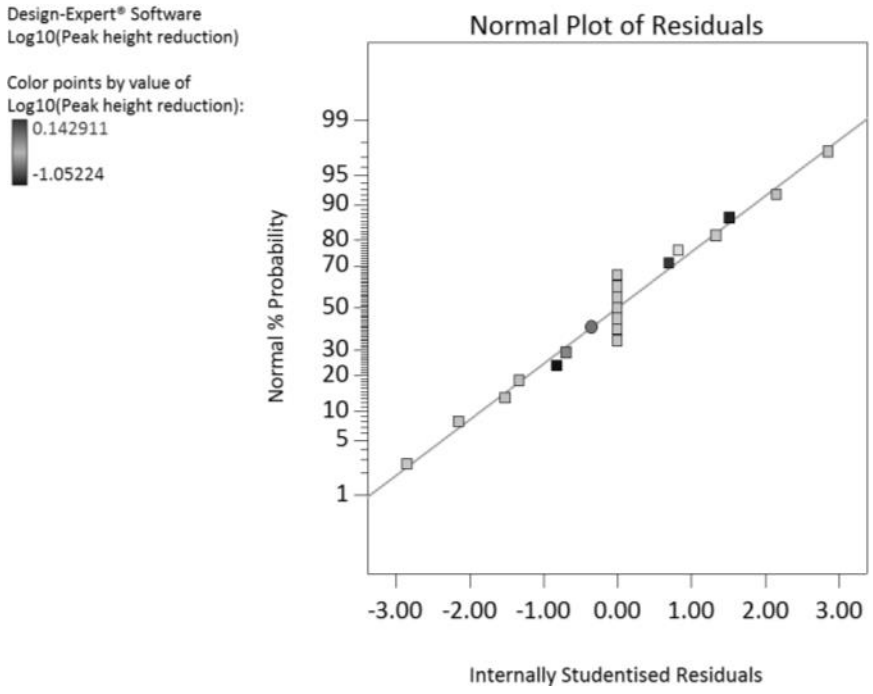

Figure 4.113 – Normal probability plot of peak height reduction datapoints.

Figure 4.113 shows an excellent fit to the guide line, with little to no scatter and no S-curve, indicating a very strong normal distribution. Scatter is most impressive, relative to the Ra and MR units as depicted in figure 4.114. The absence of *any* megaphone pattern is reassuring.

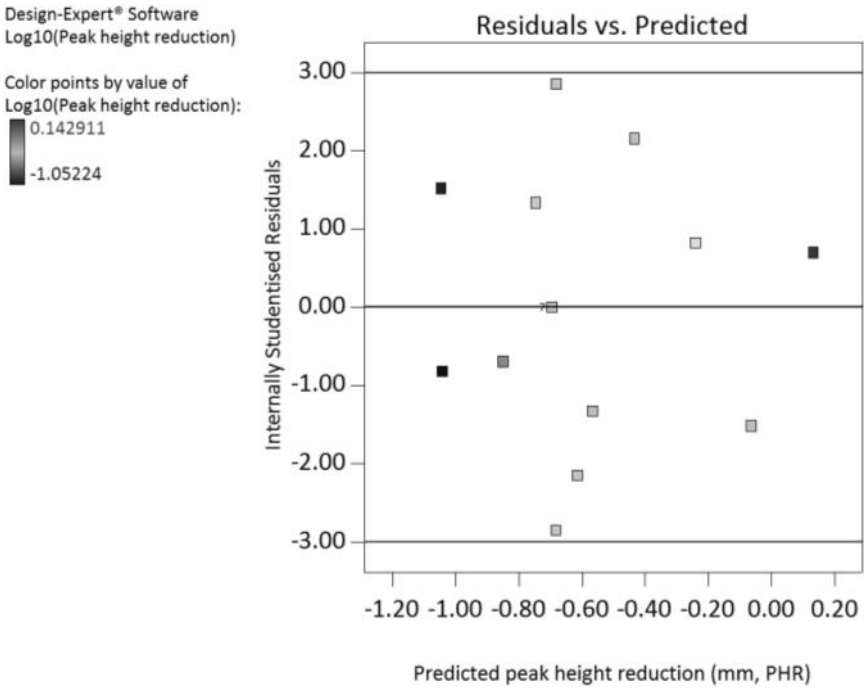

Figure 4.114 – Studentised residuals against predicted peak height reduction.

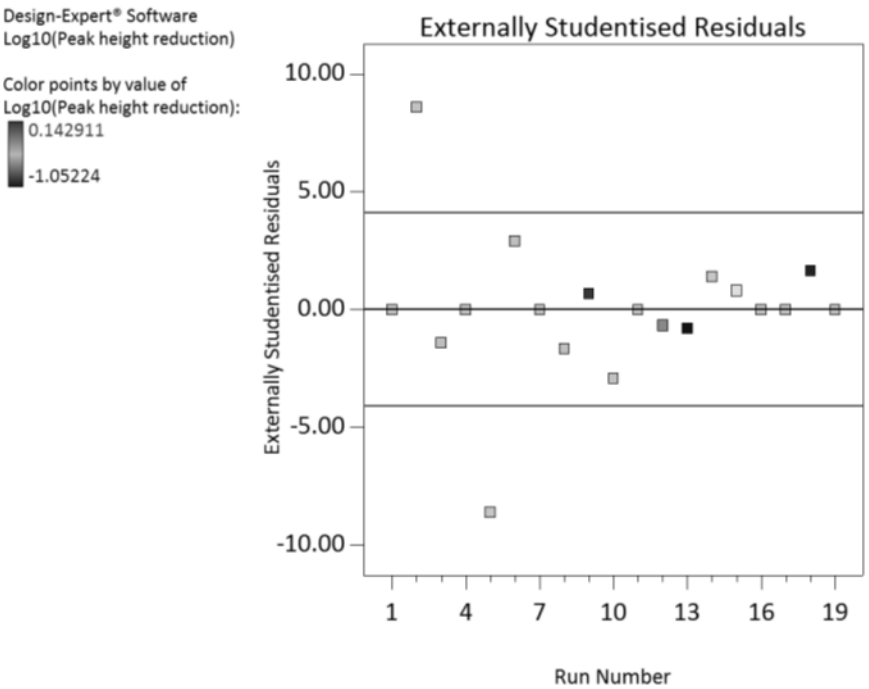

Figure 4.115 – Externally studentised residuals against run number.

Figure 4.115 highlights two erroneous points in the 8 and -8 regions at run 2 and 5. While these points are outliers, they do correspond with high magnitude responses in the experiment and they have undergone a transformation – there is no reason to remove the runs as the limited runs of the design leave it open to being disproportionately affected by the removal of responses, particularly ones characterising aggressive behaviour. It is recommended that if no special cause is found, then points should remain in the dataset. The data is transformed by a log function as per figure 4.116.

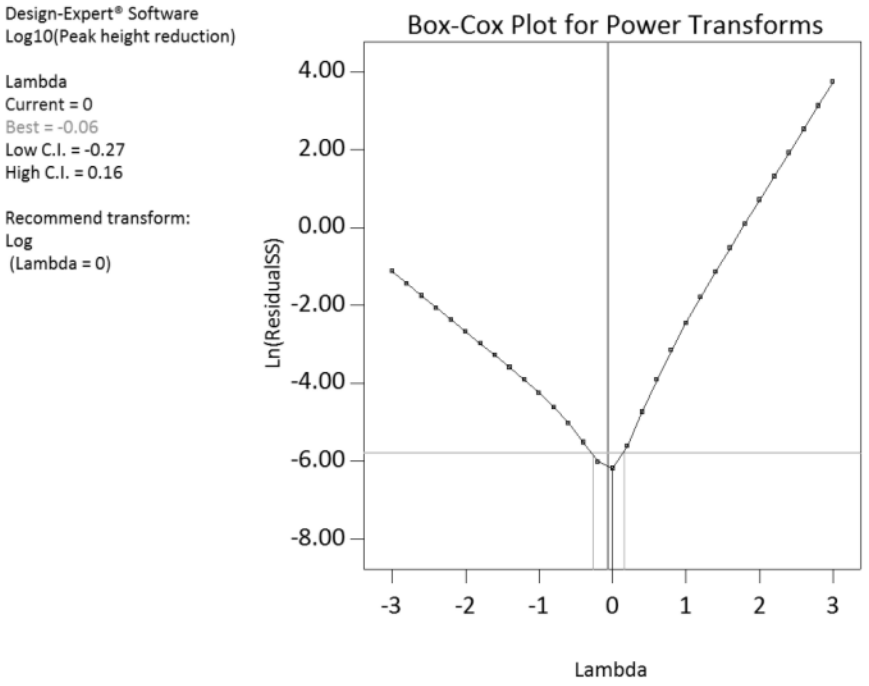

Figure 4.116 – Box-Cox power transform plot for peak height reduction dataset.

4.7.3 Modelling and interactions.

Describing process behaviour is achieved by initially using partial sum of squares ANOVA to identify significant terms and their weighting in the described equations throughout this section. Two factor interaction plots are shown at appropriate levels to describe effects and predicted versus actual value plots are used to show the accuracy of the prediction model.

4.7.3.1 Modelling and interactions of average roughness dataset.

The terms MP, GF, GS, MP-GF, MP-GS, GF-GS, MP^2, GF^2 and GS^2 are shown to be significant, while the model F-value of 260.36 implies strong significance of all terms combined, adding weight to the concept that AFM is driven by a great number of factor interaction, not just in machine parameters, but in the media configuration also.

Table 4.27 – ANOVA partial sum of squares type III.

Source	Sum of squares	Degrees of freedom	Mean square	F value	P value (prob>F)
Model	2.25	9	0.25	260.36	< 0.0001
A-Modifier percentage	0.30	1	0.30	315.39	< 0.0001
B-Grain fraction	0.21	1	0.21	217.41	< 0.0001
C-Grit size	0.82	1	0.82	853.35	< 0.0001
AB	0.11	1	0.11	115.25	< 0.0001
AC	0.23	1	0.23	243.53	< 0.0001
BC	0.30	1	0.30	309.00	< 0.0001
A^2	0.044	1	0.044	46.26	< 0.0001
B^2	0.035	1	0.035	36.27	0.0002
C^2	0.14	1	0.14	144.17	< 0.0001
Residual	0.0087	9	0.001		
Lack of Fit	0.0059	3	0.002	4.36	0.0595
Pure Error	0.0027	6	0.0005		
Corrected Total	2.26	18			

The predicted R^2 value of 0.9564 equates to a 95.6% surety of model accuracy as presented in equation 4.34. The predicted and adjusted R^2 are in very strong agreement.

Table 4.28 – Deviation and predictability figures.

Standard deviation	0.031	R-Squared	0.9962
Mean	0.43	Adjusted R-squared	0.9923
Coefficient of variation (%)	7.18	Predicted R squared	0.9564
Predicted residual sum of squares	0.099	Adequate precision	53.320

$$Ra = 0.94 - (0.037 \bullet MP) + (0.007 \bullet GF) + (0.0005 \bullet GS) - (0.001 \bullet MP \bullet GF) - (0.00005 \bullet MP \bullet GS) + (0.00003 \bullet GF \bullet GS) + (0.001 \bullet MP^2) + (0.0004 \bullet GF^2) + (0.0006_{x10^{-3}} \bullet GS^2) \quad (4.34)$$

Modifier percentage and grain fraction appear to be the two factors responsible for the final viscosity (or range of) for the media – their interaction in figure 4.117 presents a plot with constant grit size of $\bar{x}$=250μm (F60) whereby softening the carrier and increasing grit volume improve surface finishing ability – the opposite is true when softening the carrier but reducing grit quantity – the surface becomes rougher. It can be summarised as low-MP and low-GF is slightly less capable than high-MP and high-GF, although this statement may change based on grit size constant.

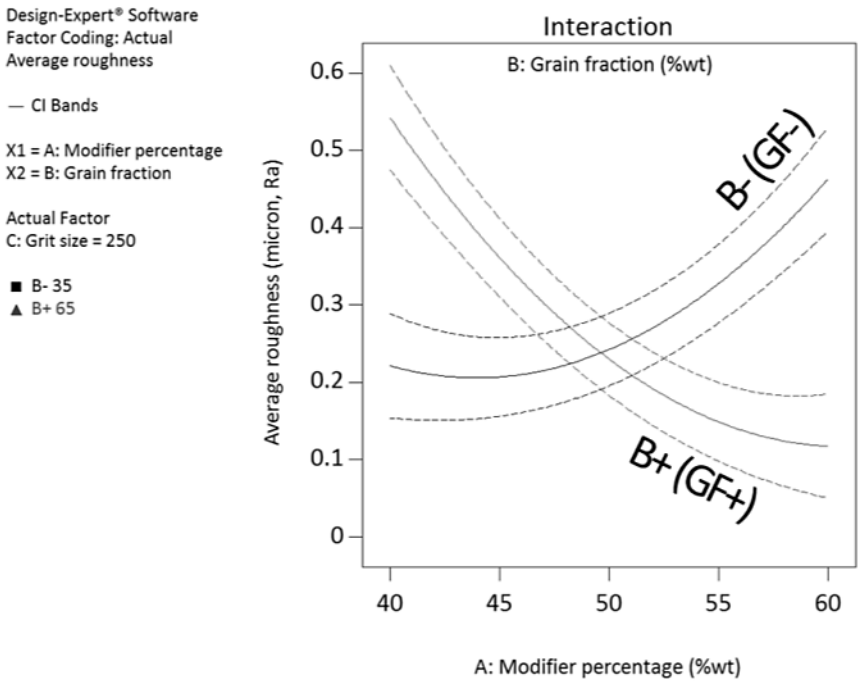

Figure 4.117 – Interaction between MP and GF for average roughness.

Modifier percentage and grit size (figure 4.118) have the same relationship – one might suggest the increase in grit size increases grit-grit interaction, whereas the previous plot increased grit-grit interaction by increasing number of particles. The effect in figure 4.118 is valid at 35%wt GF. As reduction in roughness is the target of surface finishing, the take-away from this plot is that low-MP and low-GS are equally as capable as finishing as high-MP and high-GS.

Grain fraction and grit size (figure 4.119) are, like the other interactions, almost equal and opposite; low-GF and high-GS are conducive to a good surface, while the same can be said of high-GF and low-GS. With a constant of MP=60%wt, the carrier in the plot is relatively soft – reducing MP will stiffen the carrier and increase the aggression of the

media, although the abrasive potential difference allows the 1.1mm grit to enact anywhere between 1µm and 2µm Ra finishes, while the 0.05mm grit is restricted to less than 0.3µm, regardless of GF.

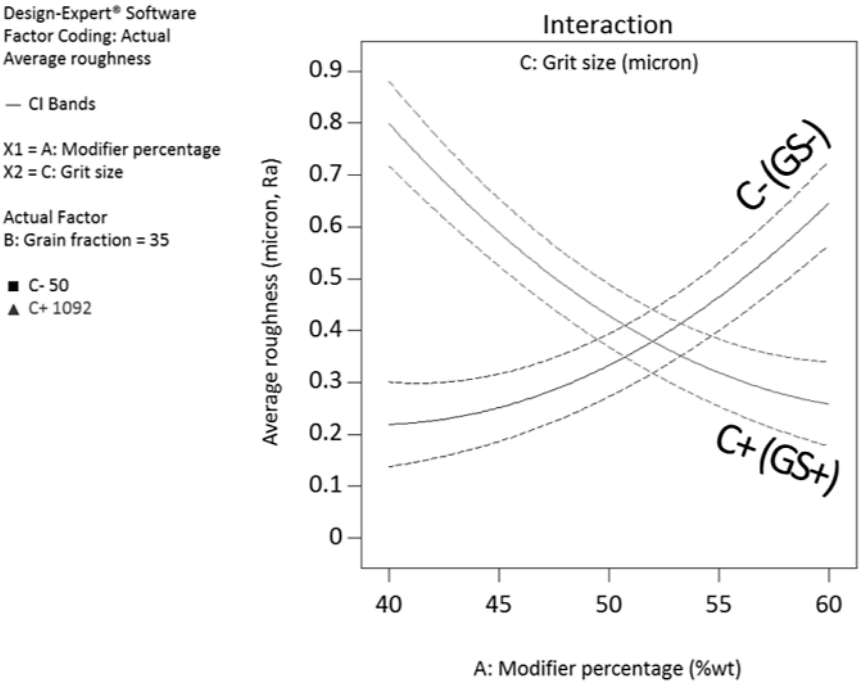

Figure 4.118 – Interaction between MP and GS for average roughness.

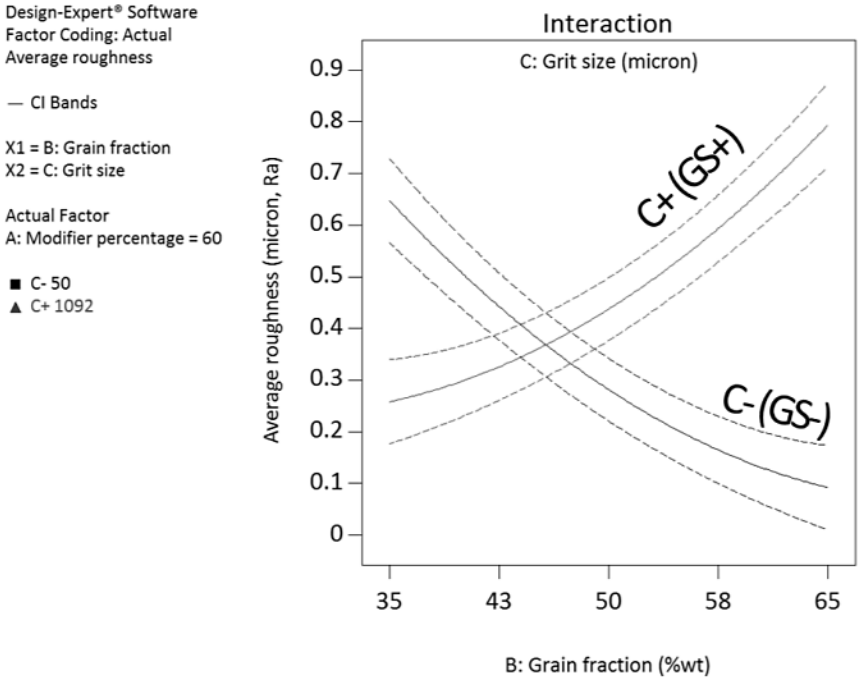

Figure 4.119 – Interaction between GF and GS for average roughness.

Applying the equation in 4.34, plots the points as shown in figure 4.120 – all points are tightly bunched on the best fit line, and while the mid-range is not well-represented, the top-end predictions give confidence that the model represents the space well and that the fit is good.

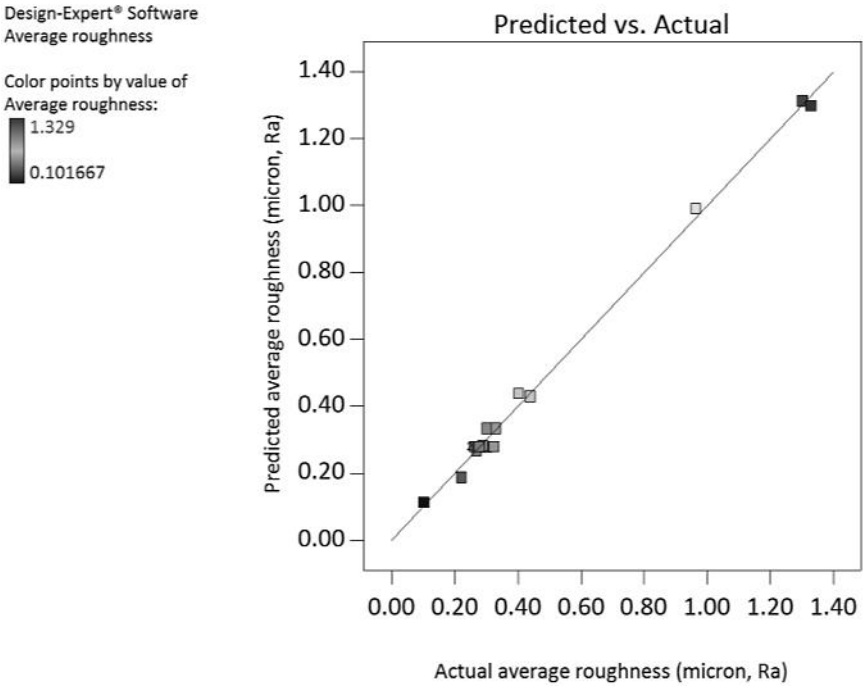

Figure 4.120 – Predicted average roughness versus actual.

4.7.3.2 Modelling and interactions of material removal dataset.

All terms are significant in the MR dataset – with the model F value at 134.17, the there is only a 0.01% chance this has occurred due to noise. F value represents explained variance over unexplained variance, thus a higher number is better. Model reduction is unnecessary as all terms are significant, and as shown in table 4.30, the data fits the quadratic model to a predicted R^2 of 99%, adjusted R^2 of 98.5% (that variation explained by the model and adjusted for the number of terms) and predicted R^2 of 88% (which should be within 20% of adjusted, as it measures the variation in the new data output by the model).

Table 4.29 – ANOVA partial sum of squares type III.					
Source	Sum of squares	Degrees of freedom	Mean square	F value	P value (prob>F)
Model	7.21	9	0.80	134.17	< 0.0001
A-Modifier percentage	1.19	1	1.19	199.94	< 0.0001
B-Grain fraction	3.21	1	3.21	537.98	< 0.0001
C-Grit size	0.80	1	0.80	133.80	< 0.0001
AB	0.60	1	0.60	100.90	< 0.0001
AC	0.25	1	0.25	42.69	0.0001
BC	0.10	1	0.10	17.17	0.0025
A^2	0.048	1	0.048	8.09	0.0192
B^2	0.64	1	0.64	107.34	< 0.0001
C^2	0.16	1	0.16	27.14	0.0006
Residual	0.054	9	0.006		
Lack of Fit	0.054	3	0.018		
Pure Error	0.000	6	0.000		
Corrected Total	7.26	18			

Table 4.30 – Deviation and predictability figures.			
Standard deviation	0.077	R-Squared	0.9926
Mean	1.69	Adjusted R-squared	0.9852
Coefficient of variation (%)	4.57	Predicted R squared	0.8816
Predicted residual sum of squares	0.86	Adequate precision	37.663

$$MR^{-1.99} = 2.741 - (0.015 \bullet MP) + (0.008 \bullet GF) - (0.001 \bullet GS) + (0.003 \bullet MP \bullet GF) + (0.048_{x10^{-3}} \bullet MP \bullet GS) - (0.02_{x10^{-3}} \bullet GF \bullet GS) - (0.001 \bullet MP^2) - (0.002 \bullet GF^2) - (0.7_{x10^{-6}} \bullet GS^2) \quad (4.35)$$

Figure 4.121 views the interaction between MP and GF for material removal. While grit size is a constant ~700µm (F24) (a relatively common multipurpose grit) the plot shows extreme results; with low-MP and low-GF, i.e. with stiff carrier and little grit, the addition (or subtraction) of modifier (MP) does nothing to change the level of MR. Logically, this statement can be explained by the lack of cutting edge in the media – because the opposite end of the spectrum shows a strong response to addition of grit. Maintaining a high MP (soft) carrier, the grit is powerless to act – however, as carrier is stiffened, MR exponentially increases, proving that low-MP is conducive to greater MR. As previously in the roughness dataset, a reduction in grit size throttles the upper limit of MR. Industrially, this means high MR operations require low-MP carriers, larger grit or where machine and geometry limit the practicalities of this, an increased proportion of smaller grit will allow the engineer to counteract the limit.

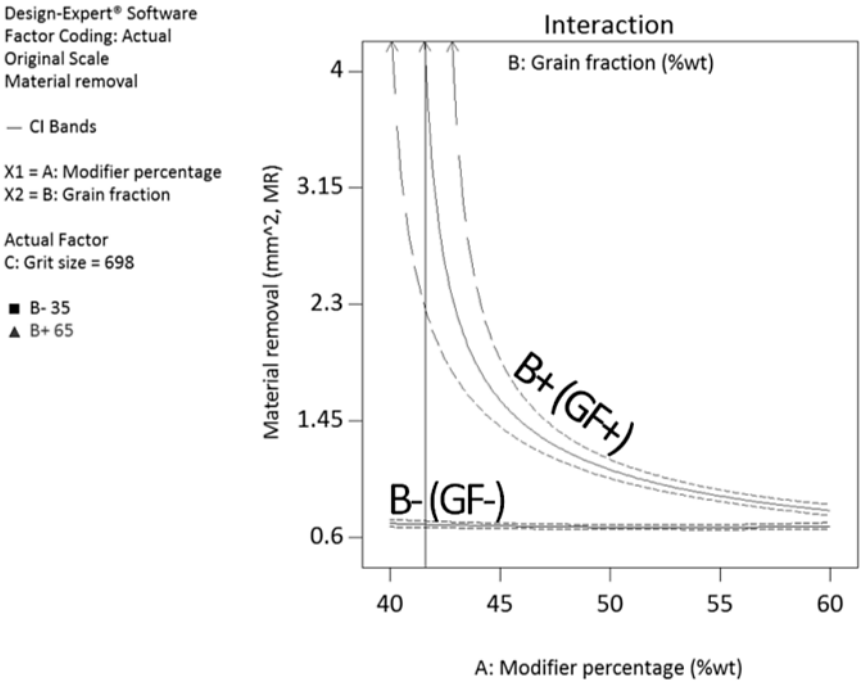

Figure 4.121 – Interaction between MP and GF for material removal.

Interaction between MP and GS (figure 4.122) highlights a similar effect as in figure 4.121. The dominant MP restricts the potential of GS (despite being at GF=59%wt). In practical terms, media temperature could be reduced to increase viscosity if MP is already high, although throttling by GS is still seen to reduce the capability of low-MP.

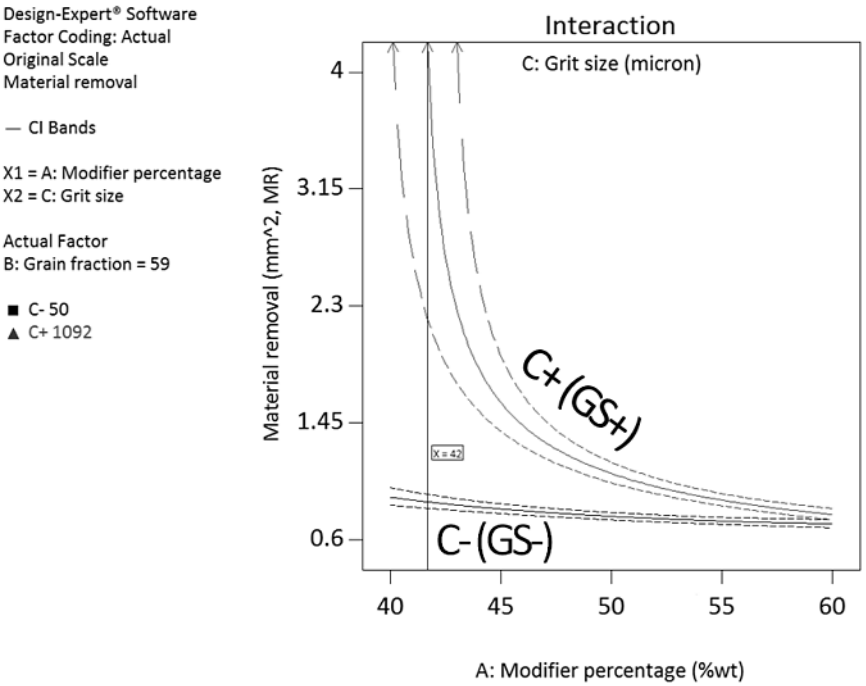

Figure 4.122 – Interaction between MP and GS for material removal.

Mirroring the effect seen previously, GF against GS (figure 4.123) represents GF acting as MP has done – to increase viscosity – while GS remains the throttling factor in terms of achieving MR. In production, opportunity to add grit to media is afforded, allowing post trial and error corrections to be made if insufficient MR has been realised.

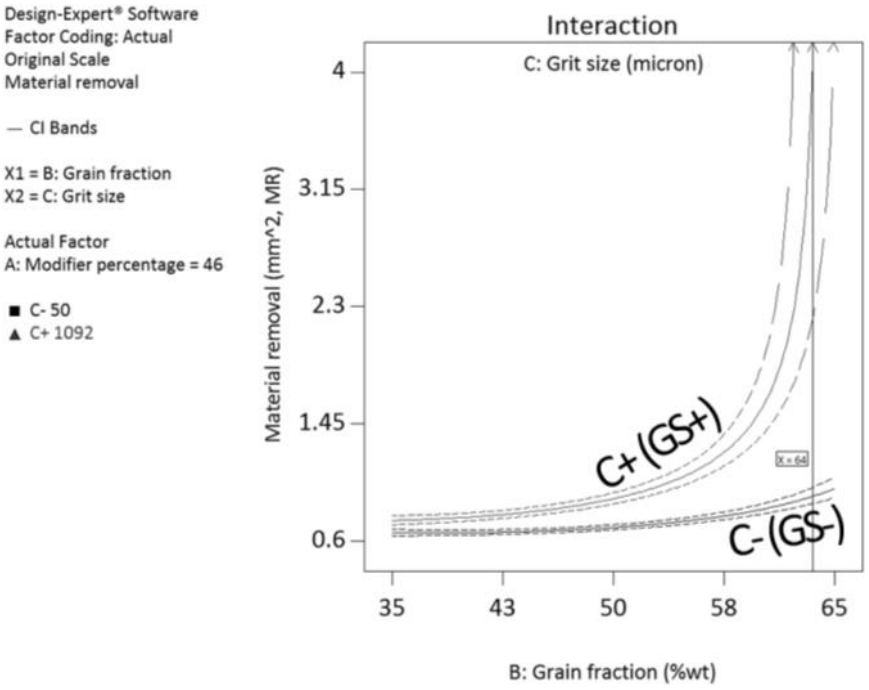

Figure 4.123 – Interaction between GF and GS for material removal.

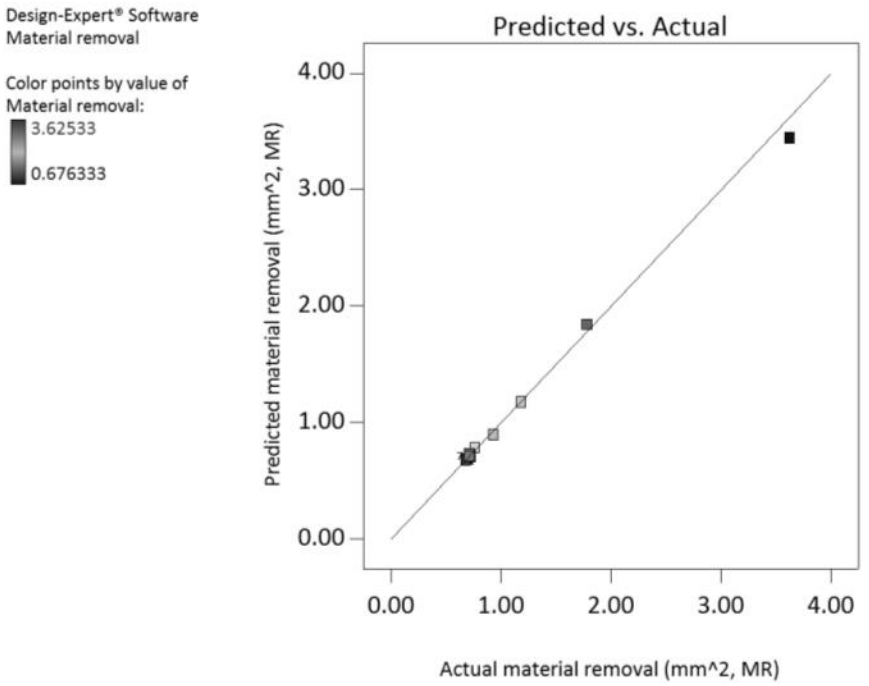

Figure 4.124 – Predicted material removal versus actual.

The points in figure 4.124 are well-conformed to the line of best fit, although the mid-range is heavily underrepresented – only two points describe the effect beyond 1.5mm^2, however their fit is strong and the average is taken from the three repetitions in the modified experimental structure, providing greater confidence in the used values.

4.7.3.3 Modelling and interactions of peak height reduction dataset.

While this dataset proves to have the best conditions for variance, it also presents a case for model reduction, unlike the other units – terms AC, BC, C^2 are insignificant and the only reason for their inclusion in the model terms is to support hierarchy for the quadratic model, typical in the RSM design. The model F-value of 232.27 indicates the model is significant and could only be derived by noise by a chance of 0.01%.

Table 4.31 – ANOVA partial sum of squares type III.

Source	Sum of squares	Degrees of freedom	Mean square	F value	P value (prob>F)
Model	1.53	9	0.17	232.27	< 0.0001
A-Modifier percentage	0.32	1	0.32	437.87	< 0.0001
B-Grain fraction	0.68	1	0.68	922.52	< 0.0001
C-Grit size	0.32	1	0.32	439.23	< 0.0001
AB	0.089	1	0.089	121.31	< 0.0001
AC	0.0017	1	0.0017	2.34	0.1607
BC	0.001	1	0.001	1.32	0.2802
A^2	0.0047	1	0.0047	6.42	0.0320
B^2	0.11	1	0.11	145.59	< 0.0001
C^2	$48.9_{x10}{}^{-9}$	1	$48.9_{x10}{}^{-9}$	$66.47_{x10}{}^{-6}$	0.9937
Residual	0.0066	9	0.0007		
Lack of Fit	0.0066	3	0.0022		
Pure Error	0.000	6	0.000		
Corrected Total	1.54	18			

R^2 of 99.6%, adjusted R^2 of 99.1% and predicted R^2 of 93% are good values for model variation. The disagreement between adjusted and predicted is approximately 6%, which is insignificant – usually the adequate precision should be greater than four.

Table 4.32 – Deviation and predictability figures.

Standard deviation	0.027	R-Squared	0.9957
Mean	-0.61	Adjusted R-squared	0.9914
Coefficient of variation (%)	4.40	Predicted R-squared	0.9314
Predicted residual sum of squares	0.11	Adequate precision	60.043

$$Log_{10}PHR = -1.01 - (0.0005 \bullet MP) + (0.002 \bullet GF) + (0.0007 \bullet GS) - (0.001 \bullet MP \bullet GF) - (0.004 \bullet MP \bullet GS) - (1.99_{x10}^{-6} \bullet GF \bullet GS) + (0.0003 \bullet MP^2) + (0.0007 \bullet GF^2) + (0.385_{x10}^{-9} \bullet GS^2) \quad (4.36)$$

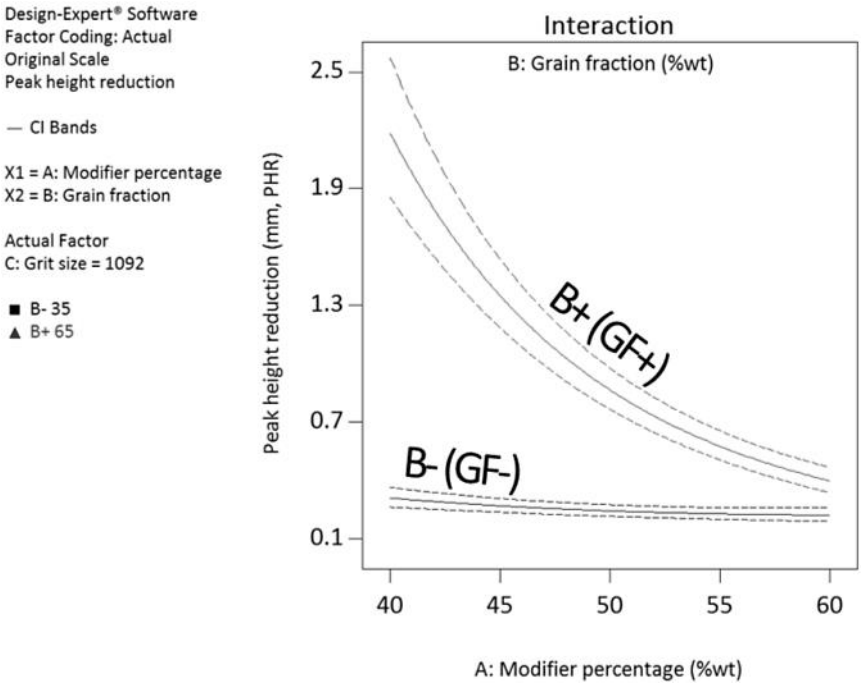

Figure 4.125 – Interaction between MP and GF for peak height reduction.

Considering a constant GS of 1.1mm, PHR is maximised by maintaining a low-MP and high-GF (see figure 4.125). PHR values at MP=60%wt are comparable, where MP limits the ability of grain to act on the surface, irrespective of volume. In a surface finishing environment, this may be useful, however in edge-rounding it is not – in order to ensure PHR capability, the correct GF and GS must be set, in accordance with MP driven by machine pumping ability. Practically speaking, the GF can be increased post-batch manufacture; simultaneously increasing viscosity, number of cutting edges and counteracting the mixed modifier percentage. Operating temperature can play a role.

Figure 4.126 presents MP against GS, showing the strength of GS as a driver of PHR, while simultaneously showing how easy it is to limit is by softening the carrier (high-MP). The C- in this plot is of a larger gradient than others – this is due to the restriction being lifted on the abrasive potential of 0.05mm grit by increasing the number of grains. The increased model error in the larger responses (LHS for both curves) is symptomatic of the greater error seen in the actual values. In practical terms, irrespective of MP or GF, increased PHR can be achieved from a batch of media by increasing GS.

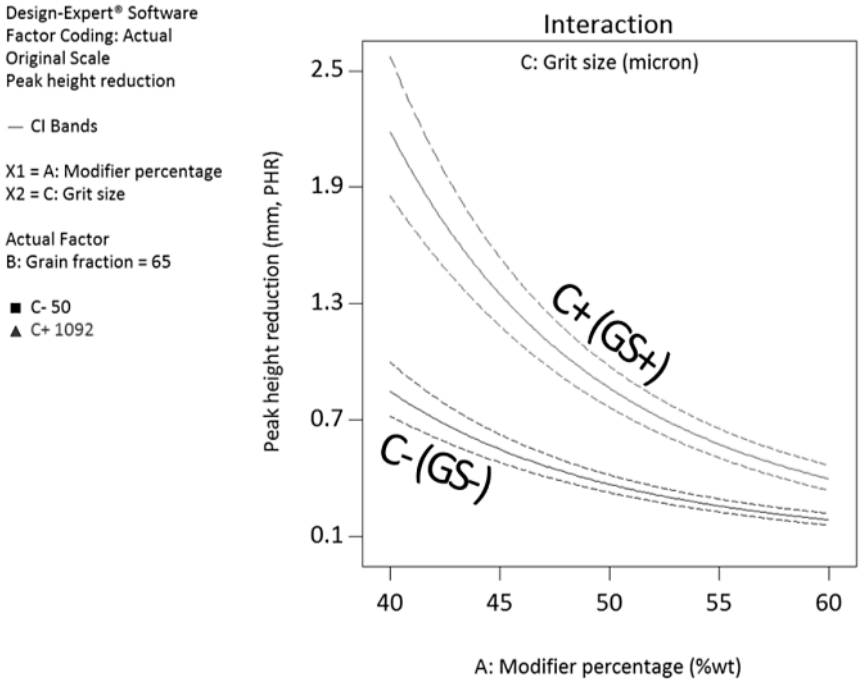

Figure 4.126 – Interaction between MP and GS for peak height reduction.

In agreement with the previous plots, figure 4.127 shows how GF is capable of throttling performance as easily as MP can. With low-GS, the PHR potential is low but can be impressively amplified by addition of more of the same size grit. The same effect is present in high-GS, except in this plot, the gradient differential is less extreme.

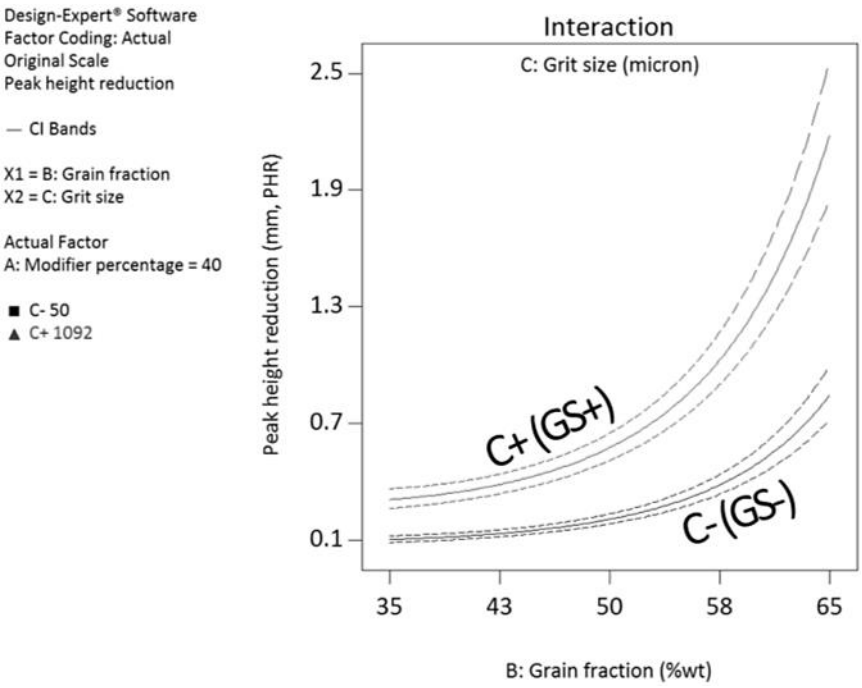

Figure 4.127 – Interaction between GF and GS for peak height reduction.

The spread of points on the best fit line of figure 4.128 is greater than Ra and MR, especially at the lower end, but comparable when viewing the mid- to high-end. The points are well-positioned, suggesting the model is strong.

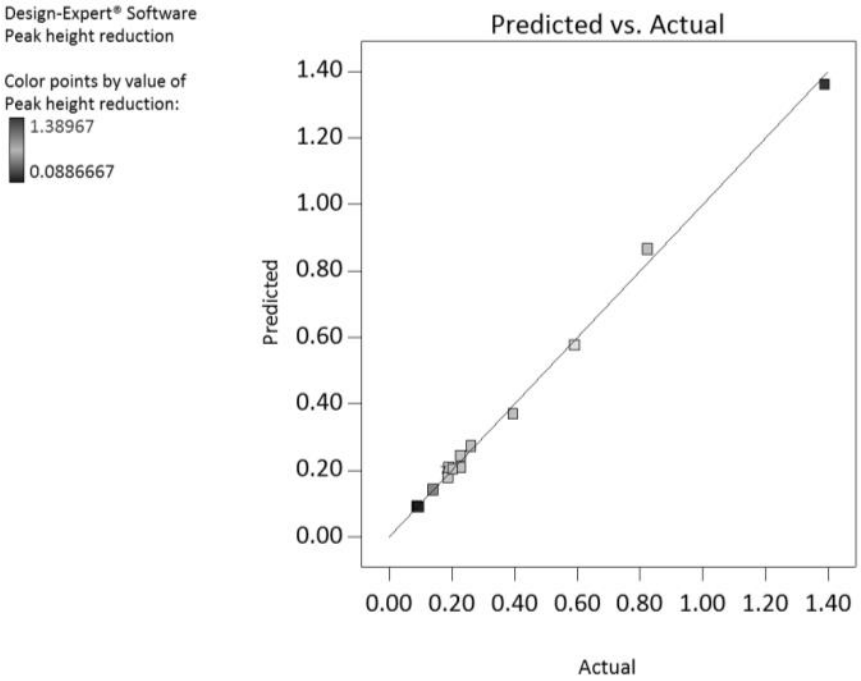

Figure 4.128 – Predicted peak height reduction versus actual.

4.7.4 Data interpretation and conclusions.

To conclude the analysis section, several key points are discussed not present in the main body. Factors such as surface texture, complex relationships and manufacturing targets are considered.

4.7.4.1 MP, GF, GS relationship.

While all three factors are shown to influence the response value, it is important to remember the dynamic between the three inputs. It can be said that motion is applied to carrier, then carrier applies motion to grit and grit then interacts with the surface. It is also true that none of the media parameters physically alter during processing – however, the experimental cell configuration creates its own unique environment.

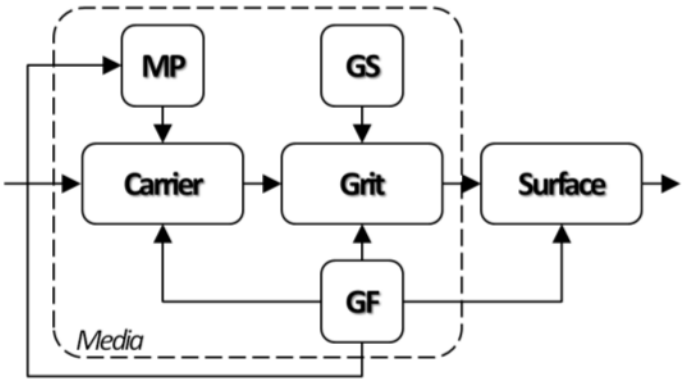

Figure 4.129 – MP, GF, GS relationship.

While MP, GF and GS remain as process inputs, and each are weighed out appropriately before mixing, further influence takes place upon mixing – MP is known to affect viscosity and strong conclusions can be drawn that increased MP softens the carrier reducing the ability of grit to act, however, once GF at -1, 0 and +1 levels are added to a given MP with fixed GS, the viscosity will vary. GF's effect on media viscosity is also manipulated by GS, and furthermore, controls rate of surface change.

4.7.4.2 Amplifying properties of GF.

Results clearly show the effect of GF to be an amplifier for the manifested effect – if surface finish is the target, increased GF will allow the effect to be achieved above and beyond an arbitrary fixed MP and GS level. The same is true for MR and PHR. It is unclear as to whether the improved rate of change is brought about by the increased volume of cutting edges, or the increased viscosity caused by additional solid phase material in the media.

4.7.4.3 Control via two factors.

Interactions show that only two parameters really need to be controlled to gain a desired finish. The extents of change witnessed in the interactions plots suggest the levels of two factors can be manipulated to achieve a response within the range – potentially useful if GS is too large for a workpiece feature, MP is too low for machine pumping capacity or if stock of grit is insufficient to gain a desired GF.

4.7.4.4 Surface texture control.

Six unique types of finish are seen in the results obtained from the focusing tool of the WLI system – in image A of figure 4.130, the best finish of the population is seen; however the streaks are comparable to that of the system using 1.1mm GS. In image B, machining marks remain, and only an undulation where media has flowed over the milling cutter step-over is seen. This could be improved by increasing GF or reducing MP. Image C is the roughest of the population and contains deep scores in random paths of between 0˚ and 30˚ of the flow direction – increase in GF will improve finish and retain MR/PHR abilities, if the machine is capable.

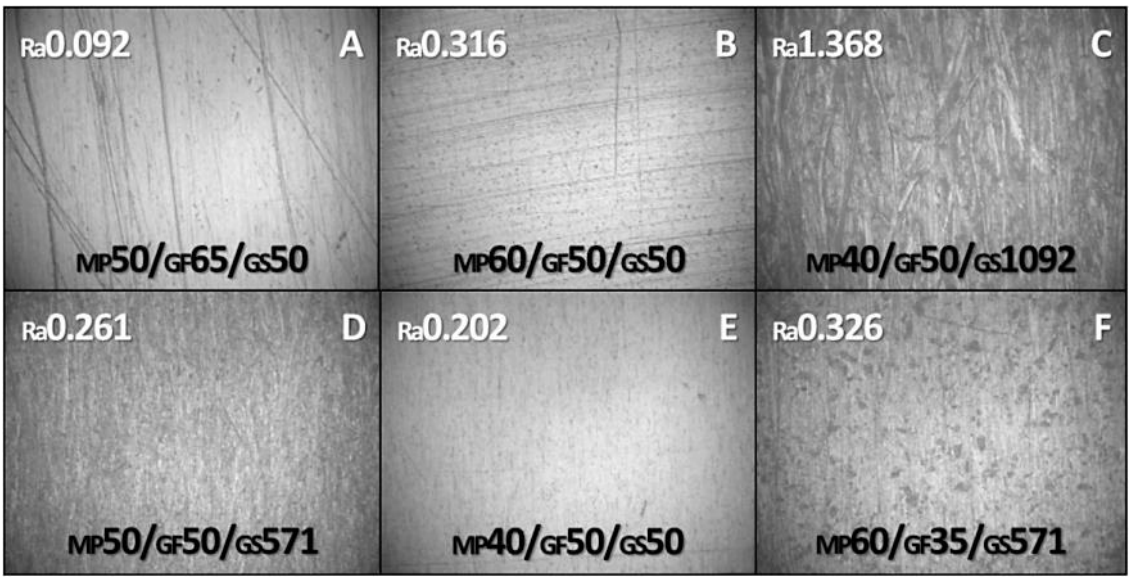

Figure 4.130 – Surface texture comparison. All images captured are 1mm^2 from CCD camera.

Image D in figure 4.130 is from the experiment centroid – this finish is typical of the vast majority of AFM operations, and while not as smooth as A or E, the finish is uniform and product is easily managed – it also provides a good start for a multipurpose configuration. Image E contains arguably the cleanest and most uniform surface finish and texture – undoubtedly, the 0.05mm GS aids the transition to the better finish. Image F is the only GF=35%wt cell – the texture shows darker scattered spots across the surface which may be attributed to soft carrier and less frequent grit-surface interaction.

4.7.4.5 Transferability and combining good finish with good MR/PHR.

The plot in figure 4.131 is useful to identify the cells where good MR/PHR has not come at the cost of poor finish – only one cell appears to buck the trend; values 12, 13 and 14, equivalent to cell treatment combination number six (image A, figure 4.130) with MP=50%wt, GF=65%wt and GS=50µm. Reasons for the results of 0.1µm Ra occurring alone are likely based on the uniqueness of the GF=65%wt and GS=50µm combination – no other runs contain this GF and GS. The only other comparable set is MP=50%wt, GF=35%wt and GS=50µm, where only GF has changed – producing an average roughness of 0.3µm Ra, allowing the conclusion to be drawn that high GF results in more work per cycle, but the level of indentation remains controlled by media viscosity – a function of GF and MP. Connotations of this include increased processing time in surface finishing applications where square edges are to be maintained, while benefits include simultaneous edge-rounding and finishing are able to be achieved, pressure capacity permitting.

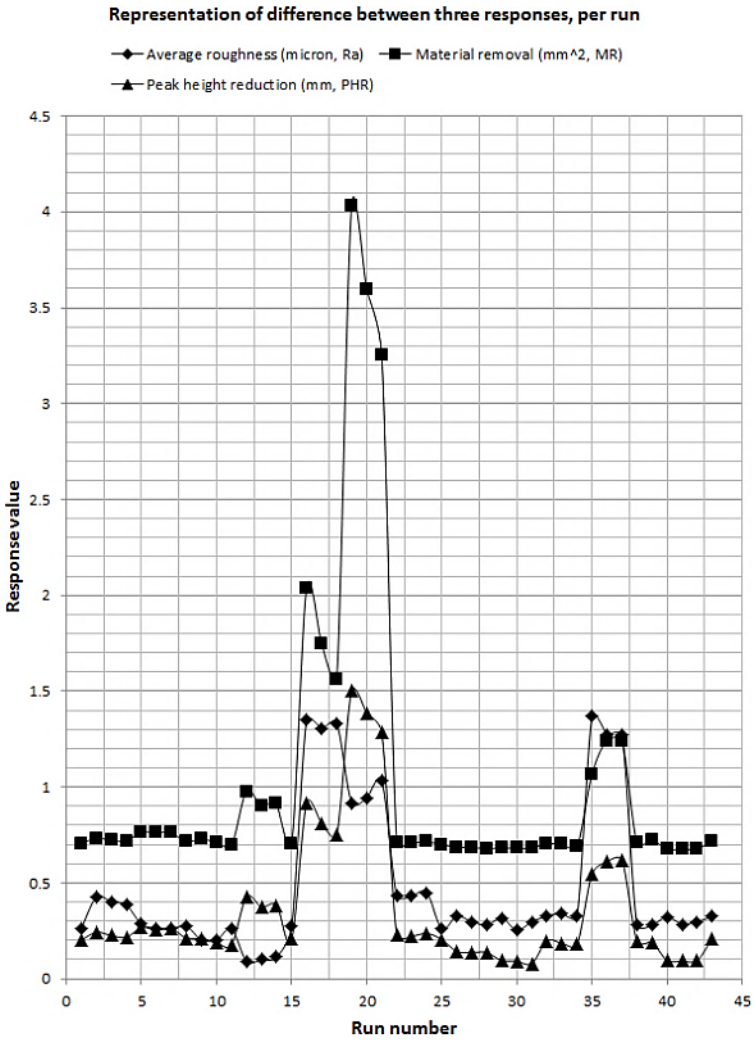

Figure 4.131 – Representation of difference between three responses, per run.

4.7.5 Populating the full factorial design for simulation.

Further to 4.4.7, the principle of extending the Box-Behnken into a full factorial structure is seen to be reasonable given the positive error and prediction values achieved in the modelling exercise (see appendix and chapter five theory). This allows like-for-like comparison between the 13 actual values and 14 theoretical, providing some interesting comparisons.

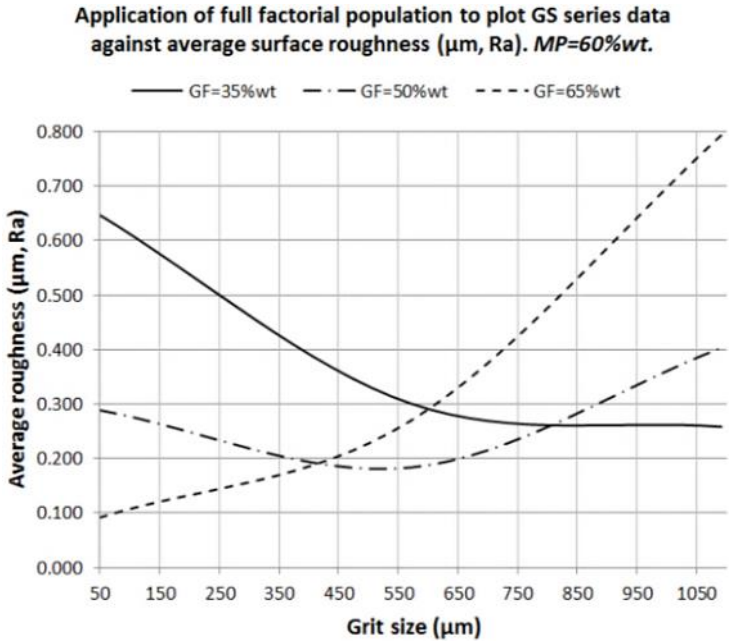

Figure 4.132 – Full factorial derived GS series against Ra.

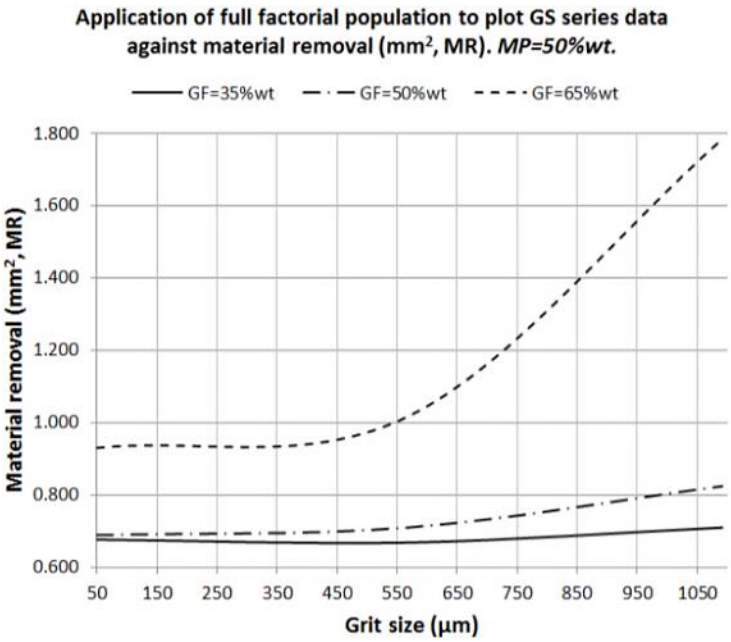

Figure 4.133 – Full factorial derived GS series against MR.

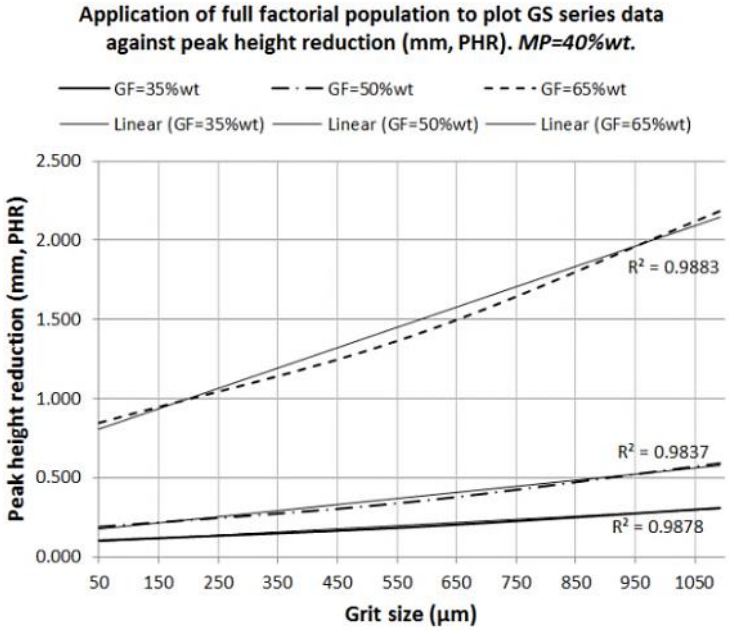

Figure 4.134 – Full factorial derived GS series against PHR.

Figure 4.132 presents three curves, all at MP=60%wt. Of the nine values required to plot, four are actual and five are predicted (GF=50%wt contains two actual) – the consistency between curve shape indicates good agreement between predicted values (both outer and centre), particularly given their extreme levels at opposite ends of the process space. It is clearly depicted that with increasing grain fraction, the curve rotates anti-clockwise about a central fulcrum which shifts down with increasing fraction; this translates to increased GF causing small GS to realise better finish and high GS to realise worse finish.

Figure 4.133 highlights an apparent threshold in GF acting to increase MR – a limited increase is seen between 35%wt and 50%wt, although between 50%wt and 65%wt, the effect occurs at a greater gradient, approximately 75%, as opposed to the 16% seen at GF=50%wt and 6% seen at GF=65%wt. As this gradient is not enacted until grit size reaches approximately 0.5mm, and all batches are the same in volume (19.5L), it is postulated that increased erosion can only be realised by a combination of increased viscosity and grit-grit interaction.

Figure 4.134 contains linear best-fit trends intended to show the removal pattern in PHR; all three lines fit to a linear model at a minimum of 98%, showing that GS as a factor drives a constant effect throughout the GS spectrum. Rate of change however, is driven by GF and while constant, where GF=65%wt, the response is ~270% greater than where GF=50%wt, whereas GF=50%wt is only ~90% greater than GF=35%wt. MP=40%wt in this plot, and it can expected that the percentage change would be less when checking softer (high-MP) carrier variants.

4.8 Summary.

This chapter has presented early inconclusive attempts at identifying standard methods of obtaining data from the AFM machine with respect to the three main factors identified as velocity, temperature and quantity. Further, the subsequent successful experimentation has been outlined in two stages of two; two experimental plans to establish machine behaviour data and media behaviour data, and two statistical analyses with activities chosen to identify main effects, interactions, validity of data and success of modelling tasks.

While the values obtained aid the understanding of the process in terms of machine and media – the geometry is fixed, as is the sample material. Therefore, the exercises completed are of limited usefulness in the production environment, save for the immediate 'firefighting' tools – it is however, critical to understanding how viable the technique proposed in chapter three may be; literature has already identified that material removal in AFM is confined to elastic deformation (rubbing, no removal), plastic deformation (ploughing, displacement without removal) and 'micro-cutting' (small chips), where the magnitude of each response is also shown in this chapter, together with the conditions (V, T, Q, MP, GF, GS) required to reach it.

It is evident that velocity and temperature affect the workpiece condition in different ways although with strong interactions – velocity alone has the potential to increase the depth of indentation of grit, causing a surface to become rougher, except increased temperature reduces the ability of velocity to transfer momentum; velocity increases internal friction in the carrier's internal structure, further increasing temperature, defining a threshold in velocity's ability to affect the surface as a softer carrier is noted to improve surface finish. Velocity is also shown to be limited by the media configuration it acts upon – experimentally, low velocity generates better finish than high – extension of this implies velocity should be set to zero, whereas the work on the media shows the range of finishes achieved when varying the media configuration and maintaining a constant velocity. It is difficult/nearly impossible to categorically state the effect that a single factor's level change will have on the surface – but research has shown that the greatest range of control is achieved through media configuration, with subsequent fine-tuning achieved by varying the machine parameters.

In this light, a conclusion is drawn that; 1) media grit size should be selected based on potential to generate surface finish or edge-rounding, 2) grain fraction should be maximised within the confines of machine pumping capacity (as viscosity is increased), 3) modifier percentage should be configured to be as viscous as possible within machine pumping capacity, while 4) velocity should be set to deliver the desired degree of indentation (as occurs in the machine configuration study) in surface finishing applications and to deliver the required shape of flow field in edge-rounding application, and 5) temperature should conform to maintain targets of velocity for a given media behaviour. Of the five steps recommended, quantity has been occluded –

the factor is purely the means to how V, T, MP, GF and GS affect the substrate. Sufficient duration under desired flow conditions must elapse to derive results.

As future part geometries will be arbitrary, the path to replicating the results is not proven – the effects of erosion under different conditions is shown by varying physical quantities, but these conditions do not provide the same results in every geometry. There must be an intermediary conversion stage that translates the physical flow phenomena associated with specific erosion into several simple actions that allow the application of this chapter's actual values into values that apply to any geometry, given a method to determine the physical flow phenomena in that geometry.

Chapter 5 - Modelling and Simulation

In chapter four, DoE techniques were used to numerically control the post-process condition of the standardised testpiece. The results are specific to the testpiece and the testpiece material, meaning results are only applicable to the geometrical environment used in the study, regardless of their accuracy or precision. The results are obtained in two separate experimental setups; 1) where media variables are isolated from machine variables, and 2) where machine variables are isolated from media variables. Explicit connections must be drawn to solve two problems; 1) how to join the two experiments together, and 2) determining which physical phenomena are responsible for erosion, thus providing a transferable metric by which erosion can be predicted and controlled.

5.1 Introduction

This chapter approaches the problem by converting chapter four's experiment environment into an electronic, simulated version representing the MMG corners (to an extent) of the AFM triangle. The 'geometry' corner is represented by converting the solid models used in part manufacture into a mesh of cells through which partial differential equations (PDEs) are calculated. The PDE solutions fed between cells, each passing solutions as outputs into neighbouring cells as inputs – the structure defined by the form of the testpiece and accompanying fixtures affects the vector of data transfer. 'Machine' is represented by the conditions applied to the cells – velocity and temperature are controlled. By representing the rheological behaviour (measurable and programmable) of the non-Newtonian slurry, the simulation environment gains an electronic version of the 'media' corner.

While the electronic representation appears thorough, it is only partially complete and several assumptions are made. The principles of engineering simulation and fluid dynamics are sound and proven, but in each of the MMG corners, there are elements that cannot be simulated, simply due to current limits of software capability; 1) 'geometry' cannot be corrected dynamically for in- or post-process erosion, 2) 'machine' cannot (nor need not) represent two way stroke or show interaction between extended processing time and surface condition, and 3) 'media' cannot represent the size distribution of grit, its mechanical properties, its interaction with the surface or its wear rate. These factors might be considered too limiting, but the methodology laid out in this chapter accounts for the missing factors in the electronic environment, and goes further to show how the remaining factors are integrated offline and proven against the values collected from the controlled chapter four experiments.

Existing data from previous authors would not have been useful for this research – the MMG environment within which their data is collected contains different sources of variation, but most importantly, the results come from a wholly different MMG

structure – testpiece geometry (including material, treatment condition and properties) is virtually impossible to replicate, media type is never disclosed in any transferable way (any reformulation thereof is impossible, as is adopting different parameters for study) and machine pressure, velocity, temperature and quantity are difficult to replicate.

Preparation of an *electronic version* of chapter four's experimental environment is made possible by logical extraction of simulation capability and known process behaviour. Figure 5.1 displays the methodology in the simplest form – boxes A to C represent physical activities; those that are capable of being performed in the real world as a means (or by-product) of controlled material removal, typically causing revenue-generation in the production environment. Boxes D to F are an electronic equivalent of A to C – the machine console is set by the operator to invoke piston motion and operating temperature – box D, simulation setup, is also set by an operator; more parameters are defined in box D than are defined on the machine console, although the parameters such as media configuration are implicitly loaded into box A when the operator fills the machine with media.

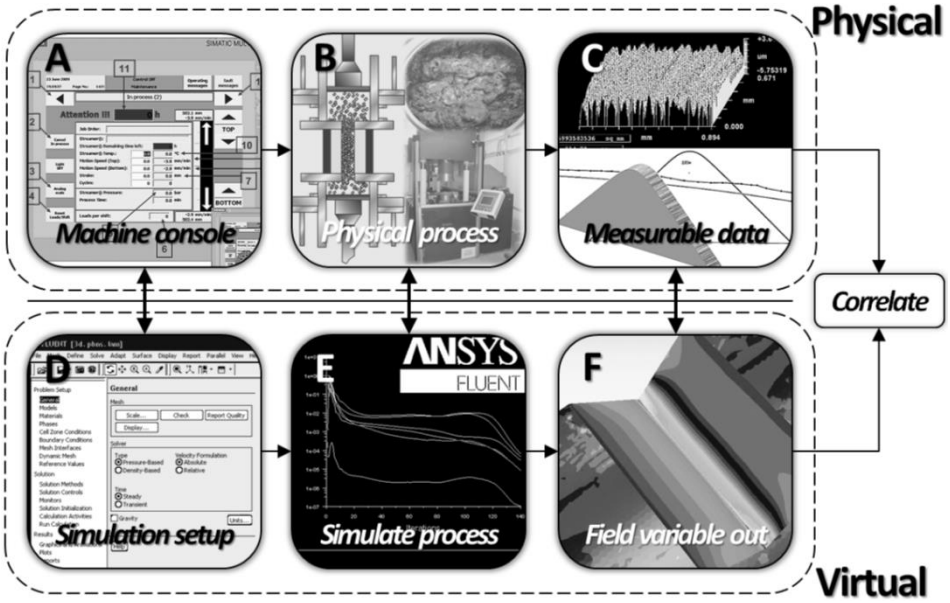

Figure 5.1 – Method of correlation between physical and simulated processes.

Boxes B and E represent the configuration of boxes A and D applied to the geometry in order to achieve an output. In the physical row, a part is clamped and media is passed through the cylinder, fixture and workpiece (geometry); in the virtual equivalent, Ansys Fluent is used to pass box D's information into the mesh (which is identical in form to the fluid-region's physical geometry). Boxes B and E can be likened to one another by describing the iterative nature of cycles – physical processing is a continual process, which will steadily march toward the final result throughout processing. Box E attempts

to solve equations using each neighbouring cell as input until they reach agreement (a result), akin to the cumulative effect of cycles applied to geometry in box B.

Boxes C and F display the results of processing – in the production environment, features are physically checked with inspection instrumentation to capture form at POIs (box C). While feature geometry cannot be measured at box F, field variables can be visualised and correlated, such as viscosity, strain rate, pressure, temperature, velocity, alongside more intangible measures such as flow field distribution and eddy currents.

Figure 5.2 – Method of correlation between physical and simulated processes.

A linear process is assembled (see figure 5.2) to summarise the transition from activities designed to collect data, and those which utilise the data. From left to right, the objective of this chapter is to firstly identify the governing flow factors (i.e. viscosity) that drive effects during physical processing. The simulation of the testpiece will allow the development of rules based on ‘erosion per unit duration/length of a processing condition’. Using knowledge of erosion caused by a processing condition, a simulation of a production part with the same electronic media and machine will help set processing parameters for complex geometry. After, the simulation will be optimised by varying any of the electronic equivalents of machine, media or geometry (i.e. the electronic equivalent of real process variables). Finally, the simulated setup will be machined and run as a manufacturing process on the physical version of the production part. Through this methodology, the aim is to develop a technique that can be easily applied to parts that require AFM, without committing to cutting metal and labour for trials. The method will allow the following in addition to savings on trial and error;

- Pre-process visualisation of effects
  Simulation can be used to judge uniformity of finish by checking velocity and pressure distribution – symmetry of flowfield about a POI gives a clear and strong indication of how tangential a radius may be.
- Tooling design optimisation
  As solid modelling allows any feature/design of tooling imaginable, tooling design can be visualised and approved prior to machining. Design of complex, deep-hole, risky and semi-automated tooling would be verifiable in a low-risk environment, without allocating productive labour.
- Cycle time reduction for high edge-rounding requirement parts
  Surface finish and edge-rounding have been shown to be almost opposing forces – where rounding is to be considered, the consequent damage to finish must be considered, and where finishing is to be considered, the lack of deburring effect must be remembered. Edge-rounding can be achieved in fewer cycles when

larger grit and greater grain fraction is used – the simulation will show the extents of surface roughening and the location, which may remain in-tolerance.

In the process of reaching this capability, there are numerous problems and offline stages required to integrate factors that are not capable of being simulated. These factors are discussed in the methodology section, 5.2.

5.2 Methodology

Simulation is not a perfect tool; output is only useful when setup is appropriate to the application. Variance exists in the CFD (computational fluid dynamics) process, as in the physical machine. Figure 5.3 presents stages of moving from a geometry designed to provide experimental data, through the CFD-preparation and data generation stages.

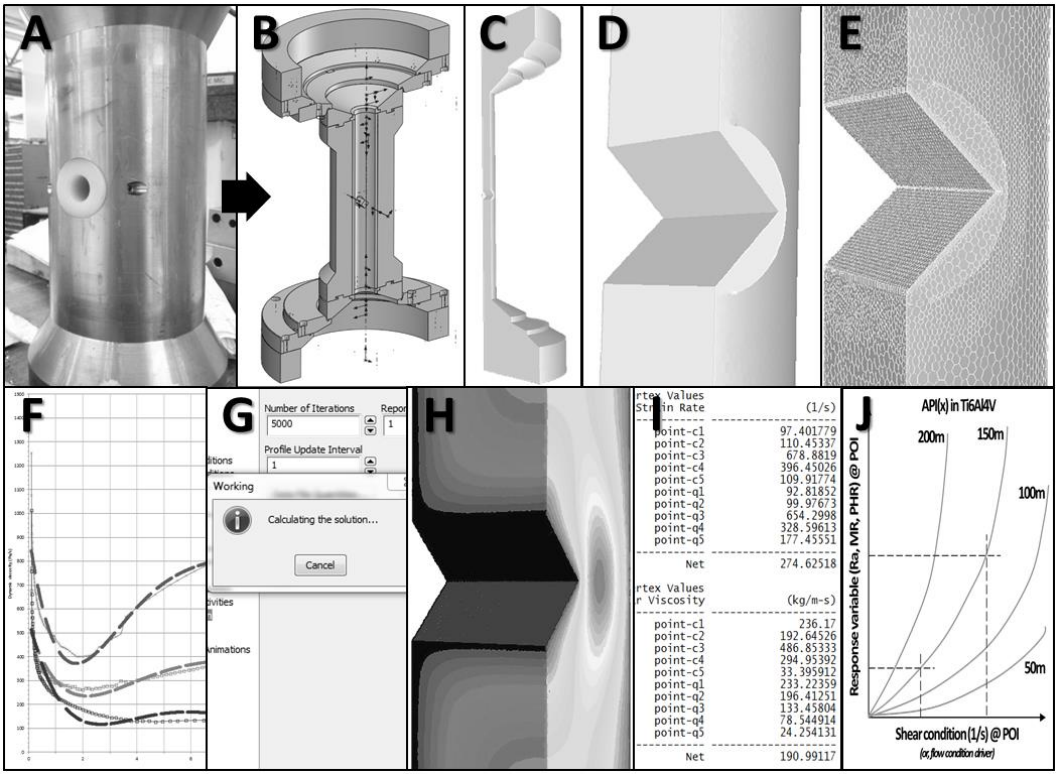

Figure 5.3 – Ten stages of data generation from a single simulation.

Two domains exist in the CFD-integration process; 1) the recognised steps in simulation used by a wide range of advanced industries (boxes A to I, figure 5.3) where solid models are converted to meshes and analysed to obtain useful field variables, and 2) where box J is included, to provide further extension of the analysis activity, for a wider reapplication of the data. Referring to figure 5.3; A – physical geometry, B – physical geometry converted to solid model (shown in section), C – solid model converted to half or quarter symmetrical model (where possible) to reduce required cell count (and thus computation time), D – close-up of two surfaces representing a quadrant of the testpiece, cut about the centreline of the flow field, E – close-up of the meshed quadrant, F – rheogram depicting an arbitrary viscoelastic behaviour, where values are placed into a look-up table for reference by the CFD solver, G – solver is ‘Fluent’, Ansys’ preferred fluid dynamics package, H – visual output of viscosity contours, I – numerical output of field variables (strain rate and viscosity pictured), and J – an example output of offline integration with processing quantity for a given API in a given material.

5.2.1 General principles of software implementation.

In the grand scheme, simulation is required to replicate the physical testpiece environment because conventional fluid dynamics equations only help to describe fluid motion in certain simple geometries, within which physical principles, i.e. tubes. The challenge in Mollart's environment is to make simulation a viable tool for predicting final condition in complex geometry. Figure 5.4 presents the method of application of simulation (term interchangeable with CFD) as applied to allow solution of complex AFM setup problems.

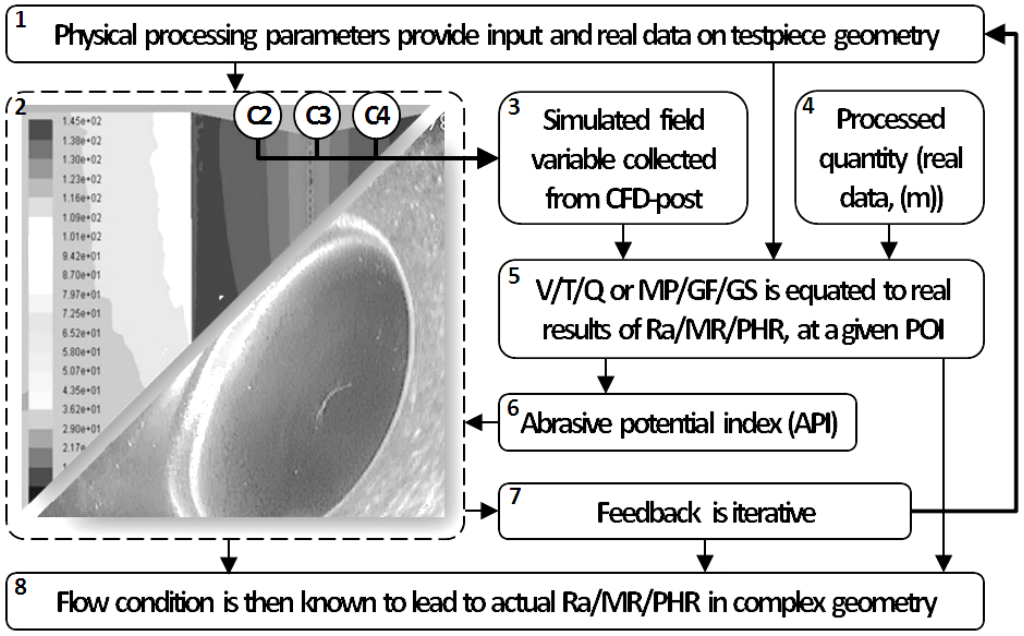

Figure 5.4 – Inclusion of simulation in CFD-aided methodology.

Beginning with the data obtained in chapter four, box 1 (figure 5.4) addresses the two physical experiments – in both, a set of controlled factors and levels supply a geometrical environment and set of processing parameters (cells) with a subsequent measurement activity providing real data at a POI (box 5), naturally found to correlate with those processing 'cells' and forms the basis for chapter four's consistent and replicable data. This understanding is taken forward to box 2 – edge rounding and surface finishing results are obtained from fixed points in the real environment, and as such are also obtained from the same points of the simulation (C2, C3 and C4). One of three inputs to box 5 is given by box 1, however boxes 3 and 4 are also required to fulfil the methodology – box 3 organises the simulation output and structures it by ignoring the quantity factor into a 3^2 velocity vs. temperature structure – more information on this approach is given in section 5.3. Effectively, the results are detached from processing quantity, as it cannot be simulated – quantity is integrated offline as in box 4. Moving knowledge of box 5 into box 6 integrates the media configuration – a method of describing the abrasive potential is considered in chapter 6. Using an electronic version

of the media (described in section 5.2.3), it is possible to describe the fluid behaviour of the media, minus any abrasive action. *If it is assumed* that the original 'chapter 4' MTT experimental media is used, then box 6 remains 'API-neutral' and a simulation of the complex geometry is carried out (return to box 2); it is known that the media flows in a particular way, as box 5 has previously merged the real data with the field variable data from the simulation – those field variables will re-appear in the complex geometry simulation, and are reverse-correlated with the real data, as in figure 5.2.

While little experience with the technique is held, the likelihood of a successful set of *machine* parameters being applied in the simulation environment is low – an initial 'best-guess' must be made, whereafter a revision should be made to the simulation parameters that delivers a more satisfactory simulation; 'satisfactory' in this context means uniformity of finish, controlled by uniformity of flow field, or similar user-judged metrics. A number of tasks need not be repeated when this process is applied in a production task – much of the data is gleamed and referred to by figures such as those at figure 5.18, 5.19 and 5.20. There are only two possibilities for infinite (iterative) setup stages;

- **Field variable responses tweaked using machine-only parameters** (velocity-temperature) only adjusts the shape and orientation of the flow field, and **does not affect the abrasive potential** of the media that the simulation is run with. If this is the case, the resultant field variables can be read off a chart (figure 5.18, 5.19 and 5.20) and *are known to match a given level of surface finishing or edge-rounding*, i.e. box 5 direct to box 8 (figure 5.4).
- **Field variable responses tweaked using media parameters** will also adjust the shape of the flow field, but by virtue of altering the GF and GS levels, even if the media is placed into the same flow condition as the next media, **the resultant 'real' Ra/MR/PHR will be different**. For this reason, where machine parameters are insufficient to deliver the required flow condition, the media configuration must be altered to extend the process capability – where media behaviour and erosion potential is known in a specific material, a plot will have been produced (figure 5.18, 5.19 and 5.20) however, when a new variant is required or a new material is being processed, integration is achieved by, 1) a short physical experiment in the test geometry (varying V, T and Q), then 2) measurement of the outputs, then 3) rheological analysis of the media (if not already available), and 4) a simulation in the testpiece geometry to determine the flow behaviour. Production of a graph (figure 5.18, 5.19 and 5.20) describing the erosion potential (in the test material) is then achievable.

While the media-change process may seem laborious, the media will never need to undergo this process again – a library of behaviour in the testpiece geometry can be built by analysing multiple media, while material changes require another short VTQ experiment where testpieces are in the same form, but different material. The simulation

only requires data for the rheological behaviour, not the abrasive potential, nor the workpiece/testpiece material.

5.2.2 System setup and hard limits of software capability.

Described previously, simulation capability is limited to exhibiting only flow condition, and additional information to transfer collected process data (for erosion) to simulated complex geometry, is performed manually, offline.

5.2.2.1 Incapability.

Methodology as developed and implemented in this work is constrained by the capability of the tool used to finalise the method and deliver the novelty of the approach. Table 5.1 categorises the 10 elements of the simulation software where its capability is insufficient, and must be further extended through offline methods. To circumvent the restrictions, methods discussed in section 5.3 are used. Some of these restrictions are intrinsic to Ansys Fluent 14.5, and some are present in the list as setting up the facility in the model adds complexity that has not been measured/verified in the physical machine environment.

Table 5.1 – Incapability of simulation.

Category	Ref.	Cannot…
Machine	1	Represent two-way stroke
	2	Display effects of quantity on post-process condition
	3	Cater for change in heater surface area with piston motion
Media	4	Mimic grit size distribution
	5	Adopt grit mechanical properties
	6	Represent grit orientation, dispersion and shape
	7	Characterise wear rate of grit
Geometry	8	Be corrected iteratively (dynamically), in-simulation
	9	Represent final erosion value
	10	Model microstructure or texture

Two-way stroke (as opposed to one-way (or unidirectional)) is a limit of the simulation software that forces the user to adopt an alternative method to incorporating the machine's total travel metric – the system also lacks a method of showing a link between total quantity and post-process condition and also the change in heating and cooling system exposure throughout the cycle as the piston motion cyclically increases then reduces the volume of media around the heat sources.

Ansys Fluent has a multiphase feature, but is typically designed for use in modelling water droplets in airfoil simulation or fuel atomisation in internal combustion engine (ICE) simulations. The grit size, size distribution, shape, dispersion, orientation-in-use,

mechanical properties and wear rate are not able to be simulated – polymer carrier behaviour *is*, and temperature-based behaviour change is also.

Following the simulation, the geometry will not have changed – unlike in the real world. Cycle after cycle, the geometry *will not* gradually creep toward rounded-edges or improved surfaces – it will simply remain 'geometrically nominal', as designed. Effects of flow on surface texture at a micro-scale are not visible in the system.

5.2.3 Operation.

Software solutions are notoriously difficult to gain replicates of operating conditions and results from the real world – figure 5.5 presents screen captures of the key setup areas in Ansys Fluent, from which a solver case can be run using the provided geometrical and rheological information, input by the user.

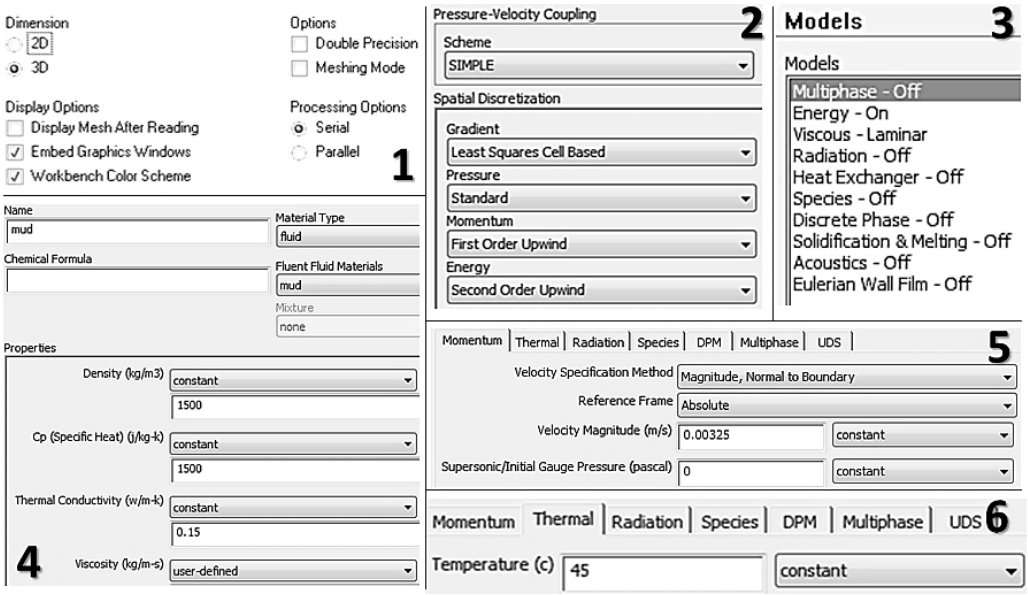

Figure 5.5 – Solver setup options (input variables) in Ansys Fluent 14.5.

Area one in figure 5.5 is the 'launcher window'. The model used is 3D, required to allow flow in three dimensions around the surface of solid model – processing options is set to serial as the computing power available in not sufficient to run parallelised. Area two describes the relationship between pressure and velocity – in AFM, the machinery delivers increasing pressure until a velocity is reached; this same approach is copied by Fluent by default, and to prevent the solution from exceeding sensible answers in the iteration process (and obtain the most suitable in-process solution), the 'least squares cell-based' method assumes a degree of linearity between cell input and output information. Area three sets the physical analyses to be performed. Energy equations and laminar flow equations are computed during the solution-derivation process. Area four considers the material types in-use, in this instance, the media (described as a fluid); their density (kept constant), the energy required to heat them

(constant), the rate at which they heat (constant) and their viscosity (shear rate and temperature dependent (empirical data applied through C file)). Area five sets the inlet and outlet pressure behaviour – momentum is set as normal to the circular pipe inlet (the media cylinder), at velocity of 0.00325m/s (195mm/min), whereas in area six, the temperature of the incoming fluid is fixed. These fields are used by the software in conjunction with user-defined geometry and fluid descriptions in order to find equation solutions that agree with all cells in the model. Once the solution is found, the error between the results is minimised and coloured plots and numerical results can be obtained by selecting field variables.

5.2.3.1 Potential for error in CFD.

As the aim is to create a virtual equivalent of the AFM machine, consideration is given to the way in which CFD aspects are interconnected, and cross-referenced with the corresponding real action. Figure 5.6 presents a visualisation of user-set inputs, the cell shape options and its propagation into a complex geometry.

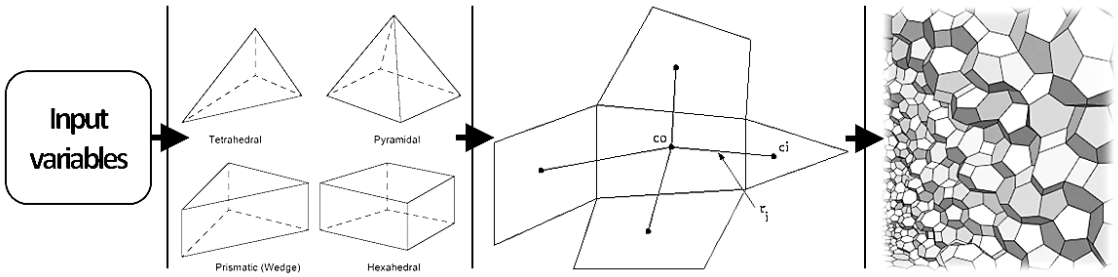

Figure 5.6 – Typical system for applying known physics to abstract geometry.

As previously shown in figure 5.5, the input variables are broad and provide a great degree of control – to an extent, real-system error can be replicated in simulation; constant values are preferred (despite the real system not adhering), and there is facility to describe transient quantities such as piston velocity using mathematical functions. Ultimately, the arbitrary nature of real-system variance is difficult to capture unless a statistical exercise is performed on each run, requiring another set of data as a function of processing conditions. Once the constant input variables and their proximity to the real values are determined, a solver passes information into the mesh for the first iteration. The mesh is comprised of a number of cells, the quantity of which is based upon the user's desired resolution at POIs. Different cell shapes fit better to features than others – the meshing stage includes a mesh-quality check, ensuring the cells are of a shape that allows reliable application of standard equations, and that the mesh is representative of the area through which fluid would flow in the real system.

Data computed in one cell is passed to the surrounding cells, dependant on which face mates with the neighbouring cells – as the system works by effectively 'guessing' whether an answer to a PDE is correct, and continually adjusting out the error levels,

there is potential to feed bad data from cell to cell. The endgame of this scenario is a ‘divergent’ solution, one where the equations do not agree and continue to increase in error – conversely, a ‘convergent’ solution is one where error reduces and a satisfactory answer is found. Results of a convergent solution are only considered sensible when a variety of processing conditions yield values that have been approximated by hand and have shown a reasonable variation in output values based on changes to simulation conditions that may also be valid in the real system – in this research, it is possible to compare the real results and check hand-calculated velocities against simulated velocities.

Other sources of error include the chosen cut-off point for iterations – as the PDEs are calculated in their entirety every iteration, a convergent simulation also reduces error in the solution every iteration. This manifests itself in changing responses variables, i.e. after 10 iterations, a POI may suggest a velocity of 2m/s exists, but at 100 iterations, a velocity of 0.5m/s may be found. To reduce the likelihood of this error, iterations can continue to be performed as shown in figure 5.7. However, using the example, between 400 and 600 iterations the results enter a phase of terminal decline where the residual error is small enough and response values (field variables, i.e. velocity, temperature) no longer change significantly. This signifies a converged solution and the results should be taken to the next phase.

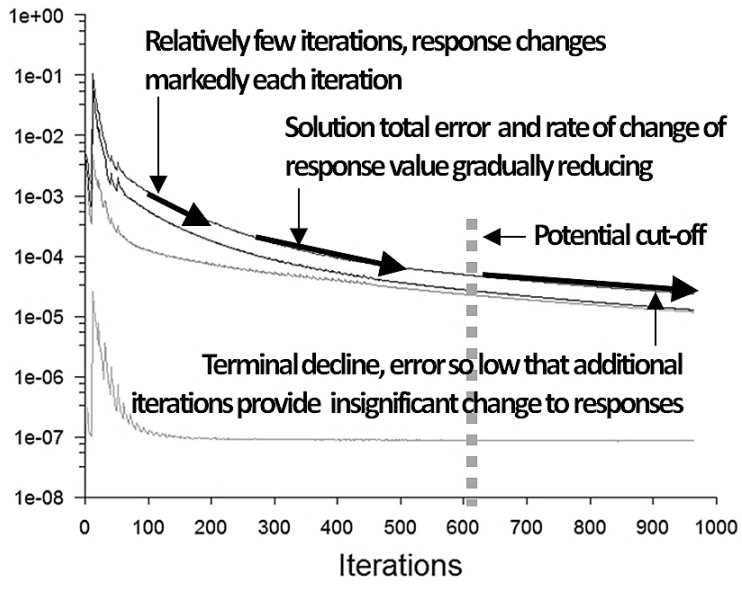

Figure 5.7 – Example residuals plot, sourced from Ansys Fluent 14.5.

5.2.3.2 Atypical changes to CFD system setup.

To reduce computational demand, the model used in this work is not a full-3D, nor a half-model, but a quarter-model. Reduction of model size reduces by extension, the cell count. Of the testpiece system, the fluid region is required to represent the flow and directional change of the media, and is therefore not suitable for a 2D simulation. This

work utilises two symmetry planes in the testpiece geometry to instruct the software to treat the planes as area through which flow may occur, albeit in a mirror image.

Truly dilatant (shear-thickening) materials are very rare, as are true pseudoplastics (shear-thinning). The behaviour of these materials are not, therefore, a common inclusion for software developers in their tools as relatively few users will use a predefined description. In order to create a virtual version of the media behaviour, (known to shear thin and shear thicken) the viscosity in a given shear condition must be provided to the software. In the research carried out, the media is tested at three different temperatures, each changing the point of thinning and thickening, raising the question of how the media best be represented, especially considering its importance to the level of erosion seen in the part. Fluent offers a tool called a user defined function (UDF) through which multiple hooks into the software are available to integrate data, coded in C-language. The C file (an example, representative of all, bar changed input values) can be found in the appendices. With the information provided to the system as described above, the simulations of methodology presented in section 4.3 are possible.

5.2.4 Data extraction.

Figure 5.8 presents a screenshot of the quarter model as obtained from Ansys, plotted in a greyscale colourmap. The view looks at the quarter model from the perspective of the centreline through to the outer diameter of the geometry. While these images are often aesthetically pleasing, they do not convey the necessary data and accuracy offered by the simulation – a closer view with repeatable position value collection is required.

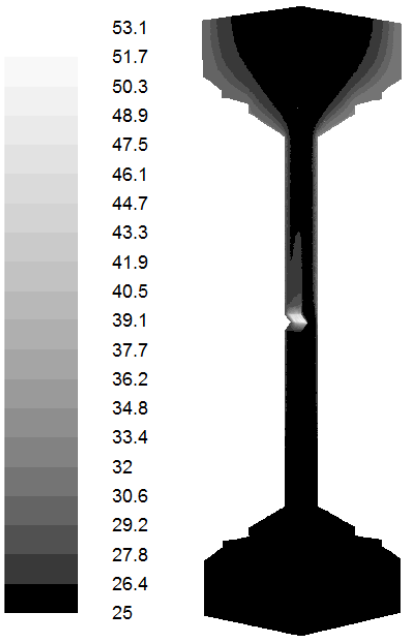

Figure 5.8 – Quarter model, greyscale colourmap, plotting temperature in degrees Celcius.

When a simulation converges, the analysis begins often with a coloured plot – this is a useful overview of the manifestation of a given field variable, but should not be relied upon for scientific work. Rather, in the case of fluid behaviour simulation, it is the concern of the engineer to obtain data for multiple field variables at the same point, following simulation of varied parameter levels for the sake of comparison. Figure 5.9 presents a close-up of figure 5.8's centre section – the area around the testpiece. In previous experiments, the data was collected physically from points as described in figure 4.4, but now a requirement exists to use the same positions in a virtual geometry, across a range of virtual samples.

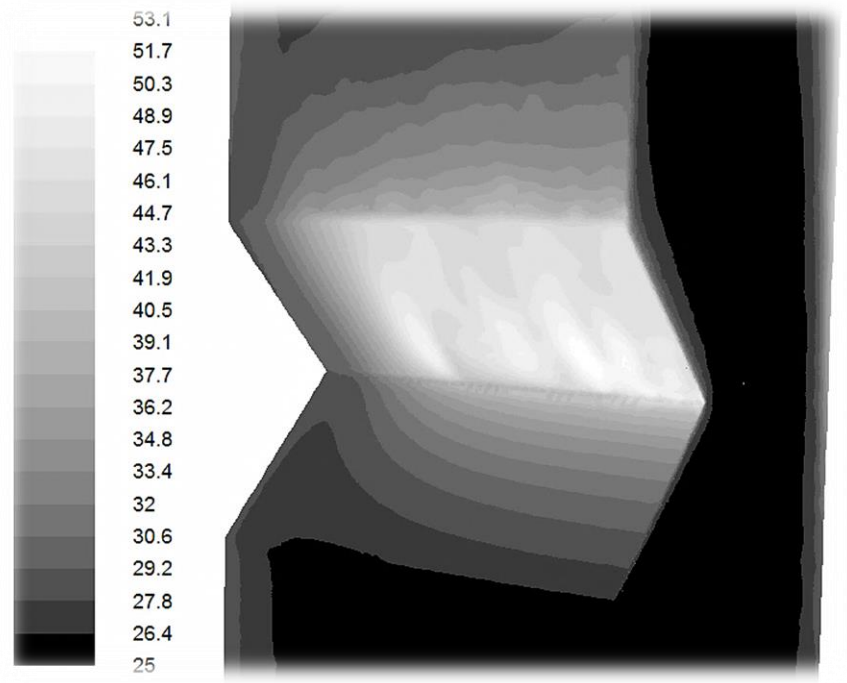

Figure 5.9 – Close-up of testpiece zone of fluid region. Output from Ansys Fluent 14.5.

Data plotted in figure 5.9 shows an arbitrarily selected trial run, where the flow of media enters from beneath and passes over the testpiece surface; the impression of the testpiece is clearly identifiable in the fluid region. As the media enters the smaller cross section, the temperature can be seen to rise from approximately the nominal pre-heated 25ºc, to approximately 35ºc in the centreline of the approach, peaking at over 53ºc at the edge-rounding point of interest. The trailing edge is exposed to the warmer media, which, judging by earlier research in this document, reduces support for grit.

Results immediately tell the viewer that temperature set on the machine is not a viable metric with which to judge estimated erosion in the job – temperature is shown to vary based on shear condition imposed by the surrounding geometry. Secondly, the result is only relevant for a one-way stroke of the machine, until single stroke results are integrated mathematically.

To move forward with these results, it can be assumed that machine parameters are known (as they are set during simulation setup (minus quantity, although known from experimental results)), media configuration is known (as the simulation only caters to rheological data, not solid matter), and testpiece material is known (as in this case, the physical measurements from experimental data are used in place of a small VT study in the chosen workpiece material and media configuration). Therefore, the engineer can use the physical measurements obtained (from the same media, the same material and the same processing parameters as simulated) to determine that if a POI is exposed to a quantity of flow at a temperature (in this example) (depicted at the POI in simulation), then erosion response is also known. Factors V, T, MF, GS and GF are not required to make the connection, as their effect is seen in the simulation's temperature (in this case) response, and in the physical measured value with which a correlation is attempted.

In application terms, these results (determined in full in section 5.3 for select material and media) would be translated into figures such as that posited in figure 5.10. These are the ultimate goal of the task, and arguably over time, a considerable volume of intellectual property would be established. Methodologically, the engineer identifies through simulation, the compromises (in the case of figure 5.10, where shear condition is considered to be the driver for erosion) necessary for a successful process;

- Given a target feature size (response variable) and a shear rate constrained by customer geometry (as seen in simulation), that the quantity of processing (time) can be adjusted accordingly.
- Given a target processing time (quantity) and a feature geometry (response variable) constrained by customer requirements, the tooling (shear condition) can be adjusted accordingly.
- Given a restricted choice of media (enforced shear condition) and quantity fixed by production time demands, the resultant geometry (response variable) can be predicted. This scenario is unlikely – processing, knowing that final geometry will be undesirable would not be performed.

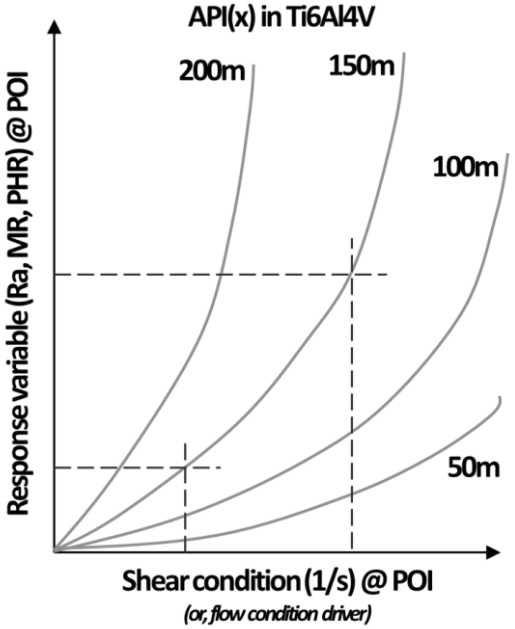

Figure 5.10 – Demonstrative example of correlation output.

However, at this point, it is unknown which field variable is considered to correlate best with the simulation output, something critical to achieving a functioning system. The temperature and shear condition field variables as shown in figures 5.9 and 5.10 may simply not be useful quantities with which to assess erosion through simulation.

Ensuring an effective analysis activity in 5.3, requires the establishment of some basic truths with which results can be interpreted in a clear and logical fashion;

- **Media configuration does not change** – MP, GF and GS are the same at any point in the job – only viscosity (MP) is altered by the environment, and the potential of the media to cause erosion is driven by the flow condition achieved.
- **Simulation is never material specific** – results for flow condition will always be bound by geometry, but never material – unless sources of heat (passive and active) are included in the simulation, the media rheology will not be influenced by workpiece material chemistry.
- **Simulation can display multiple physical phenomena** – this project is not interested in *all* outputs, but does seek to find which outputs tie close enough to be used as erosion-drivers, which is then used to predict the physical change.
- **Workpiece erosion in complex geometry occurs in the same modes as simple geometry** – assuming reasonable correlation between the simulated and physical systems is viable, erosion behaviour in one flow condition in simple geometry should be replicable in the same flow condition in another geometry – irrespective of feature size and shape.
- **Three components are necessary to create a viable production system** – 1) a VTQ dataset for the chosen workpiece material and media (workpiece material

in testpiece geometry), 2) a simulation of the chosen media in the testpiece geometry and 3) a simulation of the complex part intended for production.

- **Re-assessing erosion in new materials cannot be achieved theoretically** - without knowing the erosion in a controlled environment, the variation in material properties between supplier, measurement equipment and ambient conditions demands a new VTQ study for a given media.
- **Simulation is great for parametric studies** – where the desire is held to align a virtual model against a physical system, the opportunity within simulation to create a physical representation and vary the same parameters as in the real system is a tool that can enhance learning.

5.3 Merge of Computational Fluid Dynamics (CFD) with Physical Results.

This section details modelling, meshing, simulation and how results are extracted from the testpiece data sets – it also identifies the erosion-drivers (field variables), and how their value is combined with processing quantity to achieve a specific level of erosion in the testpiece environment. To summarise, output is applied to a demonstrative testpiece and results compared to those generated by the prediction process.

In order to generate a range of values for the output field variables and simultaneously know their resultant physical output was true and free from bias or error, the experimental conditions from the machine parameter study are used – except now, the physical effects noted will not be those of measured surface roughness or material removal, but those of the field variable, so that the field variable may be correlated with erosion, for a given quantity of processing.

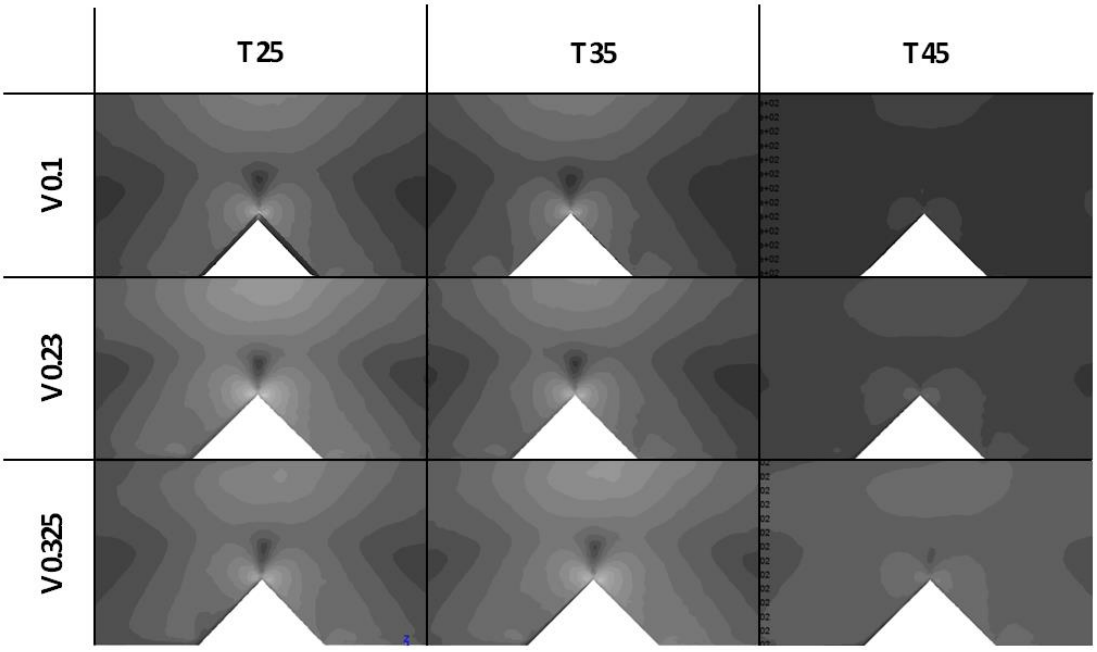

Figure 5.11 – Experimental combination simulated and resultant graphical output.

Figure 5.11 presents the graphical output of Ansys Fluent 14.5 in the form of close-ups of the testpiece section, set to display the viscosity of the media used in the experiments. As the analysis will show further on in this section, viscosity plays a highly significant role in material erosion, and helps answer the two most pertinent questions – how much erosion will occur?, and, where will the erosion occur?. The structure presented excludes quantity, and instead organises the data into a 3^2 velocity vs. temperature arrangement – this allows the engineer to obtain actual numerical values for the flow condition, collected in terms of shear rate, viscosity, velocity, pressure etc.

5.3.1 Results of simulated machine parameter study.

Numerical values sourced from simulation for the nine unique combinations of VT are provided below in table 5.2. Using the post-processing facility provided in Ansys Fluent 14.5, the results from the nine simulations are collected from three points on the mesh – C2, C3 and C4, where C2 is the leading face, C3 is the peak from which rounding is measured and C4 is the trailing face. Both C2 and C4 offer possibilities for correlation of surface roughness, while MR and PHR can only be correlated from C3.

Table 5.2 – Data obtained through simulation of testpiece points C2, C3 & C4.

			T=25˚c	T=35˚c	T=45˚c
V=0.100m/s	C2	Temp (c)	26.602	36.271	46.068
		Strain (1/s)	26.750	27.389	29.639
		Mol. visc. (Pa.s)	1817.097	782.011	167.671
		Static pres. (bar)	2.636	1.163	0.320
	C3	Temp (c)	28.825	37.214	46.234
		Strain (1/s)	130.116	129.976	169.807
		Mol. visc. (Pa.s)	5284.100	2255.993	271.991
		Static pres. (bar)	1.491	0.583	0.029
	C4	Temp (c)	28.728	37.182	46.248
		Strain (1/s)	28.848	28.770	31.441
		Mol. visc. (Pa.s)	1660.931	745.512	157.147
		Static pres. (bar)	1.080	0.502	0.174
		Total average pres. (bar)	5.857	5.857	2.610
V=0.230m/s	C2	Temp (c)	29.027	37.258	46.227
		Strain (1/s)	67.032	64.006	69.281
		Mol. visc. (Pa.s)	2994.727	1267.882	190.590
		Static pres. (bar)	9.820	4.273	0.815
	C3	Temp (c)	38.600	41.405	46.676
		Strain (1/s)	402.933	337.583	527.112
		Mol. visc. (Pa.s)	5436.702	2977.829	170.116
		Static pres. (bar)	4.334	2.087	0.084
	C4	Temp (c)	39.487	41.809	46.841
		Strain (1/s)	109.657	85.516	115.862
		Mol. visc. (Pa.s)	1572.614	887.104	105.873
		Static pres. (bar)	3.833	1.754	0.425
		Total average pres. (bar)	22.110	9.601	1.962
V=0.325m/s	C2	Temp (c)	32.179	38.559	46.396
		Strain (1/s)	106.822	97.481	110.453
		Mol. visc. (Pa.s)	3378.004	1541.252	192.645
		Static pres. (bar)	16.396	7.403	1.200
	C3	Temp (c)	46.947	46.027	47.328
		Strain (1/s)	1024.720	738.018	678.882
		Mol. visc. (Pa.s)	3641.164	1778.426	486.853
		Static pres. (bar)	3.431	2.796	0.228
	C4	Temp (c)	47.067	47.264	47.355
		Strain (1/s)	332.912	158.582	396.450
		Mol. visc. (Pa.s)	662.465	203.871	294.954
		Static pres. (bar)	6.036	2.912	0.613
		Total average pres. (bar)	37.625	16.732	2.918

5.3.2 Offline integration of field variable and quantity of processing.

Using the data from table 5.2, it must be identified which field variable(s) is responsible for driving erosion – a high goodness of fit R^2 value determines the success of a correlation activity. Using the data presented in table 5.2, the first stage to convert data is to organise it in such a way as to be useful in a spreadsheet program, presented as such in table 5.3. The table is comprised of four groups of columns; on the left (**1**), the experimental condition is given, left of centre – the simulated result (**2**) for a chosen field variable is given for the POI under study, right of centre – the quantity of processing (**3**) and right, the actual measured response (**4**) at the same position. Results are then sorted by response magnitude as displayed in table 5.4, allowing the field variable and processing quantity to be driven by response magnitude.

Table 5.3 – Example of temperature data at C2 organised for pre-correlation.

1					**2**	**3**	**4**
Experimental condition					Simulation		Actual response
Velocity			Temp.		C2 field variable	Q	
Machine values		Part					Ra
m/s	mm/min	m/s	K	˚c	˚c	m	µm
0.001417	85	0.100	298	25	25.6	40	0.364
0.003250	195	0.230	298	25	28		0.539
0.004667	280	0.325	298	25	31.2		0.515
0.001417	85	0.100	308	35	35.3		0.284
0.003250	195	0.230	308	35	36.3		0.432
0.004667	280	0.325	308	35	37.6		0.667
0.001417	85	0.100	318	45	45.1		0.270
0.003250	195	0.230	318	45	45.2		0.287
0.004667	280	0.325	318	45	45.4		0.438
Experimental conditions as above						145	0.732
							0.959
							0.554
							0.437
							0.574
							0.825
							0.242
							0.268
							0.682
Experimental conditions as above						250	1.062
							0.764
							0.665
							0.447
							1.106
							1.252
							0.305
							0.277
							0.404

Table 5.4 – Correlation of C2 temperature data with actual responses.

Temp. ˚c	Qty. m	Response µm, Ra		Temperature.metre	Response µm, Ra
45.1	145	0.242		6539.5	0.242
45.2	145	0.268		6554	0.268
45.1	40	0.270		1804	0.270
45.2	250	0.277		11300	0.277
35.3	40	0.284		1412	0.284
45.2	40	0.287		1808	0.287
45.1	250	0.305		11275	0.305
25.6	40	0.364		1024	0.364
45.4	250	0.404		11350	0.404
36.3	40	0.432		1452	0.432
35.3	145	0.437		5118.5	0.437
45.4	40	0.438		1816	0.438
35.3	250	0.447	➔	8825	0.447
31.20	40	0.515		1248	0.515
28	40	0.539		1120	0.539
31.2	145	0.554		4524	0.554
36.3	145	0.574		5263.5	0.574
31.2	250	0.665		7800	0.665
37.6	40	0.667		1504	0.667
45.4	145	0.682		6583	0.682
25.6	145	0.732		3712	0.732
28	250	0.764		7000	0.764
37.6	145	0.825		5452	0.825
28	145	0.959		4060	0.959
25.6	250	1.062		6400	1.062
36.3	250	1.106		9075	1.106
37.6	250	1.252		9400	1.252

Correlation between physical and simulated measurements from C2 and C4 should only be attempted with surface roughness data, and conversely, MR and PHR should only be correlated with C3 data. Table 5.4 considers the data required for correlation of the temperature field variable with actual *and* simulated (because they are the same) point of C2; data for simulated output of temperature is sourced from the truncated 3^2 study as above in Figure 5.11. In effect, the responses of surface finish are tied to a functional unit of the 'temperature.metre', so that an XY plot can be produced for the assessment of fit against the surface finish as measured. Figure 5.12 presents the result of correlation – the graph can be utilised by identifying the desired level of workpiece surface finish (y-axis) and reading across to the line-of-best-fit to read an x-axis value; in this instance, take a surface finish value of 0.6µm Ra, and using the third order polynomial fit (suggested to explain just over 25% of surface finish value) the y-axis reads a value of 4,800˚c/m. If the fit were considered good enough (which it clearly

isn't), then it could be said that any one of processing at; 1) 4,800˚c for 1m, 2) 25˚c for 192m, 3) 35˚c for 137m, or 4) 45˚c for 107m would achieve the 0.6µm Ra target. Unfortunately, the goodness-of-fit does not adequately account for the effect of temperature change in the system as a whole, and with a linear model with R^2=3.8%, this data should be discarded for surface finishing applications.

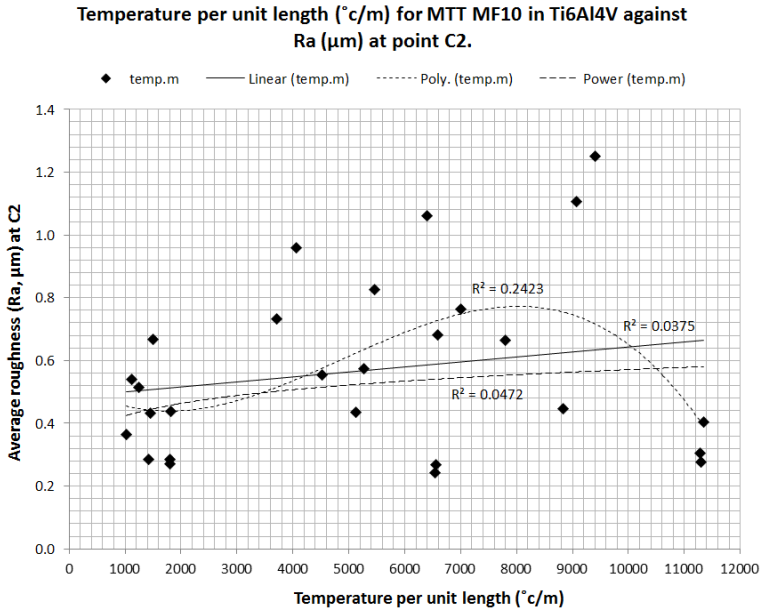

Figure 5.12 – Temperature per unit length (˚c/m) against Ra (µm) at point C2.

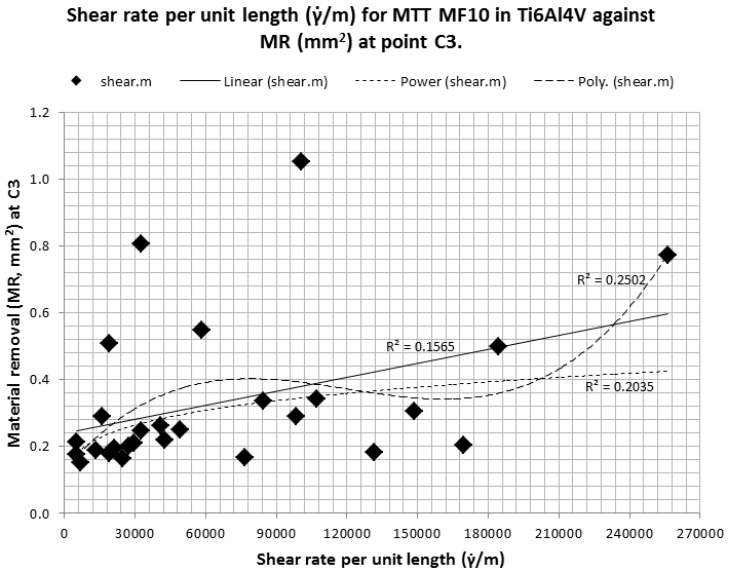

Figure 5.13 – Shear rate per unit length (γ̇/m) against MR (mm^2) at point C3.

What does this mean for further correlation work? Firstly, it is *not* the case that temperature *should* show reasonable correlation – in fact, additional research (presented in section 5.6) shows the disconnect between machine-set temperature and processing

temperature at the POI due to higher levels of viscous heating. Secondly, the mechanics of surface finishing are not temperature-sensitive – as a mechanical process and not a chemical one, the temperature is linked to the velocity distribution and viscosity, so correlation with those factors may yield better results. Examples of the same discord between some simulated outputs and actual responses can be seen in both MR and PHR datasets, as shown in figures 5.13 and 5.14 respectively – MR at point C3 is plotted against shear rate per unit length, while PHR also at point C3 is plotted against temperature per unit length. Figure 5.13 manages only an R^2=25% value for shear rate explanation of response value – if deemed to be adequately modelled, the POI could be exposed to shear rate of 2,100s^{-1} for 100m in order to achieve 0.45mm^2 of volumetric material removal. Likewise with figure 5.14, the points are too scattered to be useful. It should be re-noted at this point that increased temperature is known to reduce MR and PHR – the scatter makes the data for temperature inapplicable, but the general trend is positive. The line/curve equation would need to be inverted if data were robust.

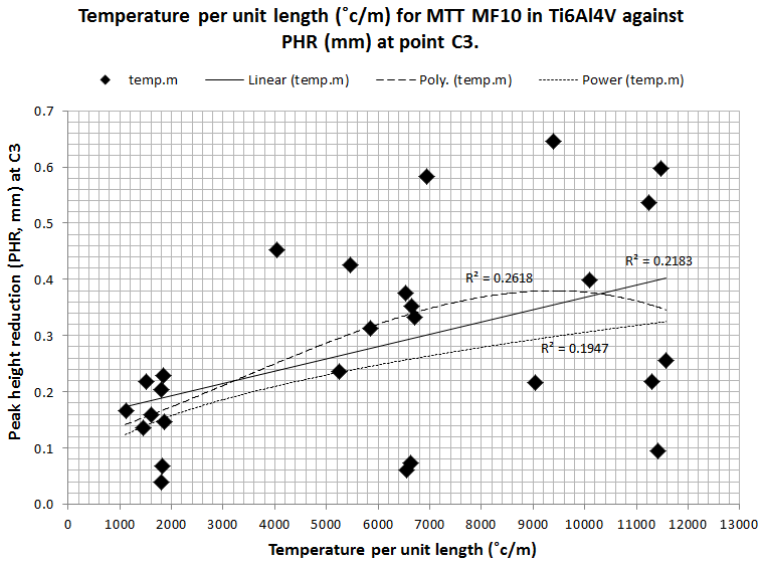

Figure 5.14 – Temperature per unit length (˚c/m) against PHR (mm) at point C3.

The previous three examples (Figure 5.12 thru 5.14) are of poor correlation – in order to adopt a single metric as a strong indicator of deterministic process performance, the R^2 value should be above 85% - not the ~25% seen above.

5.3.3 Successful correlations of derived unit with actual responses.

Through performing the exercise in section 5.3.2 through each response (surface finish (Ra) at points C2 and C4, and stock removal (MR, PHR) at point C3) for each of the variables in turn, this research work has found that media viscosity is dominant in goodness-of-fit tests with significant R^2 – while high R^2 is not automatically more

desirable than low R^2, the application in this process is looking for the strongest, most explanatory linear model, therefore a high R^2 is appropriate. Figures 5.15, 5.16 and 5.17 are the strongest correlations found between simulated and empirical data.

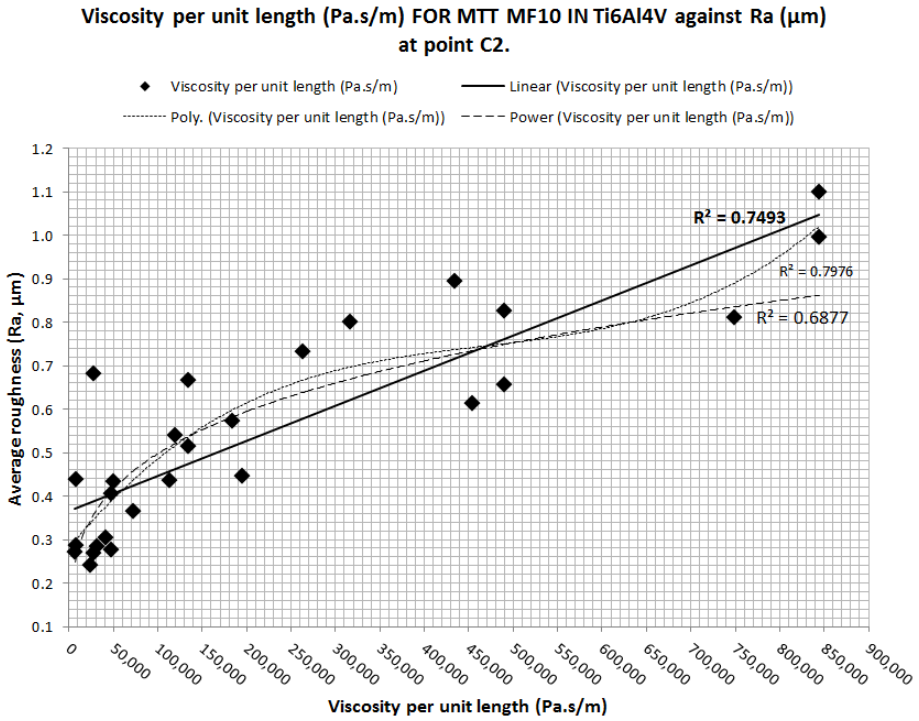

Figure 5.15 – Viscosity per unit length (Pa.s/m) against Ra (µm) at point C2.

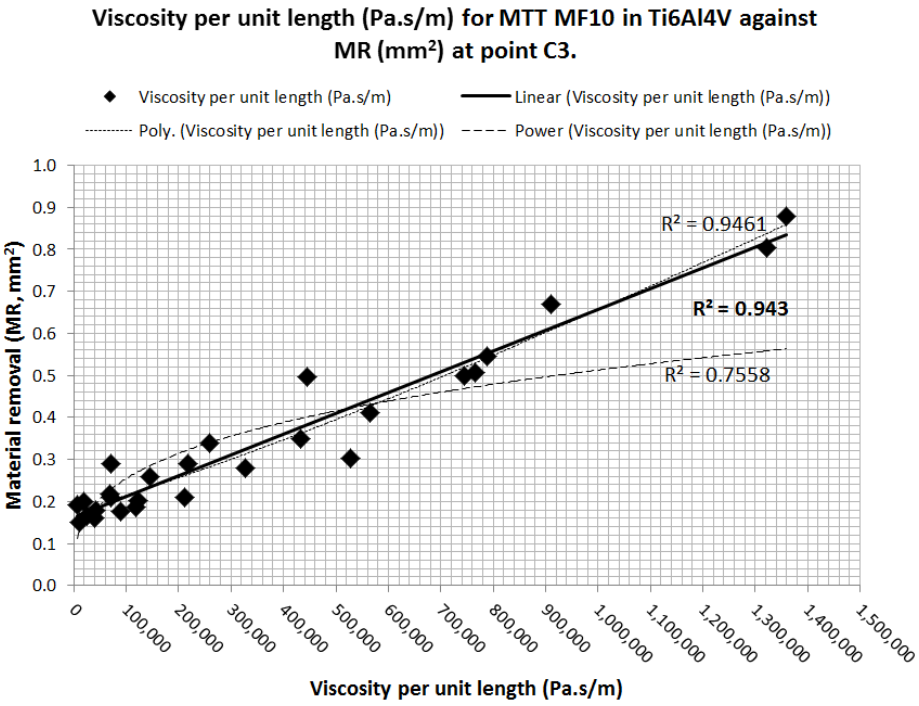

Figure 5.16 – Viscosity per unit length (Pa.s/m) against MR (mm^2) at point C3.

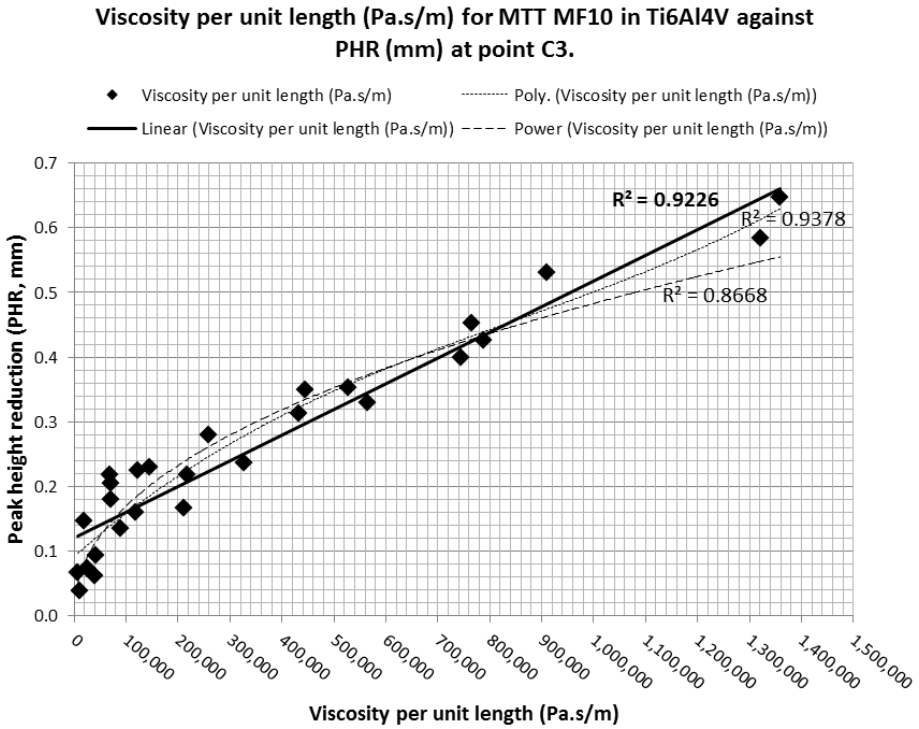

Figure 5.17 – Viscosity per unit length (Pa.s/m) against PHR (mm) at point C3.

Successful correlation of empirical and simulated data is shown to be possible. Figure 5.16 and 5.17 concern the stock removal objectives of MR and PHR – the linear model correlation of 94% and 92% respectively shows good agreement, of practical significance. As data is carried from experimental physical stages, scarcity of modelling points at the upper end of the range is a route for strengthening the model, but the same weighting of points within the process space is seen in previous work – regardless, the principle of simulated viscosity explaining over 90% of MR and PHR is proven.

Figure 5.15 surface roughness results point to a slightly less reliable dataset, one which may be affected by several issues as noted below;

- Only one value of surface roughness is integrated, either C2 or C4 – as with each stroke of the machine, both C2 and C4 swap between being the leading and trailing edge, with the consequent pressure and viscosity reduction during the trailing stroke.
- While the C2 correlation explains ~75% of finishing effect, it is difficult to say how much more would be characterised by incorporating the effect of the trailing edge eddy flow.
- Data transformation is possible, but normality of error distribution in simulated data is unknown and data is already spread through the process window. If it were to be performed, a log10 transformation to both datasets may be suitable.

The correlation exercise must now be converted to another form for reapplication.

5.4 Appraisal of CFD approach and response optimisation.

To finalise the findings within 5.3, suggested viscosity ranges are sourced from the experimental data (up to 8000Pa.s) and calculated to show relationship with a response variable for a set of processing quantities. Using the linear models showing good agreement in figures 5.15, 5.16 and 5.17, the plots in this section are the penultimate conversion into a production-useful form.

5.4.1 Conversion of CFD-derived models into functional graphs.

Figure 5.18 converts data plotted in figure 5.15. Dividing the Pa.s/m value by an appropriate (within an order of magnitude of the experimental processing levels) value for quantity, an engineer may identify a viscosity of 3000Pa.s at a POI and know that 100m of processing will likely raise the roughness to 0.6µm Ra. This of course assumes that media remains the same and material is Ti6Al4V, but as previously stated, this work now applies to any use of the MTT MF10 configuration and this grade of Ti-alloy.

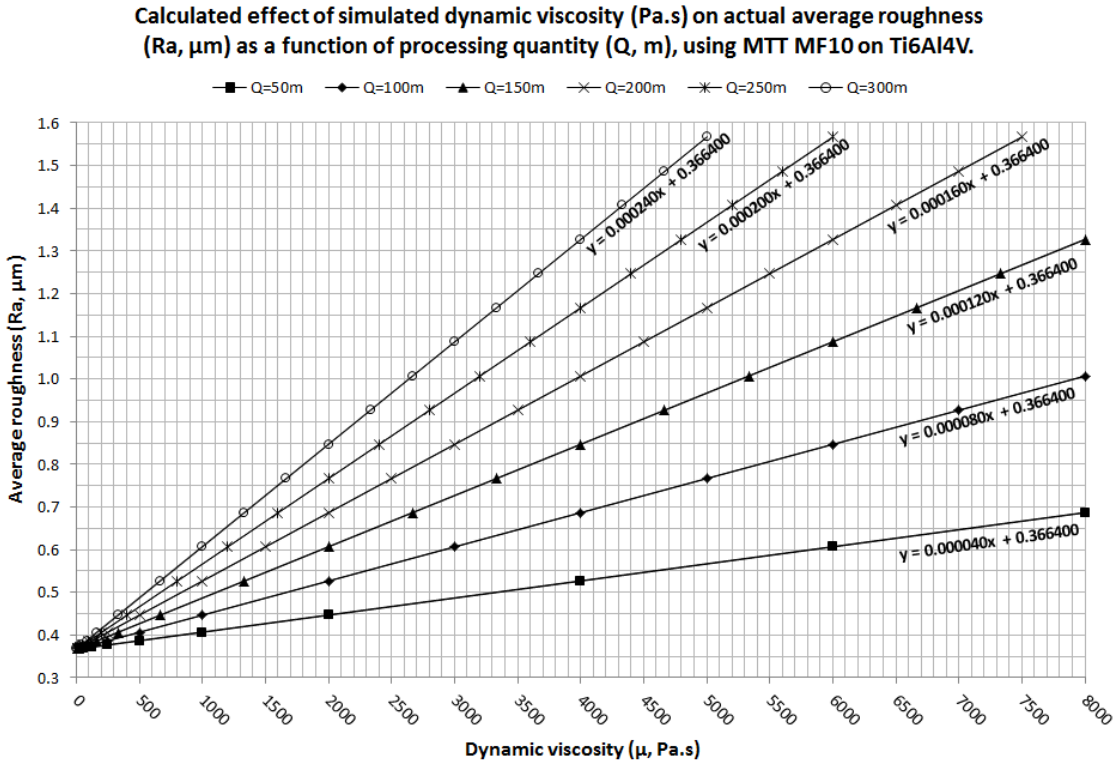

Figure 5.18 – Calculated effect of simulated dynamic viscosity on average roughness.

A typical range of acceptable industrial surface finishes are 0.3-0.8µm Ra, but more application-specific values would be provided in a commercial situation. Surface finishing is the least reliable of the three responses, so far as model correlation is considered, however the edge-rounding metrics are far more robust. Figure 5.19

considers the back-calculation of figure 5.16 – using the same methodology as per previous, while figure 5.20 considers back-calculation using values from figure 5.17.

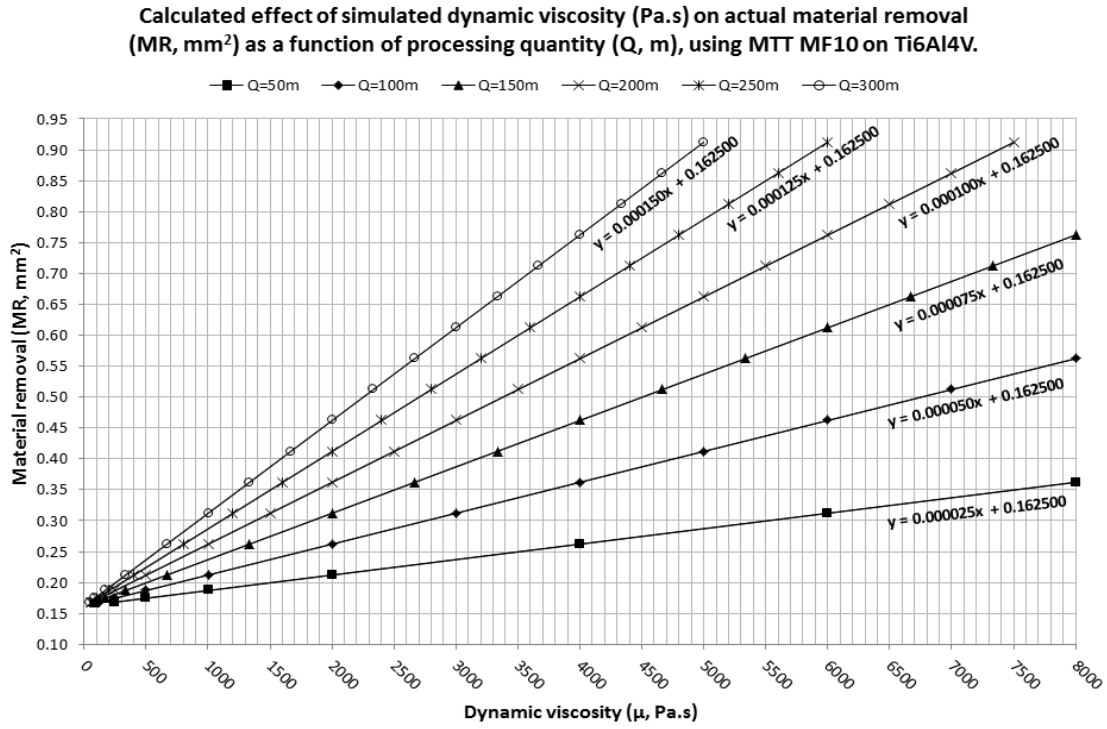

Figure 5.19 – Calculated effect of simulated dynamic viscosity on material removal.

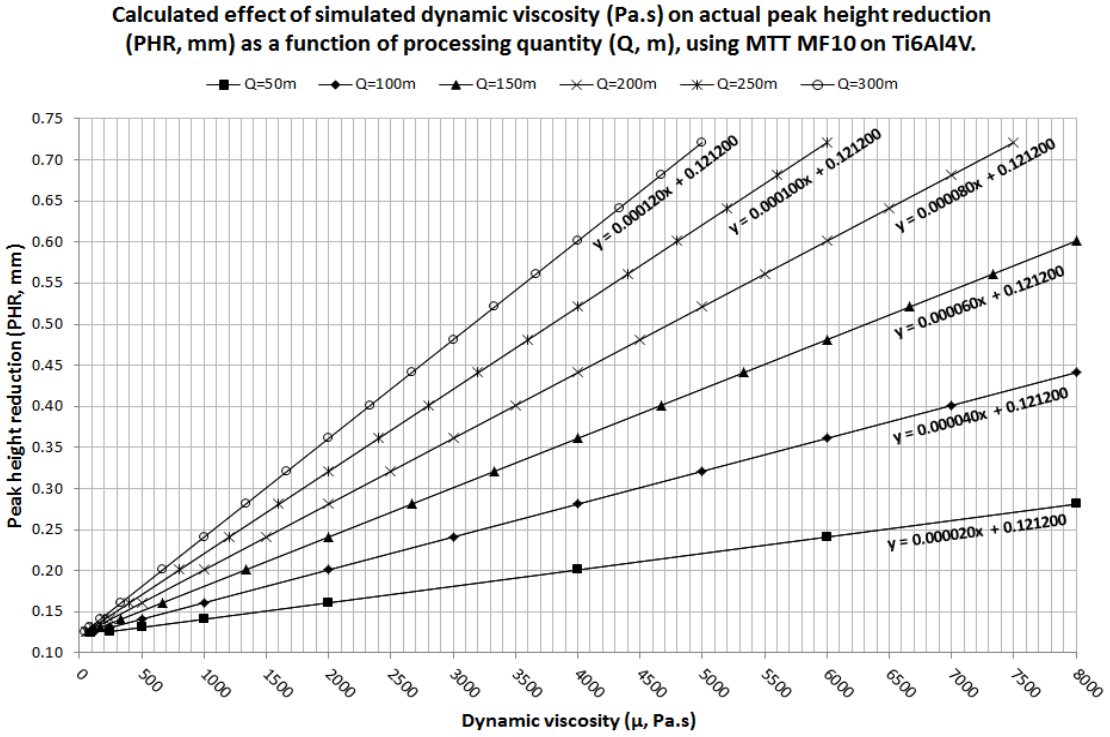

Figure 5.20 – Calculated effect of simulated dynamic viscosity on peak height reduction.

In order to interpret the results of MR and PHR, convert them into radius; the concept presented in figure 5.21 should be used. Table 5.5 provides an instant conversion.

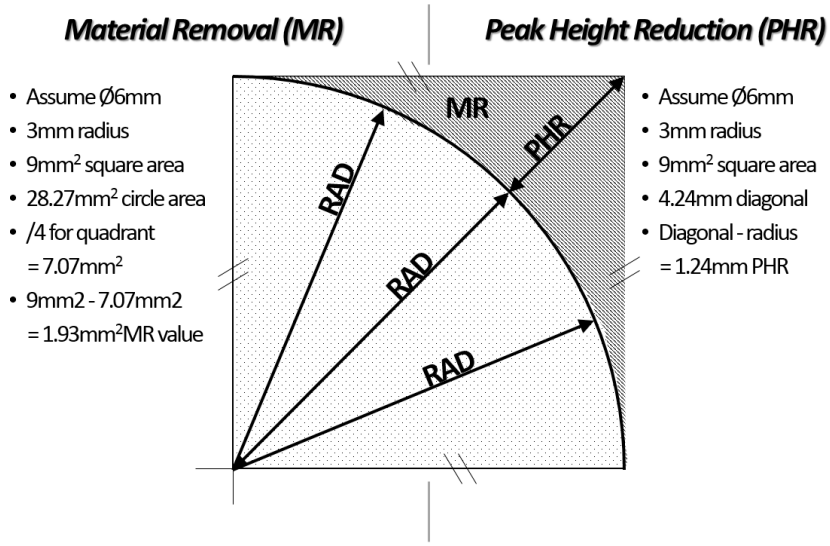

Figure 5.21 – Concept of converting MR and PHR into radius.

Values presented in previous viscosity correlation plots suggest that model data fits between radius values of 0.3-2.5mm – a highly-suitable range in practical environments.

Table 5.5 – Radius to MR and PHR.

Radius (R, mm)	Material removal (MR, mm^2)	Peak height reduction (PHR, mm)
0.1	0.002	0.041
0.2	0.009	0.083
0.3	0.019	0.124
0.4	0.034	0.166
0.5	0.054	0.207
0.6	0.077	0.249
0.7	0.105	0.290
0.8	0.137	0.331
0.9	0.174	0.373
1.0	0.215	0.414
1.5	0.483	0.621
2.0	0.858	0.828
2.5	1.341	1.036
3.0	1.931	1.243
3.5	2.629	1.450
4.0	3.434	1.657
4.5	4.346	1.864
5.0	5.365	2.071

5.4.2 Remarks on correlation activities.

In this chapter so far, several simulated field variables (temperature, strain rate, viscosity and pressure) have undergone a correlation exercise with AFM response variables (Ra, MR and PHR) in a bid to determine whether one of more fits strongly. While viscosity appears to be that factor, is there a reasoning that can be applied as to why others do not fit? Factors excluded from the analysis include velocity, as CFD assumes the boundary wall condition is 0m/s – but what of the other factors?;

- Simulated results depart from the machine GUI-set results when flow and physical phenomena combine to alter the conditions at the POI. When considering temperature, the 25˚c, 35˚c and 45˚c levels drove surface condition response in the physical experiments, but in certain circumstances (i.e. high velocity) the simulated temperature shows that all three levels for temperature rise to 47˚c. Temperature therefore will not correlate well with physical response variables, but also for the reason that temperature is a single factor and is largely influenced by other factor behaviour.
- Strain rate is a quantity that aligns with velocity only, assuming a constant volume of material is undergoing a strain force. Data presented in table 5.2 presented strain rate against three temperature and three velocity factors, where the difference between strain rate values and velocity values is significant, and the difference between those strain rate values and temperature values are insignificant. Strain rate, without sensitivity to temperature, cannot correlate effectively.
- Static pressure offers the closest match to viscosity's correlation – it can be inferred that the more appropriate variable to correlate with response variables would be the one which is most physically detached from other parameters. Pressure should drive viscosity, as the force on the material determines its viscosity, so why does pressure fall short as a determining factor? As previously discussed, the media in the process is both shear-thinning and shear-thickening, causing a low-mechanical-effort end of the process to deliver a more viscous substance than mid- and high-mechanical-effort – this would be captured by the viscosity term, but pressure would simply increase at a time when the pressure increase drove a grit-support reduction, before continuing on to increase support. Pressure would therefore be more useful if the media were linear in shear-driven behaviour.

Surface roughness is cited as the removal of peaks, and thus the researcher can expect to see a declining MRR as peak availability reduces during the surface finishing process, whereas the material removal process attempts to effectively extend an arc length of zero, to a 'tangent to tangent' length based on radius size produced, therefore increasing available surface area as it progresses. For edge-rounding responses, this length is

highly-insignificant in relation to the volume of media travelling over the surface; in surface finishing, the pre-process condition can be as high as 1.6µm Ra, but finished condition may be 0.4µm to 0.2µm – as much as 4-8x reduction in availability of peaks at process completion.

Further work may succeed by correlation of the vector quantity, 'viscosity per unit impingement angle', for surface finish, as the current work is logically difficult to determine the extents of the effect of the result from the trailing face and combine with the leading face. Upon reflection, and in the closing stages of testpiece-geometry work, surface roughness results may have suffered several causes of minor distortion and error inclusion;

- Average roughness results are all obtained from areal measurements of a 1mm x 1mm sample. Strictly, it may have been more appropriate to attempt correlation of Sa values, and use of PV (peak-to-valley), or potentially Sz or Sq. The Ra value was always taken from the centre of the square area, and may have not been a representative profile created by the process. The Ra approach is still justified however, as the production environment would be measuring with a stylus-type contact profilometer.
- Error has been stacked – each computational stage has added its own uncertainty, but the method devised does not account for an uncertainty budget, preferring nominal values sourced from acceptable error rates at each stage.
- It may be prudent, in a commercial environment to offer a form of sensitivity analysis. This would present (graphically) to a decision-maker the values of the models derived and their performance relative to the actual results.

5.5 Case study, ‘transformer shaft’.

As industrially-funded research, componentry available at Mollart Engineering is heavily oil and gas industry oriented. The component used in this study is an ideal first transfer of empirically-derived knowledge into production components. Referred to internally as a ‘transformer shaft’, the component measures approximately Ø50mm x 250mm and is manufactured with a combination of drilling, turning and milling operations, producing sharp edges in a number of locations.

5.5.1 Functional requirement and implementation of AFM.

AFM is required to apply a tangential radius on the inner edge of three slots, positioned symmetrically about the part centreline. Figure 5.22 presents a solid model in section view. The customer’s specification calls for 40-90µinch radii (1-2.25mm) – a very wide envelope within which to select a value for edge-rounding. No surface finish is specified, but remaining within the initial machined-condition of 0.8µm is preferable.

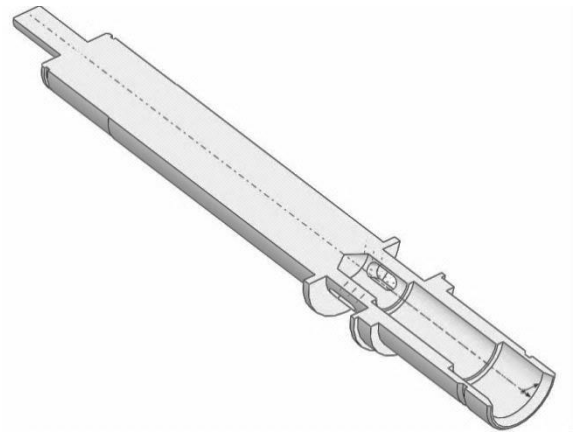

Figure 5.22 – Solid model in halved section view of ‘transformer shaft’.

5.5.2 Expectations and mitigating actions.

Using a single setup, the process model is expected to be derived without processing testpieces, using MTT’s MF10 media and in the same material as experimental work, Ti6Al4V. Fixturing to allow entry through the centre bore, the tooling ‘B’ and ‘E’ as noted at figure 5.23 is installed to prevent erosion at the locations. Media enters through a funnel form on component ‘A’, allowing media to pass through the three slots and in between aluminium tube ‘D’ and nylon sleeve ‘E’ used to contain media upon exiting. The entire system is supported at each end by two adapter plates (‘F’ and ‘G’) that direct the media upon the completion of a stroke.

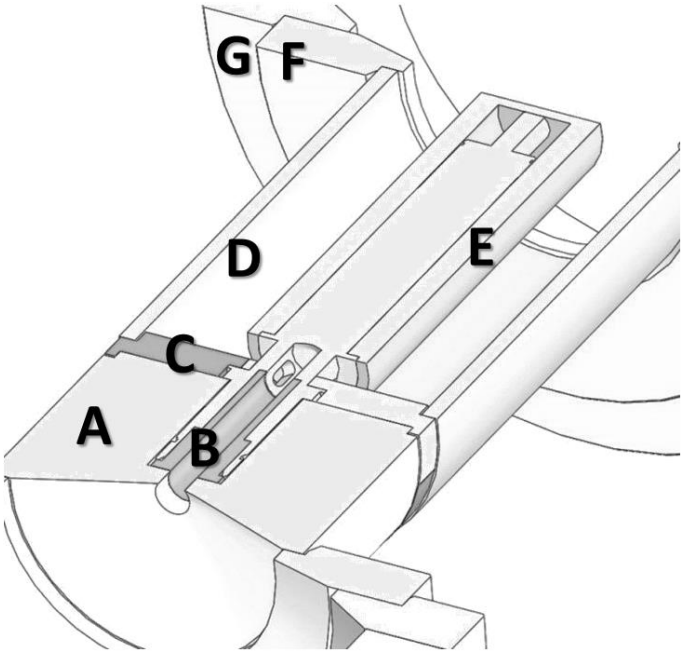

Figure 5.23 – Fully-assembled ‘transformer shaft’ and tooling in section.

5.5.3 CFD-aided process setup for transformer shaft.

Using Ansys 14.5, the model is meshed using Ansys ‘mesh’, in a half-model, i.e a single plane of symmetry is recognised throughout the model as a whole as pictured at ‘A’ in figure 5.24. ‘B’ highlights the necessity to partially model an element of the Ø250mm piston head to ensure correct simulation of media entry is achieved. At ‘C’, the mesh undergoes a localised growth rate to increase cell count, and thus resolution, at the major POI – ‘C’ is the post-process edge to measure.

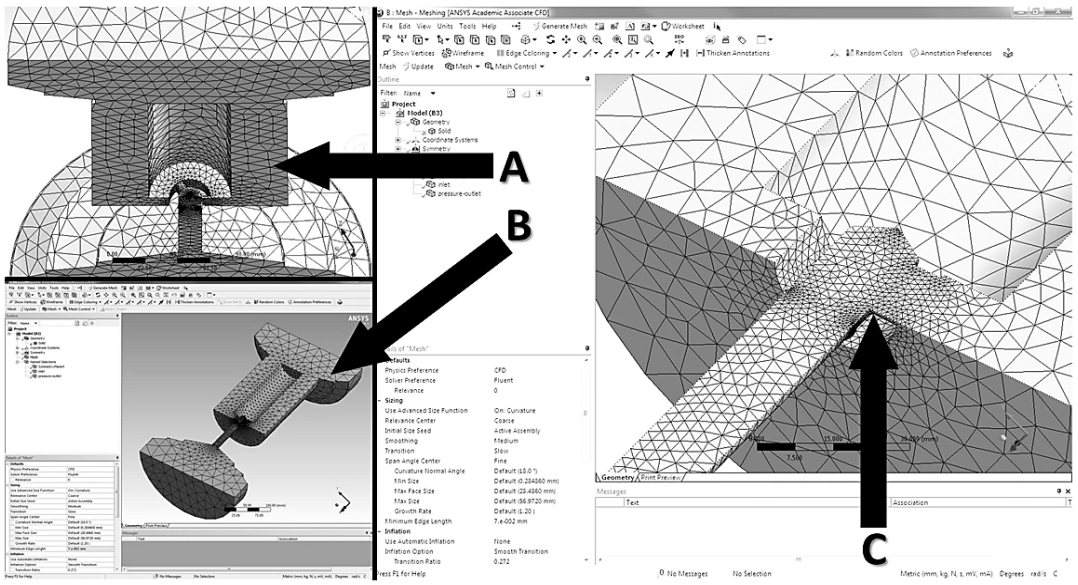

Figure 5.24 – Simulation meshing process for ‘transformer shaft’.

As per previous runs in testpiece geometry, the UDF for MF10 is loaded, so that Fluent is able to pass fluid through the component that matches the rheological responses of previously characterised processing slurry. Figure 5.25 shows the lower edge and upper edge following a converged run in Fluent, (better captured in figure 5.26) where the media inflow at the lower edge (approaching B) is shown to be more viscous at the POI (B_1) but a differential exists between B_2 and B_3, suggesting media is approaching the POI too fast and will cause a non-tangential radius. Conversely, in circle A, viscosity is lower (A_1) and a dead-spot occurs on the internal-face of A_2. Values for this simulation are provided in the next section.

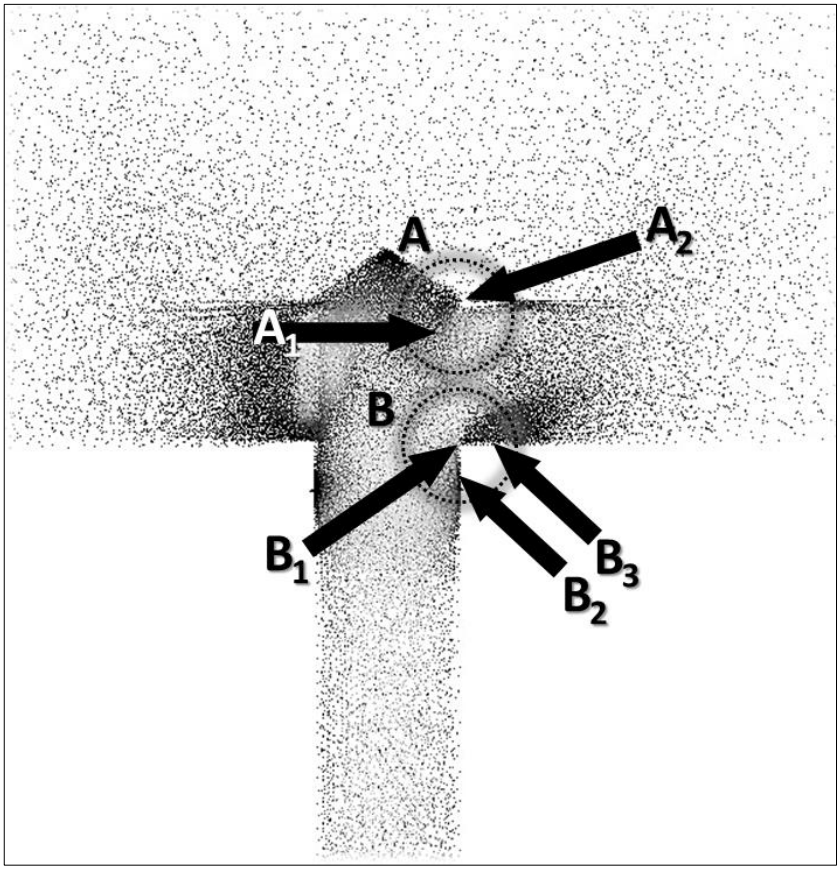

Figure 5.25 – Simulation output.

5.5.4 Results and assessment.

Based on results from the simulation, table 5.6 utilises the plot in figure 5.16, then figure 5.19 and table 5.5 to identify that within this material and media combination, the viscosity condition achieved in the simulation as set up in section 5.5.3 should be approximately 2140Pa.s, for a total length of 350m. This is based on figure 5.26 (an extended version of figure 5.19), plotted to show up 500m of processing. Using the linear equation as plotted for 350m of processing (*y=0.000175x + 0.1625*), rearranged

for x ($x=(y-0.1625)/0.000175$), it is possible to identify a target simulation value by converting the MR value to radius. In this instance, the values are provided in table 5.6.

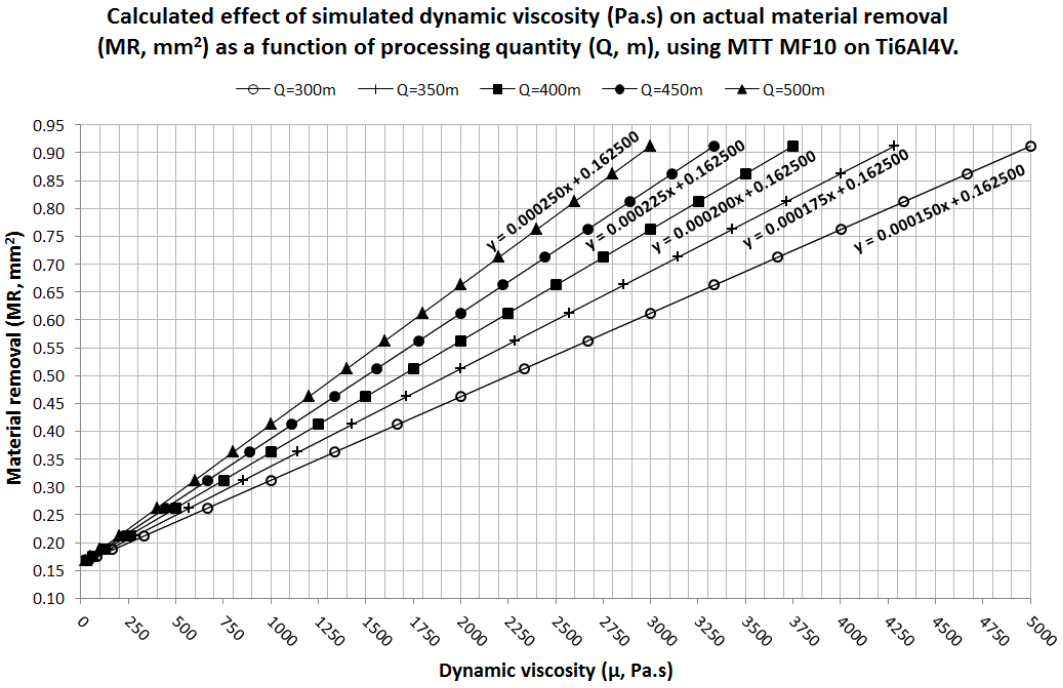

Figure 5.26 – Calculated effect of simulated dynamic viscosity on material removal, up to 500m.

Table 5.6 shows six columns – the nominal customer-specified radius value is 1.625mm, which means the tools developed are used to deliver 0.567mm^2 areal material removal. Solving for x, the process therefore demands a viscosity of 2311Pa.s for 350m. In this instance, several undocumented manipulations of the simulation were performed to reach the value, noting a manipulation in velocity and increase in temperature. The final value achieved, with a desirable flow-field shape is 2143Pa.s. Due to the wide range of responses, developing a process model to fit between the LTL (lower tolerance limit) and UTL (upper tolerance limit) is not challenging – however, the final results show how well the system can conform to a nominal target.

Table 5.6 – Viscosity to meet target customer radius.

POI	A	B	C	D	E
	Target radius	Inferred MR value	Target simulated viscosity	Simulated value	In-limit?
	mm	*mm²*	*Pa.s*	*Pa.s*	
A	1mm (LTL)	0.215mm^2	300Pa.s	-	Y
	1.625mm (nominal)	0.567mm^2	2311Pa.s	2143Pa.s	
	2.25 (UTL)	1.086mm^2	5277Pa.s	-	
B	As above				

5.5.4.1 Images and final operating procedure.

Figure 5.27 illustrates the final results, captured with an Olympus digital endoscope with Ø4mm lens, using a CCD sensor and optical fibre. No scale is provided as distortion negates useful measurement capability, but when positioned appropriately, perspective distortion is minimised and uniformity of rounding can be judged.

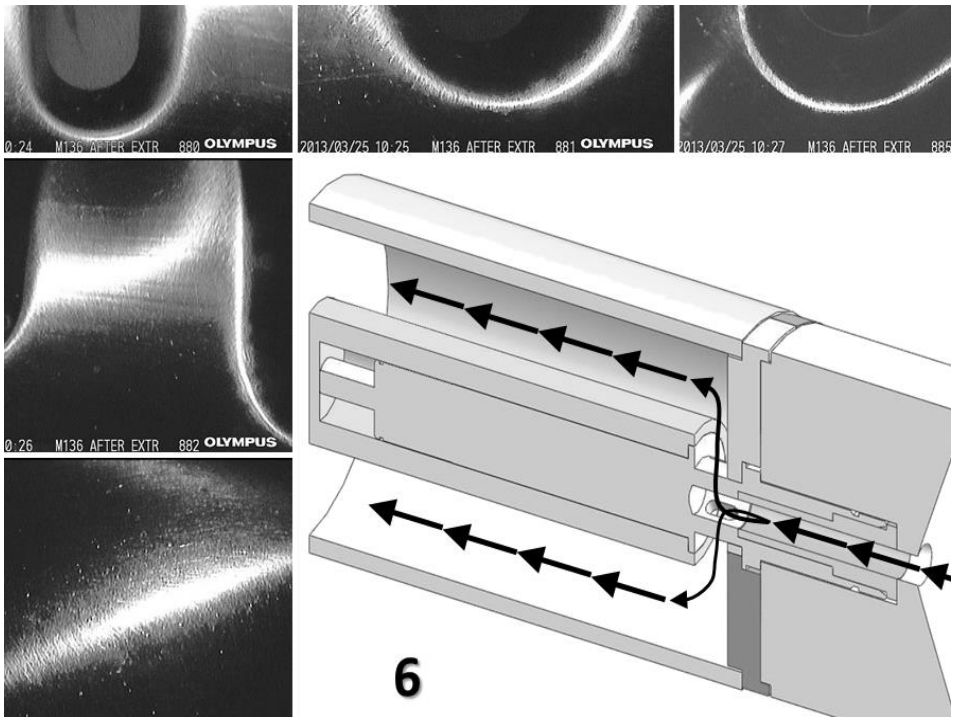

Figure 5.27 – 'Transformer shaft' final processing images.

From 1-6; 1) edge-rounding at the slot sides is shown to be highly-comparable to slot edges, 2) (inverted) top of slot receives less processing (more scrutiny of simulation about POI would be required), 3) a reduced returning piston speed allows some minor, non-functional rounding on outside of slots, 4) finish has become more reflective, measureable only by contact probe on metrology putty samples, 5) light falloff of camera gives false impression of uneven edge-rounding, and 6) direction of flow for primary intentions of rounding internal slot edges. Final system setup is in table 5.7.

Table 5.7 – Final setup for 'transformer shaft'.

Velocity		Temp.	Stroke	Cycles	Total Q	Dynamic viscosity	Media	Tooling design
Up	Down						MF10	
mm/min	*mm/min*	*˚c*	*mm*	*n*	*m*	*Pa.s*	700µm	
80	40	35	100	7	350	2140	Boron Carbide	As sim.
*System operates at simulated 32bar, but runs between 30-35bar during stroke.								
**Media volume minus fixture and part volume runs at 90-100mm stroke.								

5.6 Summary.

Through this technique, it is recognised that simulation is a production-viable, reproducible, repeatable tool to predict the surface roughness and edge-rounding in the testpiece geometry and in the transformer shaft production component. By utilising data obtained empirically concerning the effects of a configuration of abrasive media on Ti6Al4V, and applying it through a computational fluid dynamics simulation, it has been possible to identify that dynamic viscosity of carrier plays a significant (>92%) role in determining final condition.

A method has been devised whereby only partial testing is required to supplement existing simulation, rheological evaluation or erosion information, and creates the ability to catalogue (in a library) the behaviour of polymer-grit mixtures, extending to their historical behaviour for wear- and contamination-analysis. Empirically-derived charts from testpiece data offer the most robust output – they allow a lay-user with system familiarity and ability to run simulation in Ansys Fluent to identify the appropriate viscosity condition to achieve surface finish or edge-rounding. While the process shows general high levels of success, several elements should be worked on in the future;

- Further integration of media variables into the simulation, and where made possible by software, a greater range of process variables be studied to convert empirical data in an economically-restricted data set to explain the remaining ~6-8% of process behaviour uncharacterised by the research presented.
- Meshes that cater to two-way flow and iterative erosion to overcome eddy and other downstream, turbulent (or disrupted) flow patterns, currently uncharacterised and thought to be the cause of ~25% of unexplained surface roughness description. There may be systematic (structural or measurement) error present or other factors of significance, perhaps chemical relationships.
- In conjunction with the above point, a study of impingement angle effects with greater structure and control may help to understand and reinforce results recorded in complex geometry.

In the next chapter; 1) variation of media behaviour is considered, 2) requirements placed on the system to describe the configuration change are discussed, 3) media variables are analysed to identify whether abrasive potential can be described in a structured way, and 4) an additional case study is run to highlight a greater degree of complexity. Research from chapters four and five are combined to see where optimisation in both process speed and accuracy can be found – the limits of single configuration capability and single variable capability are also discussed.

Chapter 6 - Process Control, Optimisation and Case Studies

6.1 Introduction

Effective application of methodology developed in chapters four and five is crucial to developing a successful implementation of this research. This chapter aims to set-out 1) the strategy for application in an SME, for one-off, small batch and medium batch work, 2) elements of the framework requiring maintenance, external services and further development, 3) additional applications, 4) expectations and processing logic in components as-yet untested, 5) improvements to simulation system, 6) a description of the abrasive potential metric, 7) optimisation of process for speed and for accuracy, and 8) another case study, for complex geometry, highlighting areas where flow field effects are noted in simulation and corrected.

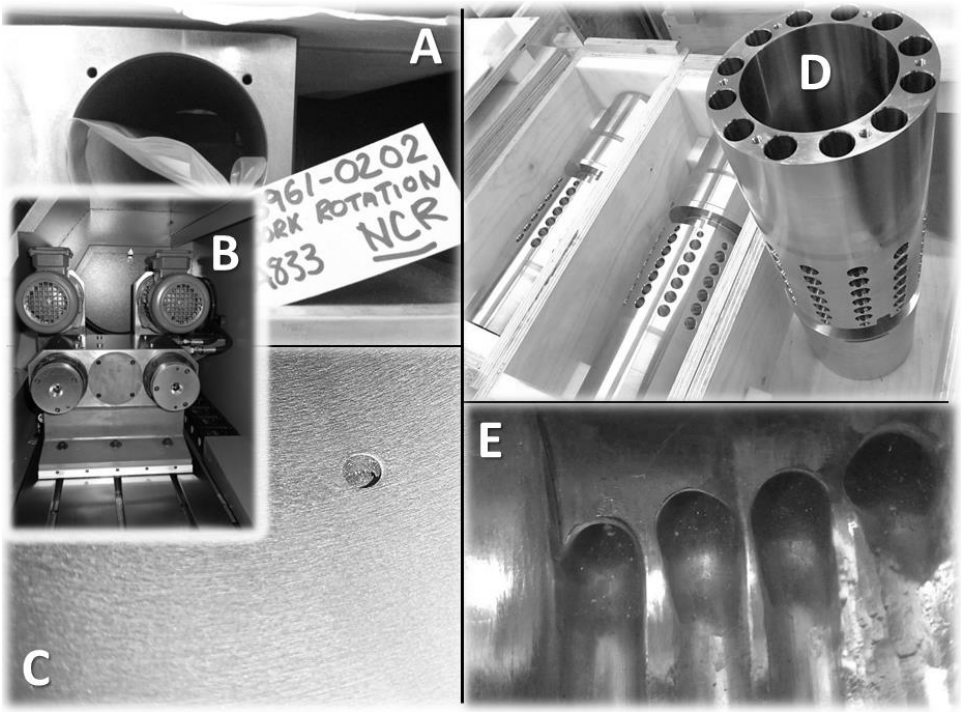

Figure 6.1 – Production challenges in a one-off and small batch work.

AFM's application is typically suited to any traditional area for loose abrasive, but as is evident in figure 6.1, internal cavities are where capability outstrips competing processes. In a machine manufacture application, images 'A' and 'B' highlight the location of surface in a machine tailstock; 'C' is the surface itself, returned to Mollart after a supplier failed to reach a predetermined surface finish. Image 'D' pictures a fracking tool where the AFM application is explained further in this chapter – economically, AFM becomes more viable with larger batch sizes, far surpassing manual processes. Image 'E' presents another difficult-to-access oil and gas component.

Converting AFM research into production-viable systems requires more than technical capability – tooling and media costs can damage the economic case, poor process repeatability may arise, unforeseen environmental variation, user-error is ever-present and where all of these don't, excessive process run-time may still occur. This chapter aims to discuss the elements of the proposed framework that, when combined, work to reduce causes of variation.

6.1.1 Production needs in an SME.

Relative to a large enterprise (LE) (>250) or a micro-enterprise (μE) (<10), the SME (50-250 employees) (where small is 11-50, medium is 51-250) bracket imposes its own set of size-specific issues on day-to-day operating conditions. In the approach to new technology *uptake*, a μE will be concerned about budget, an LE will be concerned about capability, but SMEs straddle a void where a process will likely be affordable but manpower and knowledge mean process understanding is limited, and stays that way. With respect to new technology *operation*, a μE will likely not commit unless the process is low-risk/low-complexity and some necessary skills already exist in the business, while an LE will study, train and equip to drive the success of operating a new technology. In this case, an SME will take on the technology and 'learn it' in practice, full in the knowledge of its potential. These approaches differ in terms of financial commitment and process knowledge, with three distinct approaches to dealing with the concerns of each.

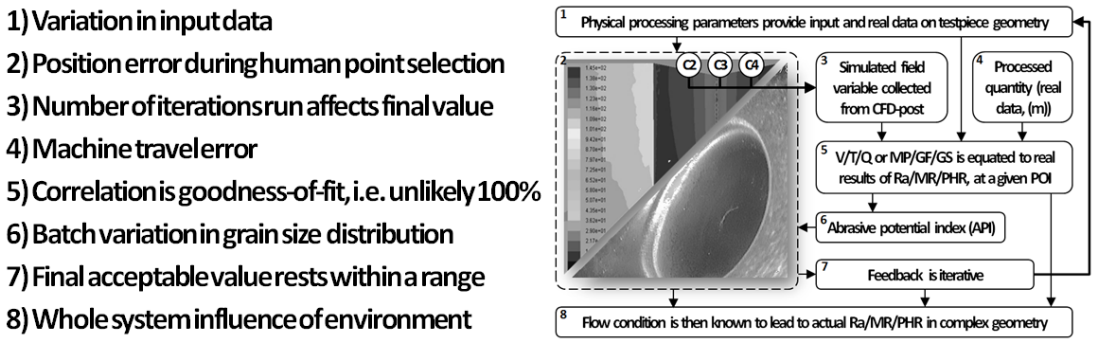

Figure 6.2 – Procedural considerations in establishing process model.

Performance in production must consider more than just studied process behaviour – figure 6.2 considers figure 5.4's actions and how results can easily be misinterpreted.

6.1.2 Framework for controlling final surface.

As detailed in previous sections, the final surface is a function of multiple variables, the levels of each determining the final cumulative effect on processing outcome.

6.1.3 Additional applications – manual internal polishing.

Consumables designed in this project's testing phase have found application in certain manual operations, typically in one-off corrections where greater tooling for automation has virtually no economic basis. The slurry, in conjunction with a tool to allow it to find crevices to fill, is effective at correcting scuffs and scratches caused in production.

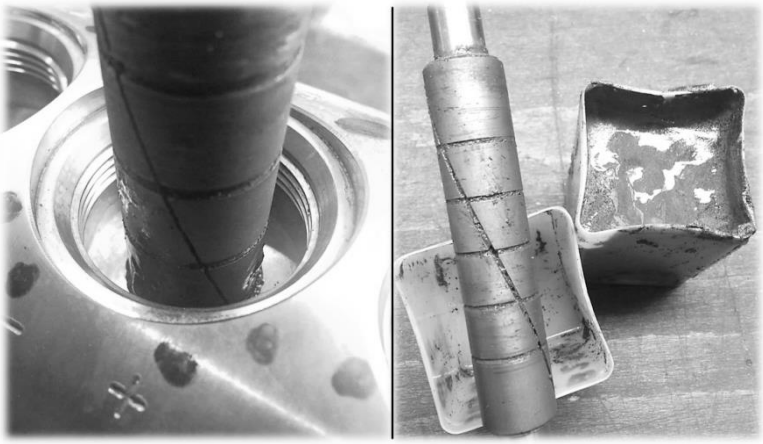

Figure 6.3 – Manual internal polishing using AFM media.

6.1.4 Additional applications – AFM trials for medical processing.

Images in figure 6.4 present a Ø10mm x 110mm sample cylinder with Ø4mm through-hole. AFM was used to process the samples to study the effects of internal (and external by other means) surface finishing on fatigue life. The results from the study were transferred by a third party to their customer, a prominent medical manufacturer.

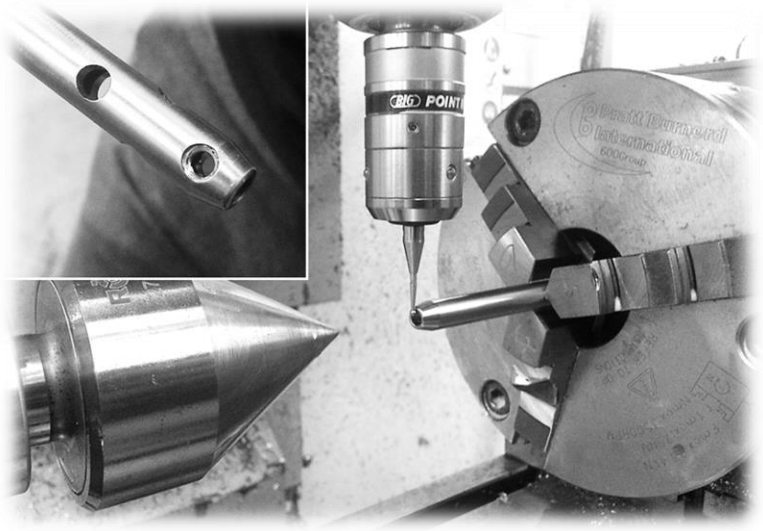

Figure 6.4 – Medical sample shaft for fatigue life testing following AFM.

6.2 Process control.

Maintaining the output of AFM to a standard is the backbone of creating a stable and repeatable process – it could be stated that a process that does not repeat, is not a process at all – rather an arbitrary output from a poorly controlled set of independent variables. In a manufacturing system, a process becomes useful when repeatability and reliability are consistent, across whichever geometries are processed.

6.2.1 Extension of process to non-tested parts.

Thus far, the methodology has been applied to testpiece geometry, within which the original data was collected, followed by a particularly suitable geometry in the same material with the same media. In order to move the setup principles to a more complex geometry, the same logic is applied, but the further away from the standard testpiece, media and material the application moves, the greater the level of data collection required, particularly in the early stages where no other data exists.

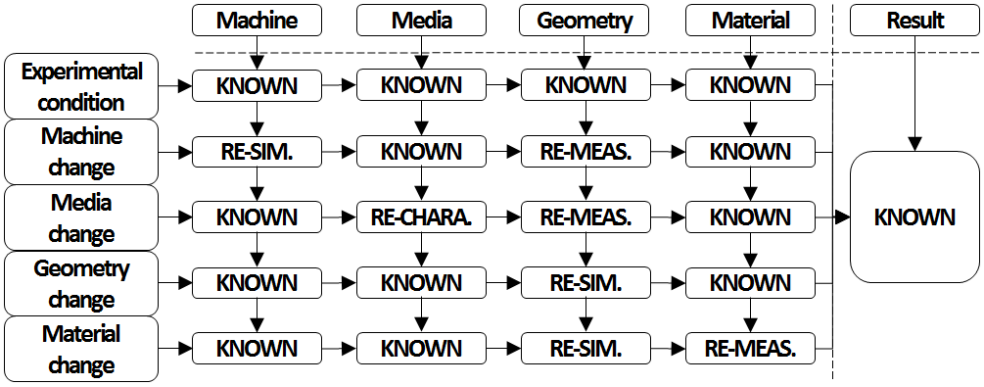

Figure 6.5 – Re-testing matrix.

Figure 6.5 offers a breakdown of the re-testing requirement when an element of the experimental system is changed. As the experimental data is collected, analysed and generally accepted to be accurate, it can be said that for each of the MMG and material categories, that the final outcome is known. If a machine change were required, the machine would require re-simulation, and media of known behaviour would process material of known properties and those samples would require re-measurement to characterise the new machine. Thereafter, the machine configuration would be known. This logic can be extended to the other rows.

6.2.2 Simulation of non-standard AFM hardware.

As presented in the literature review, many research groups across the globe (primarily in India) have developed additions to the proven hardware in the basic AFM process. Using magnetism to locally increase the motion of an iron-shot loaded media, using agitators in components to increase shear forces and using electrically-conductive media to remove material in a pseudo-ECM format are all trialled – but can they be simulated?

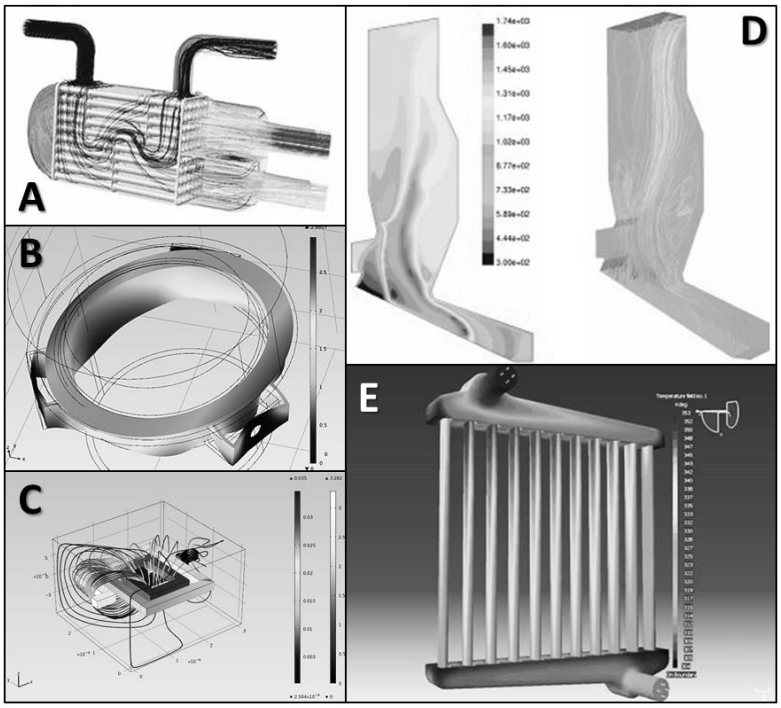

Figure 6.6 – Alternative opportunities for engineering simulation in AFM.

Figure 6.6 presents five machinery-centric examples from the Ansys Fluent package and COMSOL's multiphysics software; A) heat exchanger problems are simple and frequently performed in software – in AFM, the delivery-of refrigerant and effect-of-delivery can simulated when assessing the potential of temperature management systems, B) welded joints and surfaces undergo cyclical loading in the AFM process, to relatively high forces – Mollart's machine itself has leaked on numerous occasions – simulation can aid engineering designers in making improvements, C) modern simulation packages like COMSOL's can combine several physical simulations into one and judge their effect on one another – effect of the presence of a magnetic field through AFM hardware could be simulated to judge strength of field generated in the media, D) an Ansys Fluent example of a local shear force patterns with agitator inserted, requiring Fluent's moving mesh functions, seen mostly in internal combustion engine simulation, and E) a representative image of COMSOL's dynamic heat transfer through two phases where internal and external surfaces are able to be modelled.

6.2.3 Abrasive Potential Index (API).

Three issues exist in attempting to define the abrasive potential of a volume of grit in a body of slurry; 1) the grit may be mixed with other size ranges, 2) between batches, the grit varies by percentage volume, and 3) a single median size has upper and lower tolerance limits. The challenge in AFM is to define a single metric, so that in a situation where (crudely) a large grit is suspended in a smaller volume (relative to a smaller grit in higher volume, suspended in the same weight of carrier), it is possible to *equate* the erosion seen in a small grit suspended in a greater volume. Importance of this is seen in the production environment where the economic cost of media (typically ~EUR250/L (2013)) can be allayed by utilising existing batches for production work – however, to even the advanced-user, the ability to equate two mixtures of grit size to one another is pure guesswork.

Abrasive grains are filtered through a series of meshes, with a number of wires per inch, equating to a number of holes per inch and thus, an average square area for grains to pass through. The filtering method (FEPA) has been used for decades to sort fine powders of ultra-hard materials into groups by size. In an ideal world, the tolerances of the filtration process would be in the sub-micron range, but ultimately the process by which grit is manufactured means shape is not consistent and spherical grits are not always formed, allowing the passing of oversize greater aspect-ratio grains. This results in a median size particle with limits either side, meaning the physical standard by which all abrasive manufacturers and OEMs guide their product specification is only a nominal size, not an absolute figure. For this reason, it is statistically difficult to separate the nominal size from the tolerance limits – manufacturers provide error statistics, i.e. over 90% of a batch is at the nominal size. For this reason, the most logical approach is to define the range as the nominal, accepting that there is a source of controlled variation present.

Application of these values is most evident in the naming scheme of the media. It helps to visualise the principles of sandpaper use, whereby a single grade may be used and by varying the pressure, the removal rate changes, but the grit size remains constant. Alternatively, the pressure may be held constant, but the *potential* of the abrasive to remove material is limited by its physical size. The name *abrasive potential* is derived from this reasoning, as it encapsulates the principle of deferring MR as a function of abrasive size and volume. Assuming a reference value for abrasive potential (AP) (say, the levels of erosion seen in experimental media), a scale (an index) can be developed, whereby the change in volume and size of abrasive grit equates to a finite level of MR under a reference pressure, with predictable behaviour under pressure variation. This allows the indexing of abrasive potential (API), in a particular material, where practical usage is driven by the known results of simulation and resultant force acting on grit. Figure 6.7 below illustrates the principles of the API.

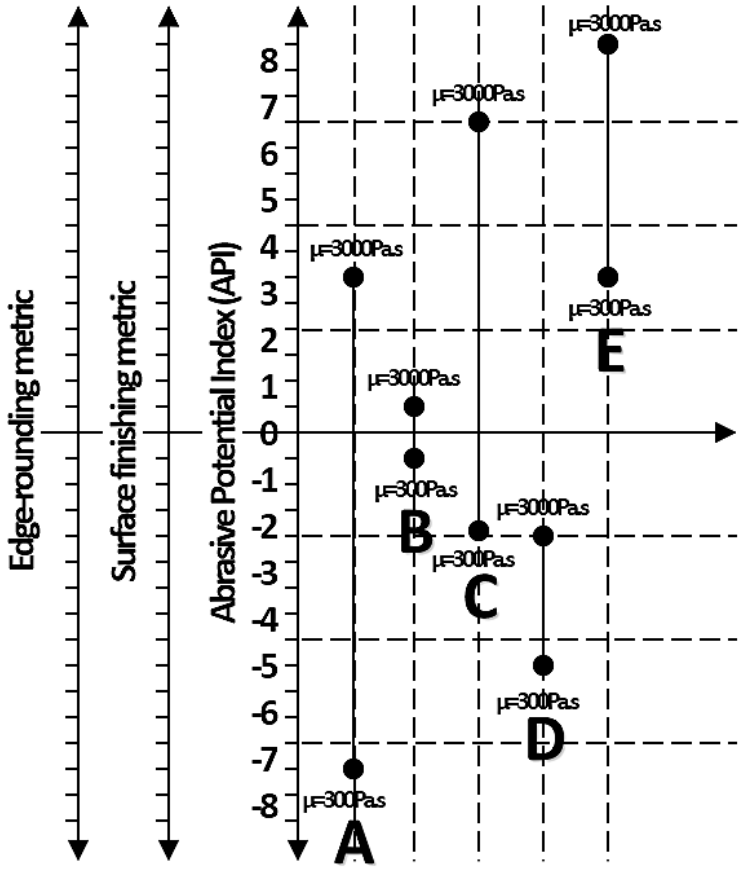

Figure 6.7 – Principle of abrasive potential index (API).

For a given viscosity condition, factors of GF and GS can be separated from their carrier (MP) influence, as the carrier's only key property is to provide support in the form of viscosity; viscosity that is measured offline and witnessed in simulation. Reference figure 6.7, letters A-E are GF-GS combinations that may be noted from any media configuration imaginable. Assuming GF-GS 'A', it can be inferred by cross-referencing against experimental results that for a given viscometric and material condition, a resultant level of MR was achieved – for the purposes of practical reference, figure 6.7 uses μ=3000Pa.s as an upper level and μ=300Pa.s for a lower level; it should be noted that GF-GS conditions A-E vary in their ability to remove material, despite processing under the same force conditions. The API gives the end-user the ability to select a media that operates in harmony with the desired process outcome and MMG constraints. An API chart is required for every new material, although the edge-rounding and surface finishing scales should be added to a single chart and offset for comparison and usability purposes. As GF-GS value may alter viscosity, this places further importance on the simulation of measured media. Method of use should be that a process developer identifies media that are capable of operating in the region of finish or rounding desired, then check in production if that media is available. Assuming that it is not, the developer may select another that is capable of operating at the same API, i.e. 'A' and 'B' are compatible, 'D' and 'E' are not.

6.3 Optimisation of CFD-aided system

Considering two methods of optimisation (by cycle time, process capability), the CFD element of the new AFM setup system is undoubtedly core to functionality – values obtained from the software are wholly user-derived; as-such, they potentially contain systematic error. This section aims to provide methods of reducing influence of error.

6.3.1 Optimisation for accuracy.

Optimisation is defined as attempting to find the highest-achievable performance by manipulating factors within a set of constraints presented. Factor manipulation in this work has already been produced, and error sources have been considered in chapter four and in figure 6.2. However, there exist several sources of CFD-specific variation that can be studied and curbed to limit the practical challenges in a production environment;

- Media behaviour can be studied at a greater actual viscosity to prevent use of extrapolated values – machinery does not currently exist to test this effectively.
- Simulated geometry is sourced from nominal CAD geometry, not actual manufactured geometry, introducing subtle flowpath geometry differences; CMM results could be integrated to modify CAD to help alleviate this.
- Introduction of further energy transfer locations on the model, i.e. incorporation of more physical phenomena such as heat transfer.
- Increase resolution of model (increase cell count and improve quality of cells) to prevent poor conformance of mesh to solid model.
- Set acceptable residual allowance during the run-stage, to prevent the decision of convergence from human influence.
- Data collection points (monitors) are added to the model manually, but where repeated running of the same geometry is concerned, the position will alter if manually re-picking the points. Software allows the consistent mapping of monitors to geometry, to be consistent between runs.

6.3.2 Optimisation for speed.

Where rough values and ‘better-than-nothing’ approaches are required, there are strategies available;

- Minimise cell count, as each iteration asks the CPU to make calculations for every cell – accuracy need not be impeded – the cells can be strategically removed (in large cavities away from any POIs). Use growth rate to effect this.
- Remove all but the most critical physical phenomena; additional study of physical effects occupies CPU cycles and increases duration to convergence.
- Limiting iterations works if a knowledgeable human is able to detect convergence (or near convergence) before a residual error value is reached.

6.4 Case study, ‘manifold’.

Research into the AFM process at Mollart culminated with the development of a process model for a new customer, sold on the capability of Mollart to provide AFM for subcontract turnkey manufacturing. The component (pictured at ‘D’, figure 6.1), is used for hydraulic fracture – repeated high temperature, high pressure load is passed through the flowlines.

6.4.1 Manifold development.

Measuring approximately Ø125mm x 500mm, 12 rows of ports normal to the OD are produced by milling and polishing. At the base of the ports (n=72) Ø3mm holes produced by EDM interconnect the individual rows. At one end, there is a T-junction, and the other, an elbow. The edges are all sharp – the drawing requires AFM to be used to finish the intersections with uniform radii no greater than 0.5mm.

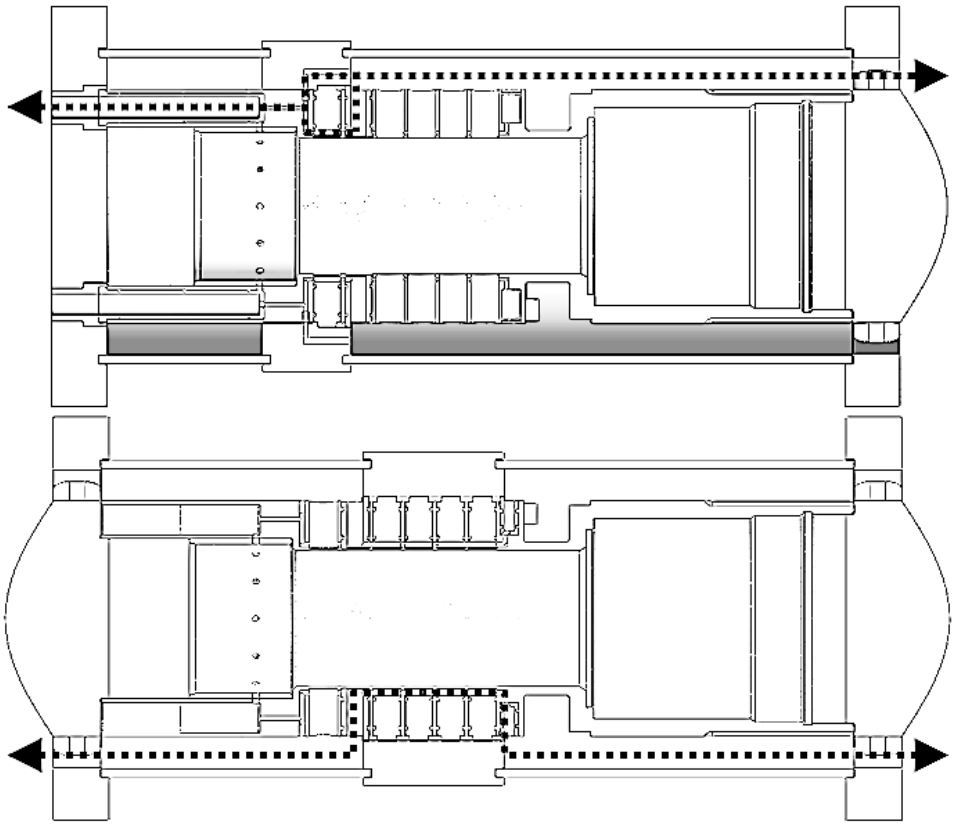

Figure 6.8 – Sections through manifold illustrating designed flowpaths.

In figure 6.8, two sections are presented, with the two setups marked by a dotted line – the flowpaths are separate and do not pass over the same features twice. This configuration is required to circumnavigate the pressure constraints calculated, as the finite capacity of the machine isn’t sufficient to deliver an appropriate flow as noted

from chapter 4's experimental work (i.e. no less that 50mm/s surface speed). The pre-simulation work is concluded by opting for a hybrid 'plug and contain' strategy where the ports are plugged to control the shape of the flow as it approaches the interconnected features, and the media is contained within aluminium tubular walls surrounding the component. This strategy is appropriate for the complex geometry at hand. A scaled down local simulation is used to ensure flow symmetry in this application.

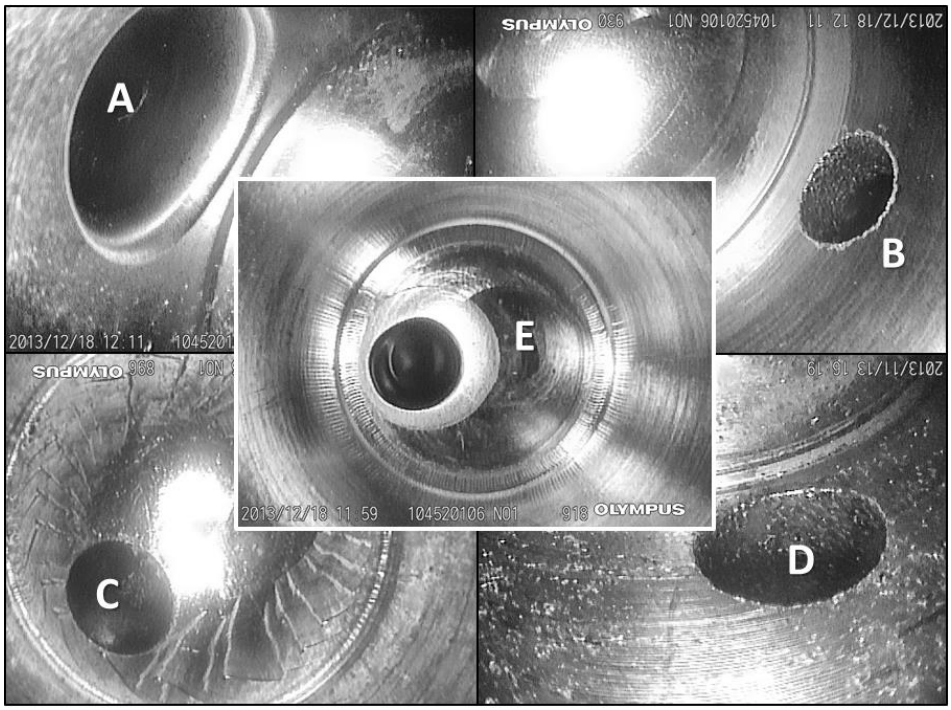

Figure 6.9 – Flow field effects when uncontrolled.

In small bores, such the Ø3mm fluid lines presented in figure 6.9, the factors of grit size, flow field shape and angle-of-attack combine to create issues that larger features are generally insensitive to. Image 'A' presents the successful and tangential rounding of the POI and image 'B' presents the typical pre-process condition. This component contains a number of holes produced by EDM, and therefore burr formation is not as significant as traditional twist-drilling, but sharp edges are still left. Image 'C' highlights a secondary aim for the AFM process, whereby 'chatter' from the milling process is left on the base of the port – AFM clears these occurrences with relative ease. Image 'D' presents a through-hole with hole-centreline in close proximity to the bottom of the port – this presents a fixturing challenge, one solved by fitting a plug with a through-hole of its own, but at a larger diameter concentric to the feature centreline. In order to maintain a circular flow-field approaching the feature, the plug appears to have a slot running through its underside – pictured in figure 6.9. Image 'E' is a side effect of tooling forcing media in a plane abnormal to the POI. The error was noted in a pre-production steel component, and tooling altered to compensate.

6.4.2 Crude oil sample collection block.

A challenge for the process at Mollart is the high-aspect ratio bores presented by the component in figure 6.10. This sample collection block is comprised of hundreds of interconnected ~Ø5mm lines for hydraulic and wires as visible in image ‘C’. Measuring over 1.6m (see image ‘A’), the physical length of the lines that are currently used (unsuccessfully) to pass media into the ports (see image ‘D’) are delivered by a fixturing arrangement that requires media to be passed through the block end-faces, causing undesirable pressure drop and viscous heating effects.

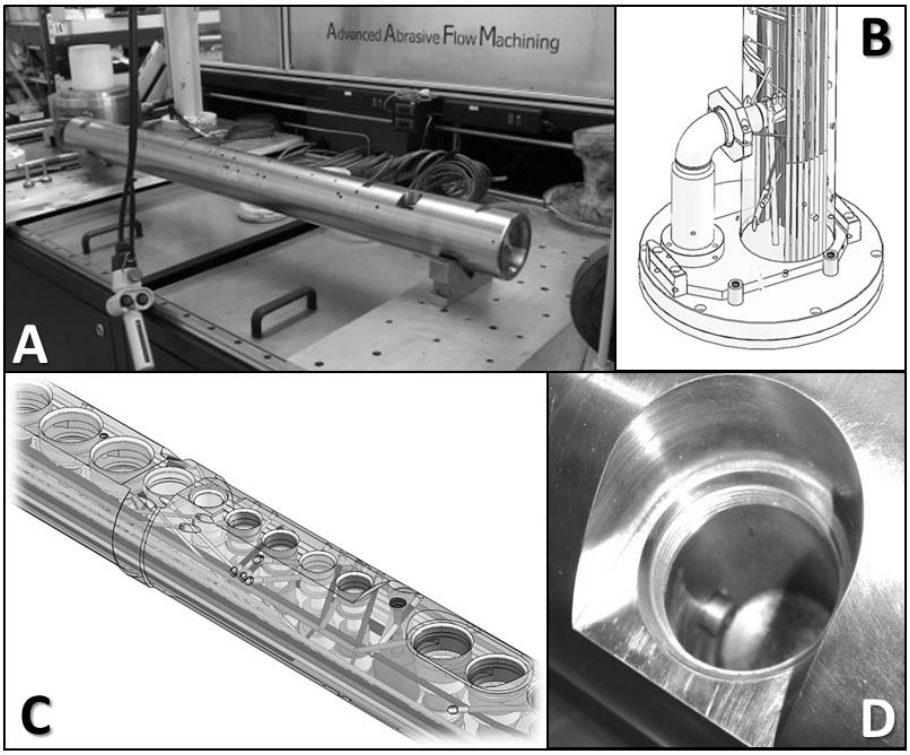

Figure 6.10 – Sample collection block appearance and proposed tooling.

Several iterations of tooling to process the part have been attempted, but the latest (and likely the last) are based on reducing pressure drop. Figure 6.10 ‘B’ presents an alternative to feed media directly into the port, while retaining the requirement to feed media through the 1.6m bores running the length of the block. An alternative and likely more successful approach is to feed media into the port (‘D’), designed so that media can also exit the part, reducing pressure drop through media transport to minimal levels.

These proposed tooling systems are yet to be designed, simulated and proven.

6.5 Summary

Abrasive flow machining is a recognised complex semi-bound abrasive machining process – its usefulness and application in a business where production volumes are low can be difficult to justify, but often in the case where part value and complexity are such that a non-aggressive, stable and manageable process is required, it is highly suitable. Its flexibility should not be underestimated, as several of the services required by AFM (i.e. documentation, an element of offline setup and stock maintenance) are considered normal to many other process (i.e. high value 5-axis milling or a new CMM program) – the technology developed must build trust in its users and the processing of the manifold is the first way this has been demonstrated.

The next chapter demonstrates the worth of the process in terms of environmental considerations and performance when compared to human labour.

Chapter 7 – Energy, Resources and Efficiency in the AFM process

7.1 Introduction

The AFM process was originally developed to automate several deburring and finishing processes present in the automotive and aerospace industry. Initially the target was honing, although it quickly became apparent that edge rounding, polishing and deburring were successful. Today, the process is adopted for any number of its uses (see table 7.1) although with relevance to Mollart, core importance lies in the ability to eradicate human-introduced variation in surface finishing and deburring in the production environment.

Table 7.1 – Techniques that AFM can replace.

Technique	Requirement	Comments
Deburring	• Carbide burrs • Power tools • Human labour	Automated operation, but poor stock removal. An initial human deburr is required.
Honing	• Hone • Honing tools • Human labour	Automated operation, difficult to know when size is achieved, polishes simultaneously.
Surface finishing	• Polishing discs • Power tools • Human labour	Automated operation, inaccessible cavities, dependent on grit size, long cycle time.
Removal of recast layer	• Shot peening • ECM • Vibratory finishing	Automated operation, grit size can control MRR, capable of processing small holes.
Radiusing	• Carbide burrs • Power tools • Human labour	Automated operation, MRR drops with increased cycle time, polishes simultaneously.

Environmental performance of the abrasive flow machining (AFM) process is currently not well understood – its flexibility as a manufacturing process has only recently been realised (Mali & Manna, 2009) in SMEs as a feasible automated alternative to deburring and polishing of complex geometry by hand (Jain, et al., 2009), and as an alternative to honing and grinding using semi-automated machinery (Cheema, et al., 2012). Economic benefit is still the main driver in the commercial uptake of environmentally-sustainable technologies (Draganescu, et al., 2003; Gutowski, et al., 2005); despite AFM's known flexibility and capability, this paper compares and critiques by, 1) assessing and comparing the requirements of competing processes (values sourced from (Gutowski, et al., 2006)), 2) their power consumption, 3) operating conditions, 4) cost of pre-requisite

ancillary equipment and 5) embodied energy and recyclability of machine structures and consumables.

Challenges facing today's environmentally-conscious manufacturers must be considered in context of economy, society, environment and technology (ESET). Looking deeper at the categories reveals Mollart's economic responsibility to itself, to continue its existence – previously the only real concern of manufacturers – and some would argue, the only real current-day concern for many. Economic performance is the register of success with customers, suppliers, lenders, the government and company employees, justifying whether a job is successful (more-so than technical accomplishment) whether employees attempt to seek new employment (retention of skills) and whether investment occurs to aid further growth.

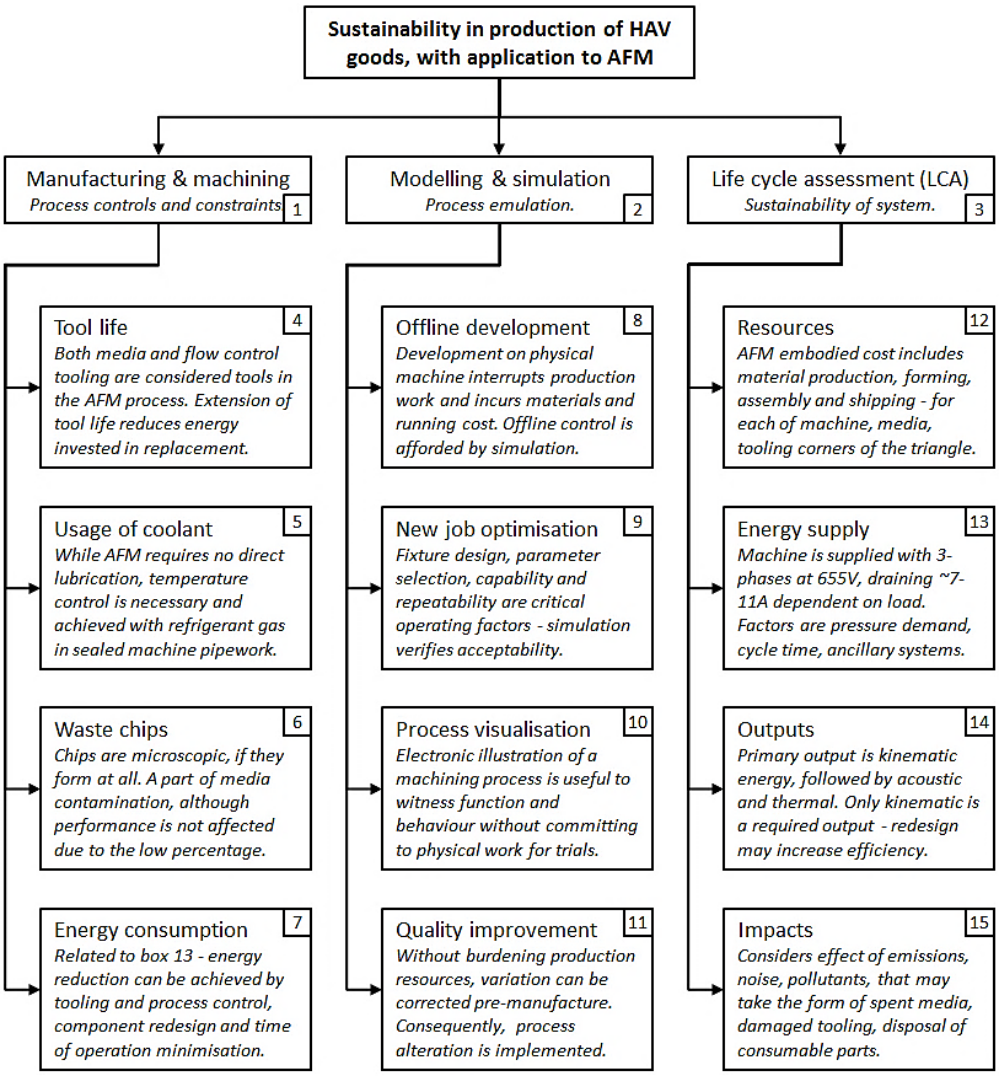

Figure 7.1 – Machining process sustainability considerations.

Societal challenges affect Mollart when access to skills is considered. The UK is known to lack engineers, at all levels – education and training of skilled-staff is a costly and

risky investment for SME manufacturers, who may move-on following training or prove difficult to train. Steady decline in apprenticeship duration and technical depth since the 1980s has reduced the pool of available skills and created a problem for recruitment in smaller SMEs, who now do/need to significantly augment college-based programmes lasting two years. Growth may be limited by this situation. Graduate employment is affected by a softening of key skill teaching throughout the formative school years, which feed into the modern open-access university system, requiring many to undertake foundation level mathematics and English to prepare them for the full degree. UK society recognises engineering as a broad term that applies predominantly to trades from automotive mechanics to air-conditioning fitters to salespeople – many argue that chartered engineers should only use the term, but one opinion is widespread and popular – that 16-25yr olds (and their parents) retain the 'oily rag' image of engineering and do not associate it with wealth creation, reducing the employment pool for companies like Mollart.

Since 1975, the term 'global warming' has been in use, accredited to Professor Wallace Smith Broecker. Environmental science and awareness in the popular media has arisen since the mid-1980s, when in 1992 global politics entered the debate at the first earth summit in Rio de Janeiro. For businesses like Mollart, the bare minimum of adhering to the law on waste disposal, noise levels and pollution control is commonplace, and accepted – with the advent of the 2004 introduction of the ISO14001 environmental management standard, larger firms have led the charge and placed requirements on SMEs to also adopt in order to win orders. The challenge for Mollart is to incorporate administratively intensive standards while operating the business – economic performance remains critical. Supporters of the instigation of such standards credit their economic impact in terms of reducing energy consumption, reducing waste and increasing efficiency, while detractors see the administrative load. Technology challenges are numerous, and can often by socially influenced – 1) alternative power generation and storage of energy are not yet ready for SME businesses, 2) environmental performance is not a significant factor in purchase of new equipment, 3) savings potential is often unclear and difficult to quantity, unlike more familiar purchase-based economising such as reduction in labour hours or materials quantity. AFM operates in an area that matches the ESET categories – the economic case is in question, as hours are spent preparing and operating an automatic machine with a trial and error requirement – Societal questions are raised over the reduction of manpower, (reducing total employment) and the automation of skills that could be taught and retained. Environmental impact is unclear as human labour and lower current consuming devices are the alternative, while technologically, confidence in the process is not inherent in new users, and takes time (and mistakes) to perfect.

7.1.1 Emerging, established and energy-saving applications of AFM.

Application to diesel and marine componentry are most common; figure 7.2 presents six active applications, 1) additive layer manufacturing (ALM) produced parts remain of poor finish, even by modern standards – with geometry producing capability beyond that of traditional machinery, the ALM process requires an equally flexible post-process such as AFM for surface finishing, 2) marine applications consist mainly of propellers manufactured in corrosion resistant materials such as brass and stainless steels. Designs attempt to reduce detrimental cavitation that leads to fatigue failure, where AFM is beneficial – improved surface finish and rounded leading-edges reduce cavitation, while compressive residual stresses are imparted, creating a surface layer of approximately 10μm with greater fatigue resistance (Baehre, et al., 2012).

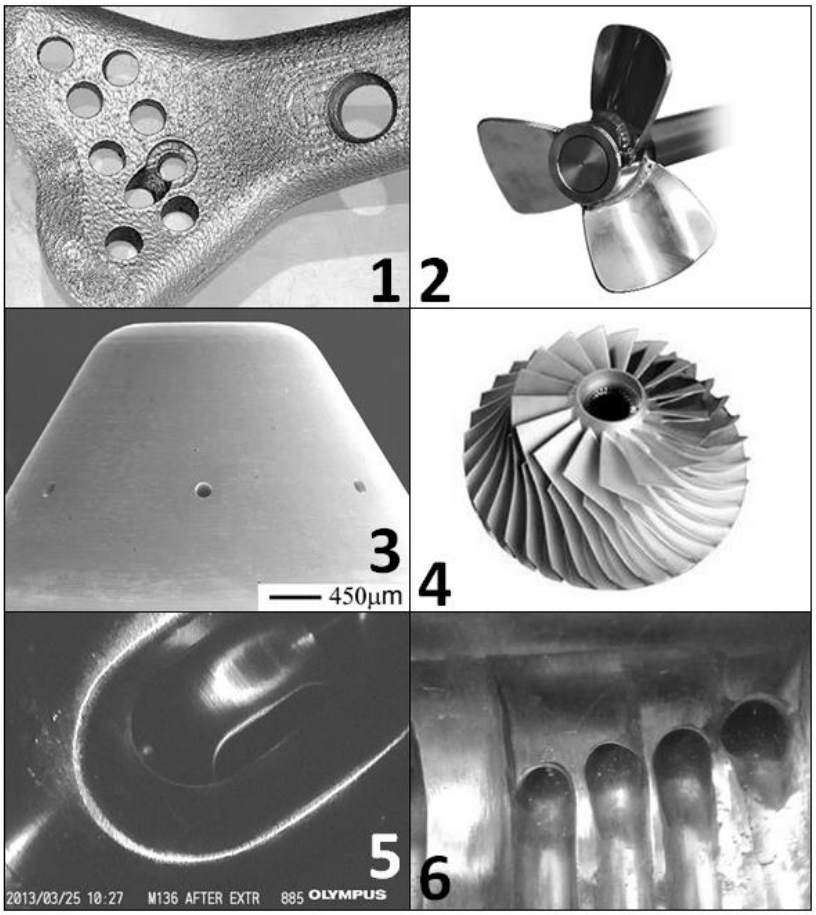

Figure 7.2 – Emerging and established applications.

3) diesel injection systems such as those produced by Bosch and Delphi seek to improve atomisation and thus improve fuel burning efficiency – modern common rail systems operate at 2000bar (Kelly, 2005) pumping fuel through injector body outlets of <Ø0.1mm where AFM assists in accurately sizing outlets and improving surface finish, 4) turbomachinery components, whether aerospace gas turbine blisks or energy-

generating steam-turbines benefit from AFM by compressive residual stress, exceptional surface finish in difficult-to-machine materials, high machine capacity and repeatability (Wilk & Tota, 2007), 5) transmission components in automotive and oil & gas industries must provide safe, rounded passages for electrical wiring – product failure has severe financial consequences, and where space is at a premium, passages are packed with thinly-insulated cabling (Howard & Cheng, 2013), and 6) oil & gas industry parts are routinely operated with liquid, gas and electronic components within millimetres of one another – a slip-of-the-hand in manual finishing can lead to >USD 70,000 of scrap, justifying the use of expensive and non-traditional automated processes such as AFM – the reduced risk and improved repeatability is of great importance to SME manufacturers

Human variation removal, risk reduction and quality improvement is the target of most AFM operators as finishing costs in manufacturing are said to comprise over 15% (Aurich, et al., 2009) of total product cost. Following success in complex geometry, more routine and established manual operations are now under consideration as candidates for replacement by AFM – the questions can be posed, "are these changes economically *and* environmentally viable?", "does the AFM process *always* exceed the suitability, capability and capacity of manual finishing?", "has the company inadvertently caused *more* damage by purchasing a dedicated machine?" and "can either process be *significantly improved* in terms of environmental performance and what are the projected gains?".

While the process improvement work will deliver the most evident results (increased utilisation of MTT machine, reduction in returned parts, reduction of re-machining operations), the consumables cost of running the machine can rise quickly, unless managed properly. The most important consumable is the reclamation and management of the abrasive media - at £1500 for 30kg, cleaning parts with chemicals will damage and waste the media. A labour intensive process is required to dig out and rescue the majority of the abrasive media.

7.2 Evaluation of energy use in manual processing

Strengths of manual finishing include virtually zero setup time, simplicity of tool application and intelligent decision making by the operator. Weaknesses are largely dependent on task – the concentration time required may extend up to three hours, putting the operator at risk of making minor or major mistakes. Where tasks on a single workpiece extend the total processing time over days (sometimes weeks) and additional shorter jobs are interspersed with the longer job, the potential for errors is further increased. Ability to handle job complexity is manual finishing's greatest strength and simultaneously its greatest weakness – this paradox stems from the minimal setup time (as human-operated hand tools are used), while work is often repetitive and un-engaging. The action of material removal is physically performed by human labour that feels tiredness, stress/pressure and typically disconnected from the wider production process.

Manual finishing utilises standard consumable tooling such as abrasive grits (i.e. aluminium oxide) supported on wire shafts by epoxy resins or other binders – they are applied by powered hand-drills and are available in infinite shapes and sizes to allow access to workpiece features. For harder materials, metallic 'burrs' are used, typically made from tungsten carbide. These are multi-flute and are somewhat less subtle than abrasive-loaded tools – they are expected to shear and chip material rather than rub, displace or grind, increasing process risk. The actions required to process the workpiece vary slightly upon each part in a batch due to human variation, leading to precision issues at the quality assurance stages. Work must be performed in a clean, quiet, well-lit, appropriately-heated, consistent and management-driven operating conditions. Cleaning requirements revolve around pneumatic airline usage and evaporating naphthalene ($C_{10}H_8$) ('panel wipe') to remove stubborn contaminants.

7.2.1 Power consumption in Joisten & Kettenbaum manual finishing tools.

Figure 7.3 presents the data collection assembly used to assess the electricity use in manual finishing; 1) power supply is delivered by single-phase AC at 240V with a power factor of 0.8, 2) current draw is read by a 'Fluke 337' true RMS clamp meter, positioned over the outlet from a standard UK three-pin plug, 3) drill speed controller is a 'Joisten & Kettenbaum Eneska 4-1' and 4) drill is a 'Joisten & Kettenbaum J-BM 50HT'. Consumption is measured in the three modes (Dahmus & Gutowski, 2004) of idle, run-time and production. Irrespective of mode, the equipment draws a consistent 0.2A, with measurement equipment error excluded by placing greater load (by hand) on an active drill, in which the current delivery increases significantly. Load upon the drill during production mode is very low, due to the fine nature of the application – power use is 0.038kW.

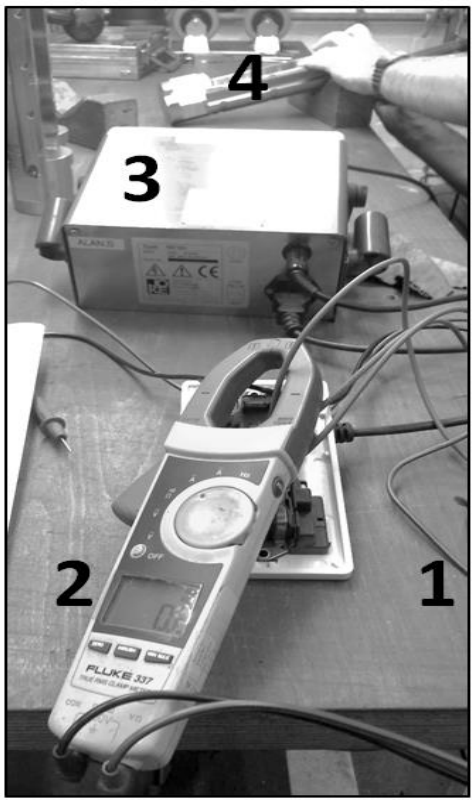

Figure 7.3 – Power metering equipment for manual finishing process.

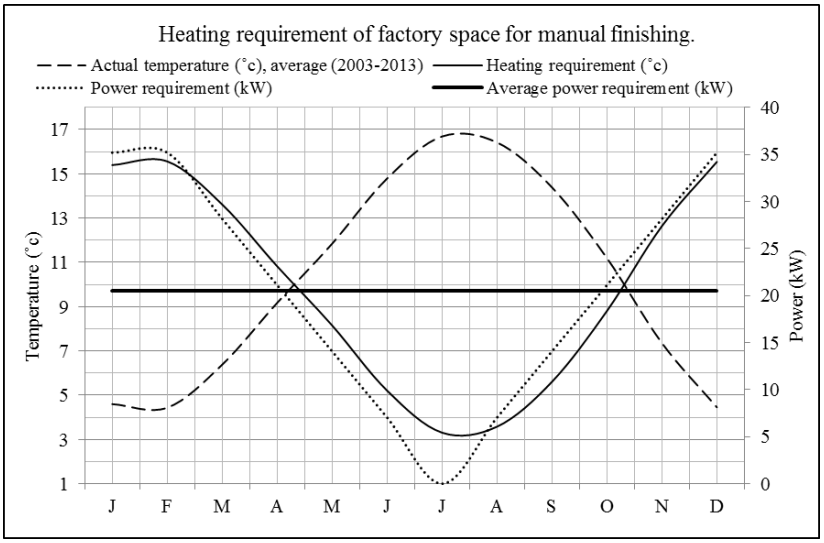

Figure 7.4 – Manual finishing heating requirement.

7.2.2 Heating the workspace for human labour.

As the process is reliant upon human labour, a gas-fired air heater is used to heat the shop space – volume is calculated at 870m^3, and is maintained at 20˚c throughout the year over a two-shift system, operating 85hrs/wk. The heater is a natural gas-fired AMBI-RAD UDSA 030 model, operating on single phase 230V, specified to regulate

2,725m^3/h and when running at maximum load, requires 35.2kW and delivers 29.2kW, making it 83% efficient. Referring to Fig. 4, Central England Temperature (CET) is sourced from the UK meteorological office (Meteorological Office Hadley Centre for Climate Change (Tim Legg), 2013) and plotted throughout the months of the year – temperatures are an average of the last 10 years since 2003. Average annual heating requirement is 9.9˚c. To calculate the energy requirement (and the power requirement in turn) from the air heater, the energy equation is used as shown in equation 7.1 to 7.3. Density of dry air at 5-10˚c is 1.2754kg/m^3 – therefore, mass to be heated is 1,110kg. Specific heat of dry air is considered at 1.005kJ/kg/˚c, while the temperature change (dt) required is (20-9.9) 10.1˚c. This results in a final energy requirement of 11.27MJ to heat the space by 10.1˚c.

$$Q = m\ cp\ dt \quad (7.1)$$

$$Q = 1{,}110 \times 1.005_{x10^3} \times 10.1 \quad (7.2)$$

$$Q = 11.27MJ \quad (7.3)$$

Where Q is quantity of energy transferred (kJ), m is mass of substance (kg), cp is specific heat of the substance (kJ/kg/˚c) and dt is temperature difference (˚c).

Values should be considered a minimum as factory has a high ceiling, poor insulation, cargo doors ajar and a mixture of ceiling heights preventing uniform temperature distribution. Equations 7.4 to 7.7 consider time required to heat the space from 9.9˚c.

$$E = P\ t \quad (7.4)$$

$$t = E / P \quad (7.5)$$

$$t = 11.27_{x10^6} / 29.2_{x10^3} \quad (7.6)$$

$$t = 386s\ (6.4min) \quad (7.7)$$

Where E is energy (kJ), P is power (kW) and t is time (s).

$$Q = U\ A\ dt \quad (7.8)$$

$$Q_{wall} = 0.317 \times 130 \times (20\text{-}9.9) \quad (7.9)$$

$$Q_{wall} = 416.22W \quad (7.10)$$

$$Q_{window} = 2.8 \times 12 \times (20\text{-}9.9) \quad (7.11)$$

$$Q_{window} = 339.36W \quad (7.12)$$

$$Q_{roof} = 0.8 \times 161 \times (20\text{-}9.9) \quad (7.13)$$

$$Q_{roof} = 1.3kW \quad (7.14)$$

Where Q is heat transfer (W), U is heat transfer coefficient (W/m^2.K), A is area (m^2) and dt is mean temperature difference (K).

Thermal transmission losses occur through the surfaces of the factory unit – equations 7.8 to 7.14 determine the losses of the walls, windows and roofing – total loss is a little over 2kW (equations 7.15 to 7.16). This value is important as the heater is not a proportionally controlled system, i.e. it does not operate continuously at a lesser rate – the maximum output is delivered until an upper threshold is met then the unit shuts off and restarts when the low threshold is met. The low threshold is the legal minimum (British Government (HMG), 2013) of 13˚c, triggering a requirement to heat the building by 7˚c when reached.

$$Q_{total} = Q_{roof} + Q_{window} + Q_{wall} \quad (7.15)$$

$$Q_{total} = 2.056kW \quad (7.16)$$

Where Q is heat transfer (W).

Heated to 20˚c with external temperature of average 9.9˚c, 7.8MJ of energy leaves the building before it reaches 13˚c (equations 7.17 to 7.19). This process takes 63min (equations 7.20 to 7.22), as determined by thermal losses of ~2kW. Once cooled, the air-blower activates and continues to burn gas generating 29.2kW for an additional 4min to raise the temperature back to 20˚c (equations 7.23 to 7.25). In summary, following the initial 6.4min period of heating from 9.9˚c, the room is left to cool to 13˚c over the next 63min. For 4min, the heater turns on, and repeats the cycle for the remainder of human occupancy – in percentage terms, 5.97% of time is spent heating and 94.03% naturally cooling.

$$Q = m\ cp\ dt \quad (7.17)$$

$$Q = 1110 \times 1.005_{x10^3} \times -7 \quad (7.18)$$

$$Q = -7.8MJ \quad (7.19)$$

$$t = E / P \quad (7.20)$$

$$t = -7.8_{x10^6} / 2.056_{x10^3} \quad (7.21)$$

$$t = 3793s\ (63min) \quad (7.22)$$

$$t = E / P \quad (7.23)$$

$$t = 7.8_{x10^6} / 29.2_{x10^3} \quad (7.24)$$

$$t = 267s\ (4min) \quad (7.25)$$

7.3 Evaluation of energy use in AFM

Mechanisation of manual finishing is the goal of AFM – as presented in table 7.1, five main operations are achievable with the process with varying degrees of convenience. In comparison to manual finishing, AFM requires three considerable time and cost investments, 1) a volume of abrasive slurry must be manufactured (if an existing configuration is not suitable), 2) tooling must be designed and manufactured, and 3) disassembly and cleaning is more demanding than the relatively dry and clean manual finishing. As with manual finishing, AFM's greatest strength is also its weakness – as tooling complexity is based on pre-process part complexity and final part condition, the effectiveness of the process is often reduced to the tooling designer's ability to engineer a desirable flow condition; the strength however, is that once a suitable result is achieved, any operator (skilled or unskilled) can load and preheat media, assemble tooling and run with confidence that components will be processed correctly.

The process is not subject to external stresses, nor does it require human operating conditions as described above. The material removal is achieved by an electrically-powered pump passing oil into a hydraulic ram with a piston mounted on the end which, to operate, is naturally more energy consuming than hand-guided drills. Dependent upon workpiece geometry and machine capacity, multiple setups may be designed to process groups of features within the maximum pressure of the machine – the cycle times are typically far shorter than manual finishing, and operations need not be run in serial; while manual finishing requires persistent human attention, the operator of an AFM machine may run operations in parallel, such as two or three unattended machining processes (also run after standard working hours) in addition to cleaning or disassembly of tooling for the next operation.

While relative procedural aspects of the two processes can be compared, repeatable quality and reduced risk in achieving the final outcome is difficult to quantify objectively. Reject rates for batches of parts can be 0-100%, while annually approximately 14% of parts require re-work – unsatisfactory ways in which manual finishing can affect the part include under-processing, over-processing and damage to surrounding features. At Mollart Engineering, this means ~GBP 1.23m can be at risk of human-induced manual finishing error. Under-processing is the simplest form of re-work which may cost 4-5hrs labour, while over-processing typically results in the requirement to add material using a welding process, usually TIG or electron beam. The costs of these operations alone can reach GBP1,000, in addition to the subsequent machining processes to correct the weld form back to the intended geometry, raising the total cost of re-work to approximately GBP1,500. As manual finishing is performed after many value-adding operations, the part's ~1,450 features are exposed to the conditions of the chosen finishing process, increasing risk of forming undesirable geometry. Customers, particularly LEs (Large Enterprises), impose strict quality management and monitoring regimes on incoming deliveries – the statistics gathered determine distribution of orders placed, and thus, the revenue potential of SMEs.

7.3.1 Power consumption in Micro Technica Duplex AFM machine.

Only electrical energy is required in AFM - the process operates in an unconditioned environment, with its own heating and cooling systems, mechanized pumping and control circuits that manage temperature and active software. The machine used in this example is a 2009 Micro Technica Technologies Duplex 250, specified to operate at 45bar or 300mm/min (whichever is reached first) with a media volume of 20L. The same Fluke clamp meter is used to collect current across three phases from the machine's electrical cabinet – three phases are fed in at 415V, with a power factor of 0.8; figure 7.5 presents the almost linear correlation between current draw and operating pressure. Draw is marginally greater when refrigerant is not running, due to a 'normally-open' valve requiring power to remain closed.

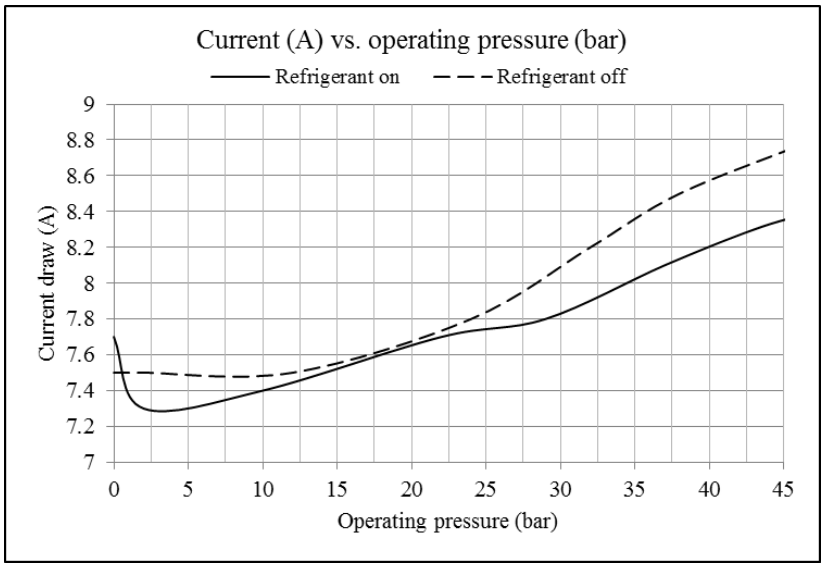

Figure 7.5 – Current vs. operating pressure.

A typical sequence of operation begins with mounting the component and tooling assembly, clamping, setting the program to run, retracting cylinders then unclamping once complete. Starting in idle mode, the machine's control is off and draws 0.75A – moving into run-time mode with control on and no material removal activity, 7.7A is drawn. Unclamping draws 8.8A, while 10.7A is drawn while clamping, likely due to increased force applied. The machine spends an insignificant time performing any of these four actions; therefore they do not comprise any part of the analysis. With refrigerant on, when machine is working with low-load but still moving, the pressure reaches approximately 3bar, demanding 7.3A – 4.198kW, whereas manual finishing operates at less than 1%. When operated to excess at an unsustainable load (45bar), 8.35A is consumed, equating to 4.802kW, but typical target is 30bar at 7.8A, consuming 4.485kW. With refrigerant off, the draw is slightly higher; 3bar, 7.5A = 4.313kW; 45bar, 8.75A = 5.032kW; 30bar, 8.1A = 4.658kW. Typical job times range from 0.5-

2.5hrs, where jobs normally require refrigerant to be active, particularly in small bore high shear-rate work (4.485kW demand) – assuming 2.5hrs, 11.213kWh is consumed, at a cost of approximately GBP 1.39, generating 4.995kgCO_2e.

7.3.2 Power consumption in alternative technologies.

Technologies for semi- and fully-automated finishing are numerous; fine machining is possible with high-quality machining centres, grinding is highly capable even with 30-40yr old machinery and electro-chemical machining (ECM) offers AFM-competitive surface finishes. These techniques vary widely in power consumption within their own class, but specific power in mechanical processes is comparable (as compared to chemical processes). Finish machining is found in the literature to consume approximately 9.59kW (Morrow, et al., 2004), grinding between 7.5-10kW (Chryssolouris, 1991; Baniszewski, 2005) and ECM at 3-100kW, converting to high current DC supply at 6-10V during processing (Mukherjee, et al., 2005).

Job complexity drives operational time, as in finish machining toolpath stepover must be minute to avoid stair-stepping; in grinding, a small mesh-size abrasive and low feed is used to minimise depth of indentation which extends process time; ECM requires complex tooling and electrolyte access – where electrode-to-workpiece gap is larger than desirable, efficiency drops as low as 10% (McGeough, 2005). All three alternative finishing processes lack the low-maintenance, surface texture generating and feature accessibility of AFM, while operating at comparable levels of power consumption and lower capability, critical when considering the cost of embodied energy described in this work.

7.4 Economic cost comparison

Three workpiece scenarios are laid out (distinguished by feature-count, processing time, tolerance-demands and setup-count) for comparison purposes – the trade-off between environmental and economic cost is described with reference to industrially-significant quality measures such as repeatability, accuracy, precision and uniformity.

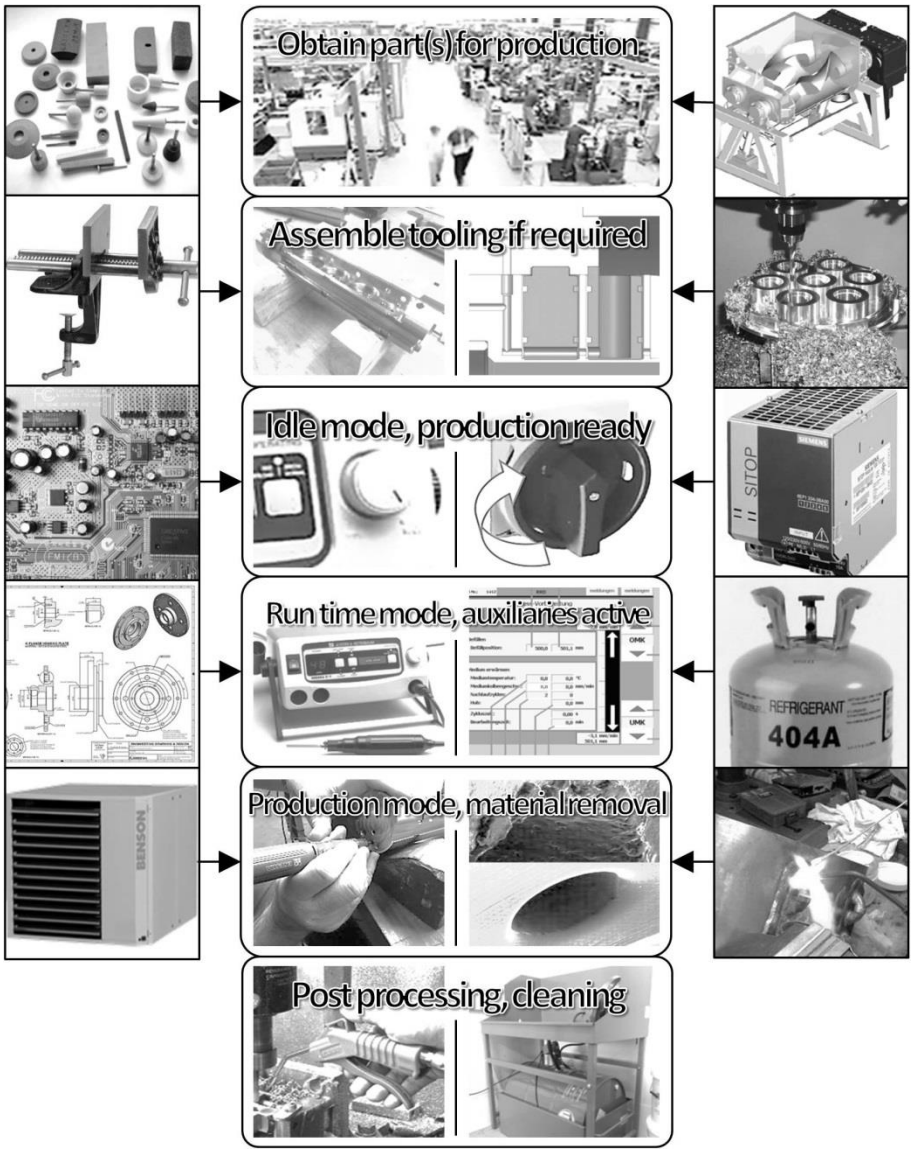

Figure 7.6 – Sequence of operation.

Availability of sufficiently-capable automated-technologies for current industrial finishing requirements is poor – multiple automated-technologies are available for different finishing operations in a range of technical complexities and price points. Where the value of machinery for a preferred automated-technology exceeds a threshold, potential purchases become unattractive to SME manufacturers in lieu of established and highly-flexible human labour. In an age of mechanised engineering,

there exists no simple solution to adopting the most suitable technology for automated finishing. Two technologies co-exist at Mollart Engineering – manual finishing by hand tools and AFM. A simplified, typical sequence of operations is presented in figure 7.6, with centre boxes representing the setup and running stages (manual left, AFM right) with main secondary requirements presented to the left (manual) and right (AFM).

Table 7.2 – Example part processing times.

Part	Manual	AFM	Complexity	Setups
A	Serial, 3.5h	Parallel, 1h	Low (batch of 7)	1
B	Serial, 15h	Serial, 2h	Medium (batch of 6)	1
C	Serial, 110h	Serial, 6h	High (batch of 1)	4

Operating manual finishing averages consumption of 2.226kW (over the course of 1h), whereas AFM averages <4kW. For a more complete example of energy consumption and cost of operation in a production environment, three example parts are set out that relate to active parts in Mollart Engineering's subcontract division as presented in table 7.2. Man hours are excluded as the comparison is intended to highlight the direct economic and environmental issues, not human cost.

Part A is a simple tube, used in a medical application for fatigue testing of material – a human operator can use an electric drill and 'flex-hone' for approximately 0.5h, while AFM can replicate the action with abrasive media to reach a required surface finish. Due to the small size and simple geometry, AFM can process the batch size of seven in parallel within 1hr, while manual finishing can only be done in serial, taking 3.5h. In this example the job is continuous; not obstructed by shift patterns and breaks, manual finishing of 3.5h means the heater is active at 35.2kW for 0.21h (12.6min), while the drills operate constantly at 0.288kW as the force to rotate a flex-hone is greater. Manual finishing therefore consumes 8.4kWh (30.24MJ) at GBP 0.46, producing 1.8kgCO_2e. AFM operates at 4.485kW for 1h, consuming 4.485kWh (16.15MJ) at a cost of GBP 0.56, producing 2kgCO_2e. In this example, manual finishing is 18% cheaper and produces 10% less CO_2e, but uses over twice the energy, taking 350% longer.

Part B is a larger titanium-alloy component comprised of an inlet and three outlets. Internal edges are to be processed around the three outlets, and are very difficult to get to by hand, yet simple by AFM. Due to a large entry bore reducing pressure drop and allowing a straight flowpath to the features, AFM can operate with less force. Manual finishing revolves around the use of electric drills with radius grinding attachments – as with part A, the process is continuous at 2.5h per part, 15h total time. Over this period, the heater is active for 0.9h (54min), while the drills operate intermittently, complemented by manually-applied abrasive cord. Drill utilisation is 75%, operating at 0.192kW – over the 15h period, this results in 2.16kWh electricity consumption. Natural gas consumption at 35.2kW reaches 31.68kWh. Manual finishing therefore

consumes 122MJ at GBP 1.74, producing 6.8kgCO_2e. AFM operates at 4.313kW, in serial for 2h; electricity consumed is 8.6kWh (31MJ) at a cost of GBP 1.07, producing 3.8kgCO_2e. In this example, manual finishing is 40% more expensive, 75% more energy consuming, takes 87% longer and produces 45% more CO_2e. Part C is considered in table 7.3 – assuming human labour per hour of GBP 25.00, man-hours for assembly are costed unlike in example parts A and B. Another titanium alloy component, the complexity requires four separate AFM fixtures, or over 110 manual hours to reach completion. In manual finishing, drills and non-powered tools are used (60% utilisation) at a low fine-finishing current consumption of 0.2A, 0.0384kW.

Table 7.3 – Complex part finishing comparison

Operation	Manual	AFM
Assemble tooling	-	1h
Machining	110h	10h (4x2.5)
Clean, reassemble	-	4h (3x1+1)*
Final cleaning	0.5h	2h
Machining duration	110.5h	10h
Total labour	110.5h	7h (1+4+2)
Business days no.	6.9	1.1
Grid electricity	0.0384kW	4.6kW
Natural gas	35.2kW	-
Total grid electricity	2.5kWh	46kWh
	1.1kgCO_2e**	20.5kgCO_2e**
		GBP 0.1239/kWh***
Total natural gas	233.4kWh	-
	43kgCO_2e**	
		GBP 0.0465/kWh***
Total power cost	GBP 11.00	GBP 5.70
Total labour cost	GBP 2,763.00	GBP 175.00
Total cost	GBP 2,774.00	GBP 180.70
Total energy	849MJ	166MJ

*Weighted to include machine monitoring
**Grid electric conversion factor of 0.44548
***British Gas values, standard tariff (Jan-2014)

Over the duration of the work, 2.5kWh is consumed, while the heater is operational for 6.63h, burning natural gas at 35.2kW, resulting in 233.4kWh. Manual finishing therefore consumes 849MJ, an energy cost of GBP 11.16, and a human labour cost of GBP 2,763. AFM operates over 10h, drawing 8A at 35bar (4.6kW), therefore consuming 46kWh of grid electricity. Activity varies while processing with AFM - there is 7h of labour to cost to cleaning, assembling and monitoring, but all processes can be performed in a little over two eight-hour shifts. See table 7.3 for detailed values. AFM is five times faster, 1/15th of the cost, 54% less generation of CO_2e and uses one fifth of the energy.

7.5 Process sustainability and embodied energy

Life cycle assessment (LCA) considers energy consumed and pollutants produced for a given process during, including and following activities beyond the end user's application (from cradle to grave) – in the case of AFM at Mollart, several key components and their principal constituent materials are presented in table 7.4.

Table 7.4 – Core materials use in AFM machine.

Subassembly	Component	Raw material
Hydraulic power pack	Hydraulic oil	75L of refined hydrocarbon
	3-phase electric motor	2kg neodymium
		2kg copper
Heating and cooling systems	Refrigerant	1.5kg R404A gas
	Induction heating mat	0.191kg nickel steel
Steel framework	Frame and cylinders	3,450kg mild carbon steel
	Fittings	50kg polypropylene
PLC control, electronics	Circuit components	2.5kg of refined silicon
Tooling	Abrasive media	10kg silicone polymer
		10kg boron carbide grit

*Volume replaced annually.

LCA often benefits from a limitation of scope, to exclude minor energy consuming activities, i.e. assembly of framework using electric drills, heating and lighting in the machine builder's workshops (distribution amongst other machines, factory space and offices) or short range transport of small consumable parts. Scope can be determined by questioning how responsible the end-user can/could/should be for the identified impacts – in this instance, Mollart chose to adopt the AFM process, setting in motion a sequence of events which led the machine builder to purchase components, component manufacturers to obtain raw material and raw material producers to mine and refine for industrial use. Mollart's liability could be considered to stretch back to the mining phase, but the onus is also on the mills, refineries, manufacturers and OEMs to ensure they minimise their impact.

Table 7.5 breaks down the contents of the machine and identifies 10 major materials groups; i.e. hydrocarbons are refined from crude oil, and production of light oil consumes 9.49MJ/L, requiring 198kWh and producing 88kgCO_2e. Total energy estimated to have been consumed while producing material for the machine is in excess of 1,800kgCO_2e, which is equivalent (The Carbon Trust, 2013) to a 17,000km flight from London to Sydney (per passenger km). Without including additional environmental burden such as pollutant from fuel used in transport or inefficient assembly practices, the values are not accrued through Mollart's actions, but by the OEM at the purchasing stage.

Table 7.5 – Core materials use in AFM machine.					
Material	QTY	Energy/QTY	Power kWh	$kgCO_2e$	Ref.
Hydrocarbon	75L	9.49MJ/L	198	88	(Szklo & Schaeffer, 2007)
Neodymium	2kg	1.1MWh/t	2.2	1	(Yanjia & Chandler, 2010)
Copper	2kg	64MJ/kg	36	16	(Williams, et al., 2002)
Gas R404A	1.5kg	-	-	5.85*	(Tassou, et al., 2009)
Nickel	0.191kg	8.7MWh/t	1.7	0.8	(Yanjia & Chandler, 2010)
Steel	3,450kg	480kWh/t	1,656	734	(Worrell, et al., 1999)
Polypropylene	50kg	81.6GJ/t	1,133	505	(Williams & Larson, 1987)
Silicon	$0.28m^2$	$0.34kWh/cm^2$	952	424	(Williams, et al., 2002)
Silicone	10kg	11.11MJ/kg	31	14	(Papaefthimiou, et al., 2006)
Boron Carbide	10kg	480kWh/t	4.8	2	(Worrell, et al., 1999)
Total	-	-	4,014.7	1,784.8	-
*Volume replaced annually (Forster, et al., 2007)					

Embodied energy as a concept leads the engineer to question whether operation consumes more energy than it took to produce, and if so, whether the operation of the process can justify the initial CO_2e penalty. If the AFM machine operated on a two-shift basis for 76h/wk and 51wk/yr, the machine would be in production mode for 80% of time – 3,100h. As an average draw of 4.485kW leads to 13.9MWh (GBP 1,722) (nearly 3.5 times as much energy as consumed in manufacture), the operating efficiency is of great importance during the use-phase. Compared to operation of the machine, approximately 6,200kgCO_2e is produced per annum – while over 25 years, the figure is 154tCO_2e putting the 'build:use' carbon equivalent ratio at 1:86. Potential to further separate the production-cost from the use-cost can be targeted using figure 7.7 – the chart uses data from table 7.5 to present materials use by share of CO_2e generation.

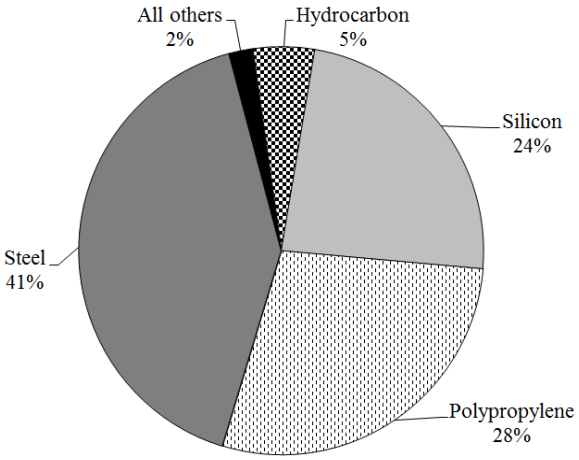

Figure 7.7 – Materials used in production.

Steel framework and machine fittings are highly energy consuming, using the electric arc furnace to smelt elements of steel and polymer production relying on initial refining of crude oil. Steel is an inexpensive yet strong and ductile construction material,

readily-recyclable and readily-available. In order to reduce the impact without using mechanically-unsuitable polymeric replacements, the only real option is to reduce overall consumption, or use different materials in a revised design. Using the (Hammond & Jones, 2008) inventory of carbon energy (v1.6a), it is possible to estimate the costs of energy and embodied CO_2e when selecting engineering materials. The values are higher than the production-only values used in table 7.5 as they include extraction, manufacturing and transportation, known as cradle-to-site. Exchanging the upper steel plate (670kg) (under bending load) for a steel I-beam, with the intention of reducing consumption and maintaining strength, should reduce by 562kg down to 108kg, saving approximately 27.2GJ. The identical steel base plate on the underside is capable of adopting the I- beam as well, and supporting steel framework is easily changed to granite – with manufacturing cost of 13.9MJ/kg, density of 2800kg/m^3 and strength in compression makes granite an attractive proposition.

7.6 Effects of ‘design for environment’ (DfE) upon process performance

Reductions in energy usage can be achieved by design changes, and increasing efficiency of individual components can significantly reduce the total energy consumption. For the following comparisons, a lifetime of 25yrs is considered, consuming 348MWh at today’s prices (total GBP 43,117).

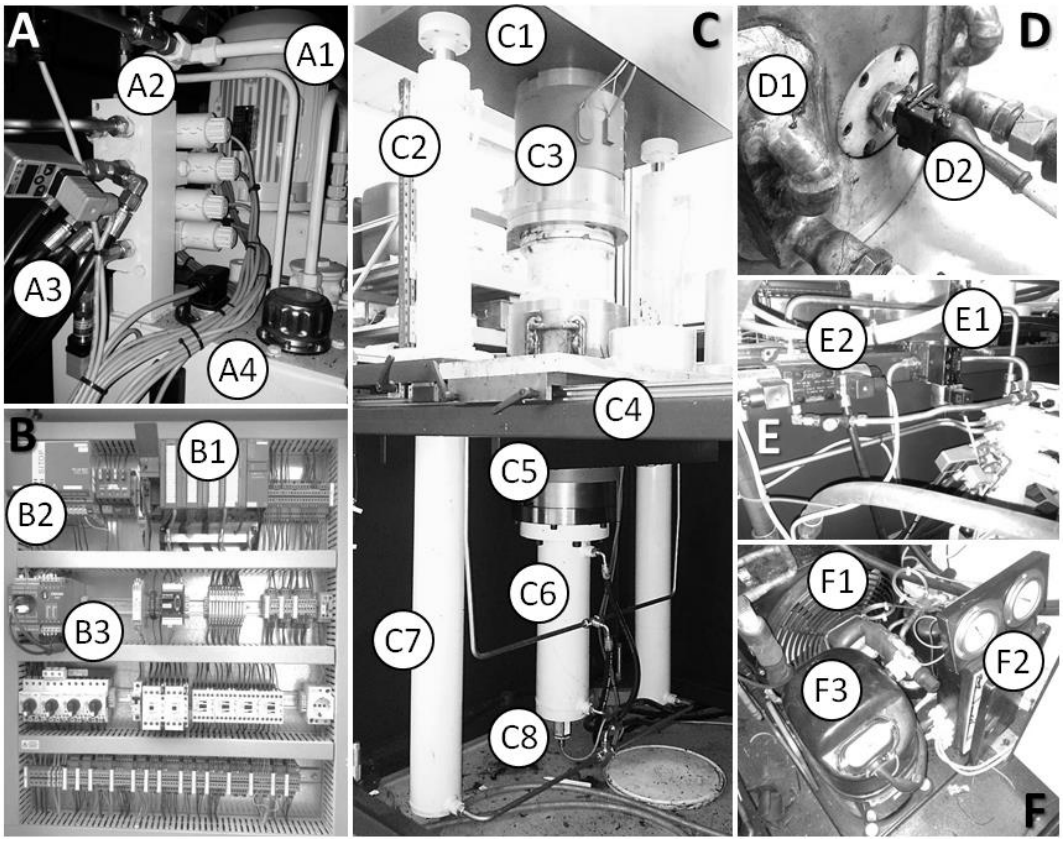

Figure 7.8 – Machine area breakdown for greening and assessment.

7.6.1 Temperature regulation system.

Regulation is performed by a permanently-on pair of silicone rubber-insulated wire heaters operating at 2x200W, accounting for 2.27A of the total 7.8A load. Cooling is performed by refrigerant gas fed through two bars over which the media flows. AFM generates thermal energy through friction; the system is weighted toward cooling by 60:40, translating to 3.4A (3.3kW). Active during 50% of the process, the current system consumes approximately 7.38MJ/h, costing nearly GBP 19,685 over machine life. Naturally, presence of active heating surfaces when cooling requirement exists is not efficient and would benefit from continuous low-energy input.

Redesigning to remove current heating and cooling systems has the potential to concentrate the consumption on a single unit, which can be specified to suit an improved efficiency target. A unit has been identified to heat and cool water, between

5˚c and 50˚c – operating at maximum input power of 9.27kW, comprised of a compressor at 2.7kW, water pump at 0.37kW, heating device at 6kW and control at 0.2kW. Cooling capacity is 7.91kW. Media chemistry, processing conditions and job geometry affect the rate of heating, therefore an example of 35˚c reduced to 25˚c is provided in equations 7.26 to 7.28. Specific heat for PDMS (Polydimethylsiloxane) is 1.552kJ/kg.K (Kuo, 1999).

$$Q = m\ cp\ dt / t \quad (7.26)$$

$$Q = (25 \times 1.552 \times -10) / 600 \quad (7.27)$$

$$Q = 0.646kW \quad (7.28)$$

Where Q is heat transfer (W), m is mass (kg), cp is specific heat (kJ/kg.K), dt is mean temperature difference (K) and t is time (s).

10min is an acceptable time to heat or cool the media in an AFM application, however, if the application is more aggressive and the rate of passive heating exceeds 0.016˚K/s (1˚c/min), more power will be consumed – an extreme example is 10˚c in 2min, requiring 3.23kW, which remains within 40% of total capacity. The change to a water-based heat-transfer fluid means the refrigerant used in the heat exchanger is sealed and does not form part of the working environment – all the nickel required in the heaters are removed and the system insulation is improved.

7.6.2 Machining strategy changes.

As shown in figure 7.5, current consumption is driven by pressure. Not all force applied by the ram is used effectively; AFM is constrained by a number of factors, perhaps the largest is the customer's geometry – it cannot be modified, and tooling must be designed to support it, however tooling can act as a funnel to feed the media over a feature, rather than allow the media free roam in and around a part. There are several sources of unnecessary pressure drop; 1) workpiece and tooling features that allow a machine to pump media onto a flat face, forcing it to find an alternative path, 2) lack of soft-start valves, forcing media into a restricting cavity (however well designed) – this reduces fatigue life of valves, tubes, pump components, tooling and carries a real risk of workpiece damage, and 3) use of tooling materials with porous surface structures, increasing friction significantly beyond that of rough metals. Polymeric materials are more elastic than most metals and more resistant to the ploughing mode of MR in AFM.

7.6.3 Wear rate on consumables.

Tooling, cylinder/pistons and media are considered replaceable elements in the AFM process. Tooling wears with use, but service life can be improved by careful design. Cylinders and pistons are in contact with media permanently. The longer they operate,

the wider they become and the rate expansion increases as the gap between cylinder and piston widens. Media is comprised of a solid and liquid phase, where the silicone-based liquid phase is susceptible to contamination, and further, degradation, by fluids commonly found in the manufacturing process. Complete removal of contaminants is virtually impossible, but altering the chemistry to one developed at Mollart Engineering has provided a resistance to rheological property changes. Pressure drop also plays a role in media life – excessive temperature generated by over-working may chemically-damage the polymer. Solid phase abrasive grains always outlast the polymer – it is possible to break down the carrier chemically and filter the grains for re-use. While the grit does not impact on figure 7.7, it is a consumable that is used continuously throughout the machine life (as is the silicone polymer) and carries a high production energy cost, as high as steel and hydrocarbon product manufacture.

7.7 Summary

Key findings in this chapter include the comparatively high energy demand from natural gas-fired warm air blow-heaters, a requirement for the heating of spaces for human labour activity. Performance is shown to be limited by design – the AFM machine in this study operates with only an additional 22% of current between idle mode and production mode (Dahmus & Gutowski, 2004) suggesting sub-assembly redesign may be of benefit. To conclude, the AFM process offers a clear route to sustainable part-finishing, low-maintenance and high potential for 'greening' when considering factors in addition to running cost.

AFM's flexibility as a manufacturing tool requires experience and basic fluid dynamics knowledge to operate, reducing the appeal to many potential users. For those users that have already invested and worked with the technology, its capability is not in question, and assessments made in this research suggest it is significantly more viable than manual processes in terms of environmental and economic cost. AFM has been considered in the 'production' and 'use' phases of operation. Key findings include;

- As applications for surface finishing on complex geometries increase with additive layer manufacturing technologies and exposure of AFM to a wider audience, the capability of AFM will lead to greater process uptake. Environmental and economic considerations must be made.
- Working conditions required for human labour increase the environmental and economic cost of manual finishing while repeatability and accuracy are no better. Initial fixturing saves material and machining cost, but when workpieces become more complex and tooling/media is reused in a repeat order scenario, AFM excels at reducing cost and increasing quality.
- Embodied energy in the process is high, roughly equivalent to a 24h airplane journey, although the long service life and potential to make CO_2e savings outweighs the initial cost.
- Potential for subassembly replacement as a means of 'greening' is high – the most promising technically as well as environmentally is the estimated 91% reduction in energy use by adopting a mode of operation similar to household combination boiler, providing a low but persistent energy input to prevent spikes.
- Priorities for further work include improved software to control machine motion, development of process simulation techniques to avoid unnecessary or inefficient tooling and retrofitting of described combined temperature regulation system.

Chapter 8 - Conclusions and Recommendations for Future Work

Industrial relevance and ‘practical novelty’ have been the key drivers of this research project; the findings have been obtained through academic means – designed experiments, scientific software and critical thought – those findings have been applied, tested and proven through industrial means, garnering a ‘stamp of approval’ in a harsh and demanding environment. This section identifies the major academic outputs and considers their importance, application and challenges a user overcomes by using them.

8.1 Conclusions.

The ten most important outputs are listed below, ranked as considered (subjectively) by the author. Outputs are mixed industrial and academic, and highlight the range of work carried out on this project. A summary is provided here;

- Geometry-independent prediction of post-process surface condition (hardware).
- Standard, non-complex testpiece design (hardware).
- Non-thermal method of media manufacture (knowledge).
- Technique for indexing abrasive potential (knowledge).
- Creation of virtual environment to preview fixture effect on flowpath (software).
- Knowledgebase framework for material erosion characteristic (knowledge).
- Causes of process deviation (knowledge).
- Formation of linear process to determine operating parameters (knowledge).
- Ranked order of effect of independent process variables (knowledge).
- Quick reference tools, derived from research output (hardware/knowledge).

8.1.1 Geometry-independent prediction of post-process surface condition.

Current academic works have proposed several models for the prediction of surface roughness, although they are largely all in a fixed geometry with no recourse for transferral of results to more complex workpieces. This leaves their work of limited importance due to poor potential for reapplication. The solution to this limitation is not to simply carry out more research in geometry representative of complex features, but to identify a technique that opens the door to any environment where fluid may flow freely. The approach in this project is to identify the process factors that are capable of replication in a simulation environment and to verify their relationship with surface condition through a virtual flow condition. Upon simulation of a complex geometry with the same simulated machine and media, the flow conditions will be visible and capable of combining with the surface condition in a simpler environment.

8.1.2 A standard, non-complex testpiece design.

Data collection proved problematic early in the project – it was known that a degree of error was present in processing factors and isolation of the effects of each could be aided by greater difference in the measured response variable. After scrapping one design for insignificant material removal and heavy post-processing requirement, the standard sample was developed and tested. There now exists a fixed manufacturing process, user-replaceable liners/bushes where the feed bore may wear, sample orientation correction, standard measurement procedures and useful measureable features without recourse for further machining to open those features to measurement instruments. The testpieces are of a size which facilitate affordable raw material purchase, in a size which the majority of modestly equipped machine shops are capable of producing with simple turning and milling operations. The raw material is also widely available in the vast majority of materials an engineering business can envisage processing. The testpiece's overall dimensions are helpful for storage and handling, and the overall dimensions of the testpiece support system allow installation on machines with piston diameters of 40mm or greater.

8.1.3 Methodology for non-thermal manufacture of abrasive media.

In a modern manufacturing environment, value is typically added through a high level of skill and experience in a specific process. In the development of an abrasive media, the main desire is to de-skill the media manufacturing process and prevent the requirement of additional time spent training in a chemical process which is far from a core-competency. If it becomes appropriate to at a later date, there is scope to upskill and develop the abrasive media as a self-sustaining product.

In this light, the subcontract relationship with Escubed will deliver a chemical product which requires no heating to produce, releases no harmful by-products, contains only readily available constituent materials and is manufactured through a simple weighing and mixing procedure.

8.1.4 Technique for indexing the abrasive potential of a media.

Current industrial research involves attempts at simulating a system whereby grit size, grit shape and grit volume are represented in a virtual media. As a by-product of this approach, an erosion model must be developed alongside greater detailed simulation of the surface structure of the workpiece materials. These requirements are currently beyond the reach of engineering simulation software packages. An alternative approach has been developed, which should also aid the transition of research into the shopfloor environment. The project approach consists of two data collection exercises through which machine parameters are varied and media configuration is varied. The constant between them is the geometry and the geometry materials, but there will undoubtedly

come a time when a media will be called-for which hasn't been tested within the confines of an experiment. It is known that media behaviour is driven not only by its internal forces, but also by external influences such as temperature and pressure. The result is that media can vary in abrasive potential, even when the contents of that media are fixed. In order to circumvent the software limitations, an abrasive potential index has been proposed which classifies the media's ability by the relationship between flow condition and abrasive quantity, where flow condition is the determinant of how the grit is delivered. The scale of abrasive potential is material-specific.

8.1.5 Creation of virtual environment to view effects of fixtures.

A by-product of the simulation system development, virtual tools and fixtures allows complex flowpath analysis. These fixture designs would have been limited to trial and error development, with limited ability for appraisal other than experiential – the technical contribution here is an optimisation of flow-field which helps to obtain uniform finishes and reduce pressure drops through identification of local blockages/restrictions. It is an iterative process, as there are often a limitless number of options when considering the parameters of a plug. The engineer must design with first principles in mind, then have their design verified virtually before proceeding with manufacture. This contribution will likely lead to highly complex tooling, ones which may not be manufacturable by traditional means – there is already effort being made to determine the feasibility of rapid prototyping plugs to allow full design freedom.

8.1.6 Development of a knowledge-base for workpiece erosion behaviour.

As an extension of the abrasive potential index, a thorough understanding of the wear resistance of particular materials in given flow conditions is invaluable. This project has seen consultation by OEMs working in the design of products that employ AFM manufacturing operations. Recently, assistance has been sought by large oil and gas OEMs in the design of a next generation oil and gas exploration tool, where there is desire to make the component more suitable for AFM. The simulation process derives nearly all of the knowledge to process a given component, but knowledge of material abrasive wear can be used in multiple ways;

- Material selection and geometry of tooling to increase durability
- Control of unwanted local erosion/ achievement of focused erosion
- Long-service components in machines erosion protection
- Understanding the trade-offs in processing time versus total erosion

8.1.7 Significant understanding of causes of process deviation (repeatability).

During discussions with the machine tool manufacturer, it has been recognised that process variance stems from three main sources. The first is within the media - polymer behaviour can vary batch to batch, and bulk behaviour can vary over time due to contaminants and loss of oils. This manifests itself in production jobs by media working fine until scheduled replacement is due, then process behaviour is not the same after the media change – it may not even be the same compared to when the previous media was new. The changes are often minor, but are down to the batch variation in industrial silicone production. The second source is largely agreed to be the machine variables piston stroke length and temperature delivery. These factors are in constant influence over a given processing length, meaning even a slight change in the two affects the overall abrasive potential of the media. The third factor is in the geometry of the production job itself – variation in burr size, surface finish or hole locations can negatively affect the AFM process. While a process model for a single workpiece (part of a batch) may be developed, there is no guarantee the process works for the next part.

These sources of error are quantified in the reports produced as part of individual work package progress, and while some error is inherently acceptable, some variation such as workpiece geometry is difficult to eliminate. Fortunately, the process methodology developed provides a range within which a specific response should be achieved – except for the rare situation where a specific surface finish or specific radius is required, the majority of the customer-required AFM features is specified as a range – this allows the process to select parameters which are known to provide the desired result, inclusive of the expected error.

Error and variance assessments have further significant benefits in future AFM development plans. Machine inaccuracies can be reduced with strategically positioned sensors, media inaccuracies can be controlled by accurate weighing and a batch viscosity check (not a rheometer check). In the future, an understanding of this deviation can be used to assess capability and aid purchase decisions of machinery that may be added to the plant list for the early subcontract service.

8.1.8 Formation of process to determine operating parameters.

Prior to this project, the ‘educated trial and error’ approach was the method of choice for establishing a process. There were many steps, involving multiple cleaning operations in-between test runs. Modifications to tooling and multiple AFM parameters were trialled. Even after that, it wasn’t possible to say which of your multiple processing steps had achieved the desired response, so a second trial was carried out, often involving reiterations to the previous ‘successful’ setup.

The answer to this unscientific approach is to adopt several of the processes from the research element of the project and propose a linear path to process setup. Assuming a

workpiece of titanium 6Al4V, the engineer takes a solid model of their complex workpiece and loads it as the geometry within the fluid simulation software package used in the previous studies. They make several initial choices for velocity and temperature, whereby the primary consideration is to ensure that the machine works within its mechanical limits – i.e. for an assumed media, ensure that pressure requirements are not excessive. A draft simulation is carried out using a media of viscosity that suits the desired flow speed. This provides a clear example of the flow condition at the POI (and everywhere else in the job). It also shows where flow is not uniform around any features that may constitute POIs – this facility allows a visual display of the effects of plugging and other tooling that may be used to divert or otherwise manage the flow as it approaches the POI. Corrections are made and a simulation is re-run. Looking at the type of surface condition desired at the POI, the engineer can adopt general findings from the experimental studies and choose a grit size and grain fraction with an API that sits within the range of the value of the desired response variable (i.e. for roughness over a surface, you may find that AP-5 provides the necessary level of abrasion within the given flow condition).

8.1.9 Ranked order of independent variables in order of effects.

Within machine and media studies, the effects of the six process variables are quantified – the magnitude of their effect is described through main effects and interactions plots. The practical application of this knowledge is in setup fire-fighting – if a setup does not yield the required results, or the engineer has been asked to complete the task in a limited timeframe, it is often useful to have ‘rules of thumb’ which can be considered as general knowledge and applied as seen fit. For example, if a surface finish improvement was required, early output shows quite clearly that raising the temperature has the greatest effect. Mean effects plots are the easiest way to graphically display these results – in terms of ranking, there is a conflict; it is easily argued that machine parameters are the simplest to change, despite potential for greater effect through media configuration change. In this case, ranked factors 1-3 would consist of machine parameters and factors 4-6 would be media parameters. Each of the factors have different and varying effects on surface condition – as surface condition is measured by roughness, peak height and material removal in this project, we can generate 18 rules of thumb (6 independent variables for 3 responses).

8.1.10 Development of quick reference process setup tools.

On the shopfloor, the complexity of research activities should ideally be hidden – it is neither helpful nor sensible to provide machine operators with all process knowledge and history of how processing levels were derived. In this vein, there are two options – either an engineer sets the process up and explicitly describes levels for machine and media, or the engineer can provide the operator with a quick reference tool which

allows the selection of levels from a number of pre-set environmental factors such a bore size, bore length, material, machine capacity, etc. Due to the variation in geometry and surface condition requirement of customer components (and the reliance on simulation for determining complex flow conditions), this technical contribution refers specifically to a number of reference tools much like an engineer’s slide rule.

8.2 Contributions to knowledge

Using the EngD handbook as prompts for headings, **original contributions** made in this doctoral thesis include;

- *Creation and interpretation of new knowledge – through original research or other advanced scholarship, that satisfies publication peer review;*
    - See publications list – two journal papers and two international conference papers published.
    - Two TSB grant applications successfully applied for and won, only one specifically for this project.
- *Systematic acquisition and understanding of substantial body of knowledge at the forefront of field;*
    - Method of utilising computational fluid dynamics (CFD) to derive a suitable process model for the productive and reproducible control of the AFM process, including identification of core physical phenomena responsible for driving erosion
    - Comprehensive understanding of effects of B_4C-loaded polydimethylsiloxane variants used to process Ti6Al4V in the AFM process, including prediction equations containing numerically-verified second order interactions (factors grit size, grain fraction and modifier concentration);
    - Equivalent understanding of machine factors providing energy input, studying velocity, temperature and quantity (verified predictions are made from data collected in Ti6Al4V substrate material using response surface methodology);
    - Holistic method of translating process data in control-geometry to an arbitrary geometry for industrial gain, extending to a framework for collecting new data and integrating into current knowledge.
- *Ability to conceptualise design and implement a project for generation of new knowledge, applications or understanding;*
    - By the time of the application, a methodology had been devised which integrated empirical data with a software-based simulated environment. Utilising computational fluid dynamics (CFD) in the process was (and is) recognised to be a novel contribution, and a reason for the TSB's acceptance of the application. Their involvement commencing September 2012 added some much needed structure, but also an additional administrative layer;
    - Application of methodology using research-derived CFD correlation, applied to complex geometry proven by measured process output.

8.3 Recommendations for future research and development.

Using STEER (socio-cultural, technological, economic, ecological and regulatory factors) and opportunities and threats identifications, this subsection address the way forward for the outputs of this research work.

8.3.1 STEER analysis.

8.3.1.1 Socio-cultural factors.

The process will offer a mechanised alternative, forcing a change of skill-set amongst the workforce. Some may consider this a negative effect, although it allows employment of low-skilled operators and re-assign the skilled to another role. This step-change in manufacturing arrangements provides customers with a surety that the parts they receive will be consistent from batch to batch. It also allow continuous improvement through logical and scientific means, instead of coping with repeatability and reproducibility issues associated with human error.

8.3.1.2 Technological factors.

In practical terms, there is an implementation perspective that requires some attention – the project is nearing the completion of datasets needed to correlate the measured results with a flow condition, length, workpiece material and abrasive potential of the media – the complicated nature of the integration activity may occur to a lesser or similar extent for every new geometry. There will need to be a two-level process setup in some cases – likely a machine operator will not need to contend with complex simulation work and will rely on a graduate engineer to deal with the initial system setup.

Conditions for long-part processing have not changed since the start of the project – we do now have a greater appreciation of the issues associated with 1.6m long bores – a proposal has been made to design an intricate fixture which excludes processing the long bores – the entry of the long bores is the POI.

8.3.1.3 Economic factors.

The process will be established in stages, as a complementary tool to current manufacturing operations – this will reduce the risk that a number of commercial customers are taken on too early, resulting in a poor output and limited success. Similar to many finishing processes, the AFM process is carried out near the end of a large number of operations, where risk to damaging features and scrapping workpieces is higher than further upstream in the manufacturing process. AFM is unique in its non-aggressive, mechanical, low material-removal-rate characteristic, reducing concerns of damaged workpieces. These parts can be of high value, and manufacturers can suffer

directly as a result of late deliveries or concession requests. Orders will reduce, so will complexity and margins will suffer as a result. AFM is a highly useful process in economic terms – not only can we reduce human labour needed, but we can also replicate the actions of several other types of machine tools - the case for labour reduction is strong and proven - AFM can carry out 5 operations & tackle multiple parts. The results achievable through the AFM process will be worth up to £150/hr, contributing to a further 25% increase year on year (2012-13; £20m) (2013-14: £25m).

8.3.1.4 Ecological factors.

Supply of chemicals in media developed is currently a shipping-heavy activity. The modifier is sourced in Belgium, the polymer from the USA and the grits from China, although all purchased through UK agents. Stock-holding arrangements will be tackled with these suppliers to minimise the damage caused by air- and sea-freight. Shorter response times should be possible when considering supply from UK-manufactured sources – sadly these heavy industries are not always available, and the polymer is a proprietary product – an alternative must be sourced, or a partner found to work on a synthesis method.

8.3.1.5 Regulatory factors.

Factors at play in the installation of a functioning AFM process include the health and safety at work act, environment act and other worker/environment protection schemes to limit exposure to harmful products in the workplace or around the factory. Special consideration must be given to the handling of some of the products in use – they are not common engineering materials and new users will need to be trained. In the area of media mixing, new machinery training must be provided, giving guidance on chemical handling and mixing techniques. The same applies to the use of specialist cleaning equipment and chemicals designed to break down silicones.

Sale of media may be subject to agreement of constituent parts suppliers, i.e. Dow Corning, Acros Organics and ABSCO materials. Further investigation must be made.

8.3.2 Opportunities and exploitation targets.

Target markets for the CFD-aided AFM process are suggested below.

8.3.2.1 Additive layer manufacturing opportunities.

Greater widespread acceptance of 3D-printing processes should be exploited – many manufacturers have been offering the service in non-functional and light-duty plastic grades for years, however with the advent of 99.9% non-porous metallic components

created through the DMLS process gaining traction with medical manufacturers, the shortcomings of the process are clear - poor surface finishes are a an unavoidable side effect of sintering a 40µm layer of powder, as you uncontrollably generate heat and sinter randomly orientated particles in the vicinity of the target.

8.3.2.2 Machinery construction.

Machines are very simple to construct – comprised of two opposing cylinders, the MTT machine's only real novelty is its moulded polymeric piston head seal and software – it is possible to improve upon these designs and through usage, offer more appropriate and customisable products to a customer base.

8.3.2.3 Modular tooling.

Designing modular, quick-release tooling may serve simple applications better than complex fixtures. Cost and lead time can be reduced, while capability may be sufficient for the job.

8.3.2.4 Media manufacture and sale.

Only two providers are known to sell media on a (highly profitable) commercial basis – configuration of media determines application suitability, and for many customers, the media they use would be the media they replace, preventing competition from third party suppliers. However, not all machines in existence are MTT or EH machines and several manufacturers do not exist anymore, so users are perhaps more willing to try an alternative product.

8.3.2.5 Alternative manufacturing processes.

The ability of the process to offer multiple manufacturing operations (lapping, honing, grinding) within limits is an attractive proposition to enhance environmental credentials and reduce energy usage.

8.3.2.6 Quality and repeatability improvement.

During previous discussions with a potential customer, awareness of customer attitudes to finishing processes has increased. Cost is not the primary concern, but quality and repeatability are. Customers are willing to pay for a better service.

8.3.2.7 Extreme complexity work.

Oil and gas customers are aware of the process and some have begun requesting its use in turnkey project work. These jobs are inevitably complex and require some planning and testing at the current level of knowledge, but greater confidence could be held in a tooling and media solution following this project. Ability to test some rather extreme designs is also made available.

8.3.2.8 Miscellaneous hardware development projects.

Throughout the course of the project, there have been numerous hardware development avenues to supplement the process and increase usability;

- High viscosity rheometer
- Lubrication in media
- Increased sensor array and closed-loop feedback to PLC to minimise high magnitude response errors
- High pressure benchtop machine to exploit medical and automotive sectors
- Studies of metallurgical effects to aid cavitation resistance in marine sector

References

Ali-Tavoli, M., Nariman-Zadeh, N., Khakhali, A. & Mehran, M., 2006. Multi-Objective Optimization of Abrasive Flow Machining Processes Using Polynomial Neural Networks and Genetic Algorithms. *Machinining Science and Technology: An International Journal,* pp. 491-510.

Arief, I. & Chen, X., 2010. *Key Parameters in Loose Abrasive Machining.* Huddersfield, UK, University of Huddersfield, pp. 1-5.

Aurich, J. C. et al., 2009. Burrs - Analysis, Control and Removal. *CIRP Annals - Manufacturing Technology,* Volume 58, pp. 519-542.

Avramescu, V. et al., 2008. *Technologies and Equipments for Complex Surfaces Nanofinishing by Abrasive Flowing with Reopectic Work Mediums.* Oradea, Romania, Oradea University, pp. 41-48.

Baehre, D., Bruennet, H. & Swat, M., 2012. *Investigation of One-Way Abrasive Flow Machining and In-Process Measurement of Axial Forces.* Saarbrucken, Germany, Elsevier B. V., pp. 419-424.

Balasubramaniam, R., Krishnan, J. & Ramakrishnan, N., 1998. Investigation of AJM for Deburring. *Journal of Materials Processing Technology,* Volume 79, pp. 52-58.

Baniszewski, B. B. E., 2005. *An Environmental Impact Analysis of Grinding,* Cambridge, Massachusetts, USA: http://dspace.mit.edu/handle/1721.1/32880.

Barletta, M., Guarino, S., Rubino, G. & Tagliaferri, V., 2007. Progress in Fluidized Bed Assisted Abrasive Jet Machining (FB-AJM): Internal Polishing of Aluminium Tubes. *International Journal of Machine Tools and Manufacture,* Volume 47, pp. 483-495.

Bin, W., Wei, C., Jin, C. & Xia, C., 2012. *A New Type of Nozzle AFM Machine Tool and Control System Research.* Chengdu, China, IEEE, pp. 2314-2318.

Brar, B. S., Walia, R. S. & Singh, V. P., 2010. *State of Art Abrasive Flow Machining.* Talwandi Sabo, India, Punjabi University, pp. 128-132.

Brinksmeier, E., Riemer, O. & Gessenharter, A., 2006. Finishing of Structured Surfaces by Abrasive Polishing. *Precision Engineering,* Volume 30, pp. 325-336.

Brinksmeier, E., Riemer, O., Gessenharter, A. & Autschbach, L., 2004. Polishing of Structured Molds. *CIRP Annals, Manufacturing Technology,* Volume 53, pp. 247-250.

British Government (HMG), 2013. *www.legislation.gov.uk - The Workplace (Health, Safety and Welfare) Regulations 1992.* [Online]
Available at: http://www.legislation.gov.uk/uksi/1992/3004/made/data.pdf
[Accessed 12 January 2014].

Campos-Amezcua, A. et al., 2007. Numerical Study of Erosion Due to Solid Particles in Steam Turbine Blades. *Numerical Heat Transfer, Part A: Applications: An International Journal of Computation and Methodology,* pp. 667-684.

Chastagner, M. W. & Shih, A. J., 2007. *Abrasive Jet Machining for Edge Generation.* Michigan, USA, North American Manufacturing Research Institution, Society of Manufacturing Engineers, pp. 359-366.

Cheema, M. S., Venkatesh, G., Dvivedi, A. & Sharma, A. K., 2012. Developments in Abrasive Flow Machining: a Review on Experimental Investigations Using Abrasive Flow Machining Variants and Media. *Proceedings of the Institution of Mechanical Engineers, Part B: Journal of Engineering Manufacture,* pp. 1951-1962.

Cheng, K., 2001. Abrasive Micromachining and Microgrinding. In: *Micromachining of Engineering Materials.* New York, USA: CRC Press, pp. 85-123.

Cherian, J. & Issac, J. M., 2013. Effect of Process Variables in Abrasive Flow Machining. *International Journal of Emerging Technology and Advanced Engineering,* pp. 554-557.

Chryssolouris, G., 1991. *Laser Machining-Theory and Practice.* 1st ed. Cambridge,MA): MIT.

Claudin, C. & Rech, J., 2009. Development of a New Rapid Characterisation Method of Hob's Wear Resistance in Gear Manufacturing - Application to the Evaluation of Various Cutting Edge Preparations in High Speed Dry Gear Hobbing. *Journal of Materials Processing Technology,* pp. 5152-5160.

CNCMedia Kft., 2011. *Renishaw PH20.* [Online]
Available at: http://www.cnc.hu/wp-content/uploads/2011/06/Renishaw-PH20.jpg
[Accessed 31 October 2013].

Coord3 Industries SRL, 2011. *CMM Scanning Deflection Diagram.* [Online]
Available at: http://www.coord3-cmm.com/wp-content/uploads/2011/10/CMM-Scanning-Deflection-Diagram11.png
[Accessed 31 October 2013].

Dabrowski, L., Marciniak, M. & Szewczyk, T., 2006b. Analysis of Abrasive flow Machining with an Electrochemical Process Aid. *Proceedings of the Institution of Mechanical Engineers, Part B: Journal of Engineering Manufacture,* pp. 397-403.

Dabrowski, L., Marciniak, M., Wieczorek, W. & Zygmunt, A., 2006a. Advancement of Abrasive Flow Machining Using an Anodic Solution. *Journal of New Materials for Electrochemical Systems,* Volume 9, pp. 439-445.

Dahmus, J. B. & Gutowski, T. G., 2004. *An Environmental Analysis of Machining.* Anaheim, California, USA, ASME International Mechanical Engineering Congress and RD&D Expo.

Das, M., Jain, V. K. & Ghoshdastidar, P. S., 2008. Analysis of Magnetorheological Abrasive Flow Finishing. *International Journal of Advanced Manufacturing Technology,* Volume 38, pp. 613-621.

Das, M., Jain, V. K. & Ghoshdastidar, P. S., 2010. Nano-Finishing of Stainless-Steel Tubes Using Rotational Magnetorheological Abrasive Flow Finishing Process. *Machining Science and Technology: An International Journal,* 14(3), pp. 365-389.

Davidson, D., 2007. Surface Condition Impacts Part Performance. *Metalfinishing,* February, pp. 22-31.

Davidson, D. & MacKay, K., 2009. Meeting the Lean Deburring Challenge. *Metalfinishing,* May, pp. 18-21.

Davies, P. J. & Fletcher, A. J., 1995. The Assessment of the Rheological Characteristics of Various Polyborosiloxane/Grit Mixtures as Utilized in the Abrasive Flow Machining Process. *Proceedings of the Institution of Mechanical Engineers, Part C: Journal of Mechanical Engineering Science,* Volume 209, pp. 409-418.

Deepak, S. S. K., 2012. Applications of Different Optimization Methods for Metal Cutting Operations - A Review. *Research Journal of Engineering Sciences,* 1(3), pp. 52-58.

Draganescu, F., Gheorghe, M. & Doicin, C. V., 2003. Models of Machine Tool Efficiency and Specific Consumed Energy. *Journal of Materials Processing Technology,* 141(1), pp. 9-15.

Duleba, B., Greskovic, F. & Sikora, J. W., 2011. *Materials and Finishing Methods of DMLS Manufactured Parts,* Kosice, Slovakia: Technical University of Kosice.

Fang, L. et al., 2009. Temperature as Sensitive Monitor for Efficiency of Work in Abrasive Flow Machining. *Wear,* Volume 266, pp. 678-687.

Finnie, I., 1995. Some Reflections on the Past and Future of Erosion. *Wear,* Volume 186-187, pp. 1-10.

Finnie, I., Stevick, G. R. & Ridgely, J. R., 1992. The Influence of Impingement Angle on the Erosion of Ductile Metals by Angular Abrasive Particles. *Wear,* Volume 152, pp. 91-98.

Fioravanti, A. & Fletcher, A. J., 1996. Thermal Investigation of a Honing Process Utilizing Polyborosiloxane Impregnated with Abrasive Particles. *Proceedings of the Institution of Mechanical Engineers, Part C: Journal of Mechanical Engineering Science,* Volume 210, pp. 43-50.

Forster, P. et al., 2007. Changes in Atmospheric Constituents and in Radiative Forcing. In: S. Solomon, et al. eds. *Climate Change 2007: The Physical Science Basis. Contribution of Working Group I to the Fourth Assessment Report of the Intergovernmental Panel on Climate Change.* Cambridge, UK: Cambridge University Press, pp. 129-234.

Galantucci, L. M., Lavecchia, F. & Percoco, G., 2009. Experimental Study Aiming to Enhance the Surface Finish of Fused Deposition Modeled Parts. *CIRP Annals - Manufacturing Technology,* Volume 58, pp. 189-192.

Gessenharter, A., Riemer, O. & Brinksmeier, E., 2003. *Polishing Processes for Structured Surfaces.* Portland, OR, USA, American Society for Precision Engineering, pp. 579-582.

Gopal, A. V. & Rao, P. V., 2003. Selection of Optimum Conditions for Maximum Material Removal Rate with Surface Finish and Damage as Constraints in SiC Grinding. *International Journal of Machine Tools and Manufacture,* Volume 43, pp. 1327-1336.

Gorana, V. K., Jain, V. K. & Lal, G. K., 2004. Experimental Investigation into Cutting Forces and Active Grain Density During Abrasive Flow Machining. *International Journal of Machine Tools and Manufacture,* Volume 44, pp. 201-211.

Gorana, V. K., Jain, V. K. & Lal, G. K., 2006b. Forces Prediction During Material Deformation in Abrasive Flow Machining. *Wear,* Volume 260, pp. 128-139.

Gorana, V. K., Jain, V. K. & Lal, G. K., 2006b. Prediction of Surface Roughness During Abrasive Flow Machining. *International Journal of Advanced Manufacturing Technology,* Volume 31, pp. 258-267.

Gutowski, T., Dahmus, J. & Thiriez, A., 2006. *Electrical Energy Requirements for Manufacturing Processes.* Leuven, Belgium, CIRP International Conference of Life Cycle Engineering (13th).

Gutowski, T. et al., 2005. Environmentally Benign Manufacturing: Observations from Japan, Europe and the United States. *Journal of Cleaner Production,* 13(1), pp. 1-17.

Haan, J. J. & Steif, P. S., 1998. Abrasive Wear Due to the Slow Flow of a Concentrated Suspension. *Wear,* Volume 219, pp. 177-183.

Hammond, G. P. & Jones, C. I., 2008. Embodied Energy and Carbon in Construction Materials. *Proceedings of the Institution of Civil Engineers,* 161(2), pp. 87-98.

Heisel, U. & Schaal, M., 2008. Burr Formation in Intersecting Holes. *Production Engineering,* Volume 2, pp. 55-62.

Howard, M. & Cheng, K., 2013. An industrially feasible approach to process optimisation of abrasive flow machining and its implementation perspectives. *Proceedings of the Institution of Mechanical Engineers, Part B: Journal of Engineering Manufacture,* 227(11), pp. 1748-1752.

Howard, M. J., Cheng, K. & Mollart, G. A., 2012. *Abrasive Flow Machining; R&D Strategy & Challenges in Industrial Applications.* Tenth International Conference on Manufacturing Research, Birmingham, Aston University, UK.

Hughes, A. & Mina, A., 2012. *The UK R&D Landscape; Enhancing Value Task Force,* Cambridge, UK: UK Innovation Research Centre, University of Cambridge.

Jain, N. K. & Jain, V. K., 2001. Modeling of Material Removal in Mechanical Type Advanced Machining Processes: a State-of-Art Review.. *International Journal of Machine Tools & Manufacture,* 41(1), pp. 153-1635.

Jain, R. K. & Jain, V. K., 2000. Optimum Selection of Machining Conditions in Abrasive Flow Machining Using Neural Network. *Journal of Materials Processing Technology,* Volume 108, pp. 62-67.

Jain, R. K. & Jain, V. K., 2001. Specific Energy and Temperature Determination in Abrasive Flow Machining Process. *International Journal of Machine Tools and Manufacture,* Volume 41, pp. 1689-1704.

Jain, R. K. & Jain, V. K., 2003. Finite Element Simulation of Abrasive Flow Machining. *Proceedings of the Institution of Mechanical Engineers, Part B: Journal of Engineering Manufacture,* Volume 217, pp. 1723-1736.

Jain, R. K. & Jain, V. K., 2004. Stochastic Simulation of Active Grain Density in Abrasive Flow Machining. *Journal of Materials Processing Technology,* Volume 152, pp. 17-22.

Jain, R. K., Jain, V. K. & Dixit, P. M., 1999. Modeling of Material Removal and Surface Roughness in Abrasive Flow Process. *International Journal of Machine Tools and Manufacture,* Volume 39, pp. 1903-1923.

Jain, R. K., Jain, V. K. & Kalra, P. K., 1999. Modelling of Abrasive Flow Machining Process: A Neural Network Approach. *Wear,* Volume 231, pp. 242-248.

Jain, R. K., Ranganatha, C. & Muralidhar, K., 2001. Evaluation of Rheological Properties of Medium for AFM Process. *Machining Science and Technology,* 5(2), pp. 151-170.

Jain, V. K., 2008. Abrasive-Based Nano-Finishing Techniques; an Overview.. *Machining Science and Technology: An International Journal,* 12(3), pp. 257-294.

Jain, V. K. & Adsul, S. G., 2000. Experimental Investigations into Abrasive Flow Machining. *International Journal of Machine Tools and Manufacture,* Volume 40, pp. 1003-1021.

Jain, V. K., Kumar, R., Dixit, P. M. & Sidpara, A., 2009. Investigations into Abrasive Flow Finishing of Complex Workpieces Using FEM. *Wear,* Volume 267, pp. 71-80.

Jayswal, S. C., Jain, V. K. & Dixit, P. M., 2005. Modelling and Simulation of Magnetic Abrasive Finishing Process. *International Journal of Advanced Manufacturing Technology,* Volume 26, pp. 477-490.

Jha, S. & Jain, V. K., 2004. Design and Development of the Magnetorheological Abrasive Flow Finishing (MRAFF) Process. *International Journal of Machine Tools and Manufacture,* Volume 44, pp. 1019-1029.

Jha, S. & Jain, V. K., 2006. Nano-Finishing Techniques. In: *Micromanufacturing and Nanotechnology.* Heidelberg, Berlin, Germany: Springer, pp. 171-195.

Jha, S. & Jain, V. K., 2009. Rheological characterization of Magnetorheological Polishing Fluid for MRAFF. *International Journal of Advanced Manufacturing Technology,* Volume 42, pp. 656-668.

Ji, S. M., Xiao, F. Q. & Tan, D. P., 2010. Analytical Method for Softness Abrasive Flow Field Based On Discrete Phase Model. *Science China Technological Sciences,* 53(10), pp. 2867-2877.

Kao, C. C. & Shih, A. J., 2007. Form Measurements of Micro Holes. *Measurement Science and Technology,* Volume 18, pp. 3603-3611.

Kar, K. K. et al., 2009a. Performance Evaluation and Rheological Characterization of Newly Developed Butyl Rubber Based Media for Abrasive Flow Machining Process. *Journal of Materials Processing Technology,* Volume 209, pp. 2212-2221.

Kar, K. K. et al., 2009b. Preferential Media for Abrasive Flow Machining. *Journal of Manufacturing Science and Engineering,* Volume 131, pp. 011009, 1-11.

Kelly, K. M., 2005. Denso Seeks Next Diesel Breakthrough. *Automotive Design and Production*, November, 117(11), p. 36.

Kenda, J., Pusavec, F., Kermouche, G. & Kopac, J., 2011. Surface Integrity in Abrasive Flow Machining of Hardened Tool Steel AISI D2. *Procedia Engineering,* Volume 19, pp. 172-177.

Kim, J. D. & Kim, K. D., 2004. Deburring of Spring Collected by Abrasive Flow Machining. *International Journal of Advanced Manufacturing Technology,* Volume 24, pp. 469-473.

Kulikov, O. & Hornung, K., 2005. *Novel Processing Aid Based on Modified Silly Putty.* Moscow, Russia, Institute for Problems in Mechanics of R.A.S..

Kumar, S. & Manna, A., 2010. *Micro Finishing by Developed Extrusion Abrasive Flow Machining Setup.* Talwandi Sabo, India, Punjabi University, pp. 112-114.

Kuo, A. C. M., 1999. Poly(dimethylsiloxane). In: *Polymer Data Handbook.* New York, NY, USA: Oxford University Press, pp. 411-435.

Lam, S. S. Y. & Smith, A. E., 1997. *Process Monitoring of Abrasive Flow Machining Using a Neural Network Predictive Model.* Miami Beach, FL, USA, Institute of Industrial Engineers, pp. 477-482.

Levko, V. A., 2009. Calculation of Surface Roughness in Abrasive-Extrusion Machining on the Basis of Contact-Interaction Model. *Aircraft Production Technology,* 52(1), pp. 59-62.

Li, J. et al., 2009. *Design and Simulation for Micro-Hole Abrasive Flow Machining.* Wenzhou, China, IEEE, pp. 815-820.

Li, J. et al., 2009. *A Method of Motion Control About Micro-Hole Abrasive Flow Machining Based on Delphi Language.* Changchun, China, IEEE, pp. 1444-1448.

Lin, Y. C., Chow, H. M., Yan, B. H. & Tzeng, H. J., 2007. Effects of Finishing in Abrasive Fluid Machining on Microholes Fabricated by EDM. *International Journal of Advanced Manufacturing Technology,* Volume 33, pp. 489-497.

Loveless, T. R., Williams, R. E. & Rajurkar, K. P., 1994. A Study of the Effects of Abrasive Flow Finishing on Various Machined Surfaces. *Journal of Materials Processing Technology,* Volume 47, pp. 133-151.

Lunn, M. F., Troup, D. P., Miller, R. A. & Delo, D. P., 2006. *Abrasive Machining Media Containing Thermoplastic Polymer.* World, Patent No. 2006007554 .

Mali, H. S. & Manna, A., 2009. Current Status and Application of Abrasive Flow Finishing Processes: a Review. *Proceedings of the Institution of Mechanical Engineers, Part B: Journal of Engineering Manufacture,* Volume 223, pp. 809-820.

Mali, H. S. & Manna, A., 2010. Optimum Selection of Abrasive Flow Machining Conditions During Fine Finishing of Al 15 wt% SiC-MMC Using Taguchi Method. *International Journal of Advanced Manufacturing Technology,* Volume 50, pp. 1013-1024.

Malkin, S., 1981. Grinding Cycle Optimization. *CIRP Annals - Manufacturing Technology,* 30(1), pp. 223-226.

Mao, T. F. et al., 2010. Experimental Investigation of Abrasive Jet Polishing on the Free-Form Machined Surfaces of SKD61 Mold Steel Using SiC Particles. *Materials and Manufacturing Processes,* Volume 25, pp. 965-973.

Mazurkiewicz, M., 2000. A Manufacturing Tool for a New Century. *Journal of Materials Processing Technology,* Volume 106, pp. 112-118.

McCarty, R. W., 1970. *Method of Honing by Extruding.* United States, Patent No. 3,521,412.

McGeough, J., 2005. *Electrochemical Machining (ECM),* Edinburgh, UK: http://electrochem.cwru.edu/encycl/art-m03-machining.htm.
Meteorological Office Hadley Centre for Climate Change (Tim Legg), 2013. *Hadley Centre Central England Temperature (HadCET) dataset,* Exeter, UK: http://www.metoffice.gov.uk/hadobs/hadcet/.

Mitchell, C. M. & Laufer, E. E., 1980. Surface Structure in an Abraded Titanium Alloy. *Wear,* Volume 61, pp. 111-124.

Mollah, A. A. & Pratihar, D. K., 2008. Modeling of TIG Welding and Abrasive Flow Machining Processes Using Radial Basis Function Networks. *International Journal of Advanced Manufacturing Technology,* Volume 37, pp. 937-952.

Momber, A. W., Mohan, R. S. & Kovacevic, R., 1999. On-Line Analysis of Hydro-Abrasive Erosion of Pre-Cracked Materials by Acoustic Emission. *Theoretical and Applied Fracture Mechanics,* Volume 31, pp. 1-17.

Morrow, W. R. et al., 2004. *Laser-Based and Conventional Tool and Die Manufacturing: Comparison of Environmental Aspects.* Berlin, Germany, Global Conference on Sustainable Product Development and Life Cycle Engineering.

Mukherjee, I. & Ray, P. K., 2008. Optimal Process Design of Two-Stage Multiple Responses Grinding Processes Using Desirability Functions and Metaheuristic Technique. *Applied Soft Computing,* Volume 8, pp. 402-421.

Mukherjee, S. K., Kumar, S. & Srivistava, P. K., 2005. Effect of Over Voltage on Material Removal Rate During Electrochemical Machining. *Tamkang Journal of Science and Engineering,* 8(1), pp. 23-28.

Nakano, Y. et al., 1991. Improvement in Dynamic Characterstics of Surface Grinding Machines with a Horizontal Spindle and Reciprocating Work-Table by Means of a New Type of Dynamic Damper. *Precision Engineering,* 13(3), pp. 177-183.

Narayanasamy, K., Raju, H. P., Srinivasa, Y. G. & Krishnamurthy, R., 2004. *Flexible Super Finishing Process For Intricate Shapes.* Orlando, FL, USA, American Society for Precision Engineering, p. N/A.

OECD, 2012. *OECD Science, Technology and Industry Outlook,* n/a: Organisation for Economic Cooperation and Development.

Oliveira, J. F. G., Silva, E. J., Guo, C. & Hashimoto, F., 2009. Industrial Challenges in Grinding. *CIRP Annals - Manufacturing Technology,* Volume 58, pp. 663-680.

Papaefthimiou, S., Syrrakou, E. & Yianoulis, P., 2006. Energy Performance Assessment of an Electrochromic Window. *Thin Solid Films,* 502(1), pp. 257-264.

Patel, K. M., Pandey, P. M. & Rao, P. V., 2009. Determination of an Optimum Parametric Combination Using a Surface Roughness Prediction Model for EDM of Al2O3/SiCw/TiC Ceramic Composite. *Materials and Manufacturing Processes,* 24(6), pp. 675-682.

Perry, K. E., 1977. *Abrasive Flow Machining Method and Tooling.* United States, Patent No. 4,005,549.

Petri, K. L., Billo, R. E. & Bidanda, B., 1998. A Neural Network Process Model for Abrasive Flow Machining Operations. *Journal of Manufacturing Systems,* 17(1), pp. 52-64.

Pontes, F. J. et al., 2010. Artificial Neural Networks for Machining Processes Surface Roughness Modeling. *International Journal of Advanced Manufacturing Technology,* Volume 49, pp. 879-902.

PriceWaterhouseCoopers LLP, 2009. *The Future of UK Manufacturing: Reports of its Death are Greatly Exaggerated,* London, UK: PriceWaterhouseCoopers LLP.

Proctor, F. M. & Murphy, K. N., 1989. *Advanced Deburring System Technology.* San Francisco, CA, USA, The Pennsylvania State University, pp. 1-11.

Rajesha, S., Venkatesh, G., Sharma, A. K. & Kumar, P., 2010. Performance Study of a Natural Polymer Based Media for Abrasive Flow Machining. *Indian Journal of Engineering and Materials Science,* Volume 17, pp. 407-413.

Raju, H. P., Narayanasamy, K., Srinivasa, Y. G. & Krishnamurthy, R., 2005. Characteristics of Extrude Honed SG Iron Internal Primitives. *Journal of Materials Processing Technology,* Volume 166, pp. 455-464.

Ravikumar, N. L. et al., 2012. Surface Finishing of Carbon-Carbon Composites Using Abrasive Flow Machining. *Fullerenes, Nanotubes and Carbon Nanostructures,* 20(2), pp. 170-182.

Rech, J., 2006. Influence of Cutting Edge Preparation on the Wear Resistance in High Speed Dry Gear Hobbing. *Wear,* Volume 261, pp. 505-512.

Renishaw PLC, 2011. *Brochure, SP25M the worlds most compact and versatile scanning probe system.* [Online] Available at: http://www.renishaw.com/media/pdf/en/0fd4b33de94b434a9e0b5b86f9447870.pdf [Accessed 31 October 2013].

Rhoades, L., 1991. Abrasive Flow Machining: A Case Study. *Journal of Materials Processing Technology,* Volume 28, pp. 107-116.

Rhoades, L. J., Nokovich, P., Kohut, T. & Johnson, F. E., 1987. *Method of Controlling Flow Resistance in Fluid Orifice Manufacture.* World, Patent No. WO 87/05552.
Ridgway, M., 2013. *Speech; British Engineering - World Class comes as Standard.* Birmingham: Manufacturing Technologies Association.

Sadiq, A. & Shunmugam, M. S., 2009. Investigation into Magnetorheological Abrasive Honing (MRAH). *International Journal of Machine Tools and Manufacture,* Volume 49, pp. 554-560.

Sadiq, A. & Shunmugam, M. S., 2010. A Novel Method to Improve Finish on Non-Magnetic Surfaces in Magnetorheological Abrasive Honing Process. *Tribology International,* Volume 43, pp. 1122-1126.

Samsonov, G. V. & Gaevskaya, L. A., 1975. Abrasive Properties of Micropowders of Refractory Metal Carbides. *Poroshkovaya Metallugiya,* 164(8), pp. 60-63.

Sankar, M. R., Jain, V. K. & Ramkumar, J., 2009b. Experimental Investigations into Rotating Workpiece Abrasive Flow Machining. *Wear,* Volume 267, pp. 43-51.

Sankar, M. R., Jain, V. K. & Ramkumar, J., 2010. Rotational Abrasive Flow Finishing (R-AFF) Process and its Effects on Finished Surface Topography. *International Journal of Machine Tools and Manufacture,* Volume 50, pp. 637-650.

Sankar, M. R., Jain, V. K., Ramkumar, J. & Kar., K. K., 2010. Rheological Characterisation and Performance Evaluation of a New Medium Developed For Abrasive Flow Finishing. *International Journal of Precision Technology,* 1(3, 4), pp. 302-313.

Sankar, M. R., Mondal, S., Ramkumar, J. & Jain, V. K., 2009a. Experimental Investigations and Modelling of Drill Bit-Guided Abrasive Flow Finishing (DBG-AFF) Process. *International Journal of Advanced Manufacturing Technology,* Volume 42, pp. 678-688.

Sankar, M. R., Ramkumar, J. & Jain, V. K., 2009. Experimental Investigation and Mechanism of Material Removal in Nano Finishing of MMCs Using Abrasive Flow Finishing (AFF) Process. *Wear,* Volume 266, pp. 688-698.

Schmitt, J. & Diebels, S., 2013. Simulation of the Abrasive Flow Machining Process. *Zeitschrift fuer Angewandte Mathematik und Mechanik,* 93(2-3), pp. 147-153.

Scott, D. A., Podany, J. & Considine, B. B., 1991. *Ancient and Historic Metals; Conservation and Scientific Research.* Marina del Rey, California, USA, Getty Conservation Institute.

Seok, J. et al., 2009. Tribological Properties of a Magnetorheological (MR) Fluid in a Finishing Process. *Tribology Transactions,* 52(4), pp. 460-469.

Sidpara, A., Das, M. & Jain, V. K., 2009. Rheological Characterization of Magentorheological Finishing Fluid. *Materials and Manufacturing Processes,* 24(12), pp. 1467-1478.

Singh, D. K., Jain, V. K. & Raghuram, V., 2004. Parametric Study of Magnetic Abrasive Finishing Process. *Journal of Materials Processing Technology,* Volume 149, pp. 22-29.

Singh, R. & Walia, R. S., 2012. Hybrid Magnetic Force Assistant Abrasive Flow Machining Process Study for Optimal Material Removal. *International Journal of Applied Engineering Research,* 7(11), pp. 1-4.

Singh, S., Shan, H. S. & Kumar, P., 2002. Parametric Optimization of Magnetic-Field-Assisted Abrasive Flow Machining by the Taguchi Method. *Quality and Reliability Engineering International,* Volume 18, pp. 273-283.

Singh, S., Shan, H. S. & Kumar, P., 2002. Wear Behavior of Materials in Magnetically Assisted Abrasive Flow Machining. *Journal of Materials Processing Technology*, Volume 128, pp. 155-161.

Sleigh, A. & Noakes, C., 2009. *Boundary Layer Theory*. [Online] Available at: http://www.efm.leeds.ac.uk/CIVE/FluidsLevel1/Unit04/T2.html [Accessed 25th October 2013].

Szabo, O., 2001. Optimisation of Technology and "Quasi Honing" of Polygon Bores. *Journal of Materials Processing Technology*, Volume 119, pp. 117-121.

Szklo, A. & Schaeffer, R., 2007. Fuel Specification, Energy Consumption and CO2 Emission in Oil Refineries. *Energy*, 32(1), pp. 1075-1092.

Szulczynski, H. & Uhlmann, E., 2002. *Material Removal Mechanisms in Abrasive Flow Machining.* St Louis, Missouri, USA, American Society for Precision Engineering, pp. 677-682.

Tassou, S. A., De-Lille, G. & Ge, Y. T., 2009. Food Transport Refrigeration - Approaches to Reduce Energy Consumption and Environmental Impacts of Road Transport. *Applied Thermal Engineering*, 29(8-9), p. 1467.

The Carbon Trust, 2013. *Conversion Factors; Energy and Carbon Conversions*, London, UK: http://www.carbontrust.com/media/18223/ctl153_conversion_factors.pdf.

Tzeng, H. J., Yan, B. H., Hsu, R. T. & Chow, H. M., 2007. Finishing Effect of Abrasive Flow Machining on Micro Slit Fabricated by Wire-EDM. *International Journal of Advanced Manufacturing Technology*, Volume 34, pp. 649-646.

Tzeng, H. J., Yan, B. H., Hsu, R. T. & Lin, Y. C., 2007. Self-Modulating Abrasive Medium and its Application to Abrasive Flow Machining for Finishing Micro Channel Surfaces. *International Journal of Advanced Manufacturing Technology*, Volume 32, pp. 1163-1169.

Uhlmann, E., Mihotovic, V. & Coenen, A., 2009a. Modelling the Abrasive Flow Machining Process on Advanced Ceramic Materials. *Journal of Materials Processing Technology*, Volume 209, pp. 6062-6066.

Uhlmann, E., Richarz, S. & Mihotovic, V., 2009b. Substrate Pre-Treatment of Cemented Carbides Using Abrasive Flow Machining and Laser Beam Ablation. *Production Engineering*, 3(1), pp. 81-86.

Walch, W. L. et al., 2002. *High Precision Abrasive Flow Machining Apparatus and Method.* United States, Patent No. 6,500,050.

Walia, R. S., Shan, H. S. & Kumar, P., 2008a. Determining Dynamically Active Abrasive Particles in the Media Used in Centrifugal Force Assisted Abrasive Flow Machining Process. *International Journal of Advanced Manufacturing Technology*, Volume 38, pp. 1157-1164.

Walia, R. S., Shan, H. S. & Kumar, P., 2008b. Morphology and Integrity of Surfaces Finished by Centrifugal Force Assisted Abrasive Flow Machining. *International Journal of Advanced Manufacturing Technology,* Volume 39, pp. 1171-1179.

Walia, R. S., Shan, H. S. & Kumar, P., 2009. Enhancing AFM Process Productivity Through Improved Fixturing. *International Journal of Advanced Manufacturing Technology,* Volume 44, pp. 700-709.

Walia, R. S., Shan, H. S. & Kumar, P. K., 2006. Finite Element Analysis of Media Used in the Centrifigal Force Assisted Abrasive Flow Machining Process. *Proceedings of the Institution of Mechanical Engineers, Part B: Journal of Engineering Manufacture,* Volume 220, pp. 1775-1785.

Wang, A. C., Liu, C. H., Liang, K. Z. & Pai, S. H., 2007. Study of the Rheological Properties and the Finishing Behavior of Abrasive Gels in Abrasive Flow Machining. *Journal of Mechanical Science and Technology,* Volume 21, pp. 1593-1598.

Wang, A. C. et al., 2009. Uniform Surface Polished Method of Complex Holes in Abrasive Flow Machining. *Transactions of Nonferrous Metals Society of China,* Volume 19, pp. 250-257.

Wang, A. C. & Weng, S. H., 2007. Developing the Polymer Abrasive Gels in AFM Process. *Journal of Materials Processing Technology,* Volume 192-193, pp. 486-490.

Wan, S. Y. M. et al., 2010. *Low Pressure Abrasive Flow Machining,* Nanyang, Singapore: Singapore Institute of Manufacturing Technology, School of Mechanical and Aerospace Engineering.

Wilk, W. & Tota, J., 2007. *Modern Technology of the Turbine Blades Removal Machining.* Sofia, Bulgaria, Advanced Materials and Operations Society (Bulgaria), pp. 347-355.

Williams, E. D., Ayres, R. U. & Heller, H., 2002. The 1.7 Kilogram Microchip: Energy and Material Use in the Production of Semiconductor Devices. *Environmental Science and Technology,* 36(1), pp. 5504-5510.

Williams, R. E. & Melton, V. L., 1998. Abrasive Flow Finishing of Stereolithography Prototypes. *Rapid Prototyping Journal,* 4(2), pp. 56-67.

Williams, R. E., Walczyk, D. F. & Dang, H. T., 2007. Using Abrasive Flow Machining to Seal and Finish Conformal Channels in Laminated Tooling. *Rapid Prototyping Journal,* 13(2), pp. 64-75.

Williams, R. H. & Larson, E. D., 1987. Materials, Affluence and Industrial Energy Use. *Annual REview of Energy and Environment,* 12(1), pp. 99-144.

Worrell, E., Martin, N. & Price, L., 1999. *Energy Efficiency and Carbon Dioxide Emissions Reduction Opportunities in the U.S. Iron and Steel Sector,* California, USA: Lawrence Berkeley National Laboratory.

Worrell, E., Phylipsen, D., Einstein, D. & Martin, N., 2000. *Energy Use and Energy Intensity of the U.S. Chemical Industry,* California, USA: Lawrence Berkley National Laboratory.

Yadav, S. K., Singh, M. K. & Singh, B. R., 2011. Effect of Unconventional Machining on Surface Roughness of Metal: Aluminium and Brass - A Case Study of Abrasive Flow. *SAMRIDDHI - A Journal of Physical Sciences, Engineering and Technology*, 2(1), pp. 53-60.

Yang, L. & Zhao, L., 2010. *The Study of Polishing and Equipment of Abrasive Flow*. Wuhan, China, IEEE, pp. 3450-3453.

Yanjia, W. & Chandler, W., 2010. The Chinese Nonferrous Metals Industry - Energy Use and CO2 Emissions. *Energy Policy,* 38(1), pp. 6475-6484.

Yin, L. et al., 2004. Abrasive Flow Polishing of Micro Bores. *Materials and Manufacturing Processes,* 19(2), pp. 187-207.

Zhang, S. et al., 2009. *Study on Abrasive Flow Ultra-Precision Polishing Technology of Small Hole*. Changchun, China, IEEE, pp. 4305-4309.

Zhong, Z. W., 2008. Recent Advances in Polishing of Advanced Materials. *Materials and Manufacturing Processes,* 23(5), pp. 449-456.

Appendix A – Copy of Four Publications Made.

ABRASIVE FLOW MACHINING; R&D STRATEGY & CHALLENGES IN INDUSTRIAL APPLICATIONS

Mitchell J. Howard
School of Engineering and Design
Brunel University
Kingston Lane
Uxbridge, UB8 3PH, UK
mitchell.howard@mollart.co.uk

Kai Cheng
School of Engineering and Design
Brunel University
Kingston Lane
Uxbridge, UB8 3PH, UK
kai.cheng@brunel.ac.uk

Guy A. Mollart
Managing Director
Mollart Engineering
Chessington Industrial Estate
Chessington, KT9 1EU, UK
guy.mollart@mollart.co.uk

ABSTRACT

Abrasive flow machining (AFM) is a popular non-traditional machining process used to finish components to a high degree of accuracy and repeatability. Geometrical complexity and part length present two significant hurdles for the process, neither of which have been tackled by commercial machine tool builders. This paper utilizes a full factorial test strategy to determine the contribution of the major machine control variables. Results show that moving media through the part as fast as possible will improve both the surface finish and deburring effect. Where geometry allows free-flowing media without constrictions, keeping media temperature as low as possible is a good approach to both deburring and polishing. Further work will be based on linking computational fluid dynamics (CFD) models with physical results in order to expediently derive correct parameter and media configuration for a given part.

Keywords: AFM, CFD, Seito

1 INTRODUCTION

The abrasive flow machining (AFM) process has cemented its place as a finishing technique with over 40 years of use. Its strengths lie in reaching inaccessible cavities, without need for specialist tools, high power-consumption, aggressive material removal (MR) methods or inducing corrosion. The mechanical nature of the process permits a wide degree of control over the effects produced by the machine, allowing an engineer to hone, polish, generate radii, deburr and remove recast layer – all with a single machine tool.

Competing technologies such as electrochemical machining (ECM) are only compatible with electrically conductive materials, suffer from high tooling and operation costs and are limited by the geometry of tools. Thermal energy method (TEM) is unsuitable for parts with thin walls, but is exceptionally quick at burr removal. Its removal mechanism relies on the mass of the burr being significantly less than the part; it is limited to deburring operations - providing a smooth radius on edges is unachievable. Magnetic deburring circulates an abrasive media within a drum of components driven by rotating magnets, although process capability is poor in small, long holes. AFM's advantage over these competing processes is its flexibility, although the vast array of parameter, media and tooling options makes it difficult for an engineer to determine suitable operating conditions. Industrially, AFM has been restricted to a trial and error approach, led mostly by commercial machine tool builders owing to the

prohibitive costs of consumables in development. Their process knowledge and development practices are justifiably retained in-house to preserve the value of their products and subcontract services. Academically, experimental testing is typically based on small motor-driven extruder screws using bench test-rigs, not commercial purpose-built machinery. Difficulties in development stem from the sheer number of process factors. By attempting to model the effects of variables and their relationships, the ultimate goal of research is to present a methodology for the accurate configuration of machine, media and part; knowledge which can be easily transferred to other machine-media-part configurations.

By working in association with a top UK engineering subcontractor, the content of this paper is based on the finishing requirements of oil and gas exploration tools, although techniques are easily transferred to aerospace, medical, defense and automotive applications. In operation, the cylindrical components (measuring up to Ø0.2x1.6m) contain hydraulic fluid, electrical cabling, solenoids and crude oil housed within an array of up to 100 ports, through-holes, blind-holes and cross-holes. Critically, it is very difficult to obtain consistent finish across all features and intersections; remaining sharp edges encourage wire insulation to be stripped, loose flashings of workpiece material can break loose, damaging pumps and hosing, and samples of oil or gas can become contaminated. Human labor is a very inconsistent method of finishing such a complex part and errors are frequently made, resulting in increased transportation and re-work costs.

2 CURRENT RESEARCH AND DEVELOPMENT STATUS

Accurate simulation of manufacturing processes allows an engineer to develop a product or process without committing material or financial resources. In AFM development, simulation focuses on determination of process parameters and their effects on the component, such as surface roughness. Jain & Jain (1999), set out to understand the mechanics of surface profile generation. Using response surface analysis (RSA) method paired with physical testing, the authors key findings include; 1) an increase in grain concentration increases the number of active grains in the media (where inactive grains are suspended away from the workpiece surface or effectively roll across the surface) and a higher velocity will increase the number of inactive grains, 2) extrusion pressure, grit mesh size and hardness of workpiece contribute to affect the possible depth of indentation and therefore the final Ramin, 3) surface finish and profile are the function of number of cycles, abrasive concentration, abrasives mesh size, extrusion pressure and reduction ratio. Reduction ratio is the reduction of cross-sectional area through which the media flows. Jain and Jain's work has received over 20 citations, and verified the core principles of AFM's surface generation method.

The use of software simulation is a promising direction for AFM process development. In recent years, the possibility to simulate viscoelastic (non-Newtonian) polymer flow has been made possible, primarily for use in the plastics processing industry. Computational fluid dynamics (CFD) was first directly applied to AFM in 2009 by Wang et al. Their paper focuses on use of a CFD package to simulate the effects of adding a "mould core" to the center of a chain link. The objective was to prove the concept that a uniform shear force acting on the part walls would lead to a uniformly polished surface. Findings show that maintaining a constant gap between core and workpiece surface generates uniform force and therefore, uniform finish.

Absent from scholarly articles are studies of how surface generation is affected in long, complex parts which suffer from pressure drop. Simulation suits the challenges of using AFM in parts with holes of aspect ratio >1:350, and to determine how the geometry affects the flow. In Jain & Jain's (1999) case, the paper focuses on the basic principles of the process, which are applicable to all AFM users. Wang et al (2009) omit the application of their results to AFM's other operations such as honing and the application of CFD models to determining surface finish in other, more complex parts.

2.1 Process Monitoring

In order to tackle the variables inherent in the process, Fang et al (2009b) utilise temperature as a feedback method. Their work highlights reducing MR efficiency in proportion with increased cycles in three tests with varying hardness steels. Key findings include; 1) high viscosity media effectively removes more material within the first few cycles. Thereafter, its MR efficiency is lower than using a higher viscosity from the start, 2) in proportion with increased cycles, media viscosity becomes less effective due to increased work, 3) through CFD simulation, it is shown that when extrusion pressure is kept constant, the media viscosity is the dominating factor in flow distribution (therefore it can be reasoned that viscosity determines the ability of a media-machine configuration to reach all features of a complex part). Somewhat contrary to Jain & Jain's (1999) viewpoint that extrusion pressure improves surface finish, Fang et al (2009b) see no significant improvement. Their analysis fails to note the link between higher velocity (caused by low viscosity) and the increase in particle rolling, further contributing to decreased work efficiency. To complement Fang et al's (2009b) work and Wang et al's (2009), we can reason that use of mould cores, or specially designed tooling to maintain cross-sectional area will increase shear stresses, increasing media viscosity and reducing work efficiency.

2.2 Performance Studies

Several researchers have focused on specific elements of the machine-media-part triangle, and produced detailed analyses. Dating from the mid-1990s, the knowledge proffered is typically situation specific, and whilst technically excellent, findings can contradict their peers. Fang et al (2009a) describes the movement patterns of ellipsoidal microgrit particles. In accordance with Jain & Jain (1999), they find reduced material hardness and increased load (extrusion pressure) conducive to reduction of rolling (increased MR).

Jain & Adsul (2000) aim to determine further core principles of the AFM process and workpiece effects. They find that MR is governed by the material's pre-process surface condition and workpiece hardness. Further, the material hardness also governs the rate of MR. Perhaps most significant for an industrial application is that the size of grit in use limits the highest achievable surface finish. Jain & Adsul (2000) state that MR and ΔRa decrease with an increase in grit mesh size. It should be noted that the authors are referring to the observed change in Ra over a number of cycles, not the final Ra value. Ra maximum should be achieved with the smallest grit available.

Jain & Jain (2001) conduct a study to establish the specific energy of the AFM process. Their findings indicate AFM to be comparable to traditional grinding operations, with the exception of higher energy where the workpiece hardness is increased. Jain & Jain (1999) discuss in further detail the MR and surface roughness. In further industrially significant statements, they highlight elements of the machine-media-part triangle and their relationships; 1) at higher value of reduction ratio (a reduction of cross-sectional area within the geometry of the part), the rate of extrusion pressure is higher, 2) indentation of grit, (irrespective of mesh size) is a function of extrusion pressure and velocity.

Geometry produced using standard engineering machine tools such as milling or turning centers will always measure different surface roughness values – not only that, but the form of the surface will vary with manufacturing method. Authors Loveless, Williams & Rajurkar (1994) provide invaluable transferrable evidence that AFM performance is limited to the surface produced prior to an AFM operation. Their work establishes that MR in AFM differs between various machined surfaces and that wire-EDM surfaces are particularly suitable. However, their work fails to draw the link between grit mesh size and MR – a fundamental concept as highlighted by Jain & Jain (1999).

Szulczynski & Uhlmann (2002) analyze the effects of three different media on a substrate. Using images of processed surfaces as their metric, the media are configured on the principle that additives (hydrocarbon oil) will reduce viscosity, and therefore produce a better polishing media, whereas minimal additive constitutes a higher viscosity media and therefore one suited to high MR for application in

deburring. These assumptions in experiment setup differ from Jain & Jain's concepts (1999, 2000, 2001) where grit size is the single contributory factor in MR and surface finish. However, Szulczynski & Uhlmann (2002), base their work on grain fraction (percentage by weight of media) and viscosity. Interestingly, their findings (with polishing media) include that no marks of rolling grains could be found on the substrate, with growing grain fraction, the surface marks become more evident. With deburring media (minimal additive), chip formation (resulting in MR) occurs in laminar flow geometry. With relevance to commercial operation, components manufactured to tight dimensional tolerances would need careful choice of media configuration to avoid scrapping.

2.3 Further research and development needs

Previous research indicates several transferrable concepts which are of industrial value and provide further direction for development. The work implies that a sweet spot exists between machine, media and part configuration, and that for each element, a correct choice exists for the intended manufacturing operation, be it honing, deburring, removal of recast layer, polishing or radius generation. Research has also implied that there is a correct grain fraction to produce a specific finish, where an excess of grain results in high MR, but scratched surfaces, and inadequate fraction results in insufficient MR and poor ΔRa. The use of simulation to aid the transferal of physical test results to a solid model in a CFD system shows promise. Wang et al (2009) used a simple mould core in a chain component, and proved that CFD simulation could accurately represent a machine operation. Thought must be given to the machine parameters used when running physical tests for the purpose of integrating into CFD simulations; other considerations include the simulation of grit interaction and motion, or whether the grain fraction and flow paths are suitable to predict the effects. Grain fraction may also affect the viscoelastic behaviour of the media. Where software packages to simulate non-Newtonian flow are unavailable, Newtonian flow can provide pressure, shear stress and flow rate data, which may be of equal value. Based on the critical review of available literature, the following research and development needs are identified; 1) methods of achieving alternative manufacturing operations such as radius generation. In a production environment, instantly available/calculable knowledge of correct operating parameters is of great value, 2) explicit discussions of transferring results of simulation of complex geometry to a physical part with success, 3) pressure drop in long components, where length (increased work and turbulence) means that temperature increases reduce MR effects and some areas of the component are left with very little deburring effect, 4) across all practical research papers, there is very little consistency of test-rigs and testpieces. While the results describe relative effects, the extent to which effects are linked may in reality show a high degree of variation, and 5) transferability studies are absent. While simple components with single faces and single-faced mould cores are modeled, papers with the knowledge and implications of attempting this with larger industrial parts (with multiple inlets, cavities and outlets) are unavailable.

3 ORTHOGONAL ARRAY TESTING AND PROCESS OPTIMISATION

Initial work undertaken to define the relationship between machine parameters and workpiece geometry effect is described here, using a standard testpiece design where a single Ø6.5mm bore was gundrilled through 250mm and counterbored at either end to Ø10mm by 80mm depth. Employing a fractionated factorial test methodology, appropriate factors and levels were chosen based on the machine's (Micro-Technica Duplex 250) maximum and minimum settings, throughput time and median values. Prior to running orthogonal array (L9) tests, the part was cleaned using panel wipe to remove any remaining oil from the gundrilling process. Once dried, all 9 holes were measured for surface roughness in Ra and Rz and an Olympus endoscope used to capture the condition of the step on the counterbore and centre bore as pictured in figure 3.

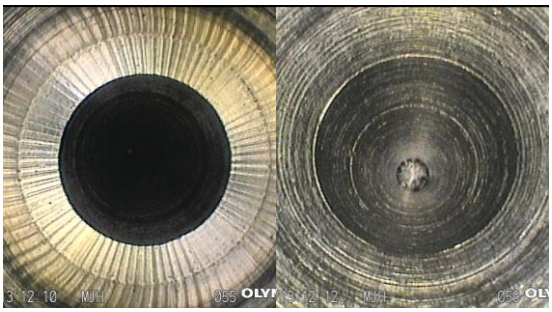

Fig 3: The as-drilled, unprocessed internal surfaces of a single bore in the testpiece block.

3.1 Results

Results of Seito analysis provide the researcher with the best combination of levels. Invariably, moving media through the part as fast as possible will improve both the finish and deburring effect. To improve finish and deburring, a higher temperature media is required at points where cavities expand, but not in straight bores and points of constriction. Where geometry allows flow without constrictions, keeping media as low as possible is a good approach to higher MR. A single manufacturing operation without inducing geometry expected from another process is possible. A single surface could be processed while allowing media to travel through other cavities, although this is a function of the part geometry.

Table 3.1: Results of Seito analysis. Best combination of operating parameters for a desired effect.

Surface	Piston Speed		Stroke Length	Cycles	Media Temp.
	mm/min		mm	#	°c
Ra	Avg.	300	200	5	25
	CB-L	300	125	5	25
	CB	300	200	15	25
	CB-U	300	200	5	25
Rz	Avg.	300	200mm	5	25
	CB-L	300	75mm	30	25
	CB	300	200mm	15	25
	CB-U	300	200mm	5	25
No Unit	CB-L	300	200mm	30	25-40
	CB	300	~	30	25
	CB-U	300	125mm	30	40

4 DISCUSSION

Based on initial work in determining the effects of machining parameters, the following findings are presented; 1) where a polishing effect is required - low temperature, long stroke length and high piston speed are beneficial, 2) where a deburring effect is required over sharp edges, a high piston speed, high number of cycles and a raised working-temperature media are beneficial, 3) in a more complex part, results point to a potential hierarchy of intersecting features, where a particular intersection will receive the highest flow rate and thus the greatest change in geometry. The answer to this lies in CFD simulation, 4) a leveling effect where a single set of parameters achieve a uniform surface finish within a cavity is difficult to achieve with machine parameters alone. In line with Wang et al (2009), a more advanced tooling setup will be required. Based on knowledge-gaps within literature and findings from experiments, the next stages of work will focus on; 1) CFD simulation upon testpiece geometry to determine parallels

between physical and Seito analysis results, 2) development and simulation of constant cross-section tooling to maintain uniform stress at the workpiece surface, 3) CFD-based parameter-media determination techniques, including viscosity of media determination, 4) how to effect an alternative manufacturing operation.

ACKNOWLEDGMENTS

The authors would like to thank the EngD scholarship programme of EPSRC and Mollart Engineering Ltd, for the support of this research work.

REFERENCES

Fang, L., Zhao, J., Li, B. & Sun, K. (2009) "Movement patterns of ellipsoidal particle in abrasive flow machining", Journal of Materials Processing Technology, vol. 209, no. 20, pp. 6048-6056.

Fang, L., Zhao, J., Sun, K., Zheng, D. & Ma, D. (2009) "Temperature as sensitive monitor for efficiency of work in abrasive flow machining", Wear, vol. 266, no. 7-8, pp. 678-687.

Jain, R.K. & Jain, V.K. (2001) "Specific energy and temperature determination in abrasive flow machining process", International Journal of Machine Tools and Mfr., vol. 41, no. 12, pp. 1689-1704.

Jain, R.K., Jain, V.K. & Dixit, P. (1999) "Modeling of material removal and surface roughness in abrasive flow machining process", International Journal of Machine Tools and Manufacture, vol. 39, no. 12, pp. 1903-1923.

Jain, V. & Adsul, S. (2000) "Experimental investigations into abrasive flow machining (AFM)", International Journal of Machine Tools and Manufacture, vol. 40, no. 7, pp. 1003-1021.

Jha, S. & Jain, V. (2004) "Design and development of the magnetorheological abrasive flow finishing (MRAFF) process", International Journal of Machine Tools and Manufacture, vol. 44, no. 10, pp. 1019-1029.

Kumar Jain, R. & Jain, V.K. (1999) "Simulation of surface generated in abrasive flow machining process", Robotics and Computer-Integrated Manufacturing, vol. 15, no. 5, pp. 403-412.

Loveless, T., Williams, R. & Rajurkar, K. (1994) "A study of the effects of abrasive-flow finishing on various machined surfaces", Journal of Materials Processing Technology, vol. 47, no. 1-2, pp. 133-151.

Rajesha, S., Venkatesh, G., Sharma, A.K. & Kumar, P. (2010) "Performance study of a natural polymer based media for abrasive flow machining", Indian Journal of Engineering & Materials Sciences, vol. 17, no. 6, pp. 407-413.

Szulczynski, H. & Uhlmann, E. (2002) "Material Removal Mechanisms in Abrasive Flow Machining", Proc. of the 17th Annual Meeting of the ASPE, St. Louis, Missouri, USA, pp. 677.

Wang, A. (2009) "Uniform surface polished method of complex holes in abrasive flow machining", Transactions of Nonferrous Metals Society of China, vol. 19, pp. 250-257.

Short Communication

Institution of MECHANICAL ENGINEERS
Journal of ENGINEERING MANUFACTURE

Proc IMechE Part B:
J Engineering Manufacture
227(11) 1748–1752

DOI: 10.1177/0954405413491957
pib.sagepub.com
SAGE

An industrially feasible approach to process optimisation of abrasive flow machining and its implementation perspectives

Mitchell Howard[1,2] and Kai Cheng[1]

Abstract

This article presents a novel industrially feasible approach to ensure that an integrated optimum configuration of machine, media and geometry is achieved for abrasive flow machining process optimisation. Historically, new part introduction requires a trial-and-error phase to develop a process model, while the proposed method identifies two key explanatory variables (edge form and average roughness) and the process conditions in which they are achieved in test-piece geometry. The method and its shop-floor implementation perspectives are evaluated and verified through computational fluid dynamics simulation and well-designed machining trials, plus reapplied to more complex workpieces. The method can significantly improve abrasive flow machining process capability, accuracy and efficiency and be used to optimise machine design, attempt radical new methods of workpiece fixturing and provide an avenue to incorporate and reanalyse the adaptations of abrasive flow machining machinery.

Keywords

Abrasive flow machining, flow deburring, process optimisation, computational fluid dynamics–based simulation

Date received: 22 January 2013; accepted: 7 May 2013

Introduction

Since its inception in the 1960s, the abrasive flow machining (AFM) process has been applied successfully to high-value manufacturing industries for the purpose of polishing, edge-rounding, honing and removal of recast layer. Especially suited to the processing of features inaccessible by hand, production methodology is well established, typically consisting of a single design stage to control the introduction of the abrasive media. With an increasing trend towards harder and tougher workpiece materials and more complex geometry, the limitations of the AFM process are becoming apparent, none more so than in material removal ability and in the flexibility of machine hardware.

In industry, the AFM process is a widely accepted form of edge- and surface-conditioning with primary application in parts with internal cavities inaccessible by traditional hand tools.[1–3] A principal concern in the production environment is the accuracy and repeatability with which an engineer can claim to control a process – AFM is subject to multi-order interactions between its (approximately) 25 variables, which dictate the final part condition.[4,5] Most of these variables are passively altered (i.e. friction accumulating thermal energy within the media), although there are three key groups of factors, which allow full control, that can be split into machine, media and geometry categories for ease of description.[6]

It is universally recognised that trial and error processes in product development are a wasteful, slow and inefficient means of gaining process knowledge and confidence;[7,8] in AFM, this is currently a prerequisite to undertaking customer work. It prevents the timely and accurate provision of customer quotations, the economic selection of materials for tooling and media (including subsequent manufacture) and the certainty of a successful outcome. The limited success of the process to date can be explained by the lack of a direct

[1]Advanced Manufacturing & Enterprise Engineering (AMEE) Department, School of Engineering and Design, Brunel University, Uxbridge, UK
[2]Mollart Engineering Ltd, Chessington, UK

Corresponding author:
Mitchell J Howard, Advanced Manufacturing & Enterprise Engineering (AMEE) Department, School of Engineering and Design, Brunel University, Kingston Lane, Uxbridge UB8 3PH, UK.
Email: mitchell.howard@mollart.co.uk

competing technology and the long-term experience of several key players. In order to progress the AFM process beyond trial and error and cope with increasingly complex geometric features and configurations, a new scientific and industrially feasible approach is essential and much needed, so as to automate the selection of parameters in the three key areas and enable the process working in a truly predictable, reproducible and highly productive manner.

AFM suffers from hydraulic system pressure drop, predominantly due to the highly viscous fluids in use, without which the grit (the cutting edge) would have an unsupportive matrix. In oil and gas industry components, some of the most difficult features to process contain holes of 5 mm diameter and 1.6 m length, making the simulation aspect of this technique of critical importance, due to multiple difficult-to-reach features. While computational fluid dynamics (CFD) simulation has been applied previously in simplistic form;[9] the methodology presented in this article is the most complete and industrially viable. Furthermore, the article discusses implementation aspects of the approach in an industrial context, providing the methodology for the integration of simulation in a greater role as a means of determining edge profile and surface roughness in the optimised AFM process.

Process factors and interactions

Control of the AFM process is restricted to modification of the variables categorised within machine, media and geometry groups, as shown in Figure 1.[6] Within machine, the engineer has four options: velocity, stroke, temperature and cycles. Within media, the engineer has four options: grit size, carrier viscosity, grain fraction and percentage of filler. Within geometry, the engineer has free reign over additional tooling, but no control over customer component geometry – this leaves part cross-sectional area, part volume and pressure drop only within partial control, but nevertheless as an independent variable. Key to providing a repeatable and stable processing environment is to ensure that parameters operate within a tolerable range, which is achieved by correct sizing of components in the system. The machine in use at Mollart Engineering Ltd is a Micro Technica Technologies 'Duplex 250D'; a 4.4 kW hydraulic motor delivers a total of 47 bar (4.5 MPa) maximum allowable working pressure (MAWP). At this limit, heat accumulation is rapid and spreads quickly – this affects other elements of the system, in particular the viscosity of the media. As an end user, machine modification is a last resort, preferring changes to media formulation and tooling to avoid excessive pressure requirements.

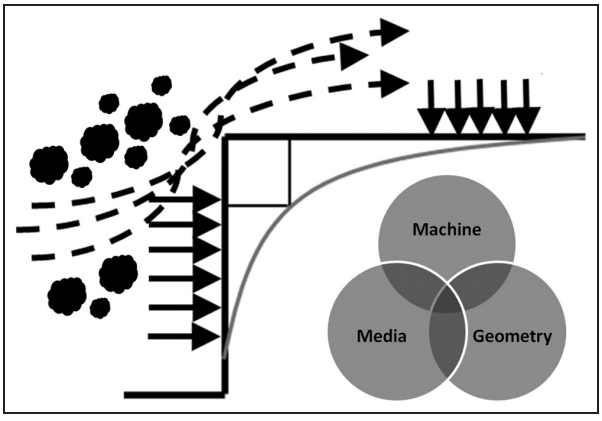

Figure 1. Schematic of square-edge testpiece geometry under conditions dictated by machine, media and geometry variables.

Data collection exercises

An experimental design is proposed to create two datasets, both specific to a given testpiece geometry and material. A three-level design is proposed to model possible curvature in the response function and to handle the case of nominal factors at three levels. Three repetitions of each trial are recommended, totalling 81 runs for each dataset. The first treats the workpieces to variations of machine parameters; velocity, temperature and length are the independent variables under consideration. Media is held constant as a control. The second dataset is formed by treating the workpieces to variations of media parameters; grit size, grain fraction and viscosity are the independents in this test. Support is received from a subcontractor in the field of product formulation in order to develop the different media required. Throughout each experiment, the testpiece and tooling must remain the same geometry and material.

The first explanatory variable of system performance is surface roughness – using a white-light interferometer (WLI) (Zygo NewView 5000), four points of average roughness (Ra) are collected from along the testpiece surface. Surface roughness is a function of the machine and tool used to create the surface initially – AFM offers greater improvement in Ra where preprocess Ra is worse and grit size in use should determine ultimate Ra. Testpieces are manufactured from a Ø16 mm bar and have a milled 10 mm^2 section, as shown in Figure 2, which allows for preprocess and post-process data collection, providing an accurate ΔRa value.

The form of the edge after processing will be paired with flow path sections from CFD-based simulations. These data, coupled with processing length information, will be useful for determining expected material removal and location of material removal. Data are collected by means of a Mitutoyo CV series Contracer, as illustrated in Figure 2. The testpieces will be measured for form after roughness measurement to avoid scoring the substrate. Tangentially formed radii are not a foregone conclusion – they are difficult (although not always *necessary*) to achieve; therefore, a single value

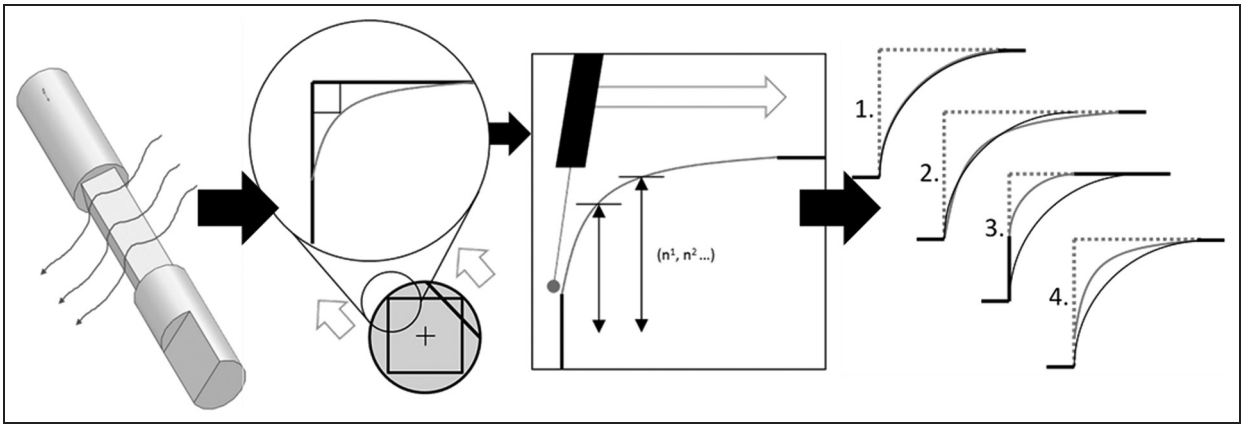

Figure 2. Testpiece form and flow direction (left), formtracer measurement technique (centre) and potential radius forms (right).
1: tangential fully formed; 2: non-tangential and out of tolerance; 3: tangential partially formed; 4: non-tangential, within tolerance.

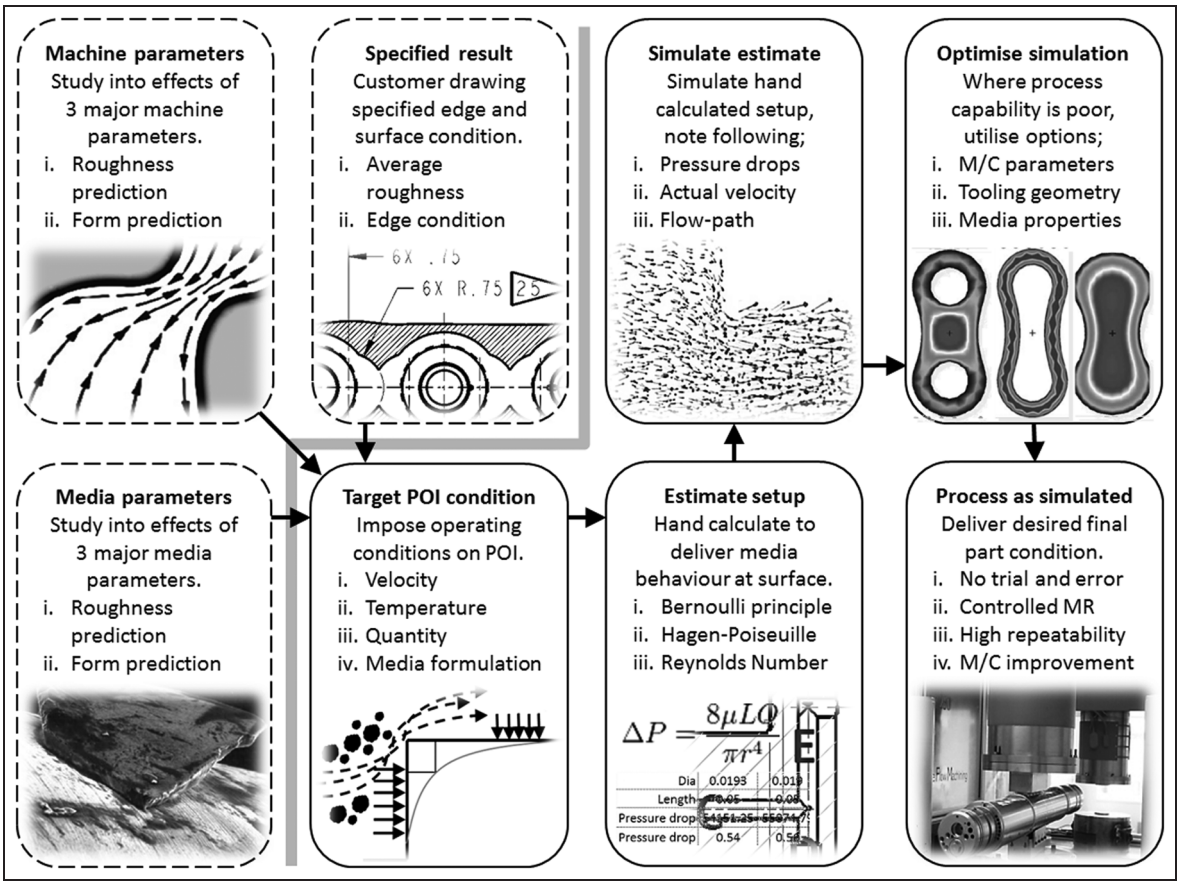

Figure 3. Integrating simulations as a means of process outcome prediction for complex geometry.
POI: point of interest; MR: material removal.

for edge form cannot be recorded – data collected from this instrument will form the mainstay of CFD-based simulations for evaluation and verification.

Interpretation, analysis and reapplication of simulation and experimental data

As depicted in Figure 3, a novel methodology is proposed to tackle the setting-up of the AFM process with greater precision. Customer requirements are an input, alongside data collected in two large-scale experiments describing the effects of varying machine and media parameters. This provides an engineer with 'target' conditions (a pressure, velocity, temperature and media formulation) that he or she must impose upon the point of interest (POI) in order to achieve a specific result – a result known to be conducive to a desired roughness or material removal profile. Once these values are chosen

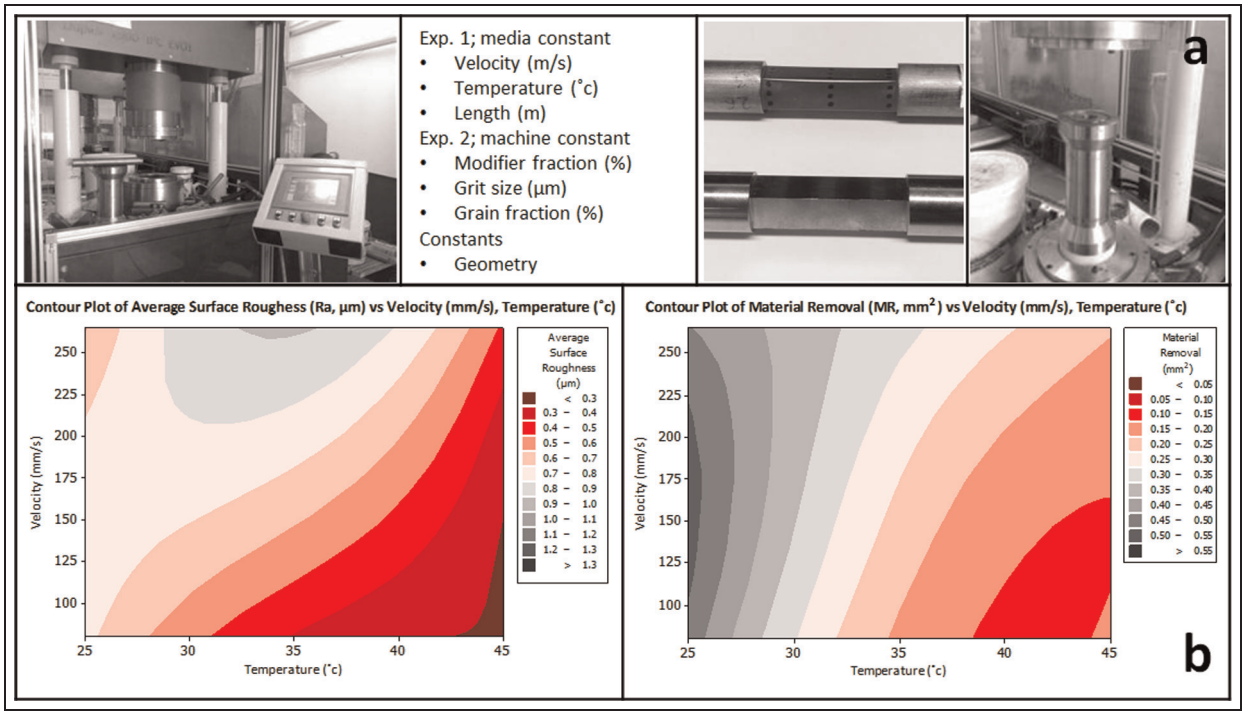

Figure 4. (a) Experimental machining and (b) results on validating the model and simulations in terms of surface roughness (left) and material removal (right).

(based upon previous experience in the specific workpiece material), basic fluid dynamics principles are employed to estimate the machine parameters necessary to deliver the required conditions at the POI. As these conditions are only relative to the testpiece geometry, CFD-based simulations are employed to extend the results of the two studies into parts that have not yet been physically processed.

As the number of features increases, their position relative to one another becomes more asymmetrical and fluid behaviour increasingly difficult to calculate by hand, making the application for CFD-based simulations clear. As the machine delivers a constant force, the media travel at the speed permitted by the volume of the cavity being processed. In order to rectify the velocity to achieve uniform processing, we introduce an additional layer of tooling (such as plugs, diverters and sheaths) – this may be used to increase the velocity at a given point with the trade-off of pressure drop, all of which is infinitely trialled in silico. In a production application, a solid model of the part to be processed will be required. The engineer will run a full simulation of the component installed on the machine, within which confidence is held due to the 'first-principles' verification of physical processing results of the testpieces. The optimum tooling, media and processing conditions can then be designed and planned for the production in a truly predictable, reproducible and highly productive manner.

Existing knowledge of the AFM process is highly fragmented, as the literature shows research carried out in select workpiece materials, with select treatments and select media configurations, none of which are replicated elsewhere. While we may partially understand a general effect of a parameter alteration, we certainly cannot quantify it with respect to the *hundreds* of other potential variables. The benefit of using CFD-based simulation is that it cancels out every variable in the geometry corner of the AFM triangle. The simulation-based approach takes measured results of the physical experimental set-up and simulates them using existing fluid rheological behaviour input methods. The simplicity of the testpiece geometry allows hand-calculated verification of parity in terms of strain rate, velocity, pressure and temperature between physical and virtual examples for all 27 unique combinations. This allows simulations on the model and further evaluation and validation, as illustrated in Figure 4, which shows the simulated and experimental machining trials for average surface roughness and material removal in reasonable agreement as progressed so far. The engineer now has the knowledge of testpiece surface conditions and resultant surface roughness and material removal rate for a given media and material – we can then work backwards for an arbitrary workpiece geometry using the optimal process variables and set-up derived through simulation.

Conclusion

This article presents a scientific-based industrially feasible approach to AFM process optimisation, which integrates the CFD simulations on accurate AFM fluid behaviour with data collected from rigorously

structured and verified machining experiments. The approach and associated techniques can significantly improve the AFM process capability, accuracy and efficiency. As a powerful tool and method, it opens the process up to new inexperienced users by increasing the ability to forecast tooling costs, processing time and consumables usage. In further applications, the technique can be used to optimise machine design, attempt radical new methods of workpiece fixturing and provide an avenue to incorporate and reanalyse adaptations of AFM machinery.

As an automated approach to the trial and error prerequisite problem, the methodology presents a highly useful and valuable technique for determining the correct processing conditions for a given set-up. The CFD simulations are applied in order to transfer the data collected in simple geometries to the increasingly more complex workpieces in the production environment. The proposed approach enables the AFM process to be operated in a truly predictable, reproducible and highly productive manner, although it is still under further development for complex components in difficult-to-machine materials such as Titanium and Inconel alloys.

Declaration of conflicting interests

The authors declare that there is no conflict of interest.

Funding

This study was supported by UK Technology Strategy Board (grant number 710231) and the UK Engineering and Physical Sciences Research Council (EPSRC) for the EngD Scholarship.

References

1. Perry KE. *Abrasive flow machining method and tooling*. Patent no. 4,005,549, USA, 1977.
2. Rhoades LJ. *Medium for process of honing by extruding*. Patent no. 3,819,343, USA, 1974.
3. Yang L and Zhao L. The study of polishing and equipment of abrasive flow. In: *Proceedings of 2010 international conference on mechanic automation and control engineering (MACE)*, Wuhan, China, 26–28 June 2010. IEEE, Beijing section CSS chapter, pp.3450–3453.
4. Arief I and Chen X. Key parameters in loose abrasive machining. In: *Proceedings of the computing and engineering researchers' conference*, Huddersfield, UK, 3 December 2010. University of Huddersfield, 2010.
5. Gorana VK, Jain VK and Lal GK. Prediction of surface roughness during abrasive flow machining. *Int J Adv Manuf Tech* 2006; 31(3): 258–267.
6. Rhoades L. Abrasive flow machining: a case study. *J Mater Process Tech* 1991; 28(1): 107–116.
7. Mali HS and Manna A. Current status and application of abrasive flow finishing processes: a review. *Proc IMechE, Part B: J Engineering Manufacture* 2009; 223(7): 809–820.
8. Cheema MS, Venkatesh G, Dvivedi A, et al. Developments in abrasive flow machining: a review on experimental investigations using abrasive flow machining variants and media. *Proc IMechE, Part B: J Engineering Manufacture* 2012; 226(12): 1951–1962.
9. Wang A, Tsai L, Liang KZ, et al. Uniform surface polished method of complex holes in abrasive flow machining. *T Nonferr Metal Soc* 2009; 19: 250–257.

Original Article

Institution of MECHANICAL ENGINEERS
Journal of ENGINEERING MANUFACTURE

Proc IMechE Part B:
J Engineering Manufacture
1–13

DOI: 10.1177/0954405414522210
pib.sagepub.com
SAGE

An integrated systematic investigation of the process variables on surface generation in abrasive flow machining of titanium alloy 6Al4V

Mitchell Howard[1,2] and Kai Cheng[1]

Abstract

This article presents an integrated and systematic investigation into the interaction and effects of the abrasive flow machining factors, through its three major process variables of the media velocity, temperature and quantity, which play an essential role in interfacing the 'machine' with 'workpiece' and 'media' corners of the abrasive flow machining triangle. The article also presents predictive models, main effects and industrially useful rule-of-thumb tools. Collectively, these variables offer machine operators the ability to manipulate the process behaviour when the opportunity to modify geometry and media levels is unavailable. In the media and geometry corners of the triangle, capital expenditure is required to adjust levels, making them economically and temporally limiting. The machine adjustments are physically limited by the hardware in use; however, this research finds that the range of response magnitude can vary significantly among the three process outcomes studied, that is, surface roughness, material removal and peak height reduction. Using a standard media and testpiece set-up, data are collected using a 3^3 full factorial experiment design and translated into a response surface design (Box–Behnken) for predictive model development. Application to oil and gas industry parts is shown whereby data are utilised to aid in the abrasive flow machining of production parts.

Keywords

Abrasive flow machining, response surface methodology, process optimisation, flow deburring, industrial application

Date received: 23 September 2013; accepted: 13 January 2014

Introduction

Modern high-value manufacturing (HVM) can be characterised by prolific use of high-performance materials, < 5 μm tolerances, costly machine–tool combinations and geometrical complexity of components and products. In many industries, in particular the oil and gas and automotive sectors, primary manufacturing methods (turning, drilling and milling) are frequently insufficient to manufacture geometry and complexity to customer specifications. These requirements stem from miniaturisation (increasing the feature set a product can offer) and design freedom offered by the capability of nontraditional material removal (MR) methods (additive layer manufacturing (ALM), electro-discharge machining (EDM), electrochemical machining (ECM) and laser-based methods).[1–4] The additional capability awarded by nontraditional methods brings their own inherent issues, the most predominant of which is feature inaccessibility, followed by difficult- or impossible-to-inspect features and third, by availability of sufficiently capable part-finishing techniques (i.e. where grinding and manual deburring may be inappropriate).[4,5]

In this light, we present abrasive flow machining (AFM) – the reciprocal pumping of an abrasive-laden slurry (~50–1200 Pa/s at ~10–200 bar) throughout an engineering component for the purpose of surface finishing, edge rounding, honing and removal of recast layer. The process is widely considered a 'black art' and while generally accepted by high-profile large enterprise (LE) manufacturers with high part volumes, establishing a presence within the high-value low-quantity world

[1]Department of Advanced Manufacturing & Enterprise Engineering (AMEE), School of Engineering and Design, Brunel University, Uxbridge, UK
[2]Mollart Engineering Ltd, Surrey, UK

Corresponding author:
Mitchell Howard, Mollart Engineering Ltd, 106 Roebuck Road, Chessington, Surrey KT9 1EU, UK.
Email: mitchell.howard@mollart.co.uk

AQ1
AQ2

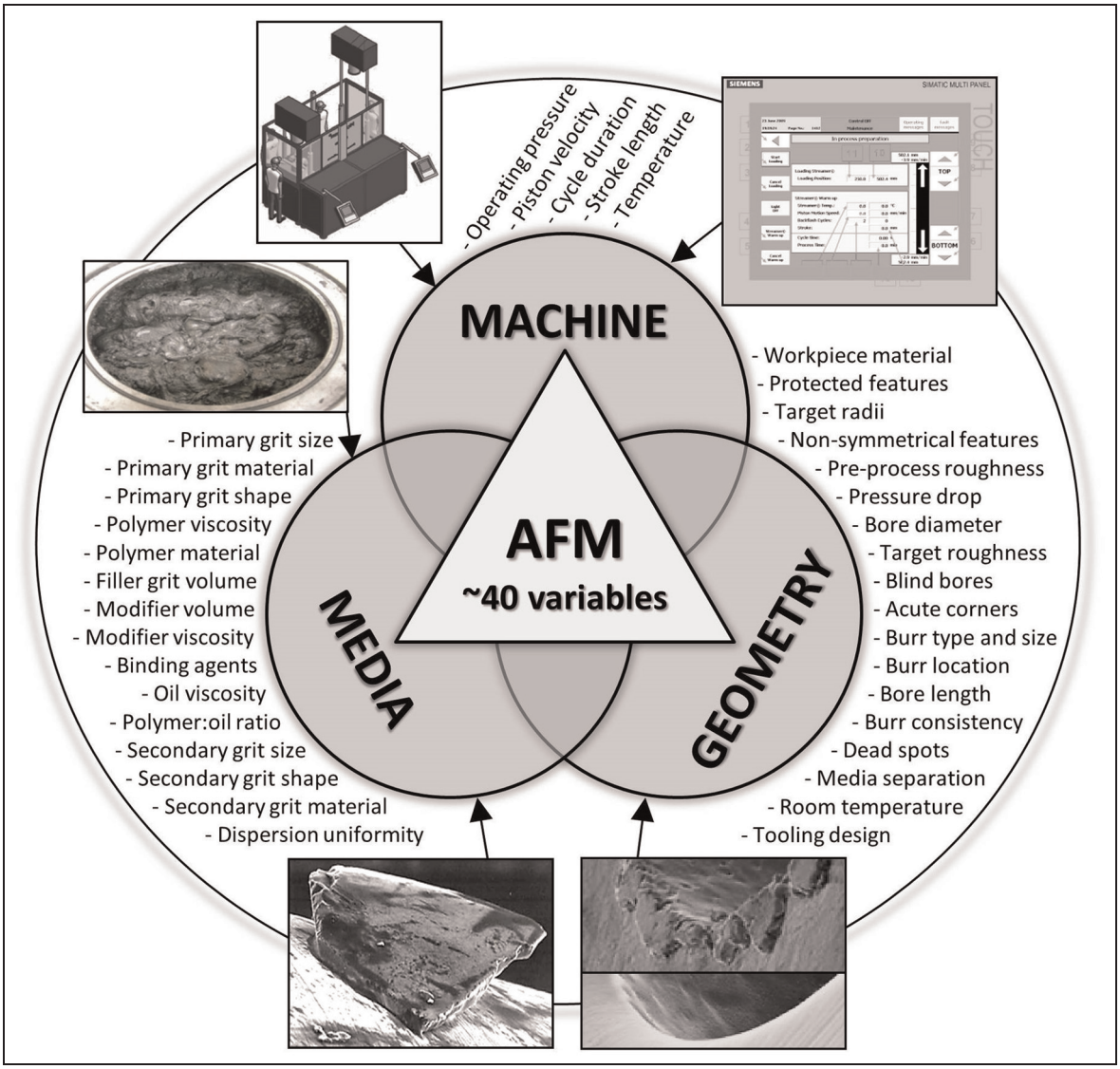

Figure 1. Identification of process variables and their intrinsic relationships in AFM.
AFM: abrasive flow machining.

AQ3

of SME HAV manufacturing has proven difficult. Key reasons for this include high capital costs through machinery, consumables (media) and fixturing costs and battling currently accepted attitudes towards the process.[4] The overwhelming factor in process uptake is process knowledge – with no fixed axes and a 'liquid cutting tool', potential users assume that operating an AFM machine can be as simple as pumping media through their workpiece. The truth is far more complex, as illustrated in Figure 1, the triangle concept illustrated describes the three corners of the process and aims to identify each element within the corner.

Multivariate processes are often difficult to understand and characterise[6] – they can be rife with systematic error and results can be misleading to a user or researcher. AFM is typical of this type of system – a level change in any of the identified variables of Figure 1 can affect multiple other factors and void any accurate process prediction. In order to provide confidence in the process, we must combine variables into more manageable units, comprising multiple fixed levels. Combining variables and fixing others implies an intrinsic relationship between those joined factors, and consideration of the effects of joining two previously independent factors must be made.

In order to progress the AFM process and improve its accessibility to lay users, the issues associated with the multiple variables must be minimised. Main technical challenges include the following: (1) determination of effect on surface for a given combination of machine–media–geometry (MMG), (2) transferral of experimental results to an untested geometry and (3) catering to arbitrary part condition[7] (burr size, surface finish) as caused by (numerous) preceding operations. This study focuses on the machine corner of the 'AFM triangle', consisting of variables such as pressure, velocity, duration, length and temperature. These factors allow the user to manipulate the final result within the

limitations of the geometry and media. Previous works[7,8–12] attempting to develop prediction models contain process factors from different corners of the AFM triangle, making it difficult to separate their findings and reapply them to other MMG combinations. Critically, the data collected in this research are to be reapplied as a benchmark in a computational fluid dynamics (CFD) simulation environment – while hand calculations and experience can often provide a user or researcher with an estimated process model, the geometry of the production components can vary in complexity – if a well-designed experiment can accurately interpolate missing values between and outside experimental levels, then we can be sure of the data quality and correlate experimental response values with simulated response values. This technique has not been previously applied and promises to lead to a full AFM simulation, providing value and viability in an industrial environment by removing costly trial-and-error steps in development of process models.

Common to all experimental investigations described above is the tendency to study groups of factors from different corners of the AFM triangle, which prevents us from isolating corners of the triangle in a simulation environment. Without knowing the effects of a complete set of machine (or media or geometry) factors, we are unable to verify experimental results against simulated results, and thus are liable to accredit changes in response variables to the incorrect factors.

Therefore, it is essential and much needed to undertake an integrated systematic investigation on the AFM process and thus develop an industrial-feasible scientific approach to render the process operating in a truly predictable, producible and highly productive manner. The research presented in this article attempts an integrated systematic investigation of the AFM system through investigating the collective effects of process variables on surface generation in AFM of titanium alloy 6Al4V.

CFD simulation-based analysis on the machine effects

As a scientific and viable production technique, readily available CFD software can be used to analyse the flow of media in an arbitrary geometry. While the rheological behaviour of the media will vary depending on its chemical makeup and grain fraction, there will always be the opportunity to determine its behaviour through simple assessment of viscosity versus shear rate, collected with a rheometer. What is unavailable, however, is the facility in software to simulate the size, shape, hardness, dispersion and general grit surface contact interaction model that the process desperately needs. Also unavailable, yet critical, is the processed length. The method presented here is the holistic embodiment of the CFD simulation-based approach as proposed by Howard and Cheng's,[13] which is an effective and *industrial-feasible* 'workaround', comprehensively integrated approach as illustrated in Figure 2.

An accurate representation of flow condition at the point of interest (POI) (in the testpiece geometry) is simulated using CFD-based simulations and checked for sensible results against measured results (collected through experimentation in entire machine process space). We then re-employ the simulation in more complex geometry, checking the flow condition at the POI. The results remain valid, assuming we are using the same media – in turn, we also retain the ability to simulate with differing machine factor values; the simulation software will display a different flow condition, and therefore we predict a reasonable result based on testpiece results and extrapolations. Geometry can also be altered infinitely at this point.

The final consideration is the integration of the grit within the media and the workpiece material. This interaction requires the addition of values that are unable to be simulated – the three factors are length, workpiece material and the abrasive potential of the media (determined by its volume and size of grit) which is an as-yet unknown quantity pending further research.

Experimental set-up and validation

Defining process behaviour through experimental investigation of all factors in Figure 1 is needlessly complex and economically costly. Instead, we identify which variables may be condensed and revise our experimental factors and levels accordingly. In the case of this research, we are looking at pressure, velocity, temperature, stroke length and number of cycles.

Procedure, design of experiments and parameterisation

In order to isolate the effects of changing machine levels, we must fix the other two corners of the triangle – the control variables. The experiment uses a media supplied by Micro Technica® Technologies GmbH, MF10-24B(60)-40B(60)-400B(40) – the naming convention of which implies an unknown (approximately 100 Pa/s) polydimethylsiloxane (PDMS) carrier and three grit sizes of Federation of European Producers of Abrasives (FEPA) mesh sizes F24, F40 and F400 (710, 425 and 17 μm). Weighting is 35% grain fraction − 65% carrier. Within the grit, there is 25% by weight of F400 as filler grit, while the larger (75%) particles provide the MR ability the media is designed to achieve.

We also control our geometry as shown in Figure 3; the media is funnelled through a series of reducing rings into the main testpiece support. This is a 40-mm tube formed of a steel body and replaceable nylon liner, with a bore crossing through halfway allowing the insertion and orientation of the testpiece. Non-Newtonian media flow through the tube causes the media at the outer

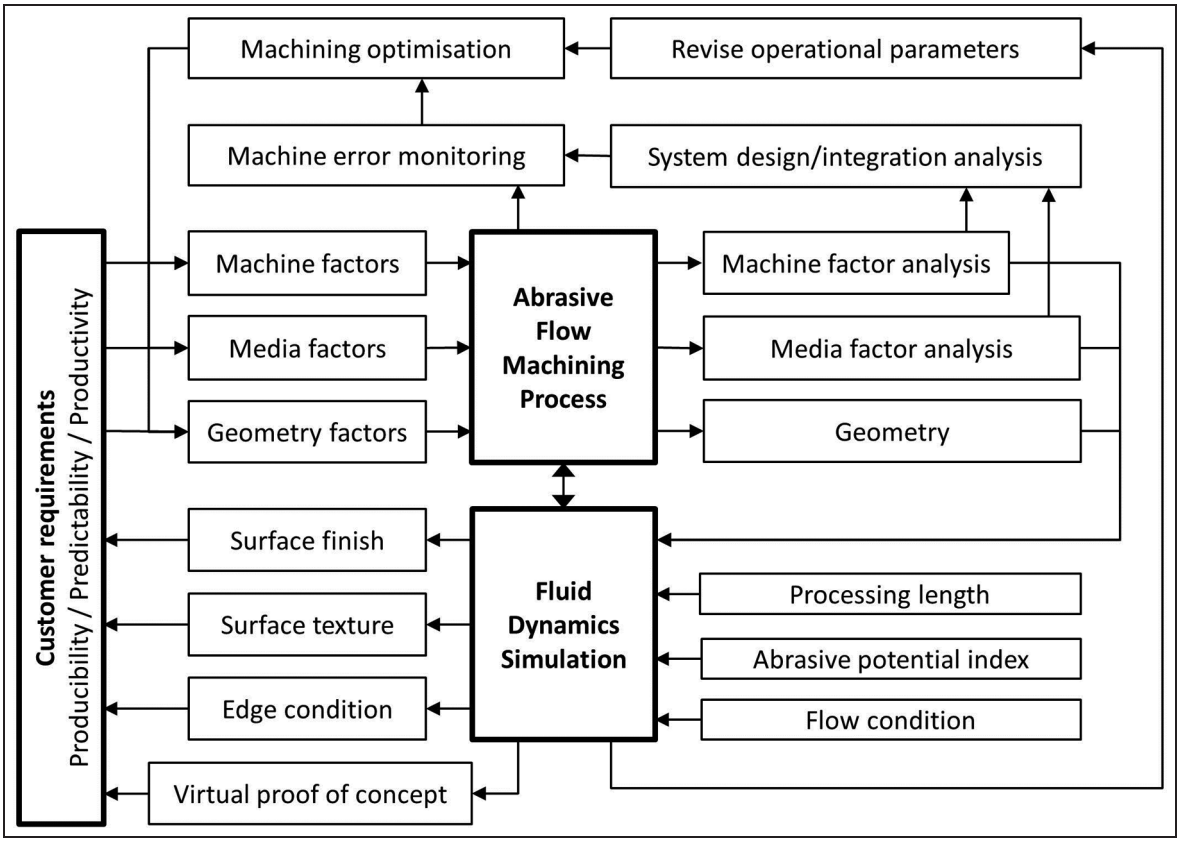

Figure 2. Map of CFD integration with AFM.

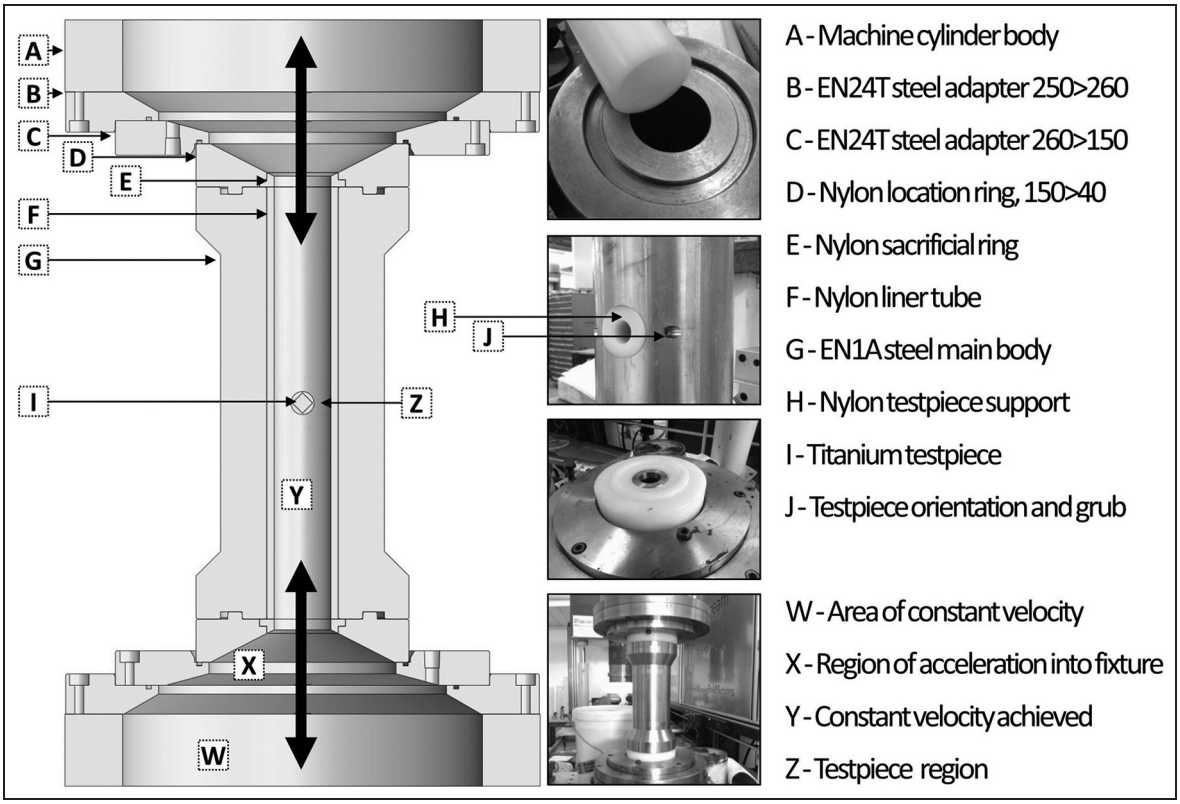

Figure 3. Experimental set-up in section view.

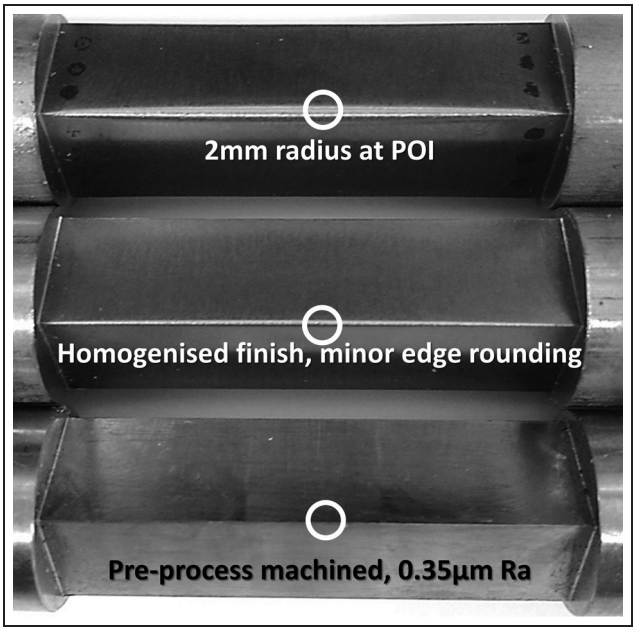

Figure 4. Titanium testpiece form; all samples contain a centre section of 10 × 10 × 40 mm.
POI: point of interest.

Table 1. Process factors and levels' selection.

Factors	Levels	Derived	M/C value
Velocity	+1	325 mm/s	280 mm/min
	0	230 mm/s	195 mm/min
	−1	100 mm/s	85 mm/min
Temperature	+1	45°	45°
	0	35°	35°
	−1	25°	25°
Quantity	+1	250 m	Stroke 150 mm, cycles 42
	0	145 m	Stroke 146 mm, cycles 25
	−1	40 m	Stroke 144 mm, cycles 7

walls to travel at reduced velocity, hence the wear pattern in the upper sample in Figure 4. Data are only collected from the centre line, to be assured that the user-set velocity is in full effect.

Variables are reduced from five to three; the stroke rate and number of cycles are compounded into a derived unit of quantity of processing (m), whereas pressure is discounted as the machinery requires a user-set velocity – pressure is delivered to reach the required level. Experimental factors are therefore set to velocity, temperature and quantity.

Prior works have shown a three-level experimental strategy to be a wise choice[10,12,14] as effects are known to be nonlinear. The minimum 3^3 requirement allows the use of response surface methodology (in the form of the Box–Behnken design), known for ease of modelling quadratic functions, functioning most reliably when levels are moderate (representative of practical process values) and greater efficiency than the Central Composite Design (CCD) when studying under four factors. Table 1 shows the selected process factors and levels.

The structure collects 12 datapoints from the edges of the process space and multiple centre points. The researchers deemed it necessary to include off-line repetitions before integrating values of higher accuracy into the process model. Level's selection was achieved by determining the least (V−, T+) and most (V+, T−) demanding to pump by trial and error. The Hagen–Poiseuille equation was used initially to help design fixture geometry using media viscosity calculated through machine back-pressure requirements – the equation only applies to laminar flow and we have exceptionally stable laminar flow of Re = 0.043.

Velocity drives the delivery of the media – we are limited to 300 mm/min (0.005 m/s) in terms of machine maximum capability; an upper level was set at 280 mm/min (0.0046 m/s) after testing with the lower level for temperature. Our fixture geometry combined with media viscosity drives a linear acceleration based on cross-sectional area (CSA) whereby the piston diameter of Ø250 mm (CSA 0.049 m^2) can be compared to the two 'half-rounds' left by the flow passage on either side of the workpiece edge of CSA (0.000696 m^2), creating a ratio of 1:70 between machine and workpiece POI. Our upper level of 0.0046 m/s is now known to be travelling at 0.322 m/s at the POI. This extends to levels 0 and −1.

Media temperature is controlled by a closed-loop system whereby a probe constantly monitors for changes, activating a refrigeration loop or deactivating to allow the permanently installed and functioning heating mats to raise the temperature. Through experience, media is known to undergo viscous heating, where operation at high pressures causes internal friction between shear planes to heat beyond the capacity of the refrigeration system. The occurrence is minimised by operating the machine within tolerable limits.

Similar to velocity, we must retain transferability in quantity, that is, our input levels must be related to the POI. Since the volume of media in the machine cylinder (0.00736 m^3 (150 mm stroke)) is greater than the volume in the fixture (0.000373 m^3), we can establish that the ratio of volume is 1:19.73. Therefore, cylinder travel drives media contact with the sample surface by this ratio, equating to a −1 level of 150 mm stroke (1 cycle = 2 strokes) at seven cycles (total of 2 m machine travel). A total of 2 m of machine travel is equal to ~40 m of processing within all surfaces in the fixture. The testpiece is processed with 40, 145 and 250 m.

Analysis of effects on surface features and process capability

Responses are recorded for three dependent variables: average surface roughness (Ra, µm), MR (mm^2) and peak height reduction (PHR, mm). These units are selected based on industrial requirements for geometry specification. Surface roughness is typically a 'no-more-than' specification, so improvement upon customer

values (or preprocess experimentally derived predictions) is acceptable. In the case of MR and PHR, edge rounding requirements in customer specifications typically specify a tangential radius between two other features where the radius value is toleranced by a range throughout which it may fall 'non-tangentially'.

Radii tolerances are based on feature function; Mollart Engineering Ltd frequently deals with components where intersecting features are responsible for carrying wires or hydraulic fluids. These functions require features that are simply rounded to an extent that insulation may not strip from wire, or that flashing and debris may not enter a stream of hydraulic fluid. MR as a response is implemented in this research for the purpose of comparing a simulated flow regime to physical MR – we evaluate the X–Y plane of the test-piece at the point of greatest velocity for greatest accuracy. PHR is an unconventional unit derived in this research for the purpose of differentiating between area reduction (catered for by MR) where the MR value may not describe the erosion of a peak – that is, MR has occurred, but the location of MR (while still high) has left a functionally undesirable edge. PHR describes the erosion level perpendicular to the flow path.

Measurement of these responses is achieved with two instruments; roughness is measured with a non-contact solution – a white light interferometer (WLI) (ZYGO NewView™ 5000). MR and PHR are measured with a Mitutoyo's CV3100 Formtracer series.

Figure 5 illustrates the mind-mapping process of collecting data from the component samples, conversions and resultant numerical outputs by using preprocess engineering analysis, shop-floor metrological measurement and post-process data processing and result's formulation.

Average surface roughness

Samples started with a consistent 0.35 μm surface roughness milled finish, resembling a reflective polished finish. Grey, non-reflective finishes were seen on all processed components, even those with improved surface finish – this points to a ploughing mode of MR, whereby the sheared surface of a milled finish promotes a mirror finish and AFM shows a dull finish (with this grit size) based on the random dispersion, size and orientation of the grains. Finish was, however, homogenous – having removed any sign of milling tool path, which has key importance in applications of cosmetic value.

Average roughness responses are collected in the range 0.239 and 1.252 μm, while standard deviation (SD) between repetitions is < 0.08 μm. Datapoints have been plotted in a run order versus response scatterplot, whereby results are spread throughout the process space, showing a low likelihood of machine bias. Figure 6 displays three WLI images, from roughest to smoothest – despite the application of F24 grit (mean size 686 μm), we are able to alter the surface condition within this range, in this geometry condition. The far left interaction plot shows that (with average quantity) roughness will linearly increase with velocity when processed at 35 °C. Velocity has little to no effect on surface roughness when operating beneath ~200 mm/s at extreme ends of the temperature scale – this can be explained by matrix and reinforcement principles; at low temperature, the matrix is stiffer, preventing free grit orientation and thus improving the shearing mode of MR – the carrier's dilatant (shear thickening) behaviour increases under increased velocity. The centre interaction plot is useful for an operator; it shows increased quantity of processing to steadily increase roughness, irrespective of velocity. The Q = 250 m line shows a tapering off, indicating an effect similar to that of using different grades of sandpaper – eventually, the grain size in media will reach a terminal roughness value, where neither quantity, temperature nor velocity had any impact. The right-hand plot shows how temperature dominates as a single factor – consisting of 30% of total effect on the surface, increasing temperature results in improved surface finish – contrary to the left plot, we may simply be placing the grits into different modes of MR; for the same grit size, a stiff matrix will provide an optically reflective surface through shearing, while a weak matrix will provide a non-reflective surface through ploughing. Both surface finishes will be the same. Temperature, velocity–temperature interaction and quantity are found to be the three most significant terms (in that order) in ability to affect surface roughness.

MR

Starting with a 90° edge positioned at 45° to the flow field, edge geometry is consistent between all samples, where error is limited to the milling machine rotary table accuracy of 5 arc-seconds, used to position the four faces of the square section. Using the Formtracer instrument output, we know that radii (where tangentially formed) range from 0.04 to 1.2 mm. Visually, it can be seen that edge rounding is not consistent along the sample length (see Figure 4), showing evidence of the non-Newtonian flow field in effect. We know that the machine's greatest influence is exerted upon the centre line of the flow field, which dictates the measurement location.

Experimental levels have provided a range of values, from 0.07 to 1.03 mm^2– SD between repetitions is < 0.059 mm^2. An increased magnitude of variation was found when processing parts for longer duration and greater velocity, while empirical evidence suggests the machinery fails to retain standards of repeatability when the machine is forced to work harder and longer.

Figure 7 shows three plots of interaction: VT, VQ and TQ. Lower left considers a constant quantity of media and shows that with increasing velocity, temperature drives MR, increasing with velocity, apart from one exception at 25 °C where MR initially increases

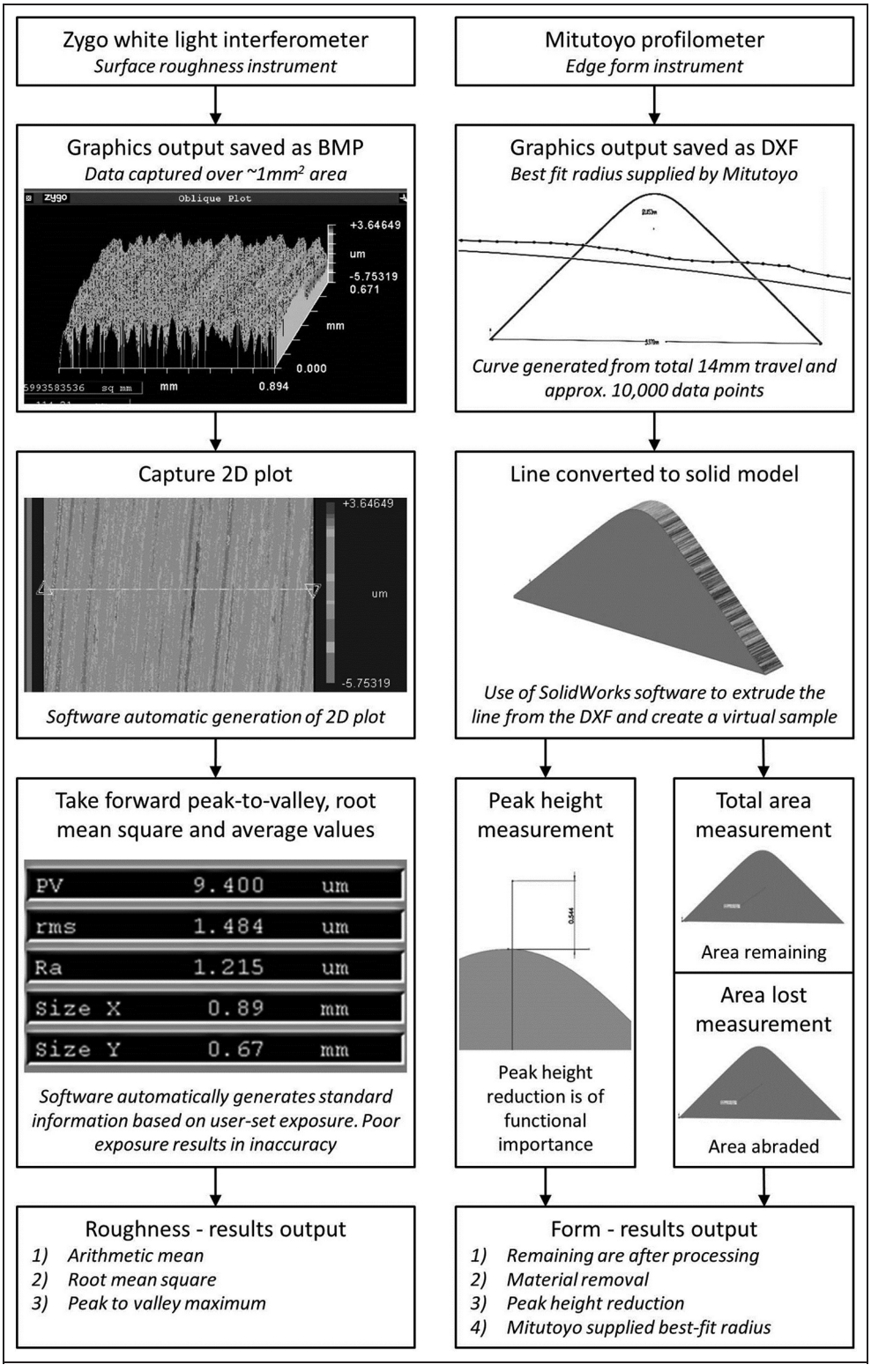

Figure 5. Process of collecting data from samples, conversions and resultant numerical outputs.
2D: two-dimensional.

then reduces – increased viscosity at lower temperature provides greater support for abrasive grit, although if the media travels too quickly, edge conformity is reduced and MR is limited. This is reinforced by considering the same VT plot in Figure 8. The half-normal plot shows that VT is responsible for 20% of total MR effect. The centre VQ plot shows that rate of change of MR increases linearly with velocity, but quantity increases roughness by 0.2 μm for every 100 m of travel. Naturally, these values are only relevant to this media and geometry, but the effect would scale accordingly elsewhere. The right-hand interaction is between

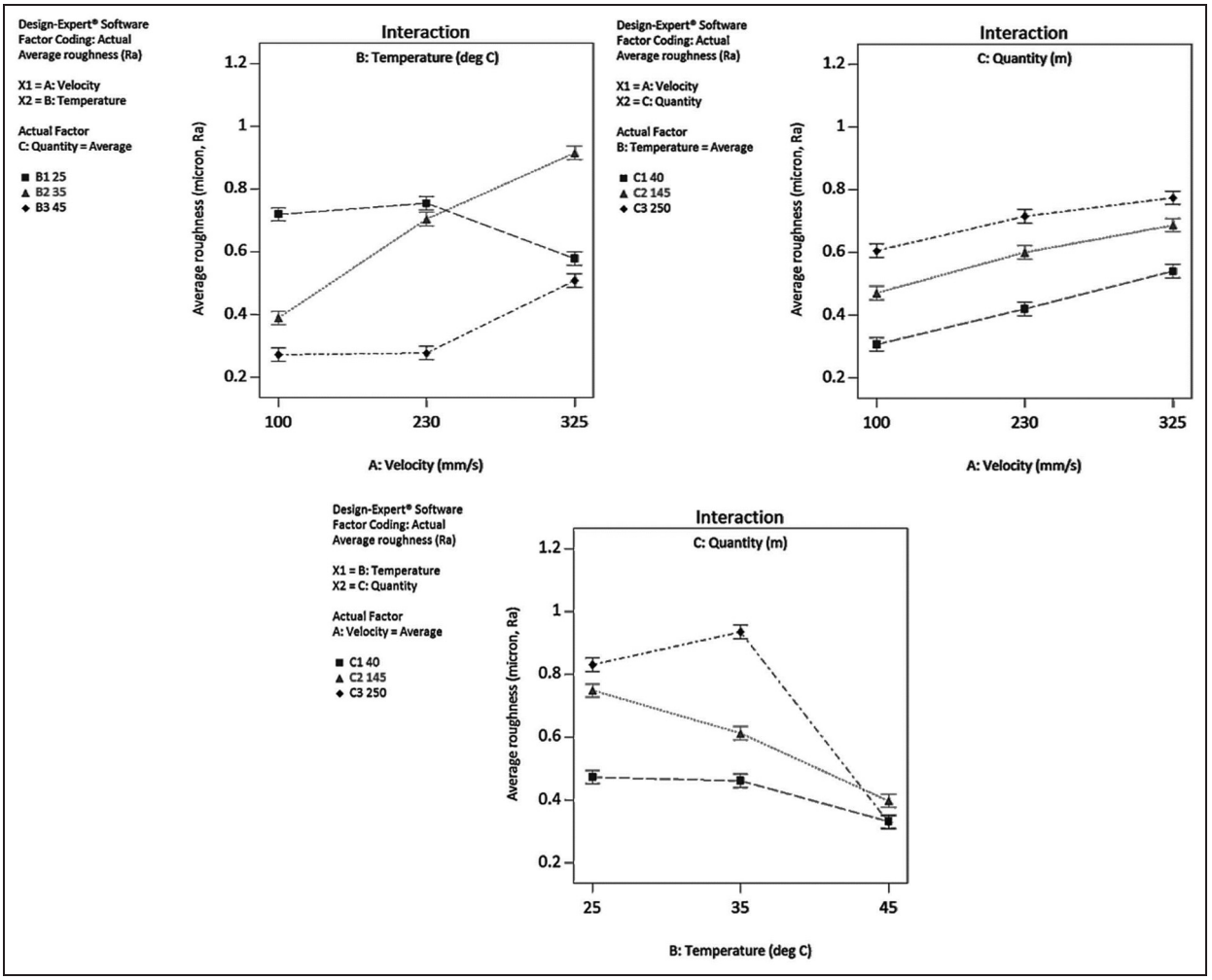

Figure 6. Three plots from a WLI and three interaction plots between velocity, temperature and quantity.

temperature and quantity; TQ is responsible for over 37% of total MR effect and shows that a higher quantity of processing will remove more material, but combined with temperature change of ~20 °C, we can more than double the effect. Approaching 45 °C, MR is poor irrespective of processing quantity. Irregularity between line gradients at different processing quantities suggests another physical phenomenon is manifested, as we expect the gradients to travel in a similar direction when treated with scaling variables. In this instance, we are likely seeing the effect of media viscosity and edge conformity.

PHR

Dimensions of the sample in processing orientation are known, where the preprocess peak condition can be overlaid on the Formtracer output – this allows a single numerical value to be measured between the previous and current peak height, which differentiates itself from MR by referring specifically to the reduction of the functionally important edge. The measurement is collected normal to the flow field, from the same data as the MR output, and therefore only in the centre of the flow field.

In contrast to the other responses, PHR offers the greatest spread of points across the process space and a maximum SD of 0.057 mm. A similar phenomenon is noted as with MR – deviation between repetitions is greater in trials of high velocity and quantity. Error is well distributed about mean values, as evidenced by bars in Figure 8.

This dataset offers a range of responses from 0.05 to 0.667 mm, allowing a significant degree of control over the edges in production parts, equating to a 1.5 mm radius. The interaction plots in Figure 8 highlight the differences in PHR to MR; PHR is driven by quantity. A total of 35% of PHR effect can be attributed to this factor. Second, the temperature–quantity interaction makes up the next 18% of the effect.

The leftmost interaction plot in Figure 8 shows that increasing velocity will generally increase PHR, and response magnitude is strongest at higher temperature, likely due to increased shear thickening behaviour under increased pressure. Looking closer at 25 °C and 35 °C highlights the same viscosity to geometry-conformity

AQ4

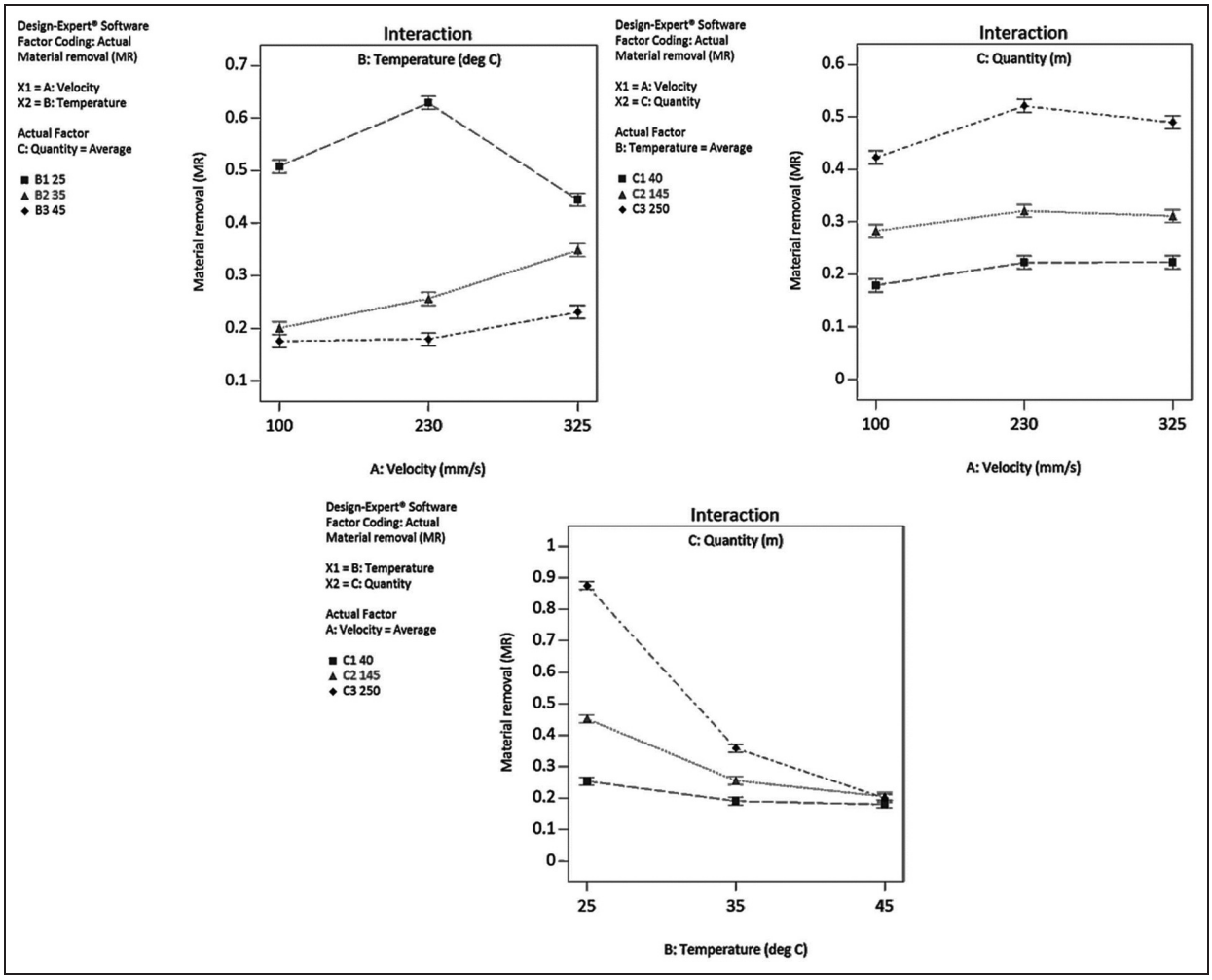

Figure 7. Three plots derived from Formtracer output and three interaction plots.

flow problem, where at 35 °C a linear improvement in PHR is achieved, but a negative response at 25 °C questions previous assumptions of 'the more viscous the media, the greater the edge rounding'. Given geometrical complexities in production parts, this is a significant finding, as it can be argued that an optimum flow field condition is necessary, one which is controlled by velocity and temperature.

The centre interaction plot identifies quantity to be insignificant to process outcome when manipulated with velocity – PHR levels are offset by varied quantity by a uniform 0.1 mm PHR/100 m quantity. Increasing velocity has no effect on gradient of response. This is useful in a production environment when a user needs to predictably gear up or gear down a response value.

The leftmost plot shows the TQ interaction, whereby PHR levels are significantly altered when low temperatures are combined with high quantities. Processing quantity can be limited by high temperatures, much as with MR; at 25 °C, 0.2 mm PHR is achieved per 100 m processing; however, that value reduces to 0.1 mm PHR per 100 m processing at 35 °C and ~0.03 mm per 100 m at 45 °C.

Predictive model

Data collection activities have provided the ability to produce type III analysis of variance (ANOVA) tables, which are re-employed with software to create predictive equations based on data best fit estimates – each of the three responses from a 3^3 full factorial design is converted into datapoints required for the response surface methodology (RSM) Box–Behnken design. Surface roughness and MR data are calculated to fit best to a linear model, while PHR fits a two-factor interaction (2FI) model

AQ5

$$\mathrm{Ra} = 0.5439 + (0.0018 \cdot \mathrm{V}) - (0.0137 \cdot \mathrm{T}) + (0.0012 \cdot \mathrm{Q}) \quad (1)$$

$$\mathrm{MR} = 0.6655 + (0.0003 \cdot \mathrm{V}) - (0.0166 \cdot \mathrm{T}) + (0.0013 \cdot \mathrm{Q}) \quad (2)$$

$$\mathrm{PHR} = 0.7585 - (0.0035 \cdot \mathrm{V}) - (0.0169 \cdot \mathrm{T}) + (0.0032 \cdot \mathrm{Q}) + (0.000094 \cdot \mathrm{V} \cdot \mathrm{T}) + (0.0000065 \cdot \mathrm{V} \cdot \mathrm{Q}) - (0.000095 \cdot \mathrm{T} \cdot \mathrm{Q}) \quad (3)$$

Naturally, these findings are only applicable to this combination of media and geometry, but critically the

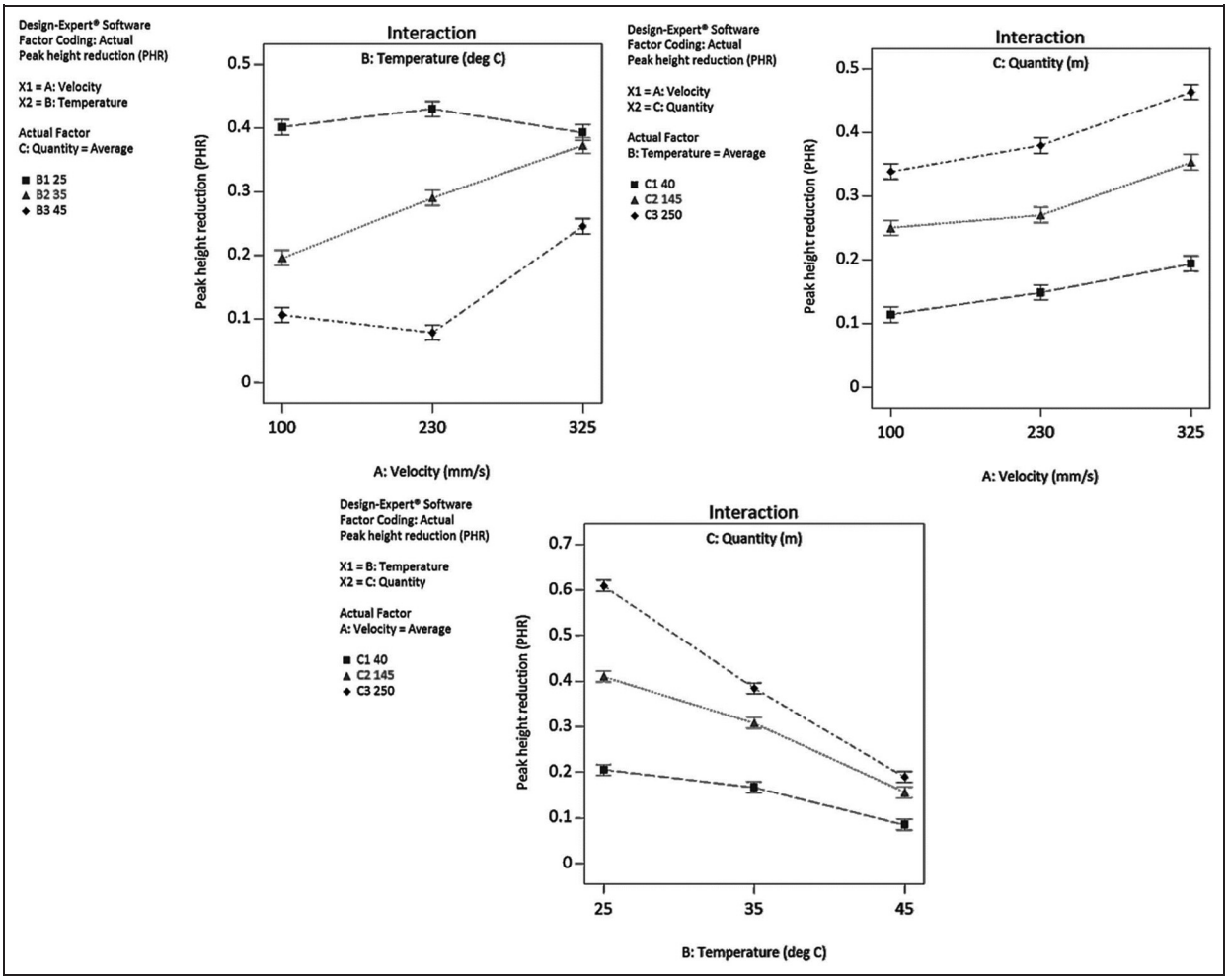

Figure 8. Three plots derived from Formtracer, solid modeller output and three interaction plots.

results are able to extend the findings of the study for the purposes of dataset extrapolation – increasing the verification possibilities where simulation of results is concerned (within limits of model error). Figure 9 displays the results of model application by plotting values of the collected datapoints with respect to the model's predicted positions – additional verification points were sourced by adopting the missing experimental configurations of the Box–Behnken from the 3^3 factorial design. Figure 9 also contains verification points, that is, points captured at arbitrary locations within the process space – these are marked on the plots; there are three unique combinations, plotted on each of the three response variable plots.

An industrial case study on an oil and gas industry component

An industrial case study is carried out by immediate transferral of the AFM approach and its industrial implementation perspectives to AFM processing of a complex oil and gas industrial exploration component. The findings discussed in section 'Analysis of effects on surface features and process capability' can be considered relevant when considering the POI in the component contains a 90° edge where flow travels at 45°, a velocity over the POI is calculable using a CSA conversion and processing volume is converted by dividing volumes. Figure 10 shows the results of 325 mm/s, 35 °C and 370 m of AFM processing of the component as required by the industrial company. Empirical evidence and prior research[15] suggest that a VQ interaction controls the differential in edge rounding between the radii of the slots and the long side – quantity discrepancies occur between the centre of the slot and the edge where a less restrictive path is found through the centre. Excessive velocity prevents the top edge of the slot from obtaining sufficient processing due to geometry-determined flow path – this can be improved by reducing velocity to allow a more uniform distribution of pressure around the inside of the port. Visualisation of this effect will be presented in further work.

Future applications of the process include surface finishing of medical-grade titanium alloy implants, produced by ALM, specifically through the direct metal laser sintering (DMLS) process. Comparatively, the material is more ductile and fracture-resistant than

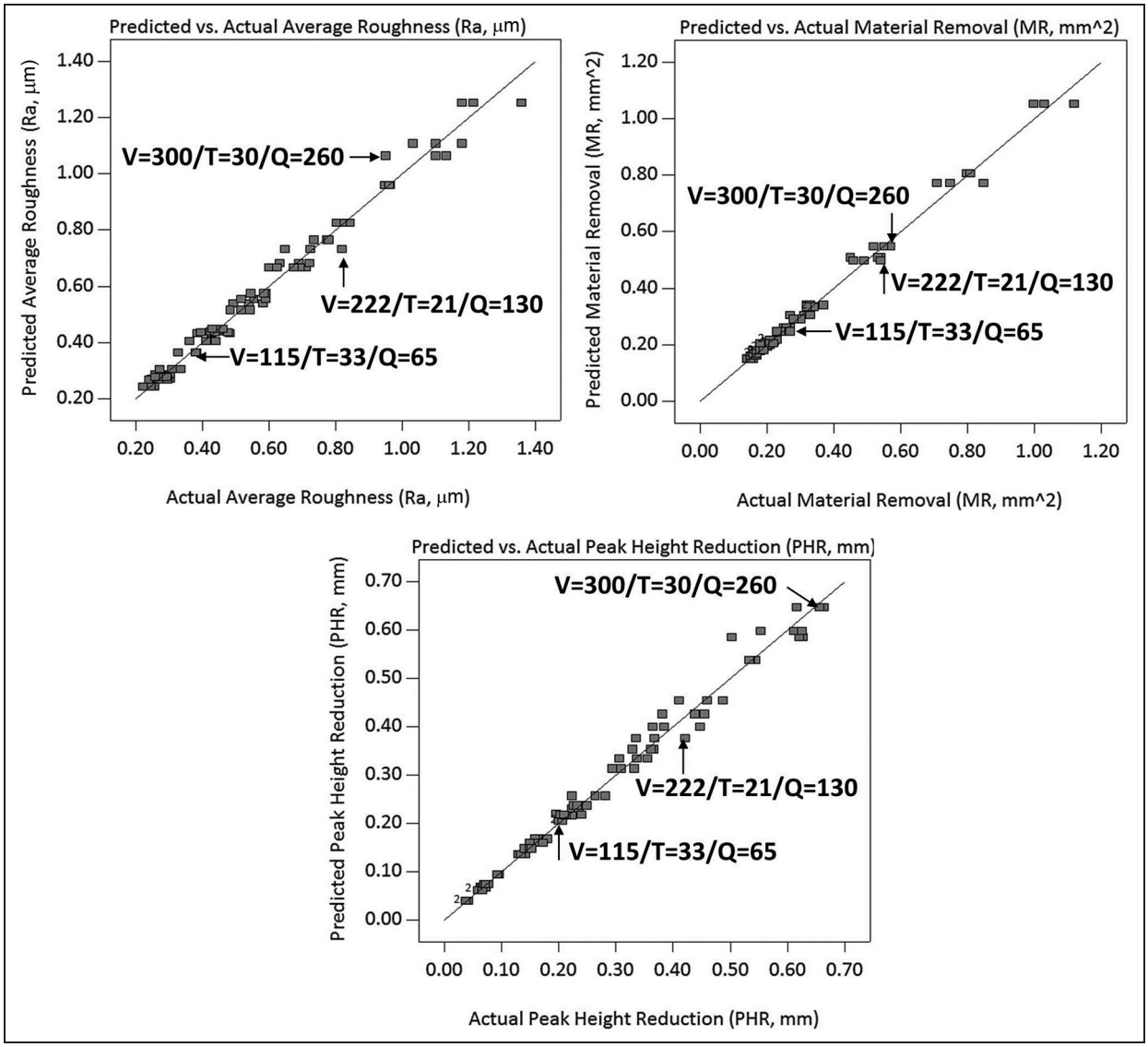

Figure 9. Plots of best fit for actual values against predicted values for responses.

common grade 5 for bone-contact applications, which theoretically demands more from the AFM process. These materials are able to be produced in the geometry used in the testpiece environment of the study presented in this article – by adopting the same test methodology, erosion achieved is known, test shear conditions are known (as the simulation does not alter) and correlation between input and output is derived – in little more than 13 samples (minimally populated Box–Behnken RSM design), it is possible to characterise AFM's capability with a new material. To enhance the level of control, an experiment has been completed to deliver equivalent data from a 3^3 RSM design studying carrier viscosity, concentration of abrasive and grit size.

Conclusion

In this article, an integrated systematic investigation is presented by focusing on the collective effects of the process variables on surface generation in AFM of titanium alloy 6Al4V. The integrated systematic approach aims to render the AFM process in a predictable, producible and highly productive scientific manner. The key variables in the machine corner of the AFM triangle are identified and studied. Each of the response variables studied scales in relative proportion with one another, proving that increased MR and PHR will result in poorer surface roughness values, for a constant media and geometry. The following conclusions are further drawn up:

- Optically non-reflective surfaces will be common in edge rounding operations without consideration to a secondary 'fine grit' stage to mimic the lapping process.
- The process is useful for cosmetic purposes to eradicate a mixture of machined surface finishes by 'overwriting' the finish with its own.

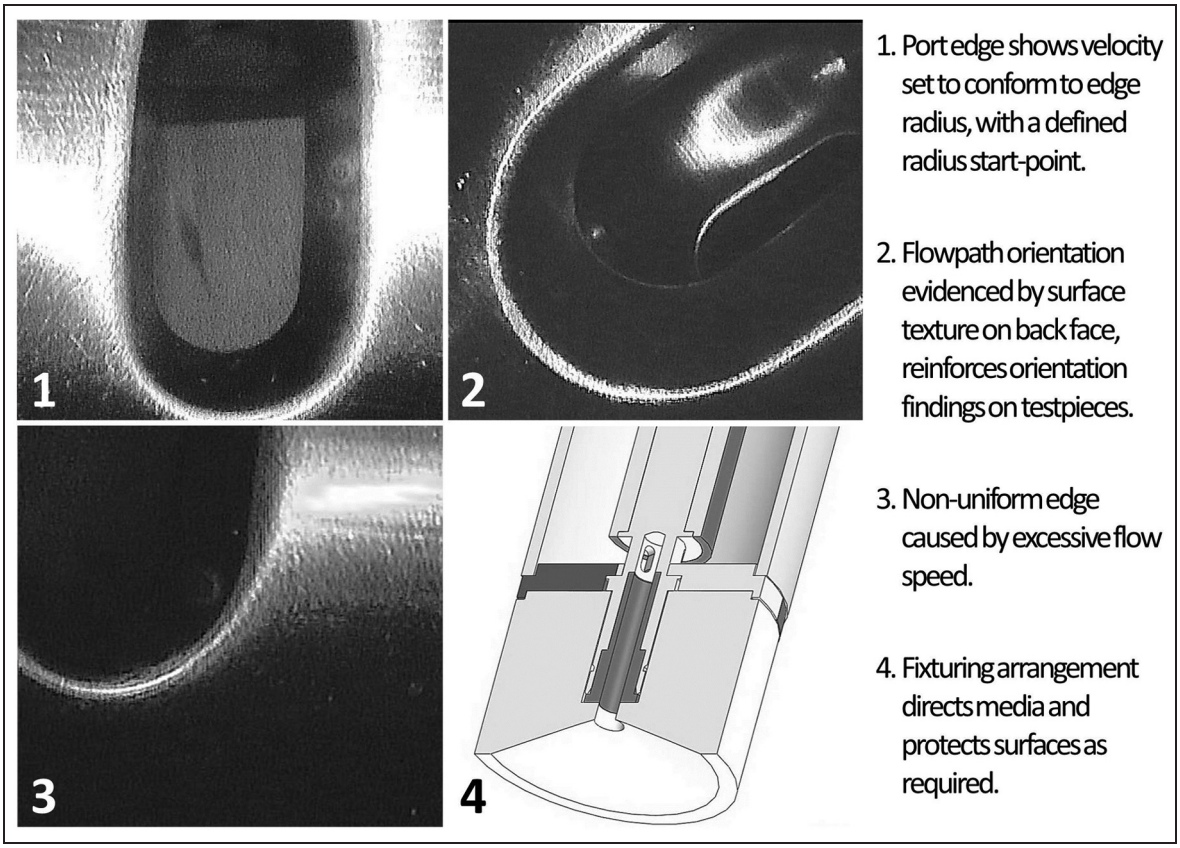

Figure 10. Areas of component inspected with Ø4 mm CCD camera on articulated head.

- For the majority of samples, roughness results exceeded the preprocess condition, calling into question the applicability of AFM for surface finishing – grit sizes and grain fractions will be studied in consequent work as prior literature shows improvements with finer mesh grit.
- Edge rounding of titanium alloy 6Al4V with media of primary grit size ~700 μm can be achieved up to ~1.5 mm, dependent upon carrier behaviour.
- Material is removed through the mechanism of ploughing and rubbing in the direction of flow as shown by the WLI images.
- Feature alteration is driven by temperature and quantity. These factors are therefore considered more critical for a production environment.
- Temperature drives surface finish in this experiment, and we know the response of viscosity to temperature to be linear, reducing with increased heat – the interaction of viscosity and grit size is therefore important to understand clearly in future work.

Furthermore, considering the importance of temperature to all responses variables, it must be concluded that rheological state of the carrier is of significant influence to process outcome. Two further research interests are identified with industrial significance, that is, a study of media factors, isolated in the media corner (as in this experiment) and a study to correlate response variable values with a simulated value to prove viscosity-edge conformance assumptions.

Declaration of conflicting interests

The authors declare that there is no conflict of interest. AQ6

Funding

The authors would like to thank the support by UK Technology Strategy Board (grant number: 710231) and the UK Engineering and Physical Sciences Research Council (EPSRC) for the EngD Scholarship. AQ7

References

1. Williams RE and Melton VL. Abrasive flow finishing of stereolithography prototypes. *Rapid Prototyping J* 1998; 4(2): 56–67.
2. Lin YC, Chow HM, Yan BH, et al. Effects of finishing in abrasive fluid machining on microholes fabricated by EDM. *Int J Adv Manuf Tech* 2007; 33: 489–497.
3. Tzeng HJ, Yan BH, Hsu RT, et al. Finishing effect of abrasive flow machining on micro slit fabricated by wire-EDM. *Int J Adv Manuf Tech* 2007; 34: 649–656.
4. Walia RS, Shan HS and Kumar P. Enhancing AFM process productivity through improved fixturing. *Int J Adv Manuf Tech* 2009; 44: 700–709.

Proceedings of the ASME 2014 International Design Engineering Technical Conferences &
Computers and Information in Engineering Conference
IDETC/CIE 2014
Aug 17-20, 2014, Buffalo, New York, USA

DETC2014-34110

ENERGY AND RESOURCE EFFICIENCY IN THE ABRASIVE FLOW MACHINING PROCESS: AN ASSESSMENT OF ENVIRONMENTAL AND ECONOMIC VIABILITY WITHIN A UK PRECISION MACHINING SME

Mitchell J. Howard
Advanced Manufacturing & Enterprise Engineering (AMEE) Department
School of Engineering & Design
Brunel University
Uxbridge, Middlesex UB8 3PH, United Kingdom
Email: mitchell.howard@brunel.ac.uk

Kai Cheng
Advanced Manufacturing & Enterprise Engineering (AMEE) Department
School of Engineering & Design
Brunel University
Uxbridge, Middlesex UB8 3PH, United Kingdom
Email: kai.cheng@brunel.ac.uk

ABSTRACT

Environmental performance of the abrasive flow machining (AFM) process is currently not well understood. Its flexibility as a manufacturing process has only recently been realised in SMEs (Small to Medium Enterprise) as a feasible automated alternative to deburring and polishing of complex geometry by hand, and as an alternative to honing and grinding using semi-automated machinery. [1-3]

Economic benefit is still the main driver in the commercial uptake of environmentally-sustainable technologies [4, 5]; despite AFM's known flexibility and capability, this paper presents systematic research by focusing on AFM including, 1) assessing and comparing the requirements of competing processes (values sourced from [6]), 2) their power consumption, 3) operating conditions, 4) cost of pre-requisite ancillary equipment and 5) embodied energy and recyclability of machine structures and consumables. Three workpiece scenarios are laid out (distinguished by feature-count, processing time, tolerance-demands and setup-count) for comparison purposes – the trade-off between environmental and economic cost is described with reference to industrially-significant quality measures such as repeatability, accuracy, precision and uniformity. Key findings in this research include the comparatively high energy demand from natural gas-fired warm air blow-heaters, a requirement for the heating of spaces for human labour activity. Performance is shown to be limited by design – the AFM machine in this study operates with only an additional 22% of current between idle mode and production mode [7] suggesting sub-assembly redesign may be of benefit. To conclude, the AFM process offers a clear route to sustainable part-finishing, low-maintenance and high potential for 'greening' considering factors in addition to running cost.

INTRODUCTION

The AFM process was originally developed to automate deburring and finishing processes present in the automotive and aerospace industry [8]. Initially the target was honing, although it quickly became apparent that edge rounding, polishing and deburring were successful. Today, the process is adopted for any number of its uses as highlighted in Tab. 1. AFM systems comprise three major elements – machine, media and geometry; the machine is typically two vertically-opposed hydraulic pistons with approximately 300mm of stroke. These units vary in maximum pressure, and a machine builder can opt to fit their own design of piston and cylinder to create a chamber within which abrasive media is stored and delivered. Media is a viscoelastic substance, comprised of abrasive microgrit (typically 0.05-1mm in size) carried by a silicone polymer, modified to achieve viscosity that pumps readily and supports the grit sufficiently to enable abrasive action upon the substrate surface. Grit measures approximately 50-60%wt [9, 10] of total

Table 1. OPERATIONS ACHIEVEABLE BY AFM.

Operation	Requirement	Concerns of AFM
Deburring	• Carbide burrs • Power tools • Human labour	Automated operation, but poor stock removal. An initial human deburr is required.
Honing	• Hone • Honing tools • Human labour	Automated operation, difficult to know when size is achieved, polishes simultaneously.
Surface Finishing	• Polishing discs • Power tools • Human labour	Automated operation, inaccessible cavities, dependent on grit size, long cycle time.
Removal of recast layer	• Shot peening • ECM • Vibratory finishing	Automated operation, grit size can control MRR, capable of processing small holes.
Radiusing	• Carbide burrs • Power tools • Human labour	Automated operation, MRR drops with increased cycle time, polishes simultaneously.

product volume. The geometry is comprised of two elements – the workpiece geometry (over which no control is held by the machine operator) and the tooling geometry, used to create a passage from cylinder to part and to create a flow condition conducive to desired processing.

Application to diesel and marine componentry are most common; fig. 1 presents six active applications, 1) additive layer manufacturing (ALM) produced parts remain of poor finish, even by modern standards – with geometry producing capability beyond that of traditional machinery, the ALM process requires an equally flexible post-process such as AFM for surface finishing, 2) marine applications consist mainly of propellers manufactured in corrosion resistant materials such as brass and stainless steels. Designs attempt to reduce detrimental cavitation that leads to fatigue failure, where AFM is beneficial – improved surface finish and rounded leading-edges reduce cavitation, while compressive residual stresses are imparted, creating a surface layer of approximately 10μm with greater fatigue resistance [11], 3) diesel injection systems such as those produced by Bosch and Delphi seek to improve atomisation and thus improve fuel burning efficiency – modern common rail systems operate at 2000bar [12] pumping fuel through injector body outlets of <Ø0.1mm where AFM assists in accurately sizing outlets and improving surface finish, 4) turbomachinery components, whether aerospace gas turbine blisks or energy-generating steam-turbines benefit from AFM by compressive residual stress, exceptional surface finish in difficult-to-machine materials, high machine capacity and repeatability [13], 5) transmission components in automotive and oil & gas industries must provide safe, rounded passages for electrical wiring – product failure has severe financial consequences, and where space is at a premium, passages are packed with thinly-insulated cabling [14], and 6) oil & gas industry parts are routinely operated with liquid, gas and electronic components within millimetres of one another – a slip-of-the-hand in manual finishing can lead to >USD 70,000 of scrap, justifying the use of expensive and non-traditional automated processes such as AFM – the reduced risk and improved repeatability is of great importance to SME manufacturers.

Figure 1. CURRENT AND EMERGING APPLICATIONS.

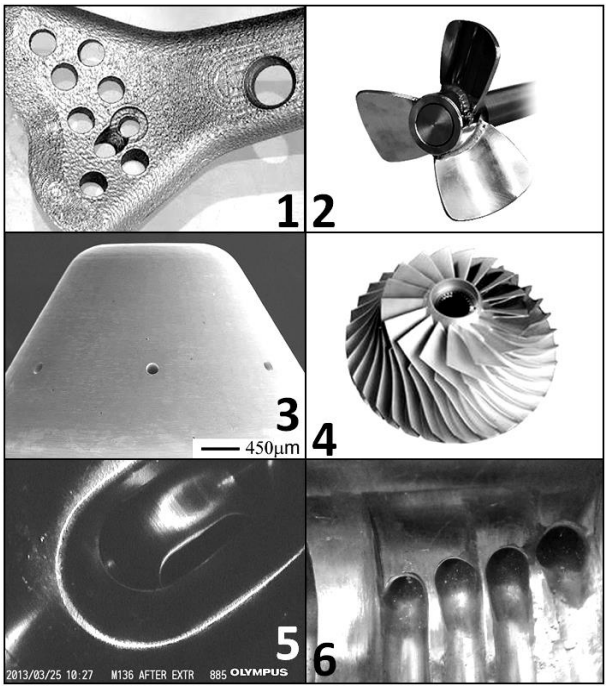

Human variation removal, risk reduction and quality improvement is the target of most AFM operators as finishing costs in manufacturing are said to comprise over 15% [15] of total product cost. At Mollart Engineering, a UK specialist precision machining SME, the AFM process was introduced to perform internal edge-rounding and polishing of complex parts, where many operations were simply impossible to carry-out by hand. Following success in complex geometry, more routine and established manual operations are now under consideration as candidates for replacement by AFM – but the authors of this paper pose the questions, "are these changes economically *and* environmentally viable?", "does the AFM process *always* exceed the suitability, capability and capacity of manual finishing?", "has the company inadvertently caused *more* damage by purchasing a dedicated machine?" and "can either process be *significantly improved* in terms of environmental performance and what are the projected gains?".

This paper identifies usage patterns, operating conditions, power consumption of manual, AFM and competing non-traditional finishing, considers a limited life cycle assessment (LCA) and makes recommendations.

USAGE PATTERNS & OPERATING CONDITIONS

Availability of sufficiently-capable automated-technologies for current industrial finishing requirements is poor - multiple automated-technologies are available for different finishing operations in a range of technical complexities and price points.

Figure 2. SEQUENCE OF OPERATION.

Where the value of machinery for a preferred automated-technology exceeds a threshold, potential purchases become unattractive to SME manufacturers in lieu of established and highly-flexible human labor. In an age of mechanized engineering, there exists no simple solution to adopting the most suitable technology for automated finishing.

Two technologies co-exist at Mollart Engineering – manual finishing by hand tools and AFM. A simplified, typical sequence of operations is presented in fig. 2, with center boxes representing the setup and running stages (manual left, AFM right) with main secondary requirements presented to the left (manual) and right (AFM).

Manual Finishing Mode of Use

Strengths of manual finishing include virtually zero setup time, simplicity of tool application and intelligent decision making by the operator. Weaknesses are largely dependent on task – the concentration time required may extend up to three hours, putting the operator at risk of making minor or major mistakes. Where tasks on a single workpiece extend the total processing time over days (sometimes weeks) and additional shorter jobs are interspersed with the longer job, the potential for errors is further increased. Ability to handle job complexity is manual finishing's greatest strength and simultaneously its greatest weakness – this paradox stems from the minimal setup time (as human-operated hand tools are used), while work is often repetitive and un-engaging. The action of material removal is physically performed by human labor that feels tiredness, stress/pressure and typically disconnected from the wider production process.

Manual finishing utilizes standard consumable tooling such as abrasive grits (i.e. aluminum oxide) supported on wire shafts by epoxy resins or other binders – they are applied by powered hand-drills and are available in infinite shapes and sizes to allow access to workpiece features. For harder materials, metallic 'burrs' are used, typically made from tungsten carbide. These are multi-flute and are somewhat less subtle than abrasive-loaded tools – they are expected to shear and chip material rather than rub, displace or grind, increasing process risk. The actions required to process the workpiece vary slightly upon each part in a batch due to human variation, leading to precision issues at the quality assurance stages. Work must be performed in a clean, quiet, well-lit, appropriately-heated, consistent and management-driven operating conditions. Cleaning requirements revolve around pneumatic airline usage and evaporating naphthalene ($C_{10}H_8$) ('panel wipe') to remove stubborn contaminants.

AFM Mode of Use

Mechanization of manual finishing operations is the goal of AFM – as presented in Tab. 1, five main operations are achievable with the process with varying degrees of convenience. In comparison to manual finishing, AFM requires three considerable time and cost investments, 1) a set volume of abrasive slurry must be manufactured (if an existing configuration is not suitable), 2) inlet tooling must be designed and manufactured, and 3) disassembly and cleaning is more demanding than the relatively dry and clean manual finishing.

As with manual finishing, AFM's greatest strength is also its weakness – as tooling complexity is based on part complexity, the effectiveness of the process is sometimes reduced to the tooling designer's ability to engineer a desirable flow condition; the strength however, is that once a suitable result is achieved, any operator (skilled or unskilled) can load and preheat media, assemble tooling and set the machine to run with confidence that components will be processed correctly.

The process is not subject to external stresses, nor does it require human operating conditions as described above. The material removal is achieved by an electrically-powered pump passing oil into a hydraulic ram with a piston mounted on the end which, to operate, is naturally more energy consuming than hand-guided drills. Dependent upon workpiece geometry and machine capacity, multiple setups may be designed to process groups of features within the maximum pressure of the machine – the cycle times are typically far shorter than manual finishing, and operations need not be run in serial; while manual finishing requires persistent human attention, the operator of an AFM machine may run operations in parallel, such as two or three unattended machining processes (also run after standard

working hours) in addition to cleaning or disassembly of tooling for the next operation.

While relative procedural aspects of the two processes can be compared, repeatable quality and reduced risk in achieving the final outcome is difficult to quantify objectively. Reject rates for batches of parts can be 0-100%, while annually approximately 14% of parts require re-work – unsatisfactory ways in which manual finishing can affect the part include under-processing, over-processing and damage to surrounding features. At Mollart Engineering, this means ~GBP1.23m can be at risk of human-induced manual finishing error. Under-processing is the simplest form of re-work which may cost 4-5hrs labor, while over-processing typically results in the requirement to add material using a welding process, usually TIG or electron beam. The costs of these operations alone can reach GBP1,000, in addition to the subsequent machining processes to correct the weld form back to the intended geometry, raising the total cost of re-work to approximately GBP1,500. As manual finishing is naturally performed after many value-adding operations, the part's ~1,450 features are exposed to the conditions of the chosen finishing process, increasing risk of forming undesirable geometry. Customers, particularly LEs (Large Enterprises), impose strict quality management and monitoring regimes on their incoming deliveries – the statistics gathered determine distribution of orders placed, and thus, revenue generation potential of SMEs.

POWER CONSUMPTION IN MANUAL FINISHING

Figure 3 presents the data collection assembly used to assess the electricity use in manual finishing; 1) power supply is delivered by single-phase AC at 240V with a power factor of 0.8, 2) current draw is read by a 'Fluke 337' true RMS clamp meter, positioned over the outlet from a standard UK three-pin plug, 3) drill speed controller is a 'Joisten & Kettenbaum Eneska 4-1' and 4) drill is a 'Joisten & Kettenbaum J-BM 50HT'. Consumption is measured in the three modes [7] of idle, run-time and production. Irrespective of mode, the equipment draws a consistent 0.2A, with measurement equipment error excluded by placing greater load (by hand) on an active drill, in which the current delivery increases significantly. Load upon the drill during production mode is very low, due to the fine nature of the application – power use is 0.038kW.

As the process is reliant upon human labor, a gas-fired air heater is used to heat the shop space – volume is calculated at 870m^3, and is maintained at 20˚c throughout the year over a two-shift system, operating 85hrs/wk. The heater is a natural as-fired AMBI-RAD UDSA 030 model, operating on single phase 230V, specified to regulate 2,725m^3/h and when g running at maximum load, requires 35.2kW and delivers 29.2kW, making it 83% efficient. Referring to Fig. 4, Central England Temperature (CET) is sourced from the UK meteorological office [16] and plotted throughout the months of the year – temperatures are an average of the last 10 years since 2003. Average annual heating requirement is 9.9˚c.

Figure 3. POWER METERING EQUIPMENT.

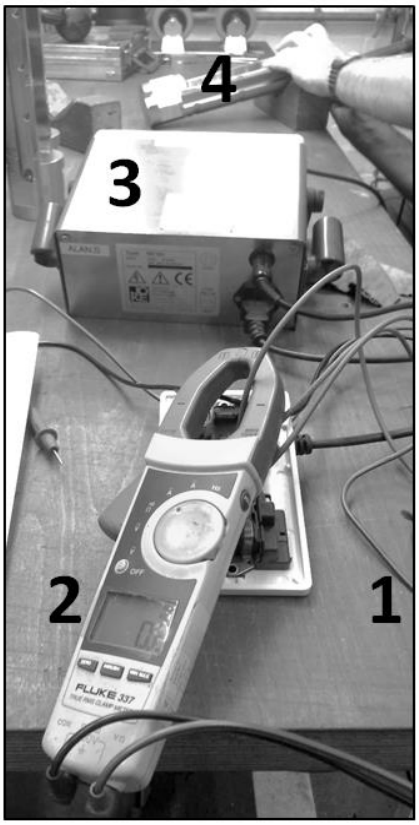

To calculate the energy requirement (and the power requirement in turn) from the air heater, the energy equation is used as shown in Eqn. (1), where Q is quantity of energy transferred (kJ), m is mass of substance (kg), c_p is specific heat of the substance (kJ/kg/˚c) and dt is the temperature difference (˚c). Density of dry air at 5-10˚c is 1.2754kg/m^3 – therefore, mass to be heated is 1,110kg. Specific heat of dry air is considered at 1.005kJ/kg/˚c, while the temperature change (dt) required is (20-9.9) 10.1˚c. This results in a final energy requirement of 11.27MJ to heat the space by 10.1˚c. These values should be considered a minimum as the factory has a high ceiling, poor insulation, cargo doors ajar and a mixture of ceiling heights preventing uniform temperature distribution. Equations (4-7) consider the time required to heat the space from 9.9˚c. E is energy (kJ), P is power (kW) and t is time (s).
Thermal transmission losses occur through the surfaces of the factory unit – Eqns. (8-14) determine the losses of the walls, windows and roofing – total loss is a little over 2kW. This value is important as the heater is not a proportionally controlled system, i.e. it does not operate continuously at a lesser rate – the maximum output is delivered until an upper threshold is met, then the unit shuts off and restarts when the low threshold is met. The low threshold is the legal minimum [17] of 13˚c, triggering a requirement to heat the building by 7˚c when reached.

Figure 4. MANUAL FINISHING HEATING REQUIREMENT.

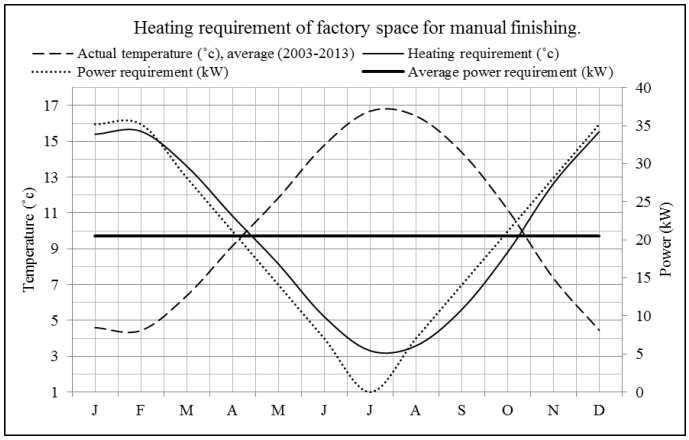

$$Q = m\, c_p\, dt \quad (1)$$
$$Q = 1{,}110 \times 1.005_{x10}{}^{3} \times 10.1 \quad (2)$$
$$Q = 11.27MJ \quad (3)$$

$$E = P\, t \quad (4)$$
$$t = E / P \quad (5)$$
$$t = 11.27_{x10}{}^{6} / 29.2_{x10}{}^{3} \quad (6)$$
$$t = 386s\ (6.4min) \quad (7)$$

$$Q = U\, A\, dt \quad (8)$$

$$Q_{wall} = 0.317 \times 130 \times (20\text{-}9.9) \quad (9)$$
$$Q_{wall} = 416.22W \quad (10)$$

$$Q_{window} = 2.8 \times 12 \times (20\text{-}9.9) \quad (11)$$
$$Q_{window} = 339.36W \quad (12)$$

$$Q_{roof} = 0.8 \times 161 \times (20\text{-}9.9) \quad (13)$$
$$Q_{roof} = 1.3kW \quad (14)$$

$$Q_{total} = Q_{roof} + Q_{window} + Q_{wall} \quad (15)$$
$$Q_{total} = 2.056kW \quad (16)$$

Heated to 20˚c with external temperature of average 9.9˚c, 7.8MJ of energy leaves the building before it reaches 13˚c (Eqns. (17-19)). This process takes 63min (Eqns. 20-22), as determined by thermal losses of ~2kW. Once cooled, the air-blower activates and continues to burn gas generating 29.2kW for an additional 4min to raise the temperature back to 20˚c (Eqns. 23-25). In summary, following the initial 6.4min period of heating from 9.9˚c, the room is left to cool to 13˚c over the next 63min. For 4min, the heater turns on, and repeats the cycle for the remainder of human occupancy – in percentage terms, 5.97% of time is spent heating and 94.03% naturally cooling.

$$Q = m\, c_p\, dt \quad (17)$$
$$Q = 1110 \times 1.005_{x10}{}^{3} \times -7 \quad (18)$$
$$Q = -7.8MJ \quad (19)$$

$$t = E / P \quad (20)$$
$$t = -7.8_{x10}{}^{6} / 2.056_{x10}{}^{3} \quad (21)$$
$$t = 3793s\ (63min) \quad (22)$$

$$t = E / P \quad (23)$$
$$t = 7.8_{x10}{}^{6} / 29.2_{x10}{}^{3} \quad (24)$$
$$t = 267s\ (4min) \quad (25)$$

POWER CONSUMPTION IN THE AFM PROCESS

Only electrical energy is required in AFM - the process operates in an unconditioned environment, with its own heating and cooling systems, mechanized pumping and control circuits that manage temperature and active software. The machine used in this example is a 2009 Micro Technica Technologies Duplex 250, specified to operate at 45bar or 300mm/min (whichever is reached first) with a media volume of 20L. The same Fluke clamp meter is used to collect current across three phases from the machine's electrical cabinet – three phases are fed in at 415V, with a power factor of 0.8; Fig. 5 presents the almost linear correlation between current draw and operating pressure. Draw is marginally greater when refrigerant is not running, due to a 'normally-open' valve requiring power to remain closed.

A typical sequence of operation begins with mounting the component and tooling assembly, clamping, setting the program to run, retracting cylinders then unclamping once complete. Starting in idle mode, the machine's control is off and draws 0.75A – moving into run-time mode with control on and no material removal activity, 7.7A is drawn. Unclamping draws 8.8A, while 10.7A is drawn while clamping, likely due to increased force applied. The machine spends an insignificant time performing any of these four actions; therefore they do not comprise any part of the analysis. With refrigerant on, when machine is working with low-load but still moving, the pressure reaches approximately 3bar, demanding 7.3A – 4.198kW, whereas manual finishing operates at less than 1%. When operated to excess at an unsustainable load (45bar), 8.35A is consumed, equating to 4.802kW, but typical target is 30bar at 7.8A, consuming 4.485kW. With refrigerant off, the draw is slightly higher; 3bar, 7.5A = 4.313kW; 45bar, 8.75A = 5.032kW; 30bar, 8.1A = 4.658kW. Typical job times range from 0.5-2.5hrs, where jobs normally require refrigerant to be active, particularly in small bore high shear-rate work (4.485kW demand) – assuming 2.5hrs, 11.213kWh is consumed, at a cost of approximately GBP1.39, generating 4.995kgCO_2e.

Figure 5. AFM CURRENT AGAINST PRESSURE.

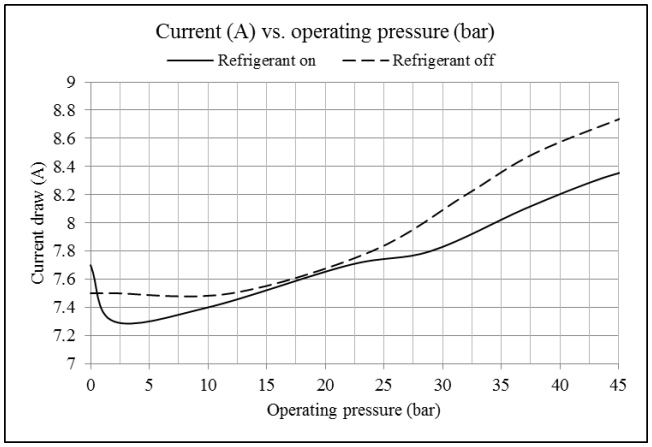

Power Consumption in Competing Automated Processes

Technologies for semi- and fully-automated finishing are numerous; fine machining is possible with high-quality machining centers, grinding is highly capable even with 30-40yr old machinery and electro-chemical machining (ECM) offers AFM-competitive surface finishes. These techniques vary widely in power consumption within their own class, but specific power in mechanical processes is comparable (as compared to chemical processes). Finish machining is found in the literature to consume approximately 9.59kW [18], grinding between 7.5-10kW [19, 20] and ECM at 3-100kW, converting to high current DC supply at 6-10V during processing [21].

Job complexity drives operational time, as in finish machining toolpath stepover must be minute to avoid stair-stepping; in grinding, a small mesh-size abrasive and low feed is used to minimize depth of indentation which extends process time; ECM requires complex tooling and electrolyte access – where electrode-to-workpiece gap is larger than desirable, efficiency drops as low as 10% [22].

All three alternative finishing processes lack the low-maintenance, surface texture generating and feature accessibility of AFM, while operating at comparable levels of power consumption and lower capability, critical when considering the cost of embodied energy described in this work.

PRODUCTION ENVIRONMENT ASSESSMENT

Operating manual finishing averages consumption of 2.226kW (over the course of 1h), whereas AFM averages <4kW. For a more complete example of energy consumption and cost of operation in a production environment, three example parts are set out that relate to active parts in Mollart Engineering's subcontract division as presented in Tab. 2. Man hours are excluded as the comparison is intended to highlight the direct

Table 2. EXAMPLE PART PROCESSING TIMES.

Part	Manual (h)	AFM (h)	Complexity	Setups
A	Serial, 3.5	Parallel, 1	Low (batch of 7)	1
B	Serial, 15	Serial, 2	Medium (batch of 6)	1
C	Serial, 110	Serial, 6	High (batch of 1)	4

economic and environmental issues, not human (social) cost.

Part A is a simple tube, used in a medical application for fatigue testing of material – a human operator can use an electric drill and 'flex-hone' for approximately 0.5h, while AFM can replicate the action with abrasive media to reach a required surface finish. Due to the small size and simple geometry, AFM can process the batch size of seven in parallel within 1hr, while manual finishing can only be done in serial, taking 3.5h. In this example the job is continuous; not obstructed by shift patterns and breaks, manual finishing of 3.5h means the heater is active at 35.2kW for 0.21h (12.6min), while the drills operate constantly at 0.288kW as the force to rotate a flex-hone is greater. Manual finishing therefore consumes 8.4kWh (30.24MJ) at a cost of GBP0.46, producing 1.8kgCO_2e. AFM operates at 4.485kW for 1h, consuming 4.485kWh (16.15MJ) at a cost of GBP0.56, producing 2kgCO_2e. In this example, manual finishing is 18% cheaper and produces 10% less CO_2e, but uses over twice the energy and takes 350% longer.

Part B is a larger titanium-alloy component comprised of an inlet and three outlets. Internal edges are to be processed around the three outlets, and are very difficult to get to by hand, yet simple by AFM. Due to a large entry bore reducing pressure drop and allowing a straight flowpath to the features, AFM can operate with less force. Manual finishing revolves around the use of electric drills with radius grinding attachments – as with part A, the process is continuous at 2.5h per part, 15h total time. Over this period, the heater is active for 0.9h (54min), while the drills operate intermittently, complemented by manually-applied abrasive cord. Drill utilization is 75%, operating at 0.192kW – over the 15h period, this results in 2.16kWh electricity consumption. Natural gas consumption at 35.2kW reaches 31.68kWh. Manual finishing therefore consumes 122MJ at a cost of GBP1.74, producing 6.8kgCO_2e. AFM operates at 4.313kW, in serial for 2h; electricity consumed is 8.6kWh (31MJ) at a cost of GBP1.07, producing 3.8kgCO_2e. In this example, manual finishing is 40% more expensive, 75% more energy consuming, takes 87% longer and produces 45% more CO_2e. Part C is considered in Tab. 3 – assuming a human labor value per hour of GBP25.00, man-hours for assembly and costed unlike in example parts A and B. Another titanium alloy component, the complexity requires four separate AFM fixtures, or over 110 manual hours to reach a finished state. In manual finishing, drills and non-powered tools are used, leading to a 60% drill utilization rate at a low fine-finishing current consumption of 0.2A, 0.0384kW. Over the duration of the work,

Table 3. COMPLEX PART FINISHING COMPARISON.

Operation	Manual	AFM
Assemble tooling (h)	-	1
Machining (h)	110	10 (4x2.5)
Clean, reassemble (h)	-	4 (3x1+1)*
Final cleaning (h)	0.5	2
Machining duration (h)	110.5	10
Total labour (h)	110.5	7 (1+4+2)
Business days (no.)	6.9	1.1
Grid electricity (kW)	0.0384	4.6
Natural gas (kW)	35.2	-
Total grid electricity (kWh)	2.5	46
	1.1kgCO_2e**	20.5kgCO_2e**
		***GBP12.39p/kWh
Total natural gas (kWh)	233.4	-
	43kgCO_2e	
		***GBP4.65p/kWh
Total power cost (GBP)	11	5.70
Total labour cost (GBP)	2,763	175
Total cost (GBP)	2,774	180.7
Total energy (J)	849	166

*Weighted to include machine monitoring
**Grid electric conversion factor of 0.44548
***British Gas values, standard tariff (Jan-2014)

2.5kWh is consumed, while the heater is operational for 6.63h, burning natural gas at 35.2kW, resulting in 233.4kWh. Manual finishing therefore consumes 849MJ, an energy cost of GBP11.16, and a human labor cost of GBP2,763. AFM operates over 10h, drawing 8A at 35bar – 4.6kW, therefore consuming 46kWh of grid electric. Activity varies while processing with AFM - there is 7h of labor to cost to cleaning, assembling and monitoring, but all processes can be performed in a little over two eight-hour shifts. See Tab. 3 for detailed values. AFM is five times faster, 15 times less expensive, 54% less generation of CO_2e and uses five times less energy.

EMBODIED ENERGY IN THE AFM PROCESS

Life cycle assessment (LCA) considers energy consumed and pollutants produced for a given process during and including activities preceding the end user's application (from cradle to grave) – in the case of AFM at Mollart, several key components and their principle constituent materials are presented in Tab. 4. LCA often benefits from a limitation of scope, to exclude minor energy consuming activities, i.e. assembly of framework using electric drills, heating and lighting in the machine builder's workshops (distribution amongst other machines, factory space and offices) or short range transport of small consumable parts. Scope can be determined by questioning how responsible the end-user can/could/should be for the identified impacts – in this instance, Mollart chose to adopt the AFM process, setting in motion a sequence of events which led the machine builder to purchase components, component manufacturers to obtain raw material and raw material producers to mine and refine for industrial use. Mollart's liability could be considered to stretch back to the

Table 4. EMBODIED ENERGY IN AFM MACHINE.

Subassembly	Component	Embodied energy
Hydraulic power pack	Hydraulic oil	75L of refined hydrocarbons
	3-phase electric motor	2kg neodymium
		2kg copper
Heating and cooling system	Refrigerant	1.5kg of R404A gas*
	Induction heating mat	0.191kg of nickel
Steel framework	Frame & cylinders	3,450kg mild carbon steel
	Fittings	50kg of hydrocarbon
PLC control	Circuit components	2.5kg of refined silicon in glass fibre and ICs
Tooling	Abrasive media	10kg silicone polymer 10kg boron carbide grit

*Volume replaced annually

mining phase, but the onus is also on the mills, refineries, manufacturers and OEMs to ensure they minimize their impact.

Table 5 breaks down the contents of the machine and identifies 10 major materials groups; i.e. hydrocarbons are refined from crude oil, and production of light oil consumes 9.49MJ/L, requiring 198kWh and producing 88kgCO_2e. Total energy estimated to have been consumed while producing material for the machine is in excess of 1,800kgCO_2e, which is equivalent [23] to a 17,000km flight from London to Sydney (per passenger km). Without including additional environmental burden such as pollutant from fuel used in transport or inefficient assembly practices, the values are not accrued through Mollart's actions, but by the OEM at the purchasing stage.

Embodied energy as a concept leads the engineer to question whether operation consumes more energy than it took to produce, and if so, whether the operation of the process can justify the initial CO_2e penalty. If the AFM machine operated on a two-shift basis for 76h/wk and 51wk/yr, the machine would be in production mode for 80% of time – 3,100h. As an average draw of 4.485kW leads to 13.9MWh (GBP1,722) (nearly 3.5 times as much energy as consumed in manufacture), the operating efficiency is of great importance during the use-phase. Compared to operation of the machine, approximately 6,200kgCO_2e is produced per annum – while over 25 years, the figure is 154tCO_2e putting the 'build:use' carbon equivalent ratio at 1:86. Potential to further separate the production-cost from the use-cost can be targeted using Fig. 6 – the chart uses data from Tab. 5 to present materials use by share of CO_2e generation. Steel framework and machine fittings are highly energy consuming, using the electric arc furnace to smelt elements of steel and polymer production relying on initial refining of crude oil. Steel is an inexpensive yet strong and ductile construction material, readily-recyclable and readily-available. In order to reduce the impact without using mechanically-unsuitable polymeric replacements, the only real option is to reduce overall consumption, or use different materials in a revised design. Using the [32] inventory of carbon energy (v1.6a), it is possible to estimate the costs of energy and embodied CO_2e when selecting engineering

Table 5. EMBODIED ENERGY IN AFM MACHINE.

Material	QTY.	E/QTY.	Power (kWh)	$kgCO_2e$	Ref.
Hydrocarbon	75L	9.49MJ/L	198	88	[24]
Neodymium	2kg	1.1MWh/t	2.2	1	[25]
Copper	2kg	64MJ/kg	36	16	[26]
Gas R404A	1.5kg	-	-	5.85*	[27]
Nickel	0.191kg	8717kWh/t	1.7	0.8	[25]
Steel	3,450kg	480kWh/t	1656	734	[28]
PP	50kg	81.6GJ/t	1133	505	[29]
Silicon	$0.28m^2$	$0.34kWh/cm^2$	952	424	[26]
Silicone	10kg	11.11MJ/kg	31	14	[30]
Boron Carbide	10kg	480kWh/t	4.8	2	[28]
Total			4014.7	1784.8	

* over 100 years [31]

materials. The values are higher than the production-only values used in Tab. 5 as they include extraction, manufacturing *and* transportation, known as cradle-to-site.

Exchanging the upper steel plate (670kg) (under bending load) for a steel I-beam, with the intention of reducing consumption and maintaining strength, should reduce by 562kg down to 108kg, saving approximately 27.2GJ. The identical steel base plate on the underside is capable of adopting the I-beam as well, and supporting steel framework is easily changed to granite – with manufacturing cost of 13.9MJ/kg, density of $2800kg/m^3$ and strength in compression makes granite an attractive proposition.

DESIGN & STANDARD PRACTICE PROPOSALS

Reductions in energy usage can be achieved by design changes, and increasing efficiency of individual components can significantly reduce the total energy consumption. For the following comparisons, a lifetime of 25yrs is considered, consuming 348MWh at today's prices (total GBP43,117).

Temperature regulation system

Regulation is performed by a permanently-on pair of silicone rubber-insulated wire heaters operating at 2x200W, accounting for 2.27A of the total 7.8A load. Cooling is performed by refrigerant gas fed through two bars over which the media flows. AFM generates thermal energy through friction; the system is weighted toward cooling by 60:40, translating to 3.4A (3.3kW). Active during 50% of the process, the current system consumes approximately 7.38MJ/h, costing nearly GBP19,685 over machine life. Naturally, presence of active heating surfaces when cooling requirement exists is not efficient and would benefit from continuous low-energy input.

Redesigning to remove current heating *and* cooling systems has the potential to concentrate the consumption on a single unit, which can be specified to suit an improved efficiency target. A unit has been identified to heat and cool water, between 5˚c and 50˚c – operating at maximum input power of

Figure 6. RAW MATERIALS BY $KGCO_2E$.

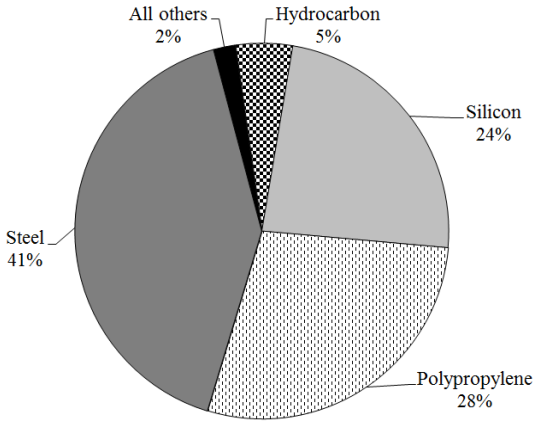

9.27kW, comprised of a compressor at 2.7kW, water pump at 0.37kW, heating device at 6kW and control at 0.2kW. Cooling capacity is 7.91kW. Media chemistry, processing conditions and job geometry affect the rate of heating, therefore an example of 35˚c reduced to 25˚c is provided in Eqns. 26-28. Specific heat for PDMS (Polydimethylsiloxane) is 1.552kJ/kg.K [33].

$$Q = m\, c_p\, dt / t \quad (26)$$

$$Q = (25 \times 1.552 \times -10) / 600 \quad (27)$$

$$Q = 0.646kW \quad (28)$$

10min is an acceptable time to heat or cool a substance, however, if the application is more aggressive and the rate of passive heating exceeds 0.016˚K/s (1˚c/min), more power will be consumed – an extreme example is 10˚c in 2min, requiring 3.23kW, which remains within 40% of total capacity. The change to a water-based heat-transfer fluid means the refrigerant used in the heat exchanger is sealed and does not form part of the working environment – all the nickel required in the heaters are removed and the system insulation is improved.

Machining strategy changes

As shown in Fig. 5, current consumption is driven by pressure. Not all force applied by the ram is used effectively; AFM is constrained by a number of factors, perhaps the largest is the customer's geometry – it cannot be modified, and tooling must be designed to support it, however tooling can act as a funnel to feed the media over a feature, rather than allow the media free roam in and around a part. There are several sources of unnecessary pressure drop; 1) workpiece and tooling features that allow a machine to pump media onto a flat face, forcing it to find an alternative path, 2) lack of soft-start valves, forcing media into a restricting cavity (however well designed) – this

reduces fatigue life of valves, tubes, pump components, tooling and carries a real risk of workpiece damage, and 3) use of tooling materials with porous surface structures, increasing friction significantly beyond that of rough metals. Polymeric materials are more elastic than most metals and are more resistant to the mode of material removal in AFM.

Wear rate reduction on consumables

Tooling, cylinder/pistons and media are considered replaceable elements in the AFM process. Tooling wears with use, but service life can be improved by careful design. Cylinders and pistons are in contact with media permanently. The longer they operate, the wider they become and the rate expansion increases as the gap between cylinder and piston widens. Media is comprised of a solid and liquid phase, where the silicone-based liquid phase is susceptible to contamination, and further, degradation, by fluids commonly found in the manufacturing process. Complete removal of contaminants is virtually impossible, but altering the chemistry to one developed at Mollart Engineering has provided a resistance to rheological property changes. Pressure drop also plays a role in media life – excessive temperature generated by over-working may chemically-damage the polymer. Solid phase abrasive grains always outlast the polymer – it is possible to break down the carrier chemically and filter the grains for re-use. While the grit does not impact on Fig. 6, it is a consumable that is used continuously throughout the machine life (as is the silicone polymer) and carries a high production energy cost, as high as steel and hydrocarbon product manufacture.

CONCLUSIONS & RECOMMENDATIONS

AFM's flexibility as a manufacturing tool requires experience and basic fluid dynamics knowledge to operate, reducing the appeal to many potential users. For those users that have already invested and worked with the technology, its capability is not in question, and assessments made in this research suggest it is significantly more viable than manual processes in terms of environmental and economic cost. AFM has been considered in the 'production' and 'use' phases of operation. Key findings include;

- As applications for surface finishing on complex geometries increase with additive layer manufacturing technologies and exposure of AFM to a wider audience, the capability of AFM will lead to greater process uptake. Environmental and economic considerations must be made.
- Working conditions required for human labor increase the environmental and economic cost of manual finishing while repeatability and accuracy are no better. Initial fixturing saves material and machining cost, but when workpieces become more complex and tooling/media is reused in a repeat order scenario, AFM excels at reducing cost and increasing quality.
- Embodied energy in the process is high, roughly equivalent to a 24h airplane journey, although the long service life and potential to make CO_2e savings outweighs the initial cost.
- Potential for subassembly replacement as a means of 'greening' is high – the most promising technically as well as environmentally is the estimated 91% reduction in energy use by adopting a mode of operation similar to household combination boiler, providing a low but persistent energy input to prevent spikes.
- Priorities for further work include improved software to control machine motion, development of process simulation techniques to avoid unnecessary or inefficient tooling and retrofitting of described combined temperature regulation system.

ACKNOWLEDGMENT

The authors would like to thank the support by the UK Engineering and Physical Sciences Research Council (EPSRC) for the EngD Scholarship. The authors would also like to thank Mollart Engineering Ltd (UK) for their continued funding and technical support.

REFERENCES

[1] Jain, V. K., Kumar, R., Dixit, P. M. & Sidpara, A., 2009. Investigations into Abrasive Flow Finishing of Complex Workpieces Using FEM. Wear, Volume 267, pp. 71-80.

[2] Mali, H. S. & Manna, A., 2009. Current Status and Application of Abrasive Flow Finishing Processes: a Review. Proceedings of the Institution of Mechanical Engineers, Part B: Journal of Engineering Manufacture, Volume 223, pp. 809-820.

[3] Cheema, M. S., Venkatesh, G., Dvivedi, A. & Sharma, A. K., 2012. Developments in Abrasive Flow Machining: a Review on Experimental Investigations Using Abrasive Flow Machining Variants and Media. Proceedings of the Institution of Mechanical Engineers, Part B: Journal of Engineering Manufacture, pp. 1951-1962.

[4] Draganescu, F., Gheorghe, M. & Doicin, C. V., 2003. Models of Machine Tool Efficiency and Specific Consumed Energy. Journal of Materials Processing Technology, 141(1), pp. 9-15.

[5] Gutowski, T. et al., 2005. Environmentally Benign Manufacturing: Observations from Japan, Europe and the United States. Journal of Cleaner Production, 13(1), pp. 1-17.

[6] Gutowski, T., Dahmus, J. & Thiriez, A., 2006. Electrical Energy Requirements for Manufacturing Processes. Leuven, Belgium, CIRP International Conference of Life Cycle Engineering (13th).

[7] Dahmus, J. B. & Gutowski, T. G., 2004. An Environmental Analysis of Machining. Anaheim,

California, USA, ASME International Mechanical Engineering Congress and RD&D Expo.

[8] Rhoades, L., 1991. Abrasive Flow Machining: A Case Study. Journal of Materials Processing Technology, Volume 28, pp. 107-116.

[9] Gorana, V. K., Jain, V. K. & Lal, G. K., 2004. Experimental Investigation into Cutting Forces and Active Grain Density During Abrasive Flow Machining. International Journal of Machine Tools and Manufacture, Volume 44, pp. 201-211.

[10] Howard, M., Cheng, K. & Mollart, G., 2012. Abrasive Flow Machining; R&D Strategy and Challenges in Industrial Applications. Birmingham, UK, Proceedings of the 10th International Conference on Manufacturing Research (ICMR2012).

[11] Baehre, D., Bruennet, H. & Swat, M., 2012. Investigation of One-Way Abrasive Flow Machining and In-Process Measurement of Axial Forces. Saarbrucken, Germany, Elsevier B. V., pp. 419-424.

[12] Kelly, K. M., 2005. Denso Seeks Next Diesel Breakthrough. Automotive Design and Production, November, 117(11), p. 36.

[13] Wilk, W. & Tota, J., 2007. Modern Technology of the Turbine Blades Removal Machining. Sofia, Bulgaria, Advanced Materials and Operations Society (Bulgaria), pp. 347-355.

[14] Howard, M. & Cheng, K., 2013. An industrially feasible approach to process optimisation of abrasive flow machining and its implementation perspectives. Proceedings of the Institution of Mechanical Engineers, Part B: Journal of Engineering Manufacture, 227(11), pp. 1748-1752.

[15] Aurich, J. C. et al., 2009. Burrs - Analysis, Control and Removal. CIRP Annals - Manufacturing Technology, Volume 58, pp. 519-542.

[16] Meteorological Office Hadley Centre for Climate Change (Tim Legg), 2013. Hadley Centre Central England Temperature (HadCET) dataset, Exeter, UK: http://www.metoffice.gov.uk/hadobs/hadcet/.

[17] British Government (HMG), 2013. www.legislation.gov.uk - The Workplace (Health, Safety and Welfare) Regulations 1992. [Online] Available at: http://www.legislation.gov.uk/uksi/1992/3004/made/data.pdf [Accessed 12 January 2014].

[18] Morrow, W. R. et al., 2004. Laser-Based and Conventional Tool and Die Manufacturing: Comparison of Environmental Aspects. Berlin, Germany, Global Conference on Sustainable Product Development and Life Cycle Engineering.

[19] Baniszewski, B. B. E., 2005. An Environmental Impact Analysis of Grinding, Cambridge, Massachusetts, USA: http://dspace.mit.edu/handle/1721.1/32880.

[20] Chryssolouris, G., 1991. Laser Machining-Theory and Practice. 1st ed. Cambridge, MA): MIT.

[21] Mukherjee, S. K., Kumar, S. & Srivistava, P. K., 2005. Effect of Over Voltage on Material Removal Rate During Electrochemical Machining. Tamkang Journal of Science and Engineering, 8(1), pp. 23-28.

[22] McGeough, J., 2005. Electrochemical Machining (ECM), Edinburgh, UK: http://electrochem.cwru.edu/encycl/art-m03-machining.htm.

[23] The Carbon Trust, 2013. Conversion Factors; Energy and Carbon Conversions, London, UK: http://www.carbontrust.com/media/18223/ctl153_conversion_factors.pdf.

[24] Szklo, A. & Schaeffer, R., 2007. Fuel Specification, Energy Consumption and CO2 Emission in Oil Refineries. Energy, 32(1), pp. 1075-1092.

[25] Yanjia, W. & Chandler, W., 2010. The Chinese Nonferrous Metals Industry - Energy Use and CO2 Emissions. Energy Policy, 38(1), pp. 6475-6484.

[26] Williams, E. D., Ayres, R. U. & Heller, H., 2002. The 1.7 Kilogram Microchip: Energy and Material Use in the Production of Semiconductor Devices. Environmental Science and Technology, 36(1), pp. 5504-5510.

[27] Tassou, S. A., De-Lille, G. & Ge, Y. T., 2009. Food Transport Refrigeration - Approaches to Reduce Energy Consumption and Environmental Impacts of Road Transport. Applied Thermal Engineering, 29(8-9), p. 1467.

[28] Worrell, E., Martin, N. & Price, L., 1999. Energy Efficiency and Carbon Dioxide Emissions Reduction Opportunities in the U.S. Iron and Steel Sector, California, USA: Lawrence Berkeley National Laboratory.

[29] Williams, R. H. & Larson, E. D., 1987. Materials, Affluence and Industrial Energy Use. Annual REview of Energy and Environment, 12(1), pp. 99-144.

[30] Papaefthimiou, S., Syrrakou, E. & Yianoulis, P., 2006. Energy Performance Assessment of an Electrochromic Window. Thin Solid Films, 502(1), pp. 257-264.

[31] Forster, P. et al., 2007. Changes in Atmospheric Constituents and in Radiative Forcing. In: S. Solomon, et al. eds. Climate Change 2007: The Physical Science Basis. Contribution of Working Group I to the Fourth Assessment Report of the Intergovernmental Panel on Climate Change. Cambridge, UK: Cambridge University Press, pp. 129-234.

[32] Hammond, G. P. & Jones, C. I., 2008. Embodied Energy and Carbon in Construction Materials. Proceedings of the Institution of Civil Engineers, 161(2), pp. 87-98.

[33] Kuo, A. C. M., 1999. Poly(dimethylsiloxane). In: Polymer Data Handbook. New York, NY, USA: Oxford University Press, pp. 411-435.

5. Zhong ZW. Recent advances in polishing of advanced materials. *Mater Manuf Process* 2008; 23(5): 449–456.
6. Ali-Tavoli M, Nariman-Zadeh N, Khakhali A, et al. Multi-objective optimization of abrasive flow machining processes using polynomial neural networks and genetic algorithms. *Mach Sci Technol: Int J* 2006; 10: 491–510.
7. Aurich JC, Dornfeld D, Arrazola PJ, et al. Burrs – analysis, control and removal. *CIRP Ann: Manuf Techn* 2009; 58: 519–542.
8. Petri KL, Billo RE and Bidanda B. A neural network process model for abrasive flow machining operations. *J Manuf Syst* 1998; 17(1): 52–64.
9. Mali HS and Manna A. Optimum selection of abrasive flow machining conditions during fine finishing of Al 15 wt% SiC-MMC using Taguchi method. *Int J Adv Manuf Tech* 2010; 50: 1013–1024.
10. Jain VK, Kumar R, Dixit PM, et al. Investigations into abrasive flow finishing of complex workpieces using FEM. *Wear* 2009; 267: 71–80.
11. Uhlmann E, Mihotovic V and Coenen A. Modelling the abrasive flow machining process on advanced ceramic materials. *J Mater Process Tech* 2009; 209: 6062–6066.
12. Wan SYM, Fong WS, Kong CJ, et al. *Low pressure abrasive flow machining*. Nanyang, Singapore: School of Mechanical and Aerospace Engineering, Singapore Institute of Manufacturing Technology, 2010.
13. Howard M and Cheng K. An industrially feasible approach to process optimisation of abrasive flow machining and its implementation perspectives. *Proc IMechE, Part B: J Engineering Manufacture*. Epub ahead of print 16 August 2013. DOI: 10.1177/0954405413491957.
14. Rajesha S, Venkatesh G, Sharma AK, et al. Performance study of a natural polymer based media for abrasive flow machining. *Indian J Eng Mater S* 2010; 17: 407–413.
15. Wang AC, Tsai L, Liang KZ, et al. Uniform surface polished method of complex holes in abrasive flow machining. *T Nonferr Metal Soc* 2009; 19: 250–257.

Appendix B – Media Manufacturing Notes.

Machine capacity of 19.64L is slightly reduced by cooling bars running through the lower cylinder – for each batch, we must aim to manufacture 19.5L. A calculator has been assembled in MS Excel which provides the information shown in table B.1 below. Experimental levels have been double checked, as have media configuration names. V1 and V2 are thrice repeated verifications of model batches.

Table B.1 – Media manufacturing guide.

Run	Uses	Media name	Polymer		Modifier		Primary grit		Filler grit	
Centroid	7	M50(50)/F30(B)(40)/F400(B)(10)	6.475	kg	6.475	kg	10.36	kg	2.59	kg
2	3	M60(50)/F16(B)(40)/F400(B)(10)	5.02	kg	7.53	kg	10.04	kg	2.51	kg
3	3	M60(35)/F30(B)(52)/F400(B)(13)	4.109	kg	6.164	kg	15.26	kg	3.816	kg
5	3	M40(50)/F240(B)(40)/F400(B)(10)	8.01	kg	5.34	kg	10.68	kg	2.67	kg
6	3	M50(35)/F240(B)(52)/F400(B)(13)	5.25	kg	5.25	kg	15.6	kg	3.9	kg
8	3	M50(35)/F16(B)(52)/F400(B)(13)	5.25	kg	5.25	kg	15.6	kg	3.9	kg
9	3	M40(35)/F30(B)(52)/F400(B)(13)	6.468	kg	4.312	kg	16.02	kg	4.004	kg
10	3	M50(65)/F16(B)(28)/F400(B)(7)	7.378	kg	7.378	kg	6.356	kg	1.589	kg
12	3	M60(65)/F30(B)(28)/F400(B)(7)	5.694	kg	8.541	kg	6.132	kg	1.533	kg
13	3	M60(50)/F240(B)(40)/F400(B)(10)	5.02	kg	7.53	kg	10.04	kg	2.51	kg
14	3	M40(65)/F30(B)(28)/F400(B)(7)	9.165	kg	6.11	kg	6.58	kg	1.645	kg
15	3	M40(50)/F16(B)(40)/F400(B)(10)	8.01	kg	5.34	kg	10.68	kg	2.67	kg
18	3	M50(65)/F240(B)(28)/F400(B)(7)	7.378	kg	7.378	kg	6.356	kg	1.589	kg
V1	3	M45(60)/F12(B)(32)/F400(B)(8)	7.953	kg	6.507	kg	7.712	kg	1.928	kg
V2	3	M55(40)/F80(B)(48)/F400(B)(12)	5.058	kg	6.182	kg	13.49	kg	3.372	Kg
Total;			96.24	kg	95.3	kg				
					127	L				
Available batch size;			22.6	kg	25	L				
Batch requirement;			4	-	6	-				
Batch unit cost;			480.2	£	186	£				
Batch total cost;			1921	£	111	£				
Per unit cost;			21.25	£/kg	7.45	£/L				

Table B.2 – Media grit size requirements					
FEPA size	Mean size µm	Requirement kg	Contingency kg	Cost per unit £/kg	Total £
F12	1600	7.71	10	28.50	285.00
F16	1092	42.68	45	28.50	1282.50
F30	571	54.352	55	28.50	1567.50
F80	165	13.5	15	29.75	446.25
F240	50	42.68	45	32.10	1444.50
F400	25	40.23	45	32.10	1444.50
				Total;	6470.25

In future it may necessary to estimate the media costs for production jobs or for customer purchase – in the case of the experiment above, containing typical values of MP, GF and GS, we can estimate a total cost of 15 batches at approximately ~£16,000, where the average batch cost is ~£1,050 and the average per litre cost (necessary for calculating the cost of filling a machine) is ~£55/L. The spread of cost is also interesting – typically 20%/8%/57%/15% (polymer/modifier/primary/filler).

Media volume and weight calculator, v1.1, 23/JUL/2013					
*Column B boxes **must** equal 100*			Weight kg	Density kg/m^3	Volume L
Media total	1	kg	1	1935.93	0.66
Grain fraction	35	% (carrier)	0.35	925.5	0.39
	65	% (grit)	0.65	2480	0.26
Filler fraction	80	% (primary grit)	0.52	2480	0.21
	20	% (filler grit)	0.13	2480	0.05
Modifier percentage	45	% (polymer)	0.1575	1140	0.14
	55	% (modifier)	0.1925	750	0.26

Calculator for media weight and volume. Yellow fields are user set.

Table above presents the total expected processing time, assuming a 15 minute media unload-clean-load cycle. Working with the constant 195mm/min piston speed and 146mm stroke and 25 cycles (workpiece 145m) processing length, a total of 43 runs will take; 195mm/min, with a total of 7.3m machine travel is approximately 40min per sample, therefore a total of 28.6hrs, or 3.5 standard working days. Including a total of 18 changes, we add 4.5hrs to the total run time.

Table B.3 – Terminology	
Base polymer	Main part of liquid phase in the media, providing the expected rheological behaviour, the base polymer provides ability to suspend solid particles.
Batch	A quantity of ~25kg, suitable for the Mollart Duplex machine to process testpieces to the same stroke length as in the machine experiments. May vary in volume slightly based on density of media constituent parts.
Bulk properties	'Bulk' references media properties as a homogenous substance, whereas non-bulk references a specific element of the media.
Carrier	Collective term for base and modifier combined. Constitutes a fraction of the media volume dependent on grit:carrier (grain fraction) weighting.
FEPA	Acronym - Federation of European Producers of Abrasives – provides the standard method of classifying grit into size groups according to their internal standard.
Filler grit	Media supplied by Micro Technica Technologies (MTT) appears to universally contain a fine grit at F400 that purportedly makes the remaining larger grits more aggressive.
Grain fraction	Term describing percentage split of media in terms of carrier:grit, by weight. High grain fraction is one whose grit percentage is higher than carrier.
Modifier	The secondary part of the liquid phase in the media. Modifier is mixed with base polymer to alter rheological properties.
Modifier percentage	By weight, the total fraction of modifying oils in the media, conducive to lowering the viscosity for the purpose of easing pumping requirements and conforming media to sharp or complex features.
POI	Acronym – Point of Interest – the generic term used to discuss the central exposed peak of the testpiece, corresponding to the virtual equivalent, and by extension, any single vertex within another geometry.
Primary grit	Media contains a main grit, typically the largest FEPA size. This grit purportedly carries out the main act of material removal.
Secondary grit	Often, a secondary material removal grit is employed with the primary and filler – MTT's response is that the grit inclusion is an experiential addition and they're not sure of the effects or reasons, to date.
Stability	The long term retention of properties while in static storage – the expectation that grit remains dispersed, oil and polymer remain mixed and the operator is able to unload a homogenous substance. Currently only proven to be stable up to 50/50 modification percentage.

Appendix C – Machine Parameter Study Data Collection.

Table C.1 Average roughness responses from n=81 samples, mean, standard deviation and standard deviation as percentage of mean. Population means also included.

#	V	T	Q	Ra_1	Ra_2	Ra_3	$\bar{x}_{Ra}$	σ_{Ra}	σ_{Ra} % $\bar{x}_{Ra}$
	mm/s	˚c	m	µm	µm	µm	µm	µm	%
1	80	25	40	0.384	0.380	0.328	0.364	0.026	7.01
2	80	25	145	0.649	0.726	0.821	0.732	0.070	9.61
3	80	25	250	1.133	1.103	0.951	1.062	0.080	7.50
4	80	35	40	0.298	0.297	0.258	0.284	0.019	6.55
5	80	35	145	0.478	0.395	0.437	0.437	0.034	7.76
6	80	35	250	0.447	0.431	0.463	0.447	0.013	2.92
7	80	45	40	0.305	0.247	0.258	0.270	0.025	9.32
8	80	45	145	0.246	0.257	0.222	0.242	0.015	6.05
9	80	45	250	0.309	0.334	0.272	0.305	0.025	8.35
10	185	25	40	0.493	0.541	0.584	0.539	0.037	6.89
11	185	25	145	0.964	0.950	0.963	0.959	0.006	0.66
12	185	25	250	0.736	0.776	0.780	0.764	0.020	2.60
13	185	35	40	0.428	0.386	0.483	0.432	0.040	9.19
14	185	35	145	0.586	0.545	0.590	0.574	0.020	3.54
15	185	35	250	1.181	1.103	1.034	1.106	0.060	5.43
16	185	45	40	0.303	0.275	0.282	0.287	0.012	4.15
17	185	45	145	0.269	0.295	0.239	0.268	0.023	8.55
18	185	45	250	0.292	0.260	0.279	0.277	0.013	4.74
19	265	25	40	0.484	0.543	0.517	0.515	0.024	4.69
20	265	25	145	0.555	0.518	0.590	0.554	0.029	5.30
21	265	25	250	0.626	0.676	0.693	0.665	0.028	4.28
22	265	35	40	0.712	0.685	0.602	0.667	0.047	7.02
23	265	35	145	0.803	0.845	0.828	0.825	0.017	2.09
24	265	35	250	1.215	1.360	1.181	1.252	0.078	6.20
25	265	45	40	0.424	0.442	0.449	0.438	0.011	2.40
26	265	45	145	0.632	0.723	0.690	0.682	0.038	5.52
27	265	45	250	0.440	0.361	0.412	0.404	0.033	8.09
						Population means	0.569	0.031	5.79

Table C.2 Material removal responses from n=81 samples, mean, standard deviation and standard deviation as percentage of mean. Population means also included.

#	V	T	Q	MR_1	MR_2	MR_3	$\bar{x}_{MR}$	σ_{MR}	σ_{MR} % $\bar{x}_{MR}$
	mm/s	˚c	m	mm^2	mm^2	mm^2	mm^2	mm^2	%
1	80	25	40	0.223	0.210	0.200	0.211	0.009	4.46
2	80	25	145	0.533	0.540	0.450	0.508	0.041	8.05
3	80	25	250	0.810	0.800	0.805	0.805	0.004	0.51
4	80	35	40	0.180	0.180	0.167	0.176	0.006	3.49
5	80	35	145	0.190	0.160	0.187	0.179	0.013	7.54
6	80	35	250	0.270	0.230	0.240	0.247	0.017	6.89
7	80	45	40	0.140	0.150	0.160	0.150	0.008	5.44
8	80	45	145	0.170	0.150	0.166	0.162	0.009	5.33
9	80	45	250	0.210	0.230	0.210	0.217	0.009	4.35

10	185	25	40	0.280	0.300	0.288	0.289	0.008	2.84
11	185	25	145	0.570	0.520	0.550	0.547	0.021	3.76
12	185	25	250	1.030	1.000	1.120	1.050	0.051	4.86
13	185	35	40	0.190	0.190	0.180	0.187	0.005	2.53
14	185	35	145	0.270	0.240	0.237	0.249	0.015	5.98
15	185	35	250	0.340	0.320	0.340	0.333	0.009	2.83
16	185	45	40	0.200	0.180	0.198	0.193	0.009	4.67
17	185	45	145	0.170	0.170	0.160	0.167	0.005	2.83
18	185	45	250	0.180	0.190	0.170	0.180	0.008	4.54
19	265	25	40	0.270	0.260	0.250	0.260	0.008	3.14
20	265	25	145	0.311	0.270	0.330	0.304	0.025	8.25
21	265	25	250	0.850	0.710	0.750	0.770	0.059	7.65
22	265	35	40	0.210	0.220	0.200	0.210	0.008	3.89
23	265	35	145	0.320	0.370	0.330	0.340	0.022	6.35
24	265	35	250	0.540	0.490	0.460	0.497	0.033	6.64
25	265	45	40	0.190	0.200	0.210	0.200	0.008	4.08
26	265	45	145	0.300	0.280	0.290	0.290	0.008	2.82
27	265	45	250	0.220	0.180	0.210	0.203	0.017	8.36
						Population means	0.330	0.016	4.89

Table C.3 Peak height reduction responses from n=81 samples, mean, standard deviation and standard deviation as percentage of mean. Population means also included.

#	V	T	Q	PHR_1	PHR_2	PHR_3	$\bar{x}_{PHR}$	σ_{PHR}	σ_{PHR} % $\bar{x}_{PHR}$
	mm/s	˚c	m	mm	mm	mm	mm	mm	%
1	80	25	40	0.180	0.159	0.163	0.167	0.009	5.44
2	80	25	145	0.487	0.460	0.411	0.453	0.031	6.95
3	80	25	250	0.621	0.627	0.503	0.584	0.057	9.78
4	80	35	40	0.142	0.130	0.134	0.135	0.005	3.69
5	80	35	145	0.233	0.226	0.250	0.236	0.010	4.26
6	80	35	250	0.224	0.210	0.213	0.216	0.006	2.79
7	80	45	40	0.042	0.038	0.038	0.039	0.002	4.79
8	80	45	145	0.059	0.059	0.067	0.062	0.004	6.12
9	80	45	250	0.209	0.240	0.204	0.218	0.016	7.32
10	185	25	40	0.227	0.234	0.195	0.219	0.017	7.76
11	185	25	145	0.456	0.438	0.382	0.425	0.032	7.41
12	185	25	250	0.665	0.657	0.617	0.646	0.021	3.25
13	185	35	40	0.150	0.157	0.172	0.160	0.009	5.75
14	185	35	145	0.294	0.310	0.333	0.312	0.016	5.12
15	185	35	250	0.447	0.384	0.365	0.399	0.035	8.79
16	185	45	40	0.066	0.073	0.064	0.068	0.004	5.70
17	185	45	145	0.078	0.072	0.070	0.073	0.003	4.64
18	185	45	250	0.096	0.092	0.095	0.094	0.002	1.80
19	265	25	40	0.228	0.236	0.224	0.229	0.005	2.18
20	265	25	145	0.366	0.329	0.362	0.352	0.017	4.71
21	265	25	250	0.626	0.553	0.612	0.597	0.032	5.30
22	265	35	40	0.207	0.207	0.200	0.205	0.003	1.61
23	265	35	145	0.336	0.421	0.368	0.375	0.035	9.35
24	265	35	250	0.544	0.533	0.535	0.537	0.005	0.89
25	265	45	40	0.141	0.152	0.149	0.147	0.005	3.15
26	265	45	145	0.337	0.307	0.355	0.333	0.020	5.95
27	265	45	250	0.223	0.264	0.282	0.256	0.025	9.63
						Population means	0.279	0.016	5.34

Appendix D – C-Language File to Describe Media in Fluent.

```
#include "udf.h"

/*  Define dynamic global variables  */

int N_points;
real tft[150][7];


/* Read  specific information from  'data.pf' and          */
DEFINE_ON_DEMAND(get_data)
{
 int i, nl, kick;
 FILE *fp1;
 char visc_file[50];

 kick = 101;
 sprintf(visc_file, "data3d.pf");

  if ((fp1 = fopen(visc_file, "r+"))==NULL)
    {
     Message("Cannot open data.pf...check file!\n");
    }
  else
    {
      Message("Reading viscosity strain rate Data ...\n");
                    nl = 0;
                    while(fscanf(fp1,  "%f  %f  %f  %f\n",  &tft[nl][0],&tft[nl][1],&tft[nl][3],&tft[nl][5]
)!=EOF)
                      ++nl;

                    kick = nl; /* global used to capture when loop exceeds data in set data */
                    Message("Number of lines in file is %d\n", nl);

                    N_points = nl;
                    i=0;
                    for(i=0; i<nl; i++)
                      {
                                  if (i==0)
                                   {
                                   tft[i][2] = (tft[i+1][1]-tft[i][1])/(tft[i+1][0]-tft[i][0]);
                                   tft[i][4] = (tft[i+1][3]-tft[i][3])/(tft[i+1][0]-tft[i][0]);
                                   tft[i][6] = (tft[i+1][5]-tft[i][5])/(tft[i+1][0]-tft[i][0]);
                                   }
                                  else
                                              {
                                              tft[i][2] = (tft[i][1]-tft[i-1][1])/(tft[i][0]-tft[i-1][0]);
                                              tft[i][4] = (tft[i][3]-tft[i-1][3])/(tft[i][0]-tft[i-1][0]);
                                              tft[i][6] = (tft[i][5]-tft[i-1][5])/(tft[i][0]-tft[i-1][0]);
                                              }
                        Message("%f  %f  %f  %f  %f  %f  %f\n",tft[i][0],tft[i][1],  tft[i][2],tft[i][3],tft[i][4],
tft[i][5],tft[i][6]);
                      }
                    Message("viscosity strain rate data read lines = %d..\n",N_points);

                }
      fclose(fp1);
```

```
}

DEFINE_PROPERTY(cell_viscosity,c,t)
{
 real mud_vis;
 mud_vis = C_UDMI(c,t,0);
 return mud_vis;
}

DEFINE_ADJUST(set_udm, d)
{
 Thread *ct;
 Thread **pt;
 cell_t c;
 int i;
 real vis25, vis35, vis45,grad;

 if ( current_iter%20 == 0 )
  {
   Message("Current iteration = %d recalculating viscosity field global var transfered = %d ...\n",current_iter, (N_points != NULL));
   thread_loop_c(ct,d)
            {
             if (FLUID_THREAD_P(ct))
               {
                begin_c_loop(c,ct)
                        {
                        i=0;
                        for(i=0; i<N_points; i++)
                         {
                                        if ((C_STRAIN_RATE_MAG(c,ct)>= tft[i][0]) && (C_STRAIN_RATE_MAG(c,ct) < tft[i+1][0]))
                                        {
                                         vis25 = tft[i][1]+(tft[i][2]*(C_STRAIN_RATE_MAG(c,ct)-tft[i][0]));
                                         vis35 = tft[i][3]+(tft[i][4]*(C_STRAIN_RATE_MAG(c,ct)-tft[i][0]));
                                         vis45 = tft[i][5]+(tft[i][6]*(C_STRAIN_RATE_MAG(c,ct)-tft[i][0]));
                                         if (C_T(c,ct)<=308.15)
                                          {
                                                grad = (vis35-vis25)/10.;  /*changed round 30sep mds*/
                                                C_UDMI(c,ct,0) = vis35+(grad*(C_T(c,ct)-308.15));
                                          }
                                         if (C_T(c,ct)>308.15)
                                          {
                                                grad = (vis45-vis35)/10.;
                                                C_UDMI(c,ct,0) = vis35+(grad*(C_T(c,ct)-308.15));
                                          }
                                        }
                         }
                        /* Message(" strain rate = %4.1f, vis = %f ",C_STRAIN_RATE_MAG(c,ct),C_UDMI(c,ct,0));*/
                        }
               }
              end_c_loop(c,ct)
               } } }
```